

UNCLASSIFIED

AD NUMBER
AD802590
NEW LIMITATION CHANGE
TO Approved for public release, distribution unlimited
FROM Distribution authorized to U.S. Gov't. agencies and their contractors; Critical Technology; OCT 1966. Other requests shall be referred to Air Force Rocket Propulsion Laboratory, Attn: RPPR/STINFO, Edwards AFB, CA 93523.
AUTHORITY
AFRPL ltr, 20 Dec 1971

THIS PAGE IS UNCLASSIFIED

AFRPL-TR-66-258

802590

SYSTEM EFFECTS ON PROPELLANT STORABILITY
AND VEHICLE PERFORMANCE

G.W. BURGE
DOUGLAS AIRCRAFT COMPANY, INC.

DAC-59314

FINAL TECHNICAL REPORT AFRPL-TR-66-258

OCTOBER 1966

"This document is subject to special export controls and each transmittal to foreign governments or foreign nationals may be made only with prior approval of AFRPL/RPPR/STINFO), Edwards, California 93523"

AIR FORCE PROPULSION LABORATORY
AIR FORCE SYSTEMS COMMAND
RESEARCH AND TECHNOLOGY DIVISION
EDWARDS AIR FORCE BASE, CALIFORNIA

Best Available Copy

6

SPECIAL NOTICES

Qualified users may obtain copies of this report from the Defense Documentation Center.

Defense Documentation Center release to the Office of Technical Services is not authorized.

Do not return this copy. Retain or destroy.

"When U. S. Government drawings, specifications, or other data are used for any purpose other than a definitely related Government procurement operation, the Government thereby incurs no responsibility nor any obligation whatsoever, and the fact that the Government may have formulated, furnished, or in any way supplied the said drawings, specifications, or other data, is not to be regarded by implication or otherwise, or in any manner licensing the holder or any other person or corporation, or conveying any rights or permission to manufacture, use, or sell any patented invention that may in any way be related thereto."

AFRPL-TR-66-258

**SYSTEM EFFECTS ON PROPELLANT STORABILITY
AND VEHICLE PERFORMANCE**

G.W. BURGE
DOUGLAS AIRCRAFT COMPANY, INC.
DAC-59314

FINAL TECHNICAL REPORT AFRPL-TR-66-258

OCTOBER 1966

"This document is subject to special export controls and its transmittal to foreign governments or foreign nationals may be made only with prior approval of AFRPL/RPPR/STINFO), Edwards, California 93523"

FOREWORD

The System Effects on Propellant Storability and Vehicle Performance program was conducted by the Missile and Space Systems Division (MSSD) of Douglas Aircraft Company, Inc., under the sponsorship of the United States Air Force Rocket Propulsion Laboratory, Research and Technology Division, Air Force Systems Command, Air Force Test Center, Edwards Air Force Base, California. The research was performed as Project No. 6753 and Task No. 750G under Air Force Contract No. AF 04(611)-10750, dated 1 March 1965, and covers work conducted from 1 March 1965 through 19 August 1966.

This report is cataloged by MSSD as Report No. DAC-59314. The authors acknowledge the major contributions to this report by Messrs. B. Schulkin, E. C. Cady, D. W. Kendle, R. H. Michaelles, P. Marvschak, J. Rhoades, S. J. Viscovich, B. R. Heckman, F. Wright, and Dr. M. Thomas.

This technical report has been reviewed and is approved by:

Edward Dahl, 1st/Lt. USAF
Project Engineer RPRPP

ABSTRACT

The objective of this program was to investigate the tradeoff between propellant storability and vehicle performance for the propellant storage and feed subsystem of a hypothetical LF_2/LH_2 space propulsion system. Detailed parametric analyses were conducted on such subsystem problem areas as booster-pump feed system utilization, feed line design, venting requirements and provisions, selection of thermal-control coatings, propellant utilization requirements, selection and design of insulation and tank supports, and pressurization system design. Each area was optimized for a spectrum of mission requirements and design ground rules. Design recommendations were derived on the basis of these results.

A full-scale, non-flightweight test article was designed, fabricated, and tested to simulate the propellant storage and feed subsystem. This apparatus incorporated, wherever practical, the recommendations of the study effort. (The simulator, which uses LH_2 and LN_2 , will be tested in the Edwards Air Force Base Space Simulation Facility to obtain experimental data for correlating certain thermodynamic analytical models used in this study.)

CONTENTS

LIST OF ILLUSTRATIONS	vii
LIST OF TABLES	xiii
Section I INTRODUCTION	1
Section II SUMMARY	3
1. Phase I -- Feed Systems	3
2. Phase II -- Feed System Line Losses	3
3. Phase III -- Venting	3
4. Phase IV -- Vehicle Thermal Control	3
5. Phase V -- Propellant Utilization System	4
6. Phase VI -- Tank Insulation and Support System	4
7. Phase VII -- Pressurization System	6
8. Phase VIII -- Test Apparatus	6
9. Phase IX -- Space Simulation Testing	6
Section III CONCLUSIONS	9
1. Phase I -- Feed Systems	9
2. Phase II -- Line Losses	9
3. Phase III -- Venting	10
4. Phase IV -- Vehicle Thermal Control	10
5. Phase V -- Propellant Utilization	10
6. Phase VI -- Tank Insulation and Support	10
7. Phase VII -- Pressurization System	11
Section IV TECHNICAL DISCUSSION	13
1. Phase I -- Feed Systems	13
2. Phase II -- Feed Line Losses	34
3. Phase III -- Venting	52
4. Phase IV -- Vehicle Thermal Control	115
5. Phase V -- Propellant Utilization	118
6. Phase VI -- Tank Insulation and Support	136
7. Phase VII -- Pressurization System	221
8. Phase VIII -- Test Apparatus Design and Fabrication	286
9. Phase IX -- Space Simulation Testing	319

Section V NOMENCLATURE	333
Section VI REFERENCES	337
DISTRIBUTION LIST	341
Appendix A: Space Propulsion System Optimization Program	347
Appendix B: Preliminary Pressure Histories	349
Appendix C: Overall System Optimization Approach	359
1. Basic Information for Optimization	359
2. Optimization Plan	359
Appendix D: Hardware Test Items	363

ILLUSTRATIONS

Figure

2-1	Configuration of Study Vehicle	8
4-1	Booster-Pump System Alternatives	14
4-2	Candidate Booster-Pump Systems	18
4-3	Parametric Weights of Basic Components	19
4-4	Component Efficiencies	20
4-5	Booster-Pump System Weights (Less Required Drive Propellant System Weights)	22
4-6	Propellant Flow Requirements for Booster-Pump System	24
4-7	Total System Weights for Candidate Booster-Pump Systems	25
4-8	Minimum Potential Weight for Booster-Pump System	27
4-9	Baseline Stage Performance Without Booster Pumps	30
4-10	Booster-Pump Optimization for Pressure-Fed Systems	31
4-11	Booster-Pump Optimization for Pump-Fed Systems	32
4-12	Comparison of LF_2 Feed Line Weight Penalties	41
4-13	Comparison of LH_2 Feed Line Weight Penalties	42
4-14	Comparison of Vent Line Weight Penalties	43
4-15	Steady-State Temperature Profiles for Liquid Fluorine Feed Line for Insulated Tanks	45
4-16	Steady-State Temperature Profiles for LF_2 Feed Line for Insulated Shroud	46
4-17	Temperature History for LF_2 Feed Line (Insulated Stainless Steel for Insulated Shroud)	47
4-18	Location of $-260^\circ F$ Point in LF_2 Feed Line	49
4-19	Total Integrated Heat Through LF_2 Feed Line (Insulated Stainless Steel)	50
4-20	Prevalve Bypass and Feed Line Relief	53
4-21	Boiloff Loss for LH_2 Feed Line (24-Hr Duty Cycles)	53
4-22	Boiloff Loss for LH_2 Feed Line (120-Hr Missions)	54

Figure

4-23	Boiloff Loss for LH ₂ Feed Line (336-Hr Missions)	54
4-24	Capillary Stability Criteria for External Disturbances	60
4-25	Mechanical Liquid/Vapor Separator	64
4-26	Thermodynamic Liquid/Vapor Separator	66
4-27	Optimum Tube Entrance Pressure as a Function of Tank and Exit Pressures for LH ₂	72
4-28	Optimum Tube Entrance Pressure as a Function of Tank and Exit Pressures for LF ₂	73
4-29	Thermodynamic Separator Length as a Function of Vent Flow Rate	75
4-30	Thermodynamic Separator Diameter Parameter as a Function of Vent Flow Rate	76
4-31	Thermodynamic Separator Tubing Weight as a Function of Vent Flow Rate	77
4-32	Thermodynamic Separator Length as a Function of Vent Flow Rate	78
4-33	Thermodynamic Separator Diameter Parameter as a Function of Vent Flow Rate for Tank Pressures of 21 and 32 p.s.i.a.	79
4-34	Thermodynamic Separator Tubing Weight as a Function of Vent Flow Rate for Tank Pressures of 21 and 32 p.s.i.a.	80
4-35	Thermodynamic Separator Tubing Weight as a Function of Conductive Diameter Ratio	81
4-36	Thermodynamic Separator Tubing Weight as a Function of Percent of Liquid Covering Separator	82
4-37	Thermodynamic Separator Response Time as a Function of Conductive Diameter Ratio for LH ₂	84
4-38	Thermodynamic Separator Response Time as a Function of Conductive Diameter Ratio for LF ₂	85
4-39	Settling Time as a Function of Acceleration	88
4-40	Total Settling (Burn) Time as a Function of Settling Motor Thrust	89
4-41	Settling Weight Penalty as a Function of Settling Motor Thrust	90
4-42	Ullage Rocket Burn Time for Venting as a Function of Ullage Rocket Thrust	92
4-43	Ullage Rocket Weight Penalty for Venting as a Function of Ullage Rocket Thrust	93
4-44	Ullage Rocket Weight Penalty for Repressurization as a Function of Ullage Rocket Thrust	94

Figure

4-45	Dielectrophoretic Electrode Configuration	97
4-46	Heat Exchanger Length as a Function of Conductive Diameter Ratio	102
4-47	Heat Exchanger Diameter as a Function of Conductive Diameter Ratio	103
4-48	Minimum Heat Exchanger Tubing Weight as a Function of Conductive Diameter Ratio	104
4-49	Installation of Thermodynamic Liquid/Vapor Separator	106
4-50	Heat Flux to H ₂ Vent Tube Capacity as a Function of Time After Venting LH ₂ Tank (1/4-in. Tube Diam)	109
4-51	Heat Flux to H ₂ Vent Tube Capacity as a Function of Time After Venting H ₂ Tank (1-in. Tube Diam)	110
4-52	Heat Flux to H ₂ Vent Tube Capacity as a Function of Time After Venting H ₂ Tank (3-in. Tube Diam)	111
4-53	Weight of Solid F ₂ Frozen to H ₂ Vent Line as a Function of Time After Venting H ₂ Tank	112
4-54	Geometry Definition	116
4-55	Space Performance Comparison of Various Thermal Coatings	117
4-56	Circumferential Variation in Skin Temperature	118
4-57	Temperature Histories of Vehicle Surfaces	119
4-58	Propellant Utilization as a Function of Fuel Bias for Pump-Fed System H ₂ - F ₂	123
4-59	Propellant Utilization as a Function of Fuel Bias for Pressure-Fed System	124
4-60	Effect of Variation in Fuel Vented with a Pump-Fed System (Fuel Bias of 60 lb)	126
4-61	Effect of Variation in Fuel Vented with a Pump-Fed System (Fuel Bias of 20 lb)	126
4-62	Variation in Engine Mixture Ratio (19 Burn-14-Day Duty Cycle)	128
4-63	Optimum Bias for a Closed-Loop Propellant Utilization System for a Pump-Fed System with Nominal Venting (H109 Program)	130
4-64	F ₂ - H ₂ Vacuum Performance	133
4-65	Concepts of High-Performance Insulation	139
4-66	Simple Model to Evaluate Effect of Insulation Placement	147

Figure

4-67	Heat Flux Comparison for Shroud as a Function of Tank Insulation Placement	148
4-68	Vehicle Configuration for Preliminary Optimization	149
4-69	Comparison of Pure He Purges and Foam Substrate with Optimum Space Insulation	153
4-70	Generalized Configuration of Insulation	156
4-71	Ratio of Contact Area to Conduction Cross-Section Area for Dimplar Insulation	162
4-72	Ratio of Contact Area to Conduction Cross-Section Area for NRC-2 Insulation	163
4-73	Ratio of Contact Area to Conduction Cross-Section Area for Mylar and Paper Spacer Insulation	163
4-74	Insulation Heat Flux for Dimplar Shroud Mounting for LH ₂ Tank	165
4-75	Heat Flux for NRC-2 Shroud Mounting for LH ₂ Tank	166
4-76	Heat Flux for Aluminized Mylar-Paper Spacer Shroud Mounting for LH ₂ Tank	167
4-77	Heat Flux for Dimplar Shroud Mounting for LF ₂ Tank	168
4-78	Heat Flux for NRC-2 Shroud Mounting for LF ₂ Tank	169
4-79	Heat Flux for Aluminized Mylar-Paper Spacer Shroud Mounting for LF ₂ Tank	170
4-80	Heat Flux for Dimplar Mounting on LH ₂ Tank	171
4-81	Heat Flux for NRC-2 Mounting on LH ₂ Tank	172
4-82	Heat Flux for Aluminized Mylar-Paper Spacer Mounting on LH ₂ Tank	173
4-83	Heat Flux for Dimplar Mounting on LF ₂ Tank	174
4-84	Heat Flux for NRC-2 Mounting on LF ₂ Tank	175
4-85	Heat Flux for Aluminized Mylar-Paper Spacer Mounting on LF ₂ Tank	176
4-86	Comparison of Correlation Equation and Computer Results	179
4-87	Model for Ground-Hold Analyzer	181
4-88	Purged Interstage Ground-Hold Test	185
4-89	Internal Heat Transfer Coefficients During Boost	187
4-90	Skin Temperature Histories During Boost	189
4-91	Total Heat Input to Propellant During Boost	190

Figure

4-92	Effects of Pressure on NRC-2 High-Performance Insulation Thermal Performance	191
4-93	Decompression Test Apparatus	192
4-94	Pressure History During High-Performance Insulation Rapid Decompression Test	193
4-95	Insulation Attachment Methods	199
4-96	Continuous Conical Tank Support	206
4-97	Study Vehicle Tank Support	207
4-98	Nine-Rod Tension Member Support System	208
4-99	Weight Comparison for Study Vehicle LH ₂ Tank Support	213
4-100	Heat Transfer Through LH ₂ Tank Tension Support Rods (Equal Strength)	214
4-101	Optimization of LH ₂ Tank Insulation	216
4-102	Optimization of LF ₂ Tank Insulation	217
4-103	Candidate Pressurization Systems	225
4-104	Thrust-Chamber Heat Exchanger Weight as a Function of Volume Flow Rate	236
4-105	Heat Exchanger Weight as a Function of He Flow Rate	237
4-106	Auxiliary LH ₂ Tank Weight	238
4-107	LF ₂ /LH ₂ Gas Generator Weight (Fuel-Rich)	239
4-108	Pressure Control Components Weight	240
4-109	He Storage Bottle Weight	241
4-110	Pressurization System Weight as a Function of Summation of Repressurization ($V\Delta P$) _T for Pressure-Fed Systems	244
4-111	Pressurization System Weight as a Function of Summation of Repressurization ($V\Delta P$) _T for Pump-Fed System	245
4-112	F ₂ /H ₂ Gas Generator Hardware	246
4-113	Program H225 Function	263
4-114	Pressurant Requirements During Outflow	264
4-115	Ullage Temperature Profiles During Outflow	265
4-116	Pressurant Requirements During Expulsion	266
4-117	Pressurant Requirements for Pressurization and Expulsion	268
4-118	Pressurization Correction Factors for LH ₂ Tank with Initial Ullage of 80 Pct	269
4-119	Pressurization Correction Factors for LH ₂ Tank with Initial Ullage of 3 Pct	270

Figure

4-120	Effect of LH ₂ Tank Pressurant on Stage Performance	283
4-121	Effect of Pressurant Inlet Temperature on Performance of Pressure-Fed System	284
4-122	Effect of Pressurant Inlet Temperature on Performance of Pump-Fed System	285
4-123	LH ₂ Tank Penetration, Support Bracket and Internal Tank	288
4-124	Completed LN ₂ Tank Assembly	289
4-125	Overall Test Apparatus Layout	292
4-126	Insulation Installation Details	293
4-127	Insulation Fabrication and Installation	295
4-128	Nearly Completed Insulation	296
4-129	Test Apparatus Propulsion System	297
4-130	Valve Module	300
4-131	LN ₂ Tank Valve Complex	301
4-132	Tank Pressure Control System	303
4-133	Estimated Pressurant Heater Capability	304
4-134	Basic Data Instrumentation Location	311
4-135	LN ₂ Tank Temperature Rake	314
4-136	Completed Test Apparatus (Front View)	315
4-137	Completed Test Apparatus (Side View)	316

TABLES

Table		
2-1	Study Phase Vehicle Parameters	4
2-2	Duty Cycle Schedules	5
2-3	Test Apparatus Design Parameters	6
4-1	Booster-Pump Systems Studied	16
4-2	Preliminary Weights of Booster-Pump Drive System	17
4-3	Typical Booster-Pump System Weight Breakdown	26
4-4	Improvements in Usable Propellant Resulting from Use of Optimum Booster Pumps	32
4-5	Preliminary Specification Data for Optimum LH ₂ Booster Pump	33
4-6	Comparison of Bare and Vacuum-Jacketed LF ₂ Feed Lines	35
4-7	Comparison of Steady-State Heat-Transfer Rates for LF ₂ Feed Line Systems	37
4-8	Comparison of Steady-State Heat-Transfer Rates for LH ₂ Feed Line Systems	38
4-9	Comparison of Steady-State Heat-Transfer Rates for LF ₂ Vent Line Systems	39
4-10	Comparison of Steady-State Heat-Transfer Rates for LH ₂ Vent Line Systems	40
4-11	Assumed Conditions for Pressure History Computations	56
4-12	LH ₂ Lost Because of Venting (Lb.)	57
4-13	Weight Penalty for Liquid Venting	57
4-14	Estimated Weight Breakdown for an LH ₂ Tank Dielectrophoretic Propellant Positioning System	96
4-15	Venting System Weight Penalty Comparison	100
4-16	Optimized Venting Requirements	113
4-17	Comparison of Optimized and Estimated Heat Fluxes for 14-Day Mission	114
4-18	Deviations Used for Determining Fuel Bias (E. M. R. 13:1)	121
4-19	H ₂ Fuel Vapor Vented	125

Table

4-20	Effect of Fuel Bias on Closed-Loop Pump-Fed System	131
4-21	Closed-Loop Pump-Fed System	134
4-22	Closed-Loop Propellant Utilization	135
4-23	Comparison of Open-Loop and Closed-Loop Propellant Utilization	137
4-24	Space Insulation System Performance Values	141
4-25	Evaluation of Placement of High-Performance Insulation on the Shroud Interior	143
4-26	High-Performance Insulation Calorimeter Tests (IRAD)	146
4-27	Insulation Correlation Equation Coefficients	178
4-28	Insulation Weight Factors	180
4-29	Ground-Hold Propellant Heating	188
4-30	Theoretical Time for Insulation Model to Reach 10^{-4} Torr With Various Overlaps (L = 48 in.)	195
4-31	Effect of Perforations on Evacuation Time	197
4-32	Tankage System Design Support Loads	204
4-33	Flight Vehicle Tank Support Member Sizes for Nine-Rod System	210
4-34	Study Vehicle Tank Support System Weights (Lb.)	212
4-35	Comparison of Tank Support Concepts	214
4-36	Insulation Optimization Results (Optimum Usable Propellant Weights)	218
4-37	Insulation Optimization Results (Sheets of LH_2/LF_2 Insulation)	219
4-38	Pressurization Media and Energy Sources	223
4-39	Pressurization System Weight Summary	233
4-40	Fixed Weight Summary	243
4-41	Pressurant Requirements	271
4-42	Comparison of Pressurant Requirements	282
4-43	Pressurant Heater Operating Characteristics	305
4-44	Feed and Vent System Components	306
4-45	Test Data Instrumentation	309
4-46	Testing Run Sequence	321
C-1	Weight Breakdown	360
C-2	Heat Leak Estimates	361
D-1	Basic Test Hardware Itemization	364

Section I INTRODUCTION

Future space missions will undoubtedly require more complex and sophisticated space propulsion systems than are currently available. These systems may require one or all of the following characteristics:

- The capability to deliver total stage velocity changes well in excess of 10,000 f. p. s.).
- The ability to provide propulsive energy after extended periods of time in orbit (in the order of weeks).
- The capability to perform high-response multiburn firings with throttling where the specific mission would be indeterminate at the time of launch into orbit.

To efficiently achieve such advanced space missions, it is highly desirable to utilize a high-energy cryogenic propellant, particularly LH_2 and LF_2 . The high specific impulse and bulk density of this propellant combination permits the accomplishment of such missions with potentially lower stage gross weight and/or higher payload weights than other candidate propellant combinations. However, orbital heating with subsequent propellant boiloff losses can seriously compromise the capabilities of cryogenic stages for extended-time space missions. LH_2/LO_2 Centaur and Saturn S-IV type stages are efficient only for missions in the order of several hours in orbit. Therefore, it is necessary to develop radically new propellant storage and feed subsystems which can retain a large portion of the cryogenic propellants for subsequent utilization.

During the past several years, a great deal of research has been underway within the aerospace community to develop the technology required to store cryogenic propellant under the environmental conditions present in space. This has covered a broad field of problems including (1) the study of low-heat input surface coating, (2) the evolution of new vehicle structural concepts which have departed from the convention integral propellant tank techniques, (3) investigations into multilayer radiation shield insulation concepts, (4) investigations into advanced techniques for controlled venting in a low-gravity environment, (5) studies of how to design feed lines for low-heat input, (6) development of improved techniques for predicting pressurant behavior and its interaction with cryogenic propellants, and (7) development of analytical tools that can assess the influence of design factors on overall system performance, and many others.

At this point in time, the accumulated technology must be extended and applied to a definitive application to establish the overall capabilities of a high-energy space stage. It is not sufficient to study an isolated LH₂ tank, but, rather, the entire propellant storage and feed subsystem must be studied as an integrated end item with respect to a specific set or spectrum of overall system requirements. Only through such a study can parameter sensitivities and interactions be rationally established. This, in essence, was the overall objective of this contract.

For an assigned spectrum of mission requirements and design ground rules, detailed studies were conducted on specific problem areas relating to propellant storability and vehicle performance. Results of the individual studies were combined in an overall system optimization to establish preferred design approaches and conditions. Because the study conclusions were based on analyses and various types of experimental data, a specific experimental test apparatus was designed and built to permit an evaluation and correlation of as many of the employed theoretical factors as possible. This test apparatus along with a test plan for obtaining the required data was sent to EAFB/RPL in August 1966 where tests will be performed at EAFB space simulation facility.

Section II SUMMARY

The objective of this program was to study the influence of pertinent system design features and parameters on propellant storability and vehicle performance for a hypothetical LF_2/LH_2 maneuvering space propulsion system with the general features itemized in table 2-1 and operating under the duty cycles covered in table 2-2. The approach taken was to (1) perform theoretical studies on each basic subsystem and use the resulting data to optimize critical parameters for the overall system, (2) design and fabricate a test apparatus for evaluating as completely as possible, in a 1-g. space simulation chamber, the analytical models used and the appropriate influence coefficients for inclusion in these models, (3) evolve a test plan for utilizing this test apparatus and coordinate with Rocket Propulsion Laboratory (RPL) personnel to implement this test plan, and (4) use the test results to correlate and appropriately modify the analytical models and to reoptimize the vehicle design parameters where necessary. This approach was implemented by a nine-phase program as summarized below.

1. Phase I--Feed Systems. The objectives of this phase were to assess the utility of LH_2 booster pump systems for a range of engine chamber pressures, to establish optimum pump types, and to establish optimum operating parameters to reduce tank pressure and thereby affect a maximum improvement in usable propellant weight. A preliminary specification was developed for the optimum boost pump system. Through this study, an assessment of vented versus non-vented tanks as well as a comparison of booster pump and an all pressure-fed system were also made.
2. Phase II--Feed System Line Losses. The objectives of this phase were to evaluate the engine feed-line propellant losses for a conventional design, investigate methods for minimizing this source of propellant loss, and select and perform a preliminary design for the approach that shows the greatest potential.
3. Phase III--Venting. The objectives of this phase were to establish the propellant losses that result from uncontrolled venting, to study various techniques for achieving efficient all gas venting and to select and perform a preliminary design for the approach that shows greatest potential in terms of maximum usable propellant.
4. Phase IV--Vehicle Thermal Control. The objective of this phase was to select the best surface thermal coating for 1-, 5-, and 14-day missions including the time degradation of coating radiation properties..

Table 2-1
STUDY PHASE VEHICLE PARAMETERS

Parameter	Magnitude
Gross weight	20,000 lb.
Payload weight	5,000 lb.
Propellant weight	12,732 lb.
Propellants	LH ₂ /LF ₂
Loads:	
• Boost	5-g axial/1-g. lateral
• Orbit	1.5-g. axial/1.1-g. lateral
Maximum diameter	10 ft.
Fuel volume	214.6 ft. ³
Oxidizer volume	128.5 ft. ³
Propellant tank pressure	250-20 p. s. i. a.
Helium storage pressure	3,000 p. s. i. a.
Fuel flow rate	4.59 to 0.46 lb. p. sec.
Oxidizer flow rate	59.65 to 5.97 lb. p. sec.
Propellant mixture ratio	13:1
Orbit:	
• Altitude	260 n. mi.
• Inclination	66-1/2°
• Suntime	66 min.
• Shadetime	28 min.

5. Phase V--Propellant Utilization System. The objectives of this phase were to assess the capabilities of an open-loop propellant utilization system and compare this in terms of maximum usable propellant, with a closed-loop system having a range of accuracy capabilities.

6. Phase VI--Tank Insulation and Support System. The objectives of this phase were to study various integrated tank insulation, penetration, and support systems and select the system that shows maximum performance capabilities in terms of usable propellant considering both theoretical and practical features of the approach.

Table 2-2
DUTY CYCLE SCHEDULES

Duty Cycle	Burn Number	Times (hr.)	Percent Total Propellant Consumed	Maneuvers		Total Avg. Propellant Flow Rate (lb. p. s.)	Fuel Flow Rate	Oxidizer Flow Rate
				Intercept	Plane Change			
A	1	0	80	3	3	6.8	0.48	6.32
	2	26	100	1	1	5.05	0.37	4.68
B	1	0	50	2	2	6.37	0.45	5.92
	2	24	100	2	2	6.35	0.44	5.91
C	1	0	20	1	0	5.30	0.38	4.92
	2	3	30	1	0	65.00	4.6	60.4
	3	6	40	0	1	3.18	0.22	2.95
	4	8	60	0	1	65.00	4.6	60.4
	5	24	100	2	2	5.44	0.39	5.05
D	1	0	10	1/2	0	6.35	0.45	3.92
	2	2.7	20	1/2	0	4.43	0.32	4.11
	3	5.4	30	0	1/2	65.00	4.6	60.4
	4	8.1	40	0	1/2	65.00	4.6	60.4
	5	10.8	50	1/2	0	6.35	0.45	5.92
	6	13.5	60	1/2	0	4.72	0.34	4.38
	7	16.2	70	0	1	65.00	4.6	60.4
	8	18.9	80	1	0	2.54	0.18	2.36
	9	21.6	90	0	1	65.00	4.6	60.4
	10	24	100	1	0	2.83	0.20	2.63
E	1	24	100	4	4	6.5	0.46	6.04
F	1	0	80	3	3	6.8	0.48	6.32
	2	120	100	1	1	5.05	0.37	4.68
G	1	120	100	4	4	6.5	0.46	6.04
H	1	0	10			6.46	0.46	6.0
	2	12	13			6.46	0.46	6.0
	3	16	16			6.46	0.46	6.0
	4	20	19			6.46	0.46	6.0
	5	24	22			6.46	0.46	6.0
	6	28	25			6.46	0.46	6.0
	7	32	28			6.46	0.46	6.0
	8	36	31			6.46	0.46	6.0
	9	40	34			6.46	0.46	6.0
	10	44	37			6.46	0.46	6.0
	11	48	40			6.46	0.46	6.0
	12	72	44			6.46	0.46	6.0
	13	78	48			6.46	0.46	6.0
	14	84	52			6.46	0.46	6.0
	15	90	56			6.46	0.46	6.0
	16	96	60			6.46	0.46	6.0
	17	102	65			6.46	0.46	6.0
	18	108	70			6.46	0.46	6.0
	19	120	100			6.46	0.46	6.0
I	1	336	100	4	4	6.5	0.46	6.04
J	1	0	50	2	2	6.37	0.45	5.92
	2	336	100	2	2	6.35	0.44	5.91
K	1	0	80	3	3	6.8	0.48	6.32
	2	336	100	1	1	5.05	0.37	4.68
L	1	0	10			6.46	0.46	6.0
	2	4.8	12			6.46	0.46	6.0
	3	9.6	14			6.46	0.46	6.0
	4	14.4	16			6.46	0.46	6.0
	5	19.2	18			6.46	0.46	6.0
	6	24.0	20			6.46	0.46	6.0
	7	28.8	22			6.46	0.46	6.0
	8	33.6	24			6.46	0.46	6.0
	9	38.4	26			6.46	0.46	6.0
	10	43.2	28			6.46	0.46	6.0
	11	48.0	30			6.46	0.46	6.0
	12	180	60			6.46	0.46	6.0
	13	240	65.7			6.46	0.46	6.0
	14	256	71.4			6.46	0.46	6.0
	15	272	77.1			6.46	0.46	6.0
	16	288	82.8			6.46	0.46	6.0
	17	304	88.5			6.46	0.46	6.0
	18	320	94.2			6.46	0.46	6.0
	19	336	100			6.46	0.46	6.0

7. Phase V.L--Pressurization System. The objectives of this phase were to evolve an analytical model to adequately describe pressurant behavior and requirements and to use this model to predict pressurant requirements and optimum pressurization system design features and operating conditions. Heated He, vaporized H₂, and alternate systems were considered.

8. Phase VIII--Test Apparatus. The objective of this phase was to design and fabricate a test apparatus which can be utilized in the Edwards Air Force Base space simulator to experimentally evaluate, over a range of operating conditions, the analytical techniques and design features evolved in the previous seven study phases.

This apparatus was essentially full-scale, non-flightweight hardware using LH₂ and LN₂ (to simulate LF₂) with the general features tabulated in table 2-3.

9. Phase IX--Space Simulation Testing. The objectives of this phase were to evolve a test plan for utilization of the test apparatus, to provide coordination of the testing at RPL, and to correlate the test results with the analytical predictions, perform necessary modifications to the analysis, and reoptimize the system parameters and design features.

This report covers the work performed under all nine phases with the exception of the test coordination and data correlation and reoptimization tasks of Phase IX. These tasks will be documented in a supplementary report following testing at RPL.

Table 2-3
TEST APPARATUS DESIGN PARAMETERS

Parameter	Magnitude
Propellant	LH ₂ /LN ₂
Propellant weights:	
• LH ₂	932 lb.
• LN ₂	6,450 lb.
Maximum diameter	10 ft.
Fuel volume	214.6 ft. ³
Oxidizer volume	128.5 ft. ³
Propellant tank pressures	250-20 p. s. i. a.
Pressurant storage pressure	3,000 p. s. i. a.
Fuel flow rate	4.59 to 0.46 lb. p. sec.
Oxidizer flow rate	33 to 3.3 lb. p. sec.
Tankage design factor	3 on ultimate at 70°F

In the course of this program maximum possible use was made of the technology evolved and technical results achieved by other R&D contracts that were related to the problem areas under investigation in this contract. Particularly close coordination was maintained with contract AF04(611)-10745 that was being performed by Rocketdyne with Douglas Missile and Space Systems Division as a subcontractor. This contract covered a system study toward basically the same type of flight vehicle. Considerable information relative to subsystem weights, vehicle configuration and duty cycle were obtained from this source. Coordination meetings were also held with Lockheed Missiles and Space Company and progress reports were exchanged with NASA contract NAS3-4199 to ensure that the latest available data on insulation system design was used. To further this objective, technology review trips were also made to NASA/Lewis Research Center, NASA/George C. Marshall Space Flight Center, and Arthur D. Little.

The study relied heavily on results from Douglas Independent Research and Development programs (IRAD) in such areas as high-performance insulation (HPI), pressurization and feed system research, and F_2 technology.

A flight vehicle configuration was prepared early in the study to maintain continuity and a common point of comparison for all the individual studies. This was modified and detailed as the study progressed and as specific items were established in this study and in the work under way under contract AF04(611)-10745. The flight configuration in its final form is shown in figure 2-1. The tabulated tank pressures were agreed upon by Douglas and RPL in the early stages of the program. The general configuration is as defined by table 2-1 and from conclusions reached under contract AF04(611)-10745. The noted skin temperatures and tank support arrangement were determined from the findings of Phases IV and VI. Although a shroud-oriented insulation is illustrated in figure 2-1, the alternate insulation location was also considered throughout the study.

TANK PRESSURE AND TANK THICKNESSES FOR PURPOSE OF THERMAL MODELING

ENGINE CHAMBER PRESSURE	TANK PRESSURE	LH ₂ TANK THICKNESS	LF ₂ TANK THICKNESS
150	235*	0.190	0.158
125	195*	0.157	0.131
60	100*	0.081	0.067
PUMP CASE	41 (LH ₂)	0.032	.03
	62 (F ₂)	0.043	.02

2014-T6 Al

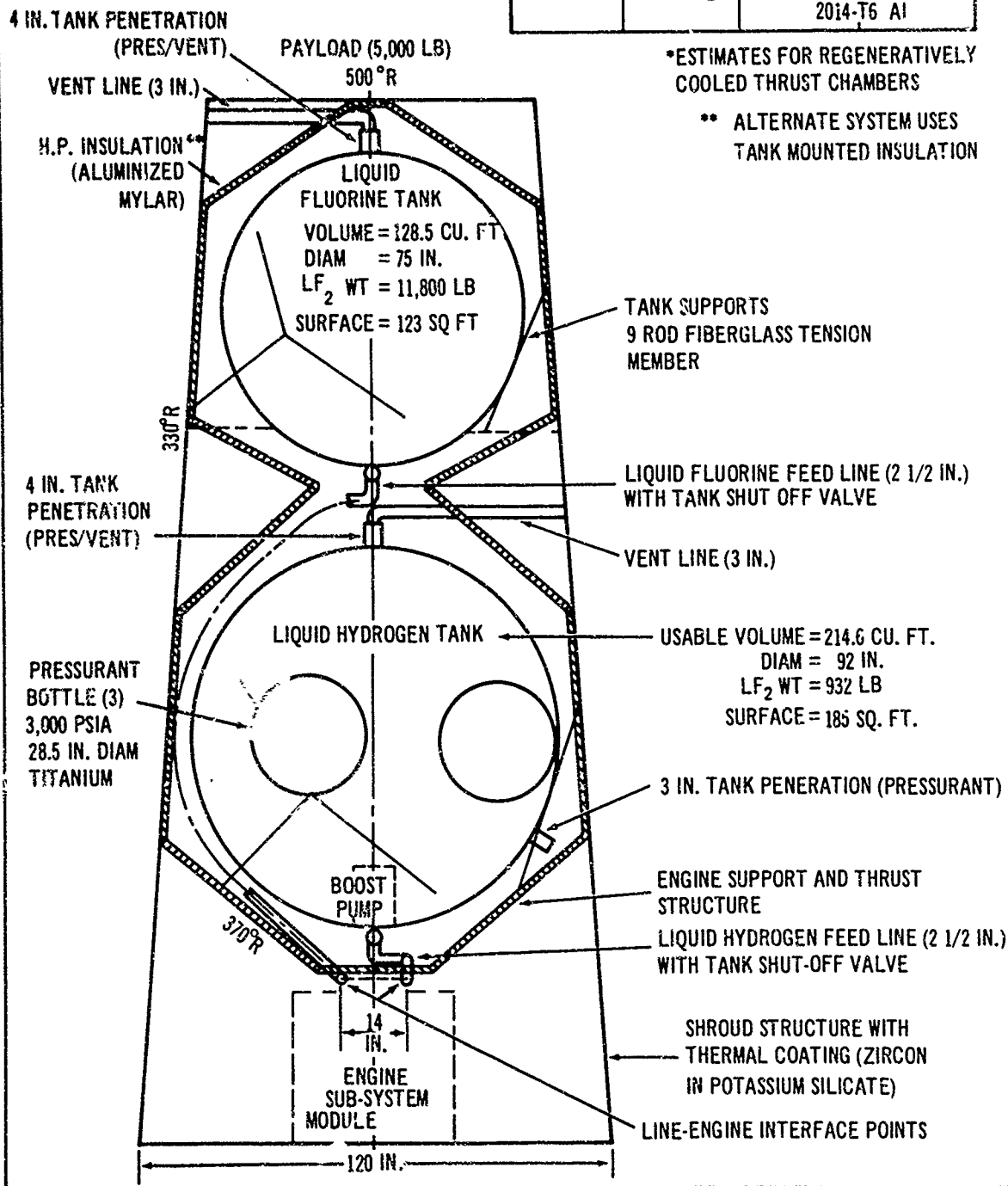


Figure 2-1. Configuration of Study Vehicle

Section III

CONCLUSIONS

Many conclusions can be drawn from the work performed under the seven study phases of the program. However, the conclusions are closely tied to the study ground rules and limitations and must be viewed with caution when departing from the assumed conditions.

The conclusions are itemized below according to study phases.

1. Phase I - Feed Systems.

- a. With both pressure- and pump-fed basic engines, independently driven LH₂ booster pumps can be used to improve overall stage performance. The magnitude of this potential performance improvement decreases as required engine inlet pressure decreases.
- b. For booster pump pressure rises of less than 30 p. s. i. , d. c. battery-driven systems are optimum. However, for pump ΔP values in excess of 30 p. s. i. , a hot-gas turbine drive using a F₂/H₂ gas generator appears optimum.
- c. With both pump- and pressure-fed basic engines, the optimum size booster pump is one that results in a LH₂ tank pressure of approximately 30 p. s. i. a.
- d. A pump-fed engine, with or without a LH₂ booster pump, yields a higher performance than any of the pressure-fed systems or any of the optimum combinations of a pressure-fed engine and independently driven LH₂ booster pump.
- e. Since low (30 p. s. i. a.) pressure tankage is optimum, a feed system using vented tanks yields higher potential performance than one using non-vented tankage.

2. Phase II - Line Losses.

- a. For long-duration missions, non-vacuum-jacketed steel feed and vent lines covered with multilayer insulation result in optimum performance with relatively low system heat input. Aluminum lines are optimum for very-short-duration missions.
- b. Tank shutoff valves with a pressure relief bypass in parallel with the tank valve are recommended.
- c. The tank shutoff valves should be opened during settling and the settling time increased to permit feedline chilldown.

3. Phase III - Venting.

- a. A limited degree of LH₂ venting will occur particularly with low tank pressures and duty cycles which require a small amount of propellant in the tank (duty cycle k).
- b. Little if any F₂ venting is required for missions of up to 14 days.
- c. Liquid phase venting of the LH₂ tank cannot be tolerated.
- d. For zero-g. LH₂ tank venting, a thermodynamic liquid/vapor separator offers maximum performance potential, although it requires development.
- e. If venting of the LF₂ tank appears likely, which would be the case only for missions longer than 14 days, the concept of using the cooling capability of the LH₂ tank vent gases to cool the LF₂ tank to prevent its venting appears feasible but also requires development.

4. Phase IV - Vehicle Thermal Control.

- a. Of the thermal coatings studied, Zr in KSi₄ yielded the best basic performance with the minimum degradation in properties for up to 14 days in orbit.
- b. Average surface temperatures on the vehicle side wall of approximately 330°R. should be expected.

5. Phase V - Propellant Utilization.

- a. If the mission is indeterminate at the time of launch, open-loop propellant utilization systems generally show greater performance potential than closed-loop systems for low tank pressures, where significant venting occurs. For pressures higher than approximately 75 p. s. i. a., closed-loop propellant utilization systems are preferred if they can achieve at least 1/2 pct. accuracy.
- b. Propellant utilization ranged from 99.1 to 99.6 pct. with fuel bias requirements ranging from 0 to 85 lb.

6. Phase VI - Tank Insulation and Support.

- a. NRC-2 and Dimplar multilayer insulation systems, using aluminized Mylar, demonstrated excellent and comparable overall stage performance, when each was properly optimized. Direct tank and shroud-oriented insulation mounting also resulted in comparable overall stage performance.

- b. A pure He interstage purge appears to offer the greatest potential for achieving thermal protection during typical ground-hold and boost-phase operation. However, future advancement in developing sealed bags could alter this general concept.
- c. To support the propellant tankage within the shroud, a point-type support system utilizing glass fiber materials yielded the maximum performance capabilities, from the standpoint of minimum weight and heat leak. A tension rod system is recommended; however, a compression member system may be equally effective.

7. Phase VII - Pressurization System.

- a. The following pressurization system is recommended for a pump-fed engine. For repressurization: heated He for both tanks using a separate F_2/H_2 gas generator heat source.

For expulsion pressurization: engine bleed GH_2 for the LH_2 tank and heated He using an engine nozzle heat exchanger for the LF_2 tank.

- b. For a pressure-fed engine, a pressurization system was recommended which uses heated He for the LF_2 tank and vaporized and heated GH_2 for the LH_2 tank, where a separate F_2/H_2 gas generator acts as heat source in all cases. The H_2 pressurant is stored as a liquid in an auxiliary tank within the LH_2 tank and pressurized by heated He.
- c. Heated GH_2 was always preferred over heated He, at the same temperatures, for LH_2 tank pressurization.
- d. Optimum inlet gas temperatures were in the order of 300 to 500°R., depending upon the tank pressure. Higher inlet gas temperatures actually result in a loss in overall stage performance using conventional inlet gas diffusers.

Section IV TECHNICAL DISCUSSION

1. Phase I--Feed Systems. For the flight vehicle under consideration, the propellant tankage constitutes approximately 10 to 24 pct. of the stage hardware weight over a tank pressure range of 25 to 250 p. s. i. a., respectively. Therefore, reductions in tankage weight can potentially result in significant increases in usable propellant weight for a fixed gross and payload weight. One often-considered technique for achieving tank weight reduction is to use a booster pump in conjunction with the engine. The booster pump supplies a certain pressure rise, ΔP , to the fluid, which can permit a corresponding reduction of ΔP p. s. i. a. in the required tank pressure.

Conventionally, booster pumps are considered with pump-fed engines where the booster pumps supply relatively low heads, in the order of 5 to 25 p. s. i. a. These use motor-driven pumps supplied with electrical power by combinations of batteries and engine turbopump-driven generators. There is no practical reason, however, why larger booster pumps with a completely independent drive system could not be used with pressure-fed engines. In reality, such an approach is an attempt to evolve a system that is a compromise between an all-pump and an all-pressure fed system.

To evaluate this approach, it was decided to consider the use of booster pumps only on the LH₂ side of the system. Two factors led to this decision: (1) because the LH₂ tank weight is nearly twice that of the LF₂ tank, most of the weight reduction benefits would result in the LH₂ system; and (2) the development problems for efficient booster pumps for LF₂ service are relatively unexplored and a large area of uncertainty would be raised by including them in the study.

a. Preliminary Candidate-System Screening Study. A vast number of hardware items can be assembled to form a booster pump system. To establish what should be studied in detail, a preliminary screening study was performed to identify a reasonable number of candidate systems. Figure 4-1 shows the breakdown of the booster pump system defining three areas: (1) the pump, (2) the pump drive, and (3) the energy source. The pump drive may be either an a. c. /d. c. motor or a turbine using hot or cold gas. Maximum variation occurs in the energy source area. For d. c. motors, a battery, an engine-driven generator, or a turbogenerator may be used. For an a. c. motor, a turbogenerator, a battery/inverter, or an engine generator plus a battery/inverter starter may be employed. Turbogenerators require secondary energy sources such as a cold- or hot-gas energy supply. The energy source for turbine drive systems is a gas supply which may be either cold gas, such as He or H₂; or hot gas, such as the products from a combustor, or bleed H₂ from the engine. The combustors may be monopropellant or bipropellant gas generators burning a variety of propellants, including H₂O₂, N₂H₄, F₂/H₂, OF₂/C₃H₈, and others.

Submerged sump-mounted-LH₂ booster pumps have been under study for several years and have been employed in the Centaur vehicle. Such pumps have been found to be reliable and efficient, and to require minimum installation space. Therefore, it has been assumed that such a configuration would be used in this application.

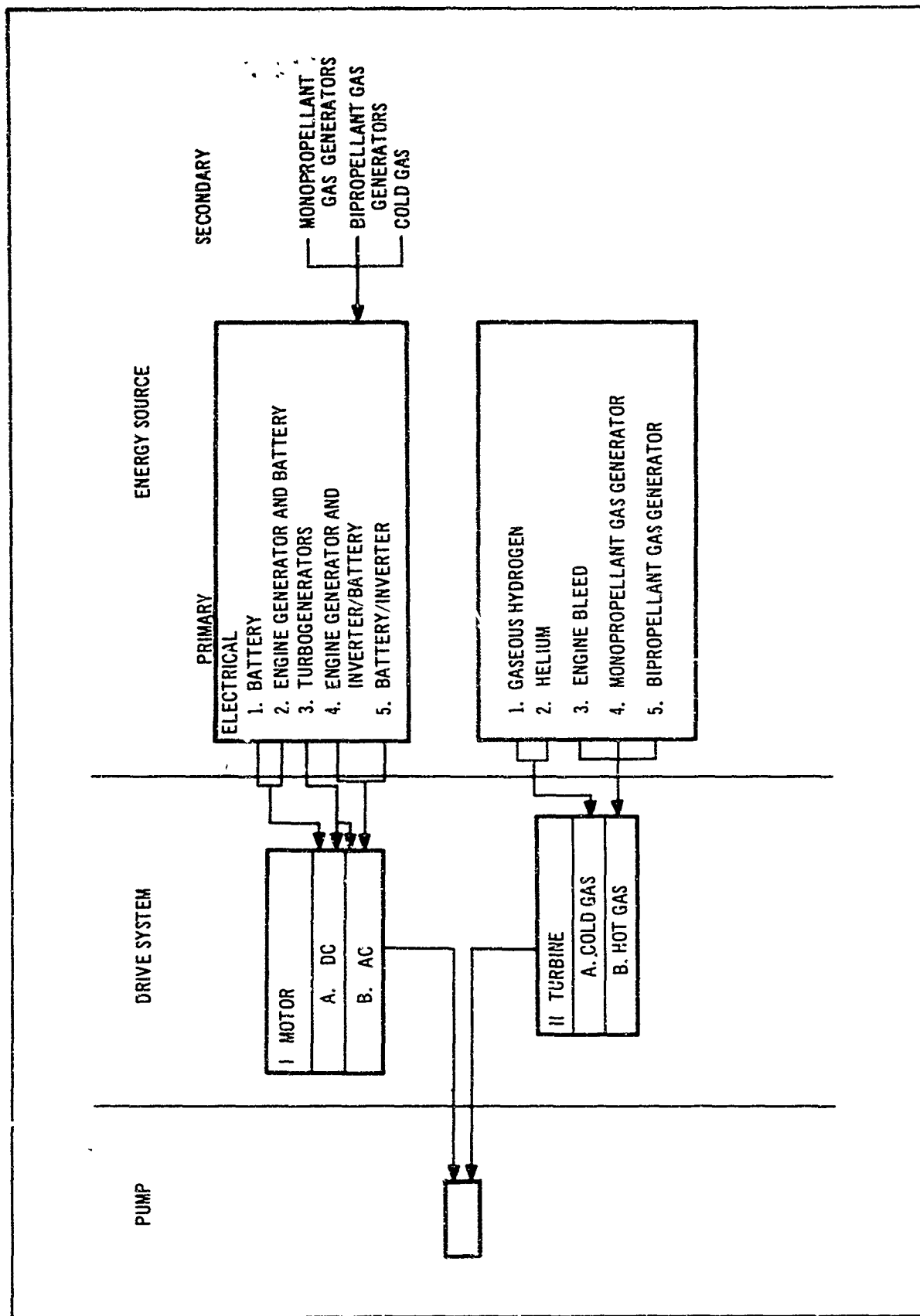


Figure 4-1. Booster-Pump System Alternatives

At this point, it was not completely obvious that any of the techniques mentioned was either far superior or inferior in a comparative sense. Consequently, a preliminary weight comparison was made for the 23 systems listed in table 4-1 and are identified according to the notation of figure 4-1. For example, system IB3 (F_2/H_2) is an a. c. motor drive that uses a turbo-generator with a F_2/H_2 gas generator. The right-hand column of table 4-1 lists the estimated weight, and table 4-2 itemizes the individual weights used. All computations were based on a 235-p. s. i. a. pump pressure rise, a full LH_2 flow rate of 4.6 lb. p. sec. and a propellant temperature of $37^\circ R$.

The significance of these weight numbers is not in their absolute value but rather in their relative values. Examination of the totals reveals that all of the cold-gas systems are considerably heavier than the rest of the proposed approaches. The weights of the others shown on the table are relatively close. Therefore, the cold-gas turbine systems were eliminated from further consideration. Because weights for electrical hardware such as motors, generators, and inverters were not estimated, the total weights for these systems are deceptively low and cannot be compared with the conventional turbine systems. Ten basic systems, not including propellant variation, were selected for further study. Schematic diagrams of these systems are shown in figure 4-2. The propellants, where applicable, were taken as H_2O_2 , N_2H_4 , F_2/H_2 , or OF_2/C_3H_8 . (OF_2/C_3H_8 was considered because it is a potential candidate for the reaction control propulsion system and, therefore, may be aboard the stage.)

b. Evaluation of Candidate Booster Pump Systems. A subcontract was issued to Pesco Products Division of Borg Warner to generate realistic parametric data on booster pump system hardware. The subcontract covered generation of appropriate weight and performance data for the selected booster pump systems. This work included information on pumps, batteries, turbogenerators, inverters, motors, and controls. Douglas retained responsibility for the propellant supply system, where required. The results of the Pesco work were provided in reference 1, and the essentials of this effort are repeated in subsequent portions of this phase description.

Figure 4-3 summarizes the basic component weights as a function of power in terms of horsepower for mechanical equipment and kw for electrical equipment. Figure 4-4 summarizes motor and pump efficiencies.

Because high horsepower-to-weight ratios can be obtained at high efficiencies with motors submerged in cryogenic liquids, only motors of this type were considered. As can be seen from the motor weight curves, d. c. motors are heavier than a. c. motors at high power levels. Also, d. c. motor weight increases more rapidly with increasing power output. This is primarily a result of speed limitations. Commutators which are required only for d. c. motors limit speed capabilities. With a. c. motors, increasing the speed permits a decrease in rotor and stator weights. For example, at 92 hp. a d. c. motor is limited to a speed of about 6,000 r. p. m., but the a. c. motor could go up to about 30,000 r. p. m. However, to avoid specialized power supplies, the speed is limited to 22,800 r. p. m. Gear boxes to step up the rotational speed are also required with d. c. motors to obtain better speed matching with the pump. This gear box weight is not included in the indicated d. c. motor weights.

Table 4-1

BOOSTER-PUMP SYSTEMS STUDIED

Identification	Description	Drive system - Weight (lb.)
IIB4-N ₂ H ₄	Hot-gas turbine	140
IIB5-F ₂ /H ₂	Hot-gas turbine	142
IB3-N ₂ H ₄	A. c. motor--turbogenerator	164 ^a
IB3-F ₂ H ₂	A. c. motor--turbogenerator	167 ^a
IIB4-H ₂ O ₂	Hot-gas turbine	171
IIB5-OF ₂ /C ₃ H ₈	Hot-gas turbine	173
IA3-F ₂ /H ₂	D. c. motor--turbogenerator	184 ^a
IA3-N ₂ H ₄	D. c. motor--turbogenerator	184 ^a
IA1	D. c. motor--battery	186 ^a
IB5	A. c. motor--battery/inverter	207 ^a
IB3-H ₂ O ₂	A. c. motor--turbogenerator	214 ^a
IB3-OF ₂ /C ₃ H ₈	A. c. motor--turbogenerator	214 ^a
IIB3	Engine bleed turbine	222
IIB3'	Engine gas generator bleed turbine	227
IA3-OF ₂ /C ₃ H ₈	D. c. motor--turbogenerator	238 ^a
IA3-H ₂ O ₂	D. c. motor--turbogenerator	239 ^a
IIA1	Cold GH ₂ turbine	687
IIA2	Cold He turbine	804
IB3-cold H ₂	A. c. --turbogenerator	873 ^a
IA3-cold H ₂	D. c. --turbogenerator	977 ^a
IB3-cold He	A. c. motor--turbogenerator	1022 ^a
IA3-cold He	D. c. motor--turbogenerator	1147 ^a
IA4	D. c. motor--engine generator	14 ^b
IB4	A. c. motor--engine generator	15 ^b

^aDoes not include certain electrical hardware.

^bStart battery weight penalty only.

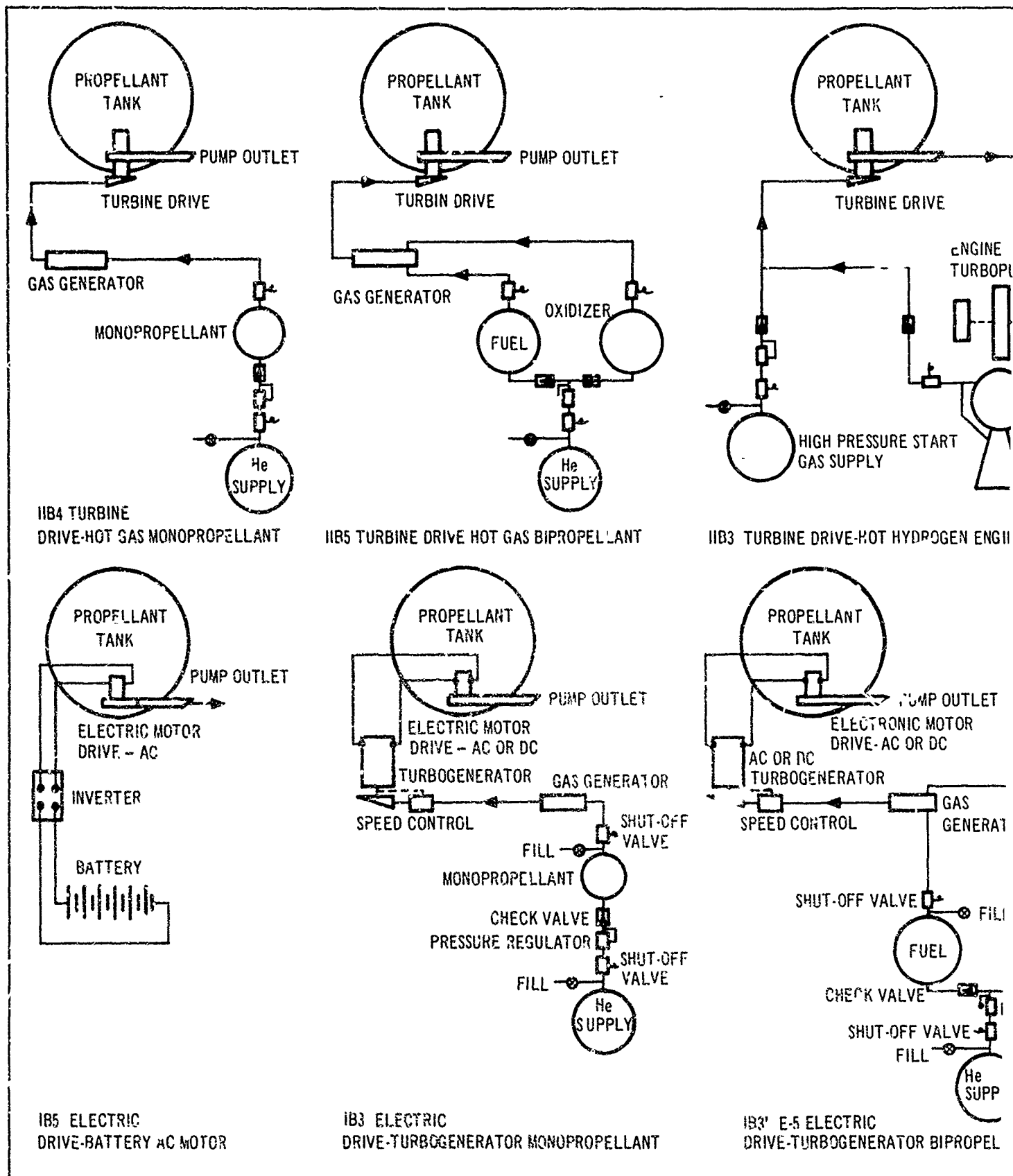
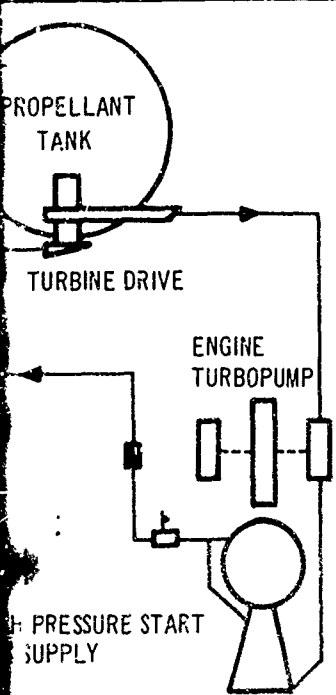
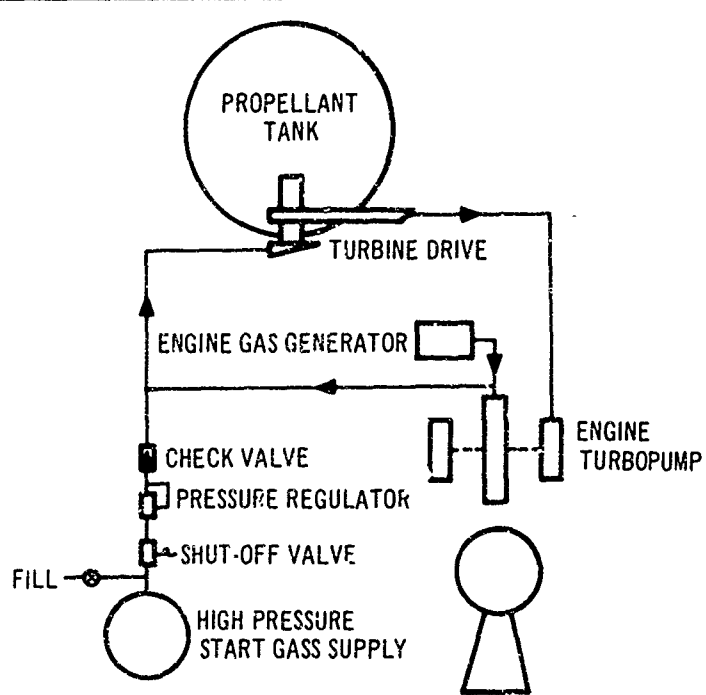


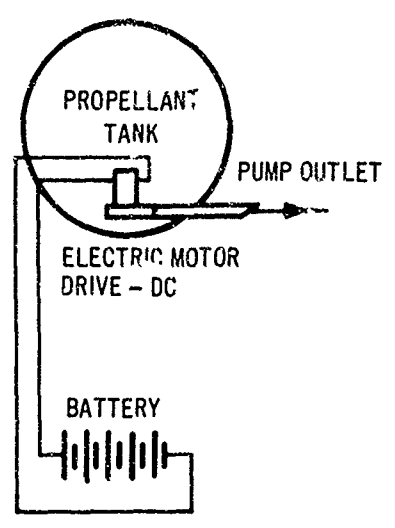
Figure 4-2. Candidate Boo:



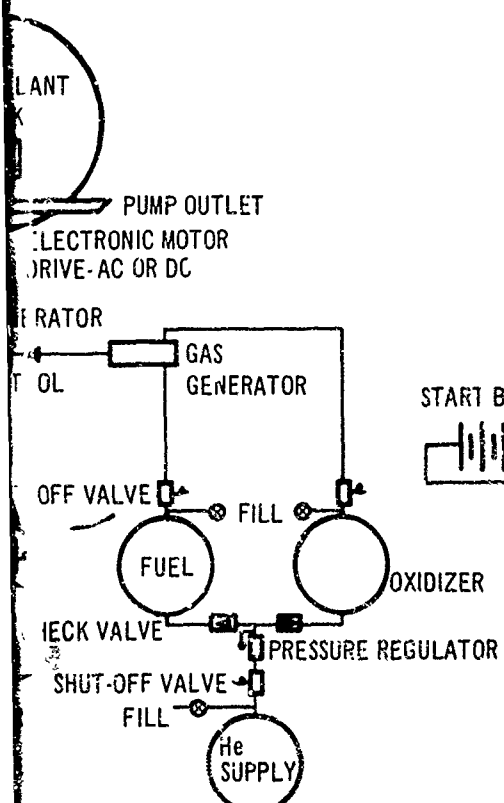
103 TURBINE DRIVE-HOT HYDROGEN ENGINE BLEED



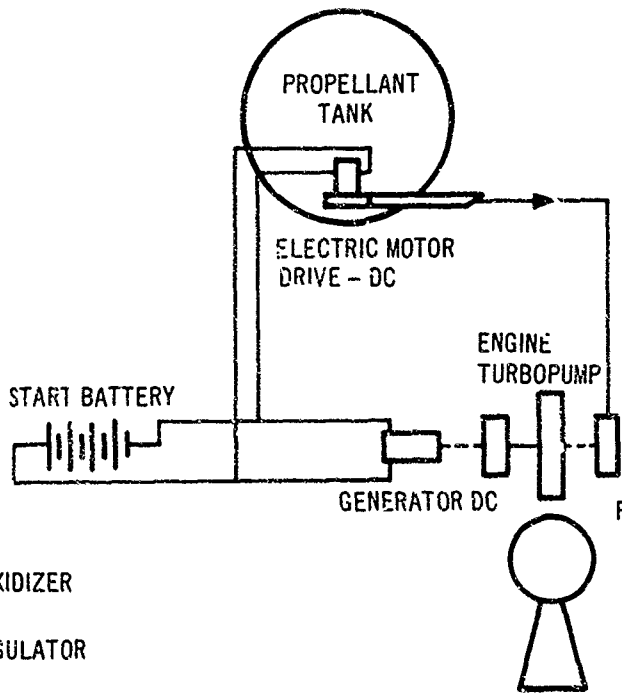
104 IIB3 T-5 TURBINE DRIVE-HOT GAS ENGINE GENERATOR BLEED



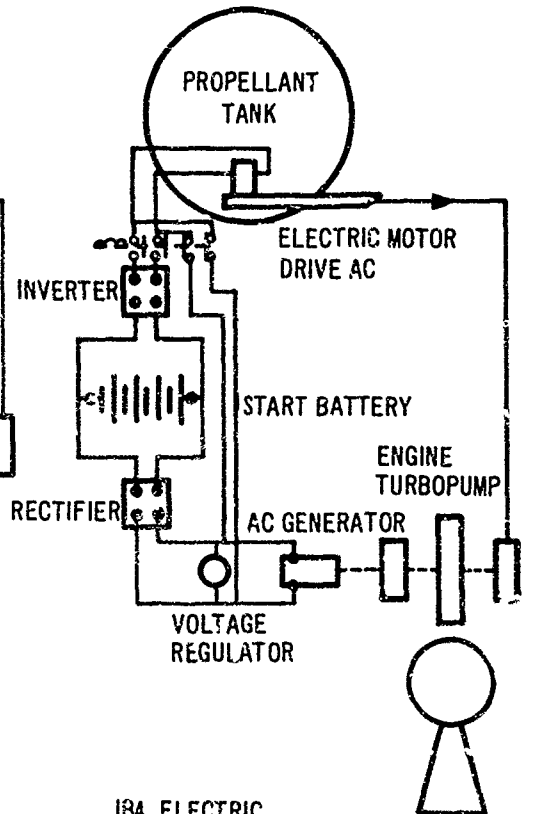
105 1A1 ELECTRIC DRIVE-BATTERY DC MOTOR



106 1A1 ELECTRIC DRIVE-GENERATOR BI-PROPELLANT



107 1A4 ELECTRIC DRIVE-ENGINE MOUNTED GENERATOR DC



108 1A4 ELECTRIC DRIVE-ENGINE MOUNTED GENERATOR AC

2. Candidate Booster-Pump Systems

B

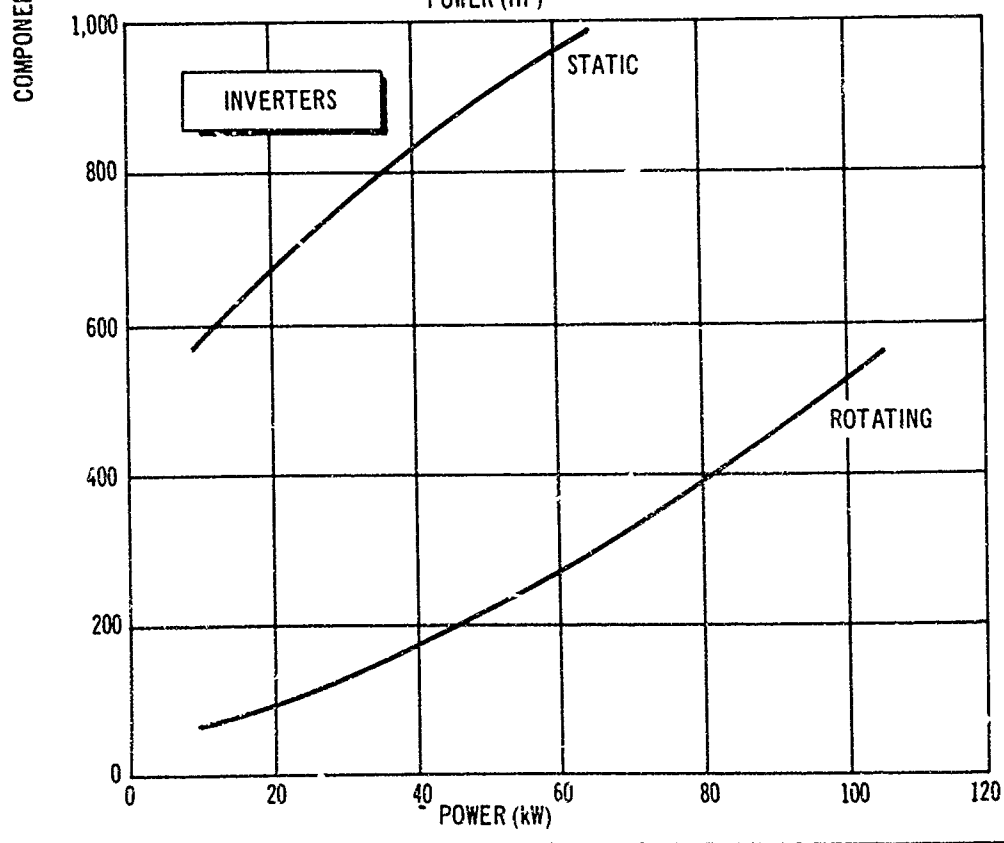
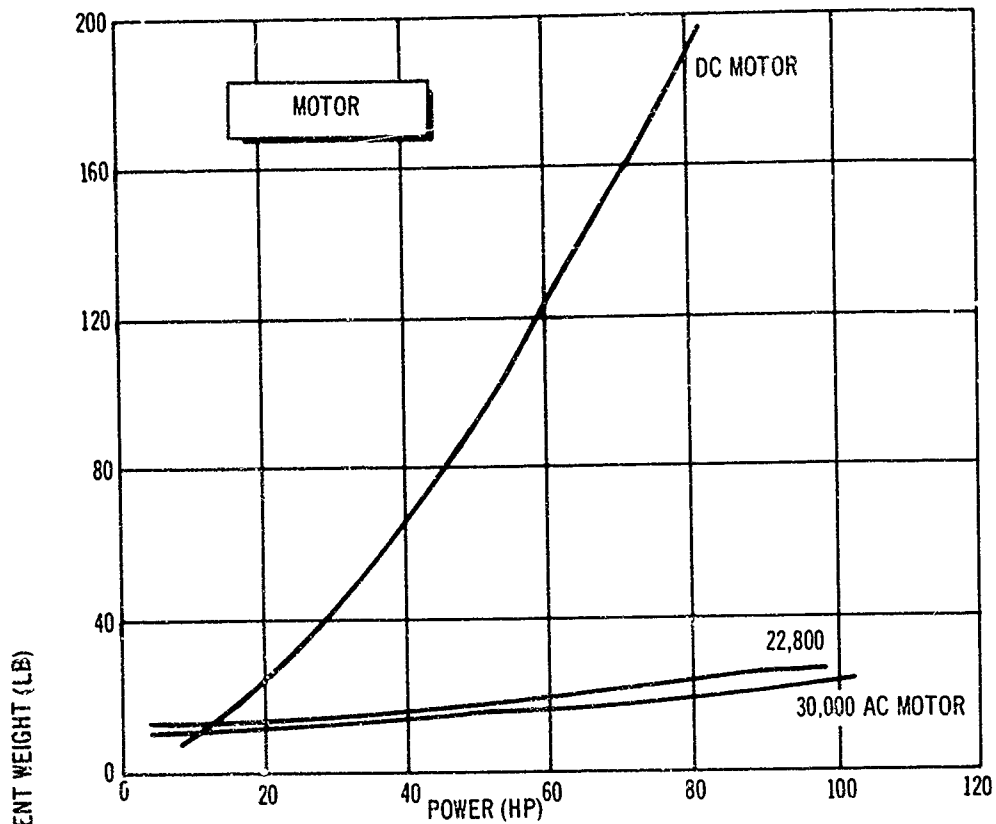
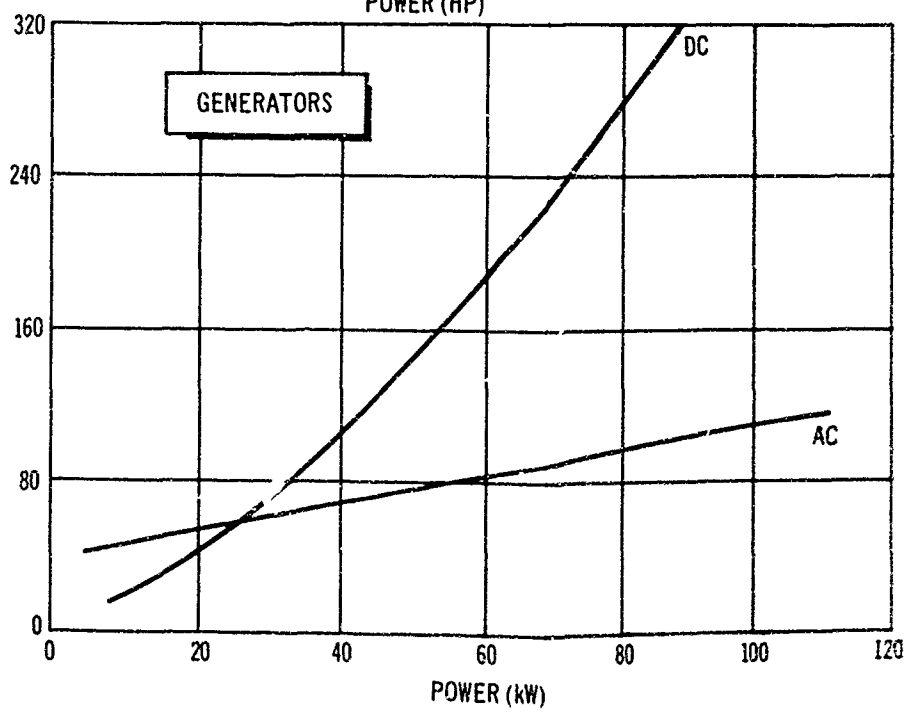
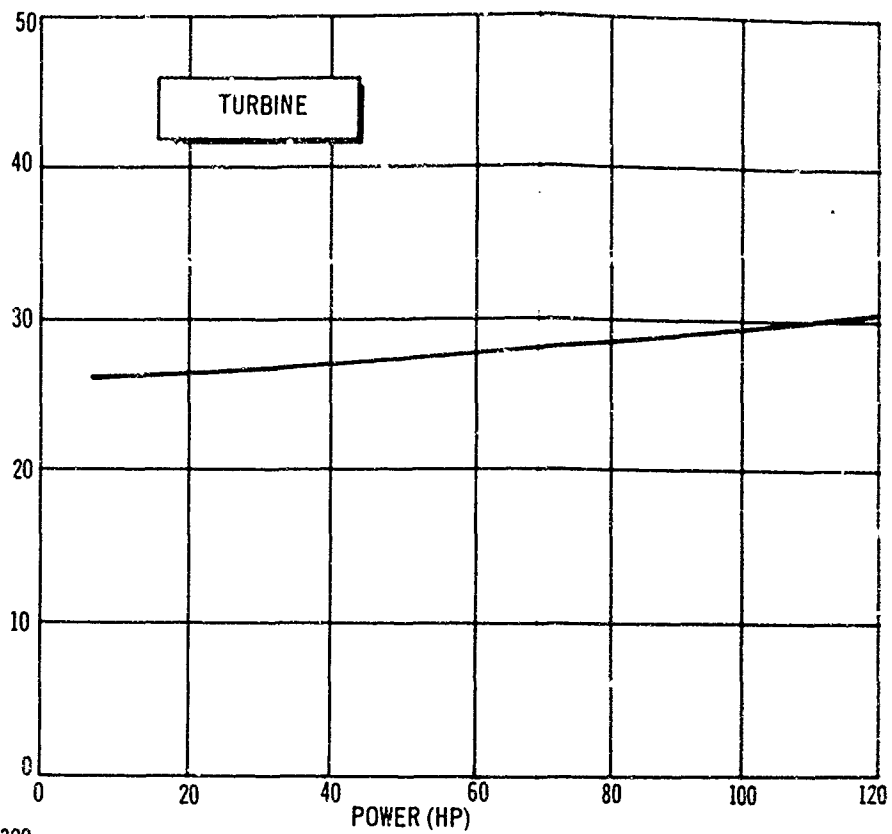


Figure 4-3. Parametric Weights of Bas

H



Parametric Weights of Basic Components

B

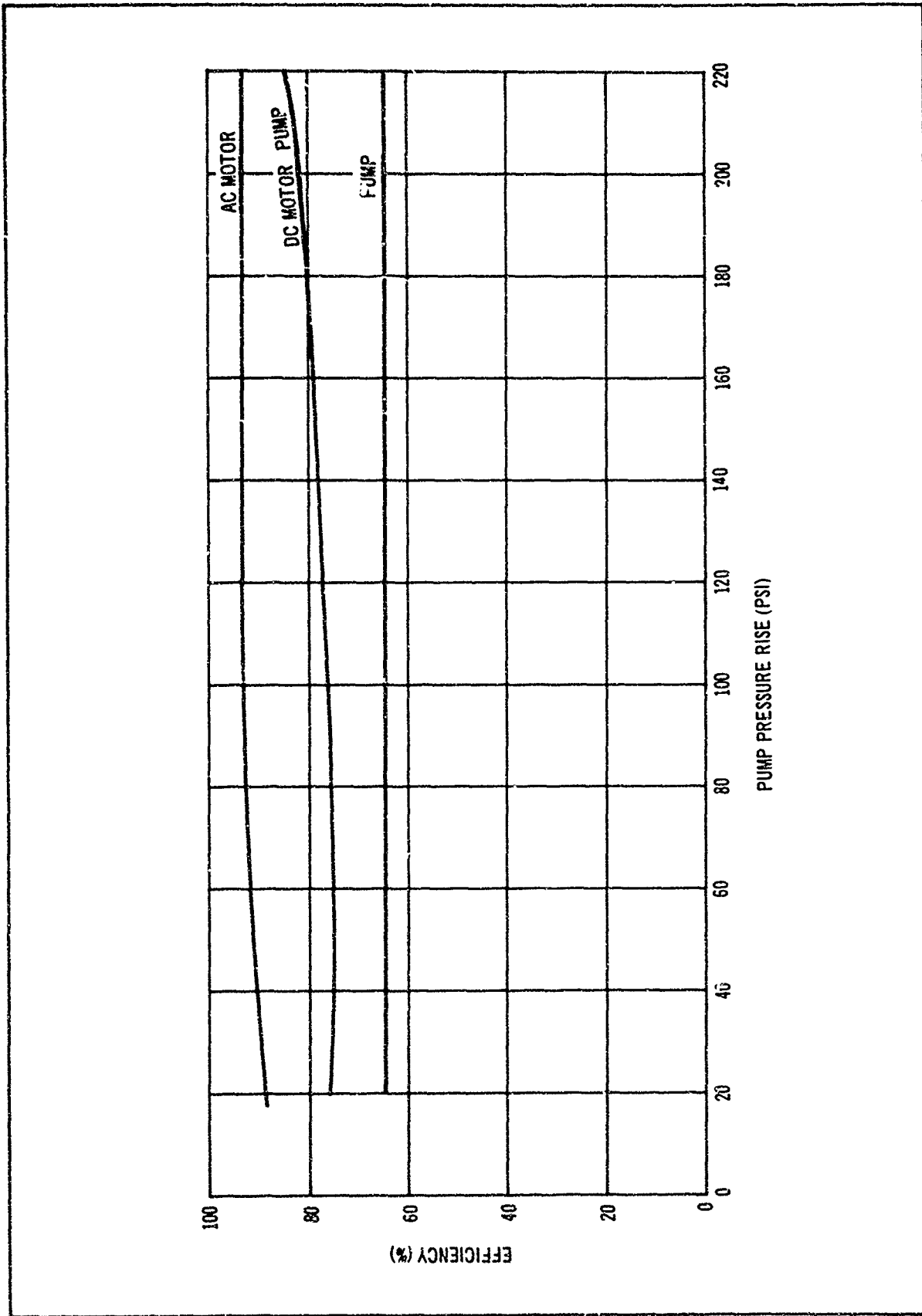


Figure 4-4. Component Efficiencies

Turbine weights were based on a multipass partial admission design with a speed limit of 60,000 r. p. m. and inlet pressures and temperatures of 400 p. s. i. a. and 1,730° F., respectively. In lieu of performing a very time-consuming optimization to arrive at turbine efficiencies, a value of 55 pct. was assumed. In some cases, this would be a conservative value.

Inverters are normally built in sizes up to 5 kw. Therefore, it was necessary to estimate weight for equipment of higher power on the basis that rotating inverters are basically motor generator devices and that the 50 pct. efficiency level, common for the small units, is also valid in the higher regimes. The weights were tailored to 200 sec. heat sink operation by taking into account the normal 150 pct. overload for a 5 min. duration usually incorporated into this class of hardware. Static inverters were found to be entirely noncompetitive with the rotating type.

D.c. generators demonstrate rapidly increasing weight with power output relative to a. c. generators because of the speed limitation, as discussed previously relative to d. c. versus a. c. motors. The weights shown were determined from available and projected hardware. Efficiencies of 75 pct. and 80 pct. for d. c. and a. c. generators, respectively, were assumed.

Battery weight estimates were based on information provided by Yardney Electric Corporation for units with Ag/Zn active ingredients and magnesium external cases. Operating voltages were limited to about 110 v. to maintain low battery currents, and it was determined that the energy capacity had to be maintained at about 17 w. -hr. p. lb. This value is primarily determined by the high discharge rate over a short period of time which necessitates a large battery plate area. An additional 15 pct. weight increase over the 17 w. -hr. p. lb criteria was included for external casing. Batteries were sized for 20 restarts. It was found that the size of the battery required for starting was the same as that of the battery required for continuous 200 sec. operation.

Pumps were sized with 2-in. discharges and with the saturated liquid assumed to be 82 p. s. i. a. with a 50° R temperature at pressures above 82 p. s. i. a. Each pump is capable of flows of from 4.59 to 0.46 lb. p. sec. Radial, mixed, and axial flow pumps with single and multiple stages were studied with specific speeds ranging from 1,000 to 7,000 r. p. m. A maximum rotational speed of 30,000 r. p. m. is considered to be a reliable operating regime within the current technology. Pump efficiencies generally were considered to be 65 pct.

Other weight items, such as gear boxes, rectifiers, and controls, were based on extrapolations of existing hardware. These hardware weights were combined to evolve system weights as shown in figure 4-5. The weights shown do not include propellant or the propellant supply, where required. For the all-electrical systems, however, the indicated weights are actually total system weights. Figure 4-5 shows clearly that the d. c. battery system (IA1) is lighter than the a. c. system (IB5). Although a. c. motors and generators are lighter than their d. c. counterparts, the added inverters in the a. c. system result in higher overall system weights. Figure 4-5 also demonstrates that motor-driven booster pumps powered by the main engine are

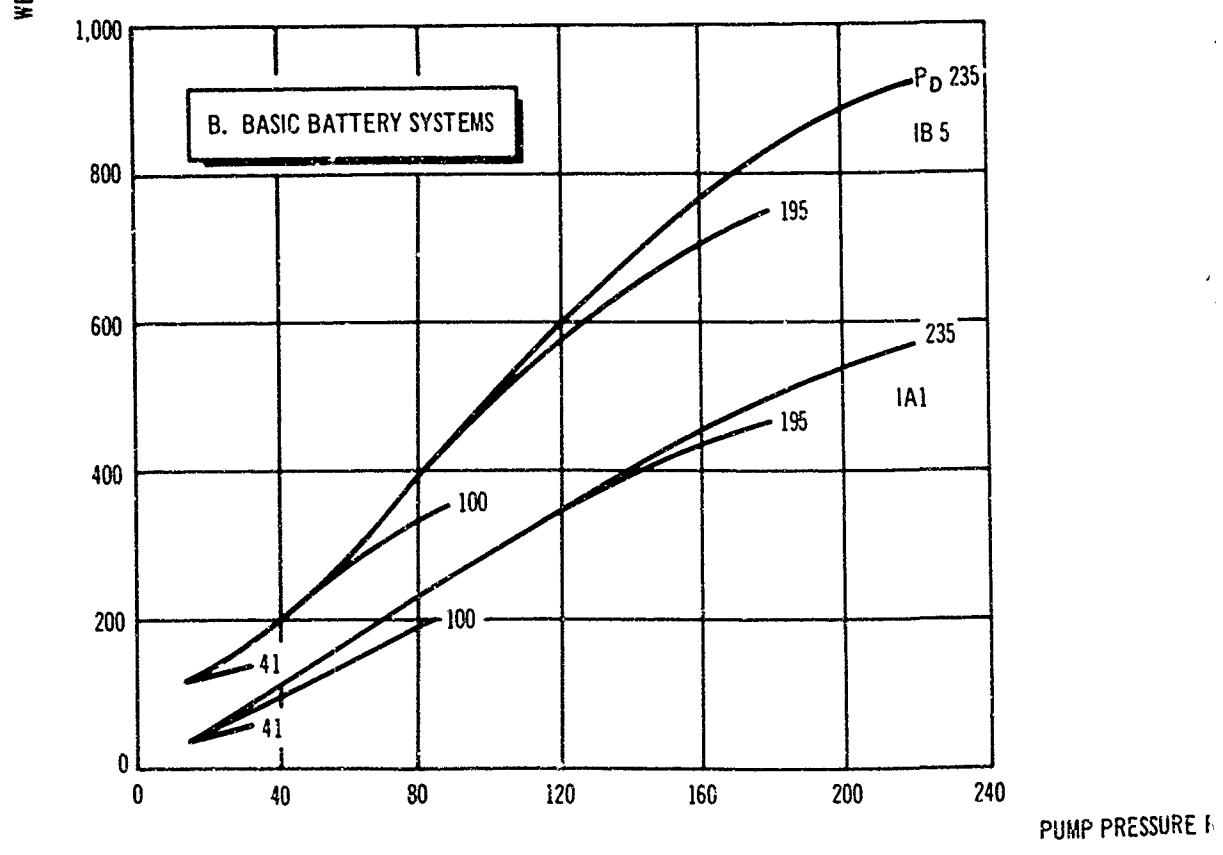
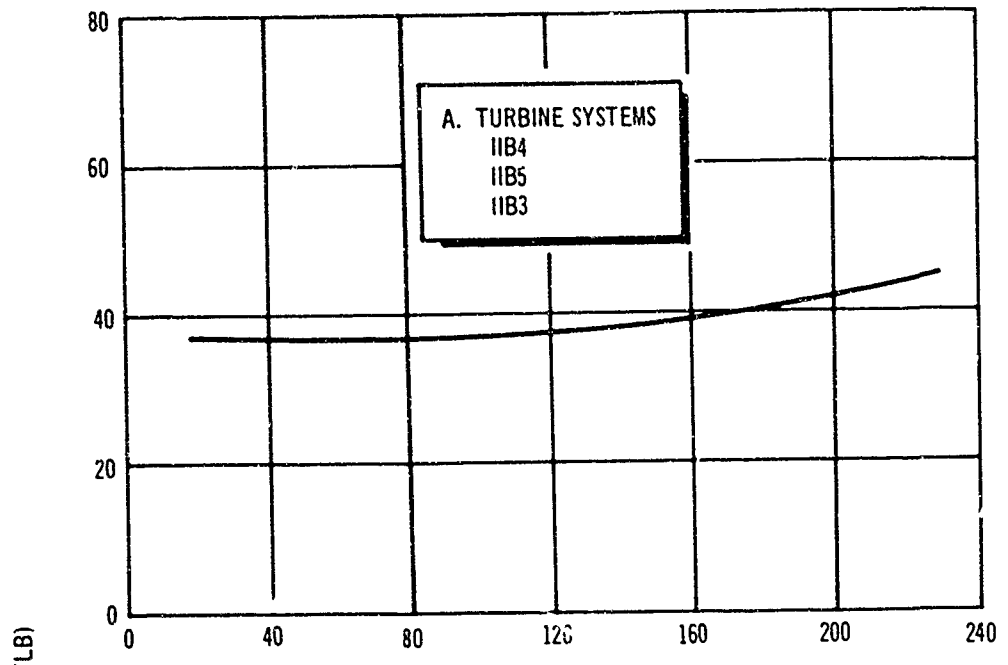
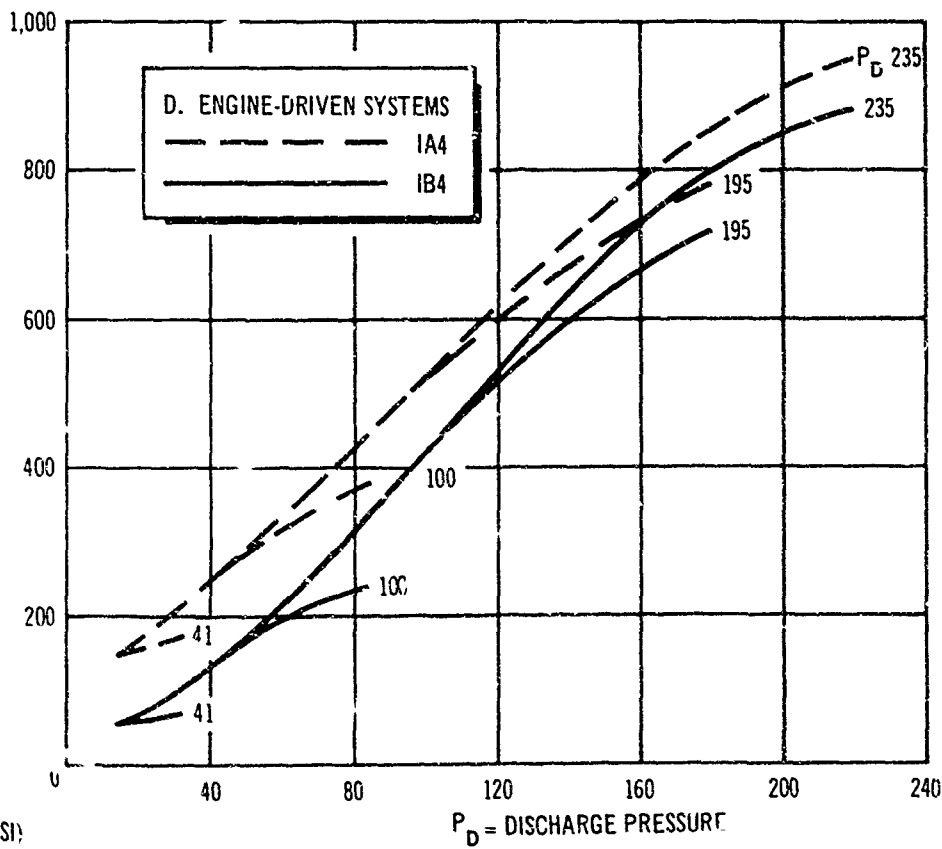
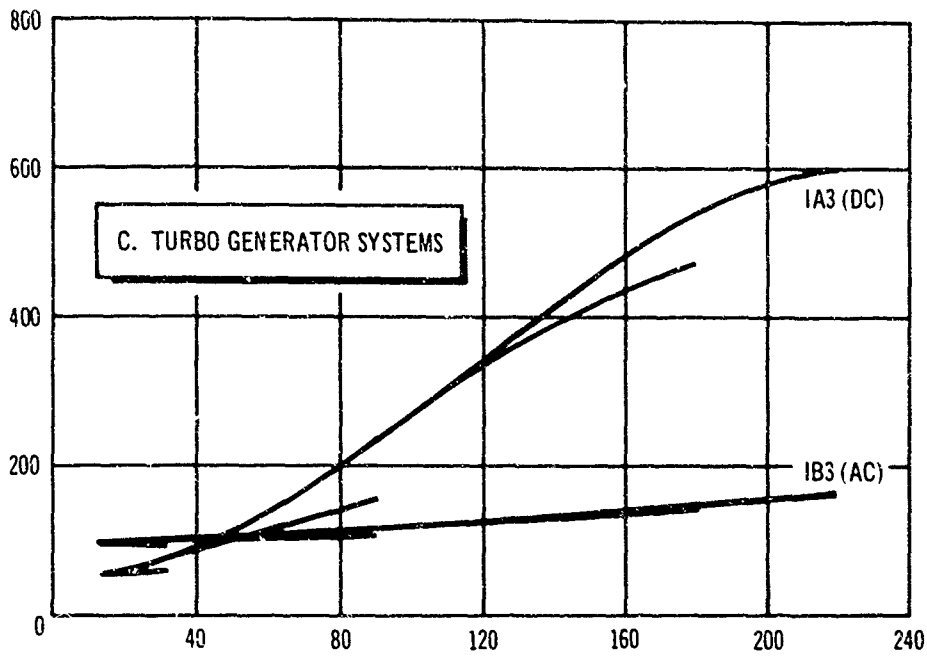


Figure 4-5. Booster-Pump System Weights (Less Rec)



Weights (Less Required Drive Propellant System Weights)

3

heavier, in all cases, than the straight d. c. battery system. This is the case because the required start battery must be as large as the battery for continuous operation, as indicated previously. Thus, the engine-mounted generator is strictly additional weight over the basic battery.

Figure 4-5 shows an interesting crossover point for the turbogenerators. At pump ΔP s below about 40 p. s. i. a., d. c. systems are lightest, but above this level, a. c. systems are to be preferred on a weight basis. Thus, the minimum weight curve for the turbogenerator system would be a broken line following the d. c. curve below 40 p. s. i. ΔP , shifting to the flatter a. c. curve above 40 p. s. i. ΔP .

Inspection of figure 4-5 permits the elimination of systems IB5, IA4, and IB4, from further consideration, leaving only hot-gas turbines, d. c. batteries, and a. c. or d. c. turbogenerator systems. It is necessary to incorporate the required propellant systems to compare these systems further. Basic propellant thermochemical data for the fluids under consideration were generated by the Douglas JA60 thermochemical computation computer program and were provided to Pesco. From this, Pesco produced curves of turbine-working fluid consumption as a function of turbine power output. By combining these with curves of pump power input versus pump pressure rise, a plot of required propellant flow rate as a function of pump pressure rise was prepared. This is shown in figure 4-6 for the maximum pump discharge (235 p. s. i. a.) for the four propellant systems under consideration. The propellant consumption is lowest for the F_2/H_2 system and highest for the H_2O_2 monopropellant system. N_2H_4 and OF_2/C_3H_8 are about the same and fall midway between the two extremes. From figure 4-6, it is possible to determine the propellant weight requirements and the weight of corresponding propellant feed system hardware. These estimates were first based on a booster pump system with a discharge pressure of 235 p. s. i. a., with a full flow 200-sec. burn time. The resulting weights for turbine systems IIB3, IIB4, and IIB5, and electrical turbogenerator systems IA3 and IB3 are shown in figure 4-7. For a comparison, the d. c. battery system, IA1, is also shown. System weight for lower discharge pressures and longer burn time at reduced flow are slightly different but reflect the same comparative trends. Table 4-3 shows the weight breakdown for system IIB5 burning F_2/H_2 to indicate weight distribution.

The curves for the turbogenerator systems, shown in figure 4.7, are a composite of two systems which accounts for the discontinuity: the first portion is the d. c. system, IA3; and the second portion is the a. c. system, IB3. This is the net minimum weight for the turbogenerator system. However, the electrical turbogenerator system is always heavier than the hot-gas turbine system. There is a distinct crossover point with the d. c. battery system which occurs at a pump ΔP of about 17 to 18 p. s. i. a. with the hot gas turbine and at 28 p. s. i. a. with the turbogenerator system. Beyond a pump pressure rise of 30 p. s. i. a., however, the d. c. battery system is noncompetitive.

It can further be seen that when a propellant system is required, the F_2/H_2 system offers minimum weight potential. This savings is small (about 6 lb. at 40 p. s. i. a) at low ΔP values, but at a ΔP of 220, the saving can be about 33 lb.

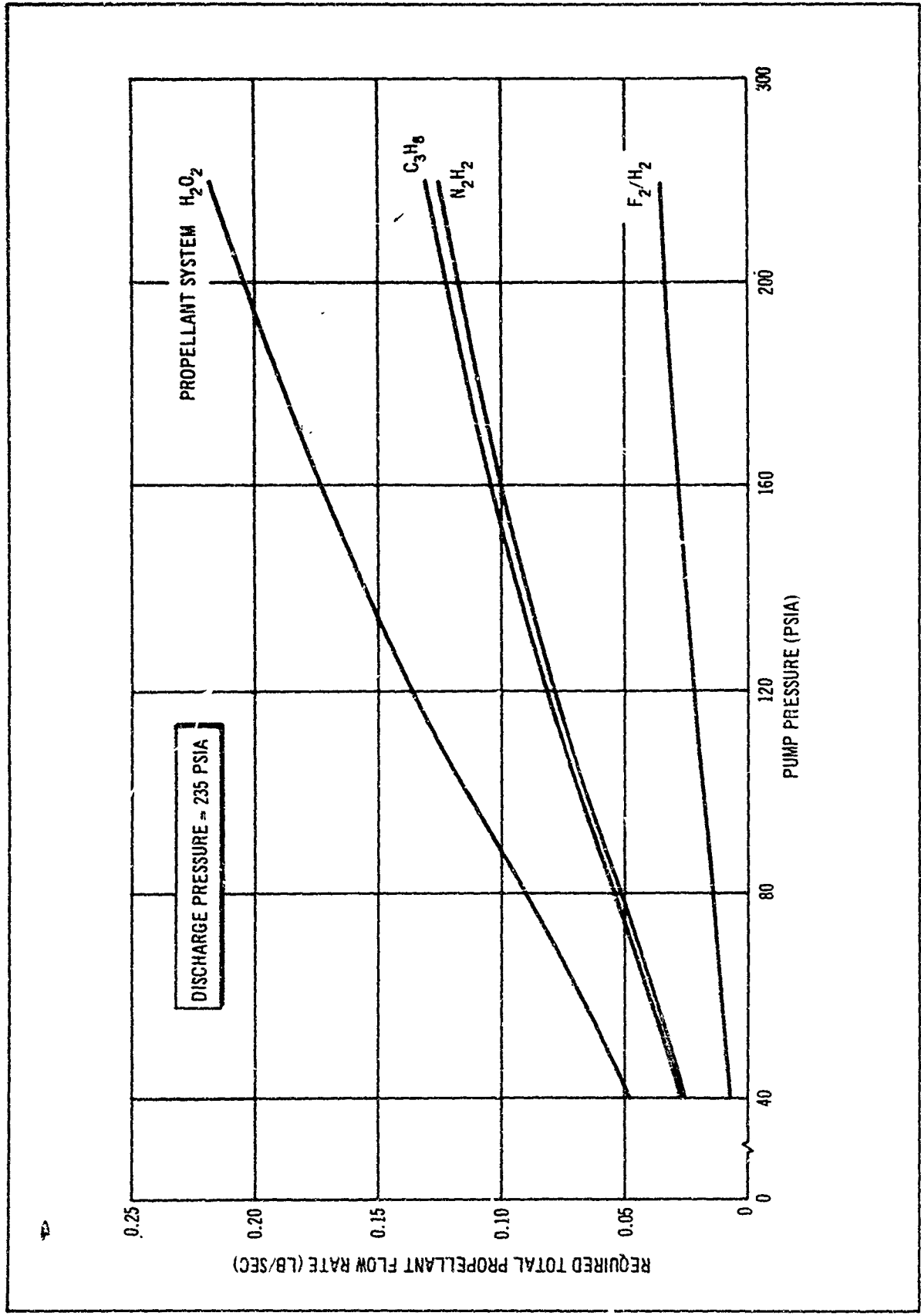


Figure 4-6. Propellant Flow Requirements for Booster-Pump System

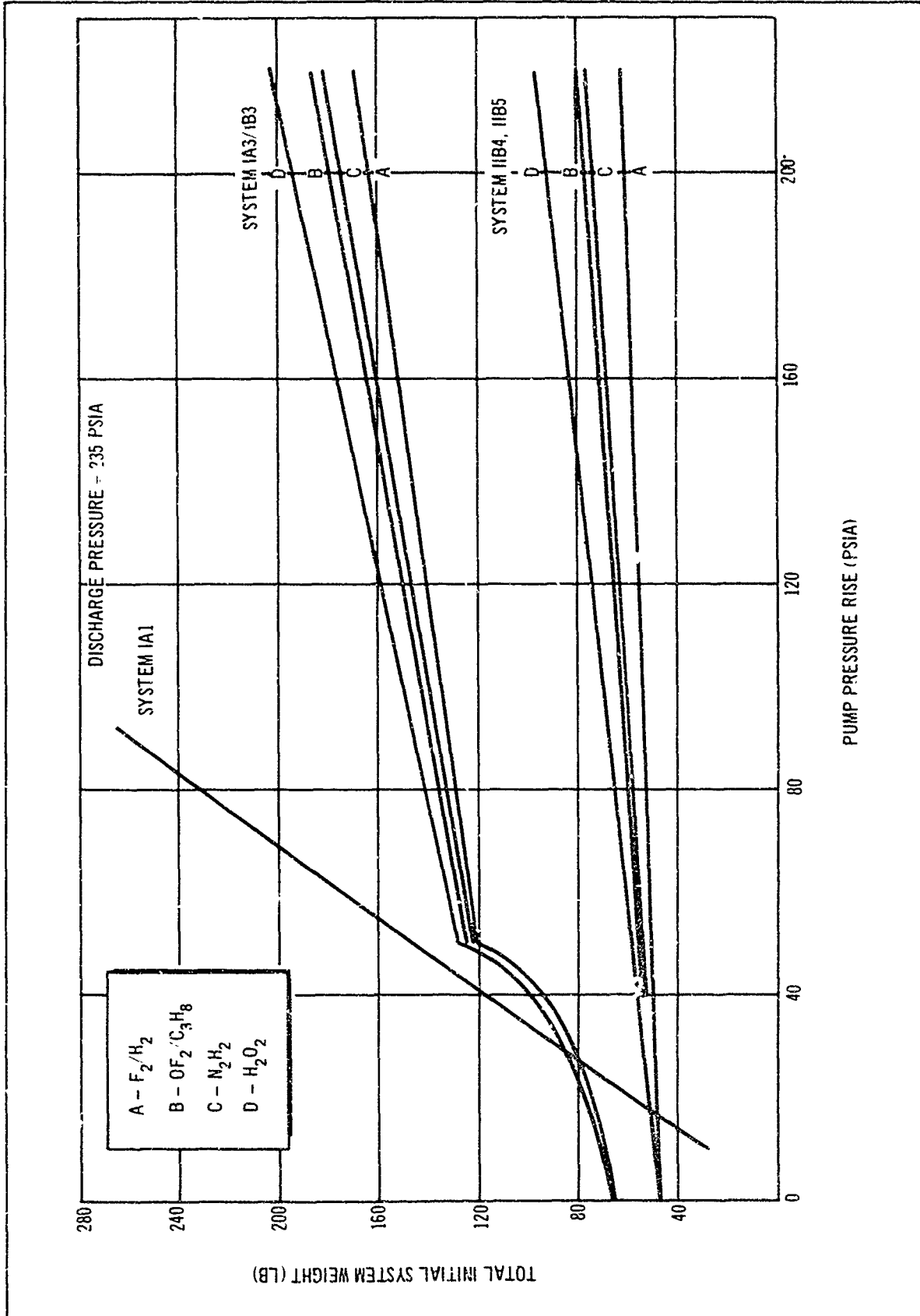


Figure 4-7. Total System Weights for Candidate Booster-Pump Systems

Table 4-3

TYPICAL BOOSTER-PUMP SYSTEM WEIGHT BREAKDOWN

Hot-gas turbine--using F_2/H_2 gas generator exhaust products	
Discharge pressure = 235 p. s. i. a.	
Pump pressure rise = 220 p. s. i. a.	
Pump/turbine complex	44 lb.
Propellant	7
Tankage	6
Miscellaneous (controls and lines)	10
Total weight	67
Dry weight	60 lb.

Independent research by Douglas on a F_2/H_2 gas generator has indicated that such a device, as would be required for the energy source, is feasible and well within the state of the art; therefore, this propellant system was selected for further use in this study. If OF_2/C_3H_8 were used in the RCS propulsion system, it would be more convenient to use this combination and accept the relatively small weight penalty.

From figure 4-7, a minimum potential system weight curve was developed as shown in figure 4-8. This does not include the effects of additional heat loads to the LH_2 which would be present for either a turbine or an electric motor-driven system. In the case of the turbine, heat would be radiated from the warm turbine hardware to the propellant tank as well as some heat conduction through the power transmission shaft. This total was roughly estimated to be 2 B. t. u. p. sec. Assuming an operating time of 200 sec. and assuming that all the heat goes into boiloff, this could cause about 21 lb. of LH_2 boiloff. For the electric motor systems, the motor inefficiency is usually felt as an additional heat load to the propellant. For a d. c. motor driving a 30 p. s. i. a. ΔP pump, the heat rejected to the propellant is about 3.5 B. t. u. p. sec. which represents a potential LH_2 boiloff of about 35 lb. For an a. c. motor, which is more efficient than a d. c. motor, the heat load to the LH_2 , for the same set of conditions, is about 2.2 B. t. u. p. sec. (a boiloff loss of 23 lb.). However, the assumption that all the heat load goes into boiloff is misleading and these losses were neglected at this point. The data of figure 4-8 was taken as a minimum potential system weight to determine if there is a range of efficient application for booster-pump systems.

c. Booster-Pump Throttling. When throttling the main engine, generally it will also be necessary to throttle the booster pump. A preliminary

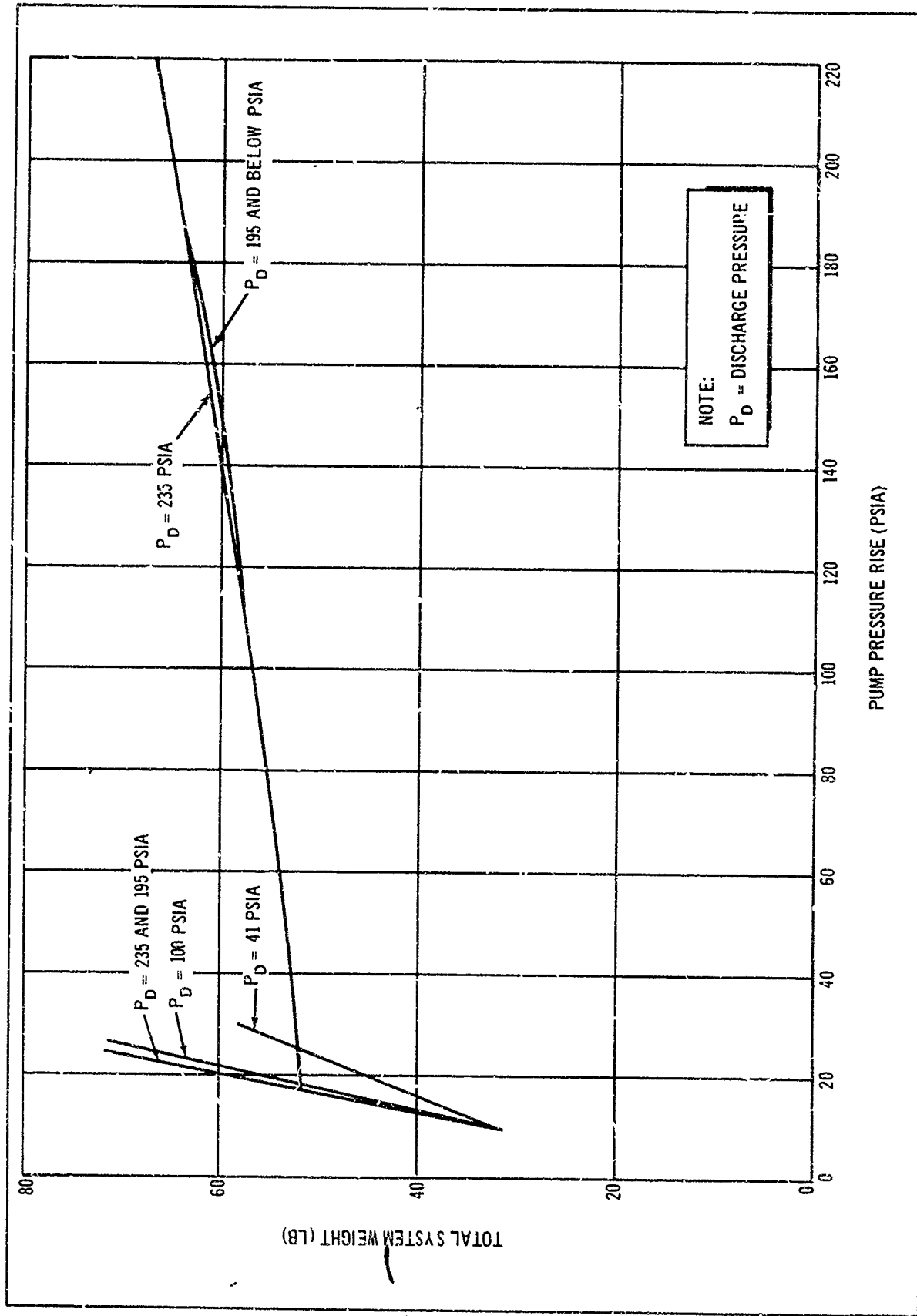


Figure 4-8. Minimum Potential Weight for Booster-Pump System

investigation of techniques for booster-pump throttling was part of the scope of the Pesco subcontract effort and was reported in detail in reference 1. The essentials of this work are summarized in this section.

There are basically three approaches that may be taken to throttle the booster pump: (1) variable pump speed, (2) pump discharge throttling, and (3) variable pump flow by-pass.

Throttling over a 10:1 ratio can efficiently be obtained by varying pump speed. The manner in which speed variation can most easily be obtained depends upon the type of drive. With a turbine system, the turbine mass flow rate would be varied. With a motor drive, voltage and frequency variations would be used for d. c. and a. c., respectively. However, the equipment to effect variation in the electrical systems is quite heavy and, therefore, not applicable in general to the flight systems being considered. With a turbogenerator system, variation in turbine speed by modulating turbine propellant flow does result in the desired electrical variations. Turbine flow control valve system weights including modulator and electrical drive would vary from about 8 to 14 lb., depending upon pump pressure rise between 0 and 235 p. s. i. a. Such a system would require development, however.

Downstream throttling and pump by-pass both employ constant speed pumps. Flow by-pass was found to result in probable instability because of operation at overcapacity. Downstream or discharge throttling is feasible and results in a decreased power input requirement for the pump, for pump specific speeds below 3,000 r. p. m. This approach is generally preferred for low ΔP booster-pump systems using battery primary power.

The details of pump throttling depend strongly upon the details of the ultimate total propulsion system that is to be used.

d. Booster-Pump Optimization. The booster-pump system was optimized considering the entire flight vehicle system using Douglas computer program H109, which is described in appendix A. The following basic conditions were assumed:

- The high-performance insulation system was of the shroud-oriented Dimplar configuration with the number of sheets optimized specifically for each tank pressure condition.
- The pressurization system was assumed to use heated He with an inlet temperature of 400° R.
- Computations were made for duty cycles A and K, which are 1- and 14-day missions, respectively. Each cycle expels the propellants in two burns, with the first burn consuming 80 pct. of the propellant immediately after orbit attainment and the second burn consuming the remainder at the end of the mission. (Duty cycle K represents the most difficult mission relative to propellant storability.)
- Other conditions such as weights and restraints are summarized in appendix B.

The first step in the optimization was to assess the performance, in terms of usable propellant, for each ground-rule LH₂ tank pressure, (41, 100, 195, and 235 p. s. i. a.) assuming no booster pump in the system. The results are illustrated in figure 4-9 which shows a marked increase in usable propellant weight as tank pressure is reduced. Figure 4-9 also indicates that pump-fed engines are superior to pressure-fed systems for the assumed conditions. For the pressure-fed cases, about 60 lb. of usable propellant is lost in going from a 1- to a 14-day mission. For the pump-fed case, the corresponding loss in usable propellant is about 150 lb. (more venting occurs in the low-tank-pressure, pump-fed case).

The pump optimization was performed by making runs on the Space Propulsion System Optimization Program (H109) for a constant booster pump discharge pressure, but by varying pump pressure rise values. This, in effect, means varying tank pressure since tank pressure = pump discharge - pump rise. Pump discharge pressures were assumed to be equivalent to the four ground-rule tank pressures. The results, in terms of maximum usable propellant as a function of LH₂ tank pressure, are shown in figures 4-10 and 4-11 for the pressure and pump-fed systems, respectively. This shows that in all cases studied, the maximum usable propellant weight results with a LH₂ tank pressure of about 30 p. s. i. a. For the pressure-fed engine systems, this means a booster pump pressure rise of 205, 165, and 70 p. s. i. a. for discharge pressures of 235, 195, and 100 p. s. i. a., respectively. For the pump-fed engine case, the optimum booster pump would have a pressure rise of about 11 p. s. i. a.

Table 4-4 summarizes the improvement in usable propellant by using the optimum booster pump for each ground-rule LH₂ tank pressure. For reference purposes, the improvement resulting from using a basic pump-fed system relative to the all pressure-fed system is also shown. This indicates that for all pressure-fed cases, booster pumps result in significant improvements with the magnitude increasing as engine delivery pressure increases. For pump-fed engines, the gain is small for the study ground rules. If a more restrictive and detailed study had been made for the pump-fed system alone, perhaps a larger increase would have resulted, but for the type of study performed, the indicated increases are within the tolerances of the optimization program and the input accuracies.

The right-hand column of table 4-4 indicates that the improvement in going from an all pressure-fed to an all pump-fed system is significantly larger than going from an all pressurized to a pressurized system augmented with a booster pump. This is not really surprising, however, since the pump-fed engine should be more efficient, but table 4-4 does show the penalty involved in not using a conventional pump-fed engine.

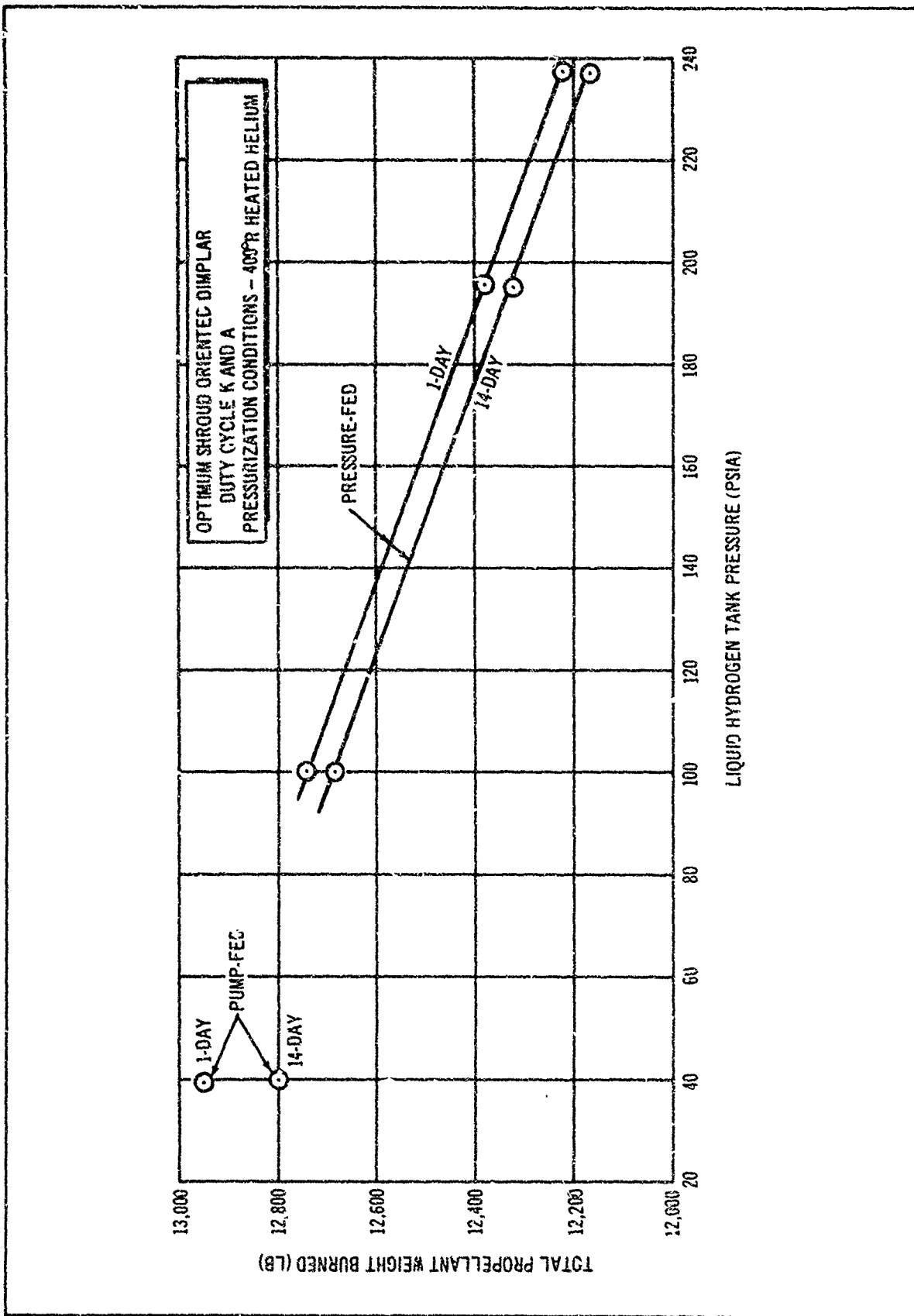


Figure 4-9. Baseline Stage Performance Without Booster-Pumps

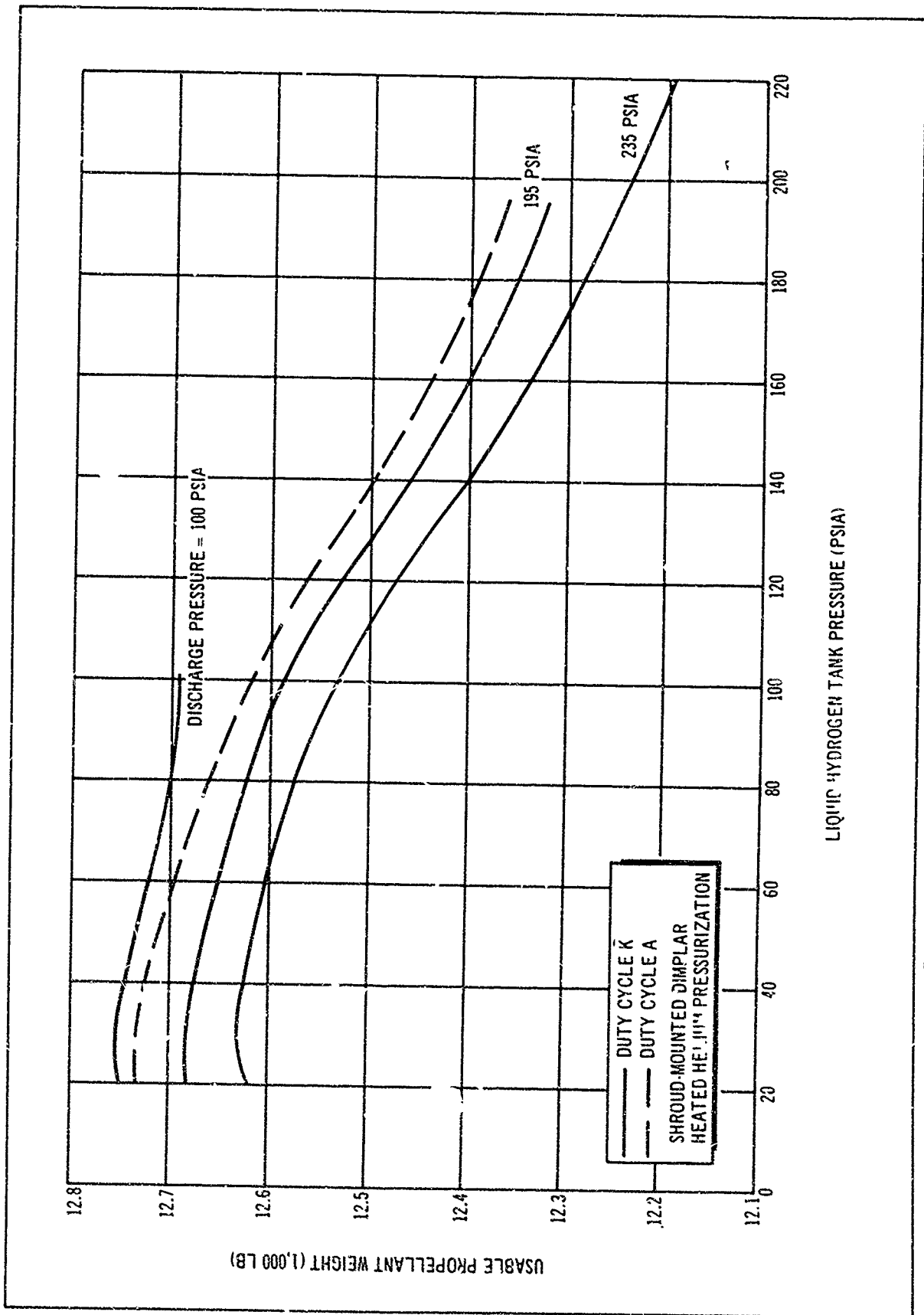


Figure 4-10. Booster-Pump Optimization for Pressure-Fed Systems

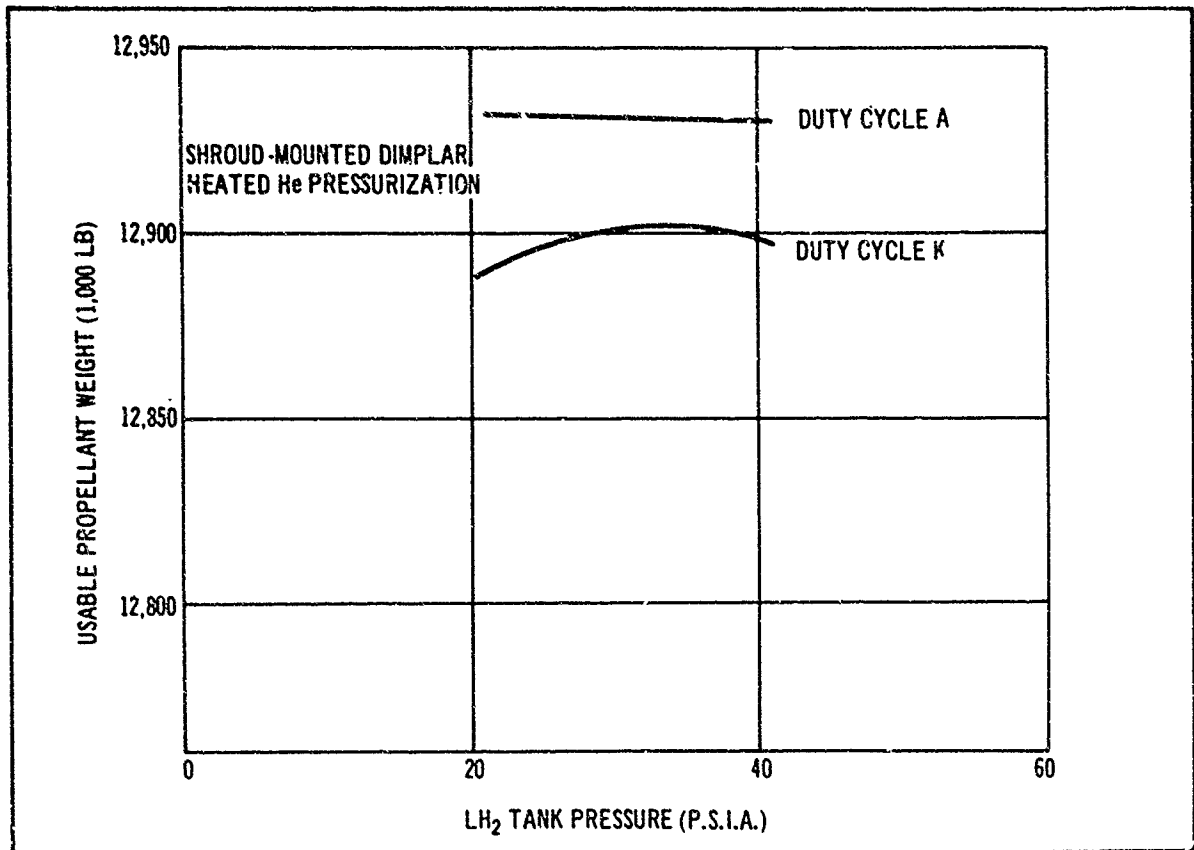


Figure 4-11. Booster-Pump Optimization for Pump-Fed Systems

Table 4-4

IMPROVEMENTS IN USABLE PROPELLANT
RESULTING FROM USE OF OPTIMUM BOOSTER PUMPS

Pressure delivered to engine	Change in usable propellant weight (lb.)	
	Use of optimum boost pump	Use of pump fed engine
235	+ 460	+ 730
195	+ 360	+ 580
100	+ 60	+ 210
41	Insignificant ^a	--

^a Within the accuracy range of the optimization.

c. Optimum Booster Pump Specification. At this point, the optimization results were reviewed with RPL, and it was decided that the pump-fed engine offered greater potentials in terms of performance than the pressure-fed engines. Therefore, only the booster pump for the pump-fed engine was considered further, and a preliminary specification was prepared for this case. Unfortunately, because of the relatively small pump required for this case, the pump system weight is probably within the accuracy of the sum total of all system weight inputs. Therefore, the information on which this specification is based is not nearly as accurate and meaningful as would be desirable.

Figure 4-11 indicates that an LH₂ tank pressure of approximately 30 p. s. i. a. is optimum for a pump-fed engine. For the baseline engine inlet pressure of 41 p. s. i. a., this means a required booster pump pressure rise of 11 p. s. i. a. This was the basis from which the specification was developed. The 11 p. s. i. a. ΔP corresponds to a pump with a maximum power rating of 2.75 hp. With this and the data contained in reference 1, the information contained in table 4-5 was evolved.

It originally had been planned to supply the optimization data to Pesco, and between Douglas and Pesco efforts, evolve a preliminary design and specification. However, since the booster pump was found to be a second-order problem, it was decided, as an economy measure, to terminate the booster pump work at this point.

Table 4-5

PRELIMINARY SPECIFICATION DATA FOR
OPTIMUM LH₂ BOOSTER PUMP

1. General Type	Submerged LH ₂ booster pump directly driven by d. c. motor and external d. c. battery.	
2. Pump	Output power Efficiency Pressure rise Discharge pressure Inlet pressure Maximum weight Maximum speed LH ₂ flow rate Discharge line size Inlet line size	2.75 hp. 65 pct. 11 p. s. i. a. 41 p. s. i. a. 30 p. s. i. a. 11 lb. 25,000 r. p. m. 0.46 to 4.6 lb. p. s. 2.0 I. D. 2.5 I. D.
3. Motor	Output power Efficiency Maximum weight Maximum speed	4.25 hp. 75 pct. 5 lb. 25,000 r. p. m.
4. Battery	Output power Maximum weight including case Maximum duration at full power Pump restarts Maximum operational battery life Environmental temperature	5.7 hp. 16 lb. 200 sec. 19 15 days 40° F.

2. Phase II--Feed Line Losses. When a propulsion system uses high-performance multilayer insulation, the total heat input to the propellant is reduced to a relatively low level. A significant portion of this resulting heat load is a direct result of conduction and radiation heat transfer through the propellant feed and vent lines. Furthermore, for a multiburn stage, the alternate filling and emptying of the feed lines influence their design criteria and requirements, both from fluid flow and heat-transfer considerations. Therefore, it is essential that the feed line be carefully designed to minimize this source of propellant heating and to satisfy operational requirements. The first step to be taken in this design is to view the propellant tank, the tank insulation, and the feed and vent hardware as an integrated system and not as distinct unrelated parts.

Line routing and sizing are relatively straightforward and determined by the general configuration and requirements of the stage. Figure 2-1 illustrates the selected line arrangement. This results in the following line lengths: $LF_2 = 173$ in., and $LH_2 = 10$ in. Fluorine vent = 50 in., and hydrogen vent = 55 in. From flow and pressure drop analyses conducted under Phase VIII, line inside diameters of 2.5 and 3.0 in. were selected for the feed and vent lines, respectively. Wall thicknesses of 0.022 in. were assumed as minimum gages.

a. Basic Line Design Study. The next step was to determine the best line materials and insulation techniques. This was accomplished by evaluating a number of candidate concepts, including:

- Bare metal lines constructed of either steel or aluminum.
- Vacuum-jacketed lines constructed of steel or aluminum. (The vacuum jacket was assumed to be 0.018 stainless steel with a 4-1/2 in. I.D. using teflon support rings every 2-1/2 ft.)
- Steel or aluminum lines with 50 sheets of NRC-2 multilayer HPI installed over the line exterior.

In all cases, an evaluation was made for location of the primary tank insulation either directly on the tanks or on the structural shrouds. It was further assumed that the LF_2 and LH_2 tanks were initially at -320°F . and -420°F ., respectively. The shroud temperatures were taken from the computations made under the Phase IV activity, and it was assumed that there was physical metal-to-metal contact with the line at both shroud and tank end. Material property data were taken from references 2 and 3.

(1) LF_2 Feed Line Analysis. The first point to be resolved was to assess the desirability of vacuum jacketing. This was accomplished by performing a thermal analysis comparing bare lines with vacuum-jacketed LF_2 lines using the Douglas three-dimensional heating computer program (JC56). The line itself and the jacket were divided into 20 equal-length heating nodes. For the aluminum lines, heat transfer was assumed to be solely by conduction, but with steel lines, both radiation and conduction were considered. The numerical results are shown in table 4-6 for four basic line designs each with and without vacuum jacketing.

Table 4-6
COMPARISON OF BARE AND VACUUM-JACKETED LF₂ FEED LINES

Feed line material	Insulation conditions	Heat transfer into line by conduction from shroud (B. t. u./Hr.)	Heat transfer into line by radiation (B. t. u./Hr.)	Net heat transfer into LF ₂ tank (B. t. u./Hr.)	Weight of LF ₂ lost in 336 Hrs. (lb.)	Weight of LH ₂ lost in 336 Hrs. (lb.)	Weight of propellant line (lb.)	Total weight line + propellant lost (lb.)
Aluminum	HPI on tanks	0.657	6.223	6.880	43.690	--	3.186	46.876
Aluminum	HPI on tanks vacuum-jacketed	0.572	6.432	7.104	44.782	--	16.462	61.244
Aluminum	HIP on shroud	6.368	-5.792	0.576	3.277	10.151	3.186	16.614
Aluminum	HIP on shroud vacuum-jacketed	6.708	-6.308	0.400	2.184	10.612	16.462	29.258
Stainless steel	HPI on tanks	0.268	1.882	2.150	13.107	--	8.975	22.082
Stainless steel	HPI on tanks vacuum-jacketed	0.268	1.722	1.990	12.015	--	22.250	34.265
Stainless steel	HIP on shroud	2.311	-2.451	-0.140	--	4.337	8.975	13.312
Stainless steel	HIP on shroud vacuum-jacketed	2.157	-2.297	-0.140	--	4.153	22.250	26.403

The weight of fluorine boiloff was computed assuming that all the heat entering the line results in liquid vaporization and boiloff. This is conservative because a large portion of the heat actually goes into raising bulk temperature and vapor pressure. However, the boiloff weight plus the line structural weight provide a good comparison criteria. Table 4-6 contains a column labeled weight of LH₂ lost which is the LH₂ boiloff resulting from radiation to the LH₂ tank from the warmer LF₂ line. This is significant only with shroud-mounted insulation. Table 4-6 indicates that although there is generally a slight reduction in boiloff loss, this is not great enough to compensate for the heavy vacuum jacketing. Because of these findings, vacuum jacketing was dropped from further consideration.

The remaining candidate line systems were analyzed in a similar but slightly more rigorous manner yielding the results shown in table 4-7. The line weight plus propellant boiloff weight is shown as a function of time in figure 4-12. As discussed above, figure 4-12 was prepared assuming that all the heat-transfer results in propellant boiloff. These results define a number of important trends. Although steel lines are heavier than aluminum, the heat leak is considerably less with steel because of its lower conductivity. Therefore, choice of line material is dependent upon mission time. For example, the results indicate that with bare lines and insulated tanks, aluminum lines would be best with mission durations of 5 days or less, while steel lines would be preferred for longer missions. With shroud-mounted insulation, the crossover occurs at about 8-1/2 days. Another noticeable trend is that when tank-mounted insulation is used, insulation of the feed line is mandatory. On the other hand, when using shroud-mounted insulation, line insulation has a very small effect, and in the case of aluminum lines, it actually represents a very slight weight penalty. Considering all the candidate approaches, the minimum potential weight would be achieved by using shroud-mounted insulation and a bare aluminum line up to 8-1/2-day missions and an insulated steel line for longer missions.

(2) LH₂ Feed-Line Analysis. The short-length LH₂ feed line was analyzed in a similar manner to that described above for the LF₂ line except that 10 heating nodes were used instead of 20. The results are summarized in table 4-8 and figure 4-13. In this case, the insulated stainless steel is preferred for all missions.

(3) Vent Line Analysis. The vent lines were analyzed in a manner identical to the feed lines. An average temperature at the shroud-vent line juncture was assumed at -130°F. and 40°F. for the LH₂ and LF₂ vents, respectively. Table 4-9 summarizes the results for the LF₂ vent line, and table 4-10 shows the results for the LH₂ vent line. The weight penalties are plotted in figure 4-14. In the case of the LF₂ vent, insulated stainless steel appears best except for very short missions. For the LH₂ side, insulated stainless steel is best for long durations but for missions shorter than 2-days, bare aluminum should probably be used.

Table 4-7
 COMPARISON OF STEADY-STATE HEAT-TRANSFER RATES FOR LF₂
 FEED LINE SYSTEMS

Feed line material	Insulating conditions	Heat conducted into feed line at thrust structure (B. t. u. p. Hr.)	Heat conducted into LF ₂ tank (B. t. u. p. Hr.)	Heat radiated into LH ₂ tank by LF ₂ feed line (B. t. u. p. Hr.)	LF ₂ Boiloff rate (Lb. p. Hr.)	LH ₂ Boiloff rate (Lb. p. Hr.)	Feed line weight (Lb.)
Aluminum	HPI on tanks	1.04	4.56	--	0.086	--	3.186
Aluminum	HPI on tanks and line	1.82	1.94	--	0.037	--	4.726
Aluminum	HPI on shroud	4.05	1.21	2.84	0.023	0.015	5.186
Aluminum	HPI on shroud and line	1.93	1.84	0.09	0.035	0.0005	4.726
Stainless steel	HIP on tanks	0.25	2.18	--	0.041	--	8.975
Stainless steel	HPI on tanks and line	0.10	0.20	--	0.004	--	10.515
Stainless steel	HPI on shroud	1.79	-0.01	1.80	--	0.010	8.975
Stainless steel	HIP on shroud and line	0.19	6.11	0.08	0.002	0.0004	10.515

Table 4-8

COMPARISON OF STEADY-STATE HEAT-TRANSFER RATES
FOR LH₂ FEED LINE SYSTEMS

Feed line material	Insulating conditions	Heat transferred into LH ₂ tank by feed line (B.t.u.p. Hr.)	Hydrogen Boiloff rate (Lb. p. Hr.)	Feed line weight (Lb.)
Aluminum	HPI on tanks	38.35	0.213	0.17
Aluminum	HPI on tanks and line	38.28	0.213	0.26
Aluminum	HPI on shroud	38.29	0.213	0.17
Aluminum	HIP on shroud and line	38.26	0.213	0.26
Stainless steel	HPI on tanks	3.30	0.0183	0.49
Stainless steel	HPI on tanks and line	3.00	0.0166	0.58
Stainless steel	HPI on shroud	3.12	0.0173	0.49
Stainless steel	HPI on shroud and line	2.99	0.0166	0.58

Table 4-9

COMPARISON OF STEADY-STATE HEAT-TRANSFER RATES
FOR LF₂ VENT LINE SYSTEMS

Vent line materials	Insulating conditions	Heat transferred into LF ₂ tank by vent line (B.t.u.p. Hr.)	LF ₂ Boiloff rate (Lb. p. Hr.)	Vent line weight (Lb.)
Aluminum	HPI on tanks	15.70	0.296	1.04
Aluminum	HPI on tanks and line	11.57	0.218	1.49
Aluminum	HPI on shroud	14.34	0.271	1.04
Aluminum	HPI on shroud and line	11.55	0.218	1.49
Stainless steel	HPI on tanks	6.72	0.127	2.94
Stainless steel	HPI on tanks and line	0.95	0.018	3.39
Stainless steel	HPI on shroud	3.76	0.071	2.94
Stainless steel	HPI on shroud and line	0.93	0.018	3.39

Table 4-10

COMPARISON OF STEADY-STATE HEAT-TRANSFER RATES
FOR LH₂ VENT LINE SYSTEMS

Vent line material	insulating conditions	Heat transferred into LF ₂ tank by vent line (B. t. u. p. Hr.)	LH ₂ Boiloff rate (Lb. p. Hr.)	Vent line weight (Lb.)
Aluminum	HPI on tanks	10.82	0.060	1.14
Aluminum	HPI on tanks and line	8.66	0.048	1.64
Aluminum	HPI on shroud	9.18	0.051	1.14
Aluminum	HPI on shroud and line	8.70	0.048	1.64
Stainless steel	HPI on tanks	4.13	0.023	3.24
Stainless steel	HPI on tanks and line	0.60	0.003	3.73
Stainless steel	HPI on shroud	1.83	0.010	3.24
Stainless steel	HPI on shroud and line	0.56	0.003	3.73

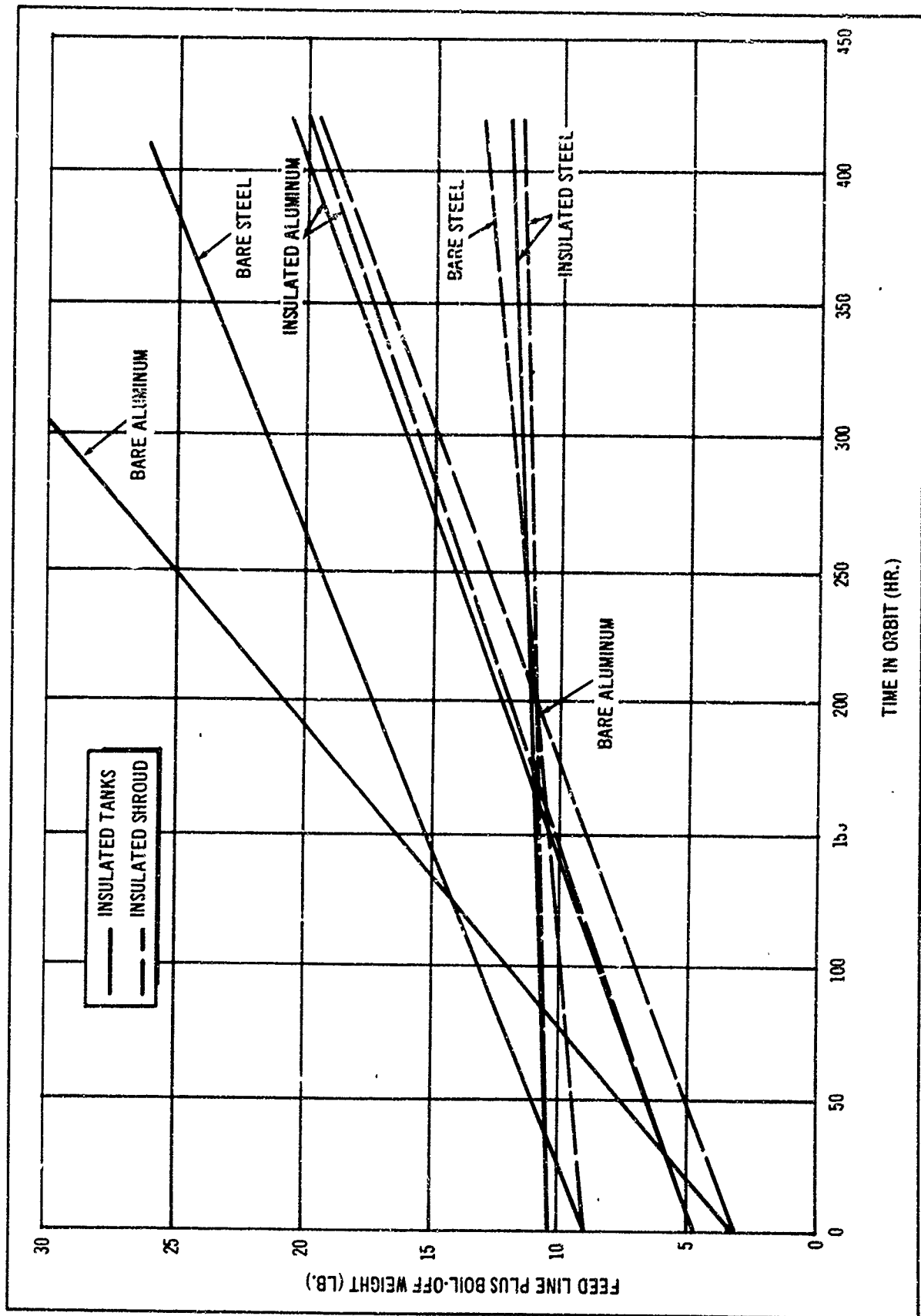


Figure 4-12. Comparison of LF₂ Feed Line Weight Penalties

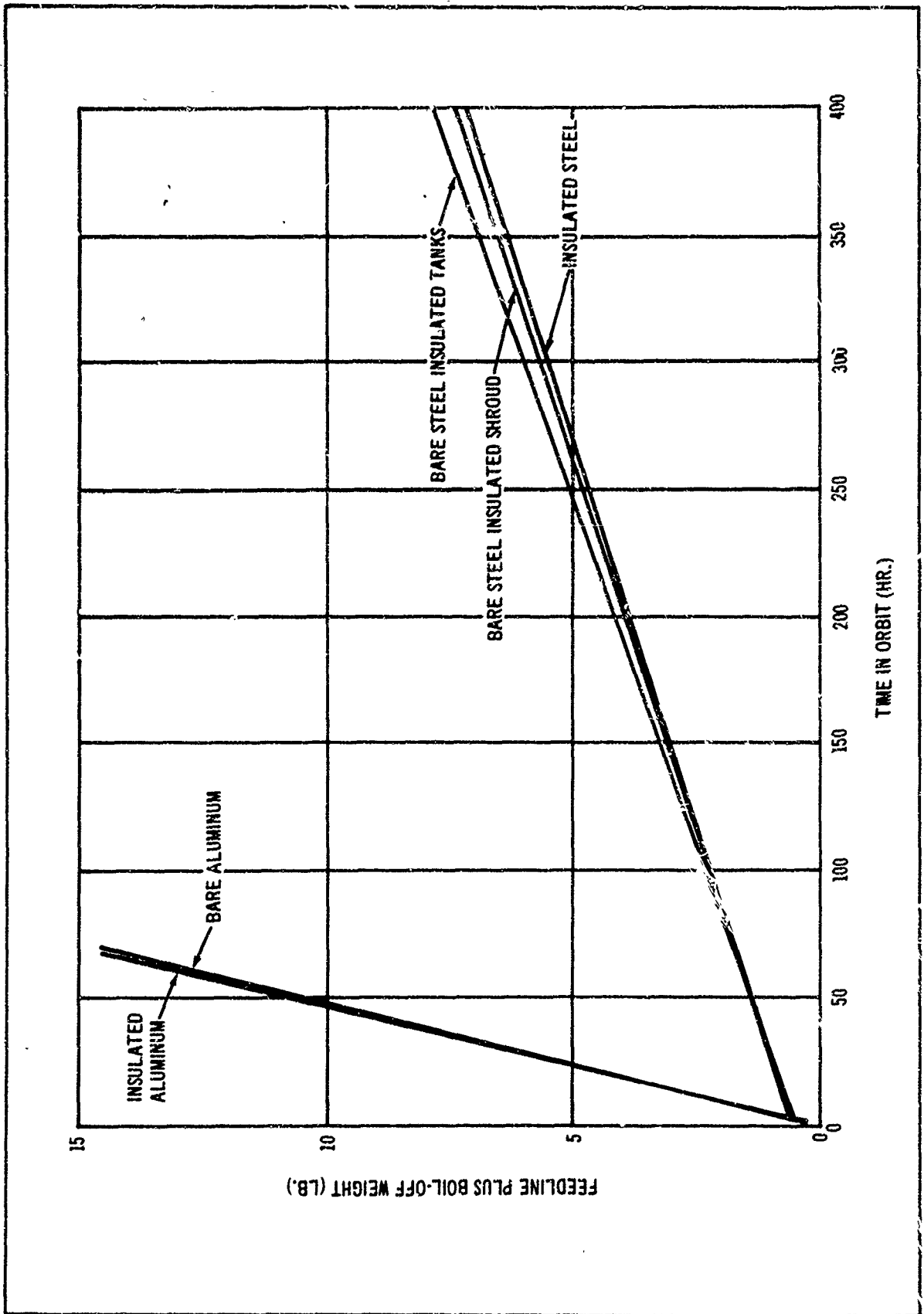


Figure 4-13. Comparison of LH₂ Feed Line Weight Penalties

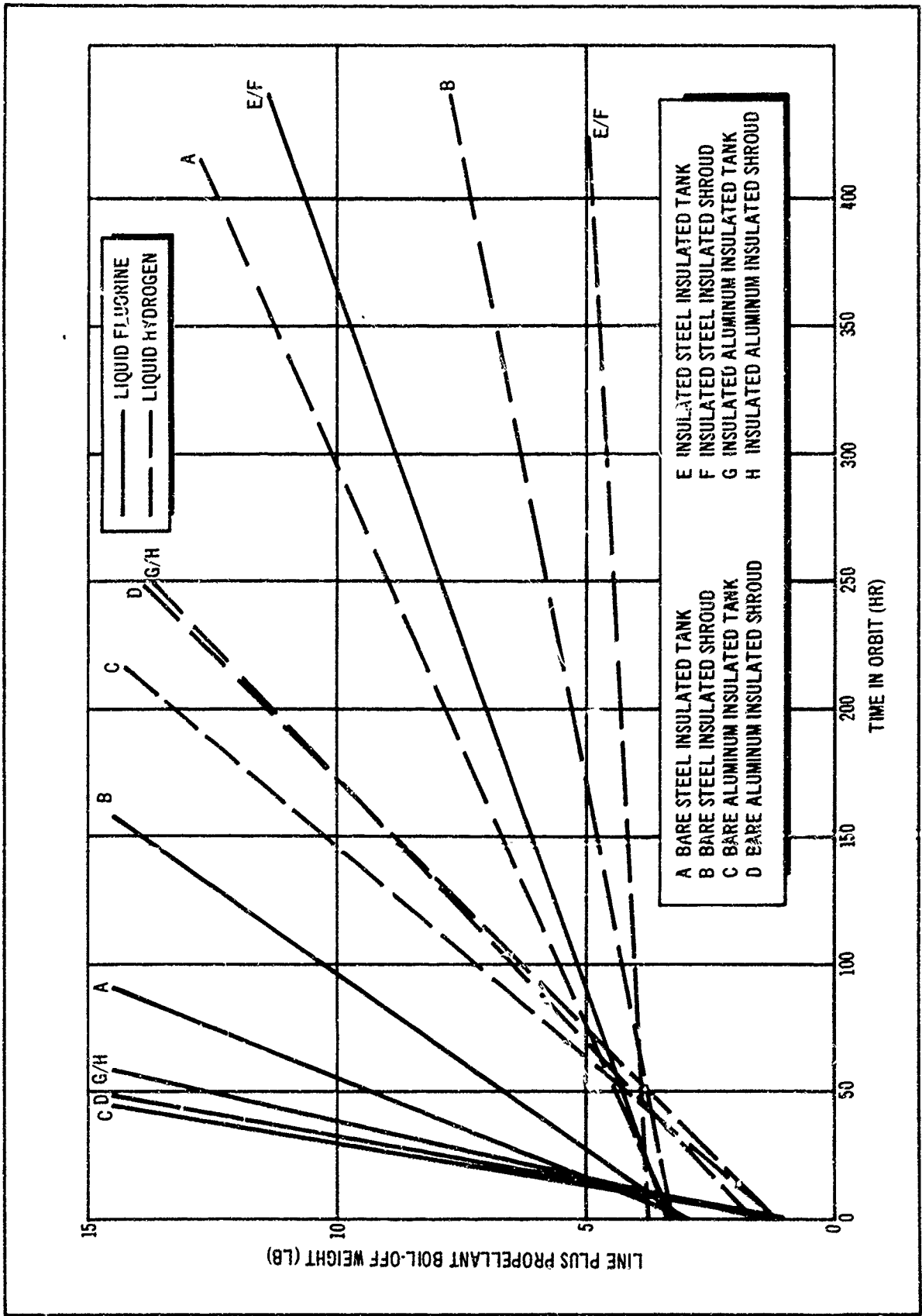


Figure 4-14. Comparison of Vent Line Weight Penalties

b. Line Heat-Transfer and Fluid Flow Phenomena. To assess the desirable operating features for the feed line system, a more detailed study of the line transient heat transfer and its influence on the fluid in the line was made. It was reasoned that after an engine firing, a favorable occurrence in the feed lines is the formation of a stable vapor region at the thrust structure that could force a major portion of the liquid propellant in the lines back into the tank or overboard. The stability and, therefore, the usefulness of this vapor region depend on the velocity of the vapor/liquid surface as it recedes from the thrust structure and on the acceleration forces present.

The differential equations governing the vapor/liquid interface movement were never completely determined owing to the complexity of the problem. In addition, the inclusion of radiation heat transfer made apparent the fact that any exact solution could only be determined using finite difference methods.

In determining the dominant factors and possible approximate solutions to the problem, it was noted that if temperature profiles for a perfectly insulated finite rod were assumed, essentially all of the liquid/vapor interface movement was due to the expansion of vapor already formed after approximately 1 ft. of the line had been filled with vapor. By assuming these profiles to be representative of the actual feed line heating, the problem could then be reduced to one of a composite finite rod initially at a uniform temperature and subjected to a step temperature change at one end.

The problem was simplified further by noting the predominant role of the metallic line with respect to the vapor in the line. The temperature history of a composite rod depends on its axial conduction and heat capacity. Since the metallic line is the major contributor to these properties, the vapor may be neglected and the line considered as a metallic tube with an effective liquid/vapor interface existing at the point on the line where the saturation temperature exists.

Both of these assumptions will yield conservative answers. By assuming no vaporization, velocities higher than the actual result since the latent heat of vaporization has been eliminated. The assumption of an empty metallic line also yields higher velocities because of the relatively large heat capacity of the vapor as compared to its axial conductivity. Thus, if the temperature profiles assumed are similar to the actual profiles encountered, this approximate solution should yield conservative estimations of the liquid vapor interface velocity.

The calculated feed line temperature profiles are shown in figures 4-15 and 4-16 for various line designs and indicate the position of the liquid/vapor interface relative to the thrust structure at steady-state conditions. This interface will be positioned near the -260°F . point (its approximate saturation temperature) on the profile. Figure 4-17 shows the transient distributions for the insulated steel line which indicates that the steady-state is achieved in about 200 hr.

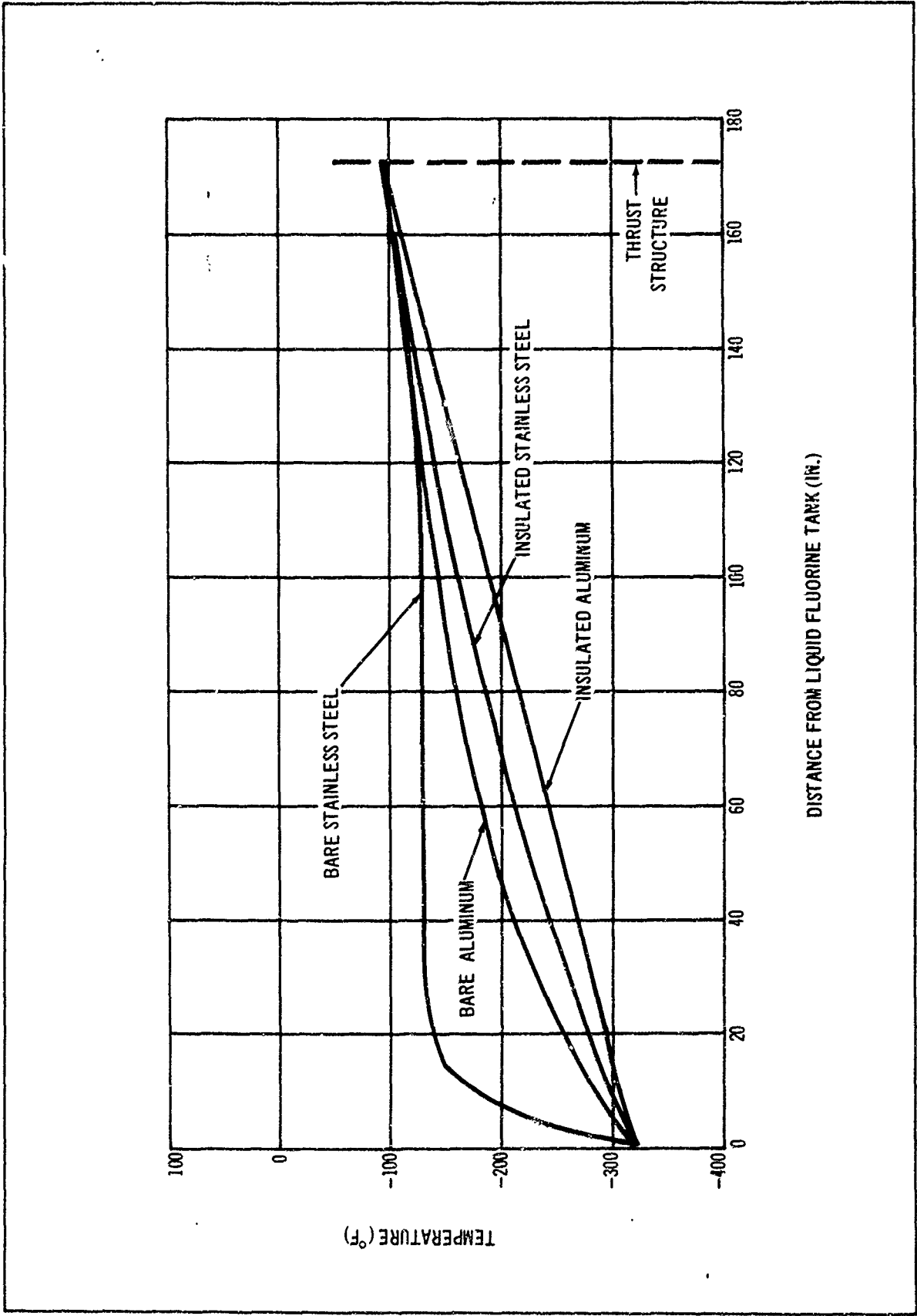


Figure 4-15. Steady-State Temperature Profiles for Liquid Fluorine Feed Line for Insulated Tanks

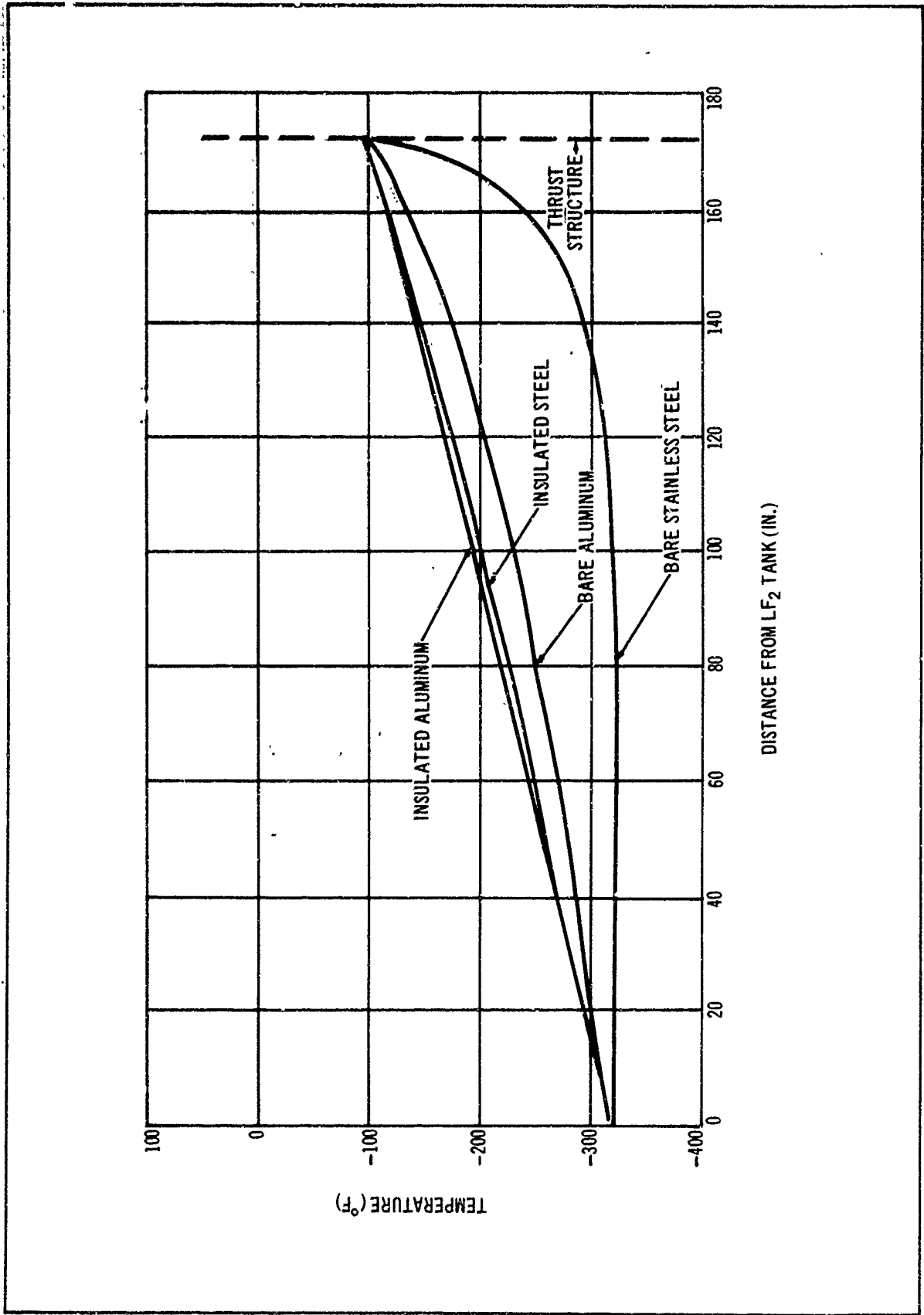


Figure 4-16. Steady-State Temperature Profiles for LF₂ Feed Line for Insulated Shroud

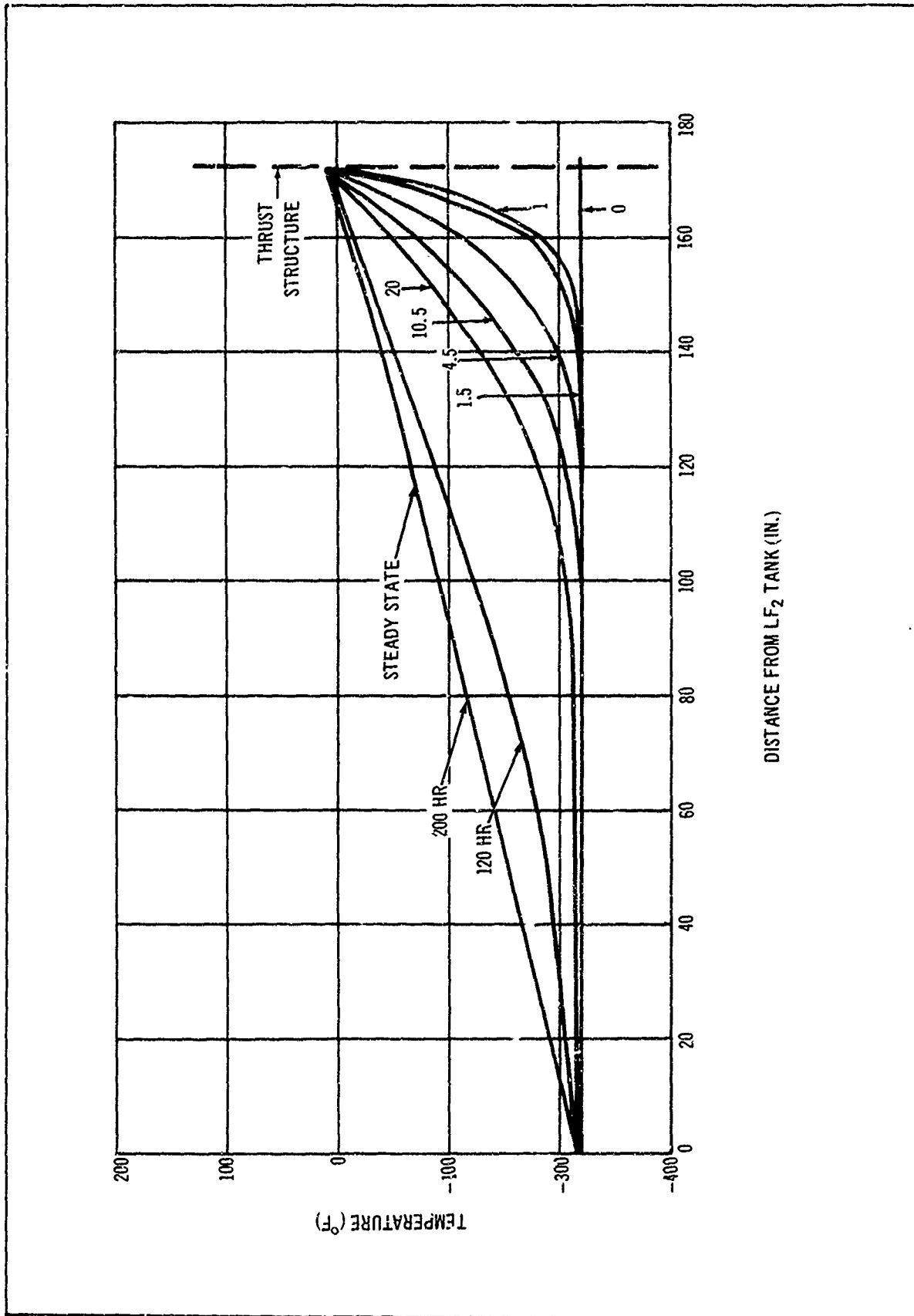


Figure 4-17. Temperature History for L.F₂ Feed Line (Insulated Stainless Steel for Insulated Shroud)

Results of line heating show that the temperature profiles assumed are nearly correct and very little propellant is vaporized after the interface recedes 1 ft. from the thrust structure. Figure 4-18 shows the growth rate of the vapor region for three stainless-steel line systems. For these small growth rates and the expected acceleration forces (less than 10^{-4} g), the interface will be stable and the vapor region will force some of the LF_2 out of the line after each firing, if relief capabilities are provided. The omitted stainless-steel system, the bare line with insulated propellant tanks, had such a high-radiation heat-transfer rate to the line that the possibility of a vapor region formation around the LF_2 existed, making this approximate solution invalid. Further investigation was not pursued on this configuration since this design did not yield favorable results at steady-state condition.

Figure 4-18 compares the solution of the insulated stainless steel line using an insulated shroud to the theoretical solution of a perfectly insulated infinite rod (dashed line). These two curves agreed fairly well initially. Since the effect of radiation is much less for the high conduction rates experienced with the aluminum lines, only the theoretical heating curve is presented for the aluminum feed lines, (figure 4-18). This shows that even for aluminum lines, the velocity 1 ft. from the thrust structure, approximately 7-1/2 f. p. r. is small enough to ensure liquid/vapor interface stability.

The assumption of liquid/vapor interface movement due to expanding vapor is not valid for the LH_2 line. This is a result of the small difference in the density of the LH_2 vapor, the LH_2 and the short length of the line. Thus, the most conservative estimate is to assume that all of the LH_2 left in the line after each firing is boiled off.

The line pressure will, in general, be above the collapsed tank pressure providing a pressure difference so that the line could be relieved back to the tank. Because the bulk of LF_2 in the tank is subcooled, the saturation point always lies within the line. This means that with a tank shutoff valve or pre-valve, the line will never be emptied passively (i. e., by self-pressurization). Furthermore, there will always be some liquid in the line which will not in any way contribute to excess heat leak into the tank since it will be in thermal equilibrium with the line.

It was previously thought that the amount of LF_2 trapped in the line could be minimized by leading the closure of the prevalve, and indeed this could reduce by as much as 10 pct. the amount of trapped LF_2 . However, it is seen from figure 4-17 that this would not alter the final condition of the liquid in the feed line and would not reduce the heat load to the tank (since it is principally through the feed line proper, not its contents). However, leading the prevalve closed would have the deleterious effect of leaving a void in the line, which would promote sloshing and unstable fluid behavior in the line immediately following engine shutdown. It is recommended, therefore, that no prevalve lead be employed and that both prevalve and engine valve be shut as nearly simultaneously as possible.

Figure 4-17 also shows that a LF_2 prevalve is not directly required for thermal reasons (provided the liquid interface is stable). On the LH_2 feed line, a prevalve is required thermally because the line boils dry very quickly and the prevalve minimizes the propellant boiled off.

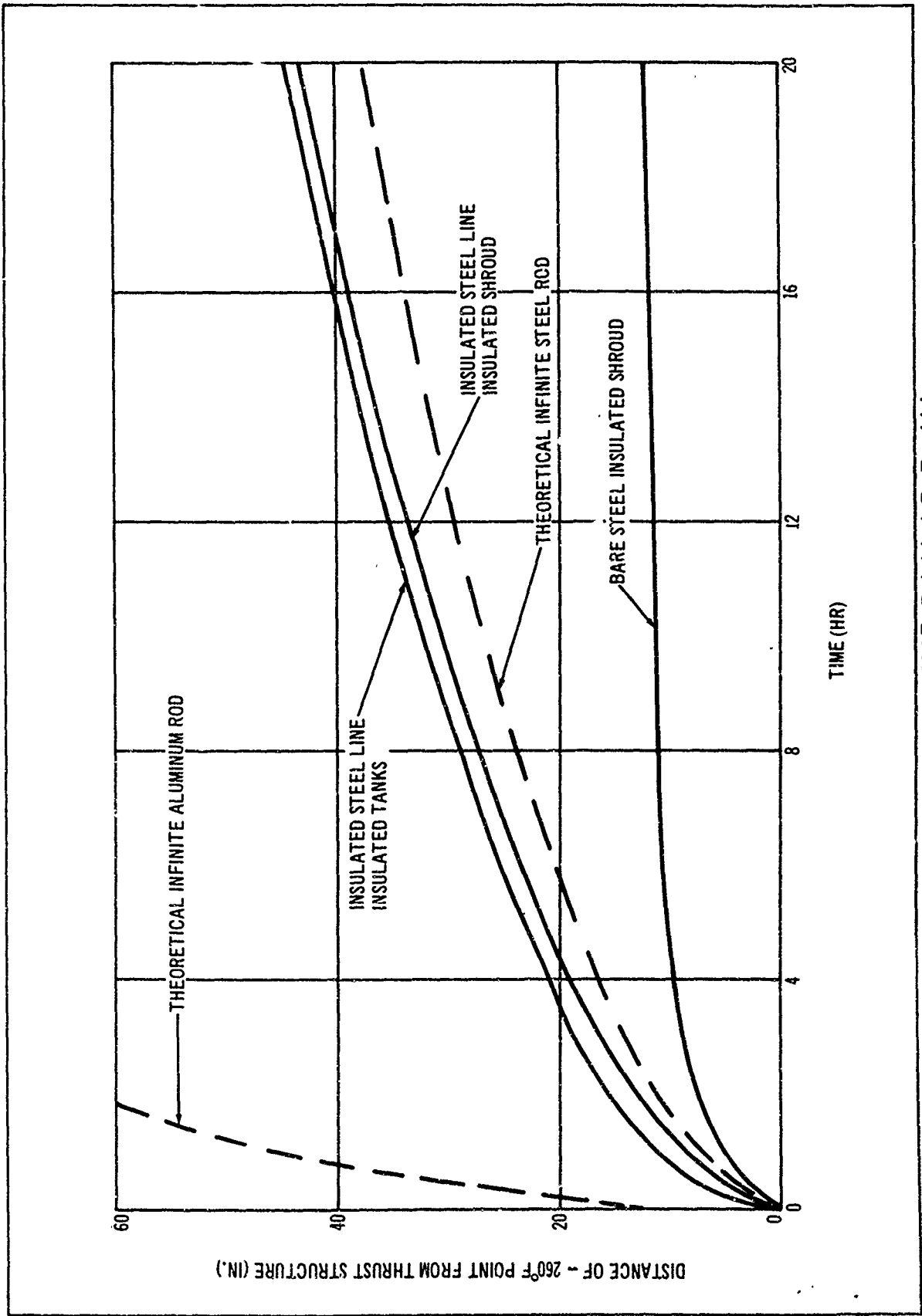


Figure 4-18. Location of -260°F Point in LF₂ Feed Line

Pressure relief of the line can be accomplished in two ways: (1) by venting the vapor (thrust structure) end to the tank, or (2) by venting the liquid (tank) end of the line to the tank. If the vapor end is vented to the tank, some of the heat input to the line may end up in the tank via the vented vapor. If the liquid end is vented, the heat into the line stays in the line and does not get to the tank, providing the liquid vent is sized for maximum vapor production, and the heating rate is low. The integrated heat input to the LF_2 line is shown in figure 4-19 and is relatively low. With liquid venting, almost all of this heat will go into warming up the line and vapor with very little going into boiloff since the liquid is in thermal equilibrium with the line. The liquid relief check valve, by-passing the pre valve, is sized to accommodate the liquid equivalent of vapor production under a peak nucleate boiling heat flux of 20,000 B. t. u. p. hr. p. ft.² to satisfy the worst case of initial boiling at the thrust structure valve face. This results in a 1/4-in.-dia. liquid relief and check valve. Once the initial vapor barrier has formed, the line heating will proceed as in figure 4-17.

It can be seen from figure 4-17 that, depending on the coast time and the line pressure, the line can be anywhere from 90 pct. full to less than 10 pct. full. This trapped propellant is a cause for some concern during propellant settling, if ullage rockets are used for settling as anticipated. The settling acceleration is about 10^{-2} g., and thus the feed line Bond number is about 48, which is marginally unstable. Thus, during settling the trapped liquid would fall into the warmer end of the pipe and vaporize, causing bubbling and geysering in the feed line. It would not help the

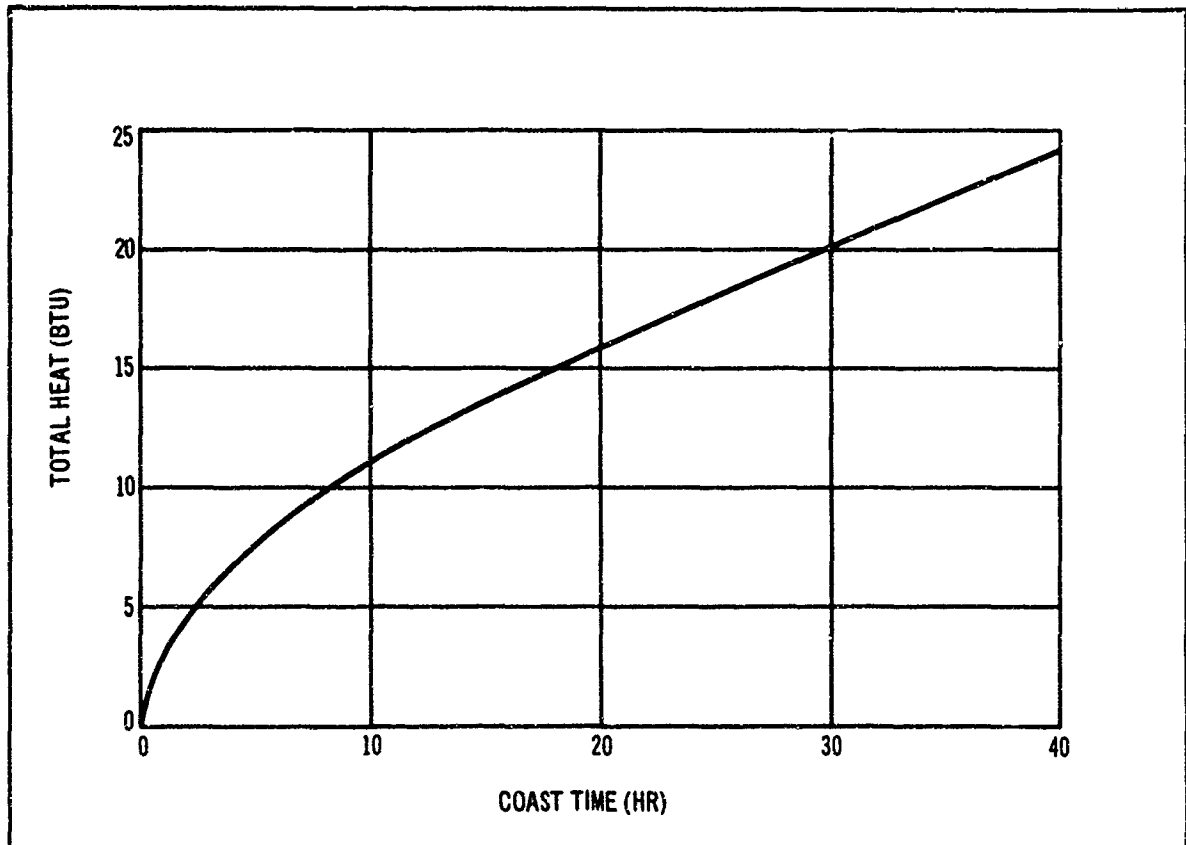


Figure 4-19. Total Integrated Heat Through LF_2 Feed Line (Insulated Stainless Steel)

situation to vent the lower end of the feed line, since the head exerted by the full liquid column under 10^{-2} g. is only about 0.1 p. s. i., and the back pressure from even a large vent line and check valve would surely exceed this for the expected vapor flow; that is, the bubbles would rather rise freely up an open 2-1/2-in. feed line than up a much smaller vent line. Therefore, it is recommended that the pre valve be opened during settling to allow unrestricted vapor egress and provide a full chilled feed line at the end of settling. The sensible heat of the line for the most empty case is about 100 B. t. u. which would vaporize something over a pound of LF_2 , creating nearly 3 cu. ft. of vapor.

This problem would not be alleviated by either (1) removing the pre valve so that the line may empty itself with an initial pressure surge under zero-g. coast or (2) actively blowing the line clear of propellant during coast. Maintaining the line in an empty condition during settling merely postpones the problem until engine start, when the engine must ingest an entire feed line full of vapor. It is felt that such ingestion would have a deleterious effect on engine reliability and performance. This would be more severe for pump-fed engines than for pressure-fed engines. Further, actively emptying the feed line serves no useful purpose since it requires that more propellant be put back into the line and thus may increase the settling time. The problem would not be substantially helped by making the feed line small enough for capillary stability during settling, since for the long coast missions, the engine would again be forced to ingest up to 90 pct. of the feed line volume of vapor.

c. Recommendations for Feed Line Operation. On the basis of the above arguments, the resulting conclusions and recommendations for feed line operation are summarized as follows:

- A pre valve, although not required thermally, should be incorporated in the LF_2 feed line to retain propellant in the line during zero-g. coast.
- The line should be pressure-relieved at the pre valve with a 1/4-in.-dia. check valve by by-passing the pre valve.
- The pre valve should be opened during the settling and the settling time increased to allow the feed line to fill and chill down prior to engine restart.
- The line should not be vented at the thrust structure end since the back pressure required would make such a vent ineffective against geysering during settling.
- The feed line should not be actively emptied by pressurization during coast.
- The feed line should not be made smaller for capillary stability during settling.
- The pre valve closure should not lead the propellant valve closure but should be closed at the same time.

Figure 4-20 illustrates a recommended conceptual design for a combination tank pre valve and line pressure relief check valve which would satisfy the above recommendations.

(4) Feed Line Restart Weight Penalties. The weight penalty actually incurred by settling the propellants prior to engine operation is primarily a function of the heat storage capacity of the line and the heat necessary to condense the vapor in the line. The worst condition that can arise is to have the line achieve steady-state conditions prior to engine operation. This constitutes the maximum heat storage condition for the line.

For the LF_2 feed line, the maximum amount of thermal energy stored by the line and the vapor is less than 50 pct. of the energy required to bring the LF_2 that remains in the line at steady-state to its saturated condition. That is, if LF_2 from the tank is forced into the line, the wetting of the line can be accomplished by using only the thermal storage capacity of the liquid originally in the line and without vapor being forced into the tank. Thus, no weight penalty for the LF_2 line would be expected for referring.

Since the LH_2 tank is at its saturated conditions, wetting the line will cause additional LH_2 boiloff. For stainless steel lines, the stored energy amounts to 10 B. t. u. In addition to wetting losses, the fuel in the line after each firing is also lost. Therefore, the total penalty for the LH_2 line is 0.2 lb. of LH_2 boiloff per firing. Figures 4-20, 4-21, 4-22, and 4-23 show the weight penalty versus time for the various duty cycles for the insulated stainless-steel LH_2 line.

3. Phase III--Venting. Venting of flight vehicle cryogenic tanks may be necessary to satisfy four individual requirements:

- To relieve tank pressure during ground loading of the propellants.
- To relieve the tank pressure buildup as it approaches the tank design pressure, as a result of heating during boost phase or orbiting flight.
- To act as a safety device in case of over-pressurization during engine operation.
- To permit blow-down of the tanks to condition the propellant (reduce propellant temperature to provide NPSH) prior to engine operation.

The last three conditions, as they apply to orbiting operation, pose particularly difficult problems for the vent system as they generally involve venting under zero-g. conditions. Under this environment, efficient venting, that is venting with negligible liquid loss, requires a reliable ullage location control system or some type of effective vapor/liquid separator in addition to the conventional vent and/or relief valve hardware. Any venting, gas or liquid, represents a loss of propellant or pressurizing gas which is no longer available for useful work. The purpose of a low-heat leak propellant storage and feed system is to reduce this loss to the point where the combined vent loss and thermal protection system weight yield maximum stage performance.

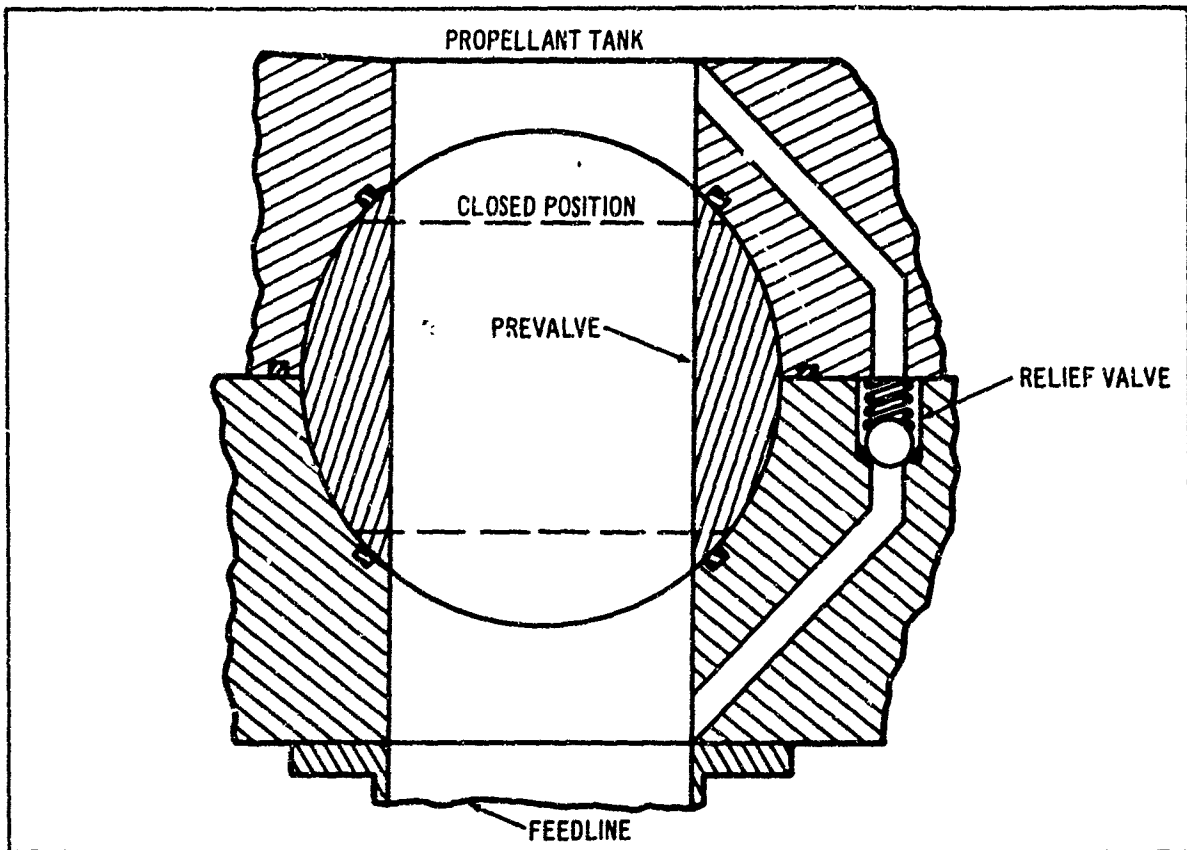


Figure 4-20. Prevalve Bypass and Feed Line Relief

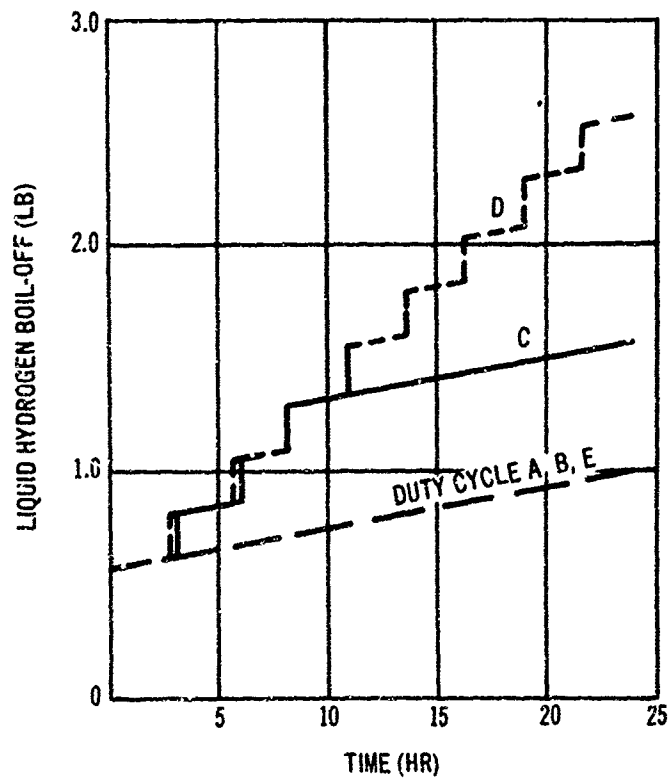


Figure 4-21. Boiloff Loss for LH₂ Feed Line (24-hr. Duty Cycle)

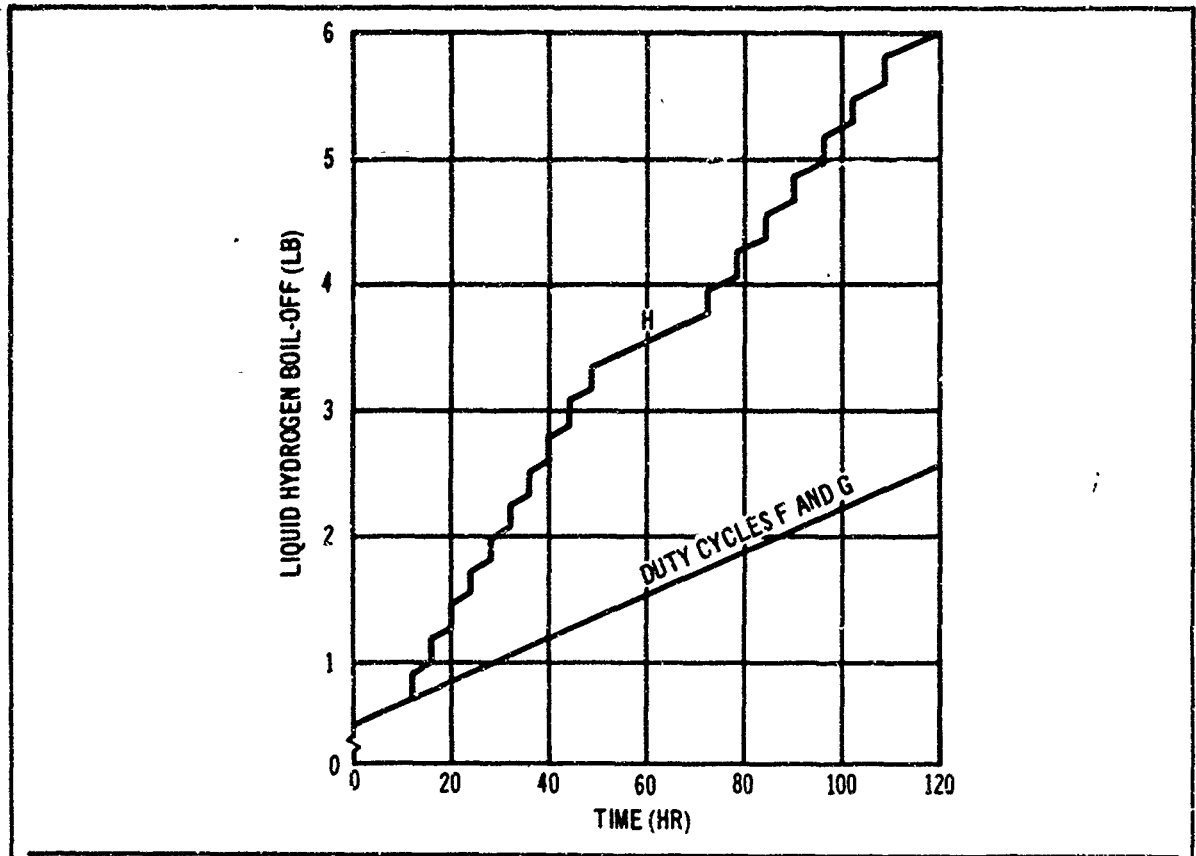


Figure 4-22. Boiloff Loss for LH₂ Feed Line (120-Hr Missions)

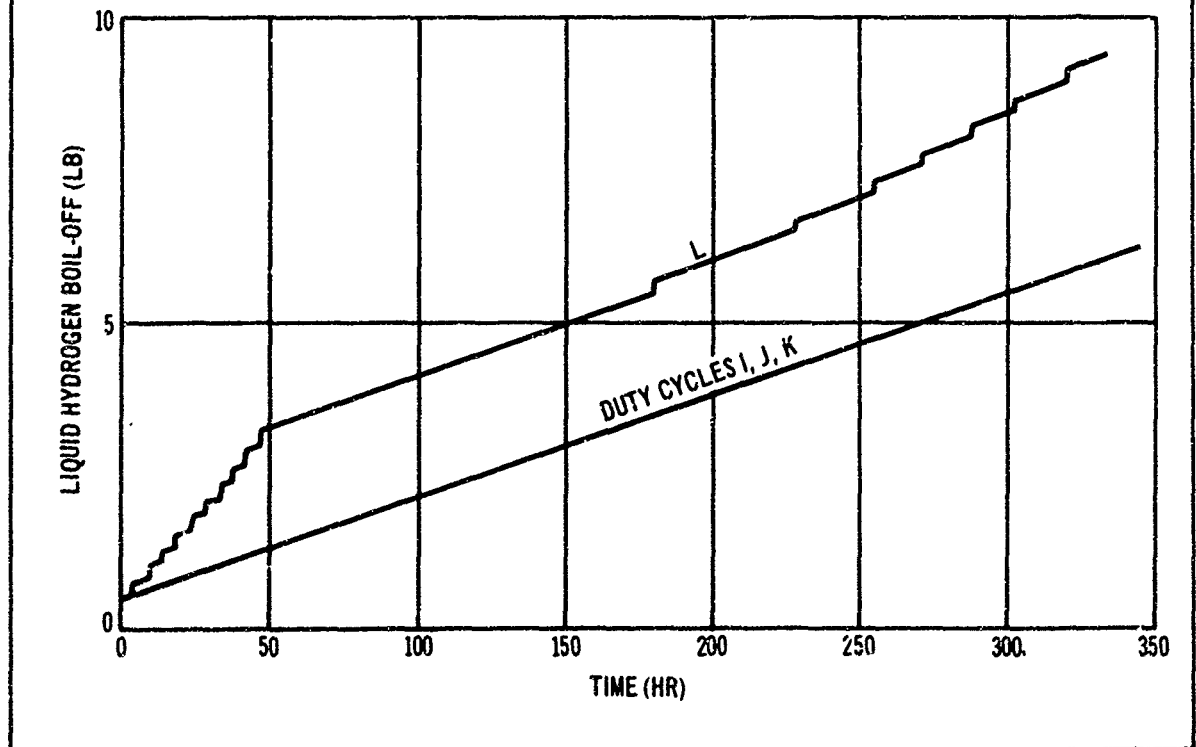


Figure 4-23. Boiloff Loss for LH₂ Feed Line (336-Hr Missions)

Two approaches may be taken to the venting problem. The first is to design the system and select the operating conditions so that the system does not require zero-g. venting. This can be done by structurally designing the tankage to accept the pressure levels resulting from the propellant heating. With this approach, no zero-g. venting is required. The alternate approach is to design the system selecting operating conditions strictly on the basis of optimization study conclusions and to design the vent with an appropriate zero-g. venting system, as required. For this study, the second approach seemed to be the most universally applicable since the ground rules involved a rather large range of base point tank pressures. Therefore, emphasis was placed on a system where zero-g. venting was a requirement, and an evaluation was initiated of the techniques for achieving venting in a zero-g. mode. To logically accomplish this, it is necessary to have a reasonably sound idea of what the venting requirements are for various duty cycles and tank pressures. If very precise accuracy were required, it would have been necessary to delay this work until the completion of all the optimization effort. This was not practical, however, and it was decided to establish preliminary venting requirements by generating pressure histories for a limiting range of tank pressures, the ground duty cycles, and an approximate overall tank heat input level which would be representative of a low-heat input stage using HPI. The other phases of the study had progressed to the point where this heat input level could be assessed with sufficient accuracy to identify the general venting requirements and to allow comparisons of the various zero-g. venting approaches.

a. Preliminary Pressure Histories and Venting Requirements.

Pressure histories were evaluated for the 12 ground rule duty cycles and pressures of 25, 75, and 250 p. s. i. a. using the Douglas H109 Multistart Propulsion System Sizing and Optimization computer program (see appendix A). Pressures were selected to correspond to the anticipated minimum tank pressure with a booster pump (25 p. s. i. a.), the level at which non-vented tank operation was thought possible (75 p. s. i. a.), and the very maximum pressure level (250 p. s. i. a.). The conditions assumed for the pressure history computations are summarized in table 4-11. The net effects of the insulation system, skin surface temperatures, and line heat shorts yield a net heat flux of approximately 50 B. t. u. p. hr. and 36 B. t. u. p. hr. to the LH₂ and LF₂ tanks, respectively. The actual heat fluxes for the optimized flight vehicle were not known at this point, but should generally be below this value, except for optimized short-duration missions. Therefore, the computed pressure histories can be used to identify those duty cycles for which venting will be required and the magnitude of the venting rates. The resulting pressure histories are shown in appendix C. For the 36 cases analyzed, none lost oxidizer and 15 lost fuel as a result of heating and/or propellant conditioning (tank blowdown) before a burn. These cases are summarized in table 4-12.

Little propellant is lost as a result of coast heating in the pressure-fed cases, and propellant losses could be reduced to zero by loading the propellant tanks at a total pressure below the run pressure. In fact, for a given mission and run pressure, the tanks could be loaded at a pressure such that the tank pressure increases to exactly the run pressure at the end of coast.

Table 4-11
ASSUMED CONDITIONS FOR PRESSURE HISTORY COMPUTATIONS

Input	Duty cycle	Pump-fed	Pressure-fed
LH ₂ temperature	All	36° R	37° R
LF ₂ temperature	--	140° R	140° R
Initial ullage percentage	--	5 Pct.	5 Pct.
Ambient H _e temperature (repressurization)	--	520° R	520° R
Heated H _e temperature	--	400° R	400° R
LH ₂ tank collapse factor	--	1.5	1.5
LF ₂ tank collapse factor	--	1.4	1.4
LH ₂ pump NPSH	--	2 p. s. i. a.	--
LF ₂ pump NPSH	--	5 p. s. i. a.	--
LH ₂ line ΔP	--	1 p. s. i.	3 p. s. i.
LF ₂ line ΔP	--	5 p. s. i.	5 p. s. i.
LH ₂ tank run pressure	A-D E-K	21 p. s. i. a. 21 p. s. i. a.	120 and 245 p. s. i. a. 70 and 245 p. s. i. a.
LF ₂ tank run pressure	A-D E-K	32 p. s. i. a. 32 p. s. i. a.	120 and 245 p. s. i. a. 70 and 245 p. s. i. a.
LH ₂ tank vent pressure	A-D E-K	25 p. s. i. a. 25 p. s. i. a.	125 and 250 p. s. i. a. 75 and 250 p. s. i. a.
LF ₂ tank vent pressure	A-D E-K	35 p. s. i. a. 35 p. s. i. a.	125 and 250 p. s. i. a. 75 and 250 p. s. i. a.

In such a case, there would be neither a venting loss or pre-pressurization penalty. More realistically, however, the mission will not be defined at the time of loading, and this ideal situation cannot be guaranteed.

b. **Assessment of Liquid Venting Penalties.** An analysis was made to determine the weight penalty for uncontrolled venting of liquid for the study vehicle duty cycles requiring venting. The analysis was based on venting 100 pct. liquid all the time and is clearly an improbable worst case. The assumption is justified, however, since the analysis has the objective of showing (with numbers) the conclusion that liquid venting positively cannot be tolerated. For five duty cycles where venting of the LH₂ tank occurred, the weight penalty based on a ratio of liquid density to vented vapor density at the vapor partial pressure is summarized in table 4-13.

Table 4-12
 LH₂ LOST BECAUSE OF VENTING (LB.)

Duty cycle	Vent pressure	Coast loss	Conditioning loss
E	75	0.4	--
	250	0.1	--
F	25	6.0	10.3
G	25	0.9	18.0
	75	0.7	--
	250	0.6	--
H	25	--	18.7
I	25	41.4	31.1
	75	3.6	--
	250	2.8	--
J	25	51.4	20.1
	75	3.4	--
K	25	57.7	11.6
	75	18.6	8.2
L	25	5.8	56.7

Table 4-13
 WEIGHT PENALTY FOR LIQUID VENTING

Duty cycle	P _T (p. s. i. a.)	W _{heating} (lb.)	W _{conditioning} (lb.)	W _{total} (lb.)
F	25	2,504	5,234	7,738
H	25	--	11,622	11,622
J	25	10,880	671	11,551
	75	551	--	551
K	25	15,350	5,207	20,557
	75	2,919	1,313	4,232
L	25	2,006	22,660	24,666

Since the normal weight of LH₂ in the tank is about 900 lb., it is clear that liquid venting will empty the tank in every case but the fourth one. The magnitude of the above numbers depends on the assumptions used for the pressurization system, which in these cases assumed heated (400°R) He.

The numbers are so large, however, that no pressurization system assumption is going to alter the essential conclusion: Liquid venting is unacceptable and some form of vent control must be utilized.

c. Study of Zero-g Venting Concepts. Having determined that zero-g venting of the LH₂ tank will be required for certain combinations of duty cycle and tank pressures and that uncontrolled liquid venting is not feasible, a study and comparison of various zero-g venting systems was initiated. This study consisted of selecting certain candidate systems, generating required performance, and weight data for each concept, and then comparing them on a weight basis for a fixed set of conditions for the venting requirements determined above.

Two basic approaches may be taken to obtain controlled low-g venting: fluid phase separation and ullage position control. In the phase separation approach, some form of separator is used to separate the gas from the liquid and ideally only the gas phase is vented. For this study, two separator concepts were selected for evaluation: (1) a mechanical device using centrifugal force to separate the different density fluids, and (2) a thermodynamic liquid/vapor separator which uses a throttling valve in conjunction with a heat exchanger using the bulk propellant as the heat sink.

In the case of ullage location control, the position of the ullage space is maintained so that it is always over the vent valve during venting, thus precluding the possibility of significant liquid venting. Three individual concepts were evaluated for ullage position controls: (1) a surface force or capillary attraction-type system, (2) an ullage rocket system which provides a sufficient g force via thrust to the vehicle to settle the liquid propellant, and (3) a dielectrophoretic system which employs a nonuniform electrical field to preferentially orient the propellants. In most of these cases, it was necessary to consider the interaction of the settling system for assuring liquid phase propellants to the engine during restart from a zero-g condition. The following sections present the basic data generated for each approach.

(1) Surface Force Concept. To control the location of propellants during periods of near zero-g for purposes of venting or providing propellants at the engine inlets for subsequent restart, concepts involving the use of capillary forces have been suggested (references 4 and 5). Capillary forces derive from the surface tension or cohesiveness of the liquid and are relatively very small, becoming important only in the absence of dynamic fluid forces and gravitational forces. Capillary forces are an inverse function of the system characteristic dimension, which makes screens attractive devices for utilization of the capillary forces, since screens can have very small dimensions, yet still allow propellant flow-through during normal-gravity operation.

This analysis investigates the potential of screens for appropriate propellant orientation for zero-g venting of the stage.

(a) Capillary Stability. For screens used as capillary devices, the stability of the liquid/vapor interface supported by the screens is the governing criteria for sizing of the openings in the screen. In a gravity field, this stability criterion depends on the Bond number, which is a measure of the ratio of the gravitational forces to the capillary forces and is defined as follows:

$$B_o = \frac{\rho g a^2}{\sigma'} \quad (4-1)$$

From reference 5, for two-dimensional screens of opening size $2a \times 2b$ with b greater than a , the interface is stable for small disturbances if

$$\rho \frac{g a^2}{\sigma'} < \frac{\pi^2}{4} \left(1 + \frac{4a^2}{b^2} \right) \quad (4-2)$$

which for b approximately equal to a , gives

$$\rho \frac{g a^2}{\sigma'} < \frac{5}{4} \pi^2 \quad (4-3)$$

Small disturbance assumptions are not always appropriate for conditions in a space vehicle propellant tank where external vibration and internal sloshing may be present. In an effort to determine the stability, criteria under external vibration were analyzed dimensionally and extrapolated to give the following criterion for approximately square openings of dimension $2a$:

$$a \leq 0.1135 \frac{\sigma'}{\rho (w\lambda)^2} \quad (4-4)$$

where w and λ are the externally imposed vibration frequency and amplitude. Equation 4-4 is plotted in figure 4-24 for LH_2 , LF_2 , and LN_2 at the most conservative conditions of σ'/ρ , namely, for saturated LH_2 at $50^\circ R$, LF_2 at $221^\circ R$, and LN_2 at $203^\circ R$.

For comparison, the spacing based on equation 4-3 for g , and $0.1 g$, small disturbances are also plotted in figure 4-24. Note that this and subsequent criteria are plotted as points since they are not functions of $w\lambda$.

For fluids in motion, the measure of interface stability is the Weber number, which relates the fluid dynamic forces to the capillary forces as follows:

$$w_e = \rho \frac{v^2 2a}{\sigma'} \quad (4-5)$$

Equation 4-5 is plotted in figure 4-24 for a Weber number of 1, which is assumed to be the dividing line between velocity-dominated and capillary-dominated forces. The velocities plotted are 3, 30, and 212 cm. p. s. or

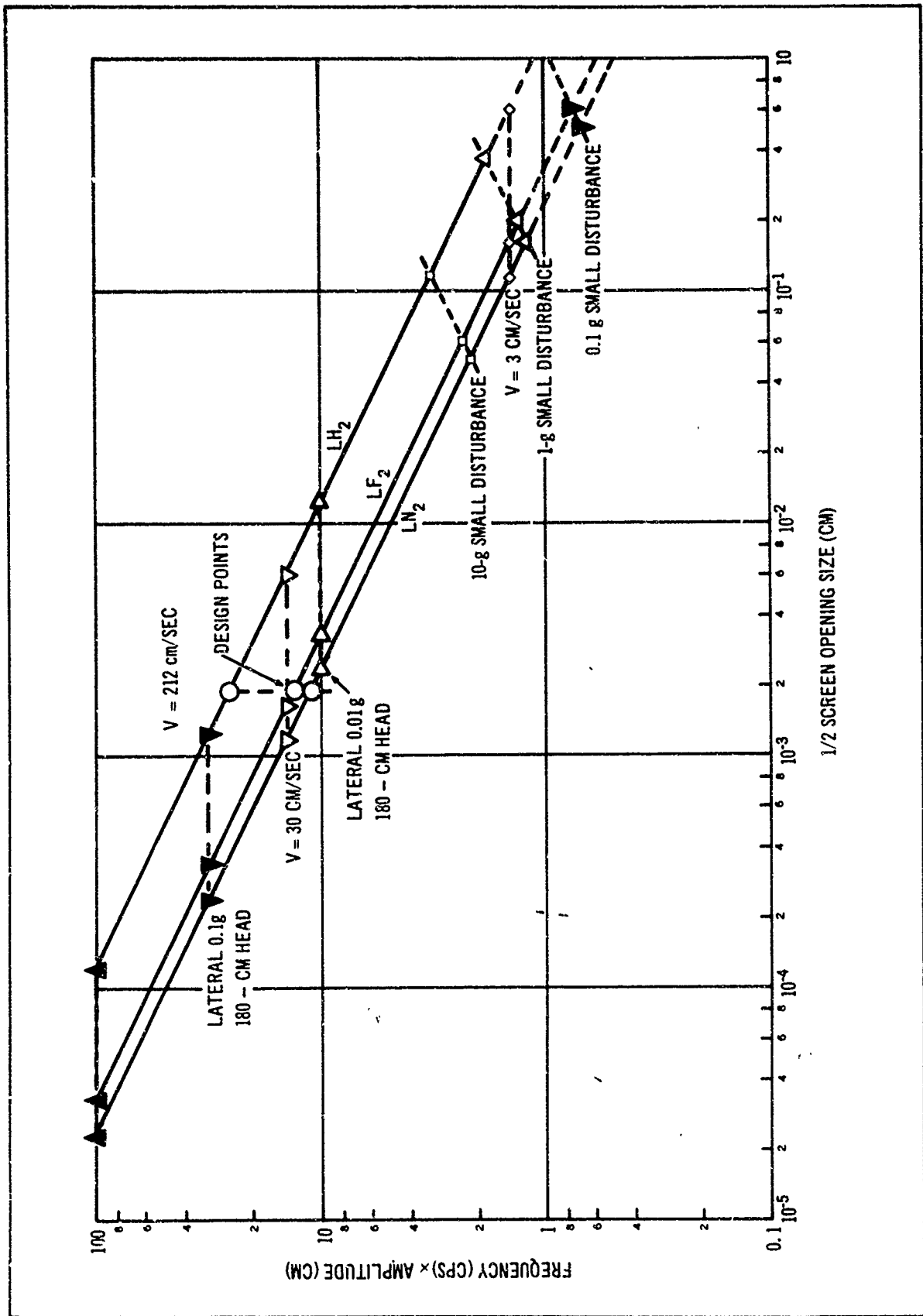


Figure 4-24. Capillary Stability Criteria for External Disturbances

0.1, 1, and 7 f. p. s., respectively. Reference 6 describes the sloshing conditions inside the Saturn S-IV and S-IVB tanks, where the fluid velocity does not exceed 1 f. p. s. It is felt that sloshing conditions inside the smaller spherical LF_2 and LH_2 tanks would be less severe, so the region of 30 cm. p. s. is chosen as a conservative criterion for the sizing of the screen openings. It should be noted that this analysis assumes a wetted screen. The behavior of liquids sloshing with some velocity against a dry screen is not completely known, as noted below in the conclusions.

Another essential screen design criterion is the ability of the screen to support lateral pressure differential or head (parallel to the surface of the screen). The pressure differential which is supported by a wetted screen is:

$$\Delta P = \frac{4\sigma}{2a} = \rho h g \quad (4-6)$$

For tanks with a diameter of 6 ft., the maximum h is about 180 cm., but this would vary, depending on where in the tank the screen was located. Equation 4-6 is plotted in figure 4-24 for an h of 180 cm. for 0.1 g_0 . Note that this range brackets the 30 cm. p. s. velocity line, and it is felt that the lateral g 's externally imposed by the attitude control system would be of the order of 0.01 g_0 or less. Thus, sizing the screen in this region would satisfy both the velocity and lateral-head screen sizing criteria.

(b) Screen sizing. Although the screen opening size can be determined based on the above criteria, the wire size necessary to support the screen against boost propellant flow pressure drop, the screen's own weight, and sloshing propellant impact loads must also be determined. A preliminary analysis showed that all the above loads were essentially insignificant and did not size the screen wire. Instead, the opening size, together with handling and fabrication limitations, sized the wire. A local screen supplier, City Wire and Iron Works, Inc., was contacted, and it was found that extremely fine filter meshes were available in 400 mesh. This is made of 304 stainless-steel wire 0.001 in. in diameter with 0.0015 in. square spaces ($a = 1.9 \times 10^{-3}$ cm.). This spacing design point is plotted in figure 4-24 and falls in the range of 30 cm. p. s. velocity and 0.1 to 0.01 g_0 lateral head acceleration. It is felt that this size screen is adequate for the design requirements of the stage.

(c) Design Parameters. Using a 400 mesh screen with 0.0015-in. spaces gives the following velocity for stability with a Weber number of 1:

LH_2	53.1 cm. p. s.	1.77 f. p. s.
LF_2	27.6 cm. p. s.	0.92 f. p. s.
LN_2	23.5 cm. p. s.	0.785 f. p. s.

For a velocity of 30 cm. p. s. , the equivalent Weber number is:

LH ₂	0.32
LF ₂	1.18
LN ₂	1.63

For 1 g_o (with small disturbances) the Bond number for stability is suitably small and is:

LH ₂	3.28×10^{-4}
LF ₂	1.22×10^{-3}
LN ₂	1.68×10^{-3}

The pressure drop through the screen for propellant flow during boost is:

LH ₂	8.7×10^{-6} p. s. i.
LF ₂	8.7×10^{-5} p. s. i.
LN ₂	7.1×10^{-5} p. s. i.

This is quite insignificant and compares as follows to the pressure supported by the screen:

LH ₂	1.33×10^{-2} p. s. i.	0.485 ft. of head
LF ₂	7.04×10^{-2} p. s. i.	0.13 ft. of head
LN ₂	2.5×10^{-2} p. s. i.	0.095 ft. of head

The equivalent lateral g.-load for a 180 cm. head which can be supported by the screen is:

LH ₂	0.0632 g _o
LF ₂	0.0208 g _o
LN ₂	0.0152 g _o

(d) Conclusions. Screens of requisite fineness are commercially available, are lightweight, and render the capillary force concept feasible but present a number of unresolved problems, as follows:

- Unknown behavior of moving fluid which encounters a dry screen.
- Keeping the screen wet at all times so that capillary forces are present; and the problem of heat transfer into the screen with subsequent drying out of the screen.
- Compatibility of fine screens with high surface-to-weight ratios with LF₂.

(2) Mechanical Vapor-Liquid Separator. A mechanical vapor/liquid separator has been considered as a method of ensuring all vapor venting in zero-g. This device is a rotating machine which centrifugally separates vapor and liquid by density difference, as shown in figure 4-25. The device may be self-powered (i. e., expand the vented vapor through a turbine which powers the separator), or it may be externally powered, for example, by an electric motor and batteries.

Pesco designed such a separator (see reference 7) to be used on the Saturn V/S-IVB to meet the following performance requirements:

- Weight: 15 lb.
- Separation efficiency: 100 pct. of inlet mixtures up to 99 pct. liquid by weight.
- Flow rate: 6 lb. p. sec. of GH_2 at 38 p. s. i. a. and 43°R .
- Pressure drop: 2 p. s. i. a. maximum.

Note that the conditions for Saturn include a high-vent rate, and thus a large vent valve, which favors the use of such rotating machinery. On the other hand, the allowable pressure drop is very small, which restricts the design of the turbine.

The results of analysis and testing of this device for the Saturn showed that separation efficiencies of 100 pct. were not possible, and that there was insufficient gas energy at high liquid qualities to drive the turbine and effect separation (in other words, high-quality liquid drowned the turbine). For the self-powered separator, the estimated performance was:

- Weight: 25 lb.
- Separation efficiency: 90 pct. for inlet qualities of up to 75 pct. providing the droplet diameters are greater than 0.1 in.
- Flow rate: design.
- Pressure drop: about 3 p. s. i. a. minimum.

It was then proposed to externally power the design for the Saturn to obtain the required performance (see reference 7). The estimated performance for an electrically powered separator was:

- Weight: 217 lb. (separator-25 lb. ; batteries-165 lb. miscellaneous electrical equipment-27 lb.)
- Separation efficiency: 80 pct. for inlet qualities up to 90 pct.
- Flow rate: design.
- Power required: 0.9 hp.

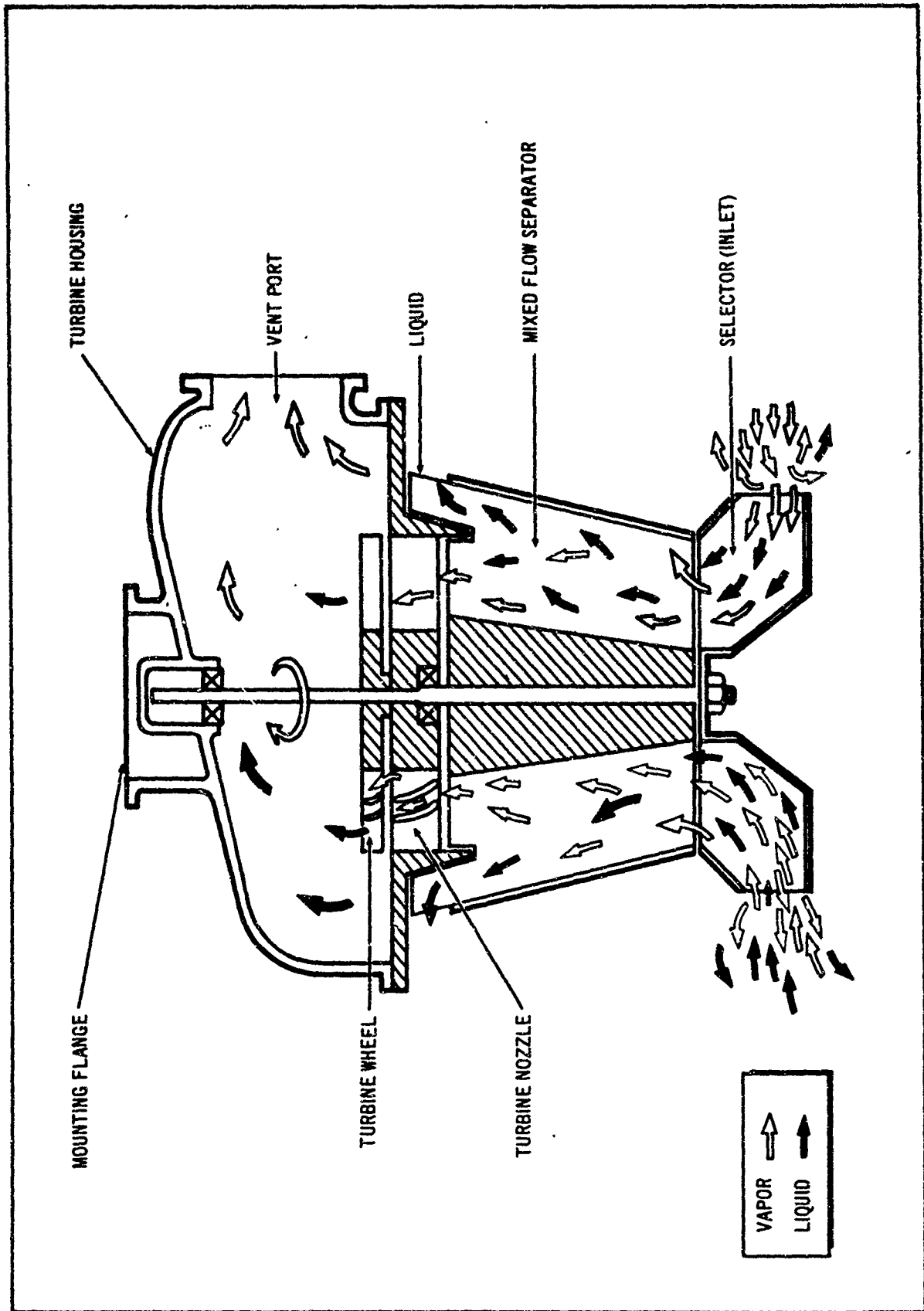


Figure 4-25. Mechanical Liquid/Vapor Separator

The applicability of such a device, either self or externally powered, to the RPL study vehicle system is very questionable for the following reasons:

- The probable steady-state rate for the study vehicle is at least three orders of magnitude below that for Saturn, which makes the rotating machinery virtually impossibly small in size.
- It may be possible to use such equipment for high flow-rate blow-down venting, but the weight penalty would be severe, since the vehicle blow-down rate is higher than the Saturn steady-state rate.

(3) Thermodynamic Vapor/Liquid Separator. A thermodynamic process vapor/liquid separator has been described in the literature (reference 8) and uses the propellant tank pressure potential, the propellant heat capacity, and a heat exchanger to effect conversion of liquid to vapor before venting, thus assuring only vapor-phase venting. The operation of the system is shown in figure 4-26, and is as follows: saturated liquid at condition A enters the vent system and is expanded to a much lower pressure and temperature (condition B) through a vent valve or regulator. This two-phase mixture enters the heat exchanger tubing (which is immersed in the vapor and liquid in the tank), where heat is transferred to the mixture because of the temperature difference between the cold mixture in the tube and the warm liquid and vapor in the tank. This heat is transferred essentially isothermally (path B to C), until the mixture in the tube reaches a condition C with enthalpy equal to that of saturated vapor at tank conditions (condition D). This vapor at condition C is then vented from the tank and vent system through a second regulator that maintains the low pressure in the heat exchanger tubing.

Note that for steady-flow operation, the system composed of the tank and vent system always discharges only vapor with enthalpy equal to or greater than that of saturated vapor at tank conditions, regardless of whether liquid or vapor enters the vent system. Thus, the vent system effectively separates vapor and liquid, venting only vapor, and is thus called a thermodynamic vapor/liquid separator. It would be more appropriate to call the system a liquid/vapor converter, since that is the system's real function. In any event, the system theoretically obviates the problem of inefficient liquid venting under zero-g. conditions, and will be analyzed below for applicability to the study vehicle system.

(a) Analysis. For steady heat leak to the propellant tank and thus, for steady vent flow, the requisite heat transfer to the fluid flowing in the heat exchanger tubing is:

$$\dot{q} = \dot{w} \Delta H = U \pi D L \Delta T \quad (4-7)$$

For the worst case of 100 pct. saturated liquid entering the heat exchanger tubing then ΔH must be at least Δh_{fg} and if the expansion shown in figure 4-26 from A to B is isentropic (the worst case), then additional enthalpy is required,

$$T ds = dh - \frac{v dp}{J} = 0 \quad (4-8)$$

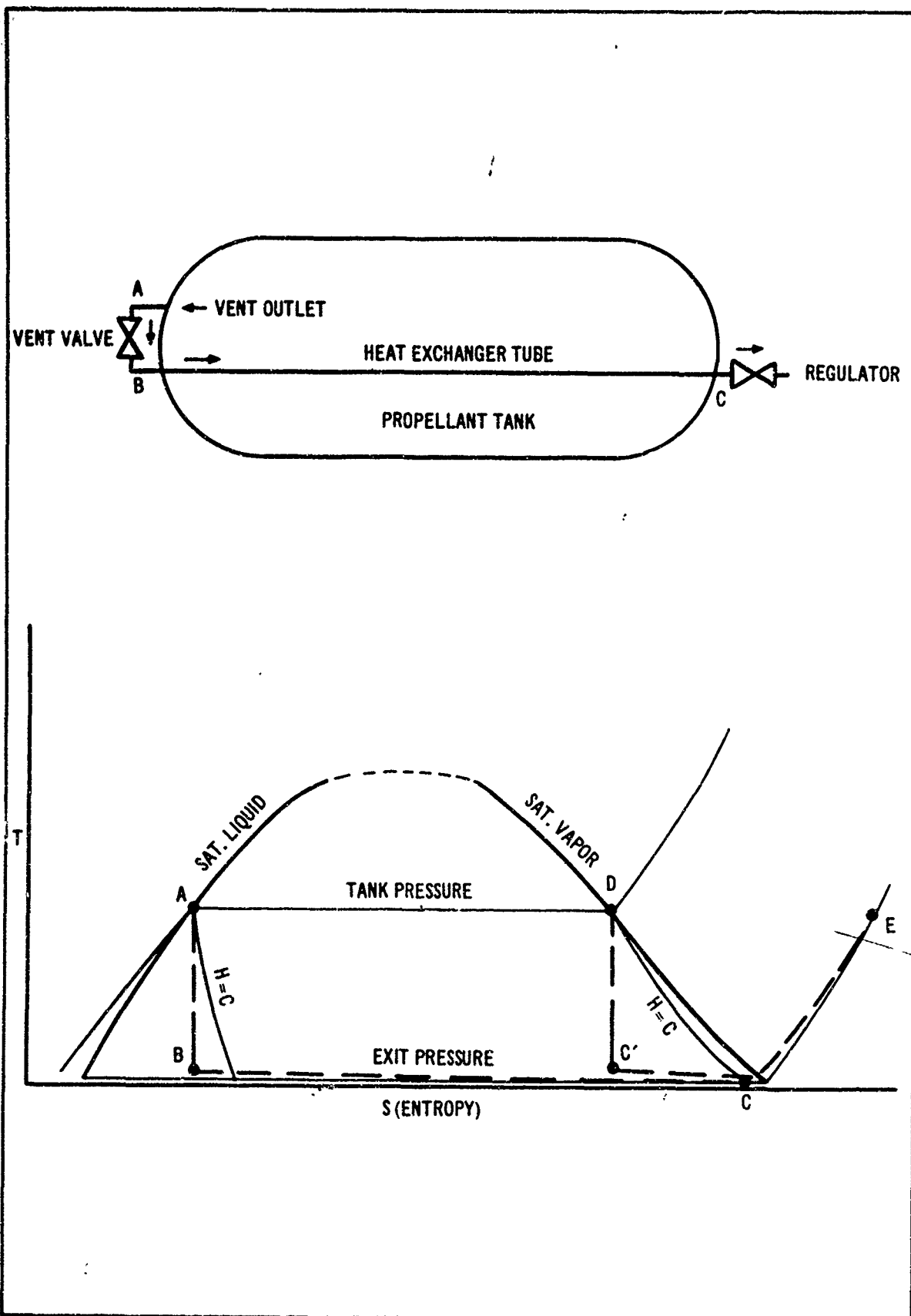


Figure 4-26. Thermodynamic Liquid/Vapor Separator

or

$$dH = \frac{v dP}{H} \quad (4-9)$$

and therefore, the maximum ΔH required is:

$$H = H_{fg} + \frac{v \Delta P}{J} \quad (4-10)$$

where ΔP is the pressure drop from P_T to P (path A to B') and v is evaluated at $(P_T + P)/2$. For the case where heat transfer to the tube from the surrounding vapor is considered, and assuming a concentric cylinder of vapor of diameter D_o , then the heat transfer to the tube is as follows:

$$\dot{q} = \frac{2\pi k_o L}{\ln D_o/D} \Delta T_o \quad (4-11)$$

and therefore, the overall heat-transfer coefficient (if conduction in the metal tube is ignored) is given by:

$$U = \frac{1}{D \frac{2k_o}{\ln D_o/D} + \frac{1}{h_i}} \quad (4-12)$$

In order to determine h_i , the nature of the flow in the tubing must be considered. For the case of cryogenic liquids or vapors, the viscosity is extremely low, and thus the Reynolds number is high and the flow turbulent even for extremely low flow rates. Assuming incompressible turbulent flow in smooth tubes, the friction factor over a range of Reynolds numbers from 2,000 to 200,000 (reference 9) and is given by the following expression:

$$f = \frac{0.184}{R_e^{0.2}} \quad (4-13)$$

The heat transfer in a tube is related to the friction in the tube by the following Reynolds analogy:

$$St C = \frac{Nu}{R_e P_r} \quad C = \frac{f}{8} \quad (4-14)$$

*The Darcy-Weisbach form (see equation 4-18).

where C is an experimentally determined constant to account for Prandtl number effects and changes in heat transfer because of the presence of two-phase flow. Therefore,

$$\text{Nu} = \frac{h_i D}{k_i} = \frac{P_r}{C} \cdot .023 R_e^{0.8}$$

$$h_i = \frac{k_i P_r}{D C} \cdot .023 R_e^{0.8} \quad (4-15)$$

and the overall heat-transfer coefficient can now be written

$$U = \frac{1}{D \left[\frac{\ln D_o/D}{2k_o} + \frac{C}{P_r k_i \cdot .023 R_e^{0.8}} \right]} \quad (4-16)$$

Substituting equations 4-10 and 4-16 into equation 4-7 results in the following expression:

$$\dot{w} \left(H_{fg} + \frac{v \Delta P}{J} \right) = \frac{\pi D L \Delta T}{D \left[\frac{\ln D_o/D}{2k_o} + \frac{C}{P_r k_i \cdot .023 R_e^{0.8}} \right]}$$

or

$$L = \frac{\dot{w} \left(H_{fg} + \frac{v \Delta P}{J} \right) \left[\frac{\ln D_o/D}{2k_o} + \frac{C}{P_r k_i \cdot .023 R_e^{0.8}} \right]}{\pi \Delta T} \quad (4-17)$$

Thus, we have the result that except as D appears in D_o/D and the Reynolds number, the length is independent of the diameter.

To evaluate the diameter, the pressure drop in the heat exchanger tubing (path B to C in figure 4-26) will be evaluated, and ignoring momentum losses, entrance and exit losses, and so forth, the frictional pressure drop is given by the following expression:

$$P - P_e = \phi f \frac{L}{D} \rho \frac{V^2}{2g} \quad (4-18)$$

where ϕ is an experimentally determined constant (or function) to account for variations due to the presence of two-phase flow. For liquids and gases, $\phi = 1$. Substituting equation 4-13 and the continuity equation

$$\dot{w} = \rho A V = \rho \frac{\pi D^2}{4} V \quad (4-19)$$

into equation 4-18 gives

$$P - P_e = 0.092 \left(\frac{\pi \mu D}{4 \dot{w}} \right)^{0.2} \phi \frac{L}{Dg} \frac{4^2 \dot{w}^2}{\rho \pi^2 D^4}$$

which reduces to

$$P - P_e = 0.142 \frac{\phi \mu^{0.2}}{g \rho} \dot{w}^{1.8} \frac{L}{D^{4.8}}$$

or

$$D^{4.8} = 0.142 \frac{\phi \mu^{0.2}}{g \rho} \frac{L}{P - P_e} \dot{w}^{1.8} \quad (4-20)$$

where, for constant diameter tubing, $\frac{\mu}{\rho}$ is evaluated at vapor conditions to give the maximum diameter.

The weight of the heat exchanger tubing is

$$W_{\text{hex}} = \rho_{\text{tube}} \psi \pi D L \quad (4-21)$$

substituting equations 4-17 and 4-20 into equation 4-21 gives:

$$W_{\text{hex}} = \pi \rho_{\text{tube}} \psi \left[\frac{0.142 \phi \mu^{0.2}}{g \rho} \frac{\dot{w}^{1.8}}{(P - P_e)} \right]^{1/4.8} \left[\frac{\dot{w} (H_{fg} + \frac{V \Delta P}{J}) \left(\frac{\ln D_o/D}{2k_o} + \frac{C}{P_r k_i 0.023 R_e^{0.8}} \right)}{\pi \Delta T} \right]^{5.8/4.8} \quad (4-22)$$

Detailed examination of equation 4-22 is in order. The term

$$\frac{C}{P_r k_i 0.023 R_e^{0.8}}$$

is of interest.

For cryogenic fluids, $C/P_r \leq 1$, and k_i is fairly small. However, the Reynolds number is large enough to be turbulent, so the term above is likely to be quite small compared to

$$\ln \frac{D_o/D}{2k_o}$$

for reasonably large values of D_o/D . For example, even for $D_o/D = 2$, and a vent flow rate of 1 lb. p. hr., the above-noted term is only about 3 to 4 pct. of the conductive diameter ratio term. Therefore, for the moment it is ignored. Further, for all cryogenic fluids (except near the critical point) or for an isenthalpic process from A to B in figure 4-26, the term $\frac{V\Delta P}{J}$ is very small compared to H_{fg} and also will be ignored. Thus

$$W_{hex} = \pi \rho_{tube} \psi \left[\frac{0.142 \phi}{g} \frac{\mu^{0.2}}{\rho} \frac{\dot{w}^{1.8}}{(P-P_e)} \right]^{1/4.8}$$

$$\frac{\dot{w} H_{fg} \ln D_o/D}{2 k_o \pi \Delta T} \quad 5.8/4.8 \quad (4-23)$$

Note that the ΔT in equation 4-23 is the temperature difference from A to B in figure 4-26 (a conservative assumption based on a fairly small pressure drop in the tube from B to C). This temperature difference is related to the pressure drop from A to B based on the properties of the fluid, thus;

$$\Delta T = \text{function } \Delta P = \text{function } (P_T - P) \quad (4-24)$$

Therefore, equation 4-23 reduces to:

$$W_{hex} = \text{Constant} \left(\frac{1}{P - P_e} \right)^{1/4.8} \left[\frac{1}{\text{function } (P_T - P)} \right]^{5.8/4.8} \quad (4-25)$$

Clearly, as P gets larger, the diameter decreases, and the length increases, and if P gets smaller, the reverse occurs. Therefore, there must be some value of P at which the weight of the tubing is a minimum. To determine this P value, the functional relationship between pressure and temperature must be determined or postulated. Examination of vapor pressure curves for cryogenic propellants shows that over a wide range of conditions (away from the critical point) the pressure and temperature are related by:

$$T = a P^b \quad (4-26)$$

and equation 4-25 becomes:

$$W_{\text{hex}} = (\text{Constant}) \left[\frac{1}{P - P_e} \right]^{1/4.8} \left[\frac{1}{a(P_T^b - P^b)} \right]^{5.8/4.8} \quad (4-27)$$

Examination of the variables in the Constant shows that they are all dependent on either P_T or P_e which are assumed known, and thus are independent of P or essentially constant. Differentiating W_{hex} with respect to P and equating to zero gives:

$$\frac{1}{\text{Constant}} \frac{d W_{\text{hex}}}{d P} = 0 = (P_T^b - P^b) - 5.8 b (P - P_e) \frac{P^b}{P}$$

or

$$P^2 - \frac{P_T^b}{1 + 5.8b} P^{2-b} - \frac{5.8b}{1 + 5.8b} P_e P = 0 \quad (4-28)$$

Thus, solving for P for any condition of P_T and P_e gives the minimum weight system, and will give the heat exchanger length, diameter, and weight based on equations 4-11, 4-14, and 4-16.

Calculations for Specific Applications. For the propellants of interest for the study vehicle, the relationships between vapor pressure and temperature are assumed as follows:

$$\text{LH}_2: \quad T = 21.9 P^{0.1935} \quad (4-29)$$

$$\text{LN}_2: \quad T = 96 P^{0.135} \quad (4-30)$$

$$\text{LF}_2: \quad T = 109 P^{0.123} \quad (4-31)$$

The optimum tube entrance pressure P for minimum weight is plotted as a function of tank pressure P_T with exit pressure P_e as a parameter for LH_2 , and LF_2 in figures 4-27, and 4-28. The tank pressures chosen for the study are those for which venting is most likely to be required, namely: 75 p. s. i. a. for the pressure-fed case, and 21 p. s. i. a. (LH_2 tank) and 32 p. s. i. a. (LN_2 , LF_2 tank) for the pump-fed case (with boost pumps). The choice of exit pressure is more difficult: clearly the lower the exit pressure, the lower the weight, with the minimum occurring if P_e is set at the triple point pressure. Practically, of course, the exit regulator would be set somewhat above the triple point so that local low-pressure regions in the regulator would not cause icing inside the regulator. If the question of testing and checkout of such low-pressure (vacuum) regulators is considered, it may prove desirable to set the regulator to a value as high as 15 p. s. i. a. for ease of testing. To obtain conservatively high weights for the study vehicle, and for ease of computation, the exit pressure will be arbitrarily set at

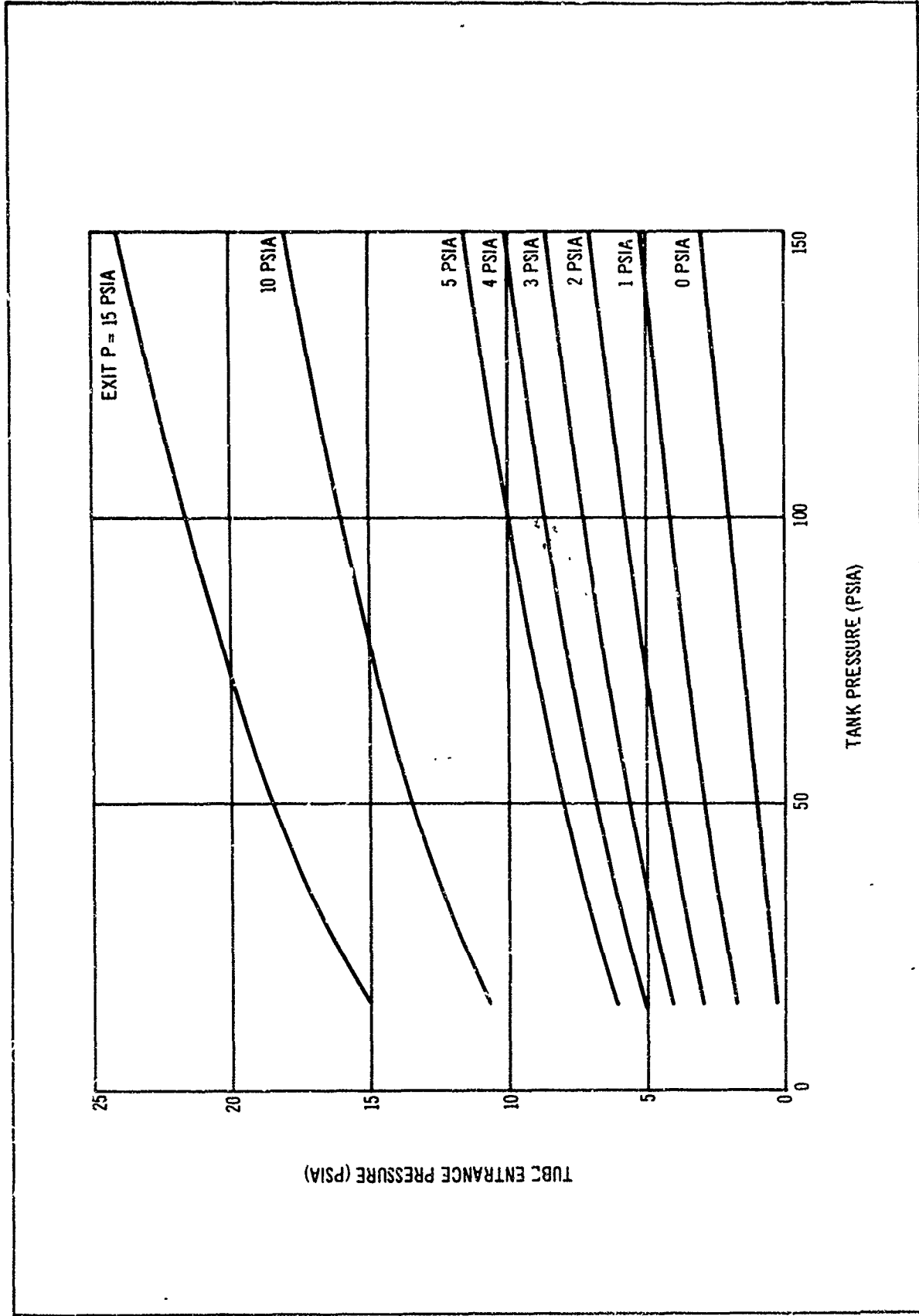


Figure 4-27. Optimum Tube Entrance Pressure as a Function of Tank and Exit Pressures for LH₂

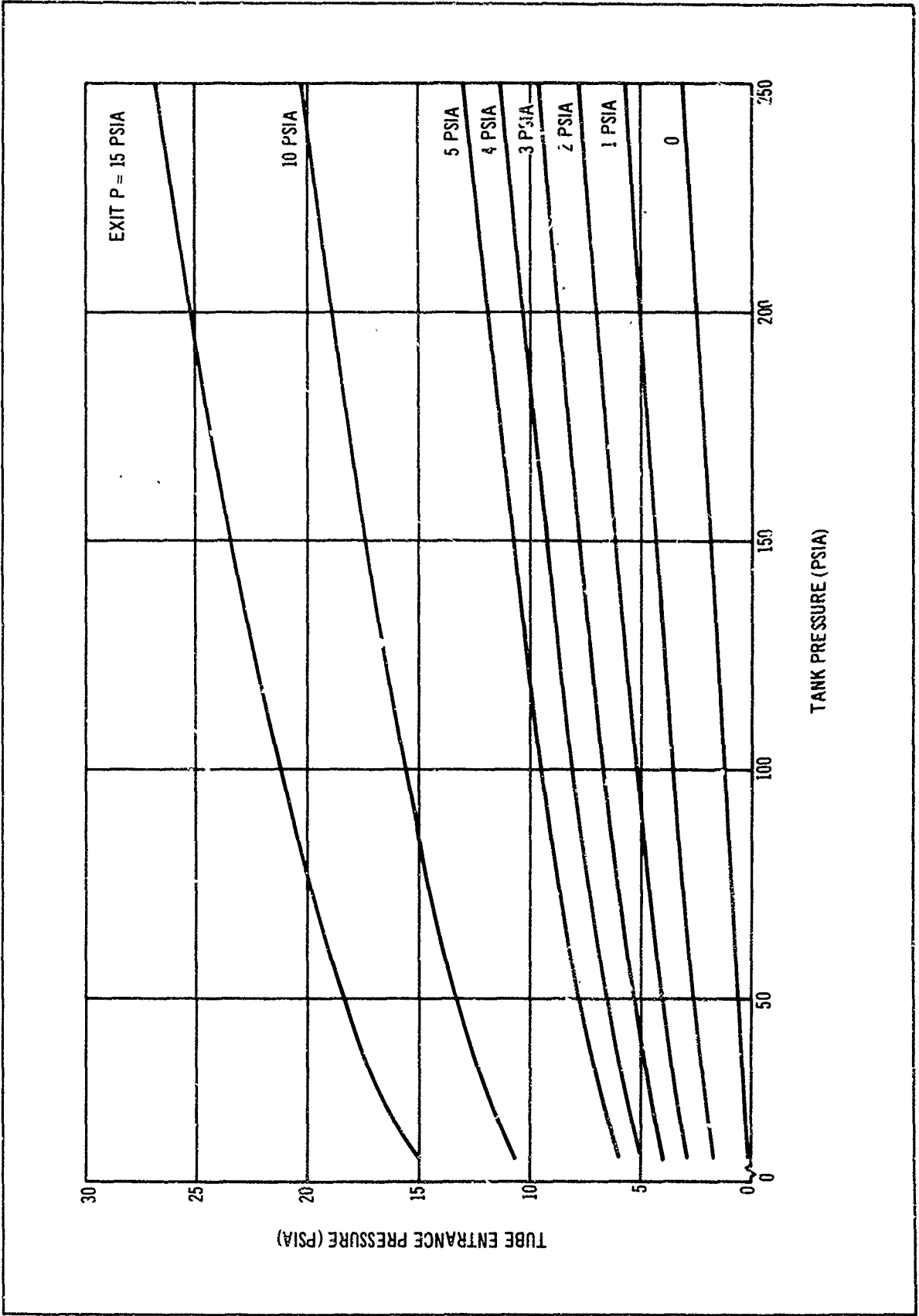


Figure 4-28. Optimum Tube Entrance Pressure as a Function of Tank and Exit Pressures for LF 2

15 p. s. i. a. for the calculations which follow, even though this severely penalizes the low-pressure LH_2 system.

It is felt that a value of the conductive diameter ratio equal to 1 ($\ln D_o/D = 0$) is of academic interest as the lower limiting value for infinite heat transfer in the tank, but is of little practical interest. Therefore the conductive diameter ratios of 2 and 100 have been selected as reasonable practical limits, and thus the dependence of the heat transfer on the inside heat transfer coefficient has been ignored. The tubing diameter has been parameterized to include ϕ and it is seen that because of the small power on ϕ , the diameter is relatively insensitive to changes in ϕ . For purposes of calculating the weight of the tubing for the heat exchanger, ϕ was arbitrarily set at 1.0, and the weights were based on aluminum tubing with 0.01 in. wall thickness. This minimum wall thickness provides sufficient strength up to diameters of nearly 1 in. for the high-pressure cases.

The tubing length, diameter parameter, and weight as a function of vent flow rates are plotted in figures 4-29, 4-30, and 4-31 for the high pressure (75 p. s. i. a) cases, and in figures 4-32, 4-33, and 4-34 for the low-pressure cases. The variations in tubing weight as a function of conductive diameter ratio for a vent flow rate of 1 lb. p. hr. are shown in figure 4-35 for all cases.

All previous computations have assumed that the tubing is completely covered by vapor in the propellant tank. If some portion is covered by liquid, the required heat exchanger length and thus weight are less due to the increased conductivity of the liquid. Conservative design would be based on all vapor, unless the tank design was such that some portion of the tube was positively submerged in liquid. Figure 4-36 shows the reduced weight possible with increasing amounts of liquid covering the tubing for LH_2 .

Off-Design Performance. The preceding analysis has been based on assumptions of steady-flow, steady-state heat transfer, and 100 pct. saturated liquid entering the heat exchanger tubing and being converted to 100 pct. saturated vapor. The question arises as to the performance of the system should saturated vapor enter the heat exchanger. For 100 pct. saturated vapor entering the system, the process will be along path D-C-E in figure 4-26, with E being at a temperature somewhat below the temperature of the tank. The pressures in the system will be essentially the same, but because of increased temperature, the superheated vapor at E has a lower density than the saturated vapor at C. This means the flow rate through the second regulator will be less for fluid at condition E, and thus, for 100 pct. saturated vapor entering the system, the vent flow rate will be reduced. However, the enthalpy of the vent flow at condition E is greater than that at C, and this will compensate for the reduced flow as follows: the ratio of the existing heat flux obtained with condition E to that required at condition C is:

$$\frac{\dot{q}_E}{\dot{q}_C} = \frac{\dot{w}_E (H_{fg} + \Delta H_{C-E})}{\dot{w}_C H_{fg}} \quad (4-32)$$

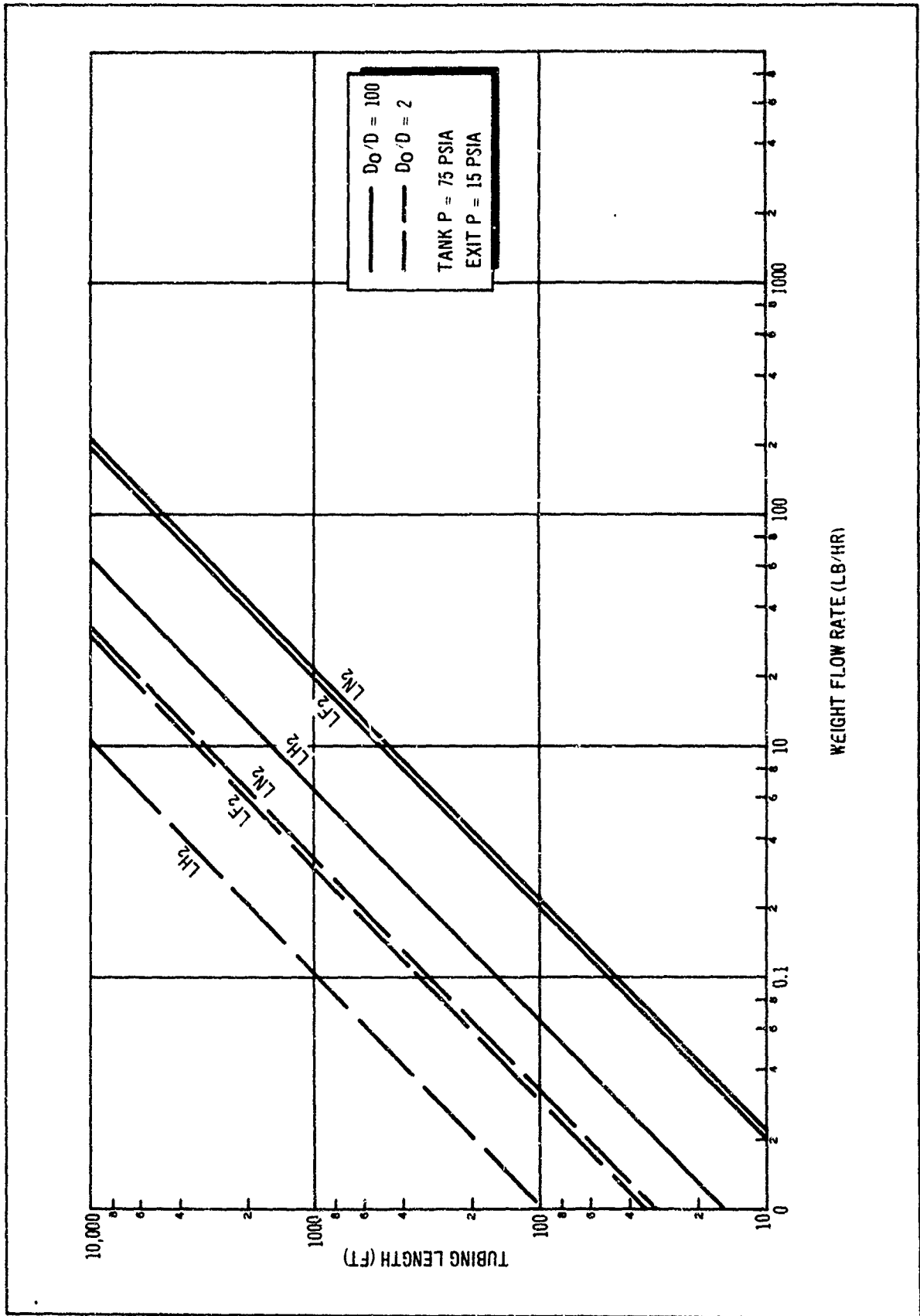


Figure 4-29. Thermodynamic Separator Length as a Function of Vent Flow Rate

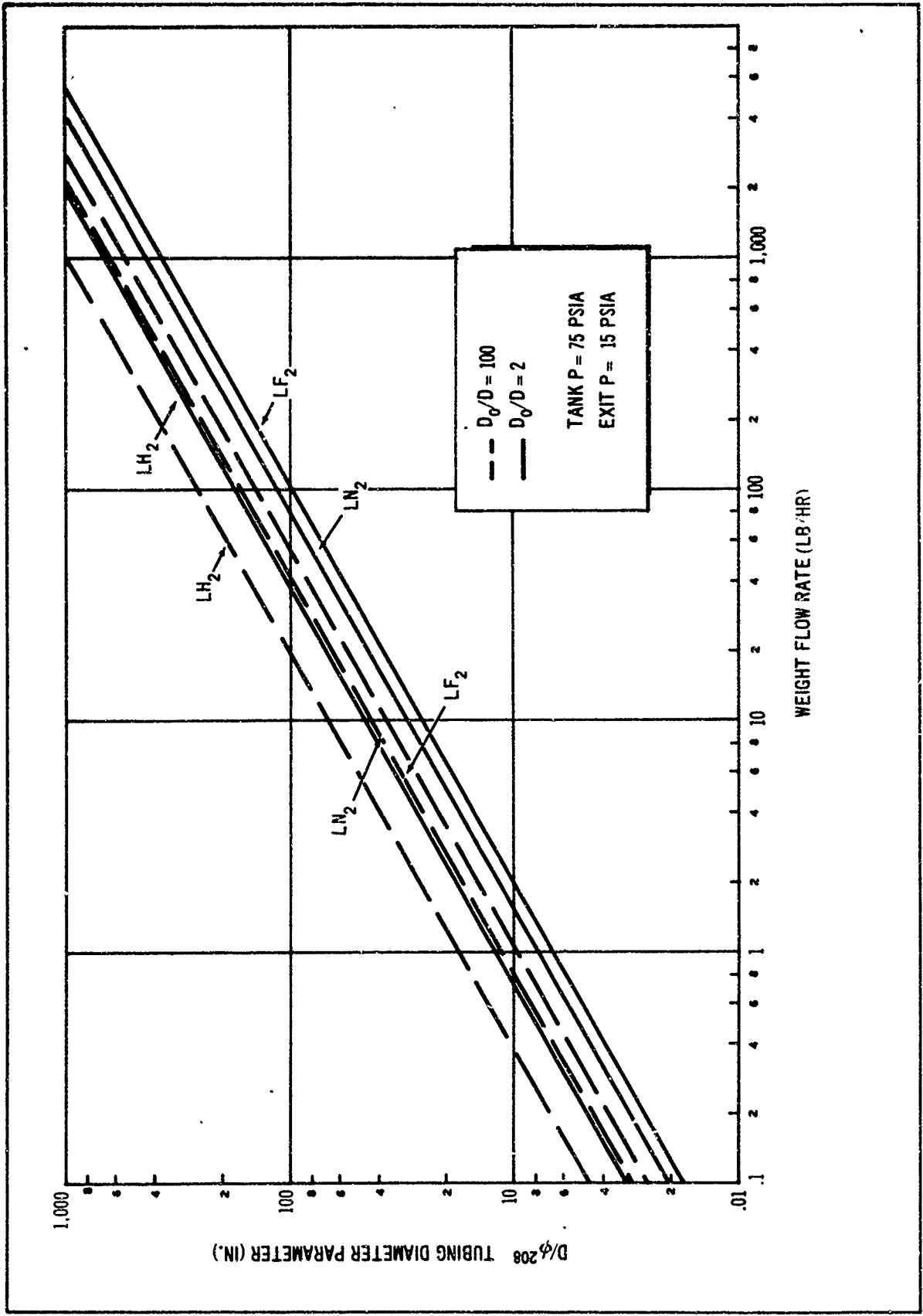


Figure 4-30. Thermodynamic Separator Diameter Parameter as a Function of Vent Flow Rate

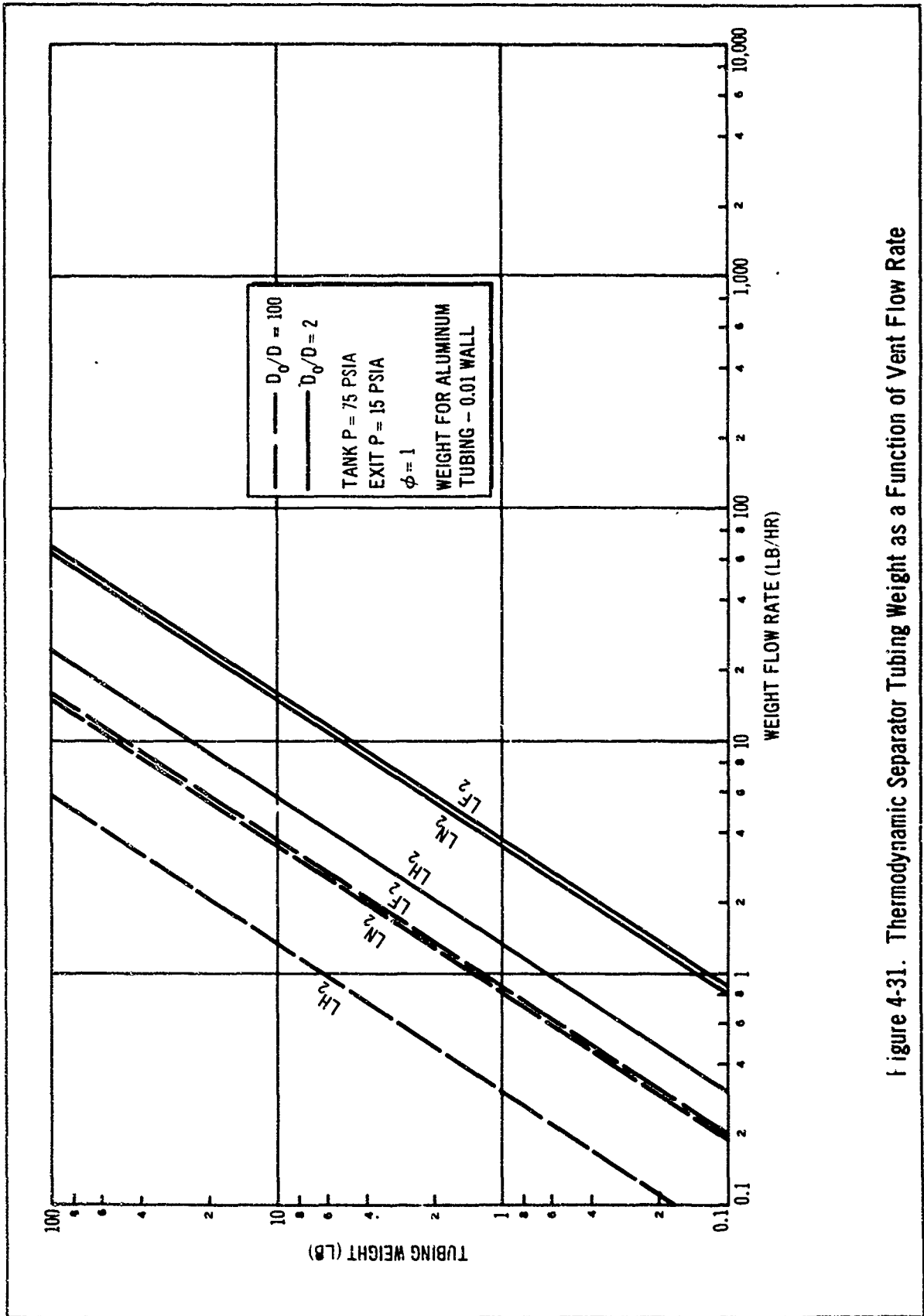


Figure 4-31. Thermodynamic Separator Tubing Weight as a Function of Vent Flow Rate

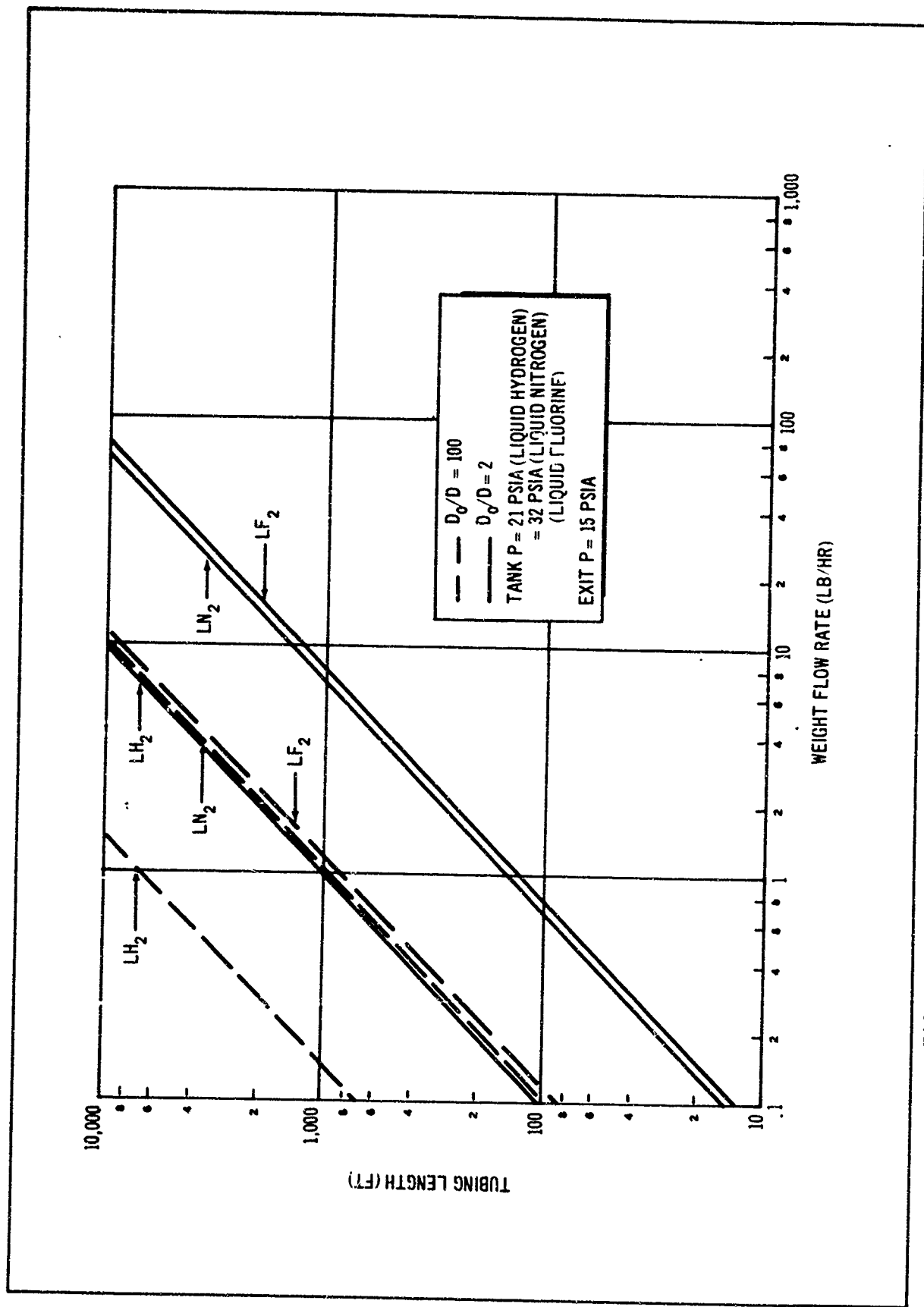


Figure 4-32. Thermodynamic Separator Length as a Function of Vent Flow Rate

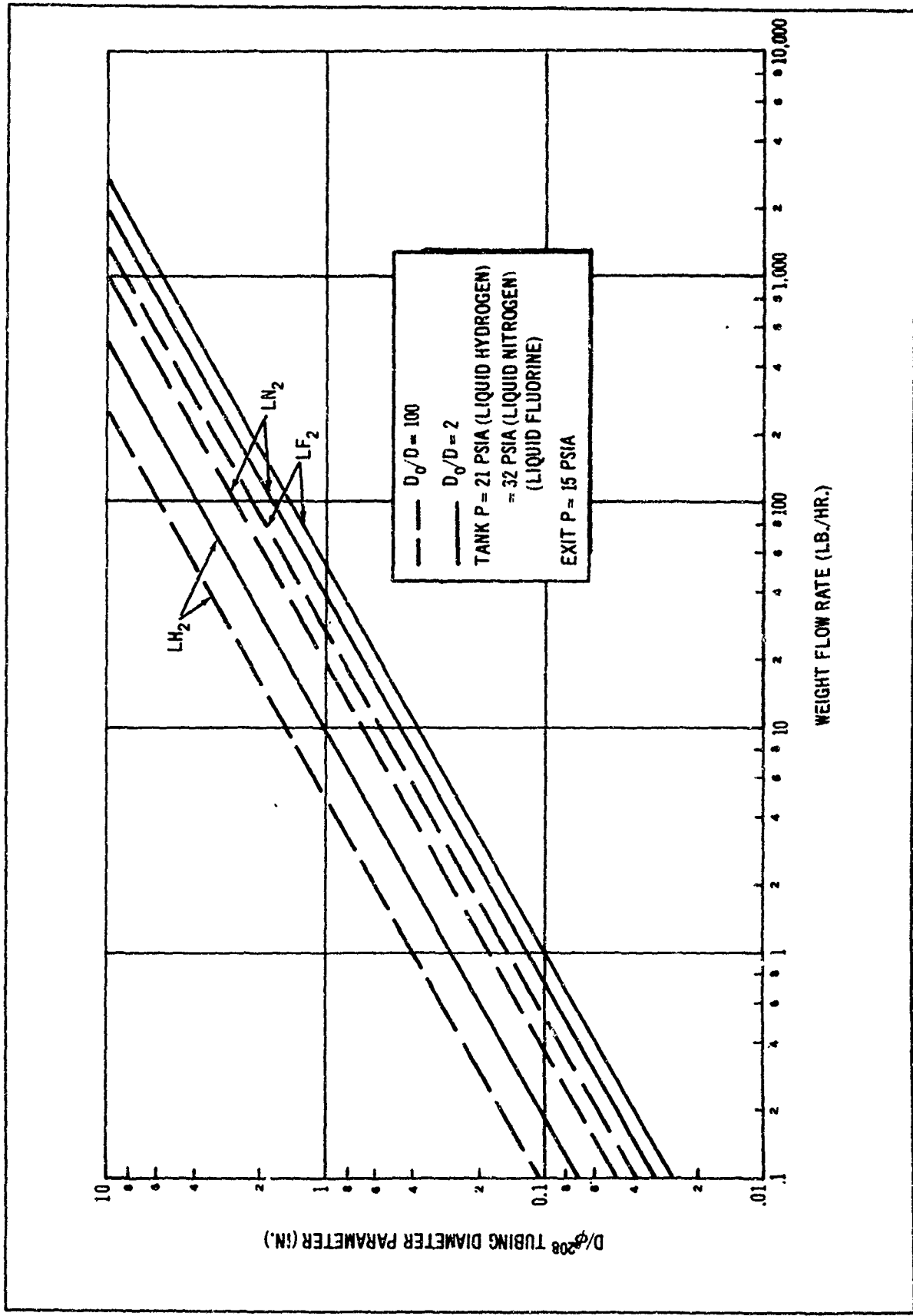


Figure 4-33. Thermodynamic Separator Diameter Parameter as a Function of Vent Flow Rate for Tank Pressures of 21 and 32 p.s.i.a.

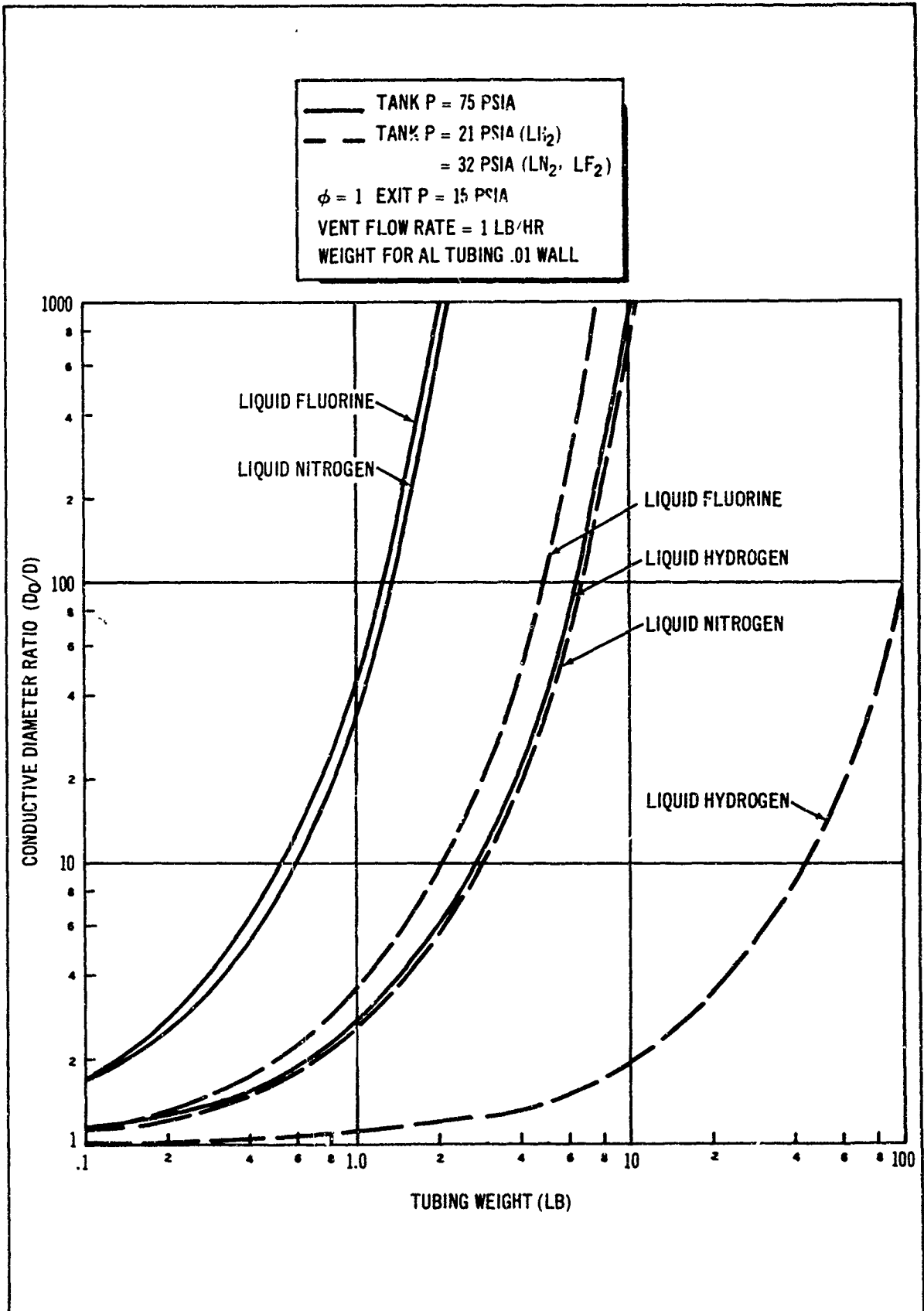


Figure 4-35. Thermodynamic Separator Tubing Weight as a Function of Conductive Diameter Ratio

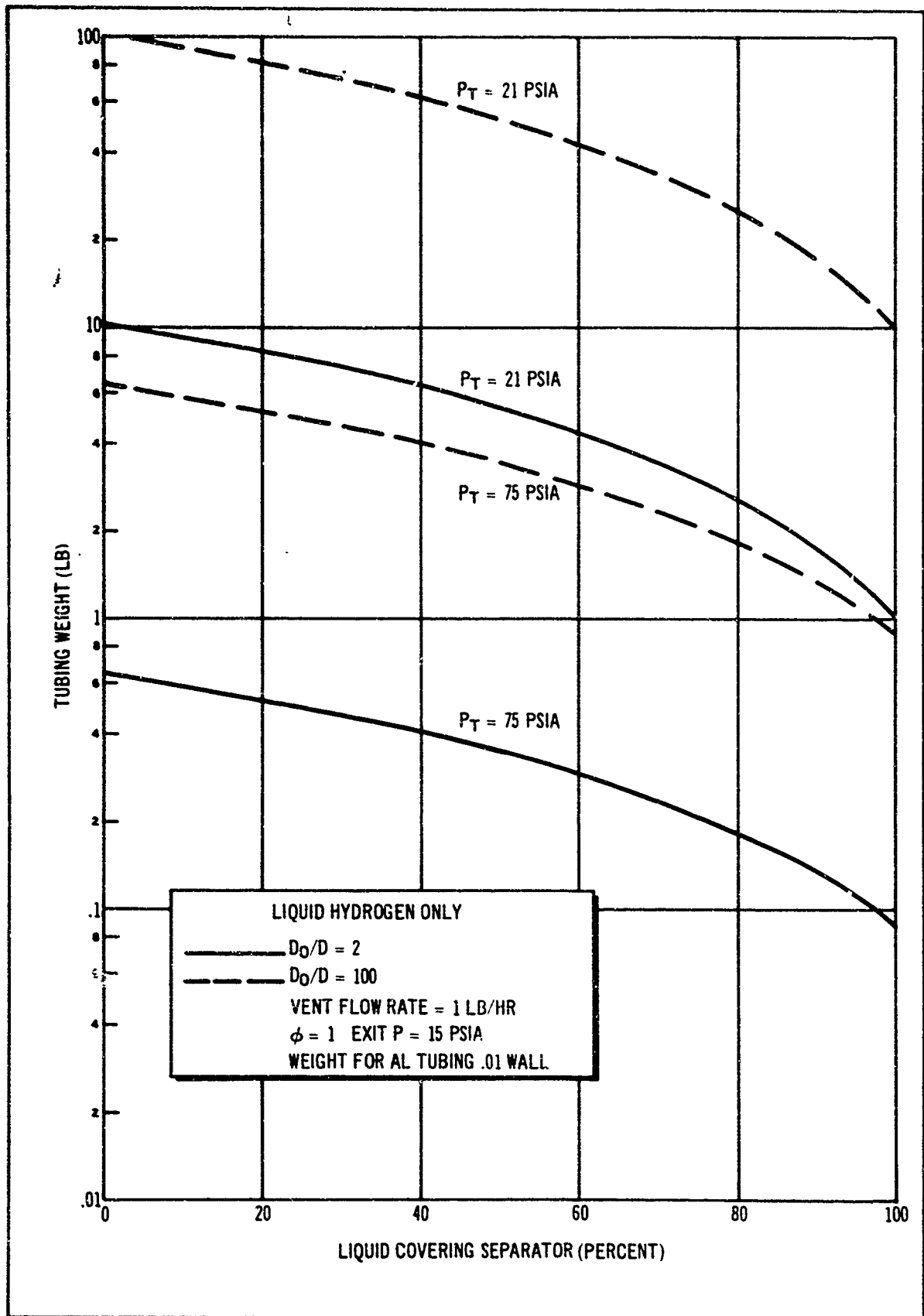


Figure 4-36. Thermodynamic Separator Tubing Weight as a Function of Percent of Liquid Covering Separator

Assuming choked flow of a perfect gas, for the vapor at C and the superheated vapor at E, the following expression holds:

$$\frac{\dot{w}_E}{\dot{w}_C} = \sqrt{\frac{T_C}{T_E}} \quad (4-33)$$

and thus:

$$\frac{\dot{q}_E}{\dot{q}_C} = \sqrt{\frac{T_C}{T_E}} \left(1 + \frac{\Delta H_{C-E}}{H_{fg}} \right) \quad (4-34)$$

For the LH₂ system at 75 p. s. i. a and 21 p. s. i. a, respectively, the ratio of equation 4-34 is 1.059 or 1.043, which implies that sufficient energy is vented under any condition of liquid or vapor entrance.

A very real problem is posed by the possibility of restrictive vapor flow at the first regulator, rather than at the second regulator. If the regulator orifice is sized for the proper flow rate of high density liquid, it will not pass the required amount of low-density vapor. The solution to this problem is found by considering a real, practical vent system. Such a system typically employs a vent valve which cracks at vent pressure and reseats at some lower pressure. Such a valve is not normally continuously open (or chattering), but opens and closes in a cyclic manner. The above problem is solved by designing the vent valve and system to a valve open time/total time ratio based on venting 100 pct. vapor at design flow rate. Then, if liquid enters, the valve open time/total time ratio simply decreases in the ratio of the vapor-to-liquid density. Therefore, the valve when venting liquid at high flow rate will just not be open as long.

The efficacy of the above solution is strongly dependent on the response time of the vent system. The true response time of a vent system is a highly complex function of the design of vent valve, tankage, duty cycle, and so forth, and is not susceptible to analysis in a general manner. There are, however, a number of characteristic times associated with the operation of the thermodynamic separator which provide valid indications of the relative response of the system. The first of these times is the average stay time of the vented liquid/vapor in the heat exchanger tubing. This time is given by the expression:

$$t_s = \frac{L}{V} = \frac{L \rho A}{\dot{w}} = \frac{L \rho \pi D^2}{\dot{w} 4} \quad (4-35)$$

The shortest stay time corresponds to a valve of ρ equal to that for vapor, which is conservative, since the average density for the liquid entrance case will be somewhat higher because of the liquid present at condition B in Figure 4-26. The stay time is plotted versus conductive diameter ratio for a vent flow rate of 1 lb. p. hr. for both high and low pressure for LH₂, and LF₂ in figures 4-37 and 4-38.

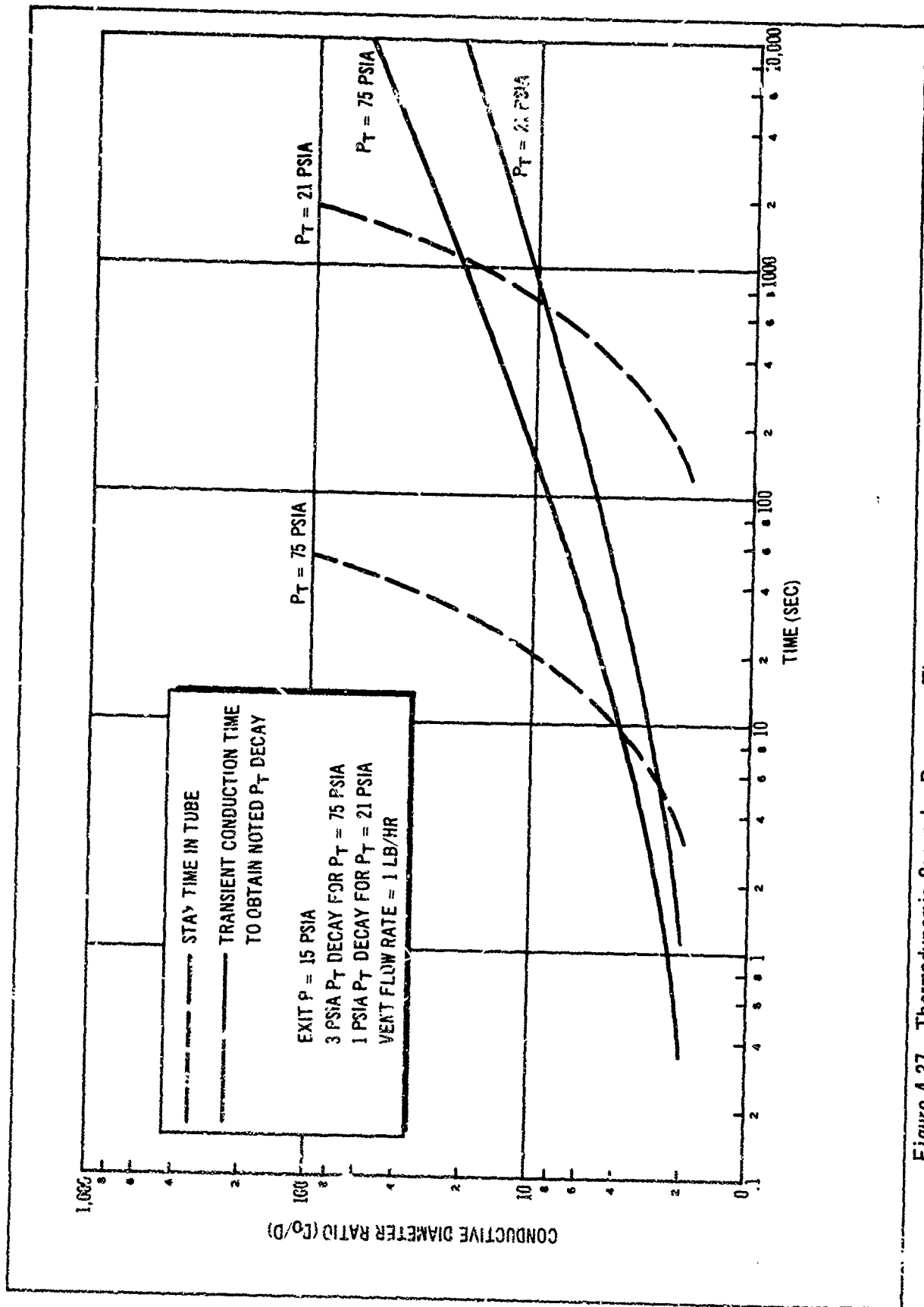


Figure 4-37. Thermodynamic Separator Response Time as a Function of Conductive Diameter Ratio for LH₂

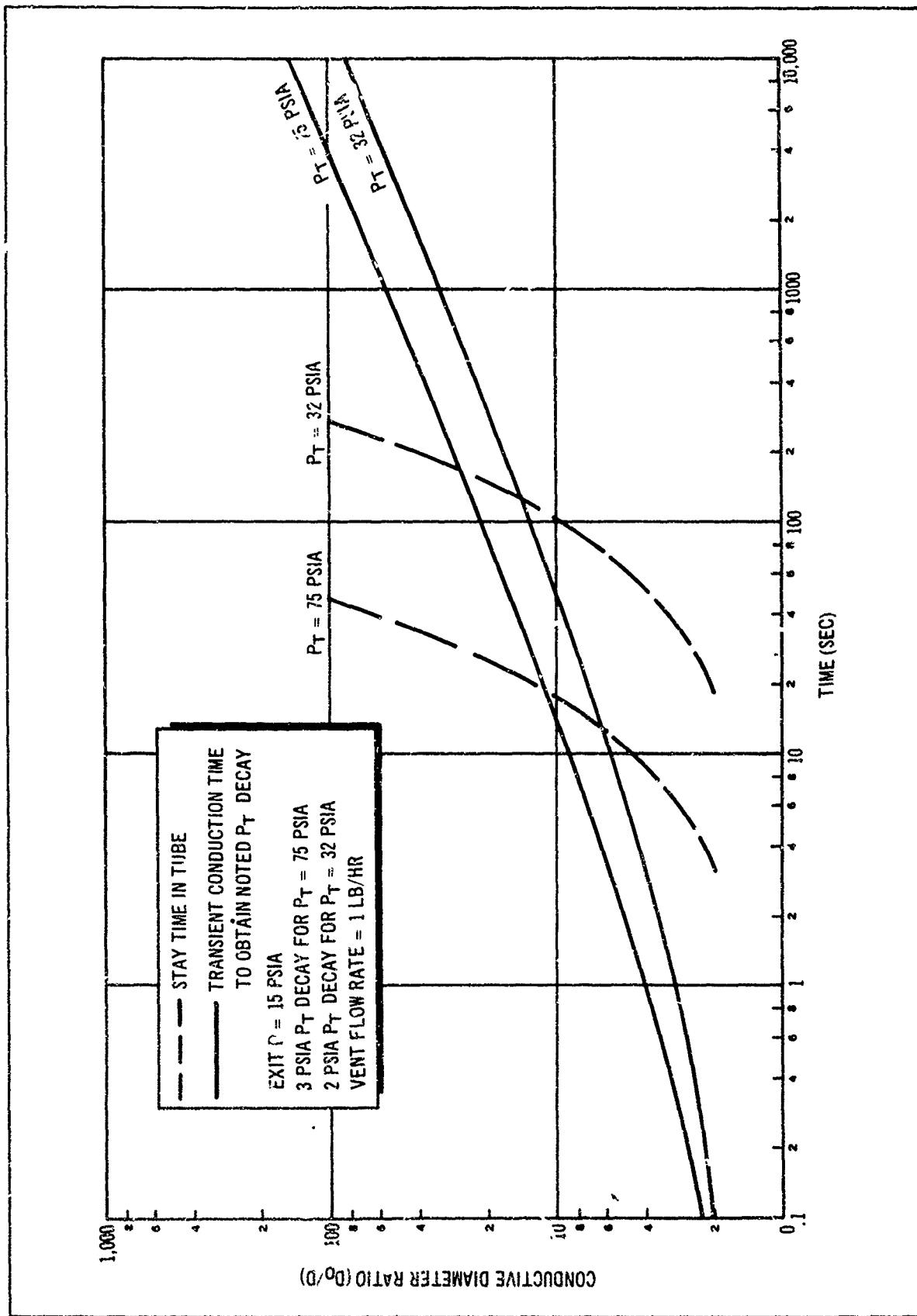


Figure 4-38. Thermodynamic Separator Response Time as a Function of Conductive Diameter Ratio for L.F.2

A more important characteristic time associated with the system is the time between opening of the vent valve and ullage pressure collapse to the vent valve reseal pressure. This time is essentially the transient heat-transfer time from the tube to the tube's region of influence characterized by the conductive diameter ratio. The model for heat transfer is as follows: a region is initially at a constant temperature and is bounded internally by a cylinder of radius a , which is maintained at some other constant temperature, (T_a) when time equals zero. Assuming that all heat transfer takes place by conduction (no convection or radiation, reasonable for zero-g. and cryogenic temperatures), the diffusive time constant ($\bar{K} t/a^2$) is related to the temperature penetration into the region. Reference 11 contains a solution to this problem, and relates ($\bar{K} t/a^2$) to the temperature ratio (T_r/T_a) and the conductive diameter ratio (D/D). The temperature ratio required is that temperature drop which will give a pressure decay to the vent valve reseal pressure. It is assumed that if this temperature decay occurs in a volume around the tube that is equal to half the volume of influence described by the conductive diameter ratio, then this is sufficient to effect the required pressure collapse in the entire volume of influence. The pressure difference between vent valve crack and reseal are assumed at the following typical values for the purpose of this analysis:

$$\text{For } P_T = 75 \text{ p. s. i. a.}, \Delta P = 3 \text{ p. s. i. a. (4 pct.)}$$

$$P_T = 32 \text{ p. s. i. a.}, \Delta P = 2 \text{ p. s. i. a. (6.25 pct.)}$$

$$P_T = 21 \text{ p. s. i. a.}, \Delta P = 1 \text{ p. s. i. a. (4.76 pct.)}$$

Based on the appropriate temperature drop to give the above ΔP , and the analysis of section 13.5 of reference 6, values of $\bar{K}t/a^2$ can be found for various conductive diameter ratios. The conductive transient time t_c , based on $\bar{K}t/a^2$, is plotted as a function of the conductive diameter ratio in the high and low pressure cases for LH_2 , and LF_2 in figures 4-37 and 4-38. It should be noted that the model assumed is a good approximation for the case of the initial vent, when, after a long coast time without venting, the tube and its surroundings are in thermal equilibrium. When the vent valve first opens the tube becomes very cold at $t = 0$, because of the high inside heat transfer coefficient. Note that the initial response time of the system is the sum of the average stay-time (t_s) and the conductive transient time (t_c) and that this is strongly dependent on the conductive diameter ratio. The response time of the system subsequent to the first vent is unknown due to the extreme complexity of the temperature distribution around the separator tube, but will be, in general, less than the initial response time. The initial vent response is the critical case, and realistic vent design will be based on it.

To evaluate the significance of the response times shown they must be compared to the time rate of pressure buildup in the tank. This time rate of pressure buildup is dependent on details of tankage design, amount of ullage at time of venting, and vent system design and cannot be evaluated at this time. However, the possible consequences of this pressure buildup

time can readily be estimated. In order to cope with a fairly rapid pressure buildup time, the designer may be forced to design the system to give a low conductive diameter ratio (see figure 4-37). To physically obtain such a diameter ratio within a given tank geometry, a much greater length of tubing may be required than is specified by steady-state heat-transfer considerations. Thus, transient conditions may size the heat exchanger and lead to much greater weight penalties.

Conclusions. The following conclusions may be reached from the above discussion:

- For the low vent flow rates anticipated for the study vehicle (of the order of 0.2 lb. per hr.) the parametric weight curves would indicate heat exchanger weights of 0.5 lb. to 8 lb. which, in absolute values are low relative to any venting system. Therefore, the thermodynamic separator appears to be very promising on this basis. The presented parametric data will be used in a detailed comparison study at the end of this phase to establish detailed weight comparisons of the various systems.
- Detail design of the system to obtain the necessary low conductive diameter ratios strongly affects the system performance and weight.
- Transient system response appears to be the governing criterion for practical system application. This criterion will be further evaluated in the system comparison stage, when vent rates, initial vent and ullage conditions, tankage design, and duty cycle will be more concretely specified.

(4) Ullage Rocket Settling. The application of ullage rockets to settle propellant to the bottom of the tank is relatively straightforward although some of the design criteria for a system of this type are at present uncertain. The required settling time for this system is a function of the thrust level applied, the gross weight at the time of settling and the ratio of tank-to-propellant volume. The relationship of these parameters is illustrated by figure 4-39. By using this information and making assumptions regarding specific impulse, the relationship between thrust and settling time can be evaluated with respect to the specific ground rule duty cycles, as shown in figure 4-40. The time shown represents the total burning time required to settle propellant for all the burns. Thus, the more burns the longer the required settling burn time for a given thrust. In examining the two different two-burn cases, it can be seen that the 80/20 burn case (duty cycles A, F, and K) require a slightly longer time than the 50/50 burn cases (duty cycles B and J) because more time is required to settle a small amount of propellant across the complete tank. Having the required total settling times, it is then possible to predict the settling weight penalty as a function of settling thrust for an assumed settling motor specific impulse. (See figure 4-41). In this case 290 sec. I_{sp} was taken for the settling motor performance assuming that a storable propellant attitude control system motor would be used for this purpose. Figure 4-41 assumes that the settling force is always such that it will produce useful ΔV for the subsequent burn. Therefore, the penalty is proportional to the difference between main engine and

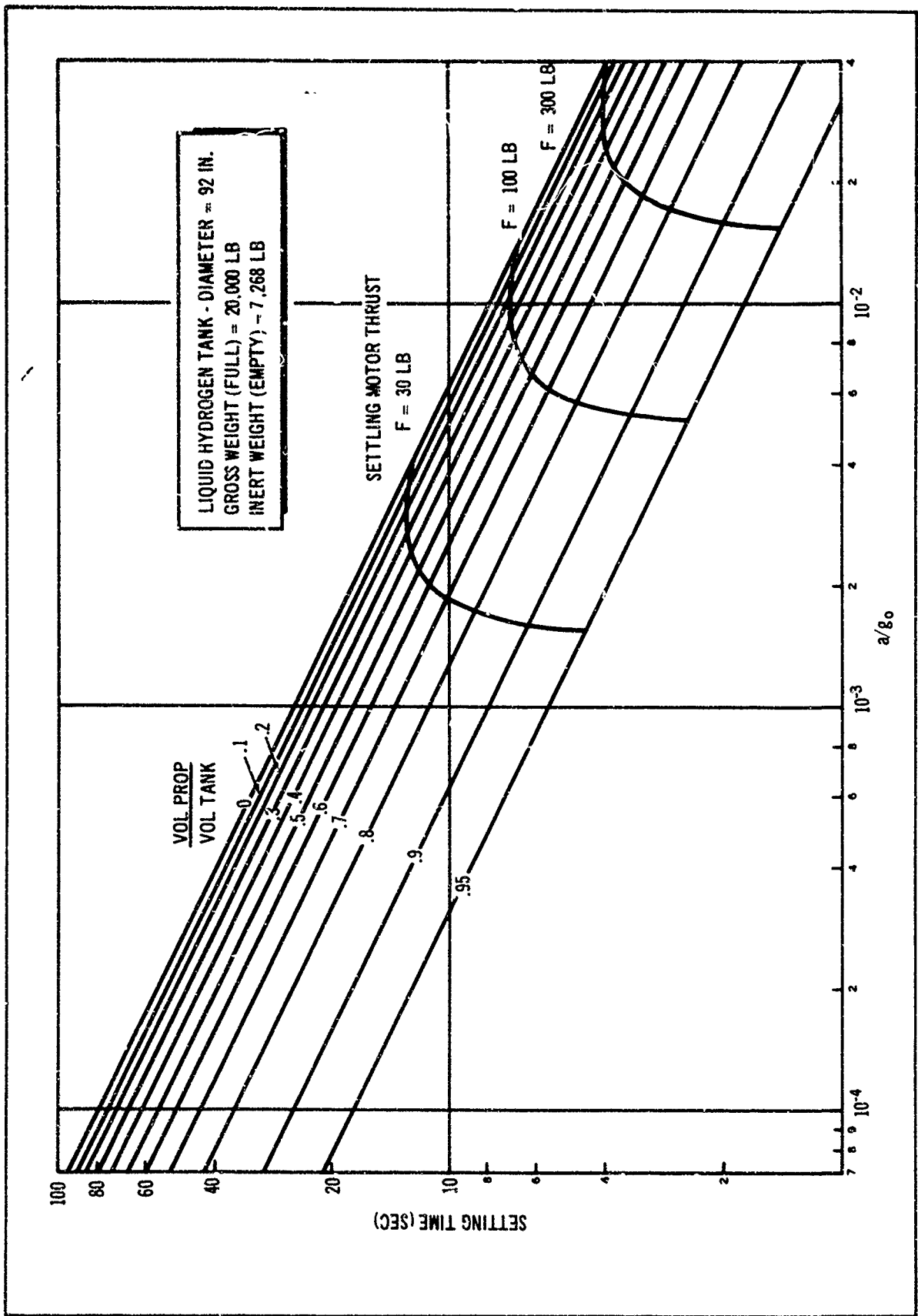


Figure 4-39. Settling Time as a Function of Acceleration

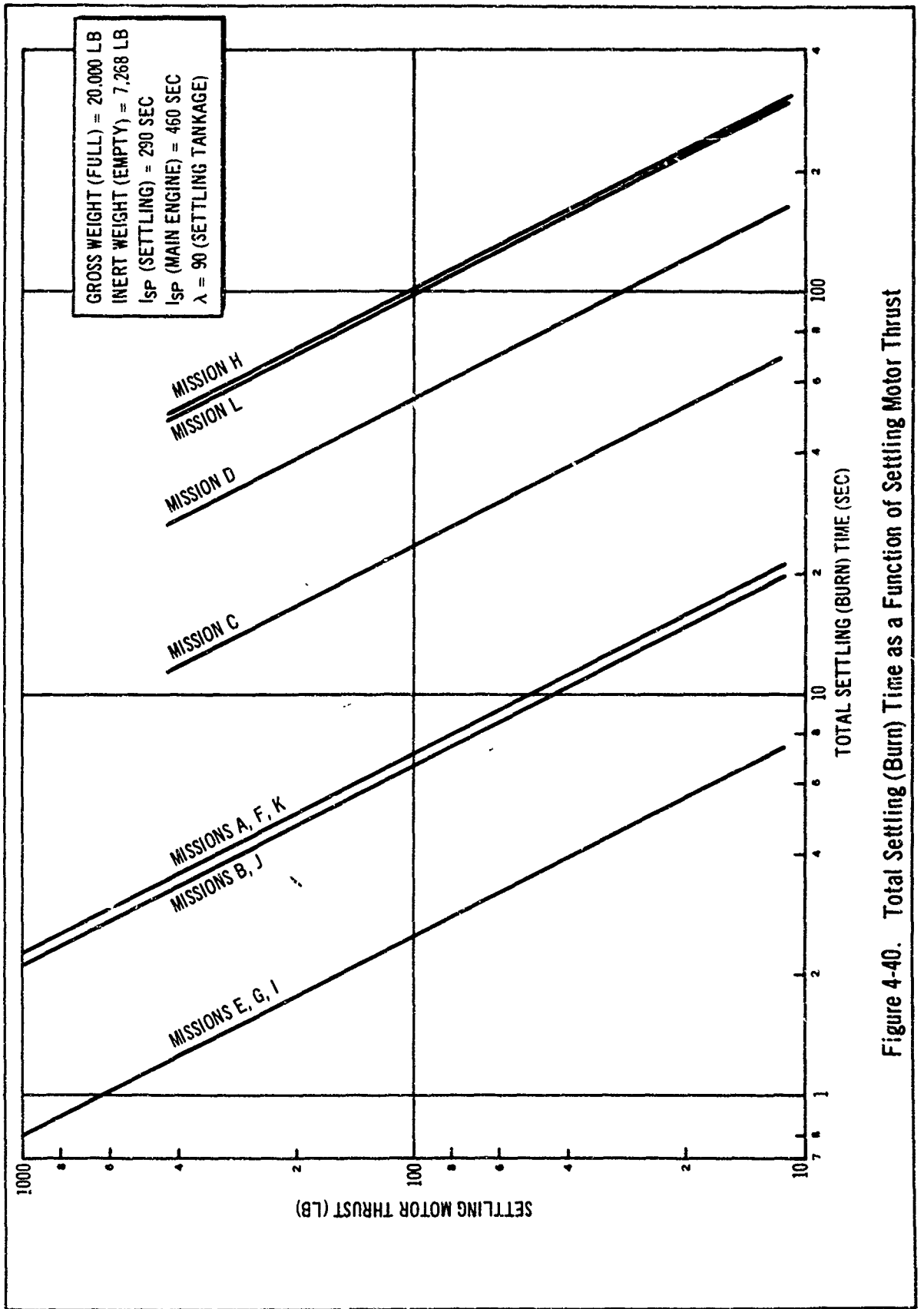


Figure 4-40. Total Settling (Burn) Time as a Function of Settling Motor Thrust

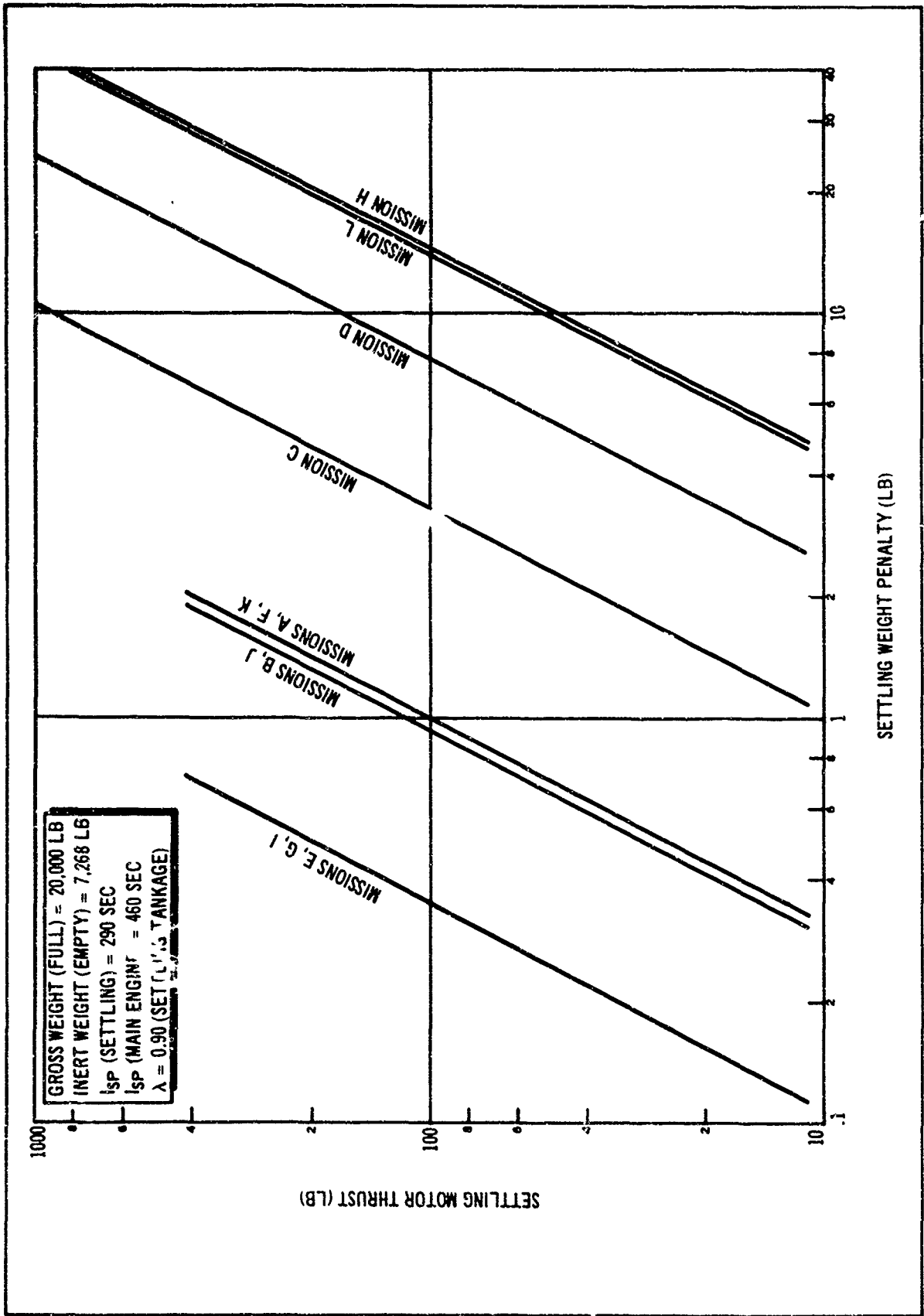


Figure 4-41. Settling Weight Penalty as a Function of Settling Motor Thrust

ullage motor I_{sp} . For coast venting this assumption may not be true and the system must be designed on the basis that the effective coast-venting ΔV is always in the opposite direction to that required for the next burn. The burn time and weight penalties for this mode of operation are shown in figures 4-42 and 4-43. The corresponding ullate rocket system weight penalties for re-pressurization are shown in figure 4-44. In this case, it is again assumed that the ΔV for settling during this time are additive to the subsequent burn ΔV .

In all of the above presented results, it was assumed that the attitude control system already on-board the vehicle would be used for settling, and no additional engine weight was included in the computer weight penalties.

(5) Dielectrophoretic Propellant Orientation. Several years ago Douglas originally proposed the idea of applying dielectrophoresis to the orientation of propellants in a low gravity environment. The basic principle here is that a continuous dielectric fluid existing in a non-uniform electrical field will be subjected to a net force in the direction of increasing field strength. Cryogenics, particularly LH_2 , are good dielectric fluids, and if a properly designed electrode configuration is provided inside the propellant tank and a voltage applied across the system, the resulting forces can be used to control the position of the contained liquid in low-g environments. A wide variety of experiments have been conducted by Douglas under Independent Research and Development Programs (see references 10, 11, and 12) and by others (references 13, 14, and 15) to indicate that such a concept is feasible.

As discussed in detail in reference 13, the total volume force \bar{F}_v , on a dielectric liquid with no discontinuities in an electric field is

$$\bar{F}_v = \rho_e \bar{E} - \frac{\epsilon}{2} E^2 \nabla K + \frac{\epsilon}{2} \nabla (E^2 \frac{\partial K}{\partial \rho}) \quad (4-36)$$

where ρ_e = electric charge density

E = electric field intensity

ϵ = capacity

K = dielectric constant

ρ = mass density

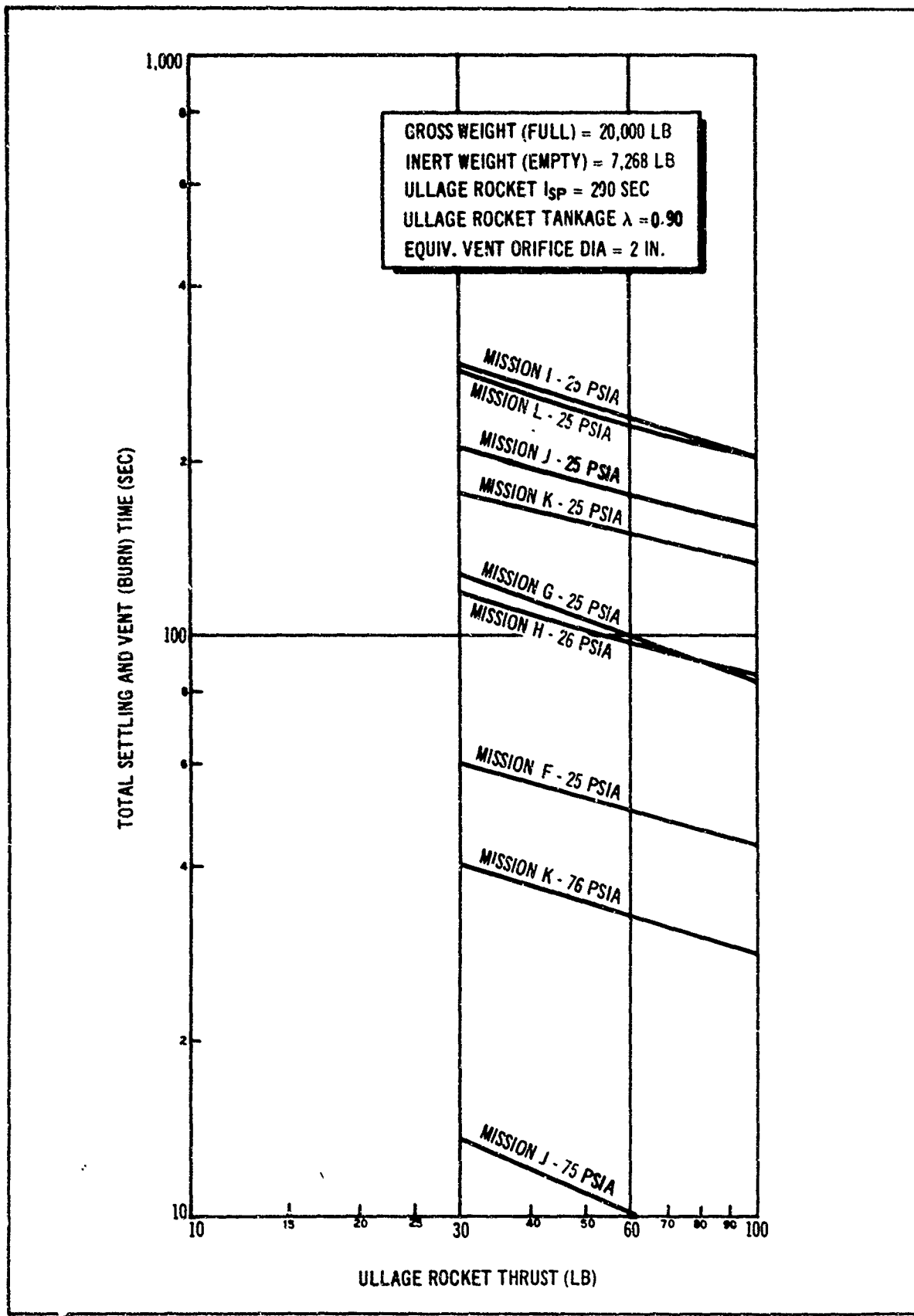


Figure 4-42. Ullage Rocket Burn Time for Venting as a Function of Ullage Rocket Thrust

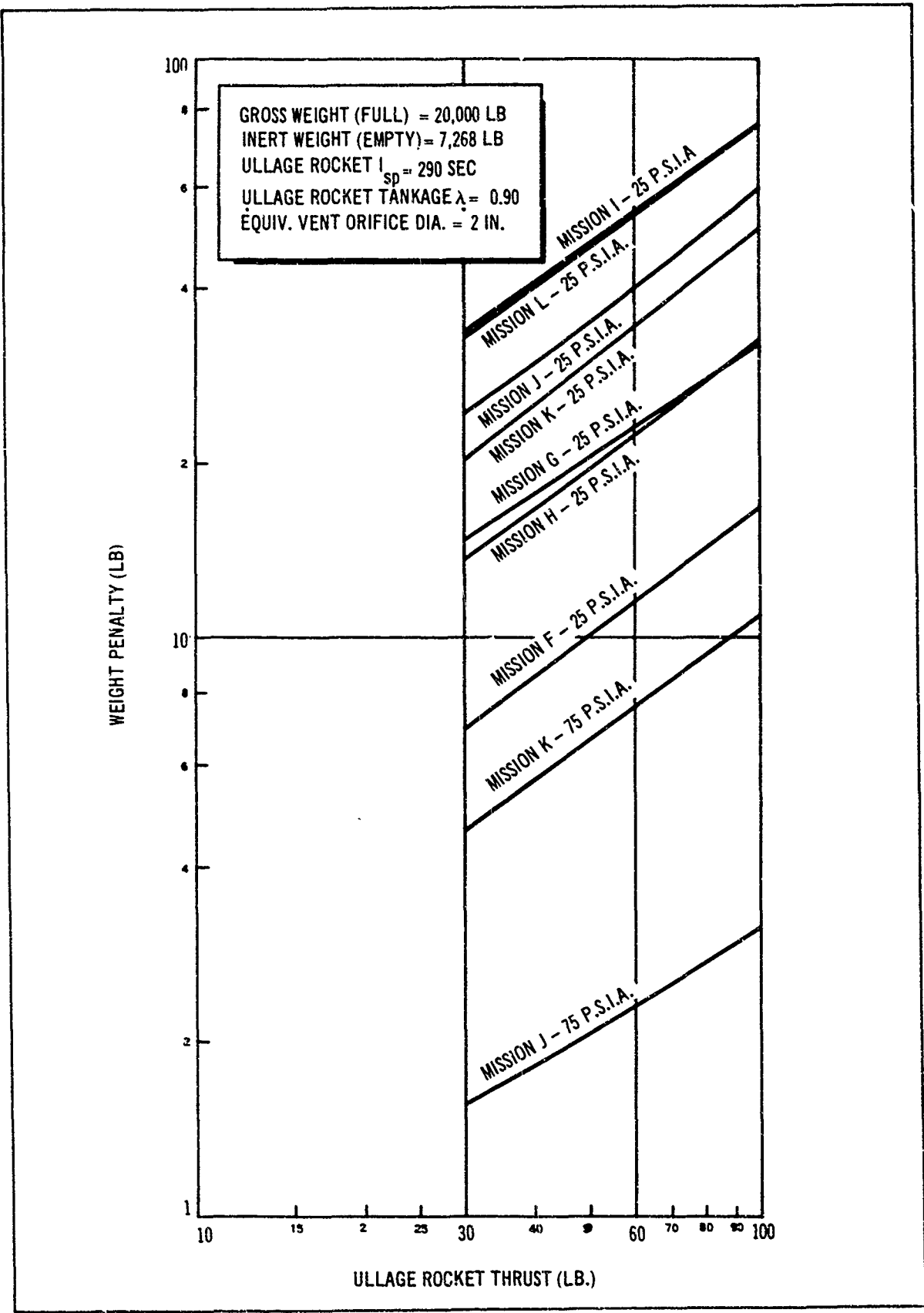


Figure 4-43. Ullage Rocket Weight Penalty for Venting as a Function of Ullage Rocket Thrust

ULLAGE ROCKET $I_{SP} = 290 \text{ SEC}$
 MAIN ENGINE $I_{SP} = 460 \text{ SEC}$
 ULLAGE ROCKET TANKAGE $\lambda = 0.90$
 NOTE: MISSIONS NOT SHOWN HAVE
 NEGLIGIBLE REPRESSURIZATION
 PENALTY

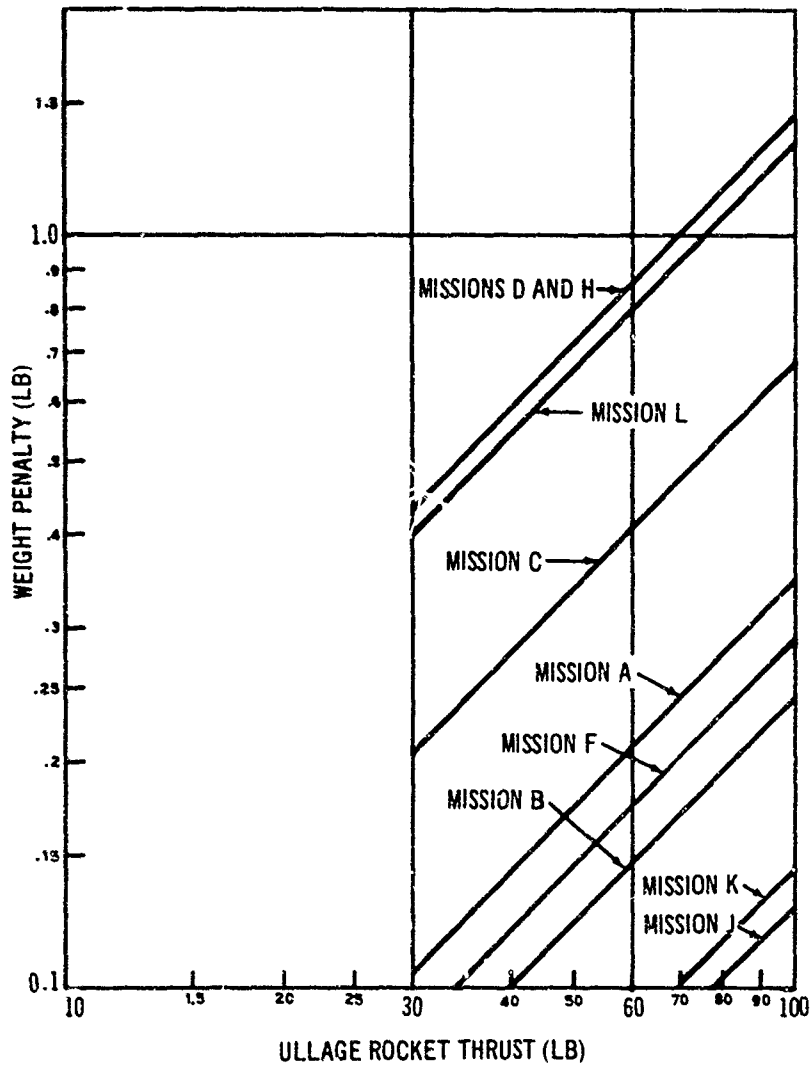


Figure 4-44. Ullage Rocket Weight Penalty for Repressurization as a Function of Ullage Rocket Thrust

The first term is the force exerted on free charges, the second term is the force exerted because of the inhomogeneity of the liquid, and the last term denotes the dielectrophoretic effect on the body in the non-uniform field. The following assumptions are made: (1) for dielectric fluids $C\rho = (K-1)/(K+2)$, where C is a constant for a particular fluid; (2) for ideal gases the free charge is negligible ($\rho_e = 0$); and (3) the liquid is homogeneous. The above equation reduces to

$$\bar{F}_v = \frac{\epsilon_0 (K-1) (K+2)}{6} \nabla E^2 \quad (4-37)$$

Thus the force depends on the square of the field intensity and is in the direction of increasing strength. The above equation may be expressed in terms of the effective g. per unit volume of liquid:

$$\frac{a}{g} = \frac{\epsilon_0 (K-1) (K+2) E^2}{6 \rho g} \quad (4-38)$$

For two co-axial cylindrical electrodes, with radii r_1 and r_2 , the voltage distribution, neglecting end effects is:

$$V(r) = \frac{V \ln r/r_2}{\ln r_1/r_2} \quad (4-39)$$

Combining the last two equations, the resulting g. level throughout the liquid is:

$$\frac{a}{g} = \frac{\epsilon_0 (K-1) (K+2) V^2}{3 \rho g (\ln \frac{r_2}{r_1})^2 r^3} \quad (4-40)$$

For example, with radii of $r_1 = 0.1$ and $r_2 = 0.5$ m. and an applied voltage of 10^6 v. the force acting on LH_2 varies from 1.35 g. at the inner cylinder to 0.1 g. at the outer cylinder.

Actual detailed analytical design of electrode configurations is not practical with current understanding of the phenomena except for relatively simple geometries such as concentric cylinders and spheres. Also, factors such as arcing, structural design and electrode support must be taken into

account. However, from limited analytical calculations and from trends observed during various phases of experimentation under the Douglas IRAD program on dielectrophoretic (DEP) propellant orientation, two conceptual electrode configurations were designed for this particular spherical tank system. The first design consists of an array of seven tubular electrodes positioned as shown in figure 4-45 and charged as noted (using a. c. power causes the polarity to alternate). With an applied voltage of 300,000 v. in the LH₂ tank, a steady downward (tangential) collection acceleration of 10⁻³g and a radial collection acceleration of 6.6 x 10⁻²g is produced. The voltage gives a breakdown safety factor of seven under worst possible conditions in LH₂. The total weight of the electrode system for the LH₂ tank was estimated at 5 lb. assuming a 1-in. -diam. aluminum tube electrode structure.

The power generation portion of the DEP system was assumed to be a high voltage a. c. electrostatic generator, powered by a solar cell array. Although voltages are high, the current requirements are quite low since all that is being done is the charging of a capacitor. The largest source of energy loss is in the generator motor inefficiency. A power requirement of 150w. was estimated which requires about 15 lb. of solar cells, assuming 100 lb/kw as the capabilities of an advanced solar cell system. Various types of specialized high voltage - low-current generators have been under study by Douglas for DEP applications. Present indications are that a cylindrical rotor-electrostatic type generator for this application could be produced for about 15 lb. Approximately 10 lb. would also be required for miscellaneous items such as controls, cabling, and so forth. Table 4-14 lists the estimated weights for a DEP system for the LH₂ tank. Since the LF₂ tank does not require venting, a system was not sized for the LF₂ tank although it would be of comparable weight.

Table 4-14

ESTIMATED WEIGHT BREAKDOWN FOR AN LH₂ TANK
DIELECTROPHORETIC PROPELLANT POSITIONING SYSTEM

Component	Tubular Electrode Design (lb.)	Disk Electrode Design (lb.)
Electrode system	10	18
Solar-cell power supply	15	15
Electrostatic generator	15	15
Miscellaneous (controls, etc.)	10	10
Total	50	58

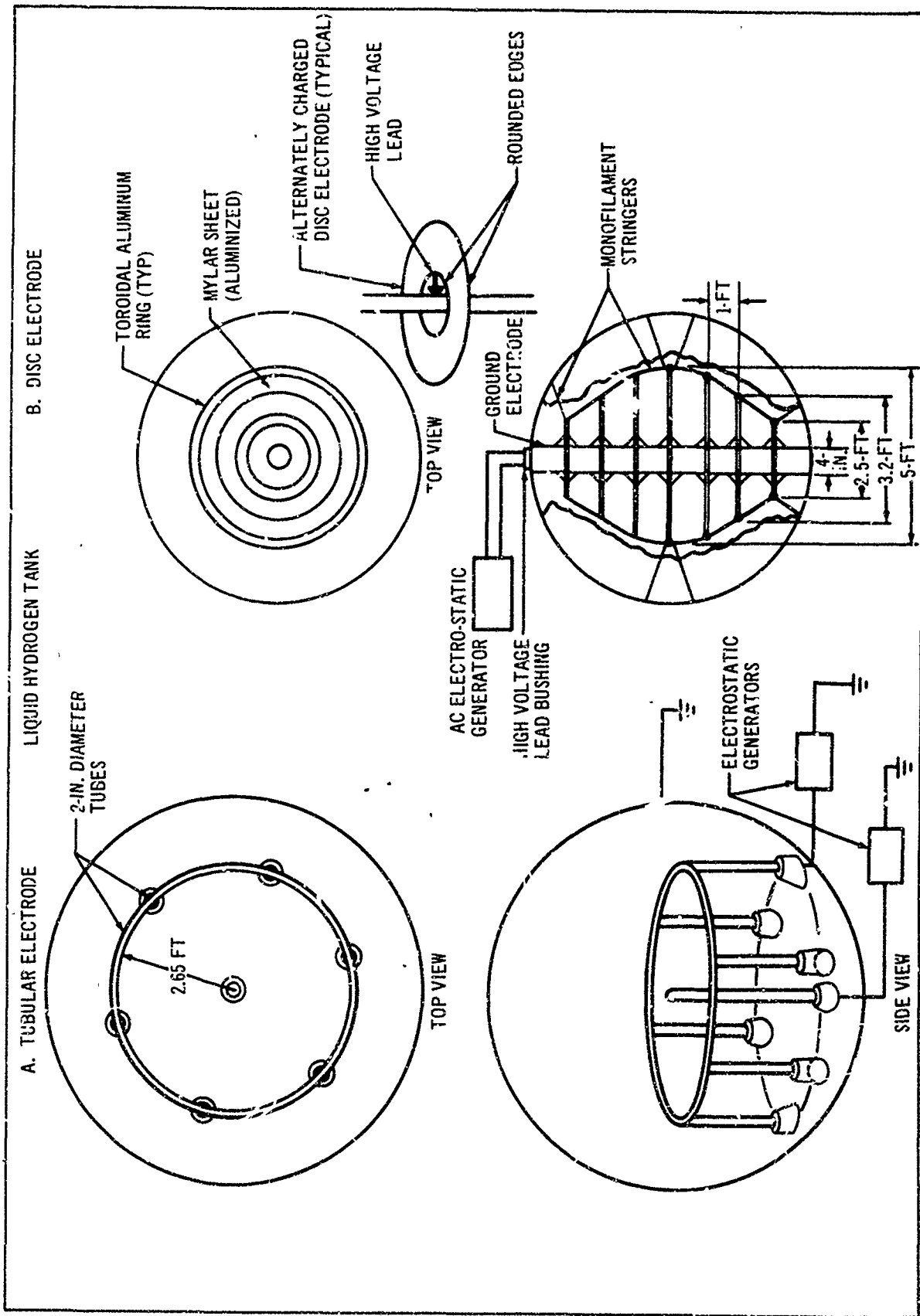


Figure 4-45. Dielectrophoretic Electrode Configuration

The second design consists of parallel disks with an axial cylindrical electrode. Liquid is collected off of the tank walls and into the center of the tank. The axial electrode induces high body forces in the radial direction (of the order of 1 g. near the electrode surface) and the parallel disks provide average forces of the order of 10^{-3} g. for voltages of the order of 500 kv. Aluminized Mylar is assumed for the electrode surface between each of the toroidal aluminum electrode supports. High-voltage leads are connected to each disk through bushings provided in the axial electrode. The disk electrode system weights are approximated in table 4-14.

The tubular electrode design of figure 4-45 is sufficient for propellant collection at the bottom of the tank for restart and venting, and provides slosh wave control at main engine cutoff. In addition, suction dip is controlled by the central electrode. The disk electrode design is more efficient, however, in the above respects and in addition performs other functions. The disk electrode configuration collects liquid for engine restart and ullage gas venting and collects liquid off of the tank wall to potentially minimize boiloff. Also, slosh wave control and suction dip control are further enhanced by the baffling effect and viscous dissipation provided by the more extended electrodes. Both electrode designs aid in alleviating boilover during rapid venting by causing more rapid vapor bubble coalescence and expulsion from the body of the liquid.

(6) Venting System Comparison. From the data generated in the preceding five sections, the various vent systems were compared on a weight basis. Since the preliminary findings of the previous section indicated that the LF_2 tank did not vent at any of the conditions studied, only LH_2 tank venting was considered. A fluorine vent line and valve system will be required to satisfy filling and emergency venting requirements.

The LH_2 tank can be vented during low-gravity coast by using one of two basic techniques: (1) discrete, high-flow, large-volume venting at intervals during coast, or (2) continuous, low-flow, small-volume venting at all times during coast. Discrete venting is considered because of the problem of efficient vapor/liquid separation during coast. For example, if ullage rockets are used to effect vapor/liquid separation, it would be desirable to vent as much as possible as rapidly as possible to minimize the ullage rocket burn time and weight penalty. It is clear that this high-flow vent technique might be wasteful for an indeterminate mission since venting might occur just before a restart command, thereby requiring additional repressurization. On the other hand, if continuous vapor/liquid separation can be assured then continuous venting of sufficient vapor to match the incoming heat load can be made with minimum losses.

Some systems, like dielectrophoretic or surface force systems, provide both vapor/liquid separation and positive liquid orientation and need no further propellant settling for repressurization and restart. Others like the mechanical or thermodynamic separators do not provide positive propellant orientation for repressurization and restart. For these systems, ullage rockets are assumed to be used for settling of propellants for restart. It is further assumed that the study vehicle is properly oriented during the restart sequence, that the thrust of the settling rockets will provide

usable measurable velocity and, therefore, reduce the settling rocket weight penalty to the ratio of the respective specific impulses of the ullage engines and the main engine (figure 4-42). Settling times and weights may have to be increased by some degree if settling and chilldown of the LF_2 feed line is the criteria. However, the worst missions shown in figures 4-41 and 4-42 are missions H and L which are 19 burn missions. The coast time between burns is short enough that the LF_2 feed line will always be nearly full, and thus the extra settling time required will be small. The penalties for settling and repressurization must be added to the penalties for those techniques which do not have positive liquid orientation.

(a) Discrete Venting. A mechanical vapor/liquid separator has been described above and provides continuous vapor/liquid separation of a sort but is considered under discrete venting because the vent flow rate required for efficient operation of such a device is much higher than the continuous vent flow rate of the study vehicle. Assuming a separator designed to the Saturn requirements, such as, 6 lb. p. sec. of LH_2 , the self-powered separator has a claimed efficiency of 90 pct. at qualities up to 75 pct. If such quality is encountered while venting the study vehicle, at least 39 lb. of excess LH_2 could be vented caused by the inefficiency of the machine. This penalty must be added to the 25 lb. weight of the separator hardware. The externally powered separator with a claimed efficiency of 80 pct. at qualities up to 90 pct. would suffer a waste propellant penalty of at least 32 lb. in addition to the enormous fixed weight of 215 lb. In addition, settling and repressurization penalties must be added giving an overall weight breakdown as shown in table 4-15.

Ullage rockets for settling during discrete coast venting were evaluated for the study vehicle (figure 4-44). During coast, it was assumed that the vehicle was randomly oriented and thus a full weight-penalty based on the ullage rockets specific impulses must be assessed. It was initially thought that the conditioning venting could be performed during the propellant settling phase and thus take advantage of the reduced penalty provided by obtaining usable thrust from the ullage rockets as described above. It was found, however, that the vent times required to obtain complete conditioning for some missions were so long that they appeared to seriously compromise the requirements for short reaction times. It was determined that for most missions minimum reaction time and minimum settling time occurred if the majority of the propellant conditioning venting occurred during coast. Therefore, the total venting requirements (both coast heating and conditioning) were divided into the number of vents which gave the minimum total time (settling plus venting) and thus the minimum ullage rocket weight penalty. Because most of these vents occurred during coast, it was assumed, conservatively, that all venting occurred during coast and that this venting incurred the full ullage rocket weight penalty. Using the ullage rocket weight penalties for the various missions as shown in figure 4-44, the total weight penalties for the worst mission is shown in table 4-15.

Table 4-15

VENTING SYSTEM WEIGHT PENALTY COMPARISON
(worst mission at settling thrust of 64 lb. ^a)

	Fixed Weight	Ullage Rocket Penalty		Propellant Penalty	Total
		Settling	Repressurization (lb.)		
Mechanical vapor/ liquid separator:					
• Self-powered	25	11.5	1	39	76.5
• Electric-powered	217	11.5	1	32	261.5
Ullage rockets	57	11.5	1	0	69.5
Surface force	20 ^b	0	1	unknown	20+
DEP	47.5	11.5	1	0	60
Thermo vapor/ liquid separator	8.5 ^c	11.5	1	1	22

^aThrust based on Maneuvering Satellite System ACS pitch-yaw engines - 4 at 16 lb. thrust.

^bBased on Maneuvering Satellite System study results.

^cIncludes 0.7 lb. for regulator - 3.3 lb. for heat exchanger - 4.5 lb. for structure, for actual design of 75 p. s. i. a. system.

(b) Continuous Venting. Surface force devices have been studied as a means of positive liquid orientation in the tank and to provide vapor/liquid separation for venting. It was found that 400 mesh screens would retain liquid under the most severe expected disturbances. However, such a screen would only retain such liquid as was trapped below it at shutdown. In order to retain all liquid in the tank the screen would have to be located at precisely the vapor/liquid interface at shutdown. If the interface was below the screen, the screen might be dry and might not hold the liquid at rebound. If the interface was above the screen, some amount of liquid would be free to float off the screen and possibly be vented. The indeterminacy of the mission (along with normal propellant usage tolerances) makes such precise location of the screen impossible. As shown in the Rocketdyne Maneuvering Satellite System study, use of a screen for H₂ propellant retention for res. is completely feasible, but retention of all liquid to allow all vapor venting is not the same thing and is clearly impractical. The weight of the Maneuvering Satellite System study surface force system is shown only for comparison in table 4-15. Since the system will not work effectively for venting, an unknown propellant weight penalty is also identified.

A thermodynamic vapor/liquid separator was sized for the study vehicle vent-rate and tank configuration. The vent rate assumed was based on venting continuously an amount equivalent to the most severe heat load encountered. The worst mission in this report was the 5-day 19 burn case which gave a vent rate of 0.425 lb. p. hr. This vent rate is more than adequate for all other venting missions.

The separator heat exchanger tubing length, diameter, and weight are shown in figures 4-46, 4-47, and 4-48, respectively, for minimum weight systems based on tank geometry. The curves shown are for the 75 p. s. i. a. and 21 p. s. i. a. systems with exit pressures of 15 p. s. i. a. and 5 p. s. i. a. It is felt that for actual systems, particularly for the 21 p. s. i. a. tank pressure, an exit pressure of 5 p. s. i. a. should be used.

Propellant settling and repressurization penalty must be assigned to this system along with the basic system weight as shown in table 4-15. Note that an additional propellant penalty is also included. This is based on the fact that tolerance in the regulator will allow some excess propellant to be vented. The estimate of one pound is extremely conservative; the actual will probably be much less. For the thermodynamic vapor/liquid separator, as is the case for all low flow continuous systems, an additional vent valve must be provided for loading and for emergency pressure relief. This vent valve will be set to vent at a pressure higher than the primary system vent pressure.

(c) Conclusions. From table 4-15, it can be seen that of the systems which will be effective in controlling vapor/liquid separation, only two have low-weight penalties: (1) the thermodynamic vapor/liquid separator and (2) the DEP system. The study vehicle is a high-performance space vehicle with very low vent requirements - optimum conditions for having a competitive thermodynamic separator system. On the other hand, the low vehicle weight makes the fairly large fixed weight of the DEP system look unattractive. The DEP system comes into its own with large vehicles and/or

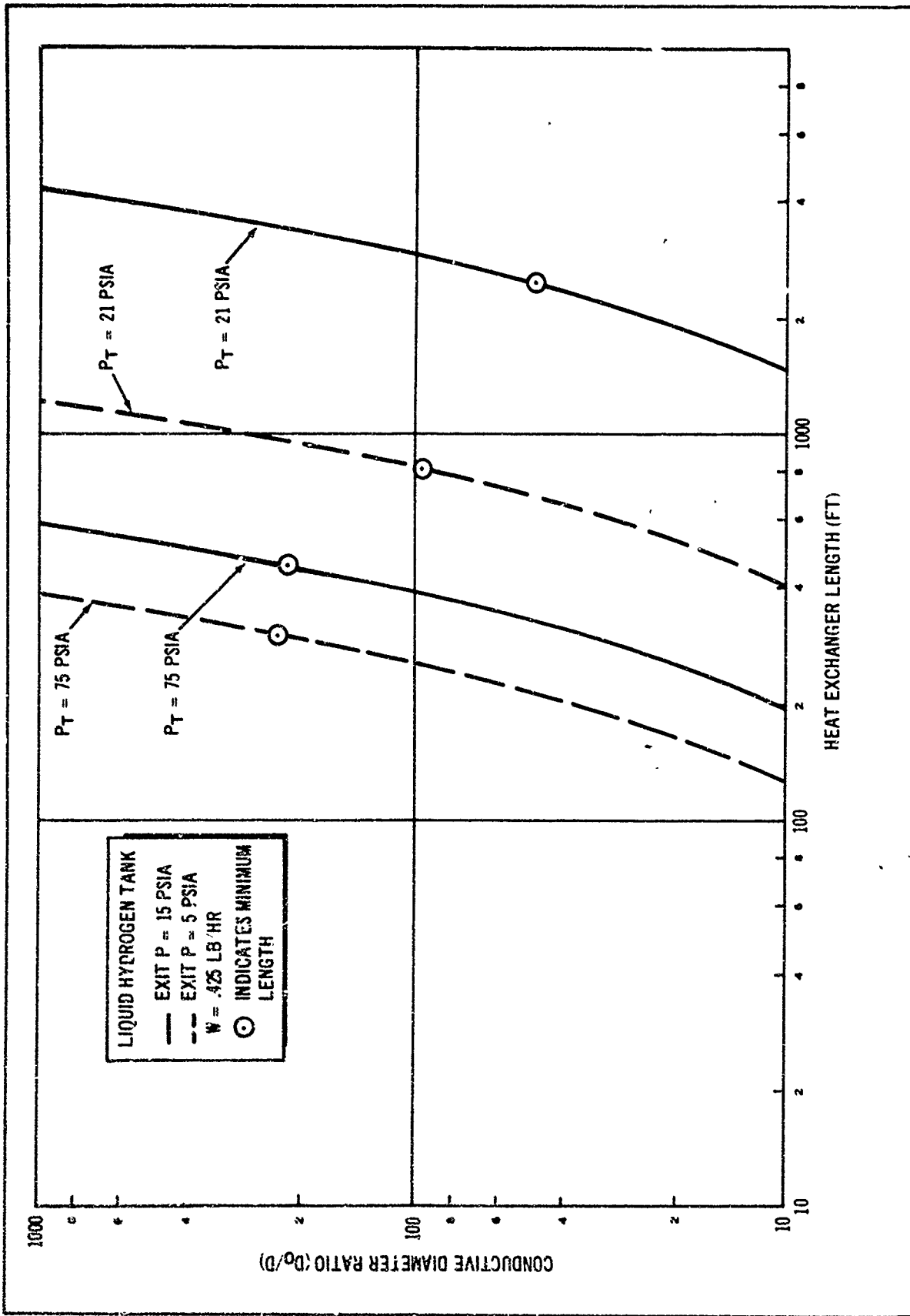


Figure 4-46. Heat Exchanger Length as a Function of Conductive Diameter Ratio

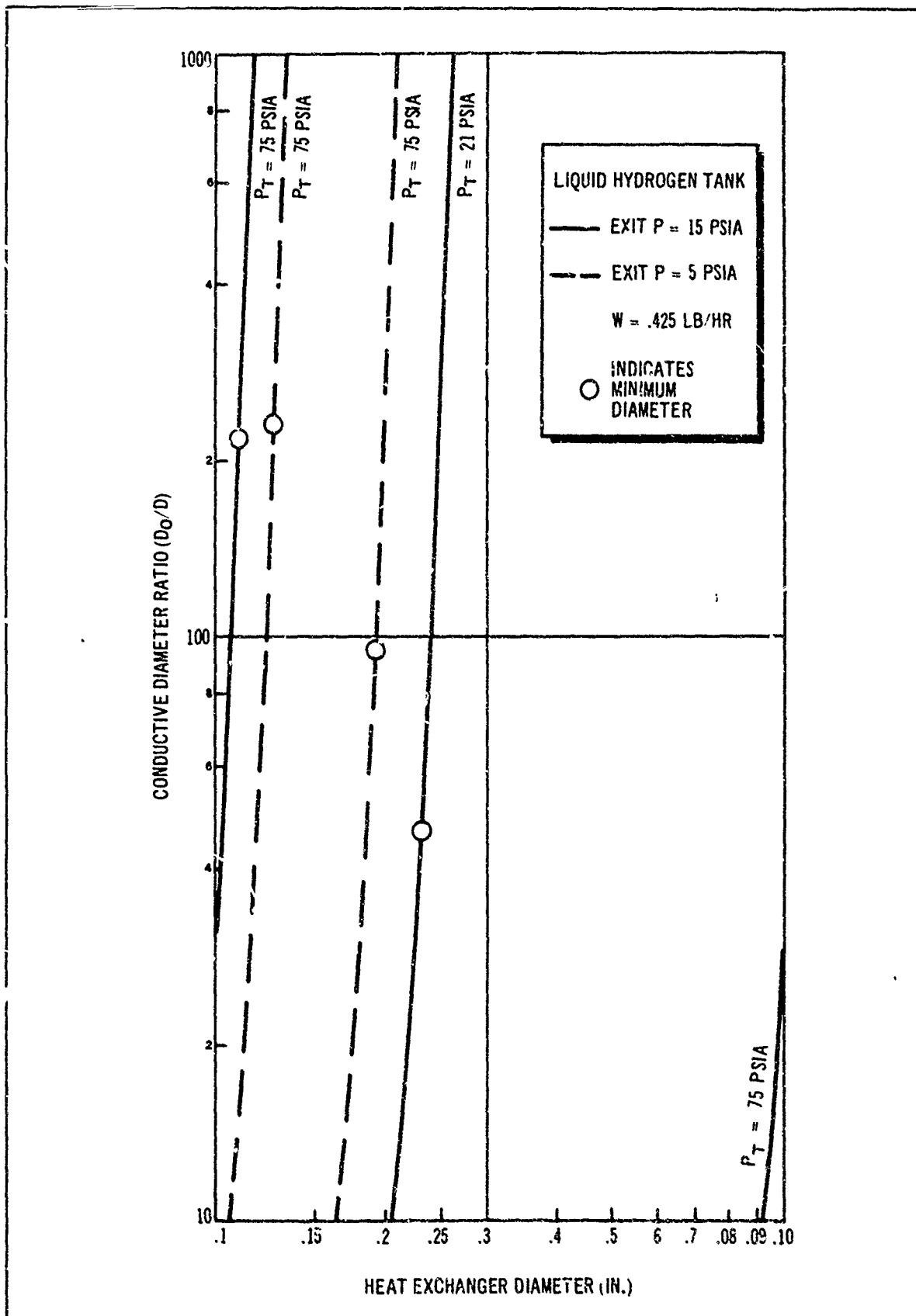


Figure 4-47. Heat Exchanger Diameter as a Function of Conductive Diameter Ratio

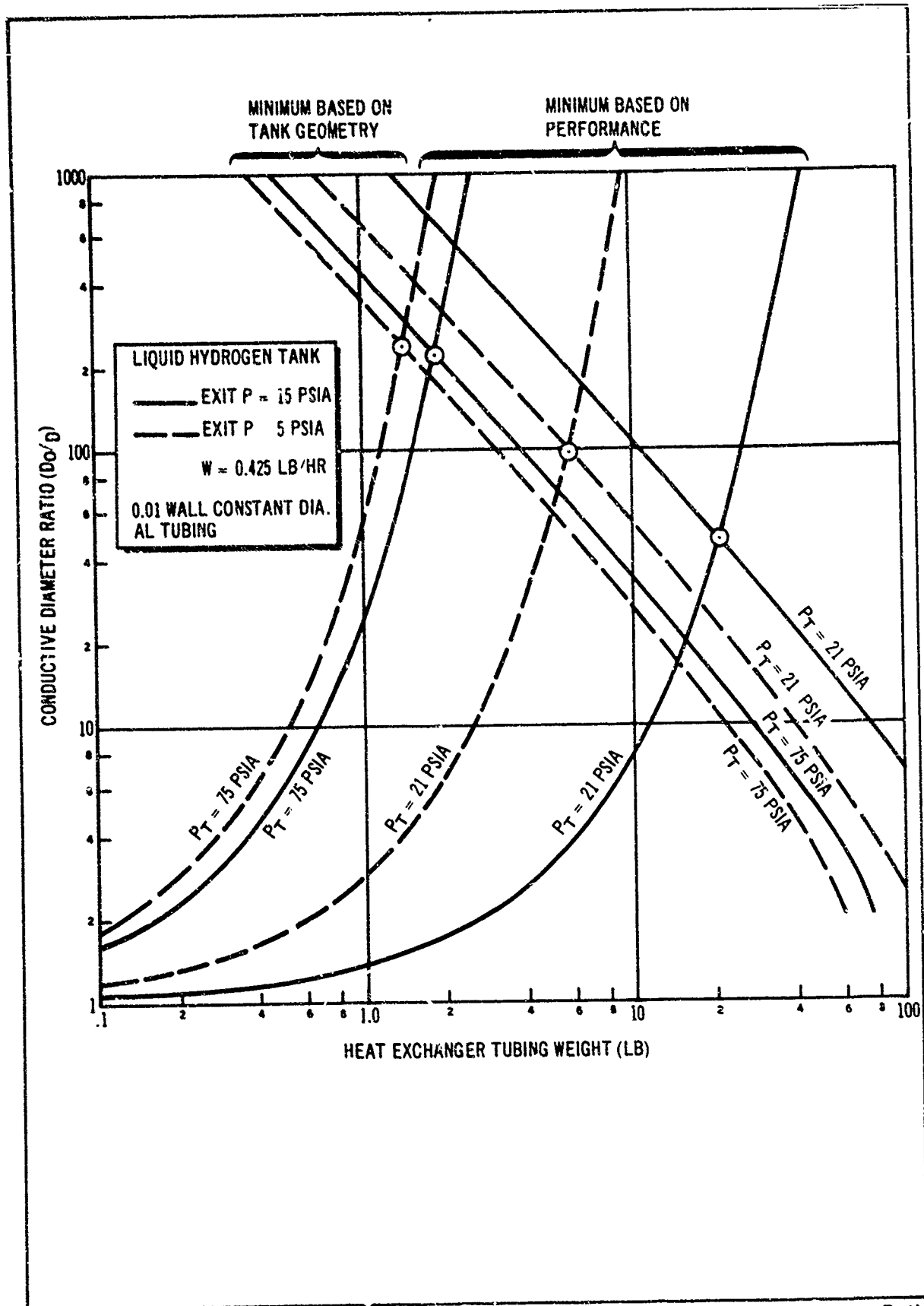


Figure 4-4): Minimum Heat Exchange Tubing Weight as a Function of Conductive Diameter Ratio

large vent rates. In the final analysis, the actual difference between the two concepts is the penalty assessed for settling and repressurization. It is possible that the optimum solution to the problem of venting and liquid orientation may be a combination of the Rocketdyne surface force system for liquid orientation and the thermodynamic vapor/liquid separator for venting. However, based on the ground rules adopted for this study, the thermodynamic vapor/liquid separator is selected as optimum for lowest weight penalty with positive control for vehicle venting.

(d) Preliminary Design of Recommended Concepts. Design of an actual thermodynamic vapor/liquid separator installation for the LH₂ tank was completed and was based on obtainable tubing dimensions and a minimum weight support system. The installation is shown in figure 4-49 and consists basically of an extruded aluminum center support column, 0.063-in. aluminum support wires attached to brackets welded to the tank wall, and a heat exchanger consisting of 3/16-in. dia. 0.022-in. thick aluminum tubing (the thinnest roll obtainable commercially), 215 ft. long, uniformly spaced in concentric rings. The tubing weight for the heat exchanger is 3.3 lb. and is suitable for the 75 p. s. i. a. system for down to 8 pct. liquid covering the tubing. The support system weight is 4.5 lb. giving a total system weight (installed) of 8.5 lb. as shown in table 4-15. The system shown would be installed from the tank bottom upward with the tubing easily formed by hand laid in, and tied down. Since all components (except bolts) are aluminum, the differential expansion problem at cryogenic temperatures is obviated. Final system hookup is to tube fittings connected to the vent valve and regulator mounted on the LH₂ tank manhole.

An alternate to this design concept would be to locate the heat exchanger on the outside of the tank wall in direct contact with the wall. However, there was not sufficient time to properly explore this approach and this would not alter the basic choice in the type of venting system to be used. This is being further studied under a Douglas IRAD program.

(e) Cooling of the LF₂ Tank with Vented H₂. From the preliminary results, it was concluded that the LF₂ tank did not require venting under any of the conditions studied. However, there were conditions where the LF₂ tank did almost vent and if heat leaks are in reality higher than anticipated or if design conditions are slightly exceeded, it is possible that the LF₂ tank may vent.

Venting of the LF₂ tank is undesirable for two reasons: (1) venting of LF₂ vapor with its high density may incur a substantial weight penalty, and (2) the vented vapor is highly toxic and corrosive, which could lead to additional problems for the structure. Elimination of LF₂ venting is facilitated by two circumstances: (1) LF₂ is typically stored in LN₂ and is thus loaded in a subcooled condition (rather than as saturated liquid-like H₂), and (2) LF₂ has a much higher boiling point than LH₂ and thus generally has less heat leak to the tank. These circumstances mean that, typically, the LF₂ tank will require venting after the LH₂ tank.

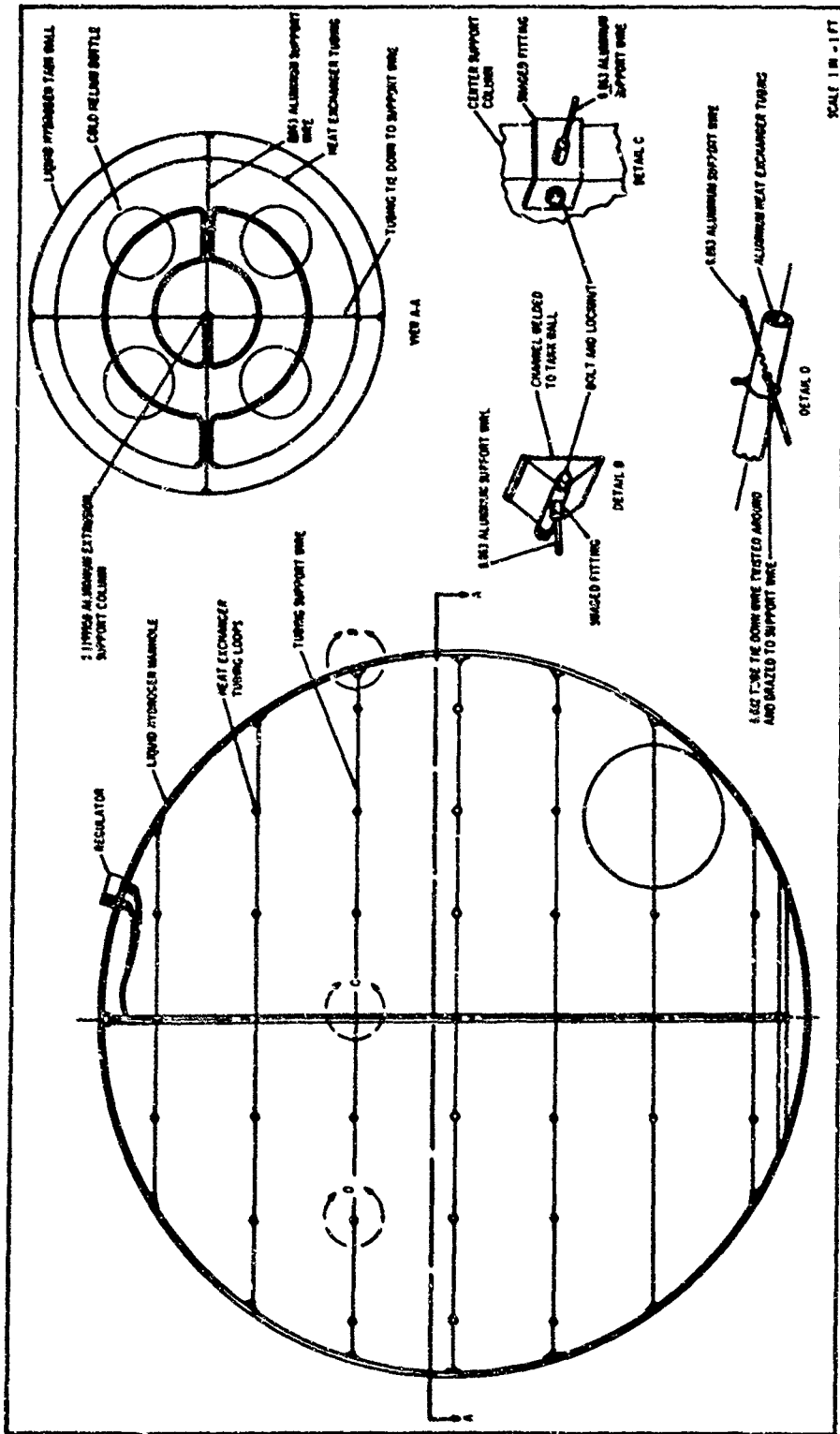


Figure 4-49. Installation of Thermodynamic Liquid/Vapor Separator

It has been proposed that the cold LH₂ vent line be routed through the LF₂ tank so that the vented LH₂ can absorb heat from the LF₂ and thus eliminate or substantially delay venting of the LF₂ tank. Routing the LH₂ vent line and freezing of LF₂ to the LH₂ vent line poses significant problems.

(1) Analysis. It was assumed that the dominant mode of heat transfer in zero-g. was conduction through the LF₂ in the tank to the vent line since it was felt that the forced convection heat transfer coefficient to the LH₂ from the vent line would be relatively large. It was further assumed that the LF₂ tank was spherical and that the cylindrical LH₂ vent line made a single straight pass through the center of the tank. Preliminary analysis had indicated that a single pass may be all that is required, and this assumption eliminates the complexity of analyzing a complicated heat exchanger. The diameter of the vent tube would be a variable, and even if a single pass of tubing did not remove heat at a rate equal to that entering the tank, it would remove sufficient heat so that venting of the vehicle LF₂ tank would be eliminated. The heat flux from a sphere to an internal cylinder, assuming constant temperature difference and conductivity, is

$$q = 8\pi k\Delta T \int_0^{(R^2 - r_1^2)^{1/2}} \frac{dx}{\ln\left(\frac{R^2 - x^2}{r_1^2}\right)} \quad (4-41)$$

where R is the tank radius and r₁, the vent tube radius. The above equation was integrated graphically for heat transfer to a variable diameter cylinder of solid F₂ at 96°R (constant) from a tank wall at saturation temperature. The conductivity was assumed to be the average conductivity based on the fractions of liquid and vapor in the tank. This is a reasonable assumption for randomly distributed vapor and liquid in the tank considering integration over the entire tank volume.

The growth of the solid F₂ layer around the vent tube was approximately computed based on the transient conduction from an internal cylinder (reference 16). The diffusive time constant for penetration of a line of 96°R temperature into the tube surroundings was computed based on a constant tube temperature equal to LH₂ saturation temperature at tank conditions. This assumption is justified as follows: the vented LH₂ temperature will rise by 26°R for a heat flux of 36 b. t. u. p. hr. (nominal heat leak into the fluorine tank) and thus the average will be in error by 13°R. However, this assumes that the vented LH₂ would be initially at saturation temperature when actually it will be much colder due to expansion through the vent valve. In fact, if the vented LH₂ was expanded from 75 p. s. i. a. tank pressure to 15 p. s. i. a. in the vent line, it would drop in temperature by 13°R, enough

to compensate for the temperature rise. The thermal diffusivity of solid F_2 was based on a thermal conductivity of 0.01 b. t. u. p. hr. -ft. $^{\circ}R$, a density of 81.1 lb. p. ft. 3 , and a specific heat of 0.32 b. t. u. p. lb. $^{\circ}R$. The solid diffusivity was an order of magnitude less than that of the liquid and two orders of magnitude less than that of the vapor, thus time-controlling. For purposes of this approximate analysis, the heat of fusion of solid F_2 was ignored, and the instantaneous heat flux through the solid F_2 coating was computed based on the instantaneous coating thickness.

The approximate maximum heat flux into the vent line versus time after venting H_2 is plotted for solid F_2 conduction controlling, and for vapor/liquid F_2 conduction controlling for vent line diameters of 1/4 in., 1 in., and 3 in., in figures 4-50, 4-51, and 4-52, respectively. The approximate weight of solid F_2 frozen to the H_2 vent line versus time after venting H_2 is plotted in figure 4-53. All computations were based on a spherical F_2 tank with a diameter of 75 in.

(2) Conclusions

- Figure 4-50 shows that a single-pass vent line of 1/4-in. dia. will probably remove sufficient heat even at low liquid fractions to eliminate any requirement for venting the study vehicle F_2 tank; however, detailed analysis using the actual venting requirements for the study vehicle should be made for a complete evaluation.
- Figure 4-53 shows that the weight of frozen F_2 increases rapidly with vent tube diameter and time; this weight penalty may be the controlling consideration. Note that even for time periods as short as 10⁶/hr., that the 1-in. and 3-in. vent lines are virtually eliminated from further consideration.
- It is felt that the hazards of F_2 ice formation and leakage risk make this technique a last-resort solution to the problem of F_2 tank venting but with proper development such an approach is feasible and deserves further study, particularly if longer duration missions are desired.

(f) Comparison of Final and Preliminary Venting Requirements.

To this point, the venting study has been conducted on the basis of the preliminary venting estimates as reported earlier in this document. These were based on an assumed constant heat input. After completion of the insulation optimization and the pressurization system optimization, a more accurate definition of the venting requirements was available. The primary difference between the final and preliminary values results from the following:

- The heat input through the optimum insulation varies depending upon the mission duration and the tank pressure level since the insulation thickness varies.
- The heat input to the propellant from the pressurizing gas varies with the inlet gas temperature, the duty cycle, and, to a certain extent, the type of pressurizing gas.

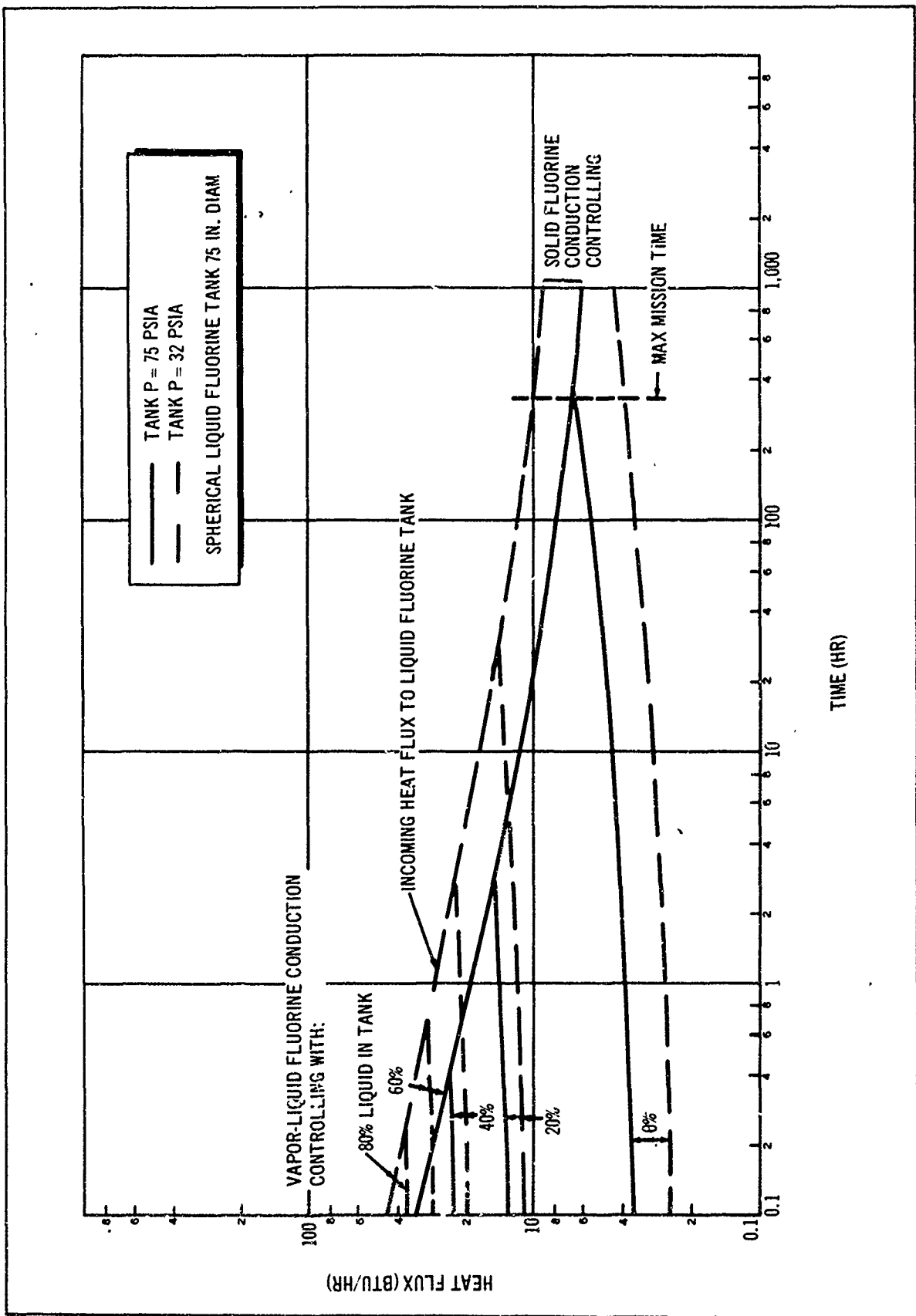


Figure 4-50. Heat Flux to H₂ Vent Tube Capacity as a Function of Time After Venting LH₂ Tank(1/4-in. Tube Diam)

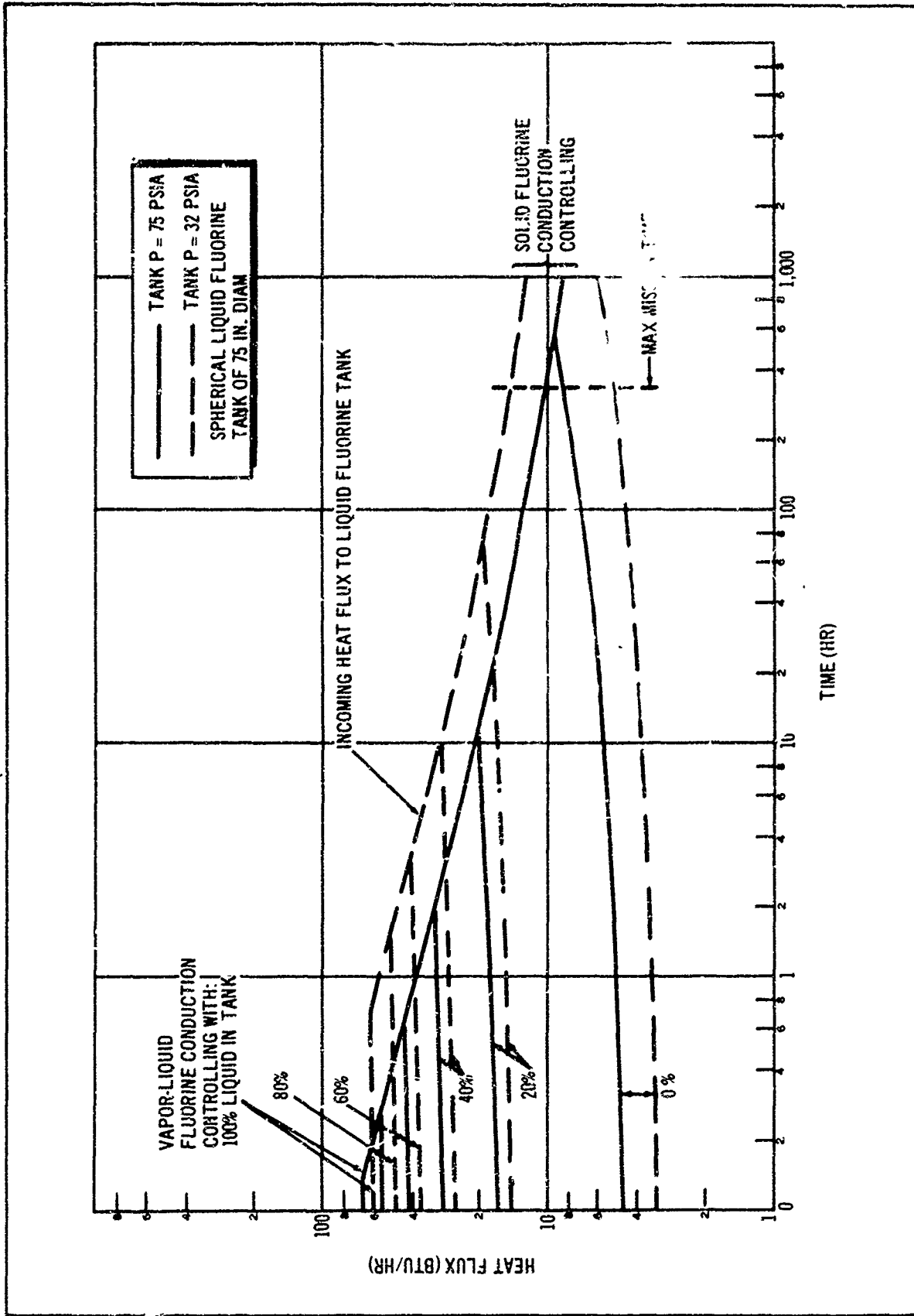


Figure 4-51. Heat Flux to H₂ Vent Tube Capacity as a Function of Time After Venting H₂ Tank (1-in. Tube Diam)

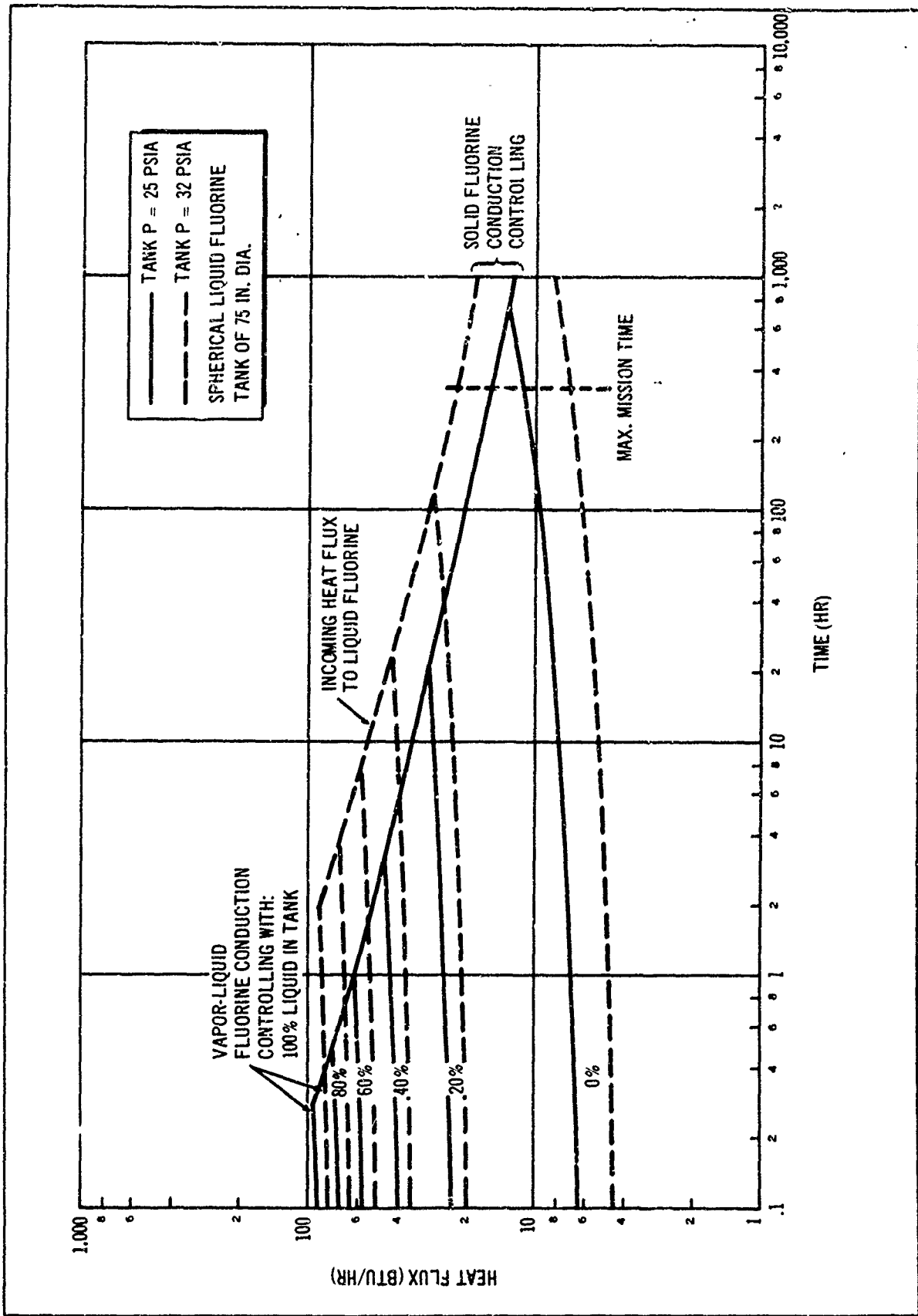


Figure 4-52. Heat Flux to H₂ Vent Tube Capacity as a Function of Time After Venting H₂ Tank (3-in. Tube Diam.)

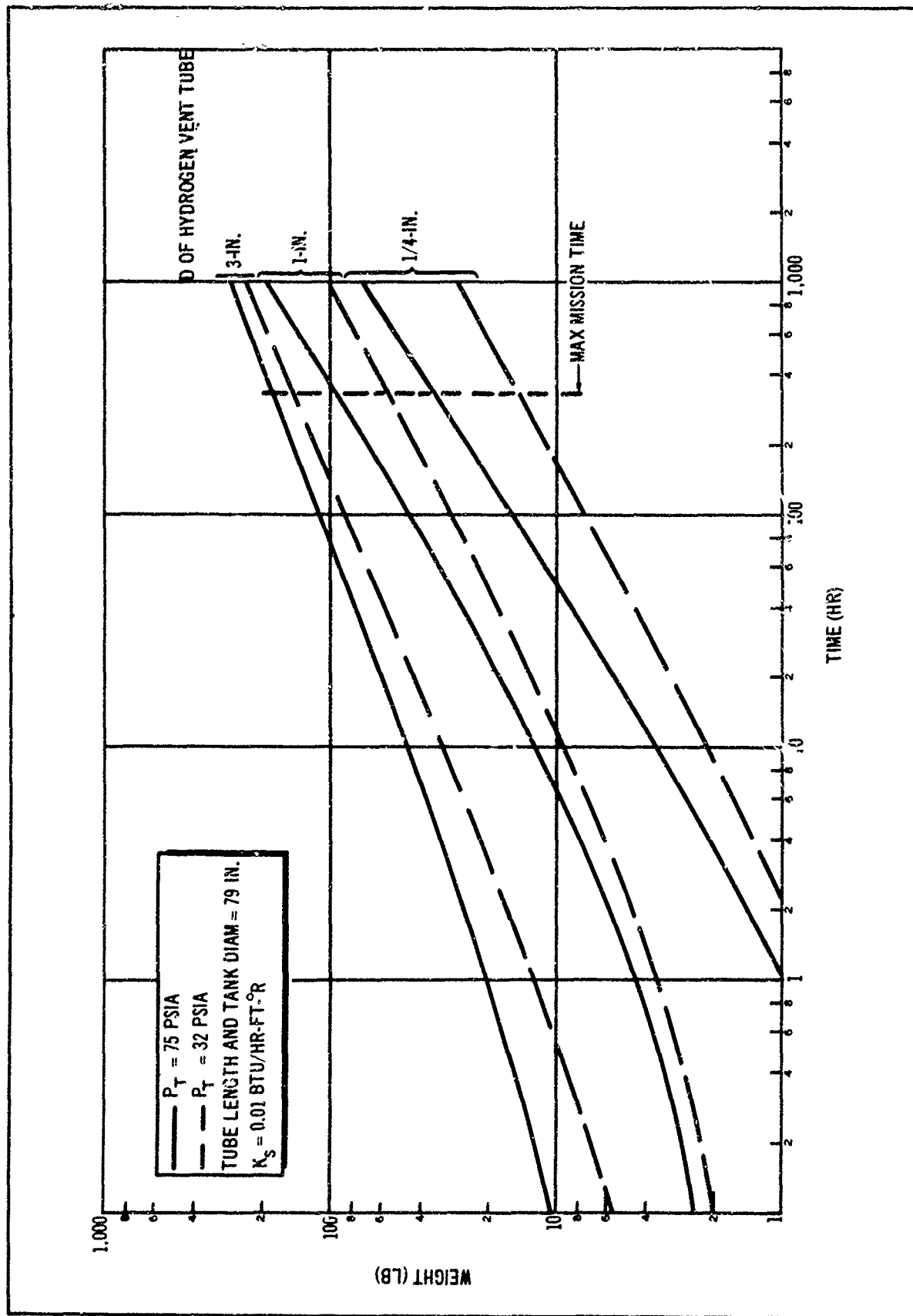


Figure 4-53. Weight of Solid F₂ Frozen to H₂ Vent Line as a Function of Time After Venting H₂ Tank

Table 4-16 lists the final venting requirements which evolved after the optimization for those duty cycles where significant venting occurred. The values shown within the parenthesis in table 4-16 are reference values from the preliminary analysis. These are not directly comparable because inlet gas temperatures and tank pressures are slightly different, but the values are in the same order. As was originally anticipated, the final venting requirements are considerably lower than the preliminary estimates, and some of the duty cycles which originally required venting did not vent in the final analysis. Duty cycles K and J are still the most critical with respect to venting. The pump-fed case for duty cycle J also requires considerable venting. All 14-day single burn missions required a slight amount of venting even for the LF₂ tank which is a departure from the original findings. However, the LF₂ tank venting is very small and could be eliminated by adding a slight amount of additional insulation. Table 4-16 also indicates the influence of inlet gas temperature on venting. High inlet gas temperatures generally lead to increased venting.

The reduction in venting over the original estimates is primarily a result of reduced heat flow with the optimized insulation. This is illustrated by table 4-17, which shows the heat flux through the optimized insulation system as compared to the originally assumed values. The final heat input is well below the assumed values particularly for the LH₂ tank.

These reductions in venting requirements should not significantly affect the previous conclusions made regarding the venting system.

Table 4-16

OPTIMIZED VENTING REQUIREMENTS

Cycle	P _t	T _{ig}	Venting Propellant Loss (Lb.)					
			All He			He(LF ₂), GH ₂ (LH ₂)		
			LH ₂		LF ₂	LH ₂	LF ₂	
1 burn (1)	235	300	1.3	(2.8)	0.2	(0)	1.3	0.2
		800	1.3		0.2		1.3	0
		1,200	1.3		0.2		1.3	0
	100	300	1.5	(3.6)	0.2	(0)	1.5	0
		800	1.5		0.2		1.5	0
		1,200	1.5		0.2		1.5	0
	41	300	b	(72.5)		(0)	1.2	0
		800					1.2	0
		1,200					1.2	0.2

Table 4-16 (cont)

OPTIMIZED VENTING REQUIREMENTS

Cycle	Pt	Tig	Venting Propellant Loss (Lb.)					
			All He			He(LF ₂), GH ₂ (LH ₂)		
			LH ₂		LF ₂	LH ₂		LF ₂
2 burn (80/20 K)	235	300	0	(0)	0	(0)	0	0
		800	5.7		0		a	a
		1,200	63.0		0		a	a
	100	300	0	(26.8)	0	(0)	0	0
		800	8.6		0		28	0
		1,200	32.0		0		a	a
41	300	b	(69.3)		(0)	25.5	0	
	800					48.4	0	
	1,200					61.1	0	
2 burn (50/50 J)	41	300	b	(71.5)		(0)	14.8	0
		800					22.3	0
		1,200					27.8	0
19 burn (L)	100	300	0		2.6		4.3	2.6
		800	1.4		0		12.7	0
		1,200	5.3		0		30.5	0
	41	300	b	(62.5)		(0)	10.0	2.6
		800					24.0	0
		1,200					33.5	0

^aCritical temperature of LH₂ was exceeded

^bPump-fed cases not optimized for He on LH₂

Table 4-17

COMPARISON OF OPTIMIZED AND ESTIMATED HEAT FLUXES^a
FOR 14-DAY MISSION (Shroud-Mounted Dimplar)

	Heat Load (B. t. u. /hr.)	
	LH ₂	LF ₂
Original estimate	50	36
Optimized values for pump-fed system	18.3	27.6
Optimized values for pressure-fed system	30.3	27.6

^aDoes not include pressurant gas heat input.

4. Phase IV--Vehicle Thermal Control. Once orbit has been attained, heat transfer to a space vehicle occurs through the mechanism of thermal radiation. Therefore, it is possible to reduce the heat flow into the interior of the vehicle by using special surface coatings which have favorable thermal properties, particularly emissivity and absorptivity. A considerable amount of work has been done in evaluating these material characteristics and studying how they are affected by the space environment. The OSO space experiments are the most notable in which promising coatings were evaluated under orbiting conditions. Data from these experiments were used in this study to determine heat inputs and surface temperature histories for the specific conditions to be evaluated.

Two distinct tasks were undertaken in this phase: (1) the optimum surface coating was determined by evaluating vehicle heat inputs for a variety of coatings as a function of time in orbit, and (2) temperature histories were evaluated for the best of the candidate coatings.

a. Coating Evaluation. At the outset of the study, the surface property and property degradation data of reference 17 were available. Additional results from OSO-II data were requested and received from the Ames Research Center (reference 18), completing the accumulation of available data.

To determine the optimum surface coatings, a simple model of the orbiting vehicle was analyzed. The vehicle was assumed to be cylinder with flat ends with its longitudinal axis aligned parallel to the velocity vector. A 260 n. mi. altitude orbit was considered with an orientation that would yield approximately 66 min. of exposure to the sun and 28 min. of shadow time.

Figure 4-54 depicts the orbit geometry utilized in the thermal analysis. The specification of the orbit in relation to positions on the Earth's surface depends on the frame of reference selected; however, for the purpose of analyzing the thermal history of the vehicle in a circular orbit, the angle between the normal to the orbit plane and the Earth-sun line uniquely specifies the orbit. This angle was determined to be 38.5° on the basis of the specified 66 min. of sunlight and 28 min. of shadow per orbit.

The initial vehicle position in orbit was arbitrarily taken as the point directly over the terminator prior to entry into the shadow. As indicated in figure 4-54, the rotation of the vehicle about its axis has been considered.

The vehicle analyzed consisted of two compartments, one containing LH_2 and the other LF_2 . The total steady-state heat transfer to the vehicle interior throughout one orbit was calculated for several surface coating conditions. The results of the analysis are presented in figure 4-55 for a number of promising surface coatings. It is readily apparent that the zircon in KSi_4 coating is the most favorable for all mission durations.

b. Determination of Temperature Histories. Surface temperatures were computed by a Douglas orbital heating computer program (JD56), using the zircon in potassium silicate coating. In addition to the conditions already specified, the forward end of the vehicle (payload end) was maintained at 40°F . The aluminum propellant tanks were assumed insulated with high-performance insulation.

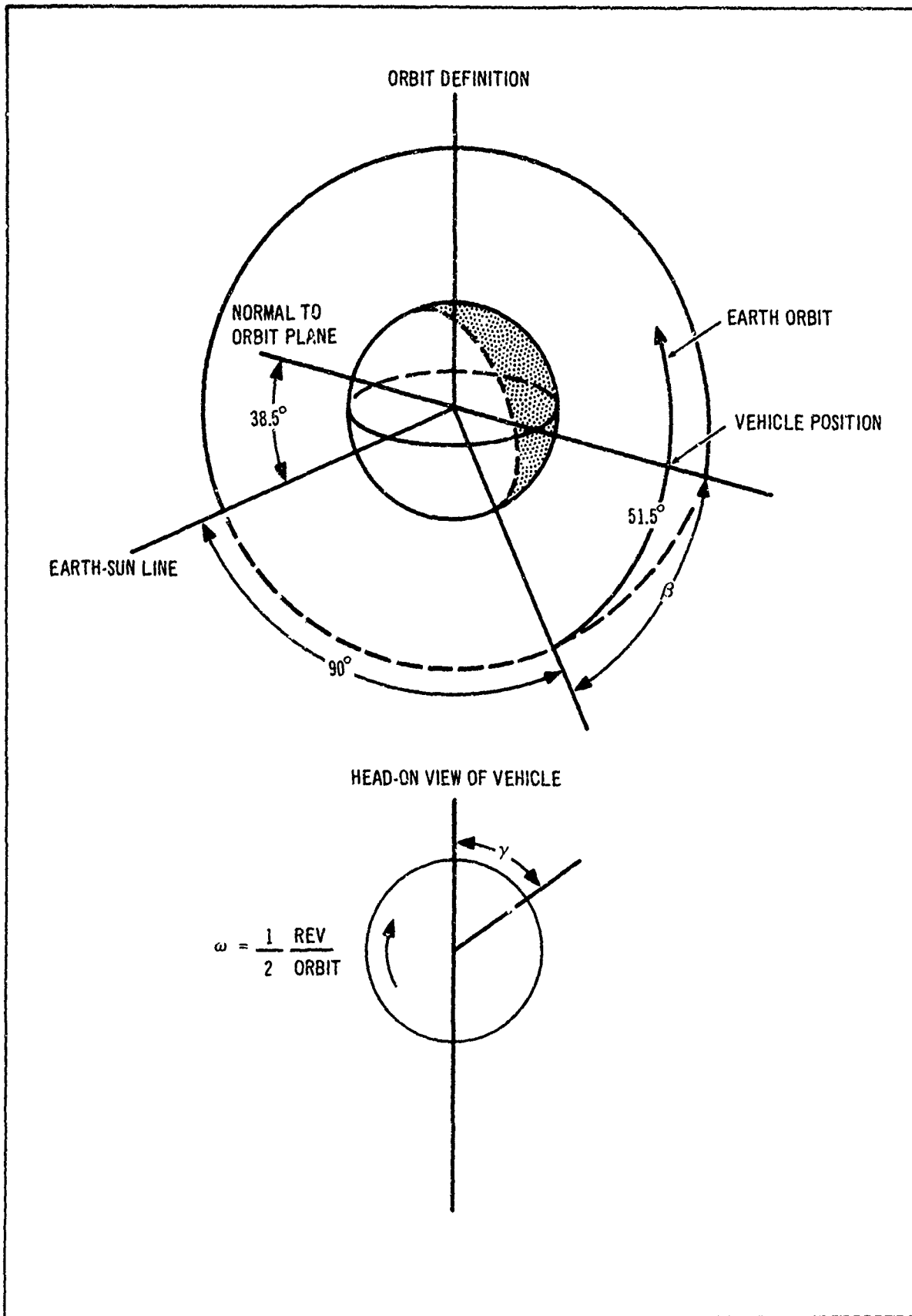


Figure 4-54. Geometry Definition

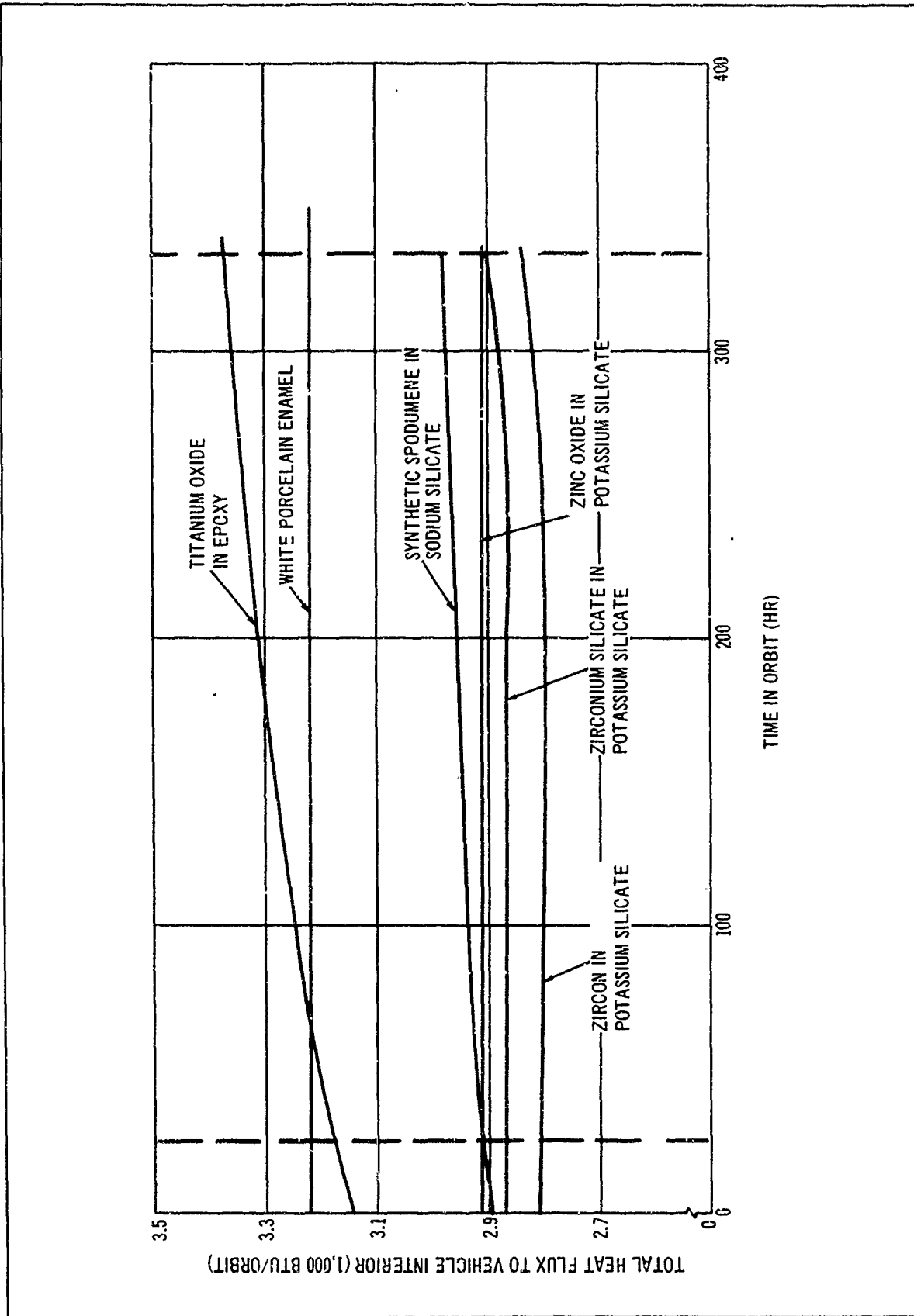


Figure 4-55. Space Performance Comparison of Various Thermal Coatings

Conduction paths from the tanks to the sidewalls and the aft end simulated steel piping. Also, glass fiber supports from the tanks to the sidewalls were simulated. The calculated surface temperatures revealed that the effect of conduction parallel to the vehicle surface was small. The longitudinal variation in sidewall temperatures was generally less than 10°F . Hence, only the sidewall temperatures at the center of the vehicle are presented in figure 4-56 and 4-57.

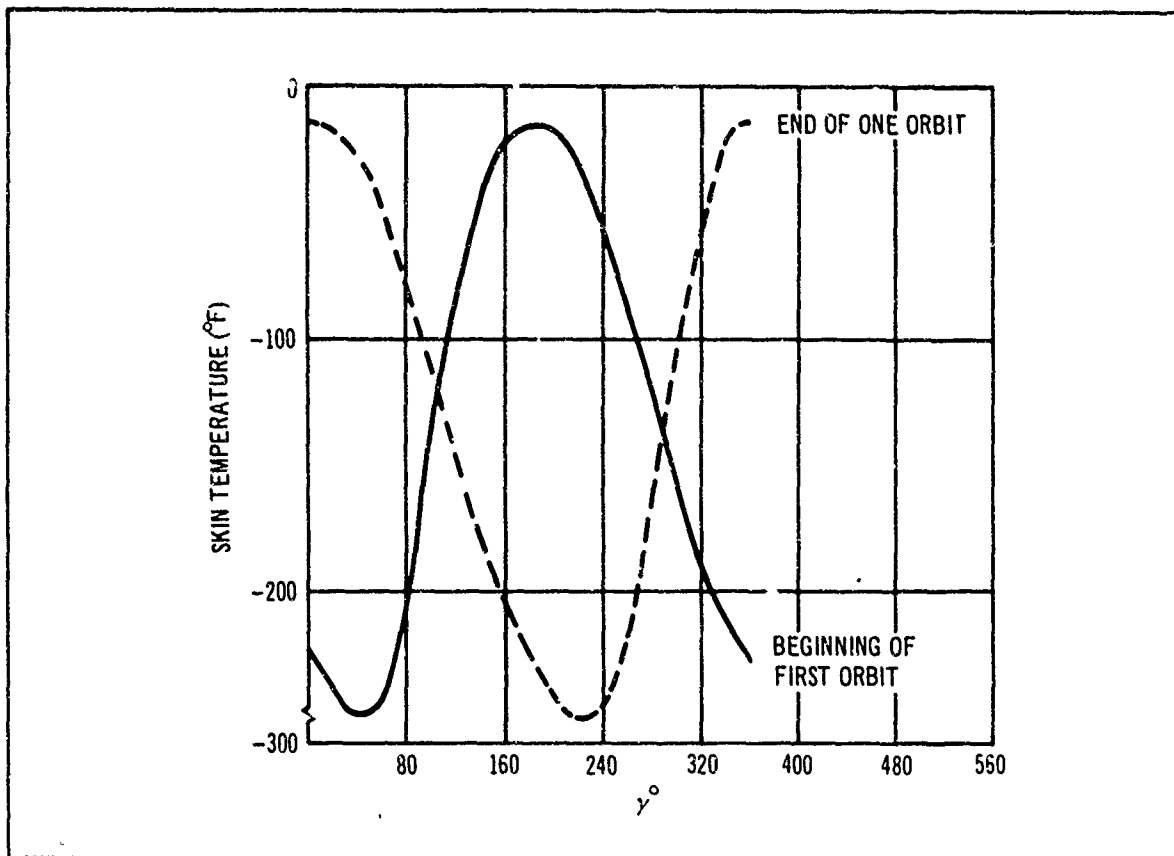


Figure 4-56. Circumferential Variation in Skin Temperature

Steady-state cycling of the surface temperatures was achieved after four orbits. In figure 4-56, the circumferential variation in sidewall temperatures is shown at the beginning and end of one orbit. In figure 4-57 the temperature histories throughout a complete two-orbit cycle are presented for three equally spaced sidewall positions, together with the vehicle end temperatures.

5. Phase V--Propellant Utilization. Propellant utilization, referred to here as P. U., is defined as the ratio of propellant consumed in flight (if the engine is allowed to burn to a propellant depletion) to the total usable propellant loaded. This is an important value since it is a measure of the total impulse available for imparting vehicle velocity. For this reason, the P. U. system is optimized for maximum performance on all rocket propulsion systems.

Determination of the P. U. for a rather broadly defined study vehicle is difficult since the results are highly dependent on the assumptions used in the analysis. For an actual vehicle, the P. U. analysis would be based on actual

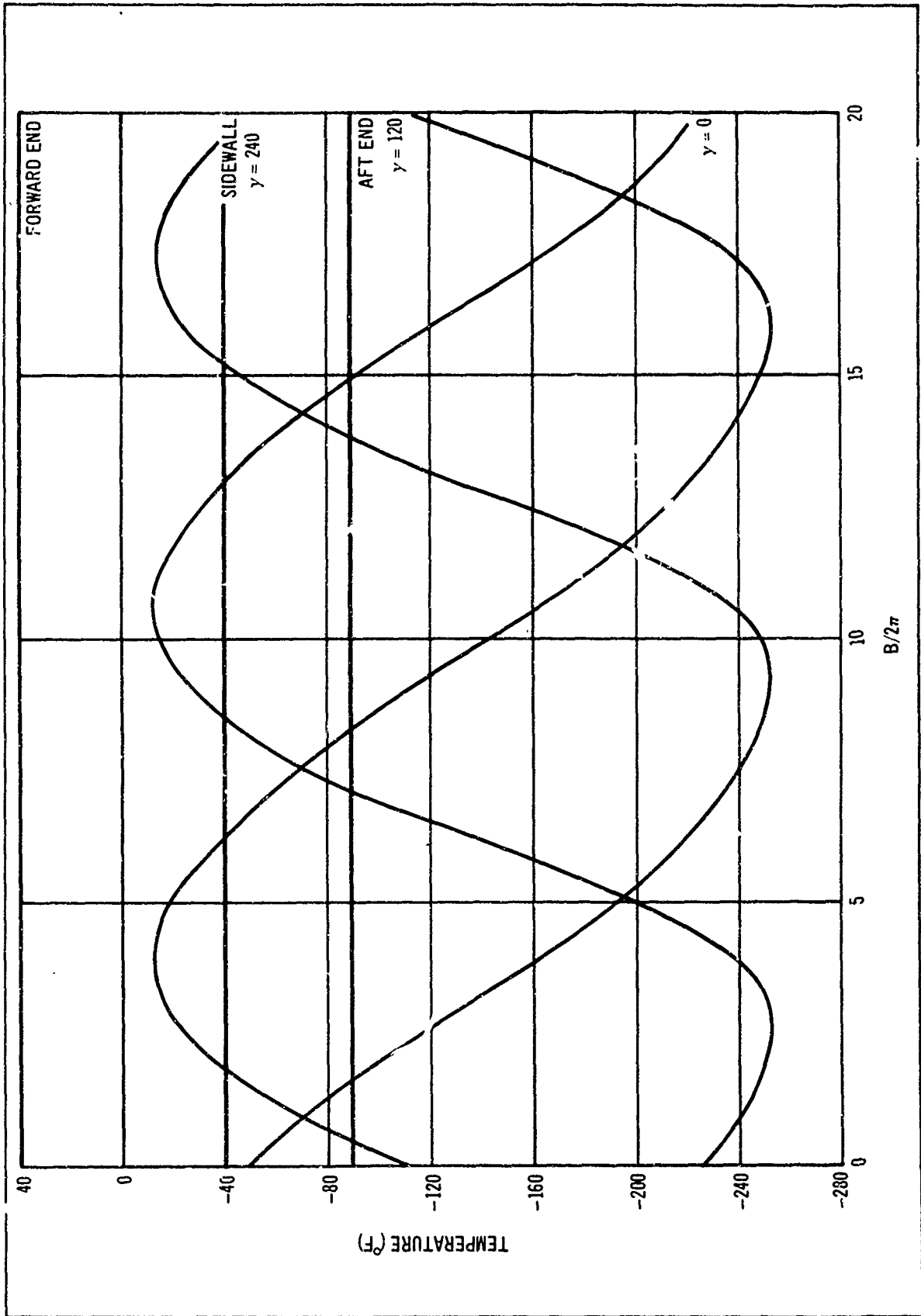


Figure 4-57. Temperature Histories of Vehicle Surfaces

experimental engine coefficients, a well defined mission including previous telemetered mission data, and a well calibrated vehicle system. Under such conditions there would be a high confidence level that a particular P. U. would be achieved. For the purposes of this analysis, assumptions were made for the pertinent experimental variables described above, and the Propellant Utilization Monte Carlo Program (F807) was used to simulate the numerous flights required to achieve a high confidence level. Thus, the P. U. values obtained are representative of the P. U. which would be realized after a number of missions and vehicles have been flown (and thus some of the bugs eliminated and some experience gained) and is probably somewhat higher than the P. U. to be expected on the initial flights. The assumptions made for the P. U. system analysis are intended to be as realistic as possible and thus result in representative values for the expected P. U.

Two types of P. U. systems are in current use: (1) an open-loop system, and (2) a closed-loop system. Both systems can produce accuracies of 99 pct. or better for properly calibrated propulsion systems, and the choice of one or the other is determined by the requirements of the specific system.

a. Open-Loop P. U. System. An open-loop system is inexpensive, reliable, and does not require black boxes or flight hardware. To attain this simplicity and reliability, it relies entirely on system predictability prior to flight, and no control of propellant utilization is possible after vehicle liftoff.

The open-loop system has been successfully demonstrated on the Thor vehicle. A guarantee of 99 pct. was established and the present P. U. average is 99.75 pct. (Whether the open-loop system would look as good with two cryogenics on Thor is questionable.) By comparison, the Saturn vehicle with its closed-loop system has a P. U. average of approximately 99.995 pct.

The accuracy of the open-loop system lies in the ability to predict the amount of propellants required to perform a given mission and the ability to load them accurately. The prediction of the propellants used in flight depends on the accuracy of the tag engine mixture ratio furnished by the engine manufacturer and the accuracy of the influence coefficients that determine the changes in mixture ratio that occur in flight as the operating conditions change. These coefficients become more and more accurate as flight experience is gained. For this study, coefficients were used which had been obtained from Bell for a H₂/F₂ engine of the 30,000-lb. thrust class. These coefficients had been used previously for the Delta II study and are shown in table 4-18.

The accuracy of loading the propellants depends on the instrumentation used to measure the specified quantities and the accuracy of the tank calibrations.

It would seem that the predicted propellants should be loaded so that, if everything operated normally, the engine would run out of each propellant at exactly the same time. This is not necessarily true, because of unpredictable variations and tolerances in the propulsion system operation conditions. Therefore, variations in open-loop propellant utilization depend on variations in tag mixture ratio, engine influence coefficients, propellant loading, and system operating conditions.

Table 4-18
 DEVIATIONS USED FOR DETERMINING FUEL BIAS
 (E. M. R. 13:1)

	Percent	Actual
<u>Pump-fed (1σ)</u>		
Oxidizer loading	0.5	59 lb.
Fuel loading:	1.32	12 lb.
• Propellant loading 0.5 pct.		
• Fuel venting 1.2 pct.		
Mixture ratio:	1.48	0.193
• Inlet conditions 1.25 pct.		
• Engine tag values 0.15 pct.		
• Duty cycle 0.73 pct.		
<u>Pressure-fed (1σ)</u>		
Oxidizer loading	0.5	59 lb.
Fuel loading:	0.77	7 lb.
• Propellant loading 0.5 pct.		
• Fuel venting 0.55 pct.		
Mixture ratio:	3.11	0.405
• Inlet conditions 1.25 pct.		
• Engine tag values 0.15 pct.		
• Duty cycle 2.83 pct.		
<u>Propellants</u>		
LH ₂ -908 lb.		
LF ₂ -11,800 lb.		
<u>Engine Influence Coefficients</u>		
$\Delta W_f / \Delta P_f$ inlet = 0.067 pct./p. s. i.		
$\Delta W_f / \Delta T_f$ inlet = -1.0 pct./°R.		
$\Delta W_o / \Delta P_o$ inlet = 0.033 pct./p. s. i.		
$\Delta W_o / \Delta T_o$ inlet = -0.3 pct./°R.		

Previous P. U. analyses have shown that with a system mixture ratio (O/F) of greater than 1.0, the open-loop P. U. can be improved by loading extra fuel (called a fuel bias). With a mixture ratio of 13, 1 lb. of fuel will combust with 13 lb. of oxidizer, or 10 lb. of fuel bias will absorb an error of 130 lb. in oxidizer usage. For this reason, a fuel bias can be used to absorb random errors in oxidizer usage and achieve higher propellant utilization.

Since the variations in the open-loop loadings are random in nature and not interrelated, the determination of the proper fuel bias and the P. U. probability cannot be handled by normal mathematical analysis. For this reason, a statistical Monte Carlo program (F807) was used to determine the optimum fuel bias and associated P. U. probability. This program has been successfully used for identical purposes on the Thor first-stage pump-fed engine and the Delta second-stage pressure-fed engine. Basically, the program consists of a set of equations defining P. U. in terms of mixture ratio, propellant loading, and burn time. One sigma variations are assigned to the variables in the equations and the program set to randomly pick a set of values for each run or flight. By repeating this process approximately 5,000 times, a P. U. probability distribution can be generated for each fuel bias.

The results for this study are shown in figures 4-58 and 4-59 and for a pump-fed system and a 250 p. s. i. pressure-fed system. The deviations used in each case are tabulated in table 4-18. An examination of the curves substantiates the fact that an open-loop system is at its best with a high mixture ratio. An increase in fuel bias absorbs all the error in the oxidizer side and leaves only the additional error of a few pounds of fuel bias that do not affect the P. U. to any great extent as the fuel bias is increased.

The deviations (table 4-18) used in setting up the Monte Carlo program strongly influence the results and must be discussed, particularly those that are peculiar to this system; namely, fuel venting effects and variations, duty cycle, and throttling variations. Other deviations, such as propellant loading deviation and initial loaded pressure and temperature deviations, were taken from Thor and Saturn data as standard percentage values.

Fuel venting is dependent on the type of pressurization system assumed, the mission, and the system pressure. For this analysis, a heated helium pressurization and ambient helium repressurization system were assumed. Under these assumptions, only a few missions vented the fuel tank; principally the low-pressure pump-fed systems. At no time did the oxidizer tank vent. The heat load to the fuel, and thus the amount vented, depends on the assumed vehicle wall temperature, and the magnitude of the heat shorts; this is one of the major system unknowns. Thus, the most conservative possible assumptions in vent rate were used. One of the most severe venting cases is mission K (80/20 burn with 14-day coast) for the low-pressure (pump-fed) case. A number of runs were made with the Douglas computer program H109, Multi-start Propulsion System Sizing Program, for this mission to determine the effect of venting or extreme changes in vehicle wall temperatures, system run, and vent pressure. The results are shown in table 4-19. The extreme wall temperature changes were selected to reflect the maximum

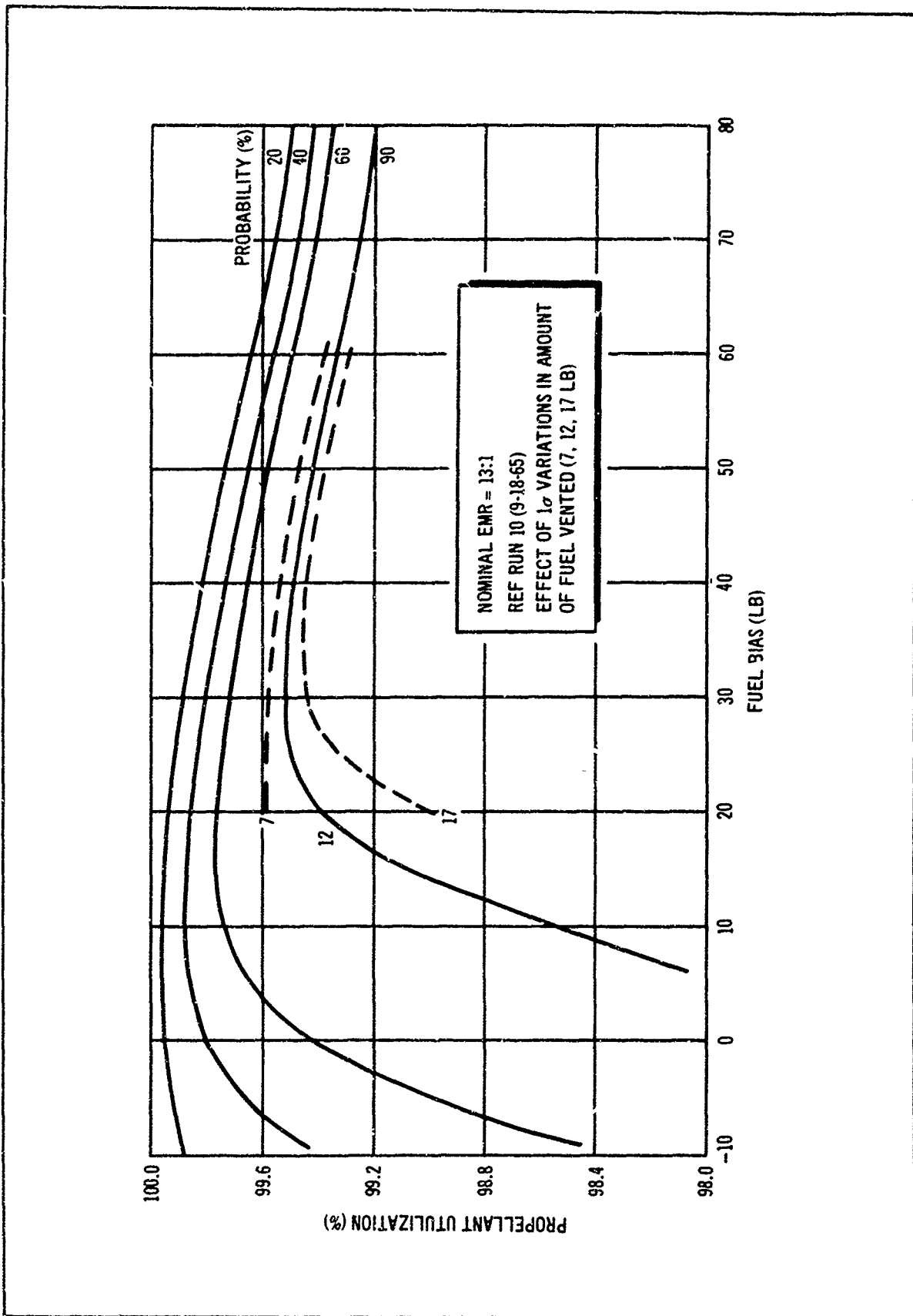


Figure 4-58. Propellant Utilization as a Function of Fuel Bias for Pump-Fed System H₂ - F₂

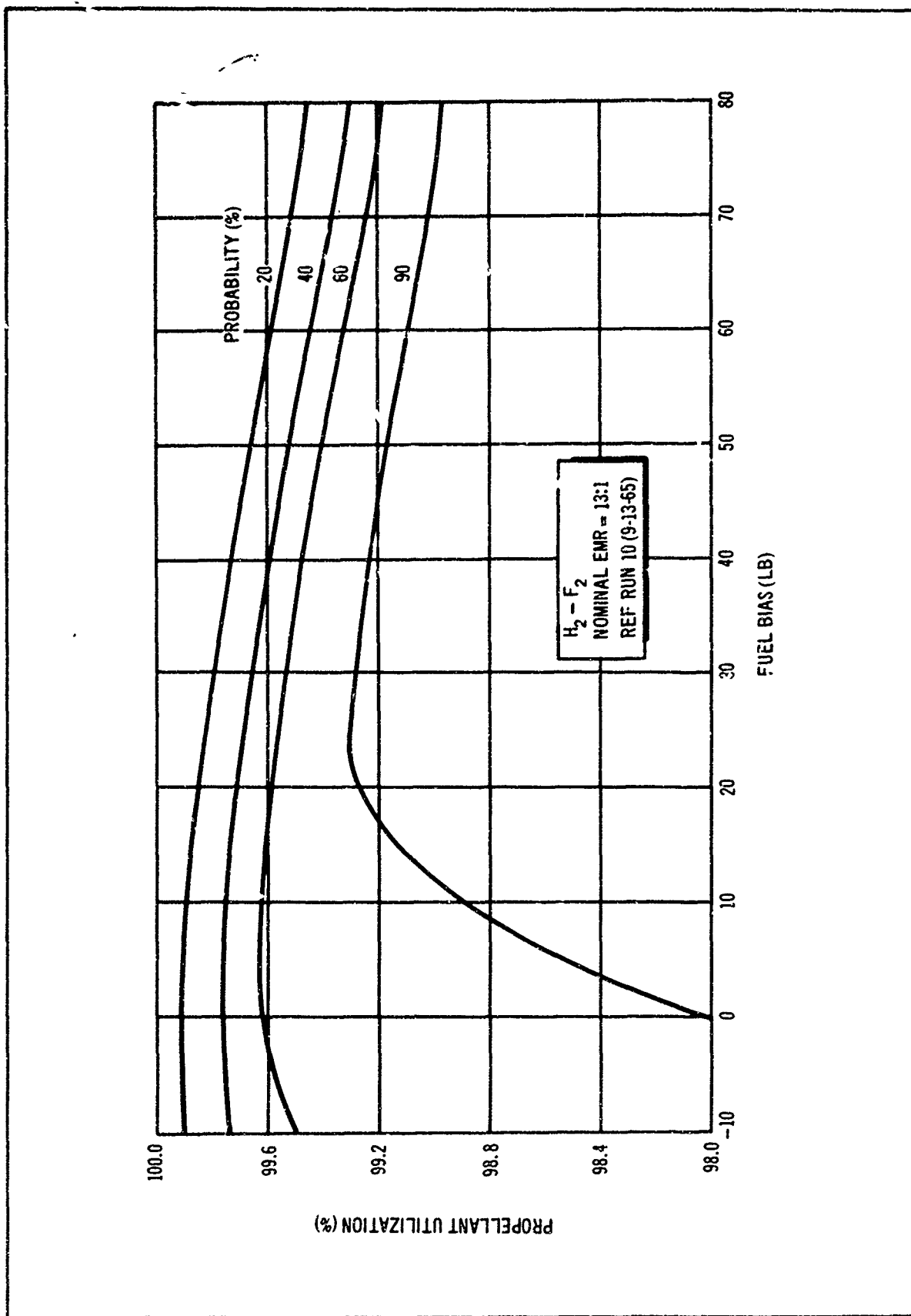


Figure 4-59. Propellant Utilization as a Function of Fuel Bias for Pressure-Fed System

heat load variation expected, rather than actual wall temperature variation expected. The maximum deviation from nominal were chosen as 3σ variations and accounted for in the fuel loading variations, since the nominal amount of vented fuel would have to be added to the open-loop fuel loading.

Table 4-19
 H_2 VAPOR VENTED
 (80/20 Run--14-day Duty Cycle)

Vent Pressure	Condition Pressure	Wall Temperature ($^{\circ}R$)		
		350	400	450
24	20	52.62	71.45	95.23
	21	51.55	70.32	94.50
	22	50.42	69.12	93.16
25	20	52.47	70.55	94.69
	21	51.15	69.96	93.45
	22	49.85	68.58	92.68
26	20	51.67	70.48	94.69
	21	51.09	69.38	93.20
	22	49.84	68.55	92.58

Since the duty cycles are so varied, the fuel vented can range from zero to the amount shown in table 4-19. This is a source of error in the open-loop system which has but a small effect on P. U. probability. This is because that extra fuel, added for venting, which is actually not vented, just acts as additional fuel bias. This effect is shown in figures 4-60 and 4-61.

In the pressure-fed engine system, the venting is reduced to a very small quantity in the 75-p. s. i. system and to none in the 250-p. s. i. system. This is reflected in the smaller sigma fuel-loading deviation shown for the pressure-fed system. No venting occurs on the oxidizer side because of the subcooled condition of the fluorine. Therefore, the only effect from heat transfer is a variation in oxidizer temperature which in turn affects mixture ratio. This effect is covered under duty cycle variations below. The temperature rise that normally occurs at the end of flight due to tank stratification is not significant because the majority of duty cycles burn only part of the propellant each time with zero-g., coast, and destratification between burns.

The biggest variable in the prediction of open-loop propellant utilization is the mixture ratio shift that occurs due to the variety of missions or duty

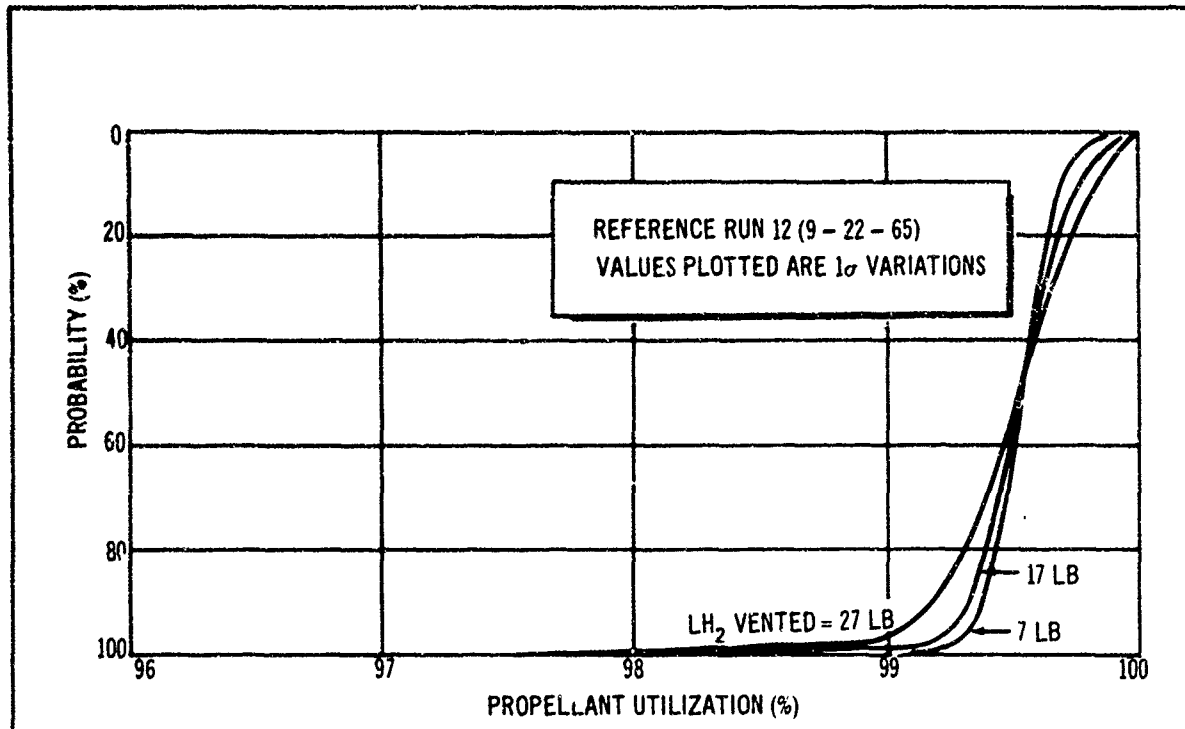


Figure 4-60. Effect of Variation in Fuel Vented with a Pump-Fed System (Fuel Bias of 60 lb)

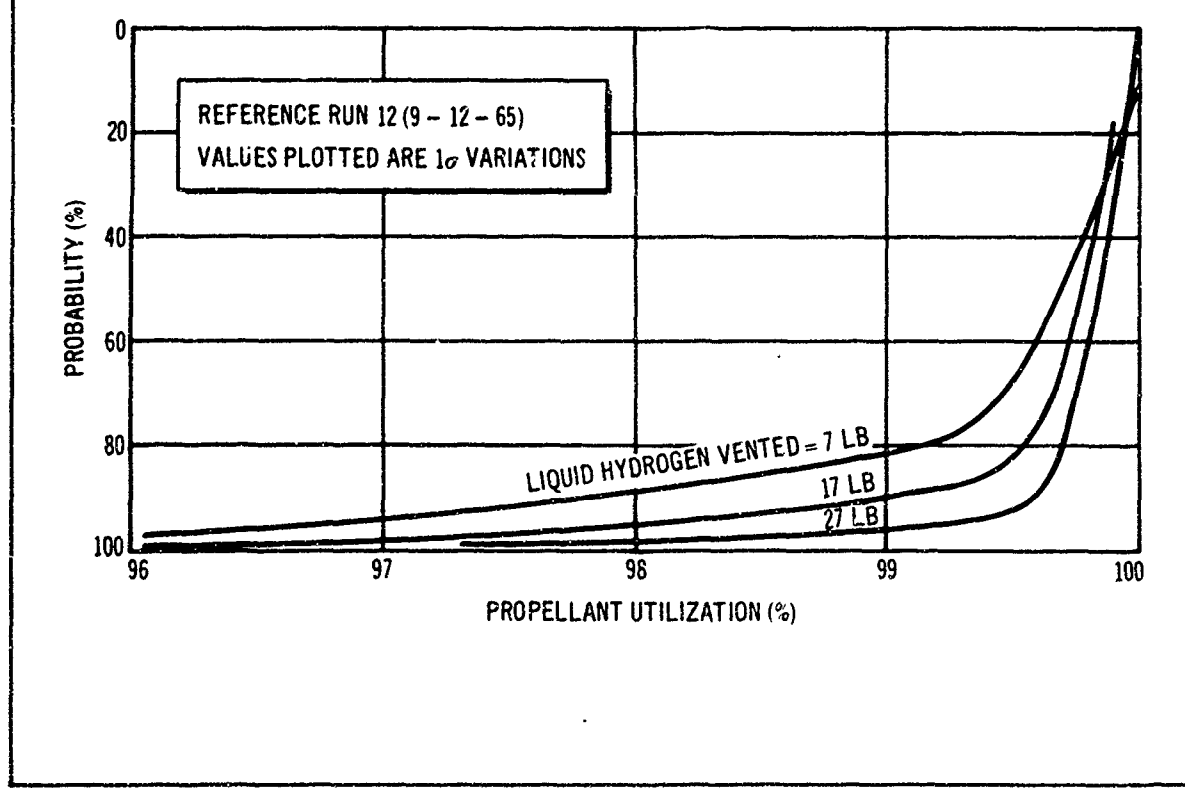


Figure 4-61. Effect of Variation in Fuel Vented with a Pump-Fed System (Fuel Bias of 20 lb)

cycles that may be assigned to the vehicle. It is assumed that the mission assignment is unknown, which means that an open-loop loading must cover all possible duty cycles at the highest possible P. U. level. The effect of this variety of missions is to make possible a large variation in propellant inlet temperature and pressure conditions which produce corresponding shifts in mixture ratio.

For the pump-fed case, the inlet pressure changes are small on the fuel side, and from 0 to 15 p. s. i. on the oxidizer side. However, the influence coefficients are so small that the inlet pressure effect on mixture ratio is comparatively small for both oxidizer and fuel. The temperature effects are quite significant. The oxidizer temperature spread is 12° and the fuel temperature spread is 2°. The spread of only 2° in fuel temperature is explained by the fact that the fuel is conditioned to provide N. P. S. H. prior to each burn in the pump-fed case. This is fortunate from a P. U. standpoint, since it results in a fairly small excursion in engine mixture ratio (E. M. R.) (see figure 4-62).

In the pressure-fed case, the oxidizer temperature spread is 20° and the fuel temperature spread is 20°. This results in a fairly large change in E. M. R. (see figure 4-62) since the influence coefficient for fuel temperature effect on mixture ratio is 3.5 times that shown for the oxidizer temperature effect on mixture ratio. Fortunately, the coefficients are of opposite sign. The flat portion of the 250-p. s. i. E. M. R. curve (figure 4-62) is caused by the fact that the burn cycles are clustered at the beginning and end of the duty cycle and relatively hot pressuring gas is being added to condition for each burn. The large spread in mixture ratio for the pressure-fed cases causes the 1- σ variation in mixture ratio to be 2.1 times as great for the pressure-fed case as the pump-fed case in the Monte Carlo program. This results in the 90 pct. probability curve being approximately 0.2 pct. worse in P. U. for the pressure-fed system (figure 4-58 and 4-59).

Selection of an actual fuel bias for the system is somewhat arbitrary in that a number of biases in a certain range can be selected which will not result in changing the P. U. probability markedly. However, the fuel bias value of 30 lb. was picked so that a large variation in fuel vented would not drop the 90 pct. probability (pump-fed case) below the 99.1 pct. P. U. level. The pump-fed case was used since it had the greatest possible variation in fuel vented. The amounts of fuel to be added to the fuel loadings were 55 lb. for the pump-fed case and 15 lb. for the pressure-fed case.

The effect of throttling was found to be minor and masked by other duty cycle and mission variations. Limited data for the RL-10 engine showed that the engine regained its nominal mixture ratio at the throttled condition after approximately 2 sec. of operation. This would result in extremely minor shifts in mixture ratio averaged over the overall burn period and would not change the results of this analysis.

In summary, the results of the open-loop propellant utilization survey indicate that a pump-fed system could attain a maximum P. U. of 99.5 pct. with a 30-lb. fuel bias at a 90 pct. confidence level, and that a pressure-fed system could attain a P. U. of 99.3 pct. under the same conditions but with a 25-lb. fuel bias.

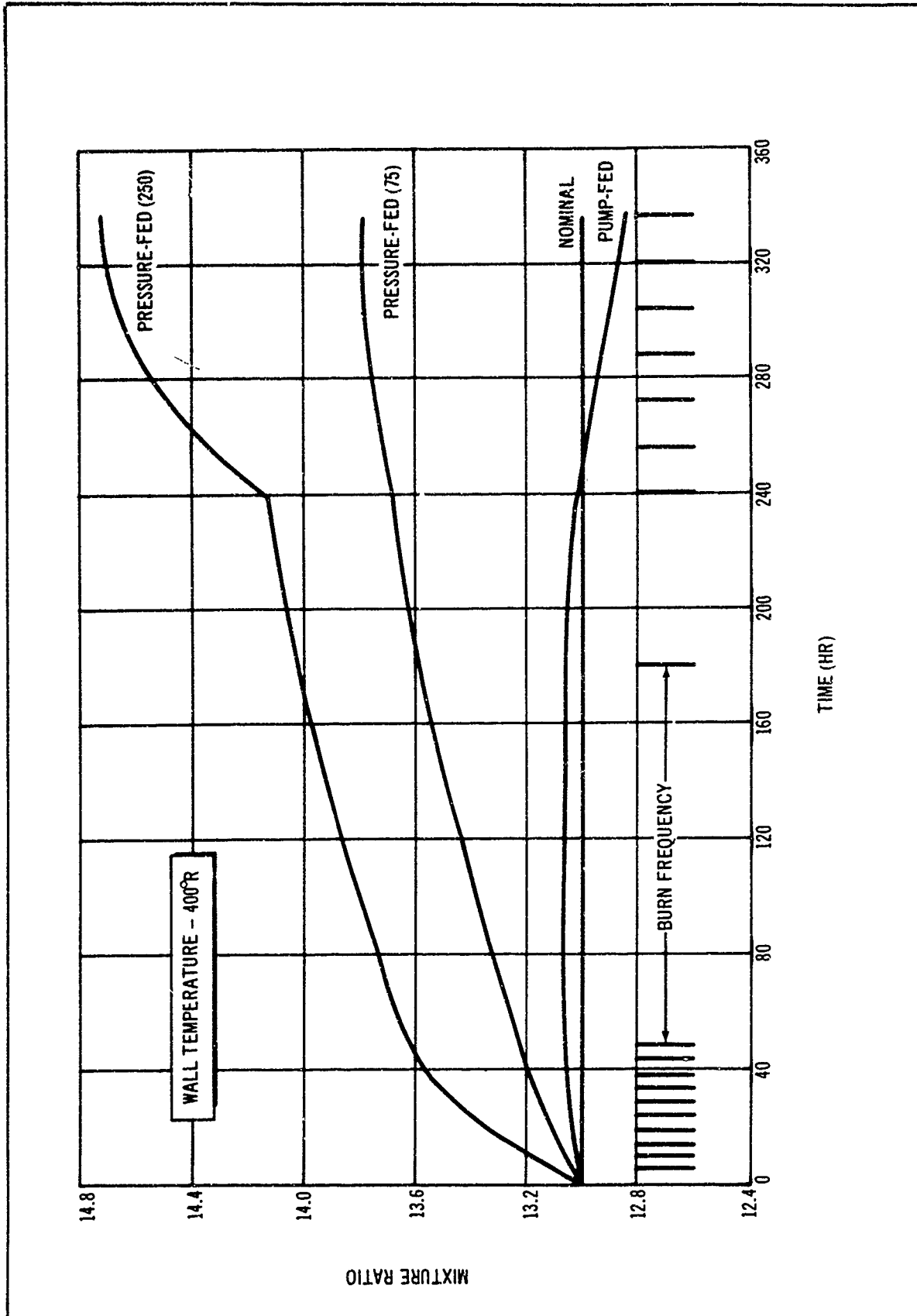


Figure 4-62. Variation in Engine Mixture Ratio (19 Burn - 14 - Day Duty Cycle)

If the system is to be mission independent, then the P. U., shown in table 4-23, could be obtained with the appropriate fuel bias.

b. Closed-Loop P. U. System. The above section discussed the open-loop system which predicted the amount of fuel to be loaded for a given oxidizer load and whose accuracy was based entirely on the validity of this prediction and the accuracy with which these propellants could be loaded.

The closed-loop system, on the other hand, does not need as exact a fuel loading, since it monitors in-flight mixture ratios and changes the engine flow rates in order to use the entire propellant load. If the initial loading is fairly accurate, the system operates at nearly nominal mixture ratio and the only penalty is the weight, cost, and potential reliability decrease of the closed-loop P. U. system. Several closed-loop P. U. systems are in operation at the present time with very high accuracies. The system on Saturn has, so far, provided a P. U. of 99.995 pct. and the Acoustica system, designed for a maneuvering satellite, claims the same 99.995 pct. accuracy.

Although this kind of accuracy cannot be matched by an open-loop system, it should be noted that the peculiar requirements of the study vehicle, with its variety of duty cycles, actually lowers the closed-loop P. U. available from a pump-fed system as much as 0.8 pct. This makes the overall P. U. available slightly less than that shown for an open-loop system. The reason for the drop in P. U. available for the closed-loop system is because the long coast periods between burns result in fairly large amounts of fuel being vented, which cannot be compensated for in the remaining burn time available. This situation was noted during two duty cycles, the 50/50 burn and the 80/20 burn 14-day missions.

With a closed-loop P. U. system capable of operating at off-mixture ratios of 10 pct. or even 15 pct., above nominal mixture ratios, it was found that the control could operate at maximum mixture ratio continuously and still not be able to burn the oxidizer equivalent of the fuel that had been vented. More important, it was found that the engine was forced to operate at a mixture ratio of 14.3 (10 pct. system) or 14.95 (15 pct. system) for the duration of the second burn period in each case, at reduced efficiency levels.

With no bias whatsoever and a nominal amount of fuel vented before the second burn period, it was found that unacceptable amounts of oxidizer would be left in the tanks (table 4-20). However, without knowing the characteristics of the closed-loop control, it was assumed that fuel could be added in excess of that required for a 13:1 mixture ratio and the control biased so that it did not see this fuel at any time in flight. This unseen fuel would offset the fuel vented, and the only penalties would be the off-mixture ratio operation of the engine and any bias fuel residual that might result.

An actual fuel bias of 64 lb. was finally established for a closed-loop system with a 10 pct. off-mixture ratio operating range as follows:

A basic fuel bias of 52 lb. was found for the 50/50 and 80/20 cases which would give a minimum fuel residual (figure 4-63) with nominal vent quantities of 69 and 71.5 lb. of fuel.

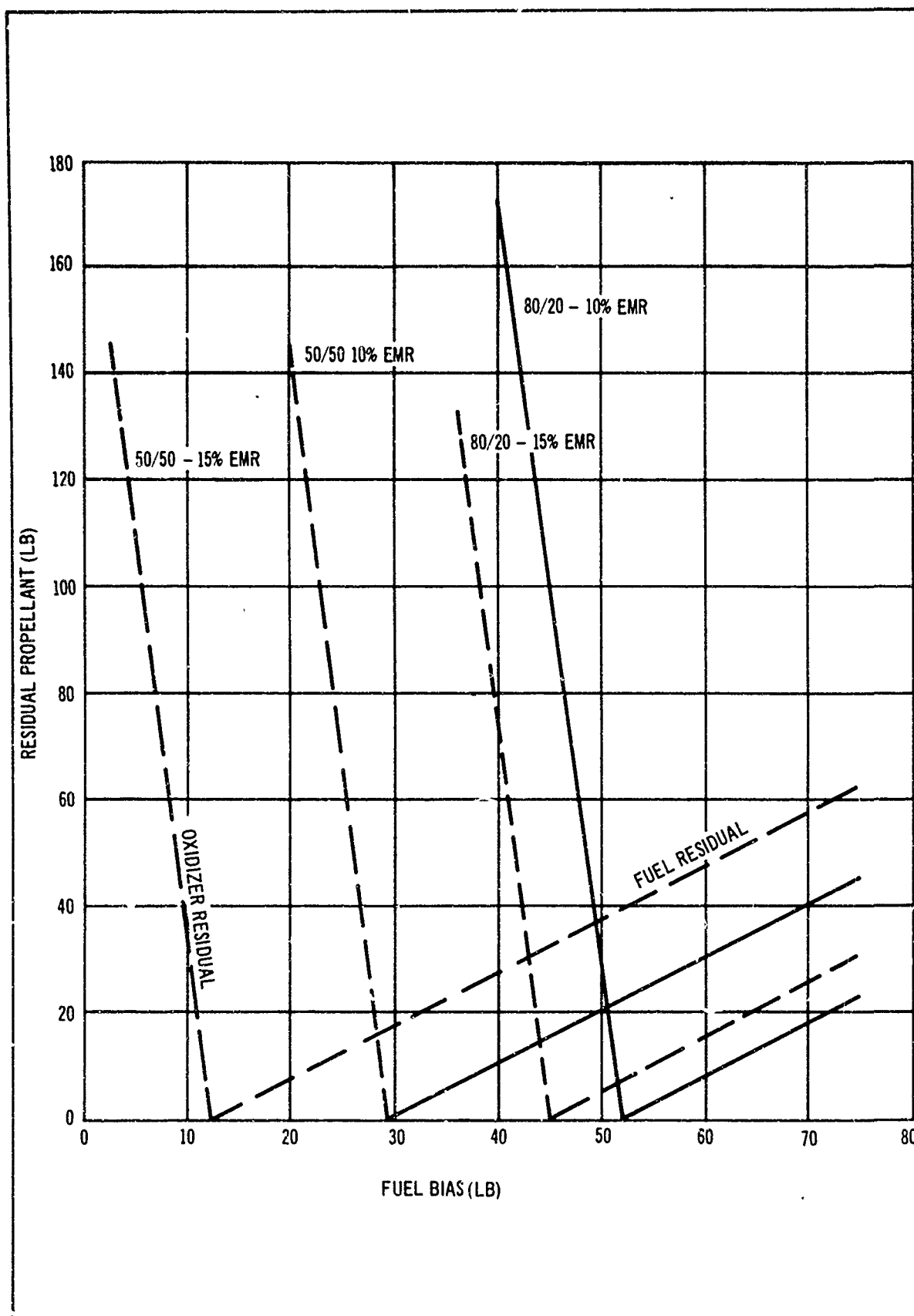


Figure 4-63. Optimum Bias for a Closed-Loop Propellant Utilization System for a Pump-Fed System with Nominal Venting (H109 Program)

Table 4-20
EFFECT OF FUEL BIAS ON CLOSED-LOOP PUMP-FED SYSTEM

Duty Cycle	Fuel Vented (lb.)	M. R. (+10 pct.)	Bias (lb.)	Residual Oxidizer (lb.)
80/20 (14 days)	69 (nominal)	14.3	0	744
	81.4 (1.65 σ)	14.3	0	922
50/50 (14 days)	71.5 (nominal)	14.3	0	431
	83.9 (1.65 σ)	14.3	0	608
80/20 (14 days)	69.0	14.3	52	0
	81.4	14.3	52	178
50/50 (14 days)	71.5	14.3	52	23 (fuel)
	83.9	14.3	52	9.6 (fuel)
80/20 (14 days)	69.0	14.3	64	12 (fuel)
	81.4	14.3	64	0 (fuel)
50/50 (14 days)	71.5	14.3	64	34.5 (fuel)
	83.9	14.3	64	22.1 (fuel)

- Variations in nominal vent quantities with 90 pct. probability limits were taken from the H109 program (± 12.4 lb.).
- A new fuel bias was established to cover the uncertainty in quantities of fuel that would be vented.

The criteria used for establishing this bias was that the minimum fuel bias of 52 lb. would be the lower 90 pct. probability limit for the highest vent condition established in the second item above. This point was chosen so that no oxidizer residuals would be obtained (at a 90 pct. probability level).

- Using the 64-lb. fuel bias, fuel residuals were obtained for the nominal 50/50 and 80/20 cases and these values statistically added with all the other duty cycles which had 64-lb. residuals. This resulted in an actual fuel residual very close to 64 lb. for all missions since the P. U. control burns everything except the fuel bias.

Once the average flight residual was established, the other penalty assessed the system was the amount of time at which the P. U. system would be operating at a maximum off-mixture ratio condition. The performance of the engine was assumed as shown in figure 4-64 on the basis of NASA experimental data and an assumed efficiency. Note that the performance drops off as mixture ratio increases. This is in accordance with experimentally observed effects and is generally attributed to increasing disassociation and ionization effects. Although the performance shown is for a chamber pressure of 50 p. s. i. a., the trend is identical for other chamber pressures. Therefore, operation at higher than nominal mixture ratio results in decreased I_{sp} which is convertible to a vehicle ΔV loss or equivalent weight penalty. Using the off-mixture ratio rise shown in table 4-21 and the performance decrease shown in figure 4-64, the velocity loss due to operation at high mixture ratio for each duty cycle was established. This number was then converted to a percentage P. U. equivalent.

In summary, the effects of (1) the closed-loop system weight, (2) the bias fuel residual to help offset fuel venting, and (3) the penalty of off-mixture ratio operation (+10 pct.) to burn excess oxidizer resulted in an average closed-loop system P. U. of 98.65 pct. (table 4-22). This applies to a 1/2 pct. basic P. U. system at a 90 pct. probability level under pump-fed conditions. Basic systems of 1 pct. and 2 pct. would be correspondingly worse.

On a comparison basis, this is slightly less than an open-loop pump-fed system where a 99.1 pct. P. U. was established. Apparently, the reason for this is that the closed-loop system is operating at an off-mixture ratio condition for a significant part of several missions, while the open-loop system is not. This offsets the advantage of the closed-loop system which burns to a zero propellant condition when given sufficient time.

If a closed-loop system with a 15 pct. off-mixture ratio control is used, the P. U. drops slightly to 98.56 pct. under the same conditions since the I_{sp} is lower at the 15 pct. off-mixture ratio condition (table 4-22).

On the other hand, the closed-loop system on a pressure-fed system appears to offer substantial improvement over the open-loop system. This results from the fact that (1) very little venting occurs with the pressure-fed system to cause problems such as those discussed above, and (2) the closed-loop P. U. control will hold the mixture ratio at 13:1 even though the engine pump inlet temperature and pressure buildups with time are such that they tend to shift the mixture ratio continually to higher values (see figure 4-62).

This shift in E. M. R. that occurs with duty cycle variations amounts to an average velocity loss of approximately 74 f. p. s. for the open-loop system or a relative improvement in P. U. for the closed-loop 75-p. s. i. system of 0.29 pct. With a 250-p. s. i. engine operating level, the improvement is even greater (0.456 pct.) since the velocity loss is approximately 120 f. p. s. for an open-loop system. This effect is independent of propellant utilization since the comparison is made on the same amount of propellants burned and only depends on mixture ratio shifts caused by changes in inlet temperature and pressure in the open-loop system.

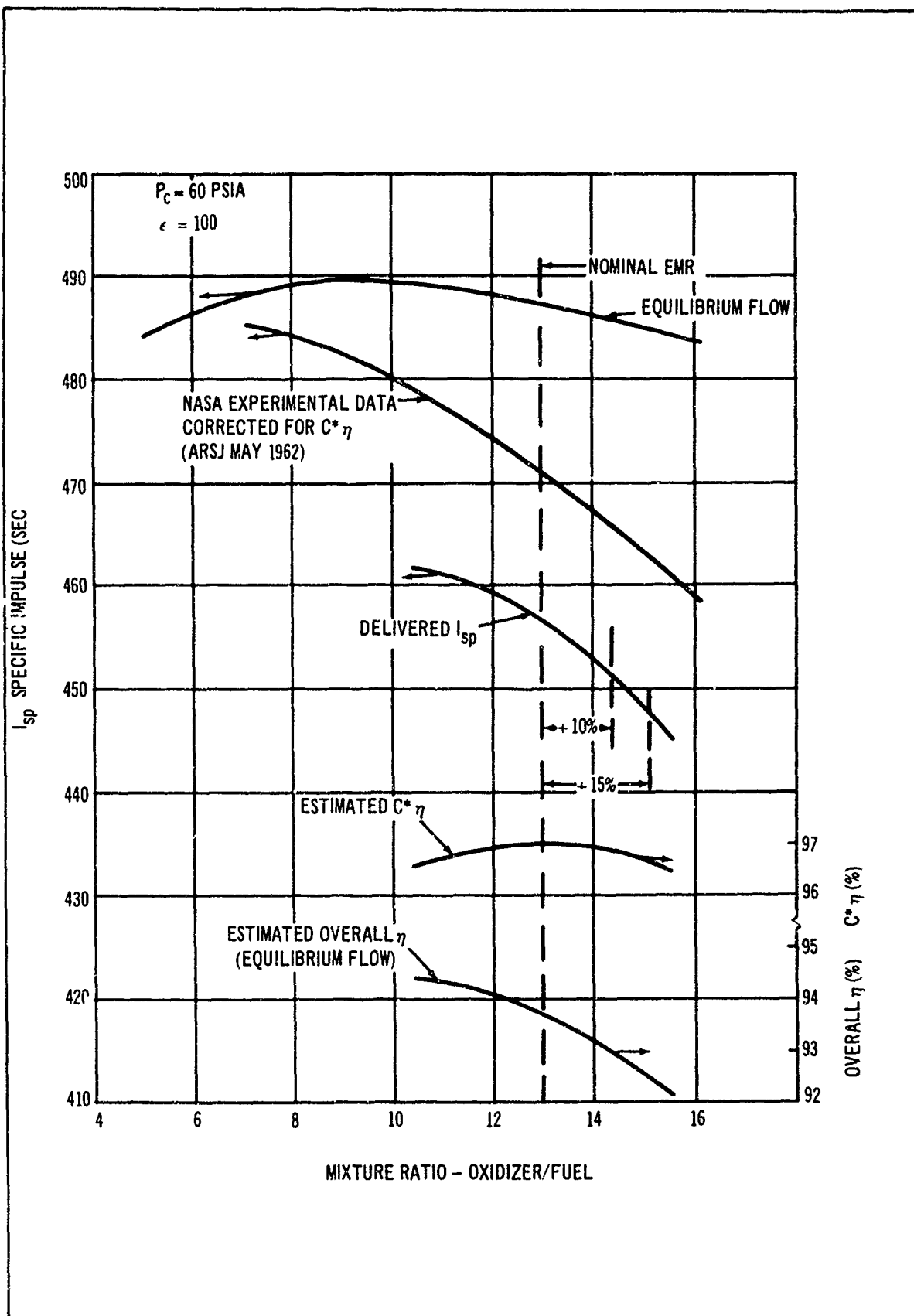


Figure 4-64. $F_2 - H_2$ Vacuum Performance

Table 4-21
CLOSED-LOOP PUMP-FED SYSTEM
 (10 pct. off E. M. R.)

Duty cycle	Vent Loss (lb.)	Fraction Off E. M. R. Time	ΔV (f. p. s.)	ΔV Loss (f. p. s.)
A	0	0	0	0
B	0	0	0	0
C	0	0	0	0
D	0	0	0	0
E	0	0	0	0
F (80/20)	16.3	0.90 of second burn	48.59	43.7
G (1)	19.0	0.21	170.07	34.0
H (19)	18.6	0.20	170.07	34.0
I (1)	72.3	0.79	170.07	134.0
J (50/50)	71.5	All of second burn (0.50)	105.00	105.0
K (80/20)	69.0	All of second burn (0.20)	48.59	48.59
L (19)	62.5	0.49	170.07	<u>83.20</u>
			Total	482.49
Average = 40 f. p. s. (for 12 duty cycles)				

Assuming a normal distribution,

$$\sigma = 43.8 \text{ f. p. s.}$$

At 90 pct. probability level,

$$\Delta V = 112 \text{ f. p. s. or } 0.42 \text{ pct. P. U. equivalent.}$$

Table 4-22
CLOSED-LOOP PROPELLANT UTILIZATION
(90 pct. Confidence Level)

	ΔV (f. p. s.)	P. U. (pct.)
<u>I. Pump-fed engine (10 pct. M. R. control and 64-lb. fuel bias)</u>		
A. Basic system (1/2 pct.)		99.725
B. Weight penalty (21 lb.)	28	-0.165
C. Operation at +10 pct. off M. R. (Isp shift of -5 sec.)	112	-0.425
D. Residual fuel (64 lb.) (1.65 σ variation in venting)		<u>-0.503</u>
Total		98.65
<u>II. Pump-fed engine (15 pct. M. R. control and 57.5 lb. fuel bias)</u>		
A. Basic system (1/2 pct.)		99.725
B. Weight penalty (21 lb.)	28	-0.165
C. Operation at 15 pct. off M. R. (Isp shift of -8 sec.)	145	-0.542
D. Residual fuel (57 lb.) (1.65 σ variation in venting)		<u>-0.450</u>
Total		98.56
<u>III. Pressure-fed engine (75-psi system, 10 pct. M. R. control and 22-lb. bias)</u>		
A. Basic system (1/2 pct.)		99.725
B. Weight penalty (21 lb.)	28	-0.165
C. Operation at 10 pct. off M. R. (duty cycle K)	26	-0.10
D. Residual fuel (22 lb.)		<u>-0.173</u>
Total		99.29
<u>IV. Pressure-fed engine (250-p. s. i. system, 10 pct. or 15 pct. M. R. control, no bias)</u>		
A. Basic system (1/2 pct.)		99.725
B. Weight penalty (21 lb.)	28	<u>-0.165</u>
Total		99.56

In several cases, it appears that the 75-p. s. i. pressure-fed system is marginal: it may or may not vent; while the 250-p. s. i. pressure-fed system shows no sign of venting. Duty cycle K for the 75-p. s. i. pressure-fed system shows 27 lb. of fuel vented before its second burn. Using the same procedure as outlined previously for calculating a fuel bias, the final result is a drop in P. U. of 0.27 pct. on an overall basis (table 4-22). While this is not a large penalty in P. U., it indicates that predictions of the amounts of fuel vented can become quite significant and should not be overlooked in the final selection of a feed system.

c. Conclusions. The overall comparison between the open-loop and closed-loop P. U. systems is shown in table 4-23. This table shows P. U. based on a bias so that optimum P. U. is obtained from an indeterminate mission. With this bias, the P. U. obtainable for each duty cycle is shown. It can be seen that the open-loop system is generally superior to a closed-loop system for low-pressure pump-fed engine systems. At 75 p. s. i., the open- and closed-loop systems are comparable; at high pressure, the closed loop is superior. This is principally caused by the fact that venting and mission indeterminacy severely penalize the closed-loop P. U. system.

6. Phase VI - Tank Insulation and Support.

a. Tank Insulation. To adequately store cryogenic propellants on board an orbiting spacecraft for periods greatly exceeding several hours, a high performance thermal insulation system is mandatory. During orbital operations, the primary means of heat transfer to the vehicle is through radiation derived either directly from the sun or reflected back from the Earth. Therefore, it has been found that an insulation system composed of a number of parallel reflective sheets contained in a vacuum has the theoretical capability of reducing the radiant input to the propellant tanks to an extremely low level. However, if conduction is permitted to occur between the sheets, either through direct sheet contact or through a significant amount of gas being present between the layers, the thermal performance of the insulation system can be greatly degraded. These factors combine to make this basic concept difficult to apply to a real system both with respect to fabrication and to make space insulation compatible with ground-hold and boost phase operation which occur in a finite pressure environment where heat transfer occurs by convection rather than radiation.

Within the past few years, a considerable amount of analytical and experimental work has been attempted to evolve a real insulation system based on the multiple reflector concept. Most of this work is summarized in references 19 through 24. Much of this work is still in progress, and as yet no consensus has been reached as to the optimum approach to this problem. It is now clear, however, that such a system can be made with the thermal, structural, and weight characteristics necessary to ensure extended duration space storage of LH_2 , LF_2 , and LO_2 propellants.

The work conducted and under way in this area has been reviewed in detail. During June, 1965, visits were made to NASA-LeRC, Arthur D. Little, and NASA-MSFC to obtain the latest information on current

Table 4-23

COMPARISON OF OPEN-LOOP AND CLOSED-LOOP PROPELLANT UTILIZATION
(90 pct. Confidence Level)

Duty Cycle	Pump-Fed Engine				75-p. s.i. Pressure-Fed Engine				250-p. s.i. Pressure-Fed Engine			
	Open Loop Ref.		Closed Loop		Open Loop Ref.		Closed Loop		Open Loop Ref.		Closed Loop	
	10 pct. M.R. Control	1/2 pct. 1 pct.	1 pct.	2 pct.	10 pct. M.R. Control	1/2 pct. 1 pct.	1 pct.	2 pct.	10 pct. M.R. Control	1/2 pct. 1 pct.	1 pct.	2 pct.
A 80/20	99.14	99.06	98.78	98.23	99.40	99.39	99.11	98.56	99.37	99.56	99.28	98.73
B 50/50	99.14	99.06	98.78	98.23	99.40	99.39	99.11	98.56	99.36	99.56	99.28	98.73
C 5 burn	99.14	99.06	98.78	98.23	99.36	99.39	99.11	98.56	99.27	99.56	99.28	98.73
D 10 burn	99.12	99.06	98.78	98.23	99.22	99.39	99.11	98.56	99.07	99.56	99.28	98.73
E 1 burn	99.10	99.06	98.78	98.23	99.40	99.39	99.11	98.56	99.40	99.56	99.28	98.73
F 80/20	99.14	98.92	98.64	98.09	99.39	99.39	99.11	98.56	99.33	99.56	99.28	98.73
G 1 burn	99.08	98.92	98.64	98.09	99.35	99.39	99.11	98.56	99.30	99.56	99.28	98.73
H 19 burn	99.13	98.92	98.64	98.09	99.28	99.39	99.11	98.56	99.04	99.56	99.28	98.73
I 1 burn	99.11	98.54	98.26	97.71	99.11	99.39	99.11	98.56	99.08	99.56	99.28	98.73
J 50/50	99.15	98.82	98.54	97.99	99.20	99.39	99.11	98.56	99.13	99.56	99.28	98.73
K 80/20	99.16	99.21	98.93	98.38	99.37	99.21	98.93	98.38	99.28	99.56	99.28	98.73
L 19 burn	99.14	98.74	98.46	97.91	99.22	99.39	99.11	98.56	99.02	99.56	99.28	98.73
Ref. (all missions)	99.10	98.63	98.36	97.80	99.30	99.29	99.01	98.46	99.20	99.56	99.28	98.73
Fuel Bias (lb.)	85	64	64	64	45	22	22	22	45	0	0	0

programs. There is an almost endless variety of detailed approaches that can be taken to involve the required insulation system. However, when considering fundamental differences and not detail variations, the basic choices are relatively few for the type of vehicle under consideration. This is illustrated by figure 4-65. This figure shows that two choices exist for the basic space insulation material; a Mylar, or other similar non-metallic film, or a metal foil such as aluminum. If the mylar film is selected, a metallizing process must be applied on one or both sides. This is generally an electrically deposited aluminum (gold and silver are also being studied). The metallized Mylar is lighter, stronger, and less susceptible to tearing than metal foil. Thus, Mylar is presently preferred.

It is next necessary to select the approach for separating the reflection layer. There would seem to be three approaches with the metallized film: (1) crinkling of the film which provides for contact only over a limited area; (2) providing a controlled permanent set in the material, which also results in a limited contact area; and (3) use of a low-conductivity separator such as a continuous paper spacer, netting material, glass fiber stripping, and so forth. Approaches (1) and (2) are similar except that setting is more rigid and controlled than crinkling. With the metal foil, an insulator separator must be used. Crinkling or setting should provide lower heat conduction and less weight, but the insulator tends to be more predictable and less susceptible to thermal degradation by crushing.

The next decision is to select the approach for adapting the space insulation system to atmospheric operation. The greatest departure in concepts is noticeable here; the following four basic selections are available: (a) a purged interstage in which helium is used to saturate the insulation with a noncondensable gas; (b) purged substrate in which a layer of low conductivity material, such as fiberglass mat, is placed between the tank wall and the space insulation and is purged with a low flow of helium; (c) a low-conductivity sealed insulation between the tank wall and the space insulation; and (d) an evacuated bag in which the entire insulation system is encased in a flexible bag and evacuated prior to loading the propellant. All of the space insulation systems are compatible with these four concepts except the crinkled mylar system which is probably not applicable to the evacuated bag concept.

Concept (a) is the simplest and lightest in weight, but the problem exists of getting purge gas initially into the system and quickly out again once the vehicle is in space. It is also somewhat inefficient as an insulation system during operation in the atmosphere. The purged substrate (b) is more complex, generally relatively heavy, and the problem of introducing purge gas still exists. Approach (c) is a good ground-hold insulation system but is heavy and has many sealing problems. The sealed bag (d) also has serious sealing problems and requires a basic insulation which is not damaged by the crushing external pressure of 1 atm. Evacuating the bag is also a problem.

Work is underway on several specific systems. The Lockheed effort for LeRC uses a IB3b system (utilizing the notation of figure 4-65), that is, a double aluminized mylar with a paper spacer and a purged fiber glass mat

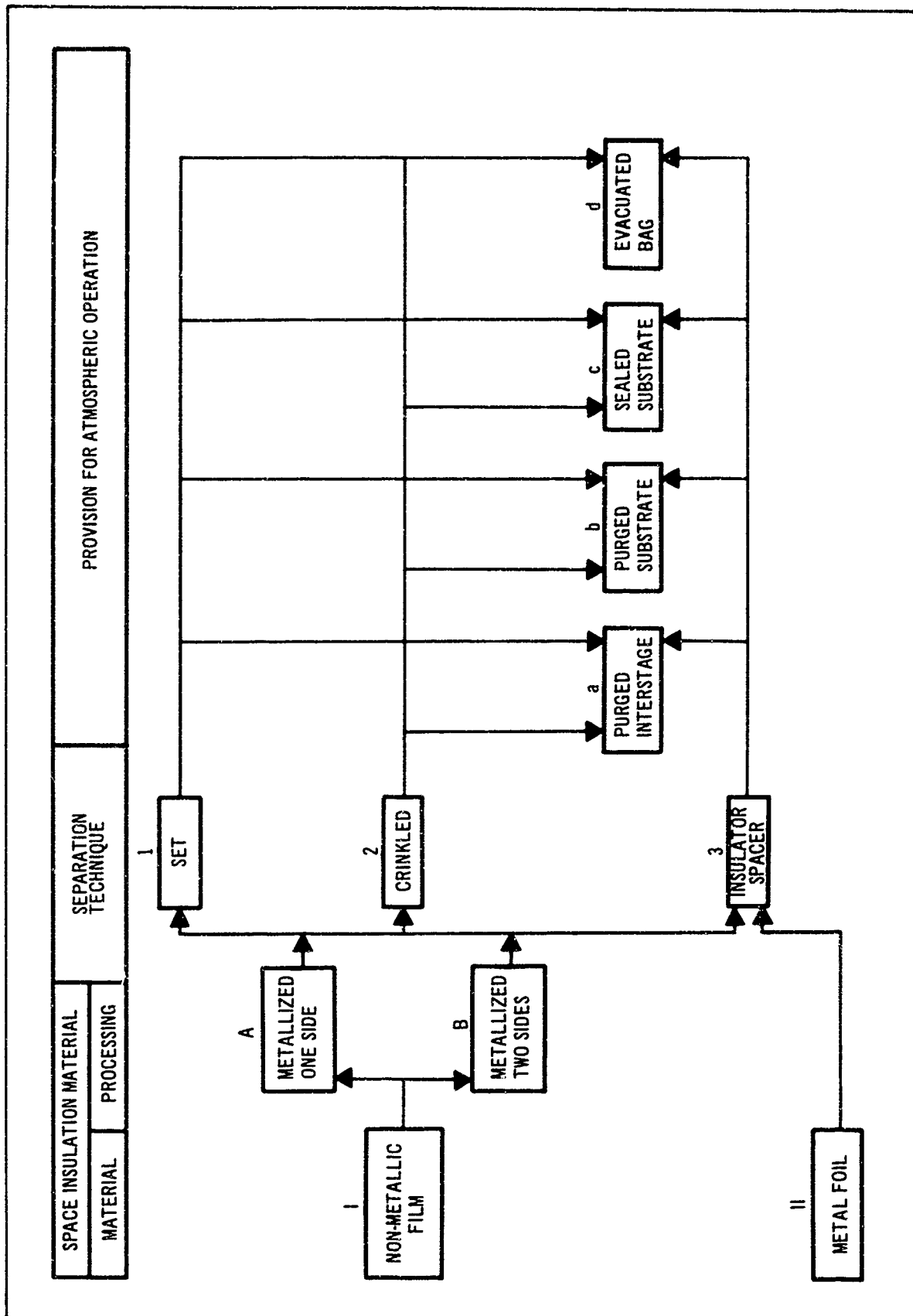


Figure 4-65. Concepts of High-Performance Insulation

substrate. The National Aeronautics and Space Administration, George C. Marshall Space Flight Center is working on a IA2c system and a IA2a system. Douglas IRAD has primarily concentrated in the past on a IA2a system. Current Arthur D. Little thinking is toward a IA2_{B3} a system.

(1) Review and Comparison of Candidate HPI Systems. Table 4-24 is a compilation of HPI data. These data are not complete as they are constantly being updated -- both from IRAD testing at Douglas and from outside sources. The sources of the data presented are: (1) aluminum foil with a glass fiber spacer -- Linde Company; (2) Mylar aluminized on both sides with dexiglass spacer -- Lockheed Missiles and Space; (3) Mylar aluminized on both sides with a nylon netting spacer -- Arthur D. Little Company; (4) Mylar aluminized on one side with a crinkling technique as a spacer -- Arthur D. Little Company; (5) Mylar aluminized on both sides with a dimpling technique as the spacer -- Douglas. Because of the difficulties and sensitivities involved in testing HPI, the comparison of conductivities of the different groups should be viewed with caution. The conductivities are best used as an intragroup comparison.

Three basic types of HPI have been selected for consideration: (1) aluminized Mylar separated by crinkling (system IA2); (2) aluminized Mylar separated by a very low conductivity material (system IB3); and (3) aluminized Mylar separated by layers of aluminized mylar which have been preset or dimpled to maintain gaseous diffusion paths and structural integrity (system IA1). The Linde insulation system is not being considered because (a) thermal shorting of the insulation becomes too critical; (b) the outer aluminum layer is prone to vibration damage; (c) outgassing of purge gas is difficult, and (d) the system generally tends to be heavy relative to the other candidates, as indicated by table 4-24. Using test results from the various sources, one can compare the insulating effectiveness for typical examples of each of the three systems.

For system IA2, test results at Douglas indicate a heat flux, q , of 0.37 B.t.u. p. ft.²-hr. for a 50-layer section of insulation (1-in. thick). Assuming that radiation is the only mode of heat transfer, we have

$$q = \frac{c}{n} \left(T_H^4 - T_C^4 \right)$$

where n is the number of layers, T_H is the hot-side temperature of the insulation, T_C is the cold-side temperature, and c is a measure of the heat transferred per unit area for a sheet. Using the above results, which were obtained with LN_2 as the cryogen and a ΔT of 395°F across the insulation, it was determined that c was equal to 2.26×10^{-10} B.t.u. p. °R⁴.

For System IB3, results from a test performed at Lockheed (sponsored by NASA-Lewis) indicate 0.3 B.t.u. p. ft.²-hr. over 30 pairs (aluminized Mylar and Dexiglass) of insulation layers. The test was performed with LN_2 as the cryogen and a ΔT of 360°F across the insulation. It is determined that c for this system is 1.13×10^{-10} B.t.u. p. °R⁴.

Table 4-24
 SPACE INSULATION SYSTEM PERFORMANCE VALUES
 (Results from several laboratory tests)

Layer Material	Spacer Technique	Layer Density (sheets/in.)	Effective Conductivity (B. t. u. /hr. -ft. - °R)	Weight (lb. /ft. ² /in.)
Aluminum foil	Glass fiber	60 80 100 120	1.8 x 10 ⁻⁵ 2.0 x 10 ⁻⁵ 2.4 x 10 ⁻⁵ 3.5 x 10 ⁻⁵	0.4 0.54 0.67 0.80
Mylar, aluminized on both sides	Glass fiber	30 50 80 100 120	2.0 x 10 ⁻⁵ 1.5 x 10 ⁻⁵ 1.5 x 10 ⁻⁵ 2.0 x 10 ⁻⁵ 3.0 x 10 ⁻⁵	0.15 0.23 0.36 0.45 0.54
Mylar, aluminized on both sides	nylon netting	25 40 60 70	1.6 x 10 ⁻⁵ 0.5 x 10 ⁻⁵ 0.4 x 10 ⁻⁵ 0.6 x 10 ⁻⁵	0.12 0.17 0.27 0.32
Mylar, aluminized on one side	crinkled	25 40 50 60 100	4.3 x 10 ⁻⁵ 2.0 x 10 ⁻⁵ 2.0 x 10 ⁻⁵ 2.7 x 10 ⁻⁵ 4.5 x 10 ⁻⁵	0.04 0.06 0.09 0.11 0.17
Mylar, aluminized on both sides	dimpled	17 30 33	4.4 x 10 ⁻⁵ 6.9 x 10 ⁻⁵ 2.4 x 10 ⁻⁵	0.126 0.222 0.244
	deepset dimple	10	9.0 x 10 ⁻⁵	0.076

For system IA1, IRAD tests at Douglas have shown that the heat flow for a typical configuration of 36 sheets of insulation is 0.26 B. t. u. p. ft.²-hr. The test used LN₂ as the cryogen and had a ΔT across the insulation of 395°F. This gave a c of 1.14×10^{-10} B. t. u. p. °R⁴. If one also considers the relative weights of the systems, the following results are obtained: if the weight of a 1-ft. square section of 1/4-mill aluminized Mylar equals 1, the weight per sheet of system IA2 is 1; the weight per sheet of system IB3 is 3; and the weight per sheet of system IA1 is 2.

Taking the products of the c values and the relative weights, we can get a meaningful measure of performance of the insulation on a weight basis. For system IA2, we get 2.26×10^{-10} ; for system IB3 we get 3.39×10^{-10} ; and for system IA1 we get 2.28×10^{-10} . This implies that the system using an insulator spacer is about 50 pct. heavier than the other two systems which are approximately equal; this difference in performance is not significant because the Lockheed system was not tested in the same apparatus used for the Douglas Dimplar and NRC-2 tests. However, system IA1 uses 1/2 mill rather than 1/4 mill Mylar sheets; therefore, it may be that 1/4 mill sheets can be used with little loss in performance.

(2) Insulation Location. The normal approach to installing multilayer insulation has been to apply the insulation directly to the cryogenic tankage. However, early in the program, it was reasoned that this was not the only possible location and that an insulation system located around the structural shell or at least removed some distance from the cryogenic tanks may have certain advantages. The pros and cons for shroud versus tank mounting are listed in table 4-25.

Quantitative descriptions of the items in table 4-25 are contained in the following discussion. The presented numerical results are based on preliminary models which may differ from item to item. Thus, the important result is the relative performance of the two systems, S (HPI on shroud) and T (HPI on tank), rather than the absolute magnitude of the separate results.

(a) Supporting Arguments.

P1 -- Ease of Compression-Free Application. Most of the heat transferred through a blanket of HPI in a typical installation results from solid conduction. To illustrate this, consider the following examples:

Dimplar -- Calorimeter Data. Tests in Douglas materials laboratories were conducted under a current IRAD program to evaluate a typical installation using dimpled Mylar insulation. A typical result was the following:

T_H	(hot wall temperature)	=	530°R
T_C	(cold wall temperature)	=	140°R
n^c	(number of HPI layers)	=	19
t	(HPI slab thickness)	=	1 in.
q	(heat flux)	=	0.57 B. t. u. /hr. -ft. ²

Table 4-25

EVALUATION OF PLACEMENT OF HIGH-PERFORMANCE INSULATION ON THE SHROUD INTERIOR

Pro	Con
P1. Ease of compression-free application.	C1. Increased area to insulate.
P2. Low shorting of insulation by supporting structure.	C2. HPI subjected to aerodynamic heating.
P3. Performance gain when HPI does not touch cold tank wall.	C3. Increased ground hold and boost boiloff.
P4. Multitemperature skin insulated optimumly.	C4. Untried system.
P5. Potential for leak detection.	
P6. Little insulation required on penetrations.	
P7. Ease of tank maintenance.	

For an ideal radiation shield of the same material, the heat flux is given by

$$q_r = \frac{\epsilon \sigma}{n} (T_H^4 - T_C^4) = \frac{0.0035}{n} (T_H^4 - T_C^4) \times 10^{-8}$$

for doubly aluminized Mylar sheets with emissivity = 0.04. Thus

$$q_r = 0.14 \frac{\text{B. t. u.}}{\text{ft.}^2 \text{ hr.}}$$

Comparing this value to above measured heat flux we find that the conductive component is

$$q_c = 0.57 - 0.14 = 0.43$$

Therefore the conductive component amounts to approximately 80 pct. of the total heat flux.

LMSC Tests of HPI System with Paper Spacers. Tests at LMSC, reported in references 21 and 22, result in the following data taken for an installation on a tank of an aluminum-coated (double) Mylar HPI using Dexiglass spacers:

$$\begin{aligned}
 T_H &= 530^\circ\text{R} \\
 T_C &= 140^\circ\text{R} \\
 n &= 30. \\
 t &= 1/2 \text{ in.} \\
 \dot{q} &= 0.30 \text{ B. t. u. p. /hr. -ft.}^2
 \end{aligned}$$

here the conductive component amounts to about 70 pct. of the total heat flux.

In contrast to the preceding values, the conductive component to the heat flux must go to zero for a contact pressure of zero between the sheets. The following is, therefore, apparent:

- Transmitted flux will depend strongly on the insulation compression.
- Current typical good installations are highly degraded because of contact between layers of insulation.

A certain amount of compression is invariably associated with wrapping insulation around a real tank or a support. Due to a topological incongruency, additional compression arises when a planar layer of HPI is applied to a spherical surface. Both problems are essentially removed when insulating the inside of the shroud. Such a system should not build up tension in the insulation (producing compression) because of the significantly different application technique. Furthermore, the shroud surfaces will be truncated cones or cylinders which present no topological difficulties such as arise with a spherical surface.

As seen by the calculations in the above examples, a compression-free installation could improve the insulating properties of an HPI blanket by about a factor of 3 (thus requiring 2/3 less insulation for the same heat-leak). The actual performance gain would be a strong function of the precise HPI application method.

At this point in time, the Douglas IRAD calorimeter tests were consistently showing Dimplar to be about twice as heavy as NRC-2 in conventional installations. However, it was expected that the spiral wrapping technique used on the calorimeter was degrading the thermal performance, particularly for Dimplar, because of the following:

- The flat reflectors in Dimplar do not give, resulting in a possible high state of compression.
- Lateral conduction effects are magnified because of Dimplar's greater thickness (conduction cross-section) and fewer shorts (conduction length).

Therefore, a special calorimeter test was made to demonstrate the performance capabilities of a compression free installation as would be expected with the shroud mounted technique. This test involved placing spacers at

either end of the calorimeter so that the insulation would be set off the cold wall. Each insulation sheet was individually installed over the supports and was cut to form a single butt joint running the full length of the cylindrical calorimeter. Each sheet was placed so that the joints of successive sheets were staggered 60 in. apart. No attempt was made to separate individual sheets but care was taken not to compress the lay-up. Each sheet was supported by looped threads hooked to rigid spoke supports. The results of the tension-free Dimplar test are given in table 4-26. For comparison, the results of the previous best performing NRC-2 and Dimplar IRAD tests are given. The Dimplar used was 0.5-mil doubly aluminized Mylar with a deep set. As can be seen, the tension-free mounting reduced the heat flux by more than a factor of 2.

P2 -- Shorting of Insulation by Supporting Structure. It has been shown in reference 25 that the high lateral conductivity in an HPI slab helps channel heat through penetrations in the insulation (support members or pipes) into the propellant tanks. The effect can be significant. For installations with about 100 HPI layers, the result of penetrations through 0.01 pct. of the insulated area is a factor of 10 increase in the heat transfer to the tank (reference 20). The model used for this computation was checked against experimental results from Arthur D. Little, Inc. (reference 26). In the ADL tests, an insulated tank was degraded with a Cu penetration and the temperature profile in the HPI was measured. Using the experimental profiles, the heat current from the HPI to the short was found; reference 26 reports the result to be 0.44 B. t. u. p. /hr. The method of reference 25 was applied to this example and the predicted result was 0.38 B. t. u. p. /hr.

When the HPI is mounted on the shroud, the situation is altered in two ways. First, many penetrations used to hold the HPI in place no longer offer conduction paths to the tank because they are only connected to the shroud. The effect is to raise the temperature of the cool layers of HPI in the vicinity of the short and to radiate some additional energy to the tank. This process of heat transfer is far less efficient than direct conduction. Second, pipes and tank supports now remain cool near the tank (see P6). Conduction of heat through these penetrations is very low because the hot areas are about ten times further from the cryogen than for the configuration with HPI on the tank.

Thus, by moving the insulation to the shroud, the severe degradation from coupling between thermal shorts and the insulation may be greatly decreased.

P3 -- Performance Gain When HPI Does Not Touch Cold Tank Walls. Whether a system of ideal radiation barriers were placed near or far from the propellant tank would not affect heat transfer. However, real HPI systems have substantial conductive components (about 75 pct.). Because of the nonlinearity of radiation heat transfer coupled with a conductive component, a performance gain can be obtained by moving the HPI from the tanks. To illustrate this effect, assume that heat transfer through HPI is 100 pct. conductive (this assumption simplifies the algebra). The systems to be looked at are shown in figure 4-66. Consider the LH₂ tank for the

Table 4-26

HIGH-PERFORMANCE INSULATION
CALORIMETER TESTS (IRAD)

Insulation system	Number of layers	Insulation thickness (in.)	Boiloff (ft. ³ /min.)	Heat flux (B. t. u. p. /hr. -ft. ²)
Shroud/mounted Dimplar (0.5 mil)	9 smooth 8 dimpled	0.9 + 0.1	0.00110	0.249
Dimplar (0.5 mil) Continuous spiral	10 smooth 9 dimpled	1.0	0.0022	0.506
NRC-2 (0.25 mil) Continuous spiral	50	1.0	0.00066	0.157
NRC-2 (0.25 mil) Continuous spiral	50	1.0	0.00072	0.166

current mission with $T_c = 36^\circ\text{R}$, $T_H = 355^\circ\text{R}$, HPI thickness = 1.6 in. (40 layers), $k = 8 \times 10^{-5}$ B.t.u./ft.- $^\circ\text{R}$ -hr. These values are typical based on current laboratory data and preliminary optimization for the 210-orbit mission (14 days). The heat flux at steady-state condition is:

System t

$$q_t = F \sigma (T_H^4 - T_t^4) = \frac{12k}{1.6} (T_t - T_c) \quad (4-46)$$

or

$$0.0035 (160 - T_t^4 \times 10^{-8}) = 6 \times 10^{-4} (T_t - 36)$$

Solving for T_t gives

$$T_t = 324^\circ\text{R}, q_t = 0.173 \text{ B.t.u./ft.}^2\text{-hr.} \quad (4-47)$$

System s

$$q_s = 0.0035 T_s \times 10^{-8} = 6 \times 10^{-4} (355 - T_s)$$

Solving for T_s gives

$$T_s = 220^\circ\text{R}, q_s = 0.081 \text{ B.t.u./ft.}^2\text{-hr.}$$

Moving the insulation to the shroud has, in this simple example, reduced the net heat transfer by one-half. Figure 4-67 displays computer-produced data for the case where the radiative component of the HPI is included. Values of k_c , the conductive contribution to the effective conductivity, vary from 6 to 8×10^{-5} B. t. u. /ft.² - °R-hr. for current good Dimplar installations. The radiative component was included in a term of the form

$$\frac{F\sigma}{n} (T^4 - T_c^4)$$

The percentage reduction in required insulation weight per unit area caused by simply moving the HPI from contact with the tank is proportional to the distance between the two curves on figure 4-67. In the range of k_c values of interest, the savings are 45 pct. (for the LH₂ tank) and 25 pct. (for the LF₂ tank). This performance increase is about the same as found experimentally (reference 27).

P4 -- Multicomponent Skin Insulated Optimumly. The configuration of the study vehicle with HPI on the shroud is shown schematically in figure 4-68. The insulation would be cut to the appropriate shape to fit along the conical sides or the disk-shaped (or cone-shaped) ends. The application method that would be used would allow application of layers of HPI along the particular surface insulated as required. For instance, the number of HPI layers along the top cone above the LF₂ tank need not be the same as the number along the vehicle sides. Furthermore, the mean temperatures of the various surfaces are quite different; thus, the optimum configuration would almost certainly involve different numbers of HPI layers at different positions around the vehicle.

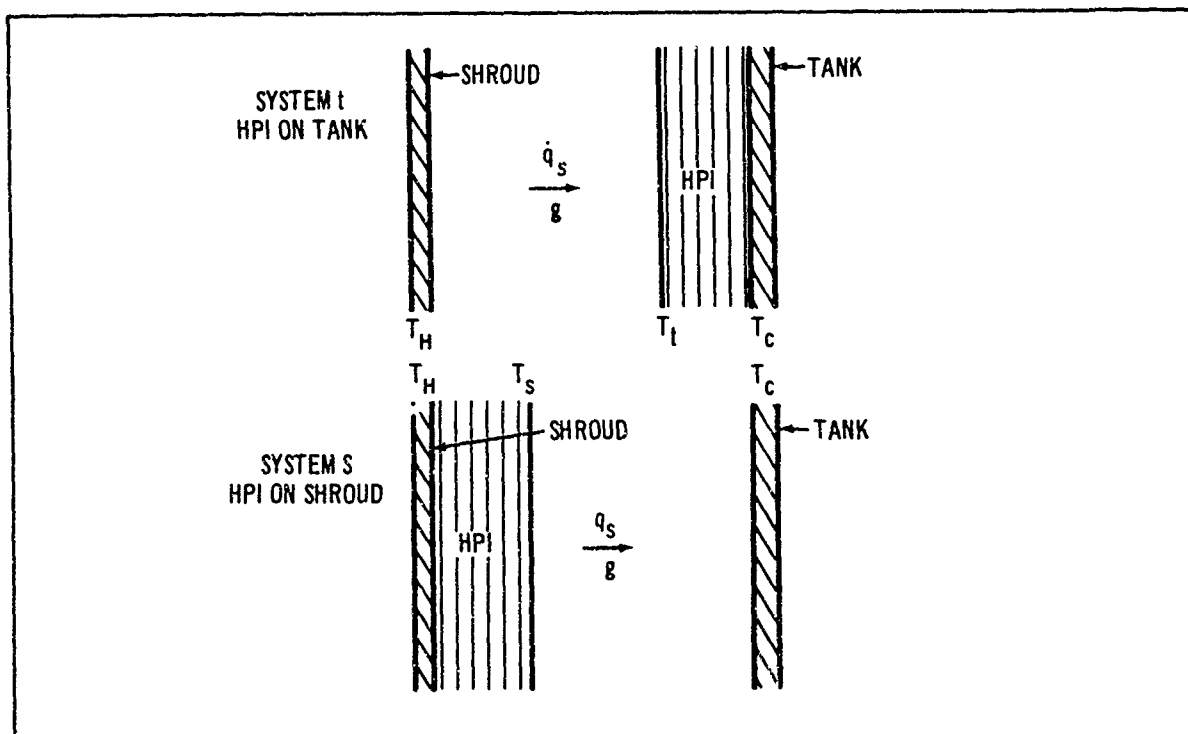


Figure 4-66. Simple Model to Evaluate Effect of Insulation Placement

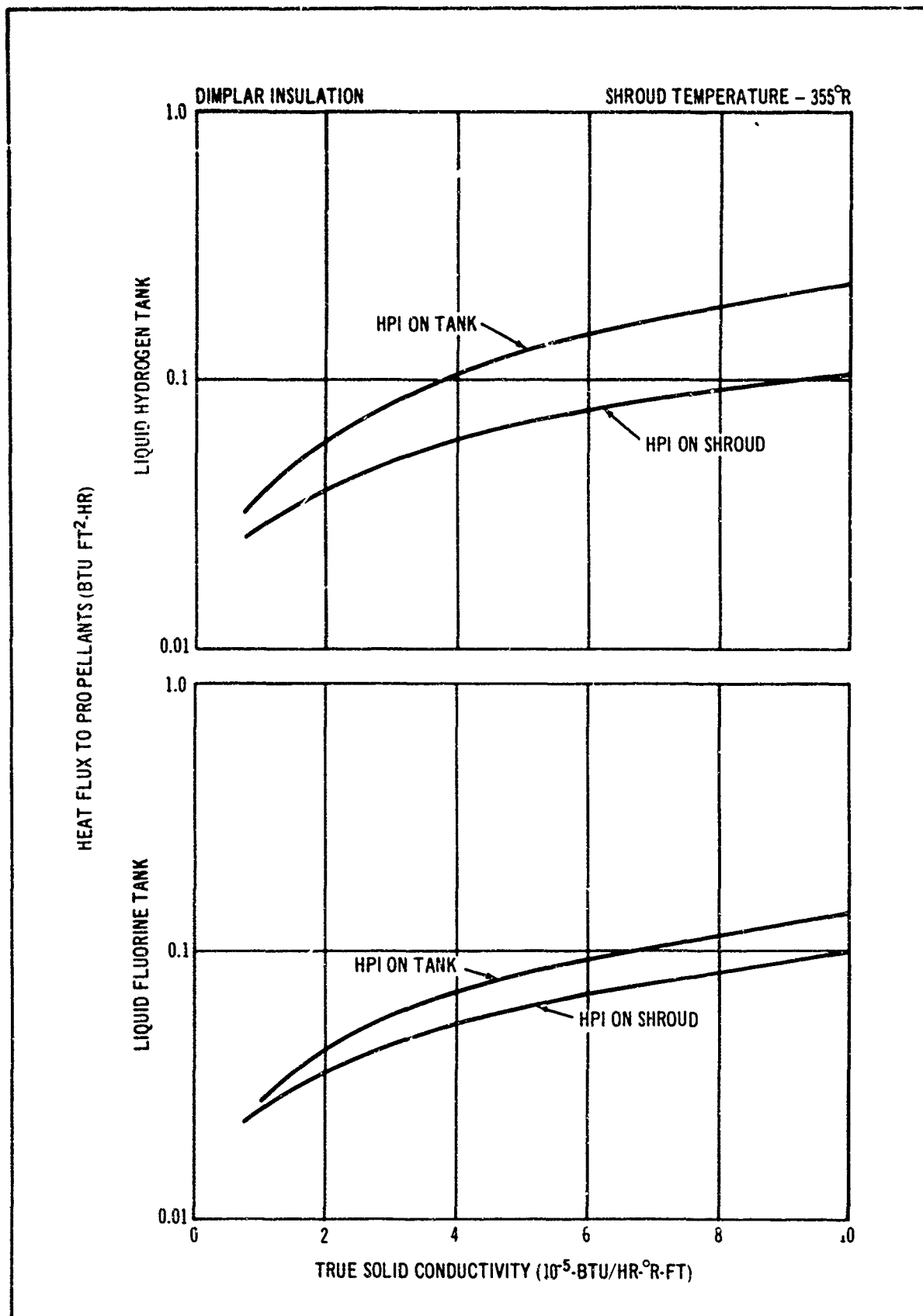


Figure 4-67. Heat Flux Comparison for Shroud as a Function of Tank Insulation Placement

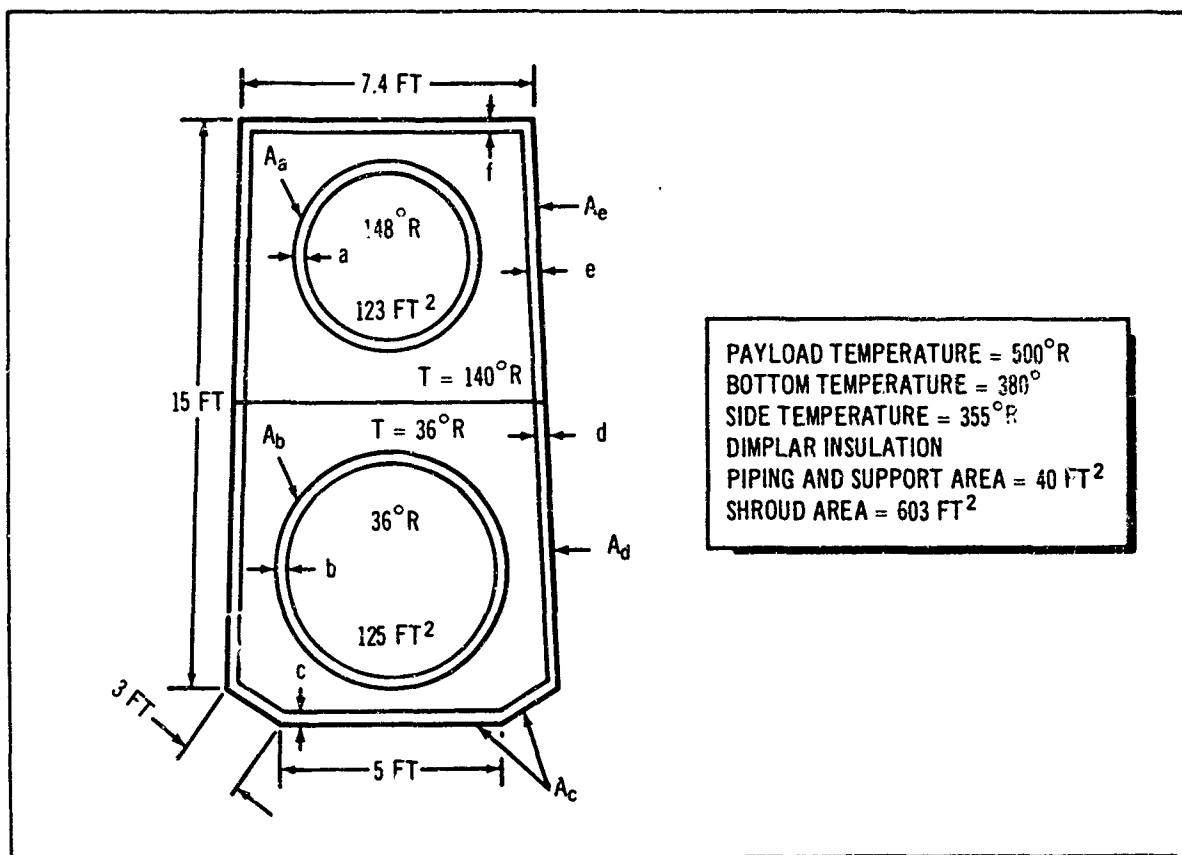


Figure 4-68. Vehicle Configuration for Preliminary Optimization

When the HPI is attached to the tank, it is impractical to insulate certain portions of the tank surface with more layers than others. Furthermore, an accurate analytic model of such a system is currently impossible. Because the insulation can be tailored when placed on the shroud, a more satisfactory performance optimization is possible. The weight savings can be large. A numerical example is shown later in this section where the net effect of area increase on the optimum configuration is calculated.

P5 -- Potentials for Leak Detection. With HPI on a tank, leaking propellant vapor will build up behind the insulation, eventually degrading the thermal performance of the HPI over a large area while slowing down the leak rate. Thus, the discovery of the leak is indirect, that is, through a slow increase in boiloff. A leak during laboratory testing will cause wasted effort, expense, and time before it would be discovered. Also, a leak existing in the flight hardware would most likely be undetected during ground hold and could result in mission failure.

On the other hand, with the insulation on the shroud, a single monitoring pressure probe in each shrouded compartment could register tank leakage. Furthermore, the region of the leak could be found by inspection of the bare tank walls. Also, if a leak occurred during ground hold of the flight hardware, a mass spectrograph probe could detect it.

P6 -- Little Insulation Required on Penetrations. When the HPI is on the tank, all penetrations must themselves be insulated. If they were not, the radiative equilibrium between the penetrations, the shroud, and the insulated tank would cause the penetrating pipe or support to be nearly as hot as the shroud to within a few inches from the tank. The heat conducted into the tank through the support under these conditions would be too great to tolerate. Thus, the radiant heating of the support must be eliminated by using HPI.

When the HPI is placed on the shroud, the field of radiant energy surrounding the support is weak. Thus the penetration requires no insulation to remain cool. Results are presented in section 4 (see figure 4-68) that show typical heating to the tanks from uninsulated supports. This heating is unimportant for this consideration and is only a few percent of the total.

Because the penetrations need not be insulated for the case of HPI on the shroud, the weight of that insulation is saved. Furthermore, the attachment of the tank to its supports and plumbing can be accomplished more easily.

P7 -- Ease of Tank Maintenance. Because plumbing and support connections to the tank are bare when the HPI is on the shroud, the tank can be removed from the shroud. Movement of the tanks can also be accomplished with minimum of risk of damage to the HPI, because most of the HPI can remain in place on the shroud walls.

(b) Opposing Arguments.

C1 -- Increased Area to Insulate. The total shroud area plus the top, middle, and bottom disks (figure 4-68) have a total surface area of 603 ft.². The total surface area of the tanks, the pipes, and supports amounts to 348 ft.². It would, therefore, appear that almost double the insulation weight on the shroud would be necessary to give the same system performance, neglecting items P1, P2, and P3 above, as that obtained with HPI on the tank. This conjecture is correct (ignoring P1, P2, and P3), but the doubled-weight system is no longer optimum. In this section, item P4 and the area increase will be considered to estimate the net weight penalty associated with insulating the shroud. Figure 4-68 identifies the insulation thicknesses and the wall areas to be used in the calculation. The surface areas shown are

$$\begin{array}{ll} A_a = 123 \text{ ft.}^2 & A_d = 207 \text{ ft.}^2 \\ A_b = 185 \text{ ft.}^2 & A_e = 207 \text{ ft.}^2 \\ A_c = 88 \text{ ft.}^2 & A_f = 49 \text{ ft.}^2 \end{array}$$

For these calculations, a pure radiation transfer equation is used with a view factor chosen to fit the existing calorimeter data on Dimplar, viz. (with T in 100°R's)

$$q = \frac{8.55 \times 10^{-4}}{t} (T_H^4 - T_c^4) \frac{\text{B. t. u.}}{\text{ft.}^2 \text{ orbit}} \quad (4-49)$$

(an orbit is 96 min.)

Temperature distributions were obtained from the data of section 4. The data of figure 4-57 can be represented with reasonable accuracy by the relation

$$T (100^\circ\text{R}) = 3.25 + 1.25 \sin \theta \quad (4-50)$$

where θ is the angular distance around the vehicle's cylindrical surface. The appropriate mean temperature to be used with the heat transfer law of equation 4-49 is found by averaging over the surface as follows:

$$\begin{aligned} \bar{T}^4 &= \frac{1}{2\pi} \int_0^{2\pi} T^4 d\theta \\ &= \frac{110}{2\pi} \int_0^{2\pi} (1 + 0.89 \sin^2 \theta + 0.022 \sin^4 \theta) d\theta \quad (4-51) \\ &= 110 (1 + 0.445 + 0.0087) = 160 \end{aligned}$$

or $T = 3.55 (100^\circ R)$

System t -- Insulation on Tank. Approximately 30 pct. of the LH_2 tank sees the bottom of the stage while about 20 pct. of the LF_2 tank sees the payload. The net heat transfer to the two tanks from equation 4-49 is (for LF_2 and LH_2 , respectively):

$$q_a = \frac{25.5}{a} \frac{\text{B.t.u.}}{\text{orbit}} \quad q_b = \frac{27.9}{b} \frac{\text{B.t.u.}}{\text{orbit}} \quad (4-52)$$

The boiloff equivalent for the most severe mission (210 orbits) is

$$W_a = \frac{30.9}{a} \text{ lb} \quad W_b = \frac{30.4}{b} \text{ lb} \quad (4-53)$$

Also the insulation weight is given by

$$W'_a = 10_a \text{ lb.} \quad W'_b = 10_b \text{ lb.} \quad (4-54)$$

Selection of the optimum insulation thickness (by minimizing $W_a + W_b + W'_a + W'_b$) yields

$$a = b = 1.7 \text{ in. Total weight} = 70 \text{ lb.} \quad (4-55)$$

System s -- Insulation on Shroud. The HPI layer separating the LH_2 and LF_2 tank compartments does not enter into the optimization as heat leaks across that layer result in zero change in the net stored heat in the vehicle. That layer is chosen just thick enough to keep the LF_2 from freezing (only a few sheets is sufficient).

The total weight penalty (insulation plus boiloff) for this case is given by

$$W_t = \frac{4.3}{c} + \frac{7.6}{d} + \frac{8}{f} + \frac{8.7}{e} + 4.1c + 9.2d + 2.62f + 9.5e \quad (4-56)$$

Minimization of W_t yields for the various insulation thicknesses is:

$$c = 1.0 \text{ in.}, d = 0.9 \text{ in.}, f = 1.9 \text{ in.}, e = 1.0 \text{ in.} \quad (4-57)$$

and the total weight is 51.8 lb.

If 0.25-mil flat sheets were used, this weight is further reduced to 44.9 lb. This compared to a W_t of 70 lb. for tank-mounted Dimplar.

Similar estimates for NRC-2 on the tank using an optimistic T^4 variation in \dot{q} assumption, give a W_t of 48.4 lb. Therefore shroud-mounted Dimplar and tank-mounted NRC-2 should be quite comparable on an overall weight basis.

C2 -- HPI Subjected to Aerodynamic Heating. During boost, the shroud skin temperatures could reach 500°F; however, Mylar fails structurally around 200°F. Thus, precautions must be taken to avoid melting of the insulation. LMSC data (reference 28) indicates that Mylar can withstand temperatures up to 300°F for brief periods. Therefore, if the HPI is not in too good a thermal contact with the shroud, it may resist the environmental heating. An alternate possibility is to use an aluminum-coated plastic other than Mylar for the first sheet of HPI that can resist the high temperature experienced. Such a material is not currently used for insulation. The boost heating calculation reported in section 4 indicates that shroud temperatures are, in fact, below the level at which this becomes a problem.

C3 -- Increased Ground Hold and Boost Boiloff. With a He-purged shroud, high boiloff rates are experienced until after the evacuating ascent into orbit. The weight penalties have been calculated in section 4 for the configuration with HPI on a tank. Figure 4-69 shows that, for a typical 300-hr. coast, the weight penalty associated with He purging varies nearly linearly from 0 to 40 pct. of the total weight penalty as the time from tank fill to He-evacuation varies from 0 to 30 min. The actual time to He evacuation is probably less than 10 min., so that the actual weight penalty is less than 10 pct. (on the order of 10 lb.).

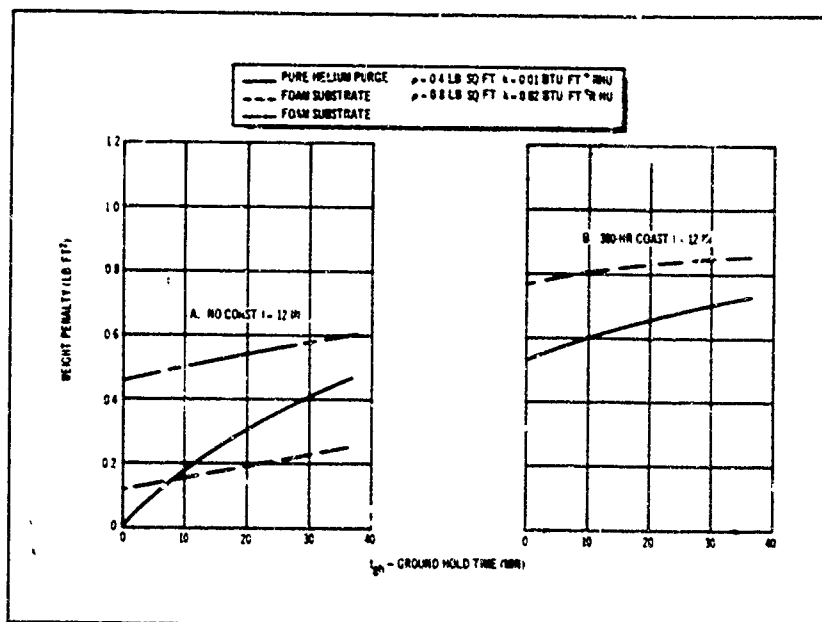


Figure 4-69. Comparison of Pure He Purge and Foam Substrate with Optimum Space Insulation

The heat transfer through the pringed, shrouded volume occurs in two modes (1) gaseous conduction inside the HPI layer and (2) gaseous convection outside the HPI layer. The effect of moving the HPI to the shroud is to make the conduction region cooler. The net effect is to increase the heat transfer; supporting calculations are below.

A hard-sphere model of the conducting helium is sufficient for these computations. Then, thermal conductivity is proportional to the square root of the temperature, that is:

$$k_c = C_1 \sqrt{T} \quad (4-58)$$

where C_1 is a constant.

The theory of free convection at cryogenic temperatures is not well defined. An estimate of the effect of temperature variation is found through correlations of room-temperature data, for example:

$$h = k_c C_2 (Gr)^n (Pr)^n (D/L)^{1/9} / D \quad (4-59)$$

where

h = heat-transfer coefficient

C_2 = constant

Gr = Grashof number $(L^3 \rho^2 g \Delta T / \mu)$

L = length of gap

ρ = density

ϕ = coefficient of expansion ($^{\circ}K^{-1}$)

μ = viscosity

D = width of gas filled gap

Pr = Prandtl number (C_p / k_c)

C_p = specific heat

n = about 1/3

(See reference 29)

The temperature dependence of h as presented in equation 4-59 is

$$h = C_3 / \sqrt{T} \quad (4-60)$$

With the insulation on the tank, the mean HPI temperature (T_1) was about 100 $^{\circ}R$ and the shroud (T_2) was about 400 $^{\circ}R$. At steady state, equations 4-48 and 4-50 combine to give

$$\frac{\Delta T \text{ (from shroud to HPI)}}{\Delta T \text{ (in HPI)}} = \frac{C_1}{C_3} \sqrt{T_1 T_2} \quad (4-61)$$

Thus, interchanging T_1 and T_2 by moving the HPI to the shroud is consistent with unchanged temperature differences across the two regions. Therefore, the net increase in heat transfer caused by insulating the shroud instead of the tank is just proportional to the increase in the mean conductivity, that is:

$$\frac{\dot{q}_s}{\dot{q}_t} = \sqrt{\frac{T_2}{T_1}} = 2 \quad (4-62)$$

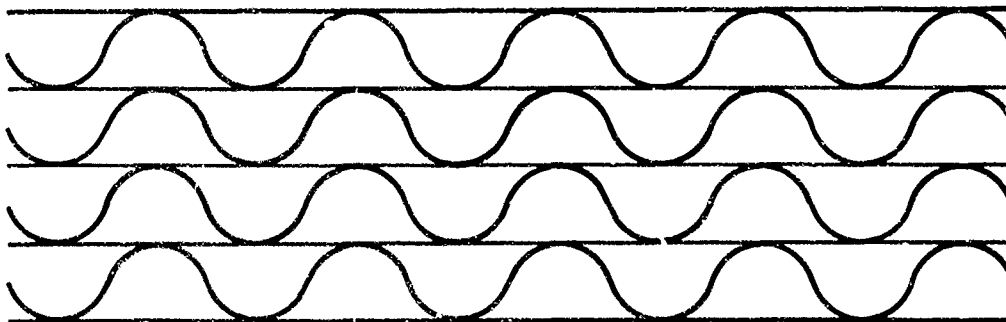
or the net ground hold and ascent weight penalty is doubled.

C4 -- Untried System. Although attempts have been made to discover and evaluate the pros and cons of the new configuration, the system is untried. The considerations of the previous sections may have overlooked important aspects of the problem. The final justification or censure of placing the HPI on the shroud must wait until the method is attempted.

(3) Basic High-Performance Insulation Thermal Analysis. To properly evaluate and compare the performance of various multilayer insulation types, it was necessary to develop an improved analytical approach for predicting basic insulation thermal performance. Such an analysis must take into account the following characteristic parameters:

- Boundary temperatures.
- Number of layers of insulation.
- Insulation packing density (layers per in.)
- Shield emissivities.
- Ratio of contact area of solid conduction to solid conduction cross-section area.
- Ratio of contact area to surface area.
- Insulation configuration parameters as illustrated in figure 4-70.

(a) Governing Equations. Consider the section of HPI shown below. This section of insulation is characterized by the fact that plain flat reflecting layers are separated by nonplanar reflecting layers.



Section of High-Performance Insulation

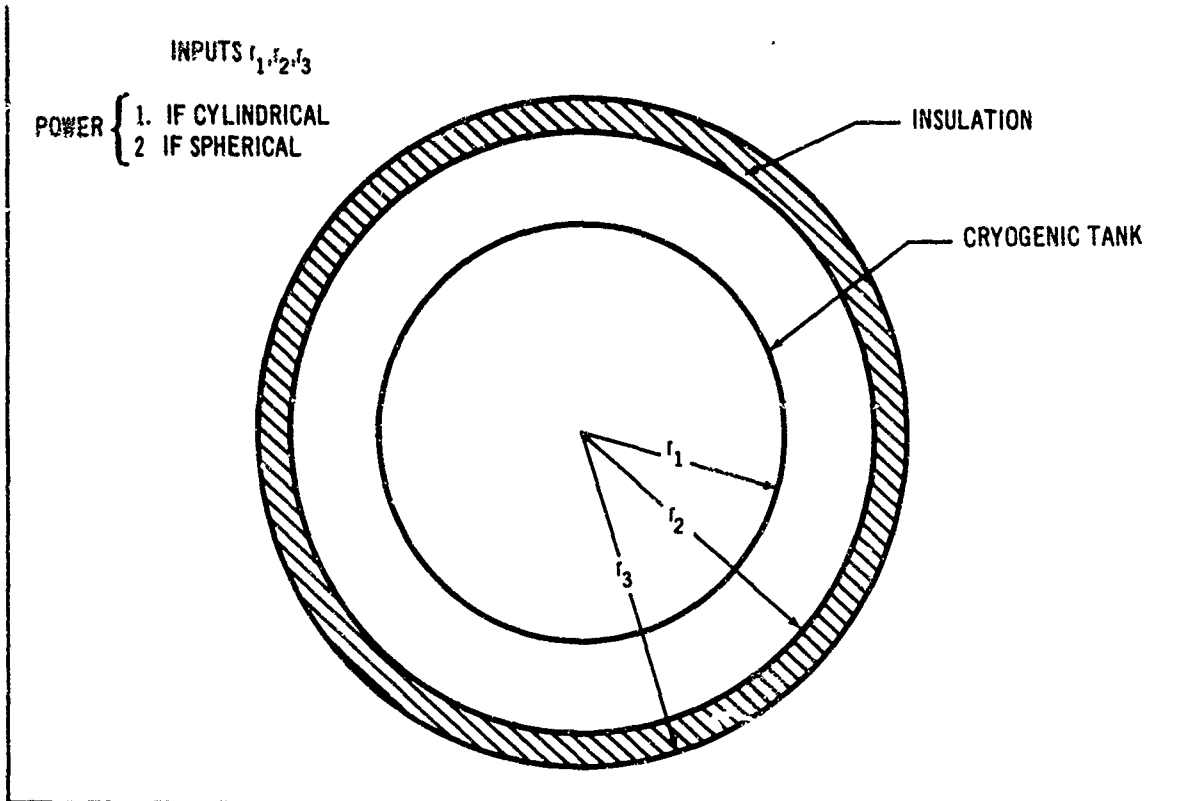
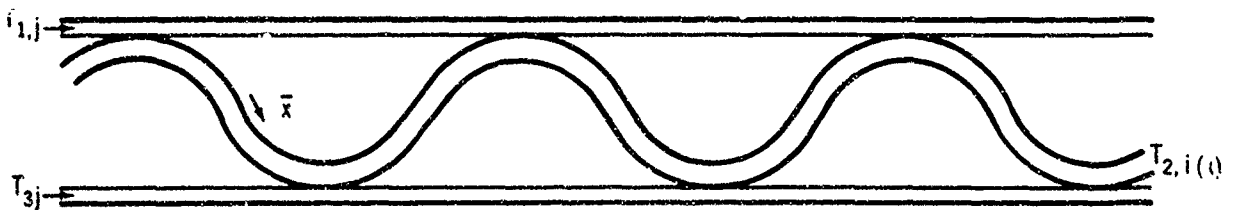


Figure 4-70. Generalized Configuration of Insulation

The separating sheets being somewhat regular enables (1) the engineer to make a reasonably good estimate of the surface contact between adjacent sheets and (2) a uniform heat flux over the surface to be established.

The problem under analysis is that of steady-state heat transfer through a section of insulation made up of $n + 1$ plain sheets separated by n nonplanar sheets. The sketch below shows three adjacent sheets of insulation.



Expanded View of Insulation

Two modes of heat transfer between adjacent sheets illustrated above are radiation and conduction. The radiation heat transfer between the sheets is:

$$\frac{\dot{q}}{A} \text{ (rad)}_i = \mathcal{F}_\sigma (T_{2,i}^4 - T_{3,i}^4) \quad (4-63)$$

or assuming

$$(T_{1,i}^4 - T_{2,i}^4) = (T_{2,i}^4 - T_{3,i}^4)$$

$$\frac{\dot{q}}{A} \text{ (rad)}_i = \mathcal{F} \frac{\sigma}{2} (T_{1,i}^4 - T_{3,i}^4) \quad (4-64)$$

where

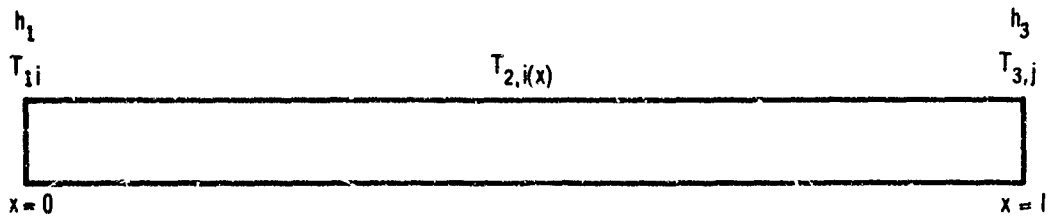
$$\mathcal{F} = \frac{1}{\frac{1}{F} + \left(\frac{1}{\Sigma} - 1\right) + X \left(\frac{1}{\Sigma} - 1\right)}$$

$$F = 1 - \frac{X-1}{X}$$

$$X = \frac{A_{1,i}}{A_{3,i}}$$

and A is one-half the surface area of the indicated sheet of insulation.

The model shown below was constructed to determine the conduction heat transfer,



Conductance and Contact Conductance (One-Dimensional Model)

The equation governing the conduction problem is the steady-state heat equation,

$$\frac{d^2 T}{dx^2} = 0 \quad (4-65)$$

The boundary conditions are,

$$\text{at } x = 0, T_{2,i} = T_{2,i}(0), q = h_1 A^* \left[T_{1,i} - T_{2,i}^{(0)} \right]$$

$$\text{at } x = l, T_{2,i} = T_{2,i}(l), q = h_3 A^* \left[T_{2,i}^{(l)} - T_{3,i} \right]$$

where A^* is the contact area and h is the contact conductance.

The solution to equation 4-65 is,

$$T_{2,i} = C_1 x + C_2 \quad (4-66)$$

Applying the boundary conditions, equation 4-66 becomes,

$$T_{2,i} = T_{2,i}(0) - \left[T_{2,i}(0) - T_{2,i}(\ell) \right] \frac{x}{\ell} \quad (4-67)$$

because a steady-state heat flow condition exists, the following relationship holds,

$$A_1^* h_1 [T_{1,i} - T_{2,i}(0)] = A_3^* h_3 [T_{2,i}(\ell) - T_{3,i}] = \frac{2kA_2^*}{\ell} [T_{2,i}(0) - T_{2,i}(\ell)] \quad (4-68)$$

where K is the conductivity of the spacing material and A_2^* is the conduction path cross-section area. Equation 4-68 can be solved for $T_{2,i}(0)$ and $T_{2,i}(\ell)$ in terms of $T_{1,i}$ and $T_{3,i}$. If we assume $A_1 h_1 = A_3 h_3$, we get

$$T_{2,i}(0) = \frac{\left(1 + \frac{A_1^* h_1}{2kA_2^*}\right) T_{1,i} + T_{3,i}}{2 + \frac{\ell A_1^* h_1}{2kA_2^*}} \quad (4-69)$$

$$T_{2,i}(\ell) = \frac{\left(1 + \frac{A_3^* h_3}{2kA_2^*}\right) T_{3,i} + T_{1,i}}{2 + \frac{A_1^* h_1}{2kA_2^*}} \quad (4-70)$$

An effective conductivity is used when necessary to consider the conduction through both the sheet material and any metallic coating which is present.

Therefore, the steady-state heat transfer between the top and bottom sheet is:

$$\frac{\dot{q}}{A_1} \frac{A_1}{A_i} = \frac{\mathcal{F}\sigma}{2} (T_{1,i}^4 - T_{3,i}^4) + Rh_1 \quad (4-71)$$

$$\left[\frac{T_{1,i} - T_{3,i}}{2 + \frac{l A_i^* h_1}{2k A_i^*}} \right]$$

where R is the ratio of contact area to total area.

At steady-state for n layers, we will have

$$T_{1,i+1} = T_{3,i}, \quad i = 1, 2, \dots, n \quad (4-72)$$

and

$$\left(\frac{\dot{q}}{A_i} \right)_{i+1} A_{i+1}^2 = \left(\frac{\dot{q}}{A_i} \right)_i A_i^2, \quad i = 1, 2, \dots, n \quad (4-73)$$

Across the void (between the insulation and the hot or cold wall), we have

$$\frac{\dot{q}}{A_1} \frac{A_1}{A_{n+1}} = \mathcal{F}\sigma (T_{3,n}^4 - T_{n+1}^4) \quad (4-74)$$

where $T_{n+1} = T_{\text{hot wall}}$ or $T_{\text{cold wall}}$

Taking stock of all the equations and the unknowns, we have:

- From equations 4-71, 4-73, and 4-74 there are $2n+1$ unknowns and n equations.
- Equation 4-72 specifies $(n-1)$ unknowns.

Therefore, we have $(n+2)$ unknowns and (n) equations. To completely solve a problem, two unknowns must be specified. These unknowns will normally be T_1 and T_{n+1} ; the hot wall and cold wall temperatures.

The procedure used to fully solve equations 4-71, 4-72, 4-73, and 4-74 is to repeatedly guess at the value of $\frac{\dot{q}l}{A_1}$ (which determines the insulation

temperature profile) in equation 4-71 until the guess is consistent with equation 4-74. When a consistent result is obtained, the correct solution has been achieved.

(b) Experimental Correlation. Because of the nature of multi-layer high performance insulation, it is impossible to accurately determine all of the input parameters which are required by the program. Because of this fact, one of the experimental parameters (the ratio of contact area of solid conduction to the solid conduction cross-section area) for each of three candidate insulation systems was determined by making the program output match experimental results.

(c) Sample Results. For a Dimplar insulation system, a heat flux to the cryogenic tank wall of 0.26 B. t. u. /ft.²-hr. was obtained using a calorimeter for the following insulation system:

Number of smooth sheets = 19

Number of dimpled sheets = 18

T_{hot side} = 535 °R

T_{cold side} = 140 °R

Insulation placement is as shown in figure 4-70 with Power = 1, r₁ = 2 in., r₂ = 2.5 in., and r₃ = 3.8 in.

An identical heat flux was obtained with the same insulation system placed directly at the LN₂ tank wall; that is, Power = 1, r₁ = 2 in., r₂ = 2 in., and r₃ = 3.3 in.

The input properties which could be determined by inspection were as follows:

- 18 layers.
- Hot-side temperature of 535 °R.
- Cold-side temperature of 140 °R.
- Effective emissivity (ϵ) of 0.04.
- Length of conduction path (l) of 0.01667 ft.
- Contact conductance (h) of 100 B. t. u. /ft.² - hr. - °R.
- Ratio of contact area to surface area of 0.0009.
- Material conductivity a function of temperature.
- Configuration parameters as shown in figure 4-70.

The computer program was then used to obtain the heat flux at the LN₂ tank wall as a function of the ratio of solid conduction area to conduction cross-section area. The results from that program indicate that the ratio sought was 166 (figure 4-71).

Values of 3,100 for NRC-2 and 436 for the Mylar-paper-spacer system were determined for the other systems from the curves of figure 4-72, and 4-73.

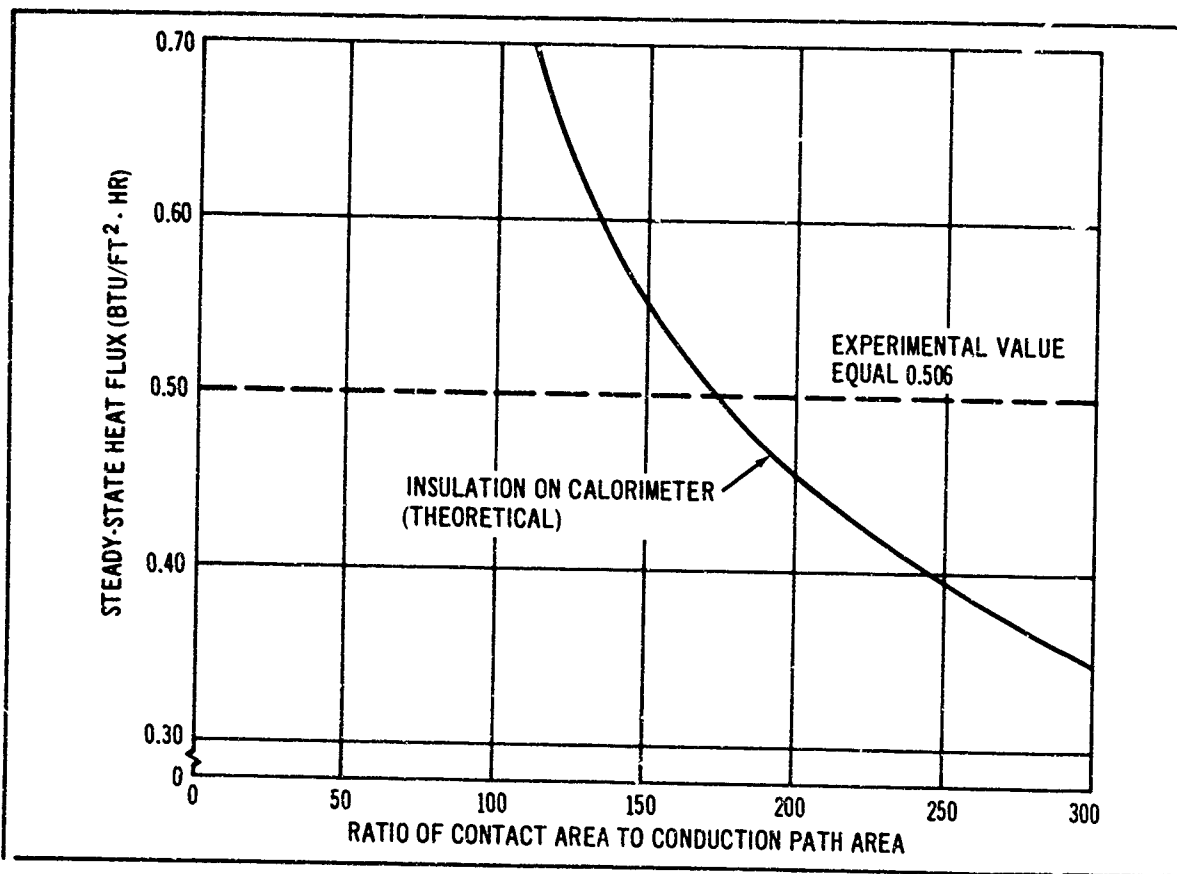


Figure 4-71. Ratio of Contact Area to Conduction Cross-Section Area for Dimplar Insulation

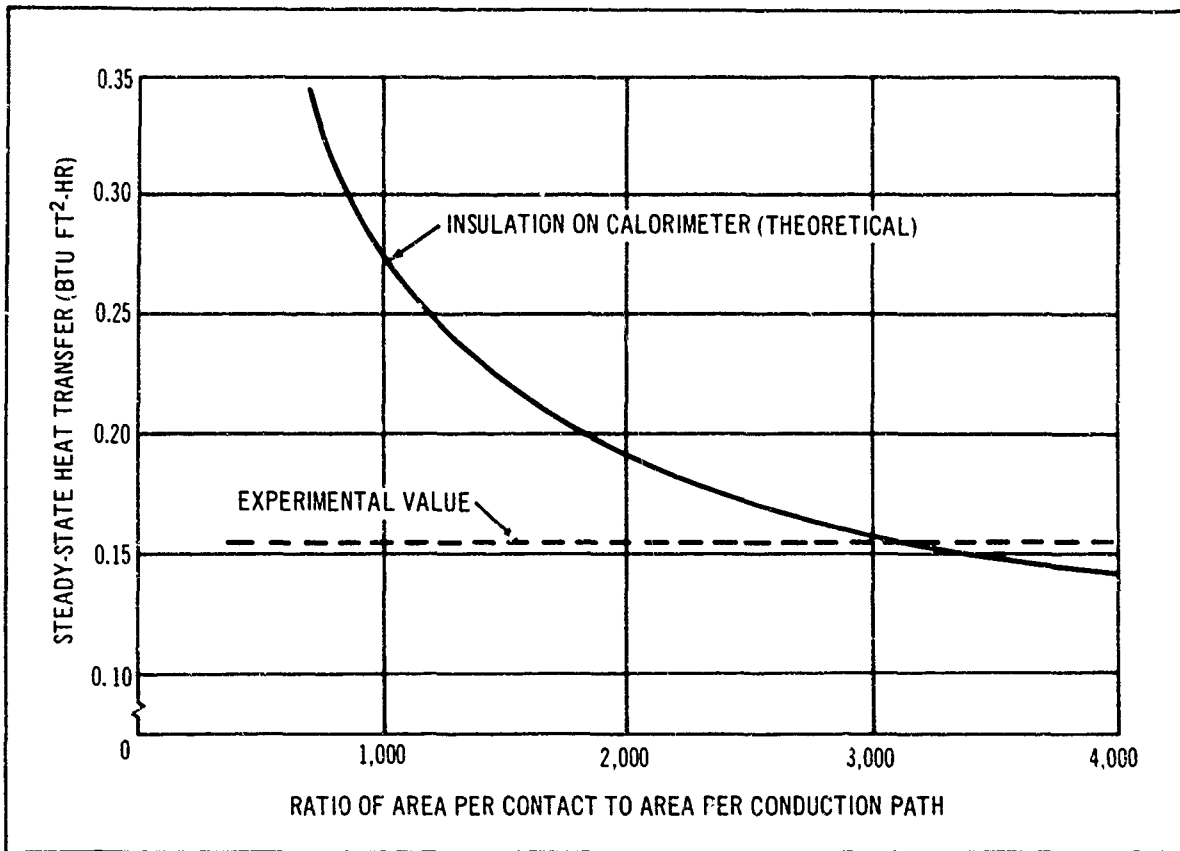


Figure 4-72. Ratio of Contact Area to Conduction Cross-Section Area for NRC-2 Insulation

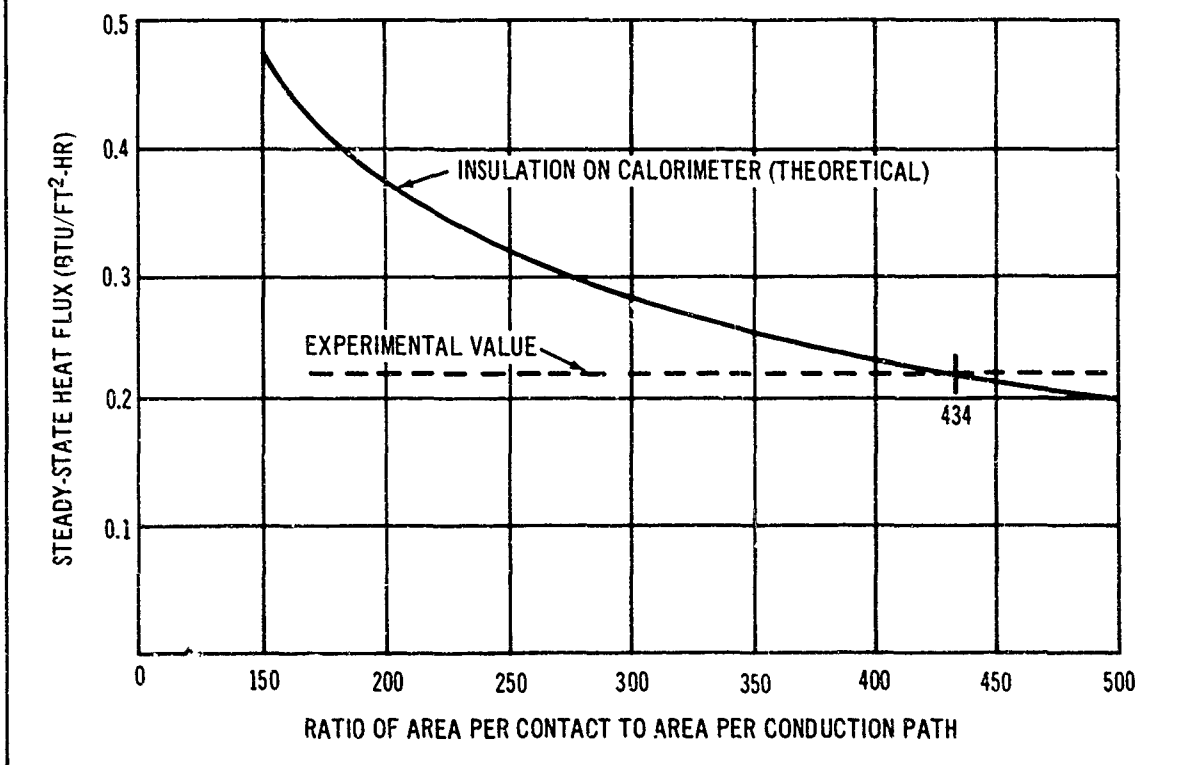


Figure 4-73. Ratio of contact Area to Conduction Cross-Section Area for Mylar and Paper Spacer Insulation

(d) Thermal Performance of the Three Candidate Insulation Systems. Once the input parameters for the three insulation systems have been determined, the performance of various amount of the insulation subjected to various temperature differences remains to be determined. This has been done for the study vehicle configuration.

Figures 4-74 through 4-76 present the heat flux to the LH₂ tank (36°R) as a function of the number of sheets of insulation and the hot-side temperature for shroud mounting of the Dimplar, NRC-2, and Mylar-paper-spacer systems, respectively. Figures 4-77 through 4-79 present similar data for the LF₂ tank (140°R). It should be noted that the heat flux plotted is the flux into the cryogenic tank and not through the insulation. Thus, the curves take into account the geometry shape factors for the study vehicle configuration.

Figures 4-80 through 4-85 show similar data for tank mounting.

(e) Development of Insulation Correlation Equation. Once the parametric data for insulation performance as summarized in figures 4-74 through 4-85 were obtained, the next task was to reduce these results into a general correlation equation which could be used to facilitate rapid tradeoff and optimization system studies using the H109 computer program.

By manipulating the insulation performance data, it was found that the insulation heat flux could be expressed by the general equation

$$\dot{q} = \frac{\gamma 10^\beta}{n^a} \quad (4-75)$$

where \dot{q} = heat flux at the cryogen tank wall in B. t. u. /ft. ² - hr.

$$\beta = \frac{a}{2} \left(\frac{T_H - 200}{50} \right)^2 + b \left(\frac{T_H - 200}{50} \right) + c \quad (4-76)$$

$$a = \frac{d}{2} \left(\frac{T_H - 200}{50} \right)^2 + e \left(\frac{T_H - 200}{50} \right) + f \quad (4-77)$$

γ = g (a constant)

n = number of layers of insulation, and

T_H = hot wall of temperature (°R).

The correlation factors for the three candidate insulation systems were evolved through analysis of basic data available from a number of sources. The factors for the aluminized Mylar-paper-spacer system were evaluated from Lockheed/NASA-LeRC published data. NRC-2 and Dimplar data being evolved under the Douglas IRAD program were used to establish the factors for these systems.

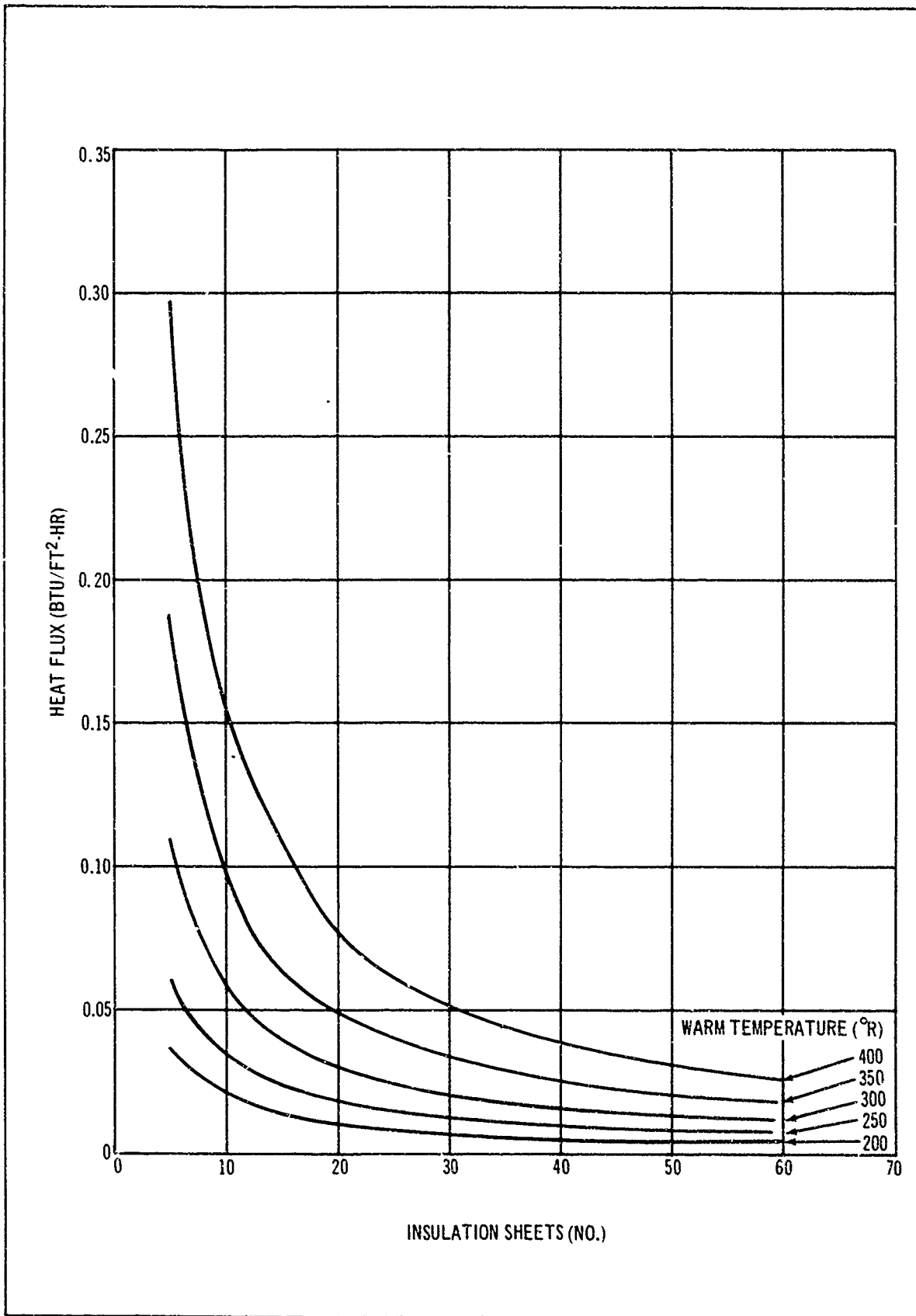


Figure 4-74. Heat Flux for Dimplar Shroud Mounting for LH₂ Tank

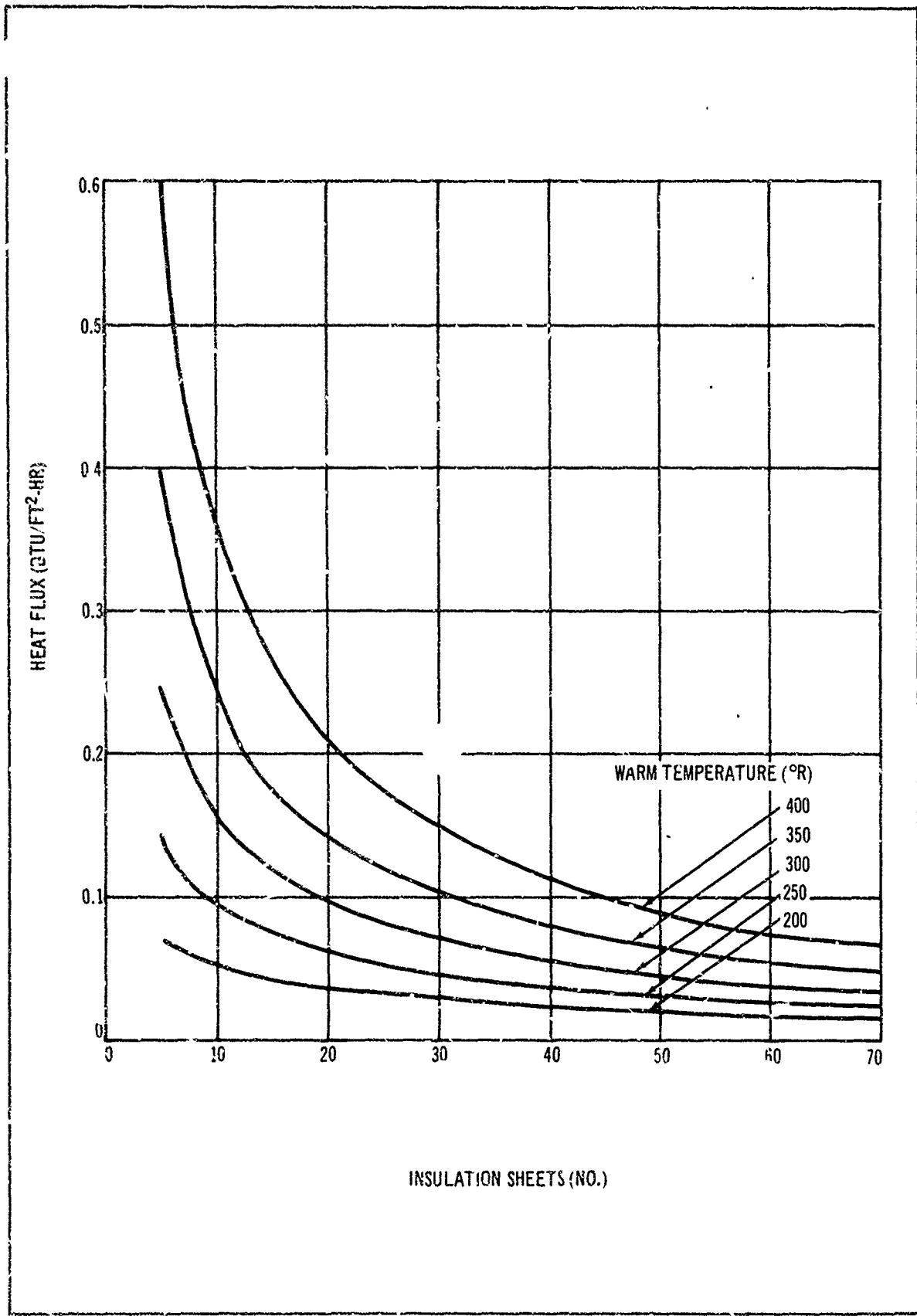


Figure 4-75. Heat Flux for NRC-2 Shroud Mounting for LH₂ Tank

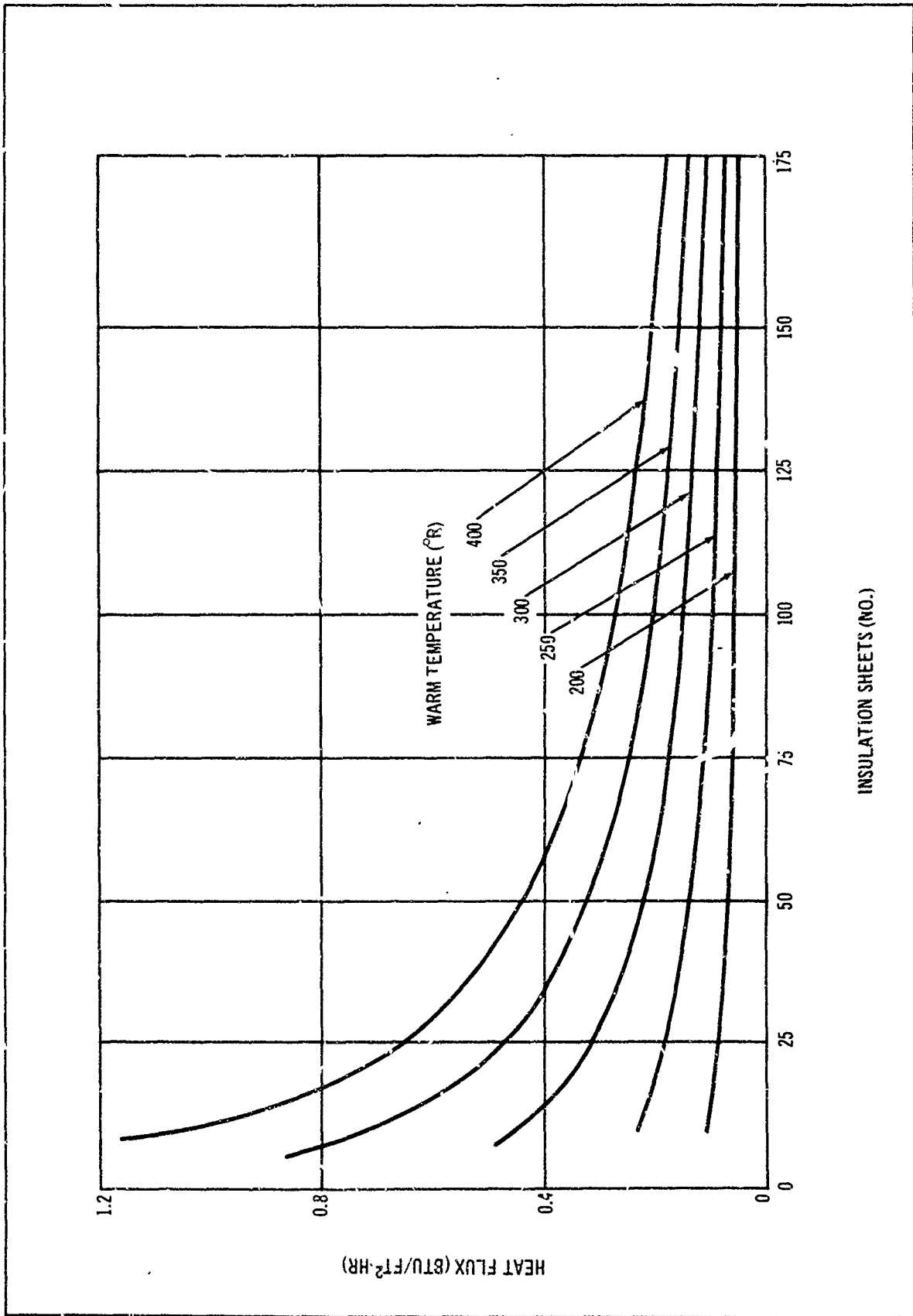


Figure 4-76. Heat Flux for Aluminized Mylar-Paper Spacer Shroud Mounting for LH₂ Tank

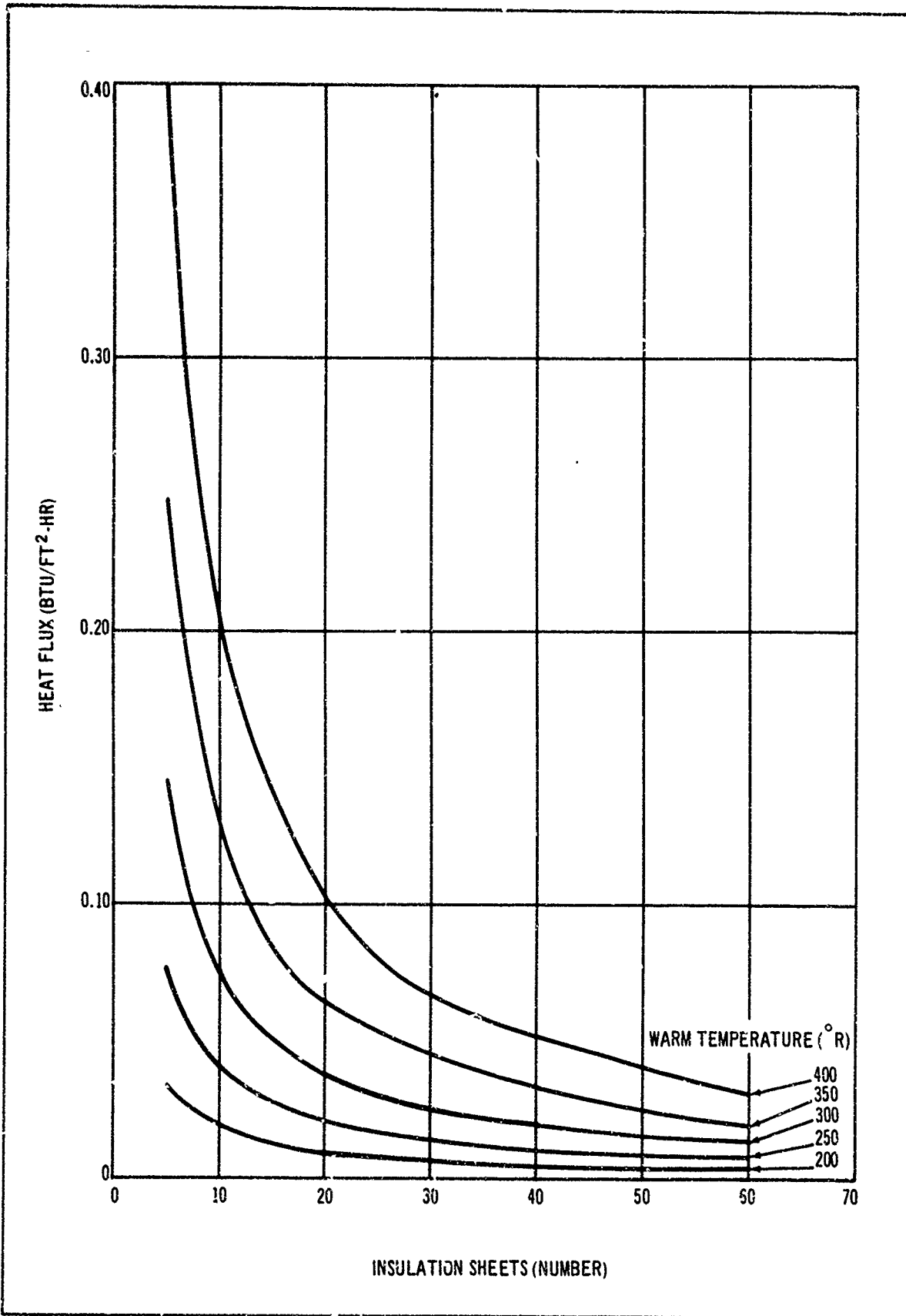


Figure 4-77. Heat Flux for Dimplar Shroud Mounting for LF₂ Tank

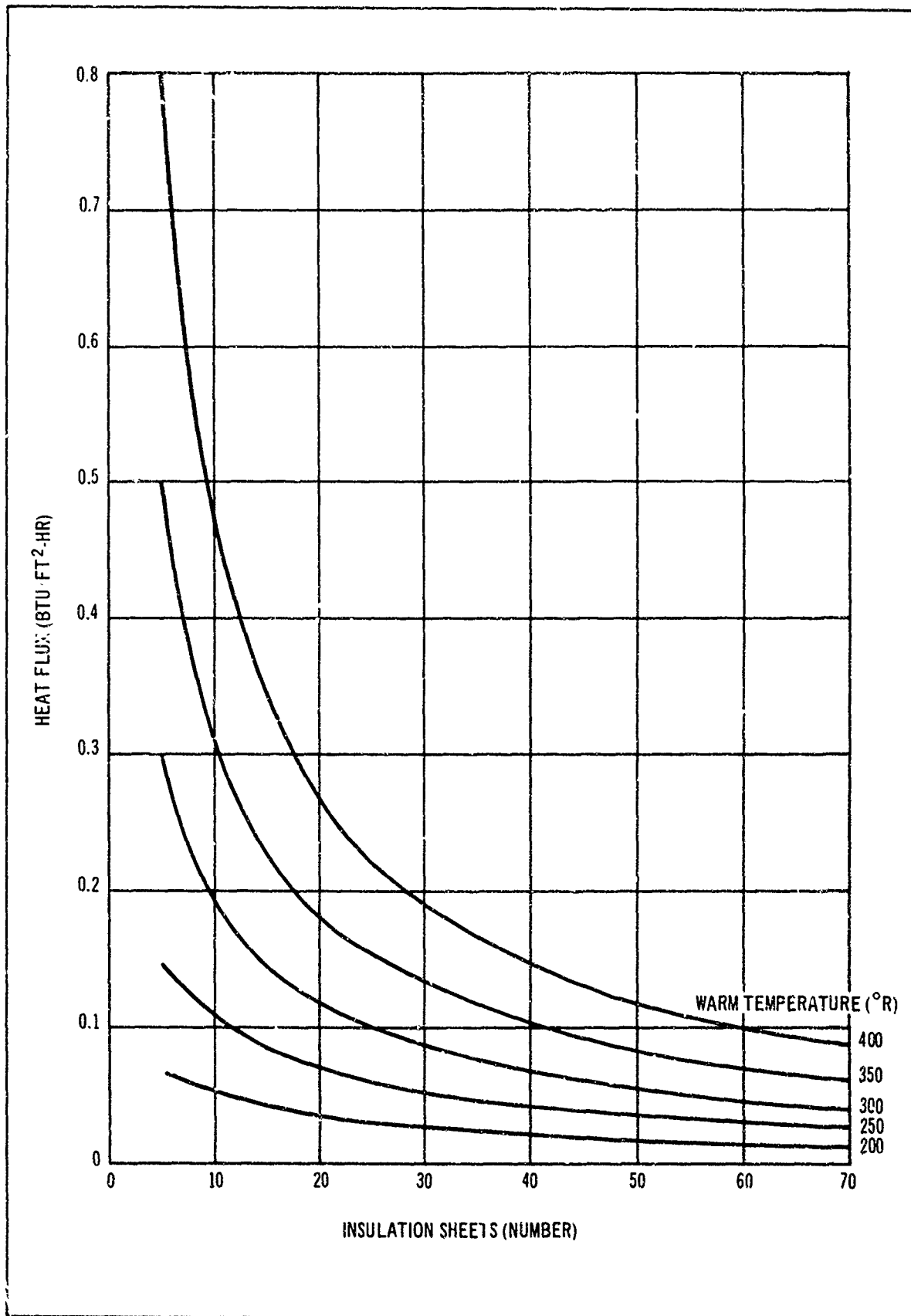


Figure 4-78. Heat Flux For NRC-2 Shroud Mounting For LF₂ Tank

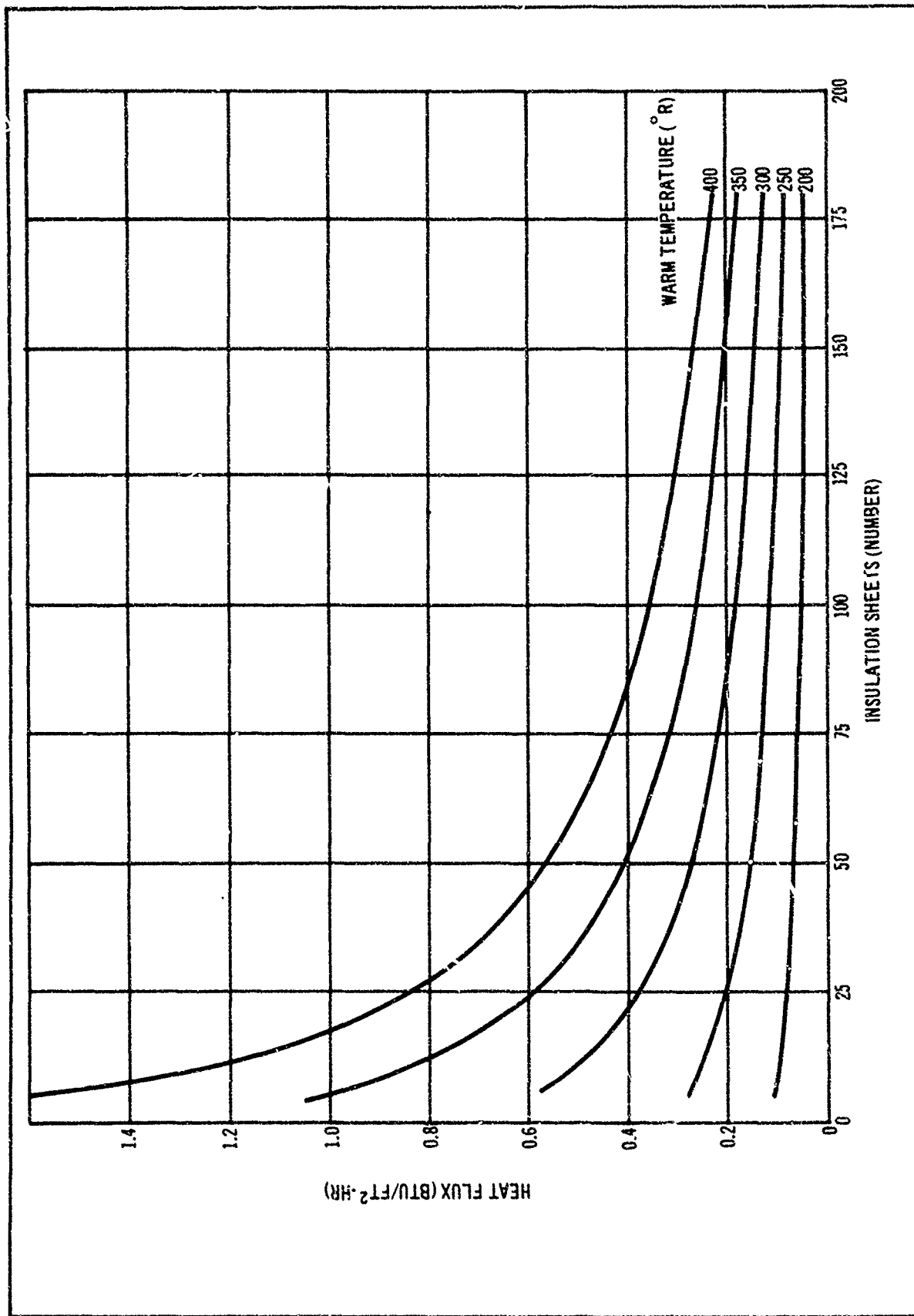


Figure 4-79. Heat Flux for Aluminized Mylar-Paper Spacer Shroud Mounting for LF₂ Tank

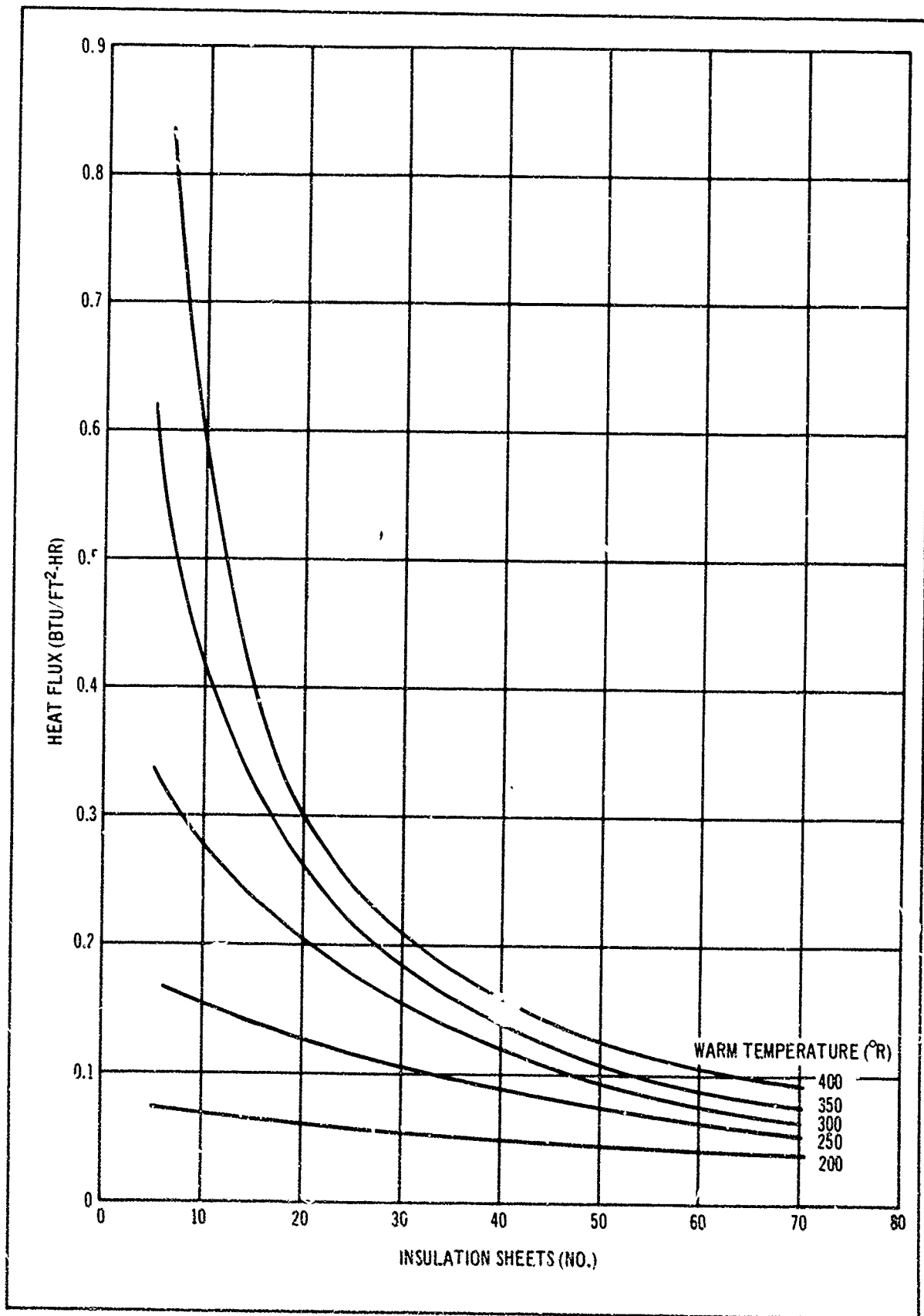


Figure 4-80. Heat Flux for Dimplar Mounting on LH₂ Tank

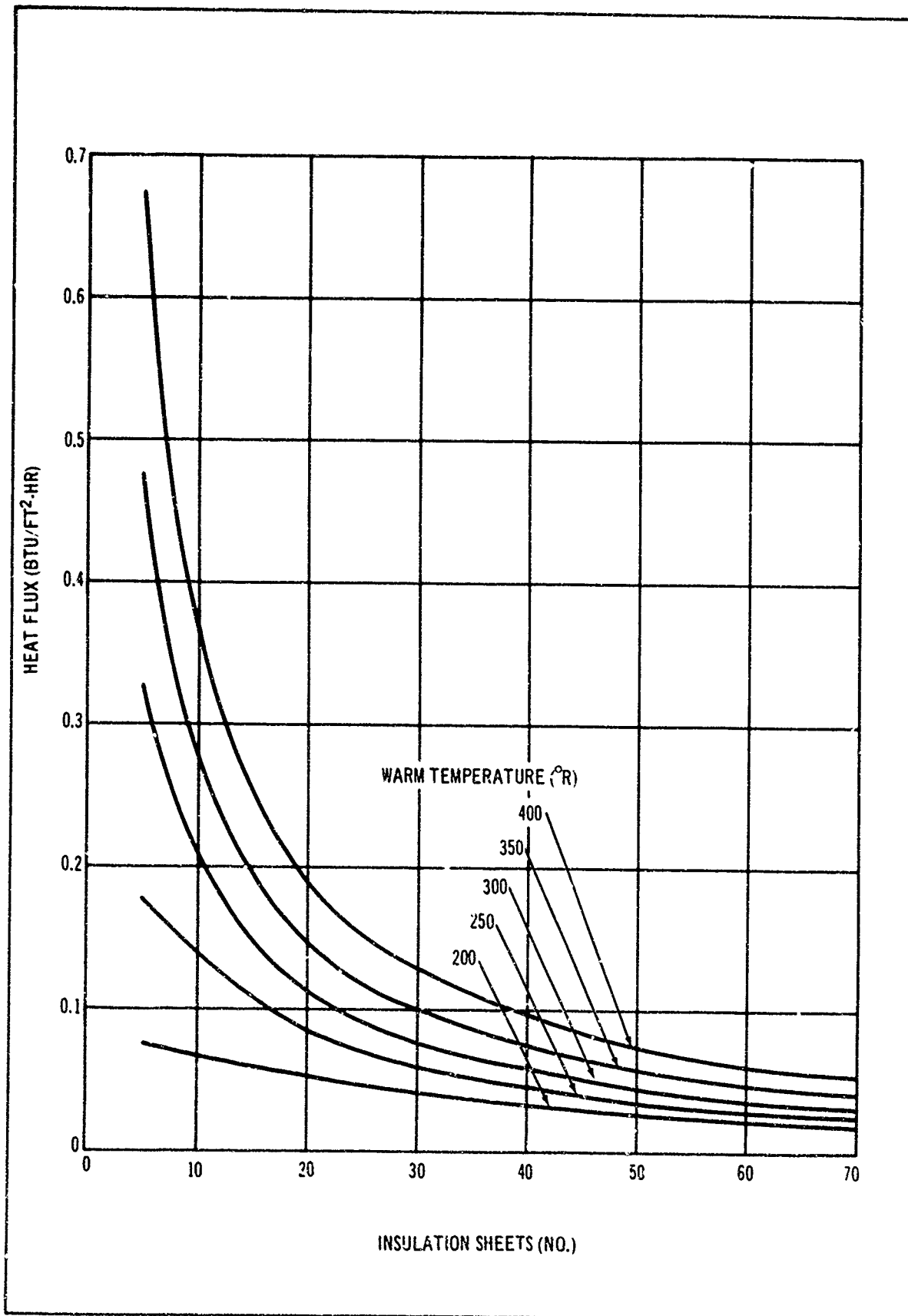


Figure 4-81. Heat Flux for NRC-2 Mounting on LH₂ Tank

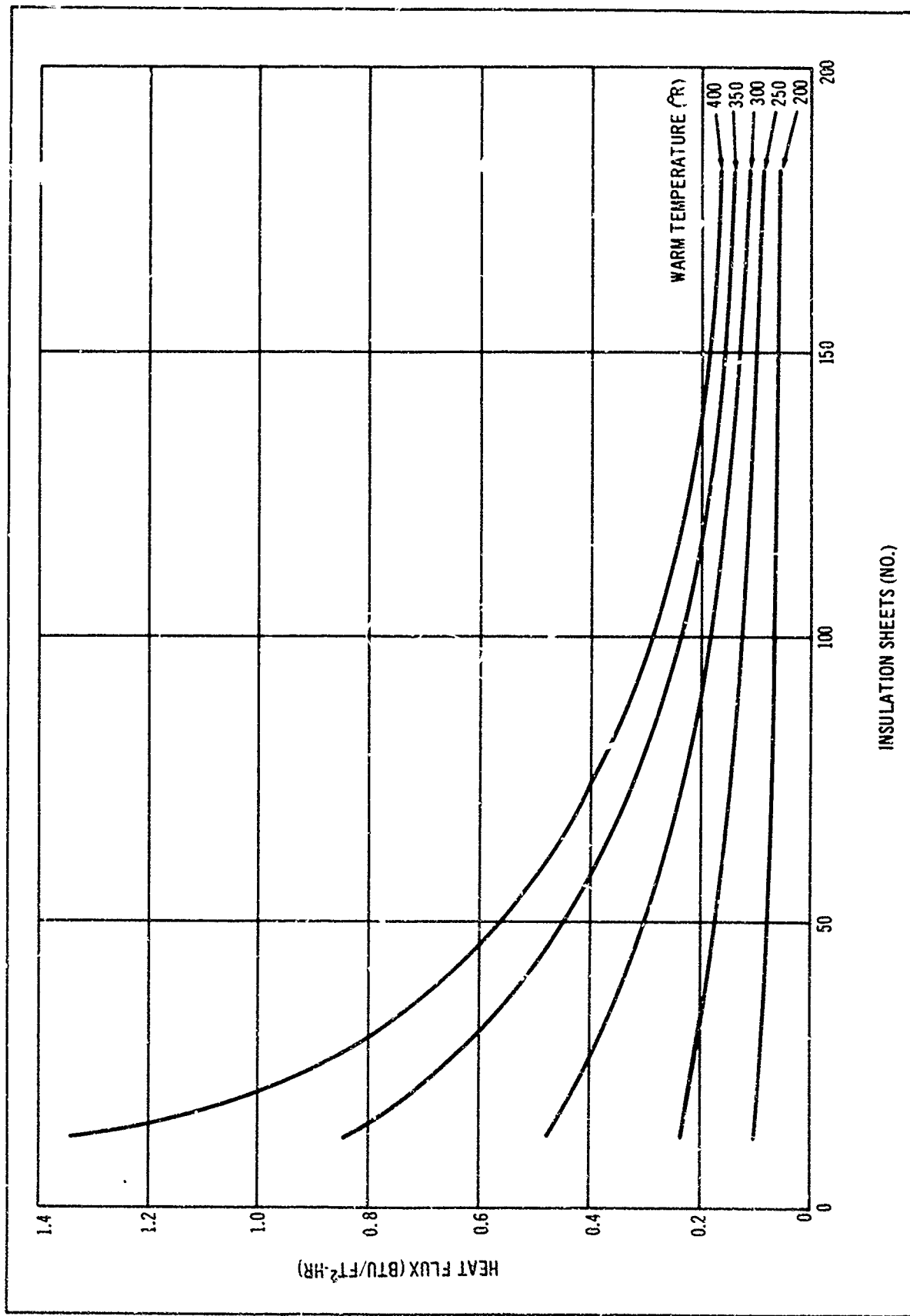


Figure 4-82. Heat Flux for Aluminized Mylar-Paper Spacer Mounting on LH₂ Tank

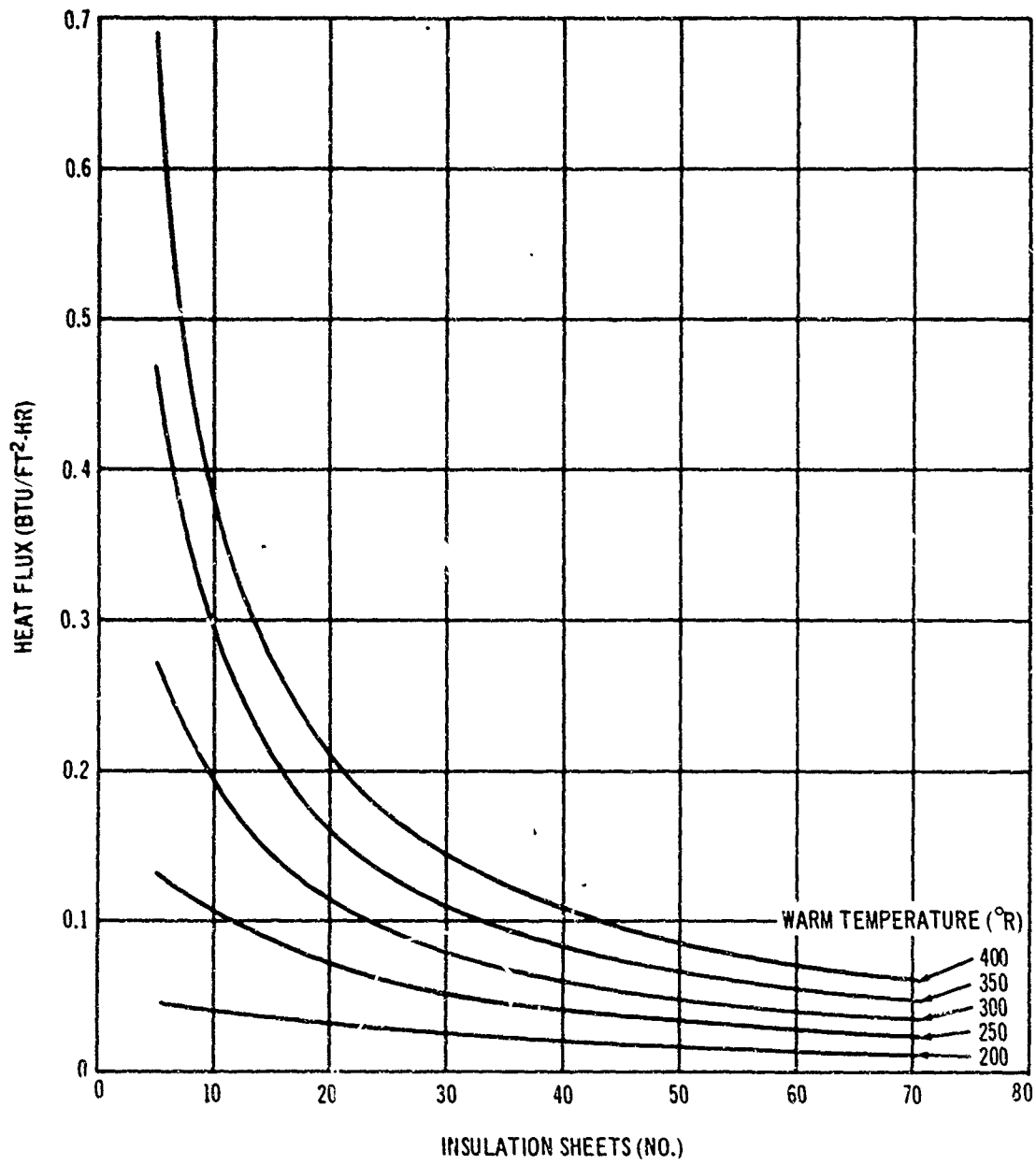


Figure 4-83. Heat Flux, Dimplar Mounting on LF₂ Tank

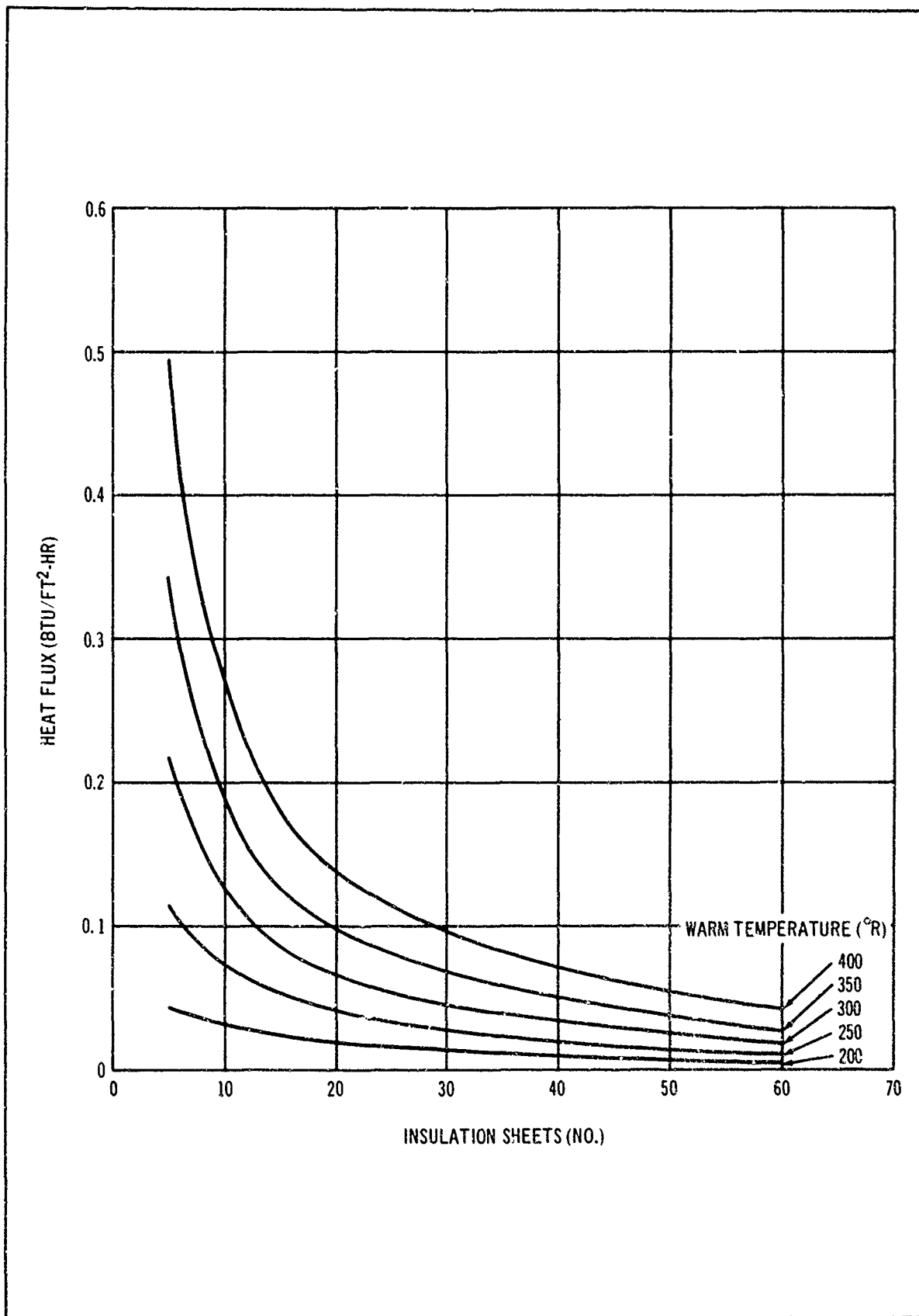


Figure 4-84. Heat Flux for NRC-2 Tank Mounting on LF₂ Tank

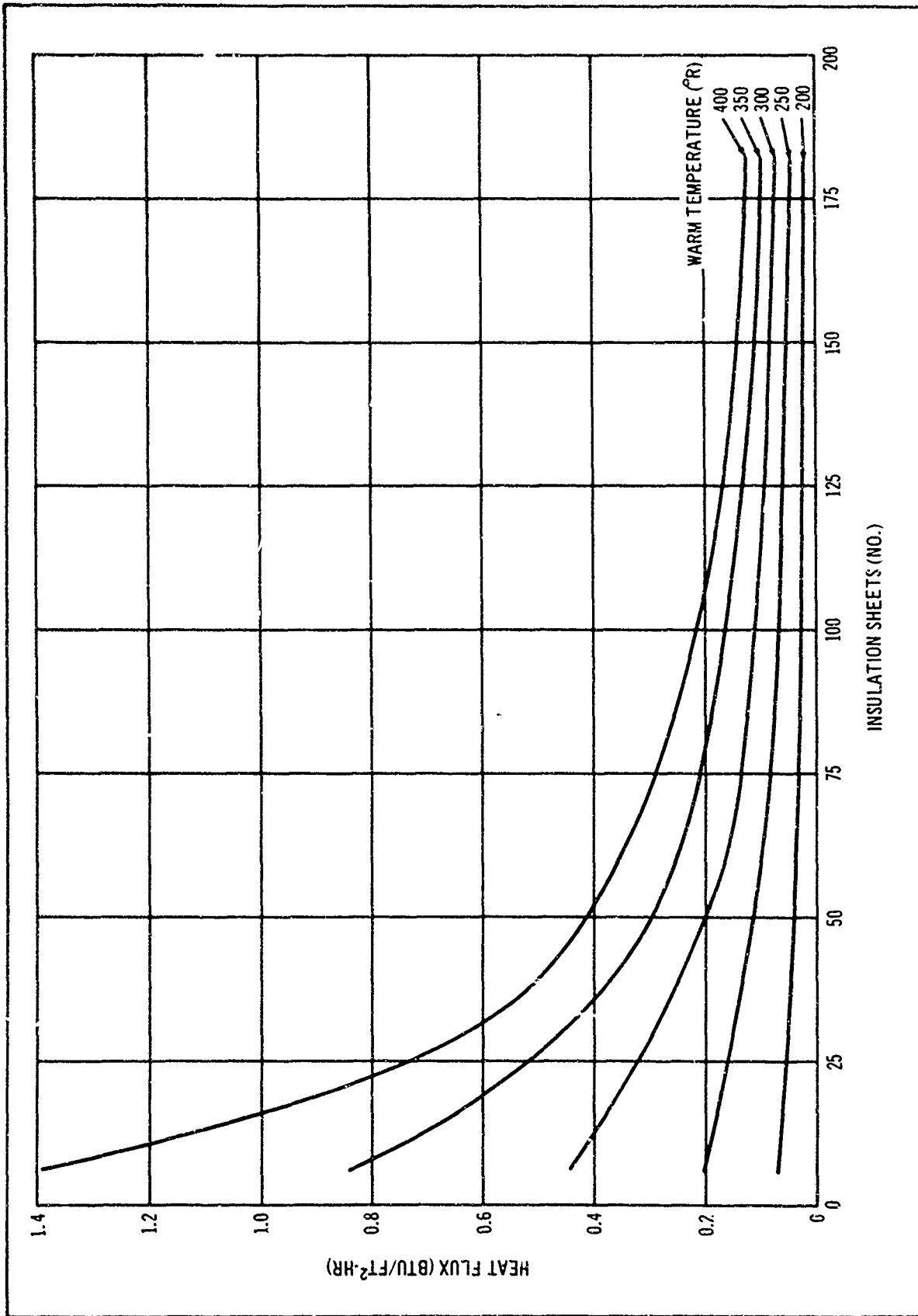


Figure 4-85. Heat Flux for Aluminized Mylar - Paper Spacer Tank Mounting on L F 2 Tank

Table 4-27 contains sets of coefficients for the correlation equation corresponding to the insulation system, the cryogen tank (LH₂ or LF₂), and the insulation location (tank or shroud).

Example: Determine the heat flux at the LH₂ tank wall for 21 layers of Dimplar with T_H = 400°R and shroud-mounted insulation.

Substituting in equations 4-75, 4-76, and 4-77:

$$q = \frac{0.1247(10) \left[-0.0365 \left(\frac{400 - 200}{50} \right)^2 + 0.343 \left(\frac{400 - 200}{50} \right) \right]}{(21) \left[-0.6 \left(\frac{400 - 200}{50} \right)^2 + 0.074 \left(\frac{400 - 200}{50} \right) + 0.819 \right]} \quad (4-78)$$

$$q = \frac{0.1247(10)^{1.08}}{(21) 0.987} = 0.0745 \text{ B.t.u./ft.}^2 \text{-hr.}$$

Equation 4-75 was coded into the overall system optimization program, H109, and the coefficient values were inserted as each insulation system was studied.

To illustrate the overall validity of correlation equation 4-75, with the insulation computer program, computations were made using each approach for shroud-mounted Dimplar on the LF₂ tank with a hot-side temperature of 300°R. The number of insulation sheets was varied from 10 to 70; the results are shown in figure 4-86. The agreement is excellent.

Table 4-27

INSULATION CORRELATION EQUATION COEFFICIENTS

	\underline{a}	\underline{b}	\underline{c}	\underline{d}	\underline{e}	\underline{f}	\underline{g}
<u>Shroud mount</u>							
Dimplar LH ₂	-0.0365	0.343	0	-0.016	0.074	0.819	0.1247
Dimplar LF ₂	-0.05	0.388	0	0	0.02	0.93	0.15
NRC-2 LH ₂	-0.0452	0.3621	0	-0.0195	0.10525	0.585	0.208
NRC-2 LF ₂	-0.069	0.438	0	-0.01875	0.0952	0.619	0.21
MPSS LH ₂	-0.086	0.468	0	-0.0301	0.1302	0.3388	0.2065
MPSS LF ₂	-0.07	0.455	0.024	0	0.067	0.386	0.219
<u>Tank mount</u>							
Dimplar LH ₂	-0.19375	0.8245	0	-0.0925	0.385	0.157	0.098
Dimplar LF ₂	-0.148275	0.6433	0	-0.061	0.225	0.527	0.1415
NRC-2 LH ₂	-0.14006	0.5623	0	-0.08525	0.27925	0.574	0.271
NRC-2 LF ₂	-0.0905	0.4544	0	-0.02875	0.10175	0.788	0.204
MPSS LH ₂	-0.20322	0.85322	0	-0.0905	0.359	0.186	0.1605
MPSS LF ₂	-0.013827	0.65235	0	-0.03825	0.17825	0.501	0.237

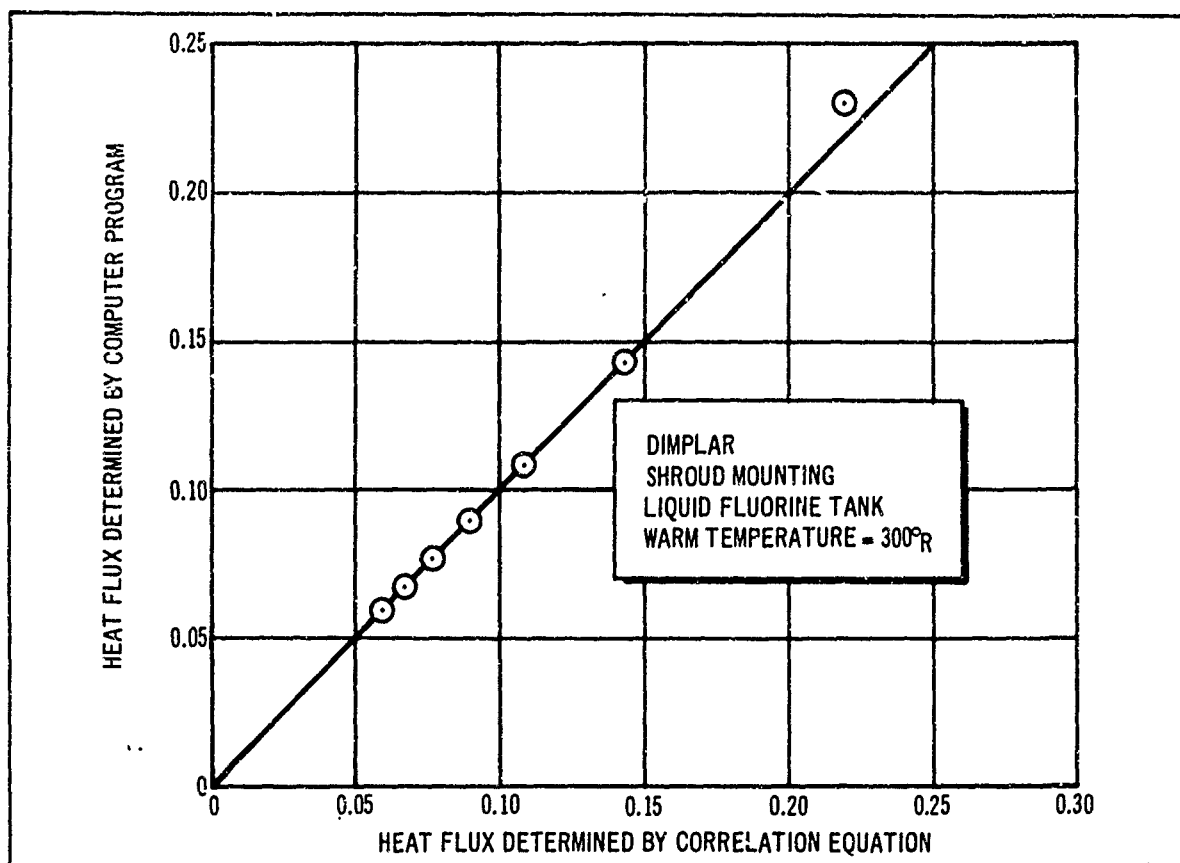


Figure 4-86. Comparison of Correlation Equation and Computer Results

(f) Insulation System Weight Factors. Basic weight information for the candidate systems was collected and is summarized in table 4-28. Also shown are the design factors for insulation areas as determined from the study vehicle configuration, an estimated factor for insulation overlap, and a factor for insulation attachment weight. This last value was based on the use of a thread and button-type attachment system and is proportional to the area to be insulated. It was assumed that the required attachment weight per sq. ft. of area to be insulated was the same for either tank or shroud mounting. The area to be insulated for the shroud-mounted case was based on the configuration shown in figure 2-1. This insulation configuration assumes that areas are provided for mounting certain components between the shroud or structural shell and the insulation where the environmental temperature is not severely low.

(4) Ground-Hold and Boost Heating Provisions. To this point, the reported work has concentrated on space environmental performance of the insulation system. However, the stage must be capable of performing under ground-hold and boost-phase operation and this can have a profound effect on the insulation system design.

Table 4-28

INSULATION WEIGHT FACTORS

<u>Basic material weight</u>		
1/4 MIL singly-aluminized Mylar (NRC-2)		0.0018 lb./ft. ² - layer
1/4 MIL double-aluminized Mylar		0.0019
1/2 MIL doubly-aluminized Mylar		0.0037
1/2 MIL doubly-aluminized Mylar dimpled		0.00396
paper spacer		0.0035
<u>Basic system weight</u>		
NRC-2		0.0018 lb./ft. ² - layer
Aluminized Mylar with spacer		0.0054 lb./ft. ² - pair
Dimplar		0.0059 lb./ft. ² - pair
<u>Design factors</u>		
Installation weight		0.03 lb./ft. ²
Overlap weight factor		12 pct.
<u>Design areas</u>		
Insulation area (uncorrected)	LH ₂	LF ₂
Tank mounted	185 ft. ²	123 ft. ²
Shroud oriented	268.5	203
Typical calculation: (20 pairs Dimplar - 500 ft. ²)		
WT = (0.0059) (20) (500) (1.12) + 0.03 (500) =		
66 + 15.0 = 81		

During ground-hold operation, the cryogenic tanks can be tapped off from the ground. For the purposes of this study, it was assumed that this could be continued up to the time of liftoff so that actual propellant loss because of ground heating could be maintained very low. However, to avoid the hazards of air liquification within the stage, purging of the interstage with N_2 and/or He is required. He alone may be used because it does not condense at either $L.F_2$ or $L.H_2$ temperatures. However, purging an entire interstage may require a considerable amount of He. N_2 may be used for primary purging with a foam substrate which is either evacuated or purged with He to limit the foamed area to a temperature no lower than the condensation temperature of N_2 ($140^\circ R$). Such a purged substrate system is described in References 21 and 22. In this case, the less expensive and more plentiful GN_2 is used for primary purging, but the weight of the substrate and its associated manifolding must be added to the stage inert weight. An evacuated and sealed substrate may also be used, but at the present state of technology such a system is not near reality. Obtaining a reliable sealed bag or other type of sealed substrate bag is the basic problem.

As part of this contract, a technology review trip was made to industrial and government centers working on problems related to this contract. The above conclusion regarding the sealed substrate was upheld--at least at this point in time--but there was a strong divergence of opinion regarding the type of purge. To permit a more rational assessment of the approach to be taken with respect to purging, approximate calculations were made comparing a good cryopumped substrate using N_2 purge to a pure He interstage purge system. Using the model as shown in figure 4-87,

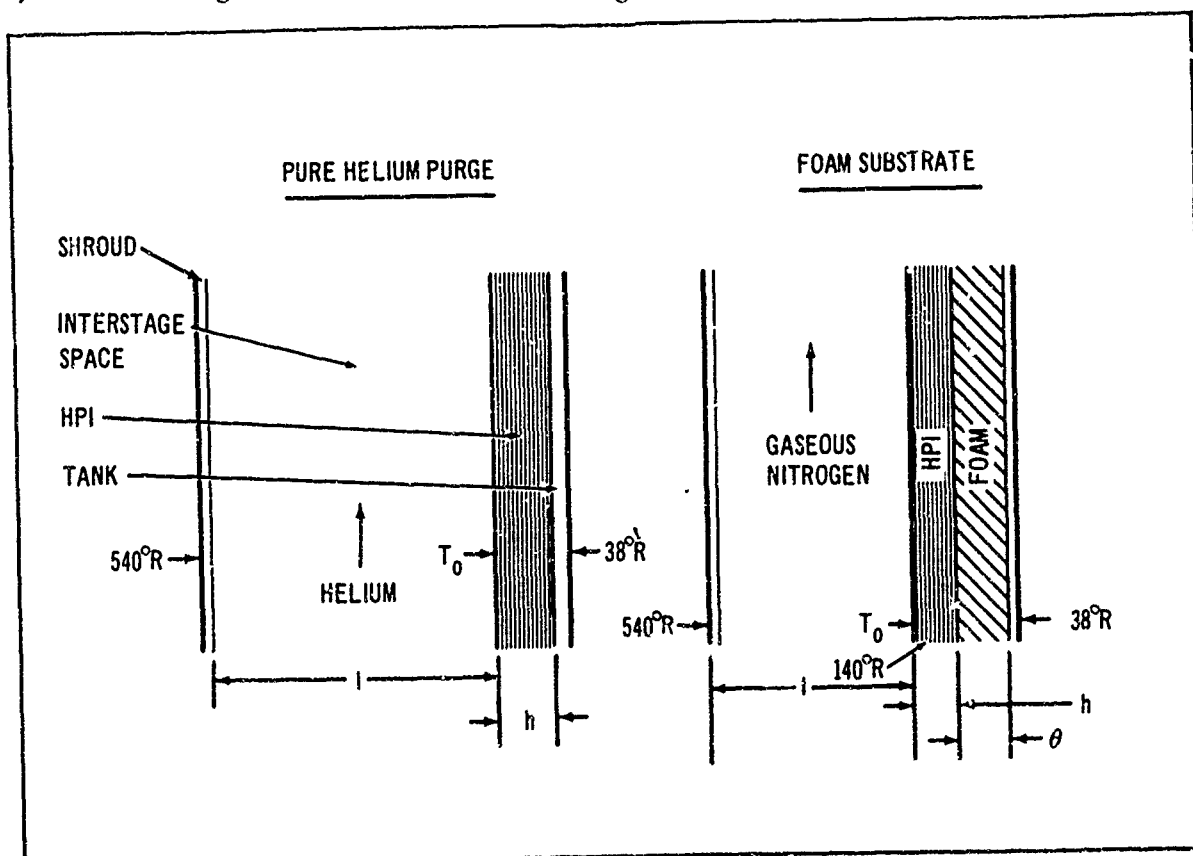


Figure 4-87. Model for Ground-Hold Analyzer

the steady-state heat flux, q , may be expressed as:

$$q \frac{\text{Btu}}{\text{Ft}^2 \text{hr}} = \frac{k}{x} \Delta T \quad (4-78)$$

Values for the three insulating elements, the foam, the high performance insulation (HPI), and the interstage space, can be obtained from:

$$q_{\text{foam}} = \frac{k_f}{\theta} (140-38)(12) \quad (4-79)$$

$$q_{\text{HPI}} = \frac{k_{\text{HPI}}}{h} (T_o - 38)(12) \quad (4-80)$$

$$q_{\text{int}} = \frac{k_{\text{int}}}{l} (540 - T_o)(12) \quad (4-81)$$

For representative conditions: $k_f = 0.02$

$$k_{\text{HPI}} = 0.06 (\text{He}) = 0.015 (\text{GN}_2)$$

$$k_{\text{int}} = 0.4 (\text{He}) = 0.11 (\text{GN}_2) \text{ (free convection)}$$

The above equations then become: $q_{\text{foam}} = \frac{24.4}{\theta} \quad (4-82)$

$$q_{\text{HPI}} = \frac{0.72}{h} (T_o - 38)_{\text{He}} = \frac{0.18}{h} (T_o - 1-2)_{\text{N}_2} \quad (4-83)$$

$$q_{\text{int}} = \frac{4.8}{l} (540 - T_o)_{\text{He}} = \frac{1.3}{l} (540 - T_o)_{\text{N}_2} \quad (4-84)$$

These can be put in terms of weights (W'), assuming that all heat goes into boiloff by dividing q by the heat of vaporization, 192.7 B. t. u. lb.

$$W'_{\text{foam}} = \frac{0.127}{\theta} \quad (4-85)$$

$$W'_{\text{HPI}} = \frac{0.72}{h} (T_o - 1.97)_{\text{He}} = \frac{0.18}{h} (T_o - 1.53)_{\text{N}_2} \quad (4-86)$$

$$W'_{int} = \frac{4.8(2.8-T_0)}{1} \text{ He} = \frac{1.2(2.8-T_0)}{1} \text{ N}_2 \quad (4-87)$$

where T_0 is 192.7°R.

For steady-state conditions equations 4-85, 4-86, and 4-87 are equal.

For the He system, equations 4-85 and 4-86 can be solved for T_0 :

$$T_0 = \frac{18.7h + .197L}{6.67h + L}$$

and from equation 4-85,

$$W'_{gh} = \frac{.72(18.7h + .197L) - .197}{h(6.67h + L)} = \frac{12.4}{6.67h + L} \left(\frac{\text{lb}}{\text{ft} \cdot \text{hr}} \right)$$

Coast boiloff weight loss, W'_c is:

$$W'_c = \frac{k_{\text{HPI}} \text{evac}(540-38)}{192.7h}$$

The conductivity of evacuated HPI is in the order of 8×10^{-5} B. t. u. ft.-hr. °F.

$$\text{Thus: } W'_c = \frac{502}{192.7h} (8 \times 10^{-5}) = \frac{2.5 \times 10^{-3}}{h} \frac{\text{lb.}}{\text{ft.} \cdot \text{hr.}}$$

The HPI weight is about $0.09h \frac{\text{lb.}}{\text{ft.}^2}$

If t_g is the ground-hold time and t_c is the coast time, the total weight penalty for the pure He purge system is:

$$W'_{he} = \frac{12.4t_g}{6.67h + l} + 2.5 \times 10^{-3} \frac{t_c}{h} + 0.09h \frac{\text{lb}}{\text{ft.}^2}$$

Using a similar approach for the N_2 purge system:

$$W'_{\text{N}_2} = \frac{2.73t_g}{6.67h + l} + 2.5 \times 10^{-3} \frac{t_c}{h} + 0.09h + \rho \theta + \left(\frac{\text{lb}}{\text{ft.}^2} \right)$$

The results obtained with these equations are shown in figure 4-69.

Computations were made for the total weight penalty versus ground-hold time where the weight penalty included boiloff and foam insulation weight. In addition to the conventional foam ($\rho = 0.8$, $k = 0.02$), a hypothetical foam with improved properties of $\rho = 0.4$ and $k = 0.01$ was also evaluated. Figure 4-69 (A) shows that with no coast considered, the pure He purge is lighter than either foam material with short hold times. The same trend is even more apparent when a 300-hr. coast is considered. Therefore, on this basis, a pure He purge system was assumed for the remainder of this study, although the difference in boost phase boiloff by using He as opposed to nitrogen was evaluated.

Early in the Douglas HPI IRAD program, the general feasibility of a He-purged NRC-2 insulation for ground-hold application was demonstrated using a 300 gal. LH_2 test tank in the Douglas Hydrogen Research Facility. The test apparatus and gross boiloff results are illustrated in figure 4-88. The tank was equipped with a cylindrical annulus into which an NRC-2 insulation was placed. Provisions were also incorporated to provide a dry ambient temperature He purge entering at the top and exiting through a bottom manifold. The annulus was purged until less than a 2 pct. O_2 content was sensed in the purge exhaust after which time the tank was filled with LH_2 . Through temperature and liquid level seasons, the LH_2 boiloff was estimated as shown in the curve of figure 4-88.

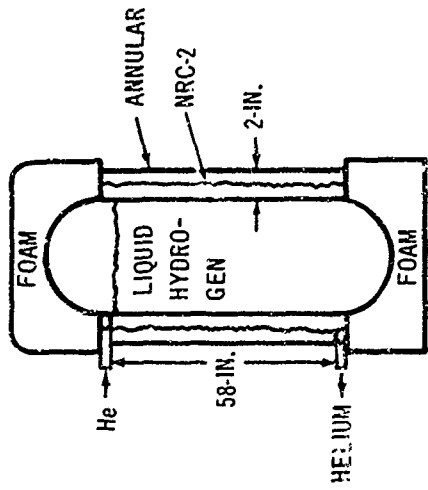
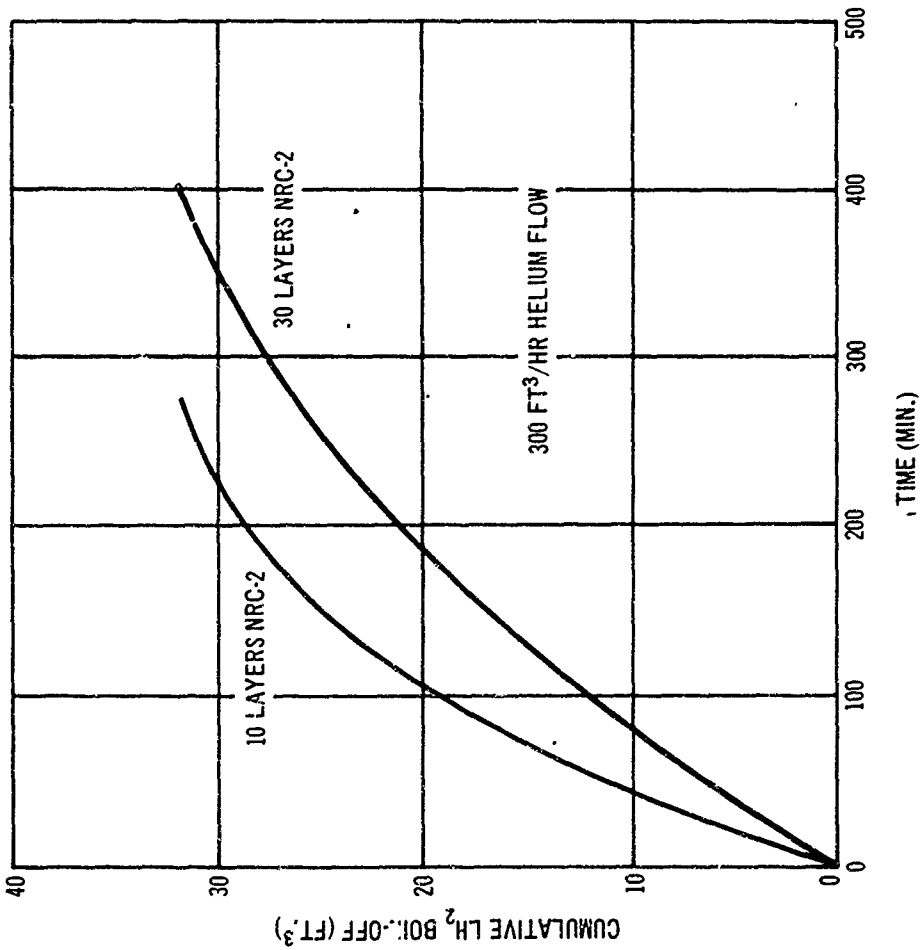
The data was also interpreted to yield mean effective thermal conductivity values with the following results:

- With a He flow of $200 \text{ ft}^3/\text{h.}$ and no HPI, $k = .38 \frac{\text{B. t. u.}}{\text{f.p.h.}^\circ\text{R.}}$
- With a He flow of $200 \text{ ft}^3/\text{h.}$ and 10 layers of NRC-2, $k = 0.27$.
- With a He flow of $200 \text{ ft}^3/\text{h.}$ and 30 layers of NRC-2, $k = 0.074$.

These values indicate that with little or no insulation, the heat transfer is slightly less than would be anticipated with a free convection analysis. With the insulation filling the annulus, as would be the case with 30 layers, the insulation acts to break up convection, and the process is close to a conduction process with a conductivity very near that of He.

The recorded temperature differences are also of interest. With a wet tank wall (37°R) the outer annulus jacket temperature varied from -280°F to -170°F for a ΔT across the purge of from 125 to 225° . If one applies directly, the results of figure 4-28 to the study flight vehicle, the ground-hold boiloff can be estimated in the following manner:

$$\begin{aligned} \text{Maximum slope of the 10 layer curve} &= 0.20 \frac{\text{ft}^3}{\text{min.}} \\ &= 0.88 \frac{\text{lb.}}{\text{min.}} \end{aligned}$$



TOTAL CYLINDRICAL VOLUME = 34.5 FT³
 TOTAL CYLINDRICAL SURFACE AREA = 45.6 FT²

Figure 4-88. Purged Interstage Ground-Hold Test

$$\text{Boiloff per effective ft.}^2 \text{ of tank area} = \frac{0.88}{45.6} = 0.019 \frac{\text{lb}}{\text{min.} \cdot \text{ft.}^2}$$

$$\text{The study vehicle LH}_2 \text{ tank area} = 185 \text{ ft.}^2$$

$$\begin{aligned} \text{Boiloff for study vehicle} &= 0.019 \times 185 = 3.54 \text{ lb. /min.} \\ &= 212 \text{ lb. /hr.} \end{aligned}$$

This value is more accurately computed below.

Heat transfer into the propellant tanks during ground hold and boost has been calculated with the aid of the Douglas JD22 computer program. This was accomplished for both He- and N₂-purged systems. Internal heat transfer from the skin to the tanks was included. These heat-transfer coefficients were obtained by modifying the coefficients obtained during a rapid pump-down of the Douglas 36-in. sphere HPI test apparatus as part of the Douglas IRAD effort.

The experimental apparatus from which the heat-transfer coefficients were obtained was somewhat different than the present system. The experimental apparatus has (1) a smaller thickness of insulation, (2) insulation on the tank, and (3) a slightly slower trajectory. A correction for insulation thickness was made by breaking the heat-transfer coefficient into a conduction and a convection component and then changing the conduction component. To be sure of obtaining conservative results, the resistance caused by convection from the skin to the insulation was neglected. An increase in the heat transfer coefficient by a factor of 2 was assumed to be the effect of moving the insulation from the tank to the shroud. The faster trajectory of the case being presently analyzed was corrected for by matching the coefficients when the free molecular flow regime became important. The shape of the time-heat-transfer coefficient curve was kept the same. The heat-transfer coefficients used are shown in figure 4-89.

Ground-hold heat transfer was calculated using the coefficients at time zero. The heat-transfer rates were then converted to boiloff rates for the H₂ and to temperature-increase rates for the F₂ since the LF is loaded in a subcooled state. These results are summarized in table 4-29. The H₂ being boiled off will be made up in the topping operation. The F₂ temperature increases appear large; however, it is loaded at a temperature of about 80°F below the tank pressure saturation temperature. It will take about 15 hours before F₂ evaporation would begin with a He-purged system. The ground-hold steady-state skin temperature value near the H₂ tank for a helium purge is -105°F. This corresponds quite well to a value of -160°F found during the Douglas IRAD ground-hold testing. This latter temperature is lower because of forced convection currents set up between the insulation and the outer skin due to relatively high purge gas flow rates.

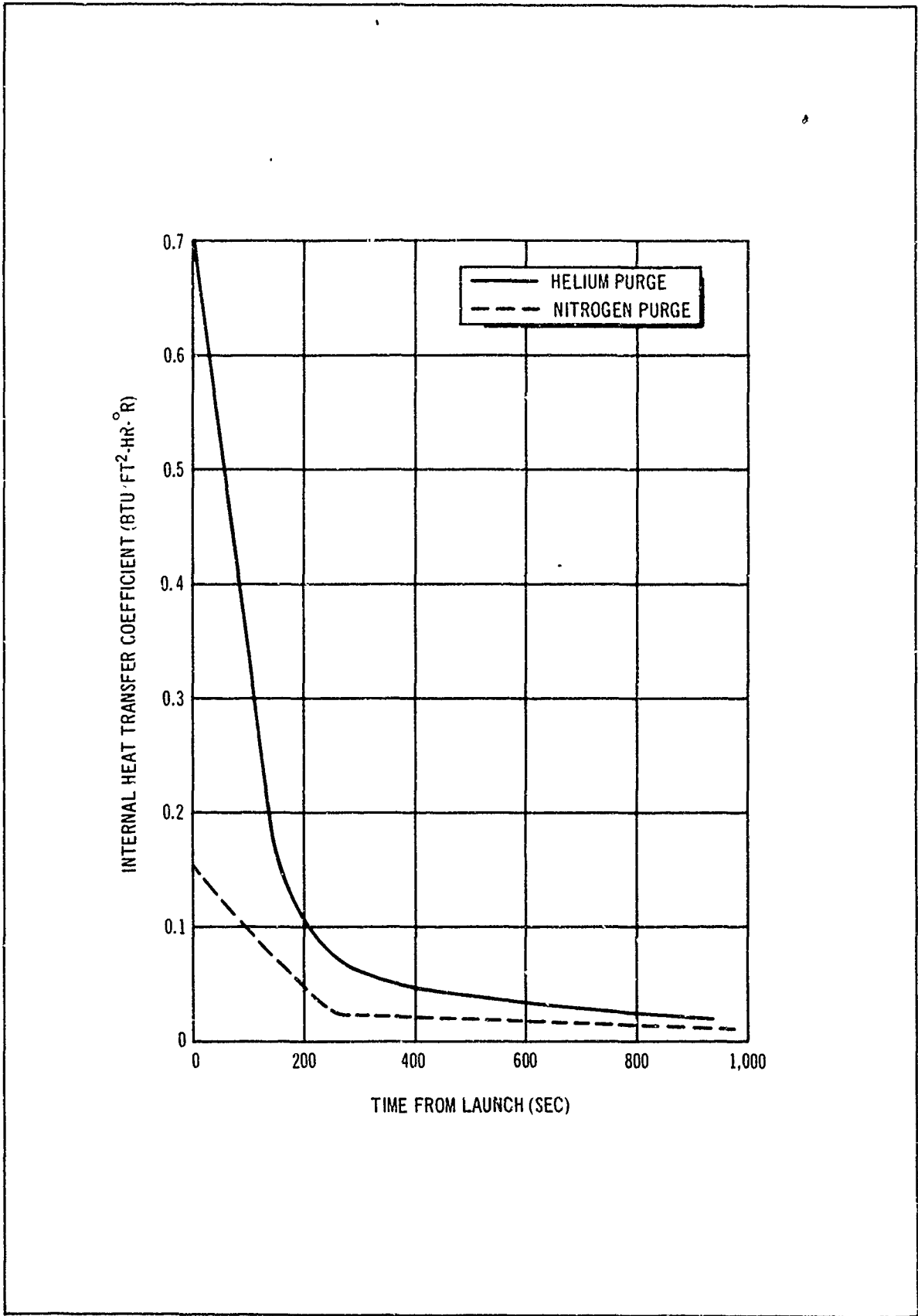


Figure 4-89. Internal Heat Transfer Coefficients During Boost

Table 4-29

GROUND-HOLD PROPELLANT HEATING

Propellant	Purge Gas	Heating Rate B. t. u. /hr.	Boiloff rate lb. /hr.	Temperature °F/hr.
LH ₂	He	37,800	197	--
LH ₂	N ₂	9,500	49.5	--
LF ₂	He	21,600	--	5.08
LF ₂	N ₂	5,500	--	1.29

Boost heating was analyzed assuming a typical Titan III-C trajectory. The results are presented in figures 4-90 and 4-91. Figure 4-90 gives the skin temperature history near the H₂ tank, and the F₂ tank. As can be seen, the highest temperature (56°F), that near the F₂ tank for a N₂ purge, is still considerably below the danger point for structural failure of aluminized Mylar. The small bumps and dips are caused by places in the trajectory when the aerodynamic heating rate falls below the interior heat-loss rate. An additional computer run was made neglecting internal heat transfer, and a maximum temperature of 140°F was reached (still quite low). Figure 4-91 shows the total heat into the LH₂. These final heat values correspond to boiloffs of 9.6 lb. for He purge and 3.9 for N₂ purge.

The extra weight of H₂ boiloff for a He purge (5.7 lb.) is considerably less than the weight of a foam substrate required for a N₂ purge system, thus further substantiating the earlier selection of an all-He interstage purge for ground-hold and boost thermal protection. Figure 4-91 also shows LF₂ total heating. These correspond to temperature increases of 0.246°F and 0.1°F for He and N₂ purges, respectively.

(5) Multilayer Insulation Depressurization. As a vehicle rises through the atmosphere, the ambient pressure drops. This creates two problems with typical HPI systems. The first problem is simply that gases which are inside the insulation blanket must escape; otherwise, the blanket may billow or balloon, and perhaps tear away from its support. Even ignoring physical damage, blankets that are very carefully arranged on the tank may become so disarrayed that the insulation system no longer functions efficiently. The insulation system must be designed to let these gases escape rapidly. The term depressurization is used to denote this process.

The second problem is keyed to the fact that multilaminar HPI systems must be evacuated to achieve high performance. More specifically, the pressure within the insulation should be 10⁻⁴ torr or less to achieve the full potential of the HPI system. The importance of maintaining or achieving a low pressure within the insulation is shown in figure 4-92 where the effective thermal conductivity of NRC-2 is plotted as a function of the internal gas pressure. The insulation system must be designed to achieve a pressure of 10⁻⁴ torr or less, as early as possible. The ideal, but probably unobtainable, case would be for the pressure within the insulation to equal, at all times, the pressure outside the insulation.

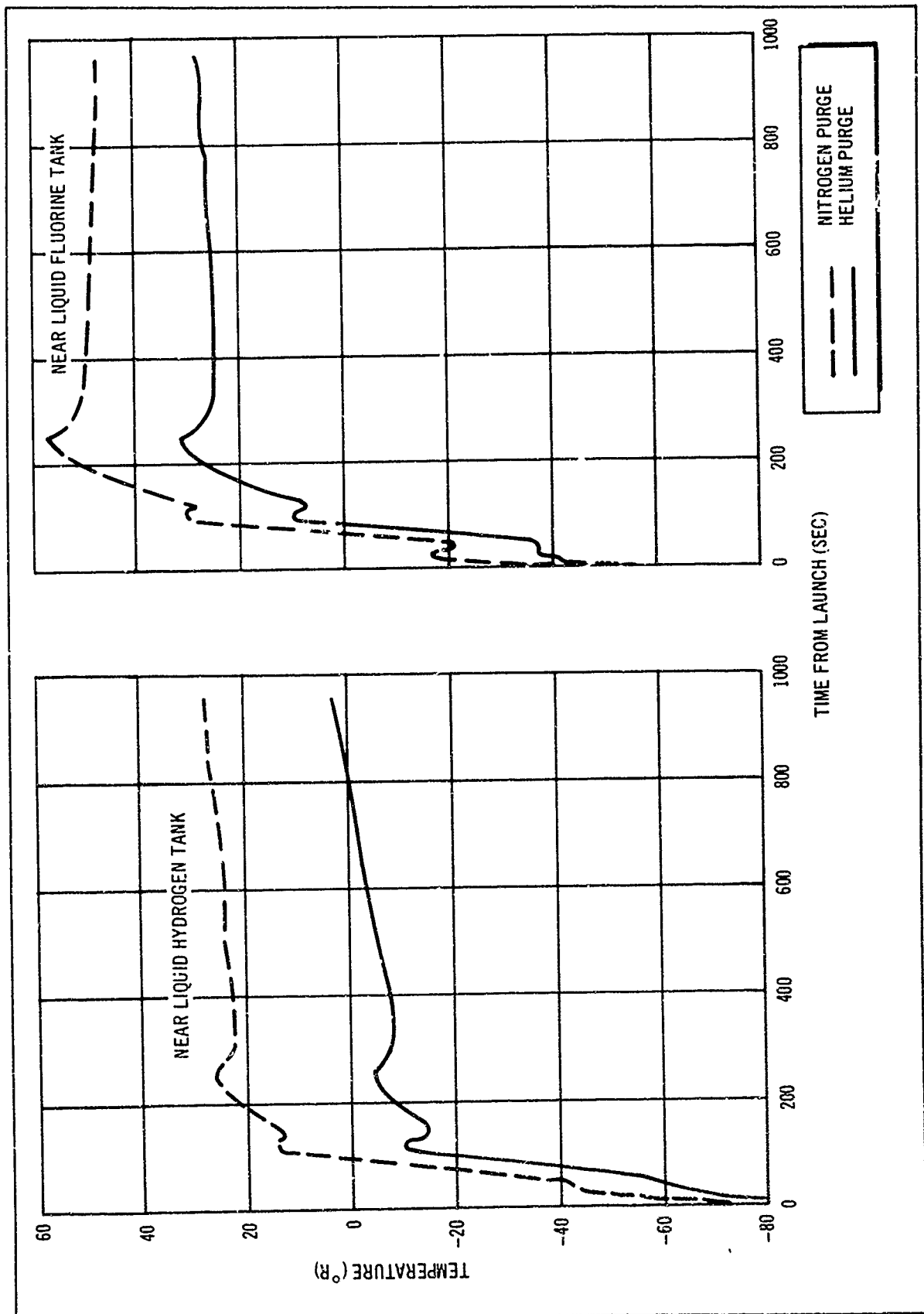


Figure 4-90. Skin Temperature Histories During Boost

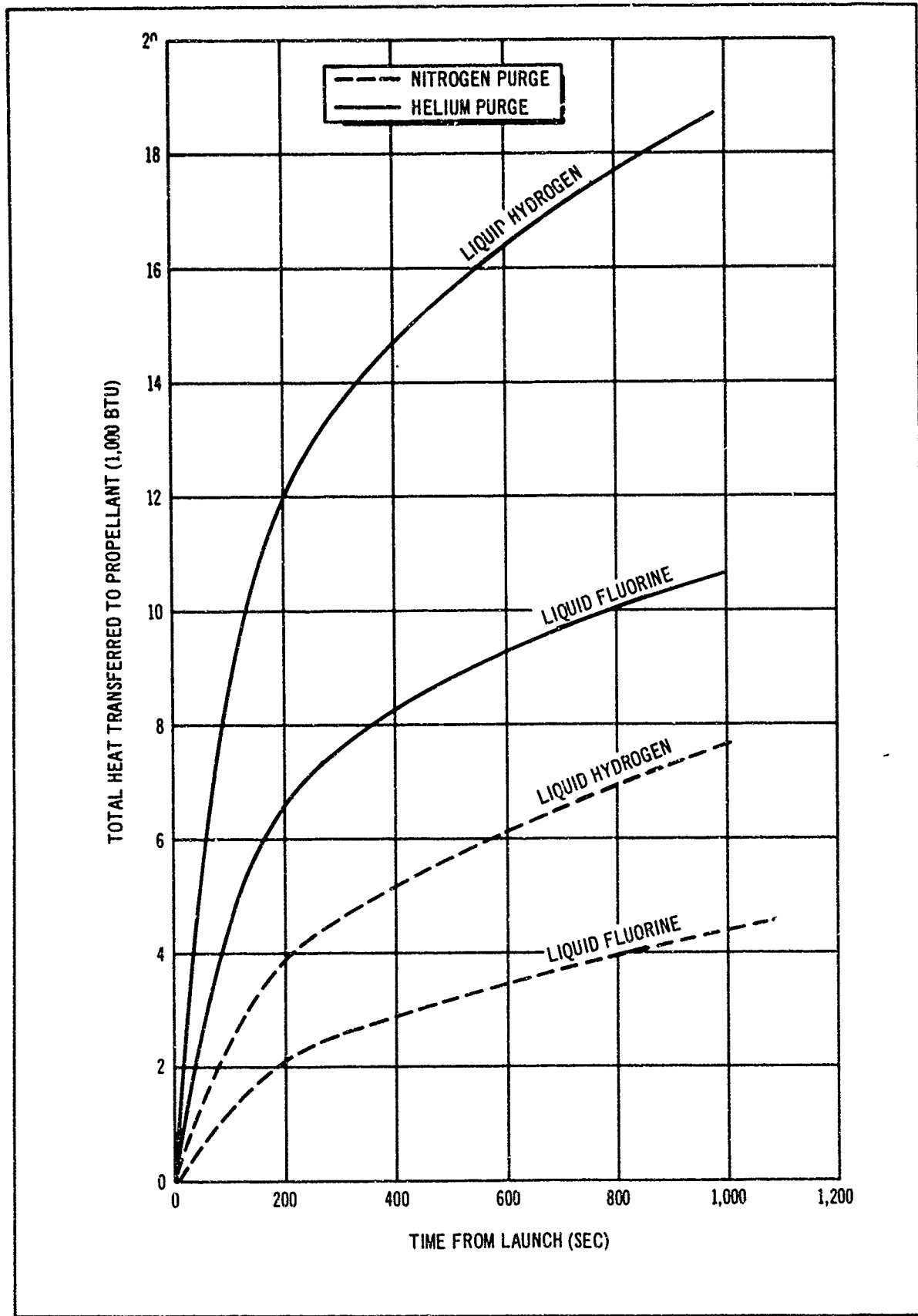


Figure 4-91. Total Heat Input to Propellant During Boost

The combined effects of degassing and depressurization are lumped into the term decompression. The line between depressurization and degassing is drawn at about 10^{-1} torr. Depressurization is primarily concerned with forces that are exerted on the insulation sheets because of pressure differences. And 10^{-1} torr is about the lowest pressure which will produce a significant force on the insulation blanket. In addition, 10^{-1} torr is the beginning of the low-pressure region where the thermal conductivity of HPI becomes dependent on ambient pressure.

For most insulations, a pressure of 10^{-1} to 10^{-4} torr means that the gases in the insulation are in free molecular flow. The mean free path of the molecules is longer than the space in between the sheets. The gases act not as a uniform fluid, but rather as a collection of individual molecules which ricochet back and forth between the insulation layers. As a result, the movement of gases within the insulation is essentially a diffusion process rather than a macroscopic or continuum flow. For pressures greater than 10^{-1} , the gases in the insulation behave as a continuous medium. They respond to pressure differences as a homogeneous fluid rather than is characteristic of the depressurization problem, while free molecular flow or diffusion is characteristic of degassing. The designer must consider this fact in picking an insulation system design.

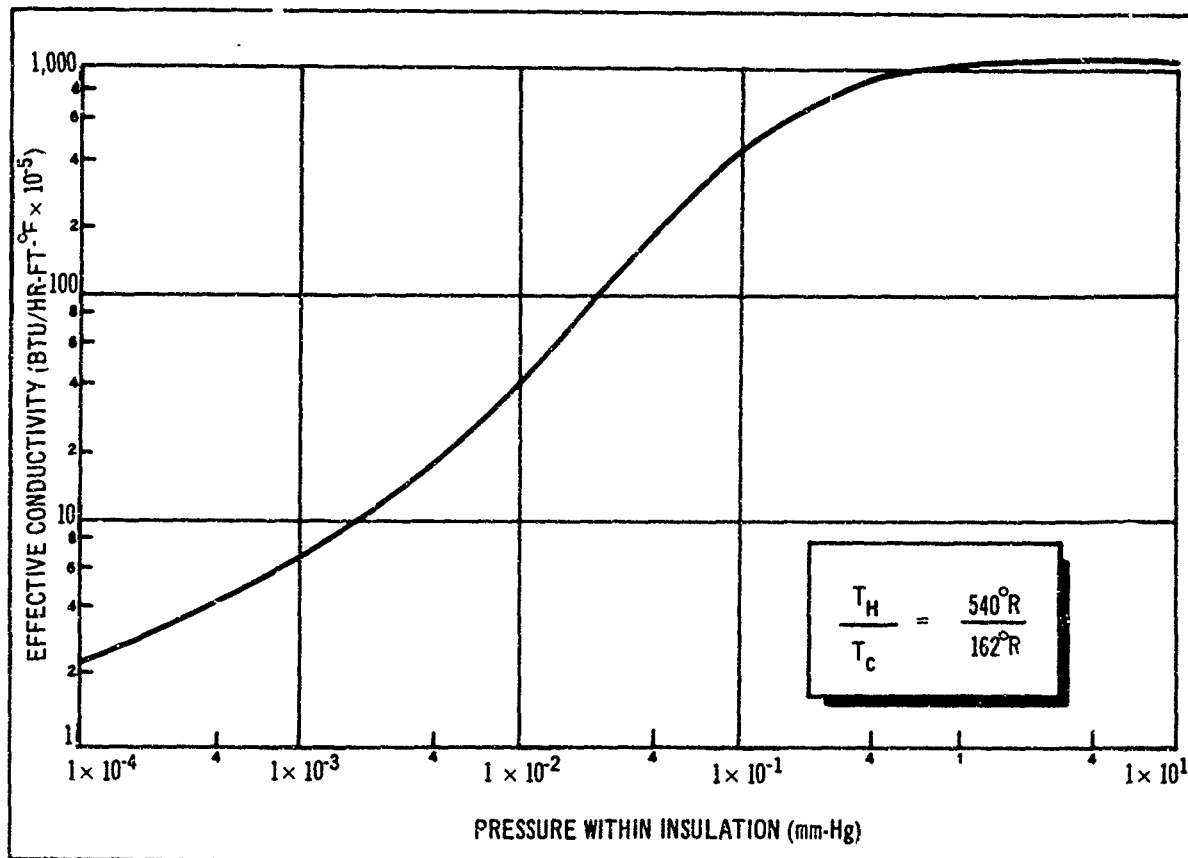


Figure 4-92. Effects of Pressure on NRC-2 High-Performance Insulation Thermal Performance

This particular problem has been under study by Douglas in its IRAD for HPI. Experiments have been underway using a degassing/depressurization test device containing a representative sample of an insulation blanket (with a joint) which is subjected to a controlled decompression schedule. Figure 4-93 illustrates the configuration of this device. Figure 4-94 shows a typical test result for a 50-layer NRC-2 blanket with a 1.5 in. overlap joint design using sets of 5 layers in an overlap.

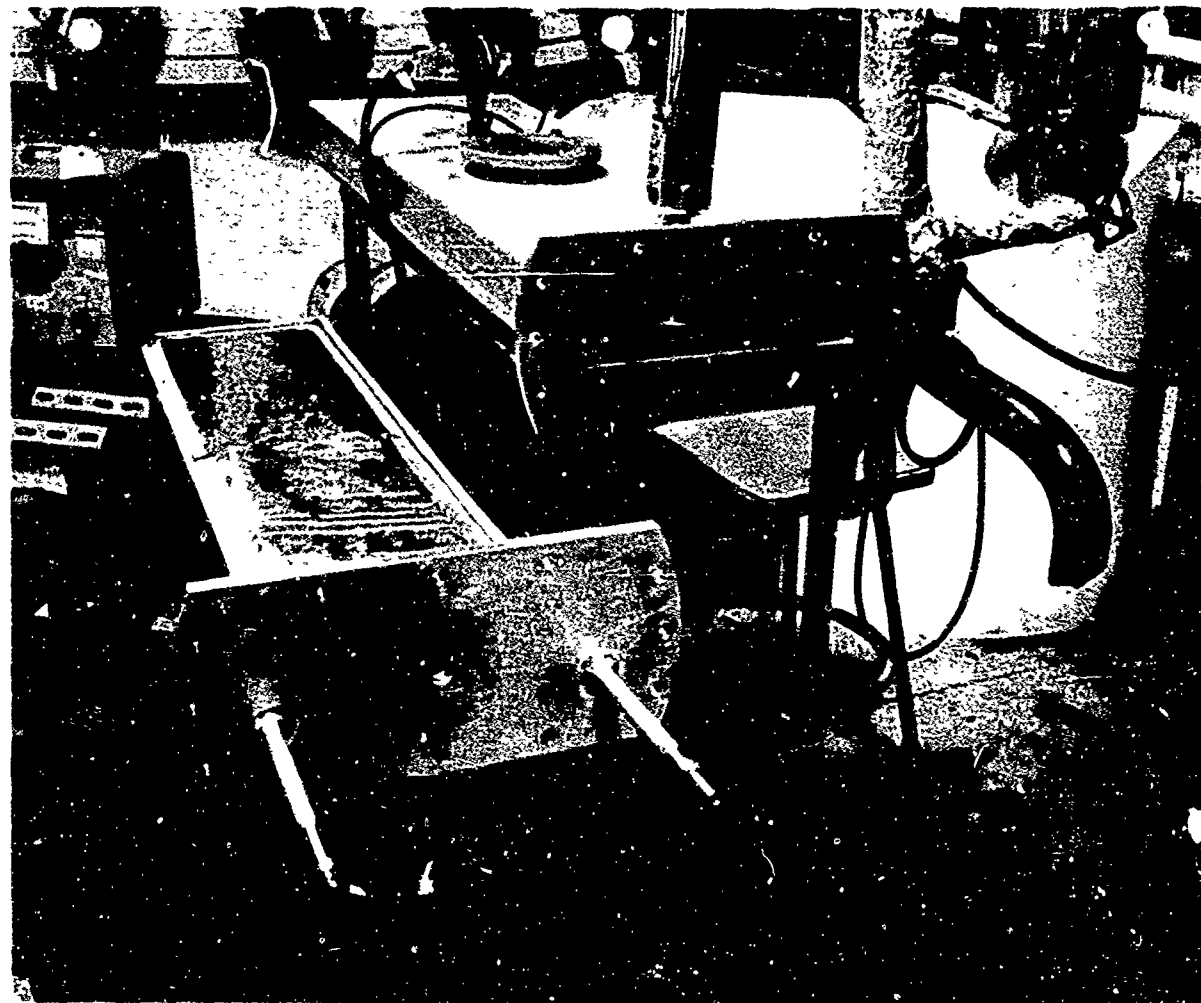


Figure 4-93. Decompression Test Apparatus

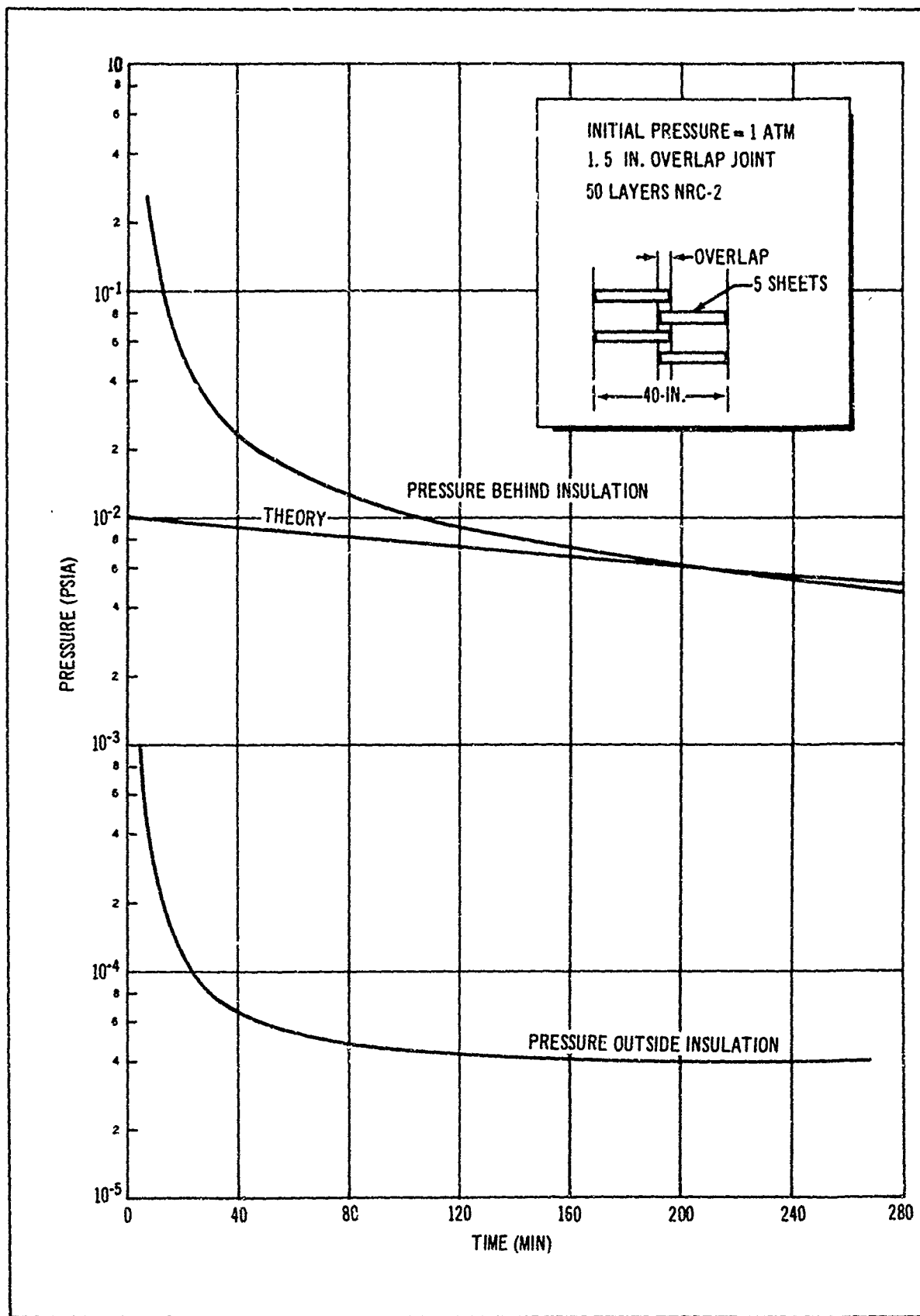


Figure 4-94. Pressure History During High-Performance Insulation Rapid Decompression Test

If the data are accepted literally, the results are discouraging. After several hours, the pressure under the insulation is still about 5×10^{-3} torr for both joint configurations. Yet the pressure outside the insulation reached 10^{-4} torr in about 20 min. An insulation pressure this high corresponds to a thermal conductivity 4 to 10 times higher than desired.

Three considerations tend to ease this situation. First, the data are not yet completely above question. The transient response of both ion and thermopile gages has not been completely defined by experiment, although this is planned. Gage and tubing volume may be influencing transient response. Outgassing within the gage and tubing could also introduce errors.

Second, the pressure is measured underneath the insulation blanket and might be considerably lower, 1 or 2 laminae away from the wall. If only a few sheets are degraded by high gas pressures, the situation is not hopeless. Poor performance on 5 out of 50 sheets would go almost unnoticed.

Third, the joint configuration used is just about the worst one imaginable from a decompression standpoint. It seems possible, if not unavoidable, to develop a joint design of comparable thermal performance and much better degassing characteristics.

Recent tests reported by Anderson and Merlet (reference 25) support the idea that, for one or more of the above reasons, the picture of insulation degassing is much brighter than is painted from the data presented here. The reference tests showed that a reasonable insulation system can achieve vacuum performance in about 2 hours after the ambient pressure has dropped below 10^{-4} torr. While this may fall short of that desired, it does give promise that with careful design the goal can be reached.

An analytical treatment of the insulation outgassing was also performed assuming a free molecular flow diffusion process within the insulation blankets. The result of the study was the equation

$$\frac{dP}{d\tau} = - \left(\frac{\pi}{2t} \right)^2 DP \quad (4-90)$$

where P is pressure, t is the HPI thickness, τ is time, and D the effective diffusion coefficient. This equation should predict the transient pressure within HPI.

Equation 4-90 is compared with the experimental data in figure 4-94. Because of the assumptions involved in deriving equation 4-90, it will only be valid for the free molecular flow portion of the evacuation which begins at about 10^{-2} torr. It is, therefore, expected that the equation will only match the measured curve in its slope $\left(\frac{dP}{d\tau} \right)$. The steady-state slopes do match 35 pct.

It was determined from this equation that the process of diffusion is very slow as long as the layers of HPI overlap, however, it was also determined that the rate of diffusion is greatly increased if a small gap (instead of overlap) exists between the HPI sheets. Table 4-30 presents the effect on evaporation time of various overlap and gap sizes for different density (sheets per in.) HPI systems. In the table, a negative overlap value is actually a gap. The dimplar shows a better theoretical venting capability because of its more rigid pre-set crinkle pattern which permits the gas flow passages to stay intact.

Table 4-30

THEORETICAL TIME FOR INSULATION MODEL TO REACH 10^{-4} TORR WITH
VARIOUS OVERLAPS (L = 48 in.)

Overlap (in.)	3	0	-1/64	-1/32	-1/16	-1/8	-1/4	-1/2	-1
Time (min.)	1,450	1,360	800	403	128	34	8.7	2.2	.53
				20 SHEETS NRC-2					
				100 SHEETS NRC-2					
Time (min.)	11,600	10,900	3,180	1,040	242	69.5	17.3	4.3	1.03
				25 SHEET DIMPLAR					
Time (min.)	198	171	156	106	49.5	15.8	4.2	1.1	.265

An analytical investigation was made into determining the effect of perforating the layers of insulation. Perforating the layers of insulation will somewhat impair the ideal insulating capability of the HPI section. However, it may be that with a proper choice of hole size and spacing the increase in diffusion will outweigh the loss of insulating capability.

Assuming a circular perforation of radius r_1 , with a spacing of 1 in. on centers, a simple sketch will show that with a 1 in. on center spacing there are four holes in every $\pi \text{ in.}^2$ of insulating material area. The ratio of perforated to total surface area is given by

$$\frac{\text{perforated area}}{\text{total area}} = \frac{4 \pi r_1^2}{\pi (1)^2} = 4 r_1^2 \quad (4-91)$$

Therefore, in a given length, L , of insulating material there will be $4 L r_1^2$ sq. in. of open (perforated) area per in. width. Because of the linearity of the equations one can superimpose the diffusion through the perforations on the diffusion that would occur without the perforations. The calculation of the diffusion coefficient resulting from the perforations follows:

$$D = 1/2 \bar{c}^* * \lambda$$

Where $\lambda^* = \frac{\text{effective distance travelled}}{\text{no. of collisions}}$

$$= \frac{2a}{\frac{L}{4L r_1^2}} = 8 a r_1^2$$

$$= \frac{\text{total distance travelled}}{(\text{velocity}) (\text{no. of collisions})} \quad (4-92)$$

$$= \frac{2a \frac{L}{L_1^4 r_1^2}}{\frac{L}{L_1^4 r_1^2} 2} = \frac{4a}{\bar{c}}$$

$$\bar{c}^* = \frac{\lambda^*}{\tau^*}$$

$$\therefore D = 1/2 \frac{\lambda^{*2}}{\tau^*}$$

or $D = 8 a \bar{c} r^4$

Using the results above, calculations have been made to determine the effect of perforations on the time to evacuation for a section of multilayer insulation. The calculations were made using a 20-sheet model with 3 in. of overlap as a base and then assuming perforations of different size (perforation spacing is 1 in. on centers). Table 4-31 presents the results of the calculations.

Table 4-31

EFFECT OF PERFORATIONS ON EVACUATION TIME

Diameter of Perforation (in.)	D_B Base System (c. p. s. ²)	D_P Perforations (c. p. s. ²)	$D_B + D_P$ (c. p. s. ²)	Time to Evacuate Without Perforations (sec.)	Time to Evacuate With Perforations (sec.)
$\frac{1}{64}$	1.195×10^{-4}	0.707×10^{-4}	1.912×10^{-4}	34,800	21,800
$\frac{1}{36}$	1.195×10^{-4}	1.13×10^{-3}	1.25×10^{-3}	34,800	3,320
$\frac{1}{16}$	1.195×10^{-4}	1.81×10^{-3}	1.82×10^{-2}	34,800	228
$\frac{1}{8}$	1.195×10^{-4}	0.29	0.29	34,800	15

Perforations and gaps in the insulation will tend to degrade the thermal performance. This then is an area where outgassing and thermal characteristics may have to be traded off.

At present, this problem cannot be resolved satisfactorily until more basic testing, such as is now under way within the Douglas IRAD program, can be completed and evaluated in order to sort out the instrumentation problems from the actual outgassing phenomena, and to clearly establish the trade off factors between outgassing and thermal performance.

(6) Insulation Attachment and Support. Insulation attachment and support concepts have been evolved and identified through Douglas multilayer insulation (RAD) program and a review of the current state of development in this area. Several attachment methods and materials have been selected as applicable for use with the three candidate insulation systems being considered in this program. These are also applicable in general regardless of where the HPI is located. The proposed fastening methods and materials are.

(a) Glass Fiber Threads. This method utilizes a fastening material of low thermal conductivity and high strength. When an insulation blanket is prefabricated, strands of threads are passed through the sublayers of sheets and knotted so that knots remain between the sublayers to aid in preventing compaction of the blanket.

(b) Nylon Studs and Buttons. This fastening method is probably not as efficient thermally as threads, but is mechanically positive in that it supports the insulation in any vehicle attitude. In this method, the studs are bonded to the tank or structural wall. The insulation is pierced and pushed onto the studs. The buttons are then secured to the ends of the studs to retain the insulation.

(c) Adhesive Tapes. Scotch 850 (Mylar with adhesive); Mystic 7000 (single faced silicone); and Mystic 7100 (double-faced silicone). These tapes are comparatively low in conductivity and are easy to apply. Small strips may be used at splices or joints to attach one sheet to another or to the mounting surface.

(d) Netting. A net type material that encloses the entire insulation. These are illustrated in figure 4-95.

Information on the practical aspects of installing multilayer insulation is not generally available because of the limited usage and experience with this type of insulation. Much of the information related to multilayer insulation application has been developed and accumulated by the insulation material suppliers treated as proprietary information. Most applications to date have been experimental in nature and, except for several programs, the details of insulation attachment and support are not available in the published literature. Of the attachment methods which are described in available published reports of related programs, many were developed to suit different insulation systems and are not directly applicable or cannot be used with confidence in this program. Therefore, it is necessary to depend primarily on information from two sources.

- Insulation material suppliers' knowledge and recommendations, based on their test results and experience. This source of information normally is not available until a firm interest is expressed in purchasing their material and services.
- The Douglas program to research and develop multilayer insulation techniques. This work has been reoriented to provide specific

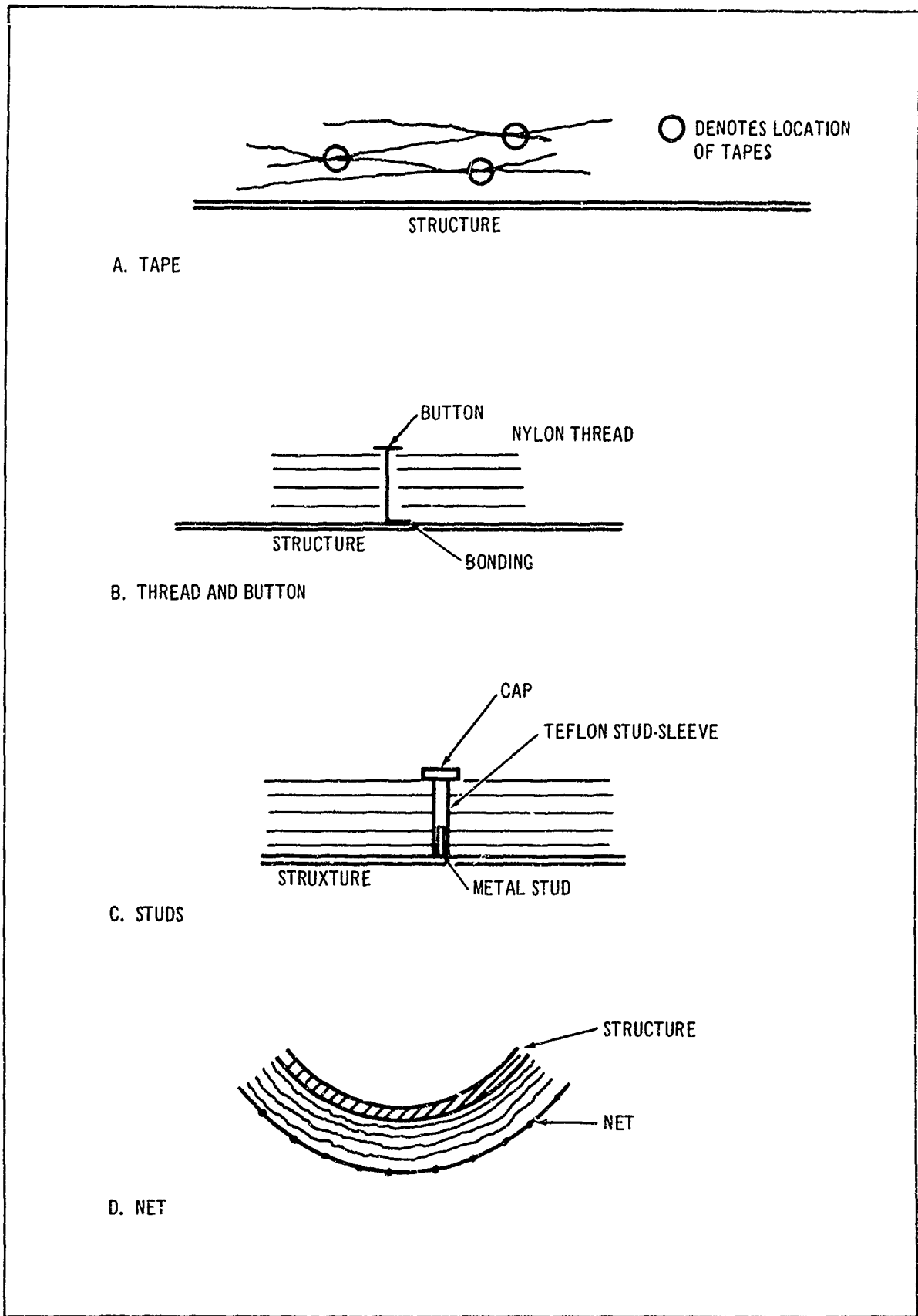


Figure 4-95. Insulation Attachment Methods

information for the contract program and to investigate new insulation materials such as dimplar.

Insulation attachment configurations are being investigated under the Douglas multilayer insulation research program. The glass fiber thread and button system for assembling insulation blankets and attaching them to a mounting surface with Velcro fasteners is being incorporated on panel specimens for testing in the 4-in. calorimeter. The basic specimen without attachments was tested previously to determine insulating effectiveness with a single seam joint. These tests have not been completed, however.

Lacking hard experimental data, an analysis was performed to predict the heat leak through the insulation resulting from penetrating the insulation as in the case of a support stud or thread used to attach and support the insulation. The following assumptions were made:

- All the heat conducted through the penetration reaches the cryogenic tank.
- The effect of the penetration will be damped out in the HPI at a characteristic distance of 2 in.
- All the HPI within the damping distance of the penetration is at a constant temperature, T .

The heat balance for the problem can be stated as,

$$0 = \dot{q}_{\text{conducted}} - \Delta \dot{q}_{\text{radiated}} \quad (4-93)$$

$$\dot{q}_{\text{conducted}} = \frac{k(T_H - T') A_{\text{conduction}}}{l} \quad (4-94)$$

$$\Delta \dot{q}_{\text{radiated}} = (\epsilon \sigma T'^4 - \epsilon \sigma T_e^4) A_{\text{radiation}} \quad (4-95)$$

$$\frac{k(T_H - T')}{l} A_{\text{conduction}} = \epsilon \sigma (T'^4 - T_e^4) A_{\text{radiation}} \quad (4-96)$$

l is the length of the short and T_e is the temperature of the inner cold face of the insulation.

Equation 4-96 expresses that all the energy coming through the penetration is radiated away by the HPI within the characteristic damping distance. Equation 4-96 can be solved for T' and the resulting heat input to the cryogen tank can then be calculated from either equation 4-94 or 4-95.

(7) Application of Analysis to a Teflon Stud. The following values were used in equation 4-96 to determine the value of T' for a teflon stud to support the insulation:

$$\begin{aligned}
 T_H &= 400^\circ\text{R.} & \epsilon &= 0.03 \\
 T_e &= 230^\circ\text{R.} & \sigma &= 0.1714 \times 10^8 \text{ B.t.u.p. hr.}^2\text{-hr.}^{-\circ}\text{R.}^4 \\
 l &= 1.25 \text{ in.} & k_{\text{teflon}} &= 0.14 \text{ B.t.u.p. hr. -ft.}^{-\circ}\text{R.}
 \end{aligned}$$

The teflon stud is 1/4 in. in diameter. Therefore,

$$A_{\text{conduction}} = \frac{\pi(1/8)^2}{144} \text{ ft}^2 \quad (4-97)$$

$$A_{\text{radiation}} = \frac{\pi(2)^2}{144} \text{ ft}^2$$

Equation 4-95 becomes,

$$102 \left(4 - \frac{T'}{100}\right) = \left(\frac{T'}{100}\right)^4 - 28 \quad (4-98)$$

and

$$T' = 322^\circ\text{R.} \quad (4-99)$$

The heat leak to the cryogen tank is

$$\dot{q} = \frac{0.14 (400 - 322)}{1.25/12} \frac{\pi(1/8)^2}{144} = 0.036 \text{ B.t.u. /hr. /stud} \quad (4-100)$$

(8) Application of Analysis to a Nylon-Threaded Button. The only quantities which change from the teflon stud applications are,

$$k_{\text{nylon}} = 0.145 \text{ B.t.u.p. hr. -ft.}^{-\circ}\text{R} \quad (4-101)$$

and with the radius of the thread 0.02 in.

$$A_{\text{conduction}} = \frac{\pi r^2}{144} = \frac{\pi(0.01)^2}{144} \quad (4-102)$$

Equation 4-95 becomes,

$$0.0068 \left(4 - \frac{T'}{100}\right) = \left(\frac{T'}{100}\right)^4 - 28 \quad (4-103)$$

and $T' = 230^\circ\text{R.}$

The heat leak to the cryogen tank is

$$\dot{q} = \frac{0.145 (400 - 230) \frac{\pi(0.01)^2}{144}}{\frac{1.25}{144}} = 0.0067 \text{ B.t.u. /hr. /button.} \quad (4-104)$$

Therefore, the heat leak per attachment point for the stud is $0.036/0.0062 = 5.8$ or nearly six times the value for the thread and button. The total heat leak attributed to the attachments can be expressed as:

$$\dot{q}_{ia} = q' \eta A_i + \theta q_i$$

where η_{in} is the attachment placement density, (attachment/ft.²), A_i is the insulation area, θ is the fractional increase in basic insulation heat leak, and q_i is the heat leak through the insulation without attachments. Unfortunately there is no completely rational method for determining q_{ia} or θ . They will, of course, vary with the type of insulation and its placement. Thread and button attachments with a spacing of about one attachment per ft.² of surface have been successfully used with a tank-mounted Mylar paper spacer system (reference 23). With this system, θ would probably be very small and possibly even negligible. With NRC-2, where compression is of major concern, θ could be quite significant. For shroud-mounted NRC-2 or Dimplar, the stud represents a much more positive support since it will not sag as would a thread. Thus a lower value of η could be used and the degree of compression could be greatly reduced resulting in low values of θ .

For a tank-mounted insulation assuming a thread and button system and no compression effects, the value of q_{ia} for the LH₂ tank would be:

$$0.0062(1)(185)+0 = 1.14 \text{ b. t. u. /hr.}$$

For a stud attachment with shroud mounting with η value of 0.5, q_{ia} would be:

$$0.036(0.5)(268.5)+0 = 4.8 \text{ b. t. u. /hr.}$$

These two values would probably be closer for NRC-2 or Dimplar since θ would have a higher finite value for the thread and button than for the stud. Also Douglas experience indicates that a lower stud spacing than 0.5 is probably adequate. However, with the knowledge now on hand, it is not possible to make rational selection as to insulation attachment.

An assessment of taping and netting techniques for insulation attachment is even more nebulous. However, as a primary insulation and support technique, these approaches seem to be less positive than either the thread and button or stud approach which actually provides a mechanical attachment at discrete points and does not rely totally on bond or glue strengths. Taping would be quite useful however for localized support and where patching is required.

b. Tank Support Study. For the class of vehicle under study, the cryogenic propellant tanks must be supported within the relatively warm structural shell in such a manner as to carry efficiently all anticipated loads on the tanks and transfer as little heat as possible from the structural shell to the tankage. This latter consideration is extremely important since heat shorting through the support system can greatly nullify the heat-transfer reduction potentials of the high performance insulation.

A brief, but intensive, survey of related programs covering the design, analysis, and testing of cryogenic tank supports was conducted (reference 27 through 30). Examination of these systems, together with knowledge gained from Douglas independent research, indicated that they did not appear to comply sufficiently with a number of features which are desirable in a thermal/structural design of this type including:

- Use of a structural material whether metallic or non-metallic, to obtain the lowest feasible thermal conductivity-to-strength ratio.
- Elimination of support member loading because of thermal contraction or pressurization of the tank.

These tank support features, of course, are supplementary to the basic structural and thermal functions of providing adequate structural support with minimum weight and low-heat leak.

To satisfy these design requirements, it was deemed appropriate to investigate a broad spectrum of possible tank support concepts and configurations. The previously mentioned survey of the present state of development of space vehicle cryogenic storage tanks revealed that, although several promising concepts are currently being considered, there is no generally accepted and proven configuration for a tank support system that is directly applicable to the study vehicle. Therefore, an independent design analysis was initiated to evolve a tank support concept that would potentially satisfy all the requirements of the system under consideration. This was then compared with respect to weight and thermal performance with other tank support concepts which were identified as promising from the noted survey.

Weight analysis of the LH₂ tank shown that the total weight to be supported varies significantly with tank internal pressure as indicated below.

<u>Pressure, p. s. i. a.</u>	<u>Total Weight, Lb.</u>
250	2,005
200	1,919
150	1,834
60	1,716

The above weights take into account the basic tank, the propellant, internal pressurant and their support, pressurant gas, and tank-mounted components. Similar numbers for the LF₂ tank are shown below.

<u>Pressure, p. s. i. a.</u>	<u>Total Weight, Lb.</u>
250	12,426
200	12,381
150	12,334
60	12,275

In the case of the LF_2 tank, the propellant weight constitutes the major portion of the load, therefore, the effects of tank pressure on support system loading is very small. Thus, the LF_2 tank support system was studied for only the maximum pressure (250 p. s. i. a.). It should also be noted that the weight to be supported for the LF_2 tank is about six times greater than in the case of the LH_2 tank. Tank weights were based on the use of 2014-T6 aluminum using the properties of the corresponding LH_2 or LF_2 cryogenic temperatures.

In designing the support system, the load conditions specified in table 4-32 were used. In addition a forward acting load of 2g was assumed for tank springback at engine cutoff. These result in the actual design loads shown in table 4-32.

Table 4-32

TANKAGE SYSTEM DESIGN SUPPORT LOADS
(250 p. s. i. a. pressure)

	LH_2	LF_2
Aft load (5g.)	10, 250 lb.	62, 500 lb.
Forward (springback)	4, 100	25, 000
Side (1.5g.)	3, 070	18, 700

The general approach taken toward structural design in the analysis phase of this program is to employ limited design analysis and weight estimation methods. This approach facilitates the determination of the weight and heat leak values for a range of design variables, which are required for the forthcoming optimization task. Since this program is not directly concerned with the actual detailed structural design of a flight vehicle, but rather with such aspects as the effect of the tank support heat leak on propellant storability and vehicle weight, complete detail design and weight calculation procedures are not essential.

(1) Selection of Candidate Support Systems. For the particular application under study, two possible basic approaches may be taken to tank support design: continuous and point support. With continuous support the tank is attached to a conical type structure around a full 360° circumferential plane. With point support the tank is supported at a number of discrete points. The application of a continuous conical support system for a similar application has been given detailed study (reference 22) and was therefore selected as one possible candidate system. Under a recent USAF/RPL

contract, AF04(611)-10745, a six-point support system using glass fiber columns was designed in some detail for a very similar vehicle and was therefore selected as the second candidate support system. These basic design approaches were adapted as necessary to this particular application, and are pictured in figures 4-96 and 4-97.

A third system applying the point support concept was specifically designed for this application. This employs a nine-rod tension support network terminating at three points on the tank.

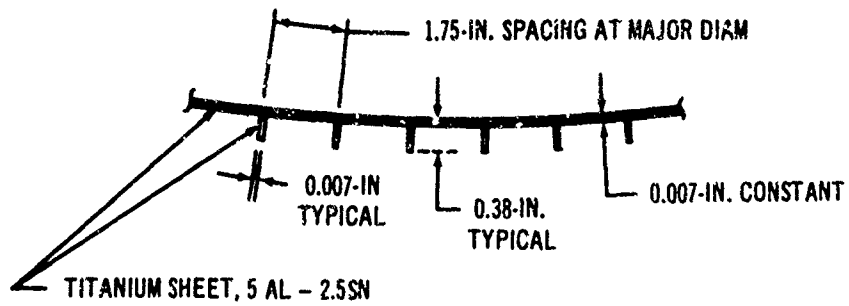
The basic relation for heat transfer by conduction through a constant area during a unit time is given by the equation:

$$q = \frac{kA}{L} (T_1 - T_2)$$

To minimize the heat conducted through the tank support, it is advantageous to minimize the cross-sectional area, A , of the support members, and use members of rather long length, L . This suggests the use of tension rather than compression members, and a system of members which will be loaded in tension to react tank inertia loads and moments in any direction. With these basic guidelines in mind, a geometrical arrangement became apparent which required the least number of structural members. Thus, the nine-rod tank support configuration indicated by the sketch in figure 4-98 was conceived as a tentative design for the study vehicle.

This system provides for attachment to the tank wall at a minimum of three points, located slightly below the tank equator, and spaced 120° apart. Three rods attach at each point and are oriented approximately as indicated in the sketch. The three upper rods serve primarily to react the major loading condition of 5-g. downward due to axial thrust during launch. A reverse or upward axial load such as would occur at boost cutoff is not reacted by the upper rods, but by the six lower rods which are angled down for this purpose. A transverse or side load in any direction is reacted by two or three of the lower rods which are most nearly parallel to the direction of loading. The upper rods are also loaded in tension by a side load, so that they work in combination with the lower rods to resist translational movement of the tank. If a loading condition induces a moment, or torque, in the tank, it is reacted by tension in two or more of the nine rods. None of the support members are required to react a load in compression nor will they be adversely affected by a small applied deflection tending to impose a compression load in them. The magnitude of moments created by side loads can be minimized by locating the center of gravity of the tank (when full) close to the plane of the tank attachment points. This can be controlled on the LH_2 tank by judicious placement of the internal pressurant tanks in the lower part of the LH_2 tank.

The geometry of the nine-rod support system was also established to accommodate overall inward and outward deflection of the tank wall caused by temperature variations and internal pressure changes. The three members at each tank attach point are oriented so that they are approximately tangential to the tank surface. As the tank attach points move radially inward



SECTION A-A

NOTE: THE EXTERNAL STIFFENERS EXTEND THE FULL LENGTH OF THE SUPPORT

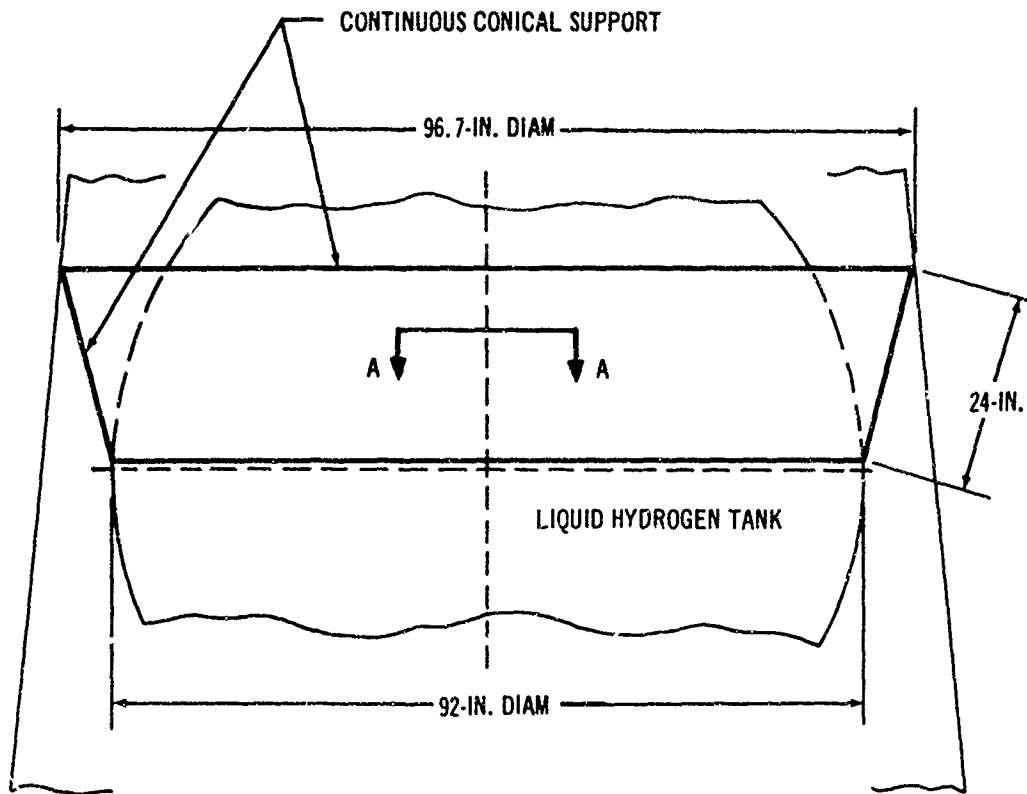


Figure 4-96. Continuous Conical Tank Support

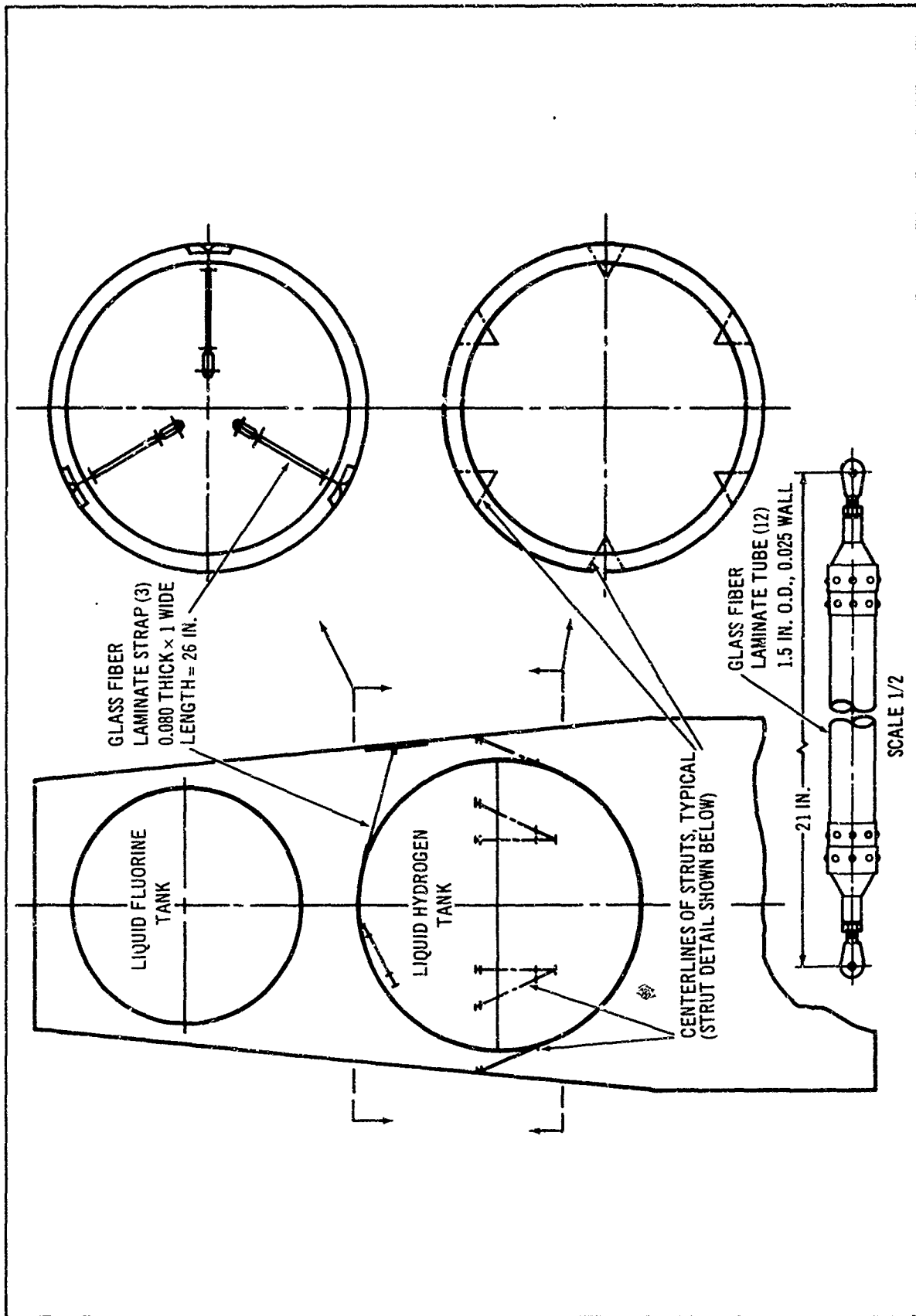


Figure 4-97. Study Vehicle Tank Support

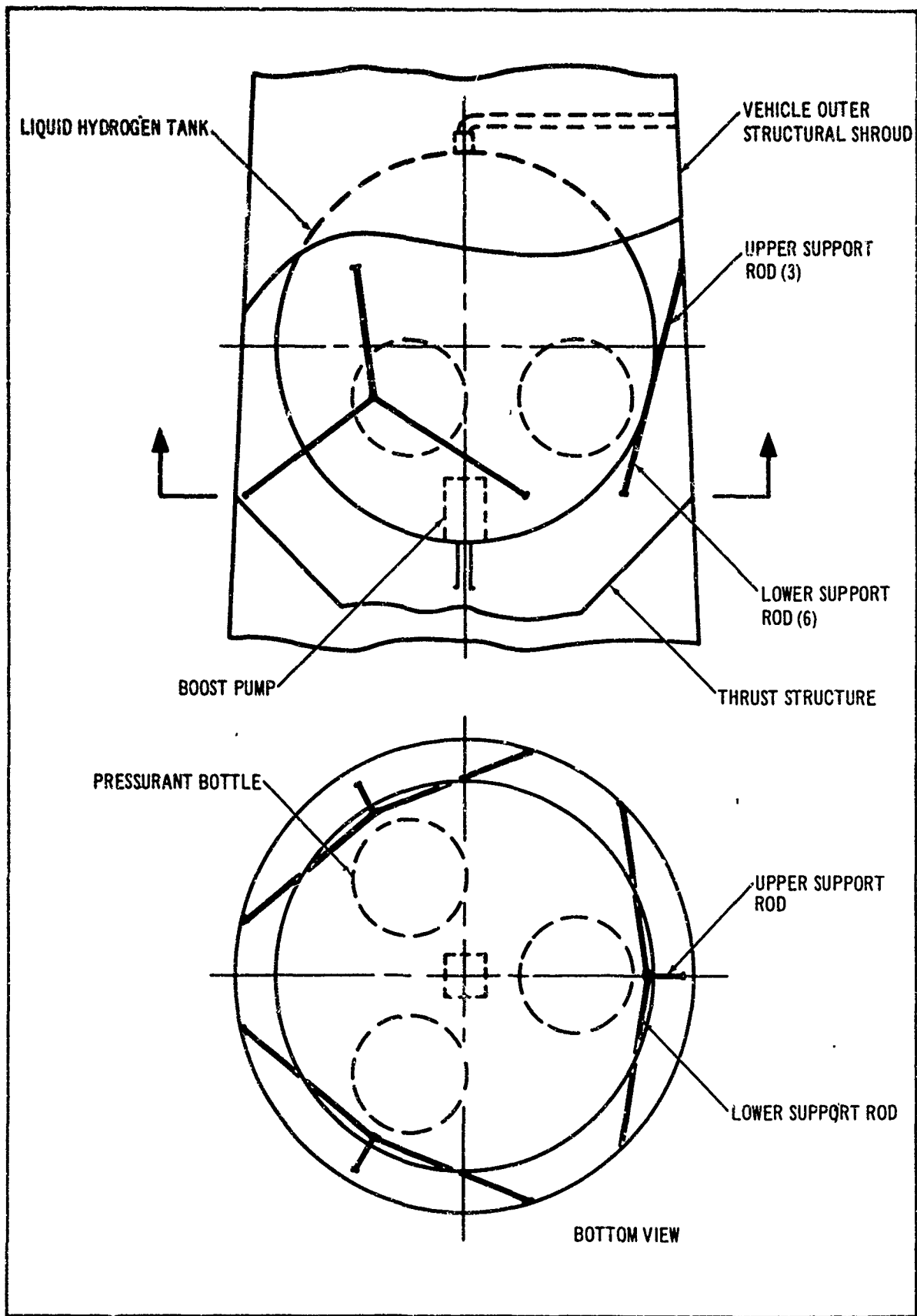


Figure 4-98. Nine-Rod Tension Member Support System

or outward, normal to the axis of the rods, the amount of deflection in the axial direction which would tend to change the length of the rod and induce a load is very small. By making slight adjustments to the initial geometry to suit the amount of radial deflection, it should be possible to effectively eliminate the problem of tank support loading caused by thermal contraction or tank pressurization.

The cross-sectional area required for the tank support for a given material tends to be reduced by utilizing a system of tension members. The tension member can be designed to withstand the maximum load at a considerably higher stress level than a compression member, which must be limited to a lower working stress to preclude failure by column buckling or local crippling. Compression members are frequently designed as tubes in order to obtain a high stiffness-to-weight ratio. The stiffness required to prevent instability failure leads to larger diameter tubes with thinner walls and, in the extreme case, the design wall thickness can become less than the minimum possible gage for certain materials and fabrication processes. Additional material and weight results from the use of such members. Another characteristic of hollow supports is that internal radiation can occur along the length of the member. It is not desirable to use tubular members to support cryogenic storage tanks if their design incurs extraneous cross-sectional area and weight, and unless the additional heat which is transmitted by radiation inside the hollow member can be effectively blocked. Tension members, on the other hand, can be solid throughout with a rectangular or circular cross-sectional shape of minimum area.

One apparent disadvantage of a tank support design having a small number of attachment points on the tank is the effect of the large concentrated loads imposed in the tank wall. The tank wall must be reinforced with pads or stiffeners to distribute the loads through the tank structure. It appears that very little analysis has been done in this area (important to considerations of support structures and vehicle weight). Analysis of this problem is being undertaken in separate Douglas programs. The tank wall reinforcement weight is presently being accounted for by use of weight factor estimates.

The nine-rod tension support system is considered to utilize either titanium or glass fiber material for the rod members. Fabricating the rods from glass fibers or tape appears to be a method for obtaining a thermal conductivity-to-strength ratio so low as to make glass fiber a more attractive material for this application than titanium or stainless steel. The selection of the materials is also dependent to some degree on whether the insulation is located on the inside of the shroud or directly on the tanks. Weight analysis of the LH₂ tank shows that the total weight to be supported varies with tank internal pressure as indicated previously.

The support member design ultimate tension member system, and the required cross-sectional areas for four materials of interest are listed in Table 4-33. The cross-section shape can be rectangular, square, or circular. The support member overall lengths are 34.5 in. for the upper members and 48 in. for the lower members. The tank support working

Table 4-33

FLIGHT VEHICLE TANK SUPPORT MEMBER SIZES FOR NINE-ROD SYSTEM

Support Member	Support Material	Design Stress P. s. i.	LH ₂ Tank												LF ₂ Tank							
			Tank Internal Pressure, p. s. i. a.																			
			250			200			150			60			250							
Upper	Unidirectional glass fiber	38,200	Ult. Load, lb.	3806	Req. Area, Sq. in.	.0997	Ult. Load, lb.	3640	Req. Area, Sq. in.	.0953	Ult. Load, lb.	3480	Req. Area, Sq. in.	.0911	Ult. Load, lb.	3260	Req. Area, Sq. in.	.0854	Ult. Load, lb.	23,600	Req. Area, Sq. in.	.62
Upper	CRES steel	36,000	Ult. Load, lb.	3806	Req. Area, Sq. in.	.1058	Ult. Load, lb.	3640	Req. Area, Sq. in.	.1011	Ult. Load, lb.	3480	Req. Area, Sq. in.	.0967	Ult. Load, lb.	3260	Req. Area, Sq. in.	.0906				
Upper	Titanium	26,000	Ult. Load, lb.	3806	Req. Area, Sq. in.	.1454	Ult. Load, lb.	3640	Req. Area, Sq. in.	.1400	Ult. Load, lb.	3480	Req. Area, Sq. in.	.1339	Ult. Load, lb.	3260	Req. Area, Sq. in.	.1254				
Upper	Aluminum	13,400	Ult. Load, lb.	3806	Req. Area, Sq. in.	.284	Ult. Load, lb.	3640	Req. Area, Sq. in.	.272	Ult. Load, lb.	3480	Req. Area, Sq. in.	.260	Ult. Load, lb.	3260	Req. Area, Sq. in.	.244				
Lower	Unidirectional glass fiber	38,200	Ult. Load, lb.	2830	Req. Area, Sq. in.	.0741	Ult. Load, lb.	2705	Req. Area, Sq. in.	.0709	Ult. Load, lb.	2590	Req. Area, Sq. in.	.0676	Ult. Load, lb.	2420	Req. Area, Sq. in.	.0634	Ult. Load, lb.	17,600	Req. Area, Sq. in.	.46
Lower	CRES steel	36,000	Ult. Load, lb.	2830	Req. Area, Sq. in.	.0786	Ult. Load, lb.	2705	Req. Area, Sq. in.	.0752	Ult. Load, lb.	2590	Req. Area, Sq. in.	.0720	Ult. Load, lb.	2420	Req. Area, Sq. in.	.0672				
Lower	Titanium	26,000	Ult. Load, lb.	2830	Req. Area, Sq. in.	.1089	Ult. Load, lb.	2705	Req. Area, Sq. in.	.1041	Ult. Load, lb.	2590	Req. Area, Sq. in.	.0997	Ult. Load, lb.	2420	Req. Area, Sq. in.	.0931				
Lower	Aluminum	13,400	Ult. Load, lb.	2830	Req. Area, Sq. in.	.211	Ult. Load, lb.	2705	Req. Area, Sq. in.	.202	Ult. Load, lb.	2590	Req. Area, Sq. in.	.1932	Ult. Load, lb.	2420	Req. Area, Sq. in.	.1801				

stress was established as 20 pct. of the material ultimate tensile strength to allow a reserve of strength for initial preloading, support member thermal contraction, and launch vibration loading.

The weights of the three candidate support systems are shown in table 4-34, and plotted as a function of tank pressure for the LH₂ tank in figure 4-99. The LF₂ system weights are not plotted since they are such a weak function of tank pressure as discussed previously. From figure 4-99, it can be seen that the weight superiority of the nine-rod tension system is directly dependent upon the use of glass fiber materials. Under these conditions it is lighter than the other two approaches.

(2) Tank Support Heat Transfer Analysis. A thermal analysis of the various tank support concepts was next undertaken. For the nine-rod system, four different materials were considered including glass fiber, steel, titanium and aluminum. The insulation was assumed to be on the shroud and all heat conducted past the insulation was assumed to find its way into the H₂ tank. A 2-in. glass fiber block was assumed attached between the shroud and all metallic supports. Surface emissivity of the support rods was varied. The results are presented in figure 4-100. These curves show that the higher conductivity materials will allow more heat input to the propellant even for low-surface emissivities. It is also observed that the effect of surface emissivity is not significant except for low values and the effect decreases with increasing support conductivity. From the figure, it is seen that an insulated, solid glass fiber support will give the least heat transfer. This support system gives a minimum heat flux of 0.0113 b. t. u. /hr. per upper support or a total of 0.082 b. t. u. hr. through all nine supports. However, for uninsulated, uncoated glass fiber, the heat input is about six times higher, and the total heat input during the 330-hr. mission would be about 162 b. t. u. The net LH₂ boiloff is slightly below 1 lb., which is almost negligible. If desired, this pound could be saved by coating the glass fiber with aluminum or gold. With even a moderately good emissivity coating, the total heat flux could be held to 0.36 b. t. u. /hr. to the LH₂ tank.

The continuous conical support for the LH₂ tank was next analyzed assuming a perfectly insulated titanium structure. This resulted in a heat transfer of 7.6 b. t. u. /hr. Preliminary computations were also made on a glass fiber conical structure which yielded a heat transfer of 1.0 b. t. u. /hr.

The six-point tubular glass fiber column system illustrated in figure 4-97 was next analyzed. This configuration was estimated to result in a heat leak of 0.62 b. t. u. /hr. which included radiation down the center of the hollow tubes. If this radiation were neglected or could be entirely blocked, the heat transmission could be reduced to 0.2 b. t. u. /hr. Blocking of the tube radiation could possibly be reduced by stuffing the tube with NRC-2 insulation.

(3) Tank Support Comparison. Table 4-35 compares the weight and heat-transfer characteristics for the three candidate support systems for the LH₂ tank. From this it can be seen that the nine rod glass fiber tension system has an edge both with respect to weight and heat flow resistance. Therefore, on this basis, the nine-rod system was selected for use in the remainder of the study.

Table 4-34

STUDY VEHICLE TANK SUPPORT SYSTEM WEIGHTS (Lb.)

Tank	Support System	Support Material	Tank Internal Pressure, p.s.i.a.			
			250	200	150	60
LH ₂	Nine-rod tension member	Unidirectional glass fiber	43.1	41.6	40.0	37.2
		CRES steel	55.0	53.0	50.9	47.6
		Titanium	51.4	49.5	47.5	44.3
		Aluminum	53.6	51.5	49.5	46.1
		Titanium	--	--	--	41.2
		Glass fiber cloth laminate	50.3	--	--	--
LF ₂	Nine-rod tension member	Unidirectional glass fiber	246.0	--	--	--
		CRES steel	300.9	--	--	--
		Titanium	284.9	--	--	--
		Aluminum	295.0	--	--	--

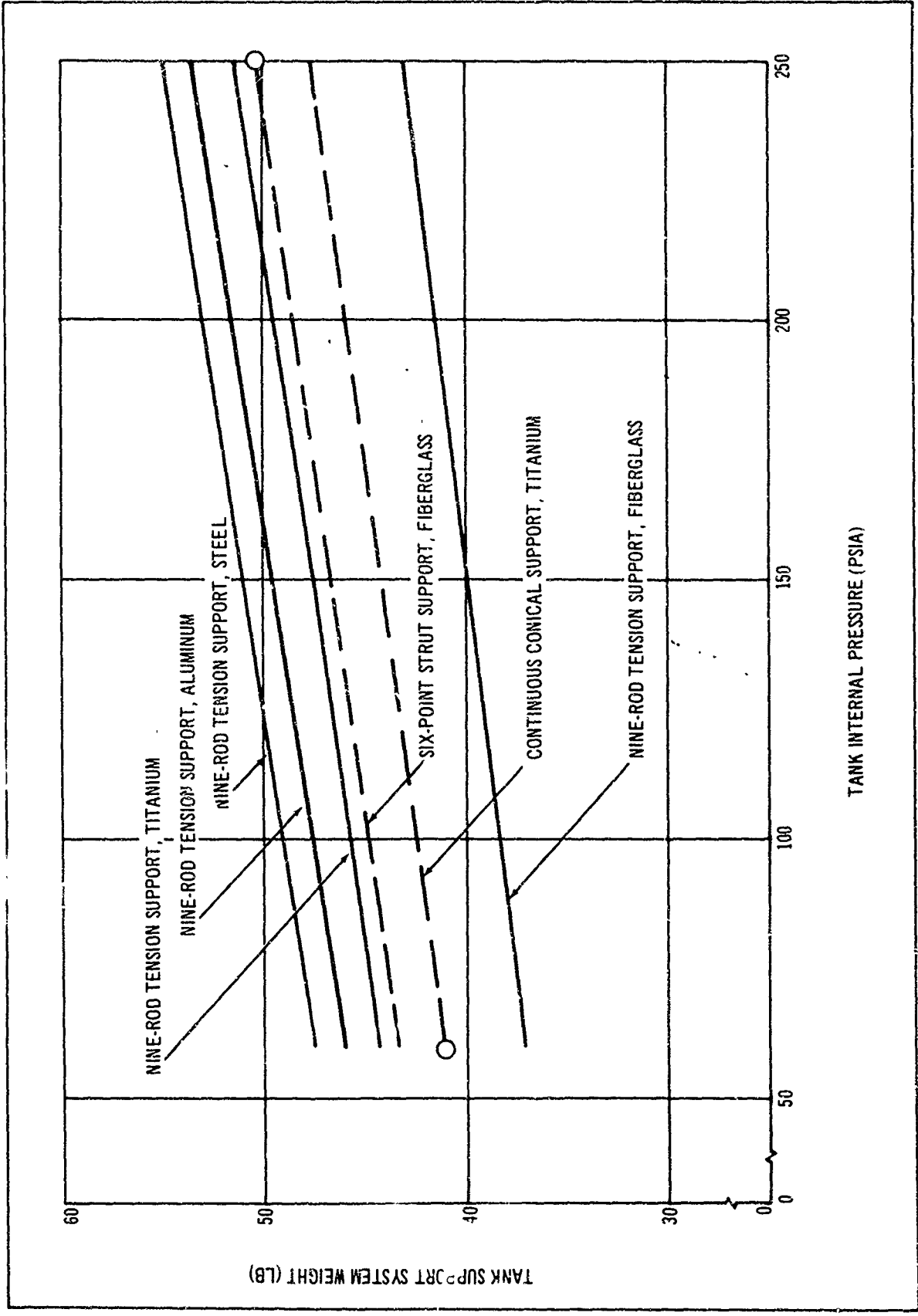


Figure 4-99. Weight Comparison for Study Vehicle LH₂ Tank Support

Table 4-35

COMPARISON OF TANK SUPPORT CONCEPTS
 (LH₂ Tank: P_T = 250 p. s. i. a.)

	Weight (lb.)	Heat Flux (b. t. u. /hr.)	
		Nominal	Minimum
Nine-rod glass fiber tension system	43.1	0.36	0.082
Continuous titanium conical system	47.5	7.8	1.0
Six-point tubular strut system	50.3	0.62	0.2

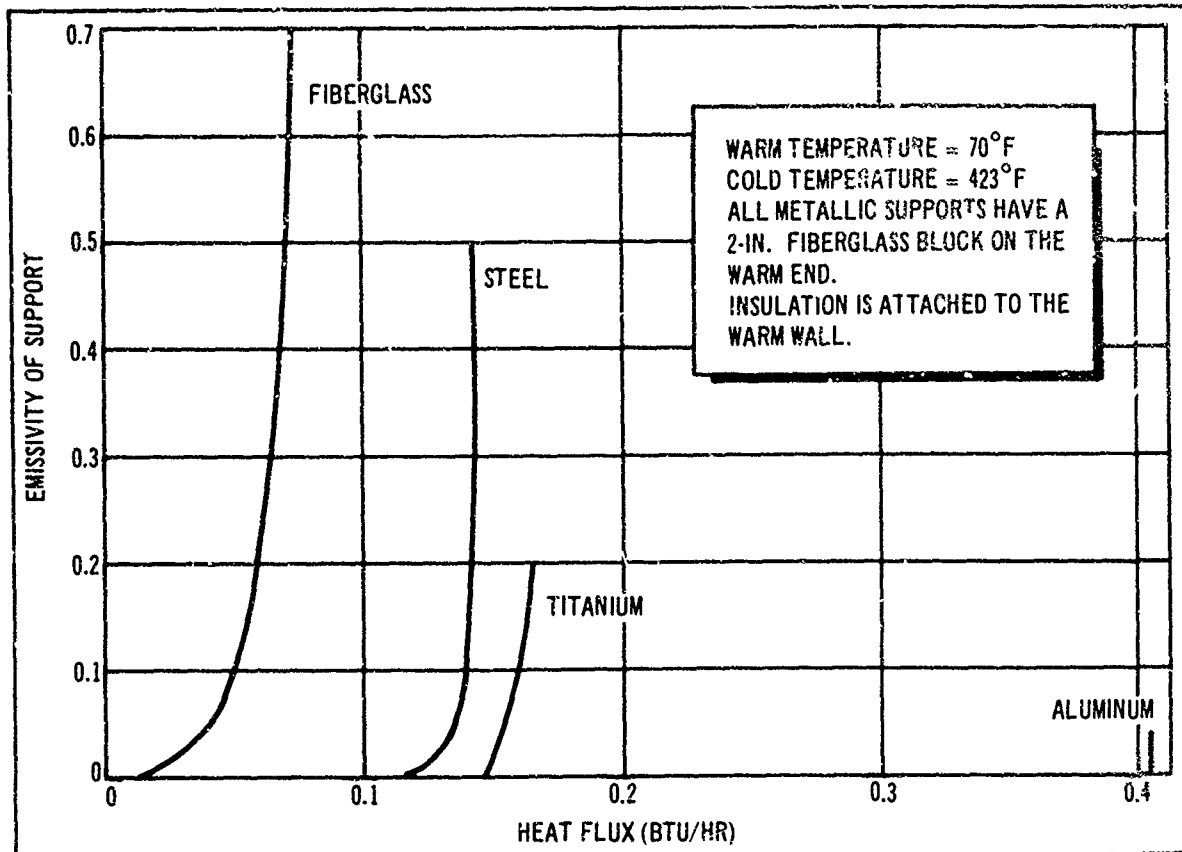


Figure 4-100. Heat Transfer Through LH₂ Tension Support Rods (Equal Strength)

It was also reasoned that this would be the preferred support system for the LF_2 tank. For the same criteria this results in a heat flux of 0.352 b. t. u. /hr. nominal.

Early in the course of this study, other more unconventional tank support ideas were given brief consideration. One of these was the idea of using a stacked washer structural concept. In this approach the tank support structure would be made up of a large number of washer or wafer type elements which would carry in compression the high loads during boost operation. During the low-g. environment in coast, the load would be relieved and thermal contact resistance between the washers would demonstrate very low heat transmission. However, the available thermal performance data on such a concept is meager and scattered and did not permit a realistic analysis. Designing a real system utilizing such a principle also involves practical problems.

The idea of a support which physically disengaged during orbit was also considered but discarded because of the design and reliability problems posed by having to couple and uncouple with a large number of burns where fast response of the stage is important. However, as seen from the above finding, the heating penalties attributable to the tank support system using rather conventional approaches are not large relative to the other sources of heat transfer.

c. Insulation System Optimization. Having all the basic insulation data now accumulated, the insulation was optimized for the overall system. This was accomplished by running the H109 computer program (see appendix A) according to the approach outlined in appendix C. The required number of reflectors or layers was optimized for a specific mission, tank pressure, insulation type and insulation location using the resulting usable propellant weight as the criteria for system performance. The general approach is illustrated below: The insulation optimization was performed assuming a nine glass fiber rod tension support system, insulated steel feed and vent lines, and a heated helium pressurization system with an inlet gas temperature of $400^\circ R$. All other conditions are as defined in appendix C. Since preliminary analyses indicated that the two-burn (80/20) mission was the most critical from a heating standpoint, this was used throughout.

The optimum number of sheets for both the LH_2 and LF_2 tanks were determined. This involved generating parametric curves of usable propellant weight versus insulation layers for the LH_2 tank with layers of insulation for the LF_2 tank as an independent parameter. Typical examples are shown in figure 4-101. Such curves were generated for each set of conditions. From such curves the optimum LH_2 tank insulation for a given number of insulation layers on the LF_2 tank could be determined. Using these values, additional runs were made with the H109 program to generate the usable propellant weight as a function of number of insulation layers for the LF_2 tank as shown in figure 4-102. This figure then defines the optimums for both tanks.

The overall optimization results, in term of usable propellant and the number of layers, are presented in tables 4-36 and 4-37, respectively.

DIMPLAR - SHROUD - ORIENTED
DUTY CYCLE K (14 DAYS)
PUMP-FED ENGINE-BOOST PUMP $\Delta P = 0$
PRESSURIZATION CONDITIONS

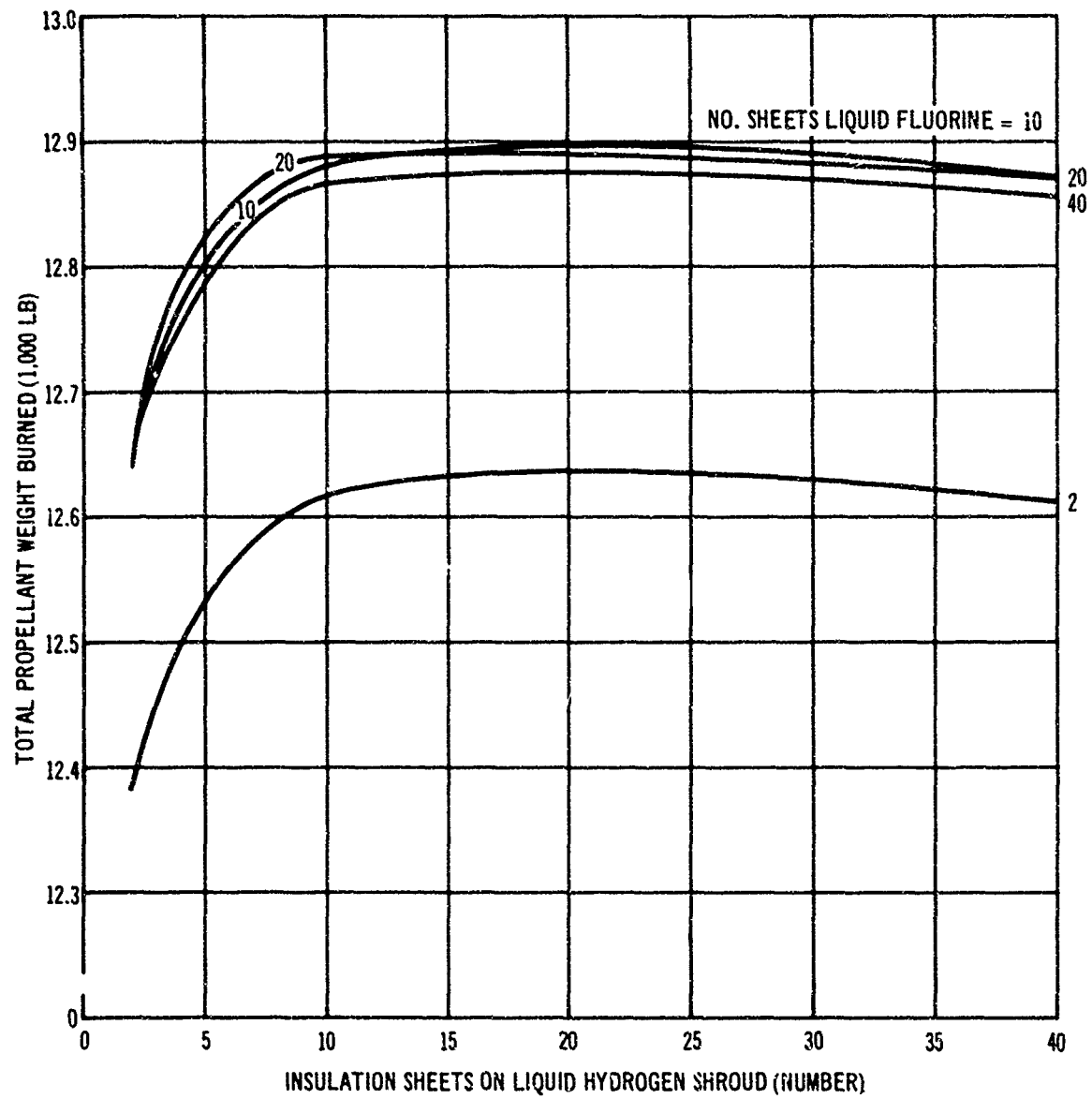


Figure 4-101. Optimization of LH₂ Tank Insulation

DIMPLAR SHROUD - ORIENTED
 DUTY CYCLE K (14 DAYS)
 PRESSURIZATION CONDITIONS - BASIC
 BOOST PUMP $\Delta P = 0$

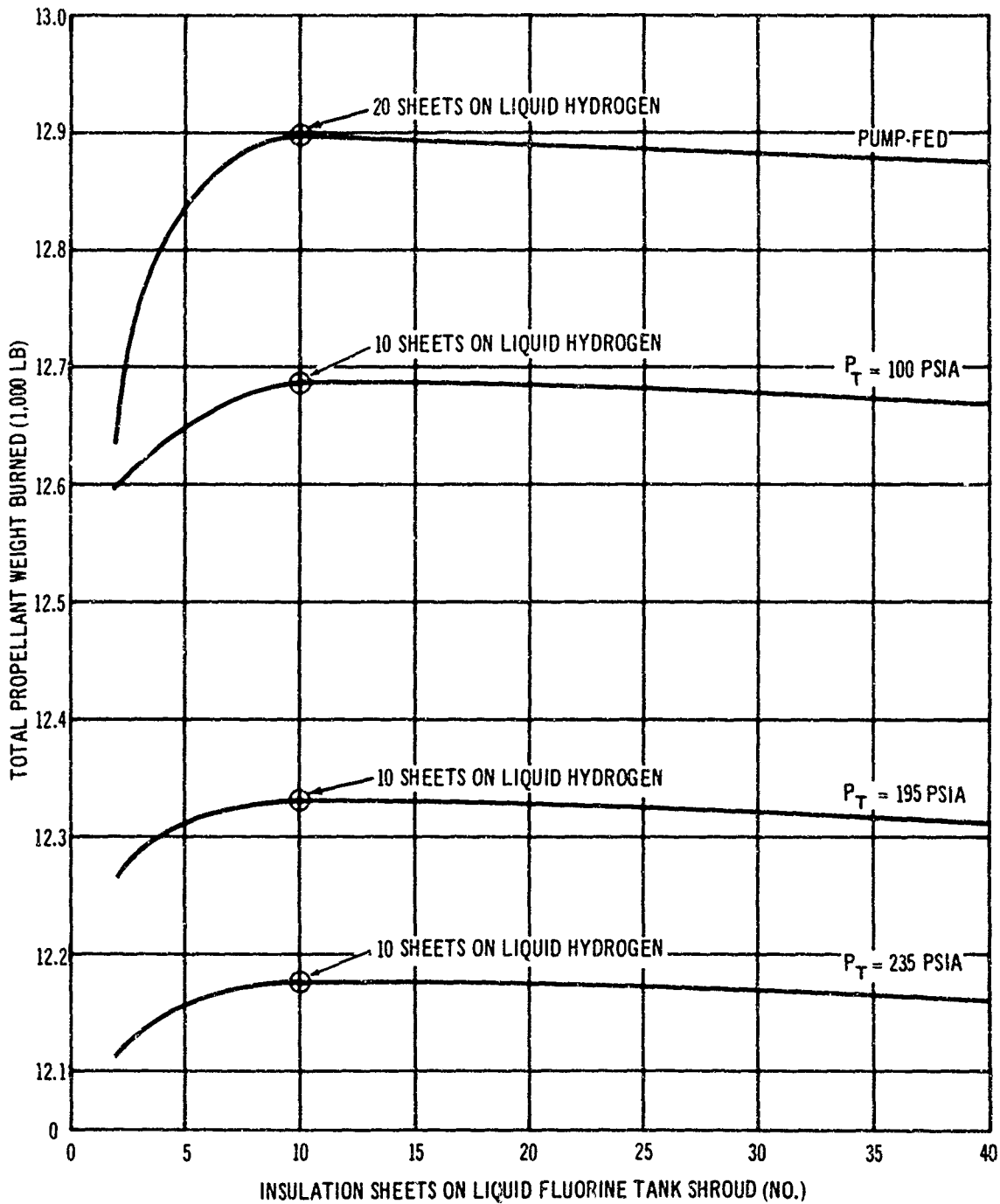


Figure 4-102. Optimization of LF₂ Tank Insulation

Table 4-36

INSULATION OPTIMIZATION RESULTS
(OPTIMUM USABLE PROPELLANT WEIGHTS)

Mission Time Engine sup. pres.	1 Day 195		5 Days 195		14 Days 195	
	Pump 100	235	Pump 100	235	Pump 100	235
Dimplar						
Shroud						
No B. P. ^a	12,946	12,740	12,927	12,715	12,898	12,687
OBP ^e	12,828	12,225	12,799	12,358	12,766	12,331
Tanke						
No B. P.	12,939	12,732	12,890	12,700	12,829	12,660
		12,216		12,338		12,300
NRC-2						
Shroud						
No B. P.	12,944	12,735	12,929	12,710	12,884	12,675
OBP	12,795	12,222	12,955	12,355	12,736	12,316
Tanke						
No B. P.	12,971	12,302	12,955	12,363	12,905	12,335
OBP	12,753					
MPSS						
Shroud						
No B. P.	12,914	12,343	12,806	12,254	12,438	11,908
OBP						
Tanke						
No B. P.						
OBP						

^aNo B. P. refers to no boost pump in the system

^eOBP refers to the use of an optimum boost pump in the system giving a LH₂ tank pressure of 30 p. s. i. a.

Table 4-37
INSULATION OPTIMIZATION RESULTS
(SHEETS OF LH₂/LF₂ INSULATION)

Mission Time Basic type used Engine sup. pres.	1 Day		5 Days		14 Days	
	Pump	Pressure	Pump	Pressure	Pump	Pressure
	100	235	100	195	100	195
				225		235
Dimplar						
Shroud						
No B.P.	1/1	1/1	10/10	10/10	20/10	10/10
With B.P.	1/1	1/1	10/10	10/10	20/10	10/10
Tank						
No B.P.	10/10	10/10	10/10	20/10	40/20	
With B.P.						
NRC-2						
Shroud						
No B.P.	2/10	10/10	10/15	15/15	40/20	20/20
With B.P.						40/20
Tank						
No B.P.	5/10	10/10		20/15	60/20	40/20
With B.P.						
MPSS						
Shroud						
No B.P.						
With B.P.						
Tank						
No B.P.	10/20	10/20	45/50	20/60	70/60	35/80
With B.P.						

Fairly complete spectrums were run for NRC-2 and Dimplar, but the Mylar-paper-spacer system was evaluated only for tank mounting. Optimizations were also run for selected conditions using an optimum booster pump.

The results shown in table 4-36 are enlightening. As would be expected, usable propellant increases as tank pressure and mission time decrease. In comparing the insulation systems capabilities for the same conditions, it can be seen that all are surprisingly close -- particularly the Dimplar and NRC-2. The difference in usable propellant between Dimplar and the MPS system is about 27 and 390 lb. for a 1- and 14-day mission, respectively, with Dimplar showing the best performance. The same differences between shroud-mounted Dimplar and NRC-2 are about 2 and 14 lb. with Dimplar again showing the best performance. The differences between tank and shroud mounting are also slight, ranging from about 7 to 20 lb., with shroud mounting being superior with Dimplar, and tank mounting being superior with NRC-2. Differences of 10 lb. or less are probably less than the accuracy band of the computer program. The following conclusions can thus be drawn:

- In terms of usable propellant weight, Dimplar and NRC-2 are comparable and both of these are significantly superior to the MPS system.
- In terms of usable propellant weight, shroud and tank mounting are comparable with shroud installation having a slight advantage with Dimplar and tank mounting having a slight advantage with NRC-2.

Table 4-37 shows that the number of reflector sheets increases as one goes from Dimplar to NRC-2 to the MPS system and as one goes from shroud to tank mounting. The greater the number of required sheets, the higher the cost to fabricate and the more severe the degassing problem; therefore, on this basis a shroud-oriented Dimplar system should be preferred. Thus, from the results shown and the previously documented discussions of pros and cons, the shroud-oriented Dimplar would seem to have maximum potential as the insulation system for this particular application.

7. Phase VII--Pressurization System. The pressurization subsystem is an important part of any propulsion system, whether the basic feed system is of the all-pressure type or the pump-fed type. The required pressurant, the gas storage and distribution facilities, and heating and control provision, as a whole, generally represent a significant portion of the stage weight. Intermittent multiburn duty cycles are generally required for the missions under investigation in this program. These cycles make the pressurization more complex than with simple single-burn velocity stages. Multiburn implies in orbit, starting with partially empty tanks. If this burn occurs at a time between tank pressure collapse and tank pressure buildup as a result of orbital heating, pressurant for pre-pressurization of the tank prior to burn must be supplied over and above that normally required for expulsion. The engine is not operating during this prepressurization period and, therefore, if heating of the pressurant is required, it must come from some independent source.

For long duration space missions with a cryogenic LF_2/LH_2 propulsion system, the heat load to the propellants must be minimized. In a multiburn mission, nearly all of the heat added to the pressurization gas will ultimately end up in the propellant for all burns except the very last. When using highly insulated tankage, this heat can be significant, relative to the total propellant heat load. Therefore, optimization of the pressurant inlet gas temperatures in this type of vehicle must be conducted with respect to overall stage performance.

This phase of the program was conducted in the following steps:

- Pressurization System Screening Study--A list of possible candidate pressurization systems was prepared and a weight analysis was conducted on each for an assumed inlet gas temperature and tank pressure, using a simplified analytical method. These were then compared on the basis of total pressurization system weight as a function of the level of work required from the system. The most promising subsystems could be identified from this comparison.
- Pressurant Requirements Analysis Program--A new computerized analysis was developed to predict the pressurant requirements for repressurization and expulsion pressurization considering heat and mass transfer to and from the ullage, and as a function of the critical variables of the system.
- Determination of Pressurant Requirement--Using the analysis developed in the second step and the general systems selected in the first step, the pressurant requirements were evaluated for each duty cycle and ground-rule tank pressure. This was done for a spectrum of inlet gas temperatures and for both He and GH_2 pressurants.
- Pressurant Gas and Inlet Gas Temperature Optimization--Using the accumulated information, the optimum pressurants and gas inlet temperatures were evaluated in terms of maximum overall stage performance.

a. **Pressurization System Preliminary Weight Screening Study.** Hundreds of different pressurization systems could be proposed for any given class of systems. However, after reviewing many possibilities, 12 individual systems were selected for study. These encompass primarily different types and combinations of heat sources and He or GH_2 pressurants. These are listed in table 4-38, and the schematic diagrams are shown in figure 4-103.

Configuration 1 illustrates a typical cryogenic pressurization system providing the maximum simplicity consistent with acceptable performance. Heated He is employed to maintain tank pressure during propellant expulsion. The helium is stored in high-pressure bottles submerged in the hydrogen tank to take advantage of the high-density storage and increased bottle strength at cryogenic temperatures. The increase in specific volume required for efficient pressurization is accomplished by passing the cold helium through a heat exchanger attached to the nozzle skirt. A constant pressurant temperature is maintained through a temperature switch/solenoid-valve combination, which allows the proper amount of cold helium to bypass the heat exchanger. Repressurization of both propellant tanks with ambient stored helium, however, is an inherently inefficient way to repressurize because of the high-weight penalties associated with warm, low-density gas storage. Therefore, several approaches for reducing the weight of the repressurization system were selected for evaluation. All of these approaches use heated gas for repressurization. These schemes are discussed in the following paragraphs.

The use of heated gas for repressurization introduces the need for an auxiliary energy source since engine heat is generally not available. Configuration 2 illustrates one energy source which is independent of engine operation.

The He used for repressurizing the H_2 tank is stored in the LH_2 tank and raised to the desired temperature in the auxiliary combustion chamber heat exchanger. The energy for heating the He is provided by the hypergolic ignition of gaseous F_2 and H_2 in the chamber. These gases are combusted stoichiometrically and diluted with He, which is stored in the F_2 gas bottle. The resultant combustion products ($\text{He} + \text{HF}$) are used to repressurize the oxidizer tank. The He reduces the combustion temperature to a tolerable level, in addition to providing the bulk of the low-density gas necessary for efficient pressurization. The HF will usually condense and freeze after contact with LF_2 ; however, HF is present only in small quantities and may not be a problem. Following repressurization and engine ignition, the cold He flow is diverted to the engine-mounted heat exchanger, where the temperature is raised to the desired level for expulsion of both propellant tanks.

Storage of the helium and the reactive gases in the low-density ambient condition is, as previously mentioned, inherently inefficient. An approach to increasing the storage density of the repressurization gases is shown in configuration 3. In this system, both of the propellant tanks are repressurized with cold-stored He by a gas generator, which is independent of the main engine. The required energy for heating the repressurization

Table 4-38

PRESSURIZATION MEDIA AND ENERGY SOURCES

Configuration No.	Tank	Repressurization		Expulsion	
		LF ₂	LH ₂	LF ₂	LH ₂
1.	Main	Ambient He	Ambient He	Heated He (nozzle heat exchanger)	Heated He (nozzle heat exchanger)
2.	Main	Gas generator exchanger (HF + He)	Gas generator heated He	Heated He (nozzle heat exchanger)	Heated He (nozzle heat exchanger)
3.	Main	Gas generator heated He	Gas generator heated He	Heated He (nozzle heat exchanger)	Heated He (nozzle heat exchanger)
4.	Main	Gas generator heated He	Gas generator heated He	Gas generator heated He	Gas generator heated He
5.	Main	Heated He (engine heat exchanger)	Heated He (engine heat exchanger)	Heated He (engine heat exchanger)	Heated He (engine heat exchanger)
6.	Main	Gas generator heated He	Gas generator heated He	Heated He (nozzle heat exchanger)	Engine bleed CH ₂
7.	Main	Twydyne exchanger (He + H ₂ O)	Gas generator heated He	Heated He (nozzle heat exchanger)	Engine bleed CH ₂

Table 4-38 (Cont)

Configuration No.	Tank	Repressurization		Expulsion	
		LF ₂	LH ₂	LF ₂	LH ₂
8.	Main	Gas generator heated He	Gas generator heated He	Heated He (nozzle heat exchanger)	Vaporized LH ₂ (nozzle heat exchanger)
9.	Auxiliary	--	Cold He	--	Cold He
	Main	Ambient He	Ambient He	Heated He (nozzle heat exchanger)	Vaporized LF ₂ (nozzle heat exchanger)
10.	Auxiliary	--	Ambient He	--	Ambient He
	Main	Gas generator heated He	Vaporized LH ₂ (gas generator heat exchanger)	Gas generator heated He	Vaporized LH ₂ (gas generator heat exchanger)
11.	Auxiliary	--	Gas generator heated He	--	Gas generator heated He
	Main	Gas generator exchanger (HF + He)	Gas generator heated He	Gas generator exchanger (HF + He)	Gas generator heated He
11a.	Auxiliary	Cold He	Cold He	Gas generator heated He	Gas generator heated He
	Main	Gas generator exchanger (HF + He)	Gas generator heated He	Gas generator exchanger (HF + He)	Engine bleed GH ₂
	Auxiliary	Cold He	Cold He	Gas generator heated He	Engine bleed GH ₂

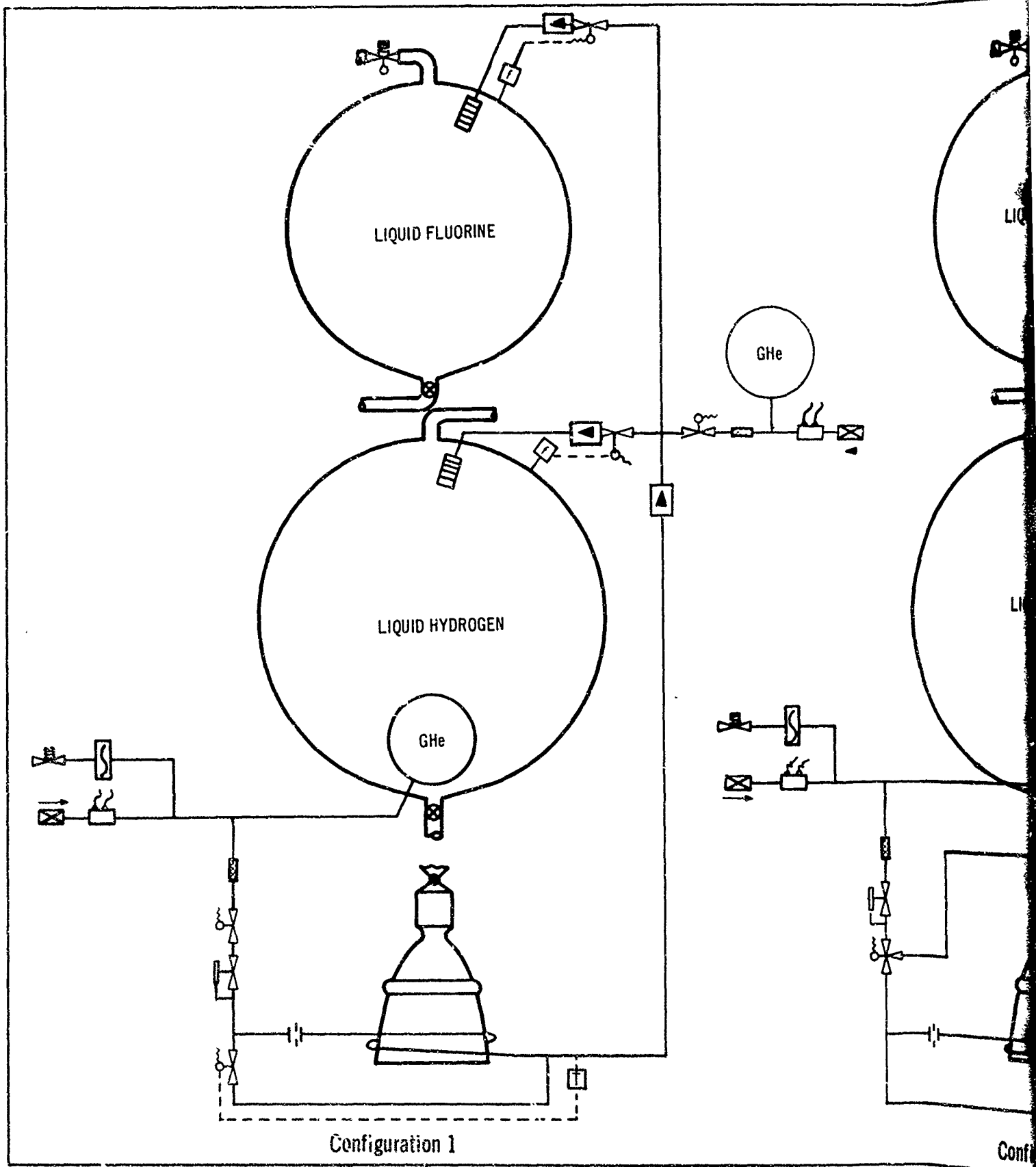
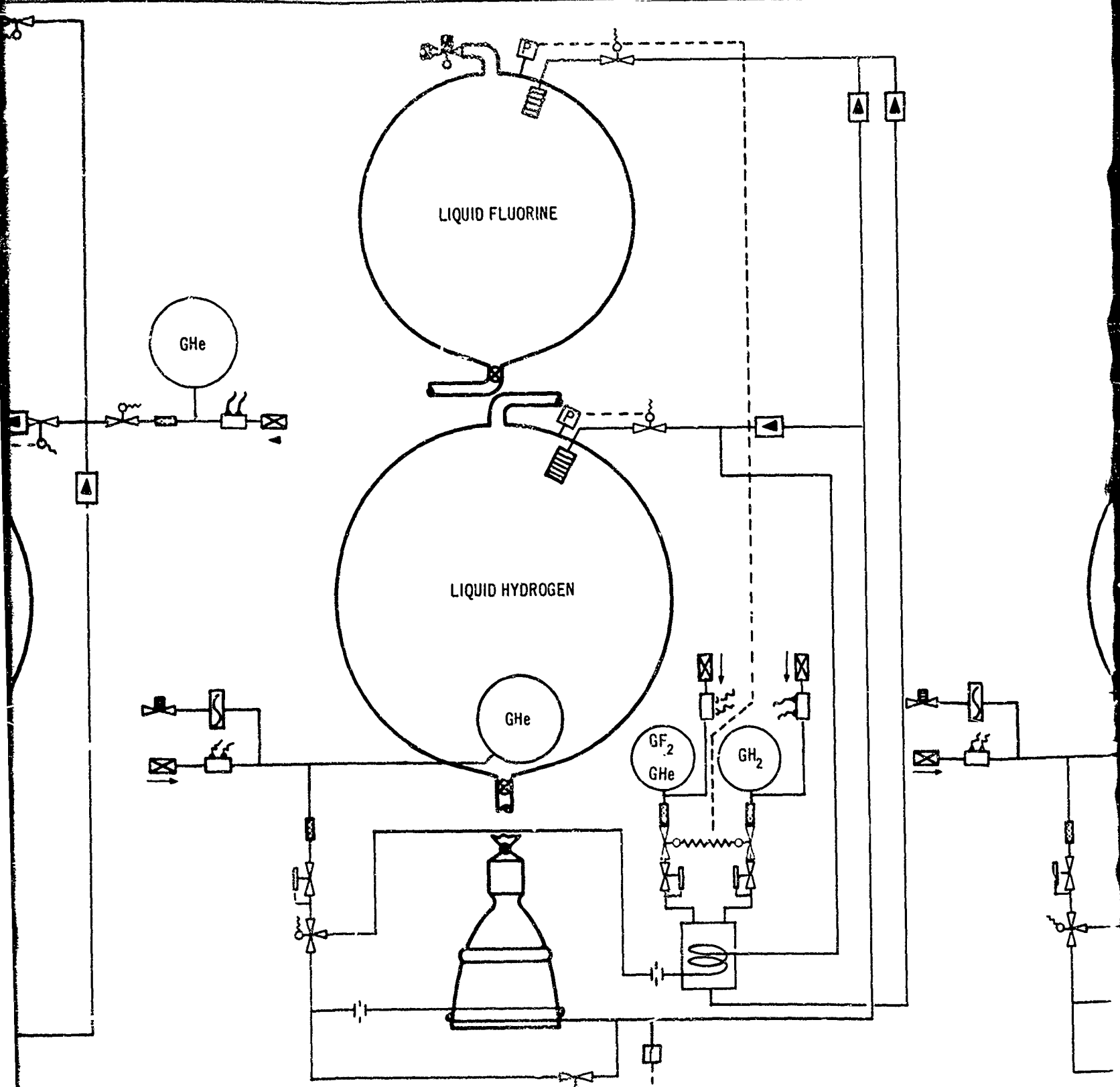


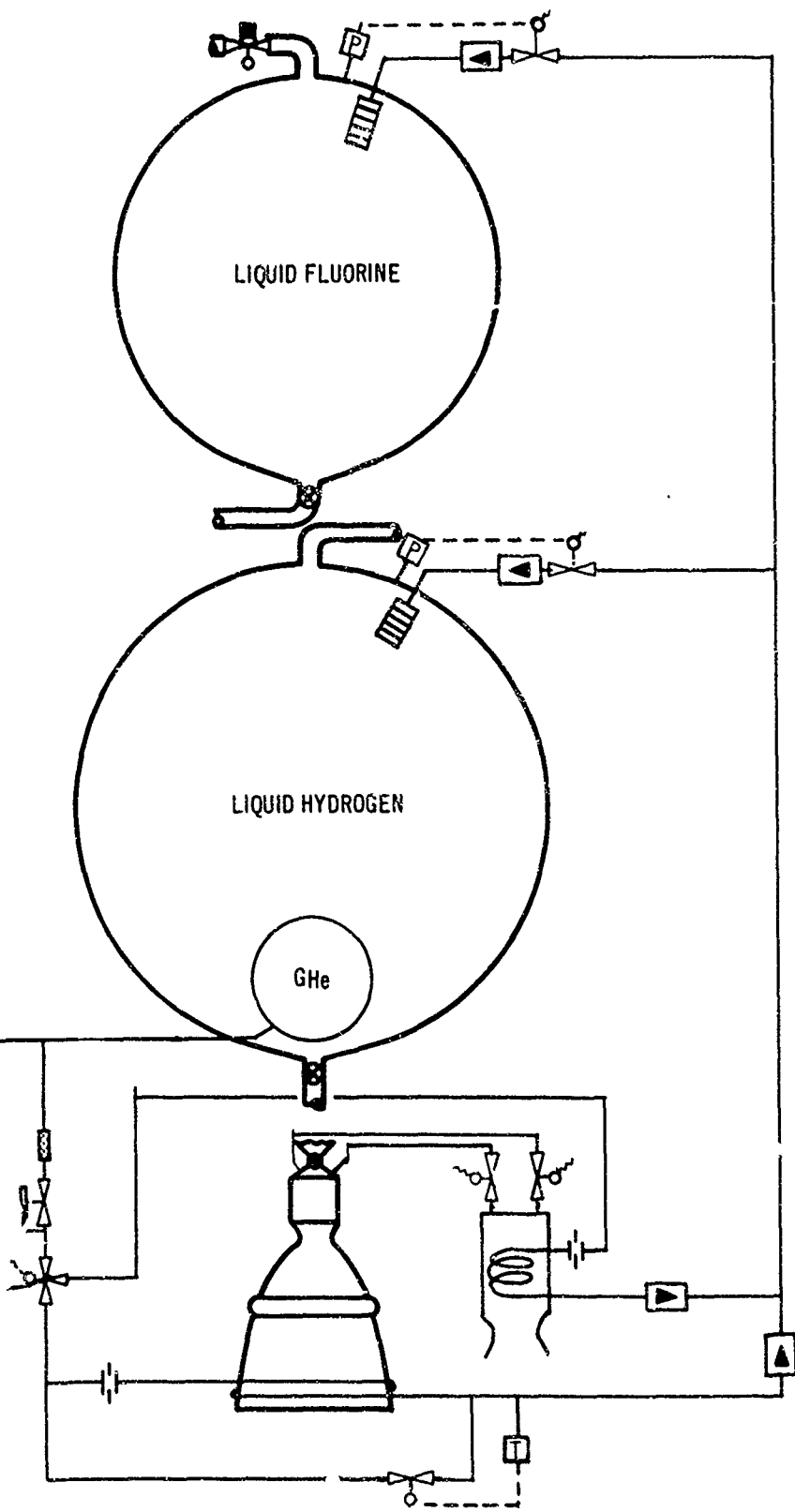
Figure 4-103. Candidate Pressurization Systems

A.

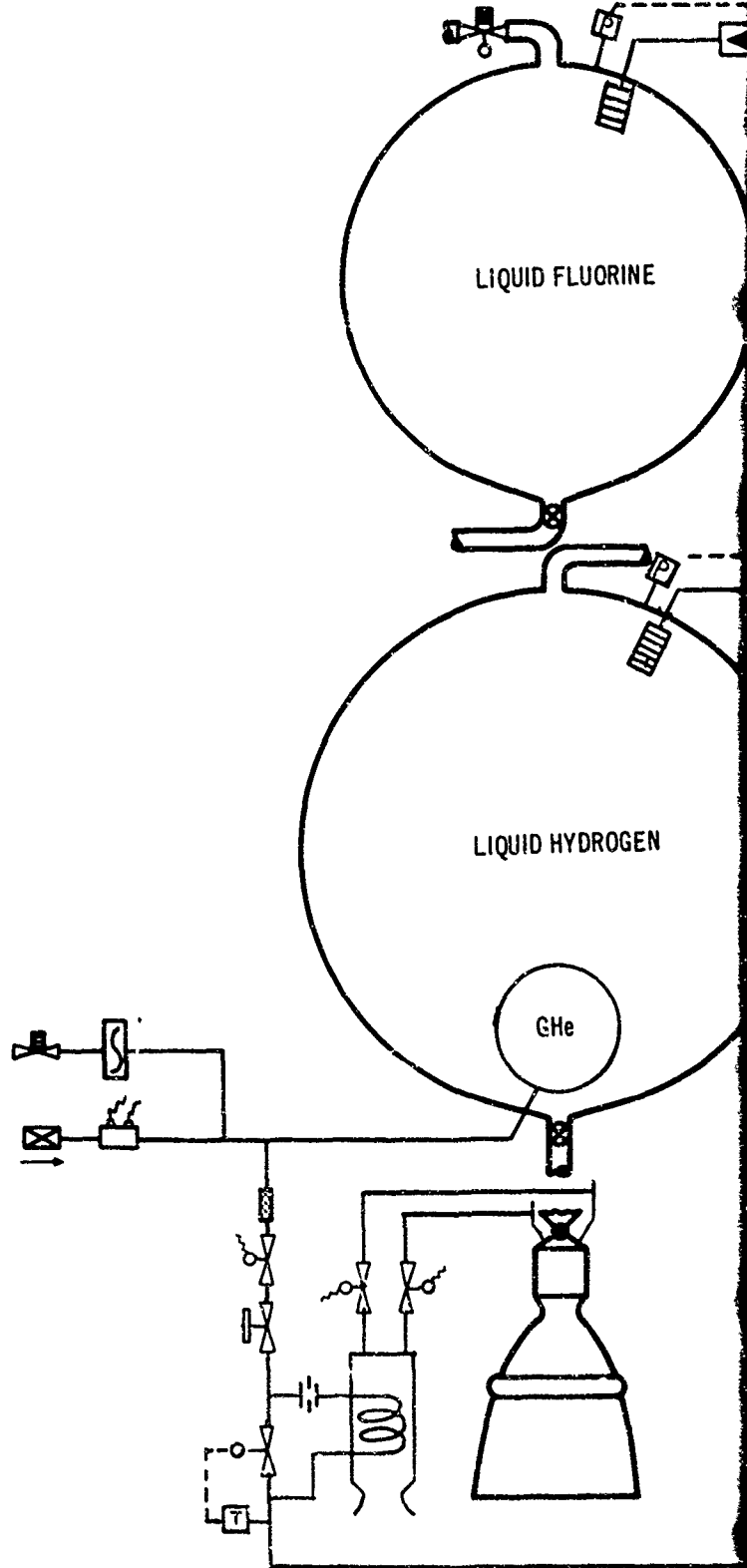


Configuration 2

b

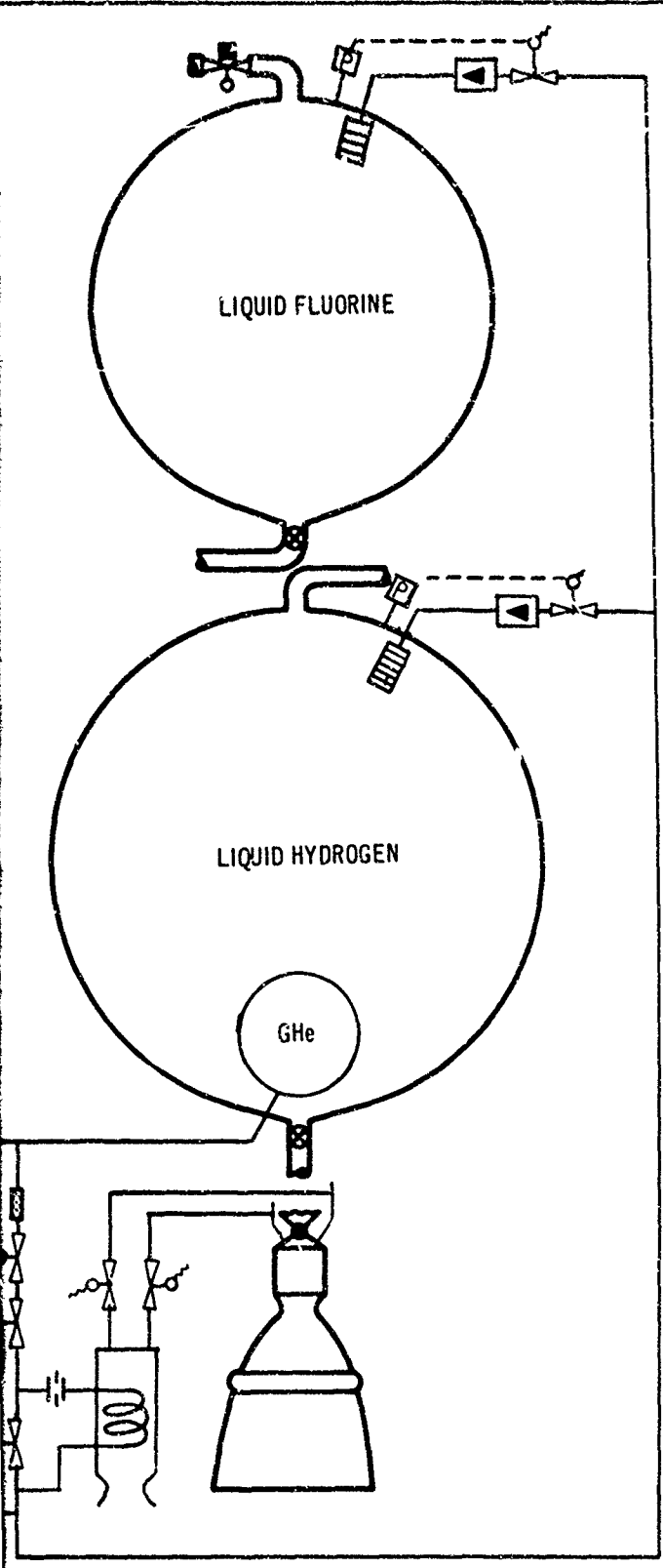


Configuration 3

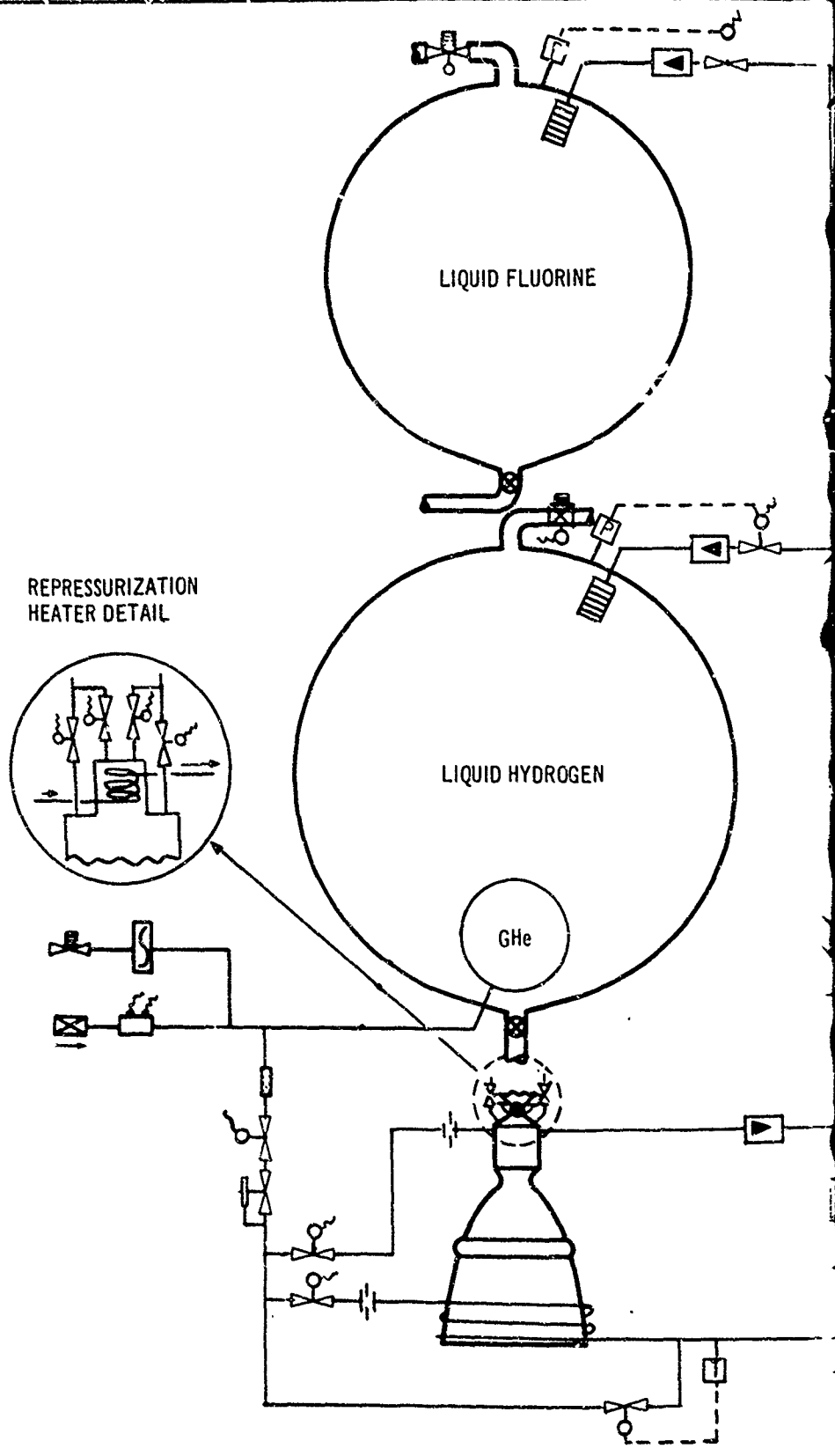


Configuration 4

C

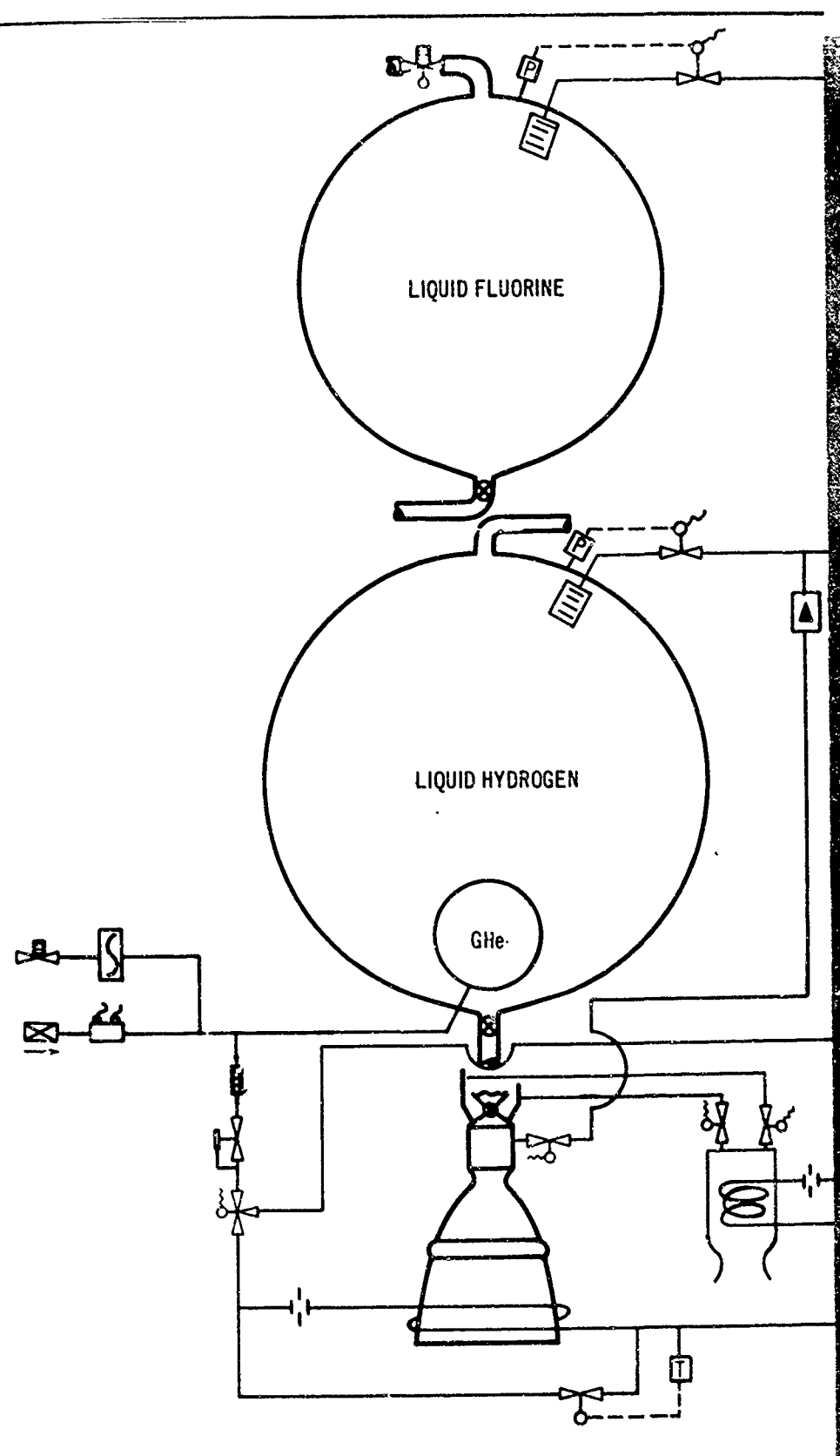
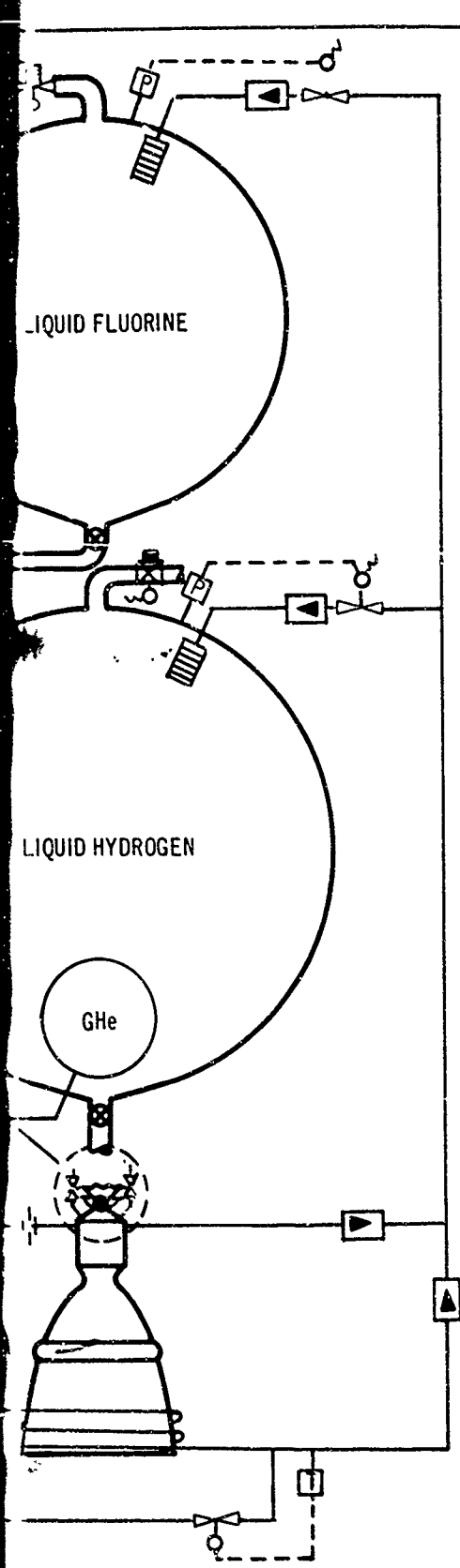


Configuration 4

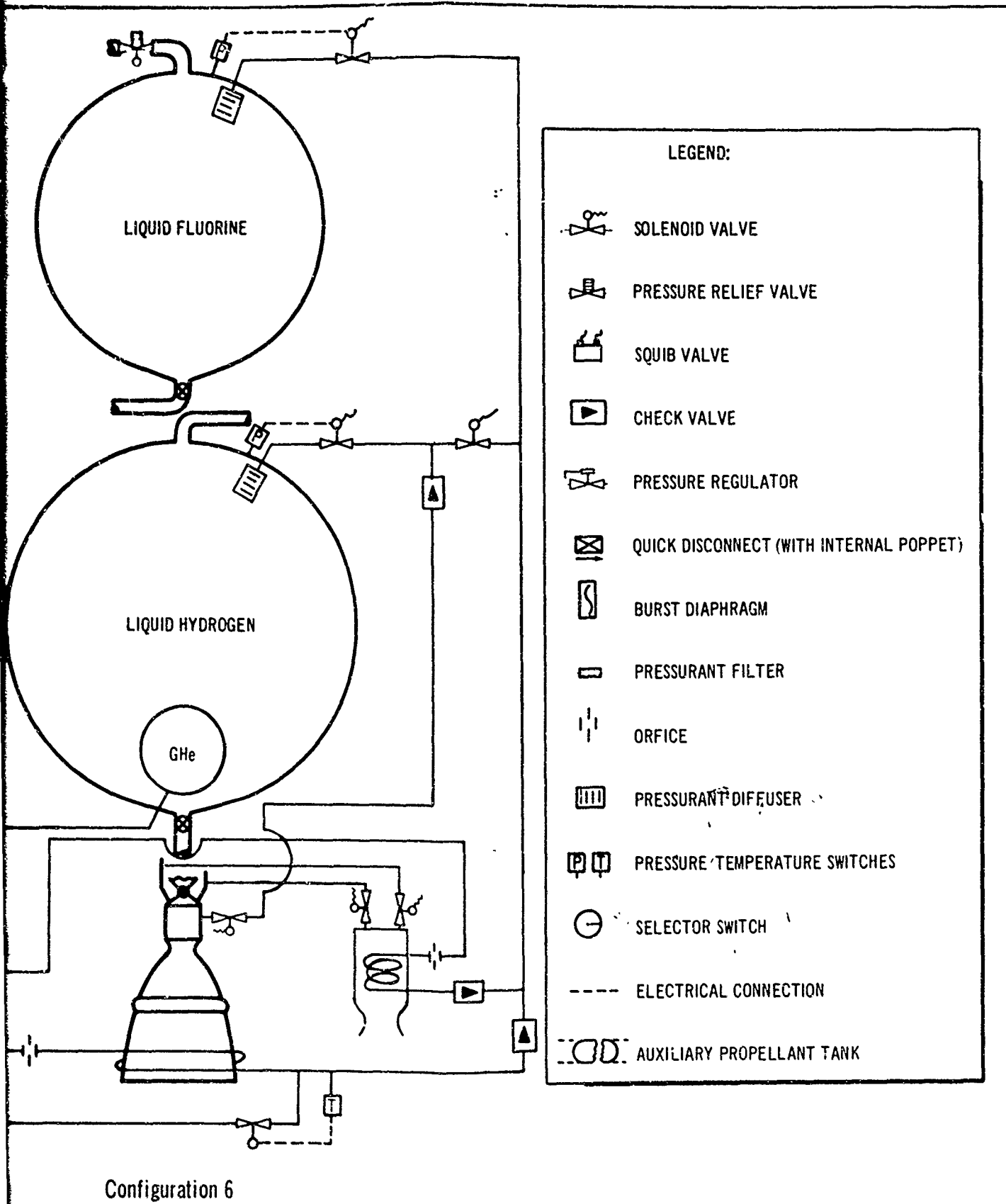


Configuration 5

D

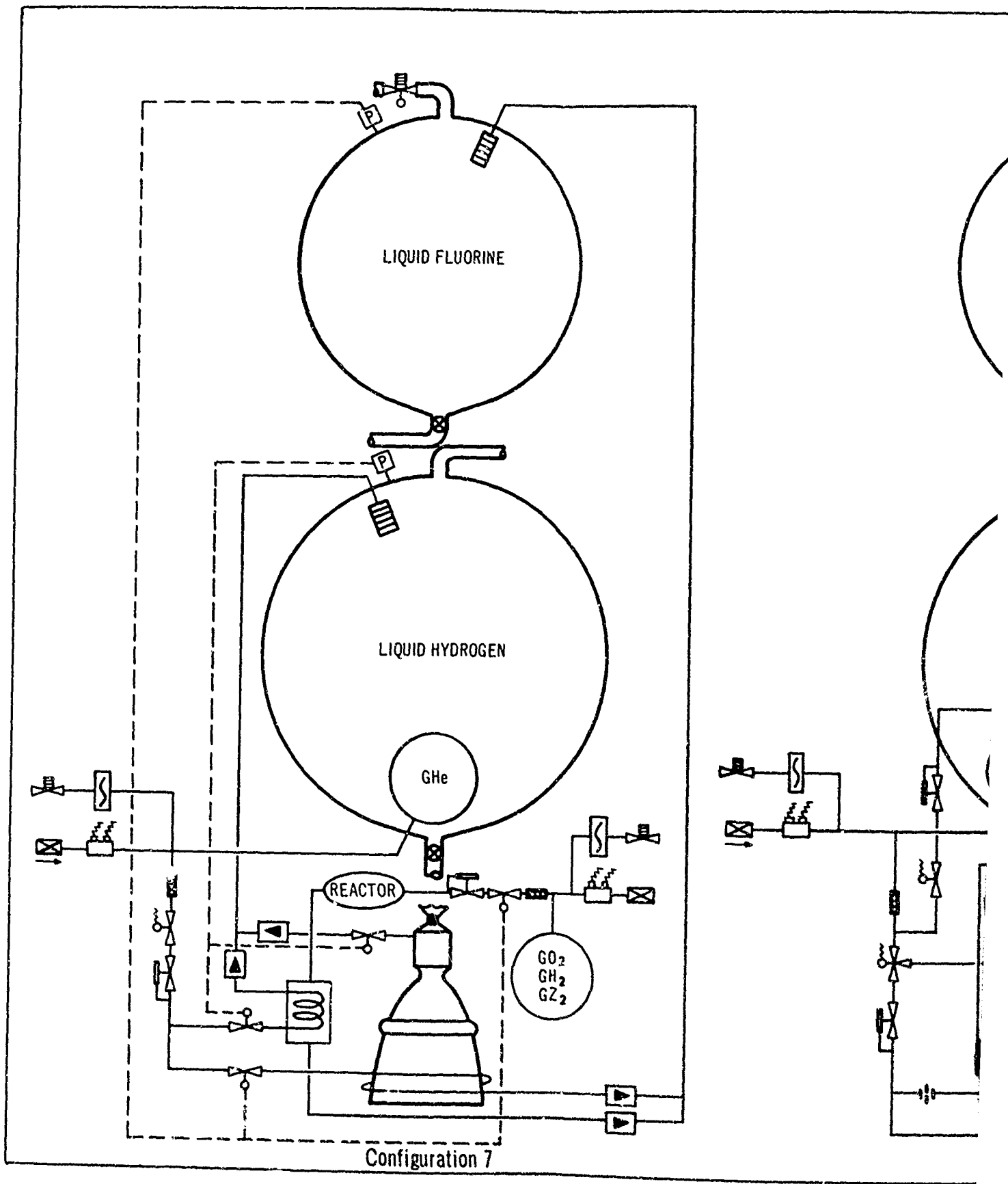


E

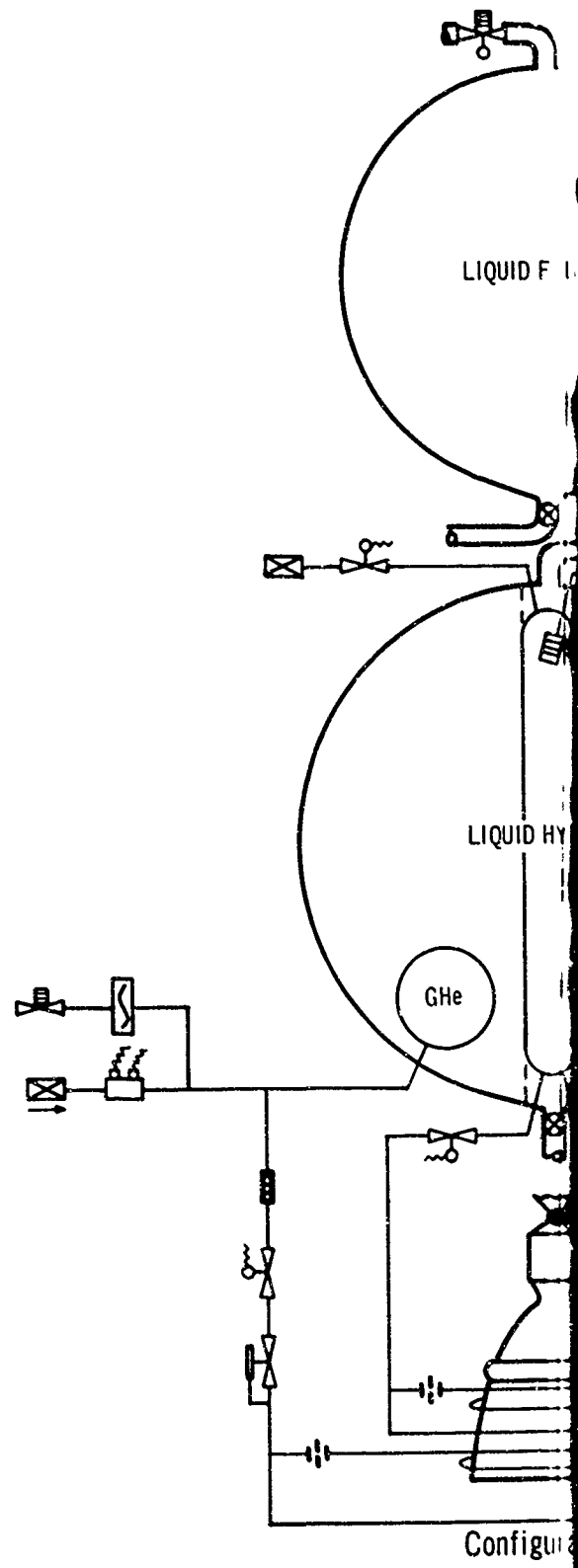
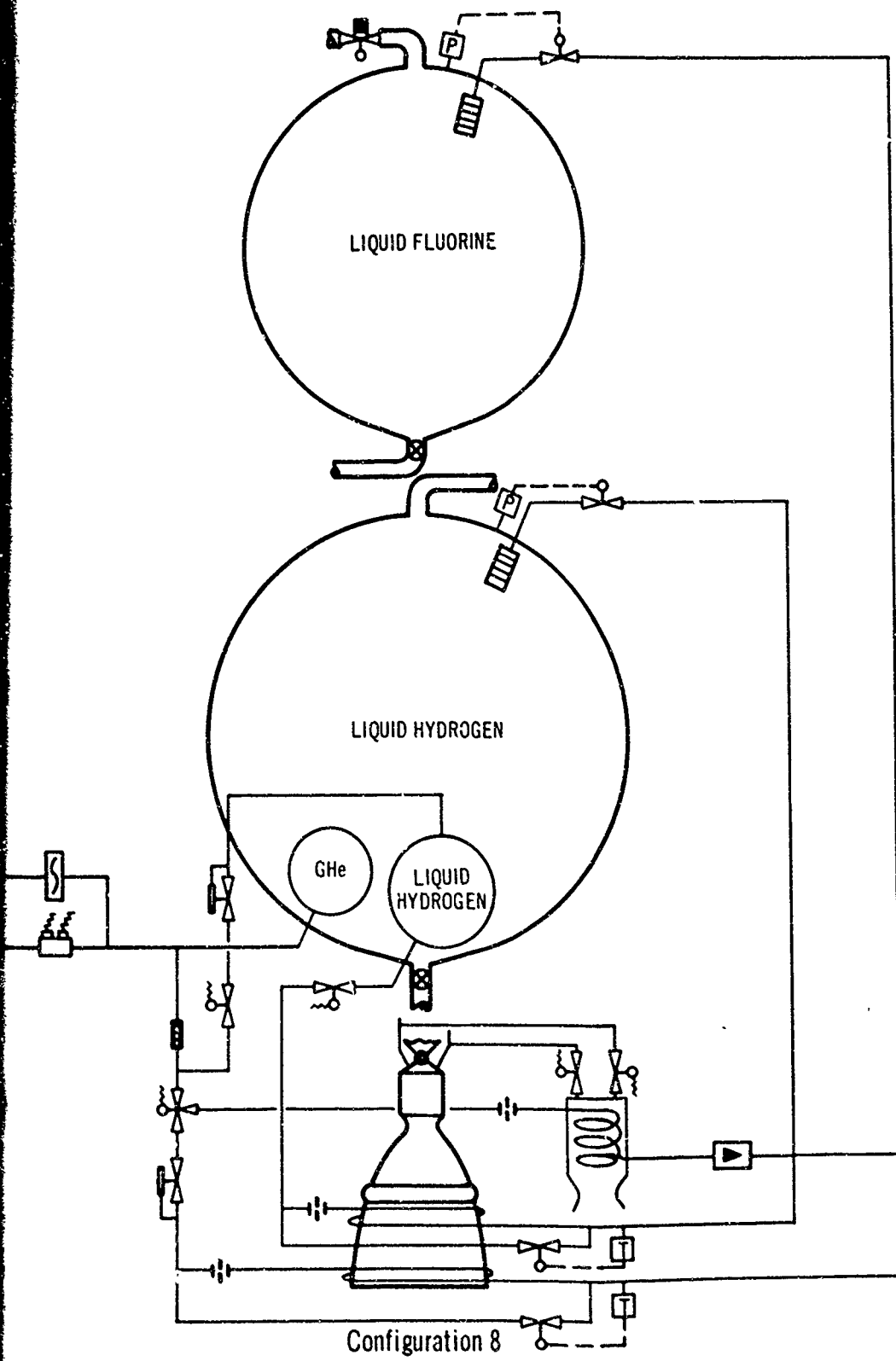


Configuration 6

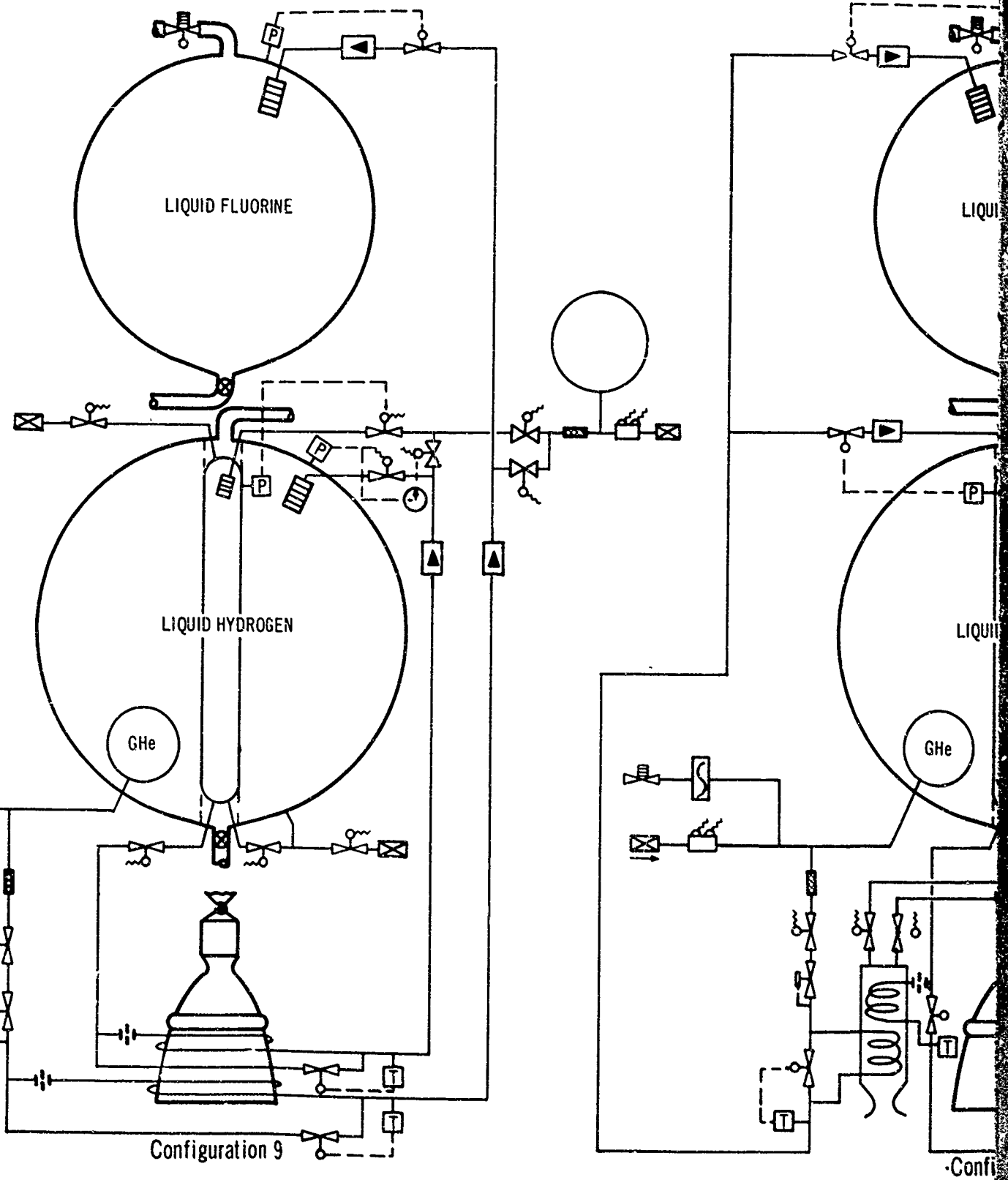
11



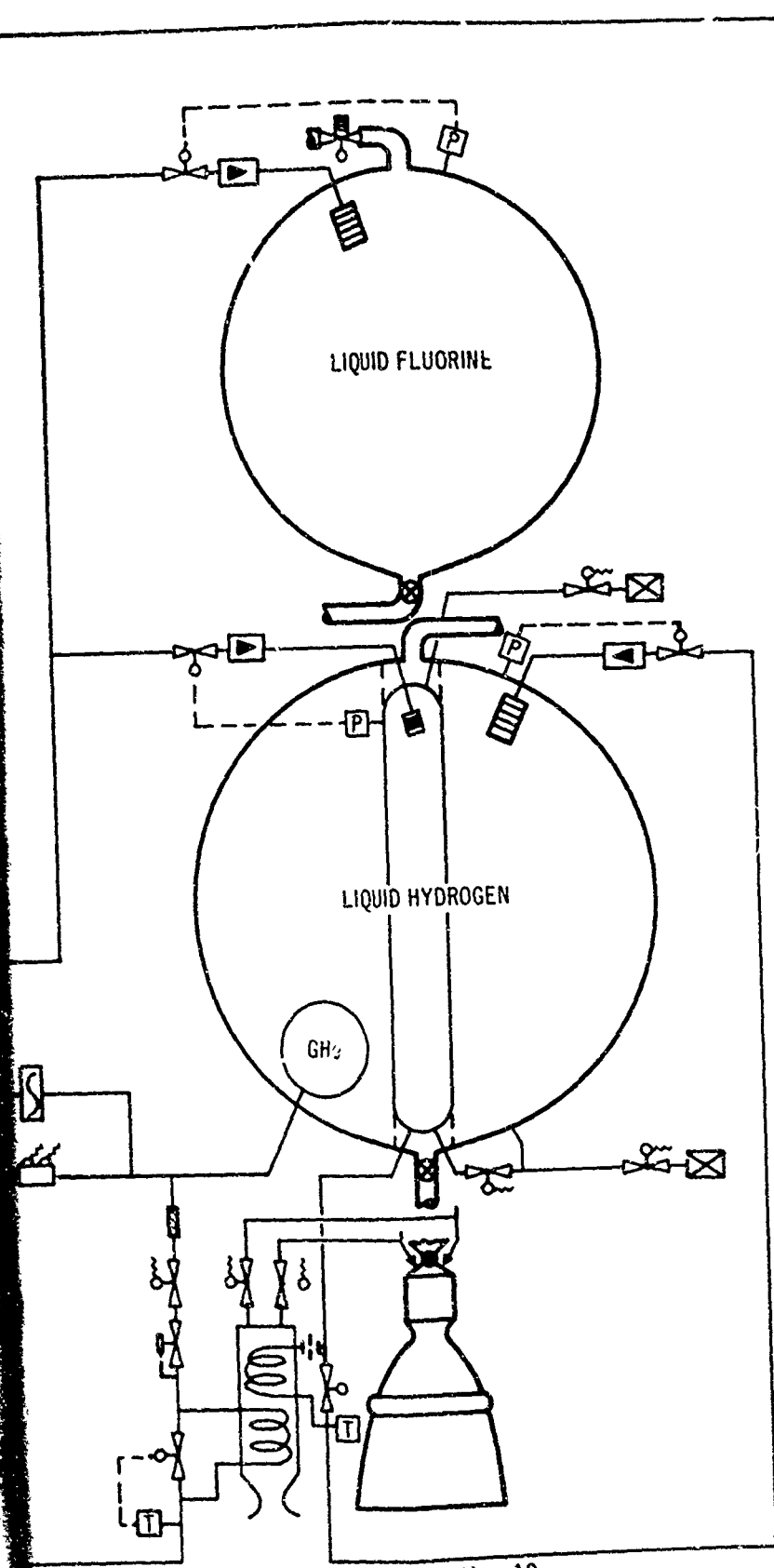
A



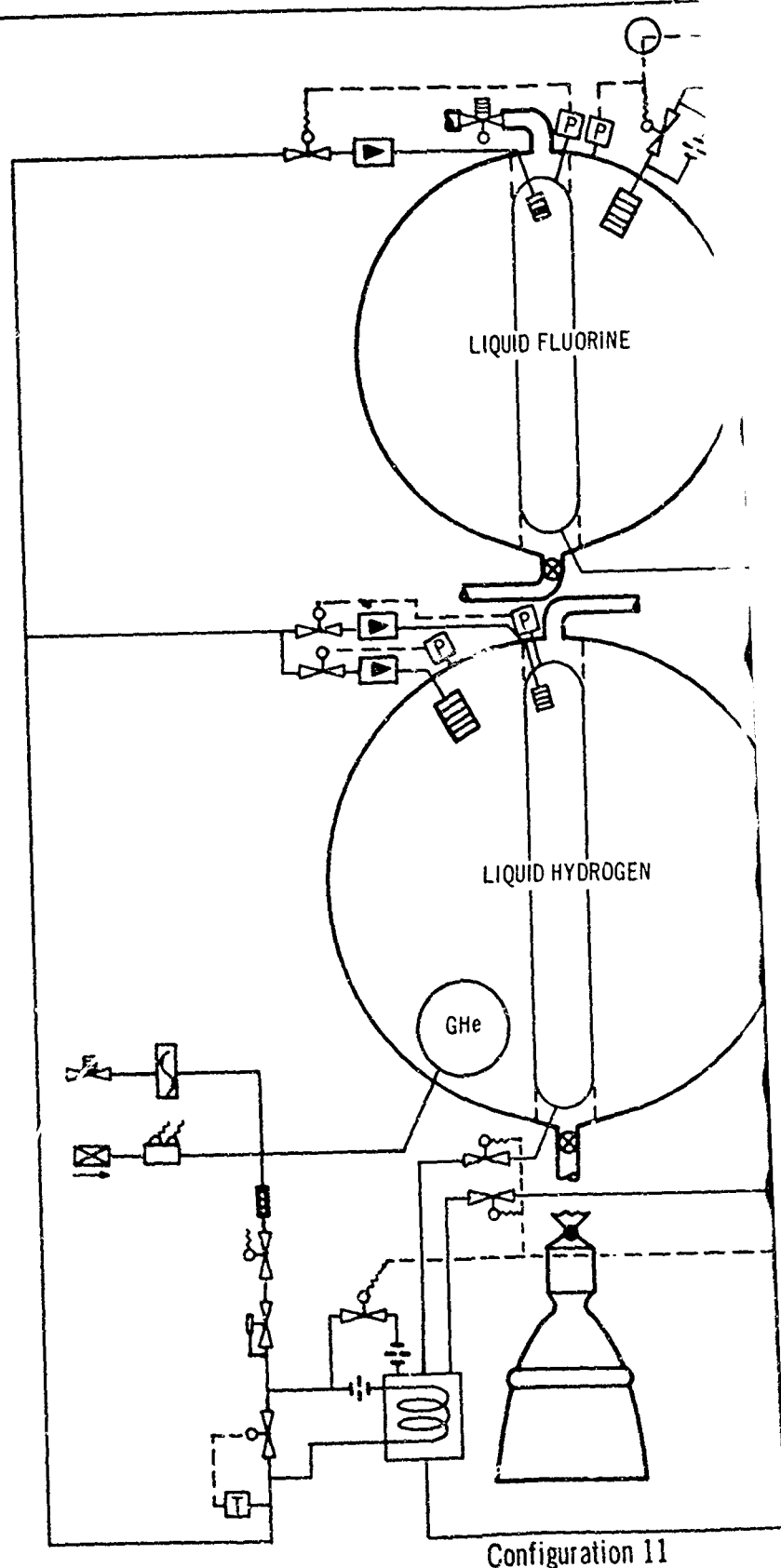
B



C

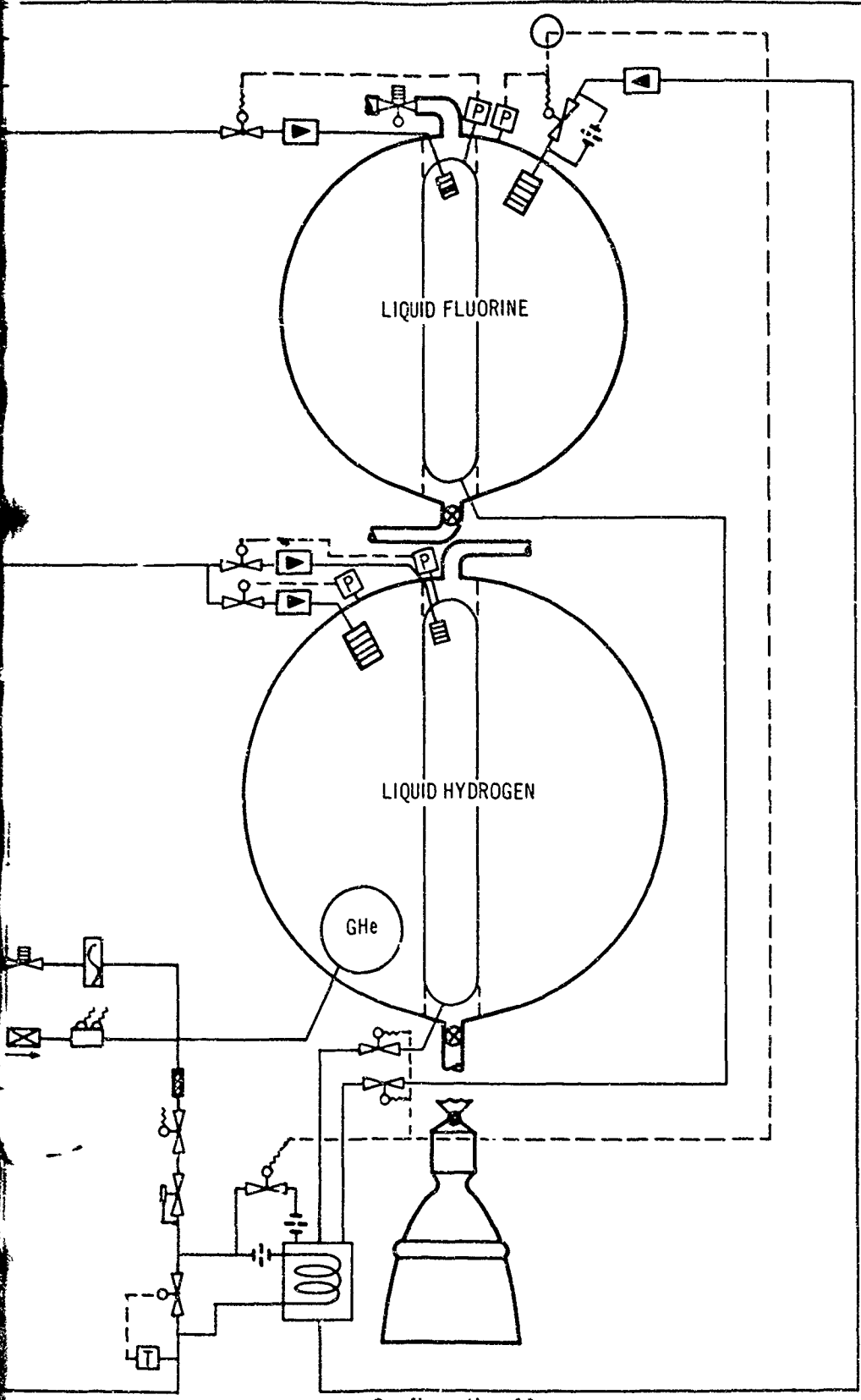


Configuration 10

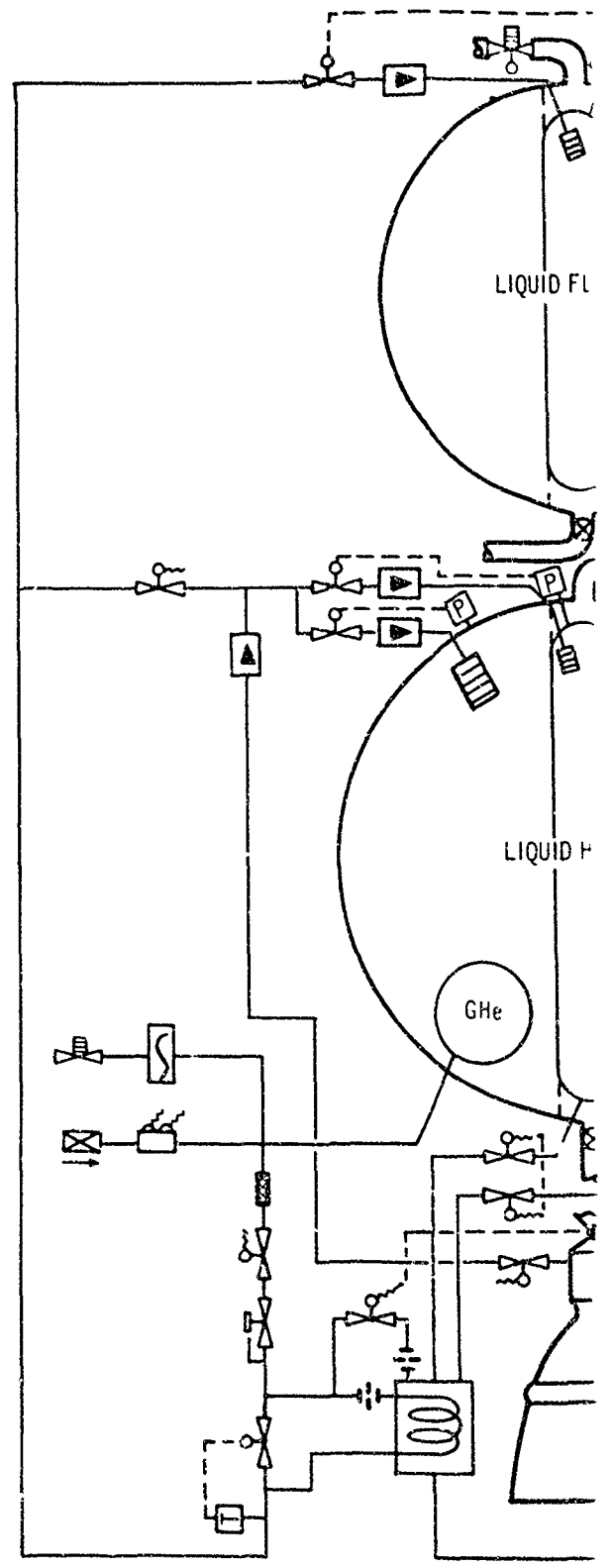


Configuration 11

D

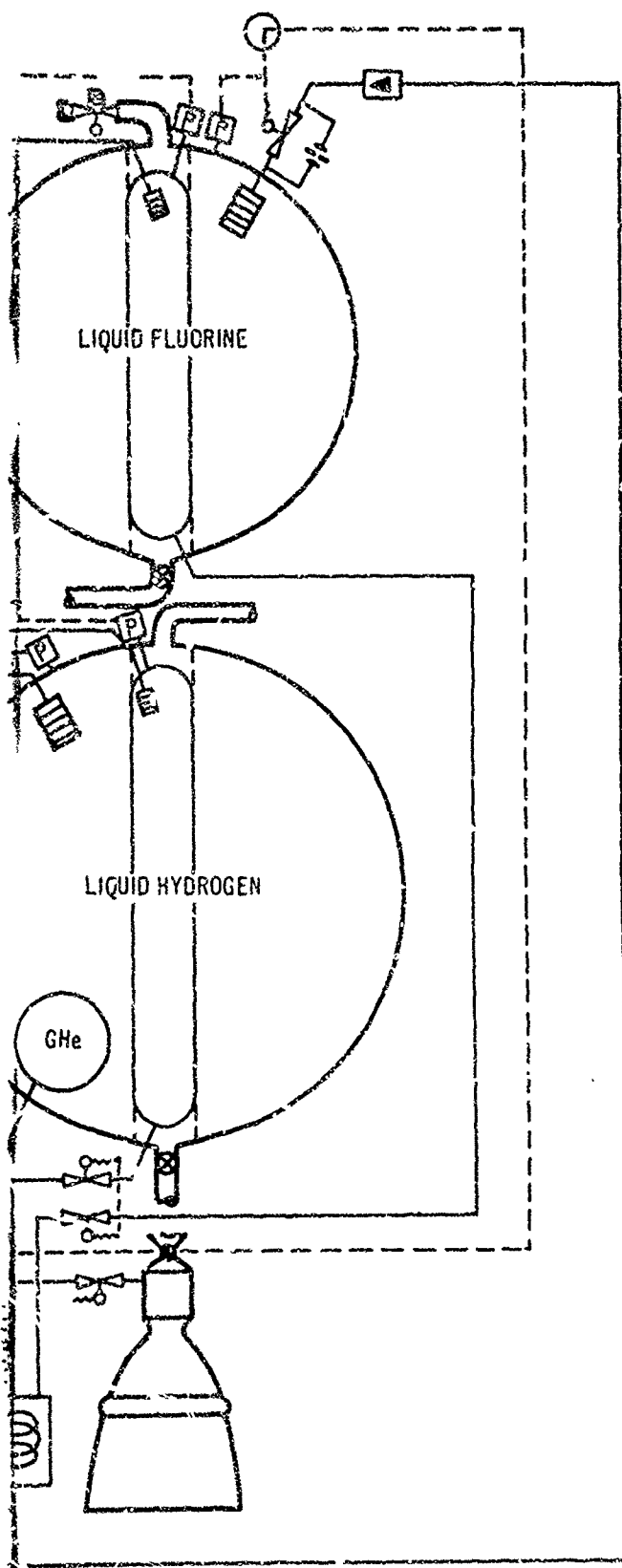


Configuration 11



Config

E



Configuration 11a

- LEGEND:
-  SOLENOID VALVE
 -  PRESSURE RELIEF VALVE
 -  SQUIB VALVE
 -  CHECK VALVE
 -  PRESSURE REGULATOR
 -  QUICK DISCONNECT (WITH INTERNAL POPPET)
 -  BURST DIAPHRAGM
 -  PRESSURANT FILTER
 -  ORIFICE
 -  PRESSURANT DIFFUSER
 -  PRESSURE TEMPERATURE SWITCH
 -  SELECTOR SWITCH
 -  ELECTRICAL CONNECTION
 -  AUXILIARY PROPELLANT TANK

Figure 4-103. Cont'd

F

helium is obtained from the combustion of LF_2 and LH_2 in the gas generator. The gas generator propellants are supplied by the main tank propellants, which are fed to the gas generator by the propellant tank head. While this gas generator feed system is relatively simple, there are several potential problems which should be investigated during development. The nature of a tank head feed system requires gas generator operation under varying propellant inlet conditions. The fuel and oxidizer inlet pressures increase, at different rates, as the main propellant tanks are repressurized, resulting in gas generator propellant flow rate and mixture ratio variations. Therefore, the resulting heat transfer to the helium changes as the tanks are being repressurized.

The absence of the inert He in the combustion chamber imposes a limitation on the combustion temperature, thus requiring a fuel-rich mixture. The nature of the combustion products may represent a problem area. Conceivably, the resultant thrust can be utilized for propellant settling during repressurization. Once the engine is operating, an engine-mounted heat exchanger is used to heat the He for propellant expulsion.

An alternate approach to configuration 3 is illustrated in configuration 4. In this system, the LH_2/LF_2 gas generator supplies the heat for both the repressurization and expulsion functions. By combining the heat source for these functions, the need for an engine-mounted heat exchanger is eliminated, as well as the additional complexity of switching between heat sources.

It may be postulated that if a gas generator can be operated on existing tank head, then the same function could be designed into the main combustion chamber for less weight penalty. This idea is presented in configuration 5. Pressurization of both propellant tanks during expulsion is accomplished by heating cold-stored He in the engine-mounted heat exchanger as described for configurations 1, 2, and 3. If the main thrust chamber is to assume the functions of the gas generator of configuration 4, it will be required to ignite at low tank pressures and sustain combustion under the same adverse inlet conditions described for the gas generator. During the period of reduced thrust operation, while repressurization is being performed, it is unlikely that sufficient heat would be available at the nozzle exit for heating the cold He. Both the heat-transfer problem and the problems associated with low-pressure operation could be overcome by employing a pre-chamber with its own propellant valves and injector. The pre-chamber would house the repressurization heat exchanger and would provide for low-level combustion. Propellant flow would be switched to the main injector upon reaching the required main engine operating pressure in the propellant tanks.

Although cold-stored heated He is a relatively efficient way to pressurize, the use of vaporized LH_2 results in a lighter system for fuel tank pressurization because of its low molecular weight. The following paragraphs concentrate on systems utilizing vaporized H_2 for pressurization of the fuel tank.

Pump-fed, regeneratively cooled engines offer a convenient source of high-pressure gaseous H_2 . The hot gas can be bled from the regenerative section, upstream of the injector, at varying temperatures, depending on the location of the port. Thus, separate pressurant storage tanks, gas generator, and heat exchanger are eliminated from the fuel pressurization system. Configuration 6 illustrates such a system. Engine bleed H_2 is used to pressurize the fuel tank during expulsion, while the oxidizer tank is pressurized with He, stored cold and heated in the nozzle heat exchanger. For repressurization, a gas generator, which operates on the main propellants (LH_2/LF_2), provides the energy required to heat the cold-stored He. As in configurations 3 and 4, the gas generator must operate fuel-rich to reduce combustion temperatures and must be capable of sustained combustion under the variable conditions experienced during repressurization.

The application of an energy source, suggested by Rocketdyne, which would circumvent these generator problems, is illustrated in configuration 7. This system (Tridyne) depends upon the stoichiometric combustion of gaseous H_2 and O_2 in a catalytic reactor. The two reactant gases are stored along with the He pressurant, in a single bottle. When released from the bottle, the gas mixture flows through the regulator and into the catalyst bed, where the H_2 and O_2 are reacted to form H_2O . The heat of reaction is absorbed by the He in the H_2/O_2 mixture. The reactor efflux ($H_2O + He$) is passed over a heat exchanger coil, which is conducting He stored in the LH_2 tank. The LH_2 stored cold helium is raised to the desired temperature for repressurization of the fuel tank and the Tridyne exhaust products are cooled for repressurizing the oxidizer tank. The water vapor in the reactor efflux may react with the LF_2 upon entering the oxidizer tank forming HF and O_2 . However, only a small amount of water vapor enters the LH_2 tank, and it is hoped that this should not pose problems. The HF and O_2 formed by the reaction may condense and freeze in the LF_2 environment resulting in basic problems during ca-g in-operation. Heated He rather than Tridyne is used to repressurize the LF_2 tank during thrusting to avoid possible clogging of the tank outlet. The system shown is pump-fed, thus engine bleed GH_2 is available for pressurization of the fuel tank during expulsion. The cold-stored He is heated in the nozzle heat exchanger for expulsion-pressurization of the oxidizer tank.

Pressure-fed engine systems cannot provide a source of high-pressure GH_2 for fuel tank pressurization. If gaseous H_2 is to be used, it becomes necessary to provide a LH_2 vaporization system. Configuration 8 describes such a concept. Since LH_2 at tank pressure cannot be vaporized to maintain its own pressure, an auxiliary tank is submerged in the LH_2 tank and is pressurized with cold He. The use of warm pressurant is precluded by the rapid pressure collapse, which would occur under the conditions. During expulsion the auxiliary LH_2 is passed through the nozzle heat exchanger where it is vaporized for fuel tank pressurization. Temperature control is maintained through a solenoid valve, coupled to a temperature sensor, which allows the required amount of liquid to bypass the heat exchanger.

Pressurization of the oxidizer tank is accomplished with cold-stored He, heated in a nozzle heat exchanger as described for prior configurations. The repressurizing medium for both main tanks is He, which is stored cold and heated in the gas generator/heat exchanger. The gas generator operates on the main tank propellants and is exhausted overboard.

It is conceivable that, under certain conditions, the weight of the auxiliary LH₂ system may be reduced through the use of a cylindrical tank, as shown in configuration 9. The mounting of spherical pressure bottles within propellant tanks results in increased system weight. In addition to the weight of mounting brackets, allowances must be made in bottle and tank thickness to withstand the additional stresses introduced by the mounting. If a cylindrical tank, fabricated from high-strength seamless tubing, were installed to take advantage of the existing dollar plates at the tank poles, a significant weight saving may be realized. The major factor, which may make this design highly competitive, is the ability to use warm gas to pressurize the cylindrical tank. If properly sized, the propellant level in the auxiliary tank would regress at about the same rate as the level in the main tank. Since the ullage of the auxiliary tank is now surrounded by a warm gas environment, there is no temperature gradient to cool the ullage gases as would be the case if the auxiliary tank was submerged in LH₂. It should be noted that these weight savings may be partially offset by the structurally inefficient nature of the cylindrical pressure vessel. Future tradeoff studies should be made to evaluate the merits of this approach. The expulsion-pressurization techniques employed in configuration 9 are similar to those of configuration 8 in that nozzle-heated H₂ and He are used to pressurize the fuel and oxidizer tanks, respectively. The auxiliary LH₂ tank, however, is now pressurized and repressurized with ambient He. Ambient He is also used to repressurize the main fuel and oxidizer tanks. With only minor system changes, heated He could be used to expel the auxiliary LH₂ for more efficiency.

Configuration 10 represents an advanced version of configuration 9, which incorporates heated gas repressurization. Cold-stored He is heated for both repressurization and expulsion-pressurization of the oxidizer tank and the auxiliary fuel tank. The main fuel tank is pressurized and repressurized with vaporized H₂ from the auxiliary LH₂ tank. In this design, the energy for all pressurant heating, during both expulsion and repressurization, is supplied by a LF₂/LH₂ gas generator operating fuel rich and exhausting overboard.

A design which could potentially improve the efficiency of the bipropellant gas generator approach is presented in configuration 11. Auxiliary propellant tanks, operating at a pressure higher than the maximum main tank pressure supply the fuel and oxidizer to the gas generator. The auxiliary tanks are required as the gas generator exhaust is to be used to pressurize and repressurize the main oxidizer tank and thereby must be available at a higher pressure. Use of the exhaust products in the oxidizer tank is made possible by stoichiometric combustion of the fuel and oxidizer and dilution with cold He. The He serves to reduce the operating temperature of the combustion chamber/heat exchanger, and subsequently provides the bulk of the low-density gas necessary for efficient pressurization. A portion of the

energy released is used to heat the cold-stored He passing through the heat exchanger. The heated He is used to repressurize and expel both of the auxiliary propellants and the main fuel supply. Initially, the repressurizing He will enter the auxiliary tanks cold because of the thermal lag in the heat exchange system, the bulk of the gas will be heated, however. Many potential weight saving techniques are incorporated into this design including: high-density pressurant storage, heated gas expulsion and repressurization, stoichiometric gas generator combustion and recovery of the exhaust products for use as a pressurant. This high degree of sophistication, however, is accompanied by a number of design difficulties. Sequencing, for example, becomes a problem with the closed circuit gas generator. It is unlikely that the system could be sized to provide simultaneous repressurization of both tanks. Since the gas generator must be shut down upon reaching operation pressure in the oxidizer tank, any remaining pressurization must be accomplished, inefficiently, with cold He. It is possible that the time lag can be predetermined and the He outlet temperature adjusted to provide the desired ultimate ullage gas temperature. A similar problem exists during expulsion. The use of pressure switch/solenoid valve pressure control is considered to be more reliable than a pressure regulator, particularly in a F₂ environment. The pulsing nature of this system could establish undesirable pressure oscillations in the gas generator. However, the problem can be alleviated by providing continuous flow through an orifice at a rate somewhat less than that required to maintain tank pressure. The amount of flow now controlled by the solenoid valve would be just adequate to maintain the tank pressure within an established band, but not sufficient to induce severe pressure oscillations in the gas generator. Another problem which may have to be solved is the possibility of mixture ratio variation from stoichiometric during the transient repressurization period. Should the system analysis indicate a significant weight saving, further investigation of these areas will be necessary.

Configuration 11a is adapted to a pump-fed system. Since engine-bleed H₂ is available, it is used to pressurize both main and auxiliary fuel tanks during expulsion. In all other respects, including the design problems, the system is identical to configuration 11.

It should be noted that, of the 12 systems, 6, 7, and 11a apply to systems using pump-fed engines. The remaining nine apply to all pressure-fed systems.

The system weight for the candidate systems were computed, using the techniques as outlined in the following paragraphs.

(1) Pressurant Requirements For Expulsion. Calculation of the pressurant required for propellant expulsion was based on the following equation for a constant tank inlet temperature:

$$W_{gu} = \frac{P_T W_P (CF)}{p_p RT} \quad (4-105)$$

where

W_{gu} = usable pressurant weight (lb.)

P_T = operating tank pressure (p. s. i. a.)

W_p = propellant expelled (lb.)

ρ_p = propellant density (lb. p. ft. ³)

R = pressurant gas constant (ft. p. °R.)

T = tank inlet gas temperature (°R.)

CF = correction factor

With the exception of the correction factor, each term is self-explanatory. The correction factor is defined as the ratio of gas weight accounting for energy exchange between the tank walls and propellant during expulsion to gas weight neglecting any energy exchange. For the initial system comparison, a tank pressure of 250 p. s. i. a. and an inlet temperature of 520°R. was selected for both tanks in the pressure-fed systems. The pump-fed system comparison was based on a tank pressure of 25 p. s. i. a. and 35 p. s. i. a. for the LH₂ and LF₂ tanks. A 520°R. gas inlet temperature was used for both tanks.

Certain systems used gas, which was stored in high-pressure containers. The initial storage pressure was taken as 3,000 p. s. i. a. and the gas in the container was allowed to expand to 300 p. s. i. a. by the end of propellant expulsion. The following equation was used to calculate the total gas weight required including the residual gas remaining in the containers.

$$W_{gBi} = \frac{W_{gu}}{\left[1 - \left(\frac{Z_i}{Z_f} \right) \left(\frac{P_f}{P_i} \right)^{1/\gamma} \right]_B} \quad (4-106)$$

where

W_{gBi} = total initial gas weight in the container (lb.)

Z_i = initial gas compressibility factor

Z_f = final gas compressibility factor

P_i = initial gas storage pressure (p. s. i. a.)

P_f = final gas storage pressure (p. s. i. a.)

γ = ratio of gas specific heats

B = storage bottle condition

A summary of the gas requirements for propellant expulsion is shown in table 4-39 for the 12 systems considered. The expulsion gas weights are based on complete expulsion of the propellant tanks. Analysis has shown that the expulsion gas required is relatively independent of the number of intermediate engine firings, provided that the tank pressure at the beginning of each firing is the same. That is, the same amount of gas is needed to expel 100 pct. of the propellant in one engine firing or 10 engine firings. Consequently, the weight for that portion of the pressurant supply system used for propellant expulsion is independent of duty cycle.

(2) Repressurization Gas Requirements. The repressurization systems shown for the 12 candidate systems consisted of either adiabatic blowdown or constant inlet gas temperature systems. The pressurant requirements for these two basic approaches were based on the following equations.

(a) Constant Gas Inlet Temperature.

$$W_{gu} = \frac{(P_{T_f} - P_{T_i}) V_u}{R T \gamma} \quad (4-107)$$

(b) Adiabatic Blowdown.

$$W_{gu} = \frac{(P_{T_f} - P_{T_i}) V_u \left[1 - \left(\frac{Z_i}{Z_f} \right) \left(\frac{P_f}{P_i} \right) \right]_B^{1/\gamma}}{R T_{B_i} \left[1 - \left(\frac{Z_i}{Z_f} \right) \left(\frac{P_f}{P_i} \right) \right]_B} \quad (4-108)$$

where

W_{gu} = usable pressurant weight (lb.).

DT_i = initial tank pressure (p. s. i. a.).

DT_f = final tank pressure (p. s. i. a.).

V_u = ullage volume (ft. ³).

R = gas constant (°R. p. ft.).

T_{B_i} = initial bottle temperature (°R.).

Table 4-39

PRESSURIZATION SYSTEM WEIGHT SUMMARY

Configuration	VAP Repressurization Ft.-Lb. x 10 ⁻⁶		WG _{Expulsion}			WG _{Repressurization}			W _{Bottle}			ΔW _P (gas generator)	Fixed Weight Hardware	Weight Total
	He	H ₂	HF/He	He	H ₂	He	He/X	He	He/X	GH ₂	Weight AT			
1	1.5 9 30	134		8.4 50.4 168				203 623 1,799						380 842 2,135
2	1.5 9 30	134		7 42 140		2.6 0.26 15.4 1.5 51.3 5.1		125 157 244	18 106 354	0.3 2 5.5			59.4	347 517 994
3	1.5 9 30	134		10.5 63 210				129 175 306				2.6 16 53	56.7	333 445 760
4	1.5 9 30	134		10.5 63 210				129 175 306				36 50 86	57.5	367 480 794
5	1.5 9 30	134		10.5 63 210				129 175 306				2.6 16 53	45	322 433 748
6	1.5 9 30	7.2	1.8	10.5 63 210				16 62.3 163				2.6 16 53	47.4	86 238 513
7	1.5 9 30	7.2	1.8	42 140		2.3 13.9 46.4		12.6 43.8 131	23 138 460				45.5	82 275 815
8	1.5 9 30	74.3	18	10.5 63 210				129 175 306				2.6 16 53	63.2	314 426 742
9	1.5 9 30	51.5	18	8.4 50.4 168				44.5 519 1,695	99 519 1,695	24			50.7	295 758 2,052
10	1.5 9 30	51.9	18	3.7 23 75	1.6 10.7 35.6			49.5 66.6 113				18 26 45	64.8	234 300 475
11	1.5 9 30	85		7 42 140		4.4 1.0 25.5 1.1 85 3.7		141 190 330					67.2	373 478 781
11a	1.5 9 30		1.8	7 42 140		4.4 0.19 25.5 1.1 85 3.7		18.2 68 208					64.4	126 214 418

γ = ratio of specific heats.

Z_i = initial gas compressibility factor.

Z_f = final gas compressibility factor.

P_i = initial bottle storage pressure (p. s. i. a.).

P_f = final bottle storage pressure (p. s. i. a.).

B = storage bottle conditions.

Equations 4-107 and 4-108 are based on no energy exchange between the incoming gas and tank walls and propellant. Because short repressurization times are anticipated, this assumption should provide realistic gas requirements. (Subsequent analysis using the H225 program have shown this to be the case). It should be noted that equation (4-108) has been slightly simplified from the equation which is used in the H109 optimization computer program. This was done to simplify hand calculations for the preliminary pressurization screening study. The total gas weight for repressurization systems using gas stored in high-pressure vessels is calculated using equation (4-106).

Equations 4-107 and 4-108 show that the repressurant gas weight, hence system weight, is proportional to the product $(P_{T_f} - P_{T_i}) V_u$. Therefore, the total system weight for a multistart mission requiring tank repressurization prior to each start is a function of the sum of $(P_{T_f} - P_{T_i}) V_u$ required for each tank prior to each burn. To solve for the system weight requires an analysis of the pressure history in each tank for all of the mission duty cycles. This analysis is included in the H109 computer program. However, the intent of this preliminary screening was to select one or two systems which will be analyzed in more detail using the H109 computer program in later computations. Therefore, to facilitate hand computation, the product of $(P_{T_f} - P_{T_i}) V_u$ was selected as the independent variable for system comparison. The system weight can be shown independent of an actual mission duty cycle. The sum of the product can be shown to be $(P_{T_f} - P_{T_i}) V_u$ which includes both the fuel tank and oxidizer tank. The repressurization gas requirements should be investigated separately for each tank. Again, because of the complex nature of the analysis, a simplifying assumption was made. The product of $(P_{T_f} - P_{T_i}) V_u$ for the oxidizer tank was arbitrarily selected as one-half the same product for the fuel tank for any repressurization cycle. The actual values for each tank will be determined as part of the subsequent pressurization system optimization study using the H109 computer program.

(3) Hardware Weights. The major hardware items include, where applicable, the heat exchangers, auxiliary gas generator, auxiliary propellant tank(s), pressurant containers, and control components. Parametric

weights which were used for these items are shown in figures 4-104 through 4-109. Weights for thrust chamber and gas generator heat exchangers are shown in figure 4-104 and 4-105. The thrust chamber heat exchanger weights are based on data obtained from engine manufacturers. The gas generator heat exchanger weights of figure 4-105 are based on extrapolated data from the Rocketdyne/Douglas MANSAT study (AF04(611)-10745).

Spherical and cylindrical auxiliary tank weights are shown in figure 4-106. These weights are based on using 6061-T6 aluminum, with a safety factor of 2.2 on the ultimate tensile strength. A minimum gauge of 0.02 in. was assumed. The assumed operating pressure of the auxiliary tank was 300 p. s. i. a. for the pressure-fed engine system and 100 p. s. i. a. for the pump-fed engine system.

The curves in figure 4-106, show that a spherical tank is lighter than the cylindrical auxiliary tank. However, a cylindrical tank offers the advantage of being able to use hot gas for auxiliary tank pressurization because the surface level of the propellant in the auxiliary tank would regress at about the same rate as the main propellant. There is essentially no temperature gradient between the hot ullage gases in the main and auxiliary tanks. On the other hand, the spherical tank should be buried within the main propellant tank to prevent heating of the auxiliary propellants by the hot ullage gases during engine operation. Consequently, cold gas would be required to pressurize the spherical auxiliary tank during operation to prevent excessive local heating of the main propellant. From a total system viewpoint, the auxiliary tank weight, plus pressurant weight, may indicate that a cylindrical tank would result in the lighter overall system weights. In addition, installation considerations may favor the use of a cylindrical tank. Unfortunately, there was not sufficient time to evaluate these details.

The gas generator weights of figure 4-107 are based on data obtained from engine manufacturers. Pending a more complete analysis, a gas generator propellant flow-rate of 0.5 lb. /sec. was used for open-loop operation (overboard dump); a propellant flowrate of 0.75 lb. p. sec. was used for closed-loop operation (LF₂ tank dump). For the open-loop system, the gas generator operating mixture ratio used was 1.2 (F₂/H₂) resulting in a combustion temperature of approximately 1,950°R. The propellant weight penalty for gas generator operation was based on the gas generator delivering an I_{sp} equal to one-half of the main-engine system. (Note: If the gas generator delivered the same I_{sp} as the main engine, there would be essentially no weight penalty attributed to the additional gas generator propellants - provided that the vehicle was properly oriented during all gas generator sequences). The stoichiometric F₂/H₂ mixture ratio was used for closed-loop gas generator operation to preclude any H₂ from entering the LF₂ tank. He was used as a diluent to reduce the inlet gas temperature to the LF₂ tank to 520°R.

Component weights were based on an arbitrary nominal line size of 3/8 in. These weights were taken from figure 4-108. Line lengths were approximated for each system and corresponding weights were calculated based on aluminum line weighing 0.03 lb. p. ft. These are summarized

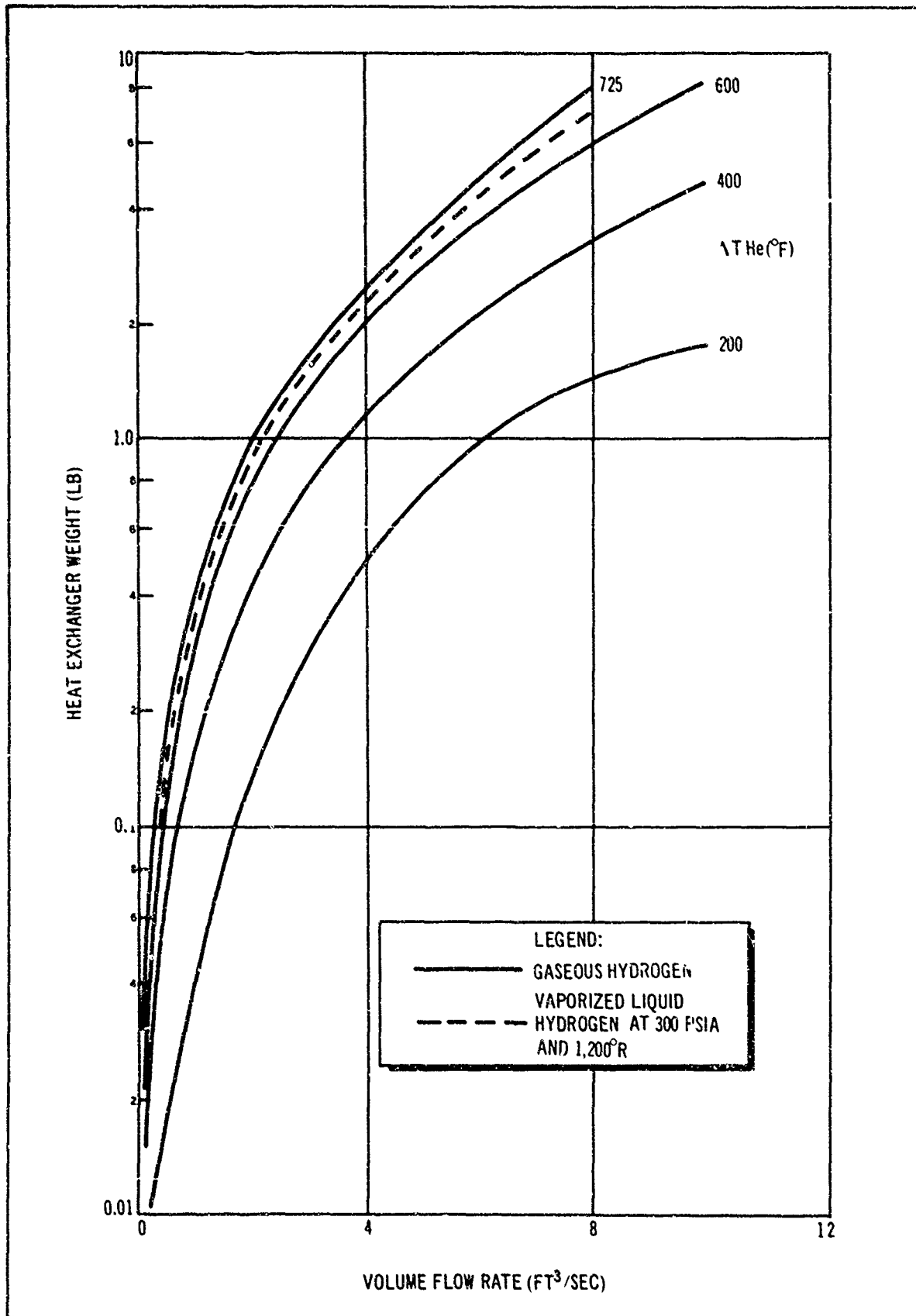


Figure 4-104. Thrust-Chamber Heat Exchanger Weight as a Function of Volume Flow Rate

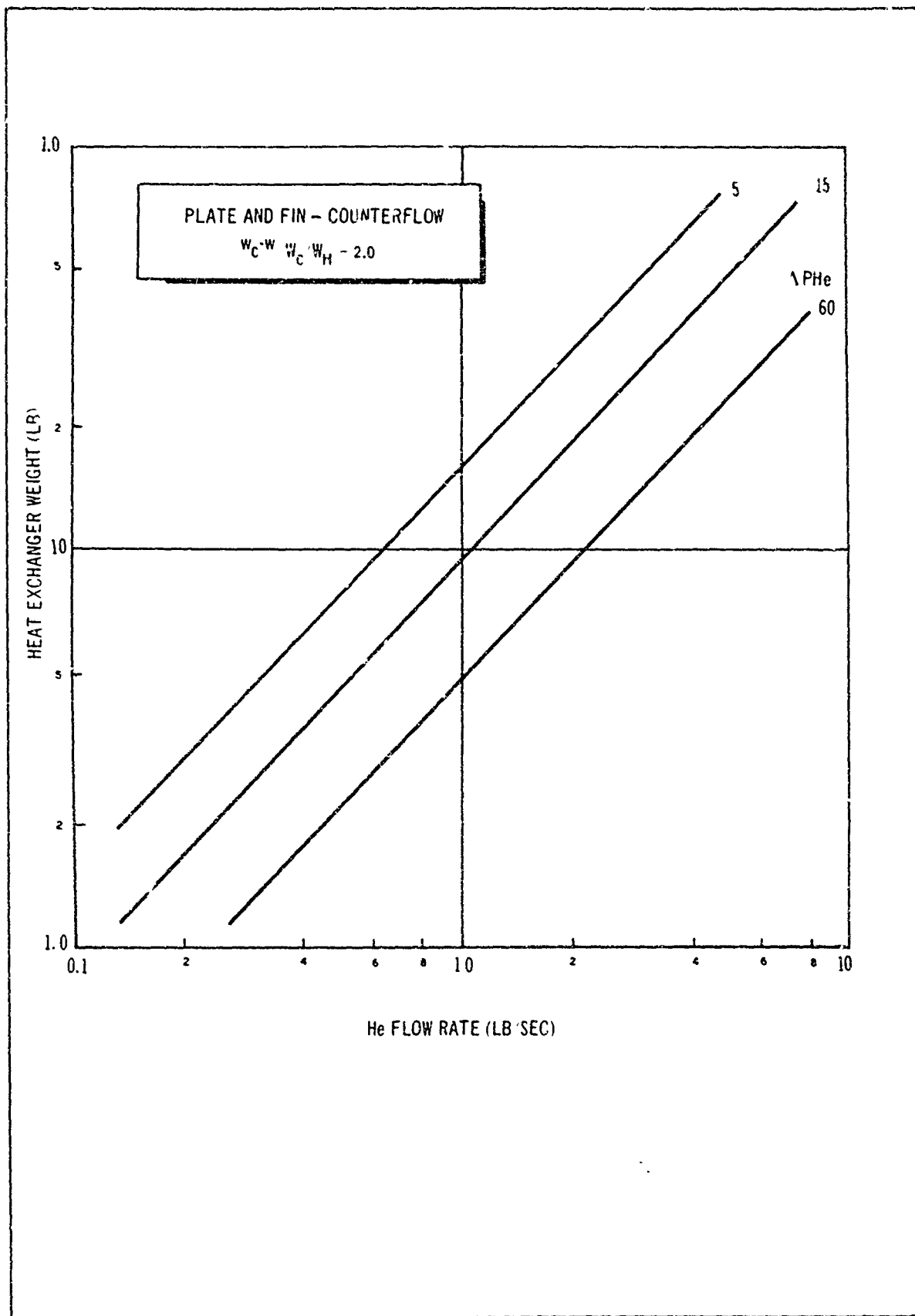


Figure 4-105. Heat Exchanger Weight as a Function of He Flow Rate

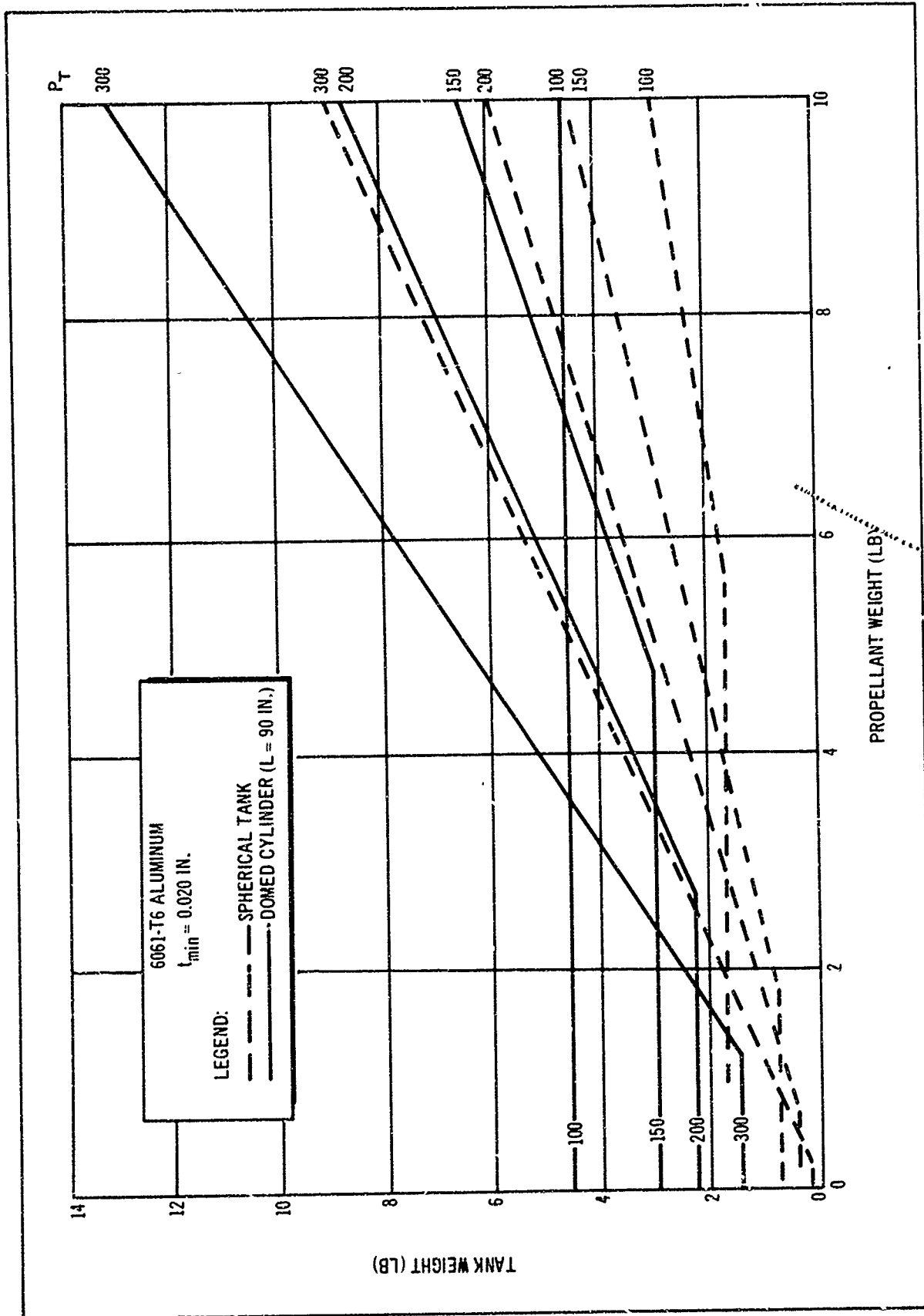


Figure 4-106. Auxiliary LH₂ Tank Weight

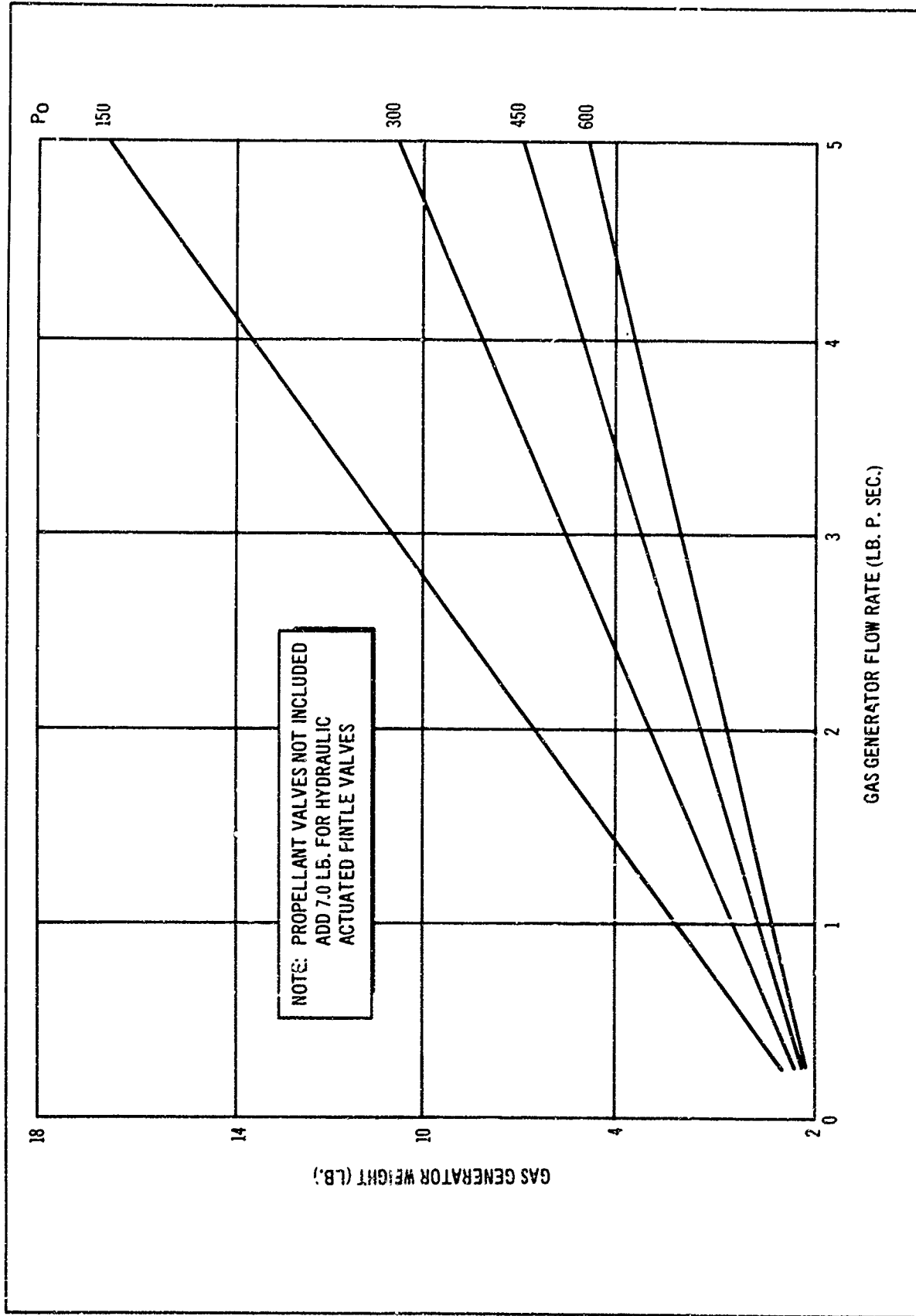


Figure 4-107. L₂/LH₂ Gas Generator Weight (Fuel - Rich)

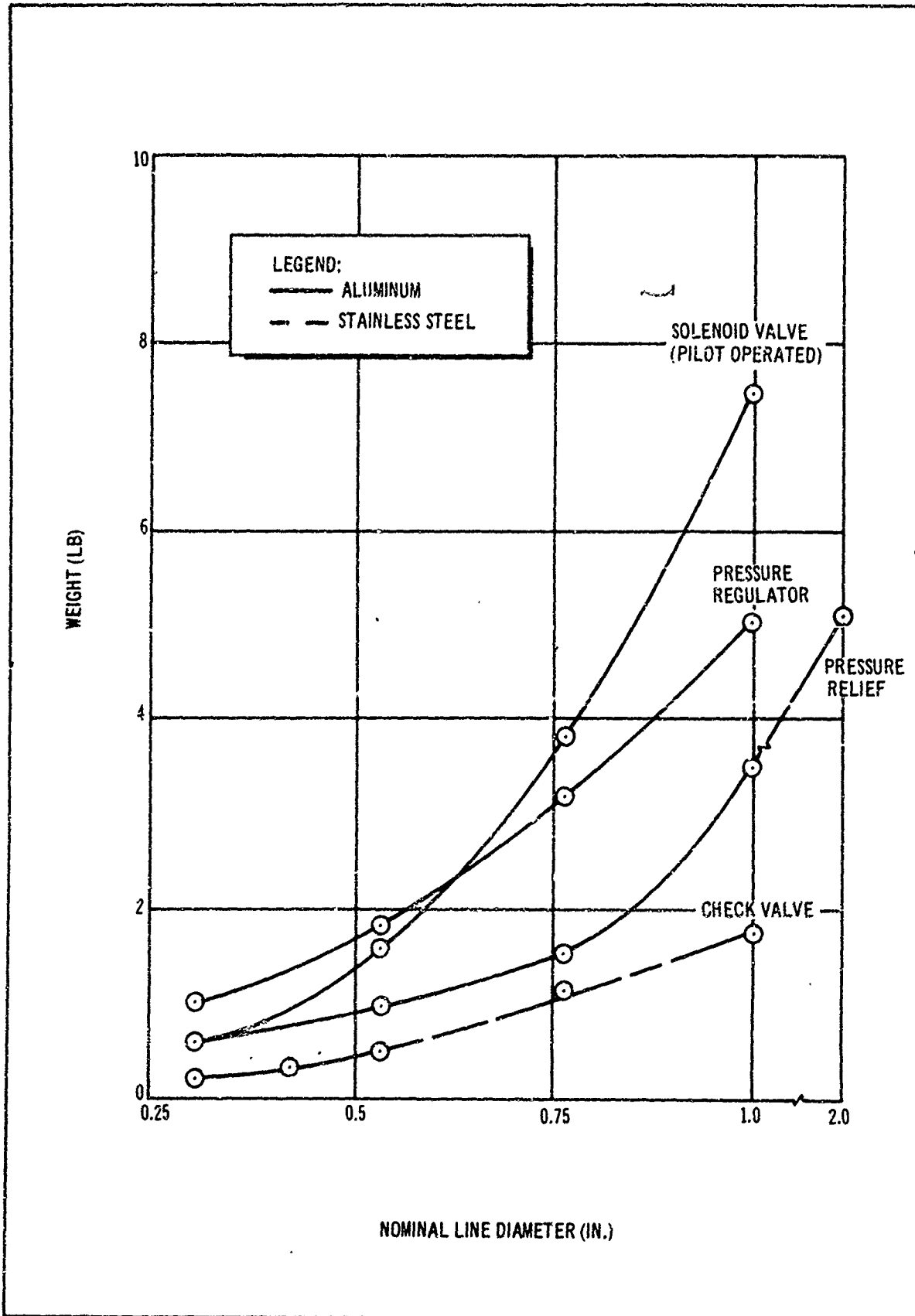


Figure 4-108. Pressure Control Component Weights

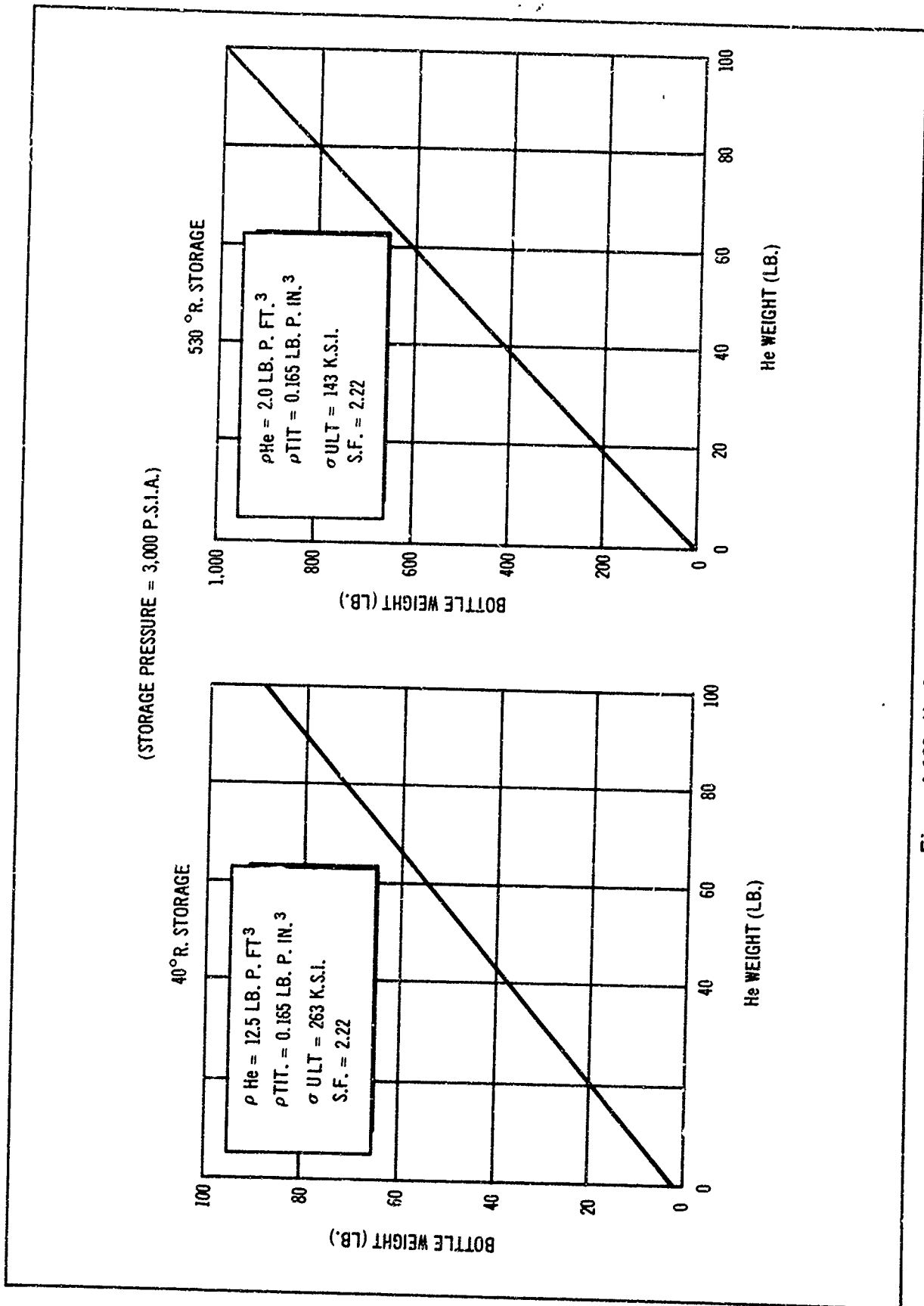


Figure 4-109 He Storage Bottle Weight

for each system in table 4-40. Pressurant storage bottle weight, which is a function of required gas weight, is shown in figure 4-109. This assumes 3,000 p. s. i. a. spherical titanium bottles with a safety factor of 2.22.

(4) Weight Comparison. The final results of this evaluation are shown in figures 4-110 and 4-111 for the pressure-fed and pump-fed engine systems. The purpose of this study was to perform a preliminary screening of the 12 candidate systems and establish a weight spectrum. Total pressurization system weight for both propellant expulsion and tank repressurization was used as the basis for system comparison. Included in the total system weight are the pressurant, pressurant container, auxiliary propellant tank, control components, auxiliary combustion devices, heat exchanger, and lines.

By noting the results for the pressure-fed system shown in figure 4-110, it can be seen that the system of configuration 9 results in the lowest overall pressurization weight. Configuration 9 uses ambiently stored He for adiabatic repressurization of both the LH₂ and LF₂ tanks. As expected, however, the ambient repressurization system weight increases rapidly as the repressurization requirements increase. A more favorable system for many duty cycles, requiring increased repressurization, is found in configuration 10. Since the most difficult duty cycle would be used to select size and design, the pressurization system, system 10, was selected for detailed study for the pressure-fed cases.

Reference to figure 4-111 indicates that the choice between configurations 6 and 7 is not governed by system weight consideration, because they are relatively close. From an ease of development viewpoint, the system shown in configuration 6 appears to be the most desirable. The only item requiring development is the F₂/H₂ gas generator/heat exchanger system. Such a device is under development by Douglas in an IRAD program. Because of the open-loop operation of the gas generator where combustion products are dumped overboard, the system control is similar to that used on current vehicles (such as Saturn S-IV and S-IVB), and does not need further development. Figure 4-112 shows the F₂/H₂ gas generator hardware being developed under the Douglas IRAD program. The generator part of this system has been successfully demonstrated. The system shown in configuration 7 has several items requiring feasibility demonstration and development. The catalytic reactor system would require extensive development. Also, temperature control of the combustion products entering the LF₂ tank is complicated because the combustion products are also used to heat He for LH₂ tank repressurization. Any change in He flow to the LH₂ tank would affect the temperature of the combustion gases entering the LF₂ tank. Another area requiring investigation is the effects of small amounts of water vapor entering the LF₂ tank. Because of these system development problems, configuration 7 is dropped from further consideration. For large repressurization requirements, configuration 11a results in substantial weight savings. However, because of the lower tank pressures required for pump-fed engine operation, high values of ΔP , at which the cross-over occurs, are not anticipated. Therefore, configuration 6 will be used for the pump-fed pressurization system optimization study.

Table 4-40
FIXED WEIGHT SUMMARY

Item	Size	Unit Weight	1		2		3		4		5		6*		7*		8		9		10		11		11a*	
			Num-ber	Weight																						
Solenoid valve	3/8	1.3	5	6.5	6	7.8	4	5.2	6	7.8	6	7.8	6	7.8	5	6.5	7	9.1	13	17	9	12	11	14	13	17
Squib valve	3/8	0.5	2	1.0	3	1.5	1	0.5	1	0.5	1	0.5	1	0.5	2	1.0	1	0.5	2	1.0	1	0.5	1	0.5	1	0.5
Press relief valve	3/8 & 3/8	8.7	3	14.8	3	14.8	3	14.8	3	14.8	3	14.8	1	14.8	3	14.8	3	14.8	3	14.8	3	14.8	3	14.8	3	14.8
Check valve	3/8	0.3	3	0.9	3	0.9	4	1.2	2	0.6	4	1.2	3	0.9	4	1.2	1	0.3	3	0.9	1	0.9	4	1.2	5	1.5
Pressure regulator	3/8	1.3	1	1.3	3	3.9	1	1.3	1	1.3	1	1.3	1	1.3	2	2.6	2	2.6	1	1.3	1	1.3	1	1.3	1	1.3
Quick disconnect	3/8	0.5	2	1.0	3	1.5	1	0.5	1	0.5	1	0.5	1	0.5	2	1.0	1	0.5	4	2.0	3	1.5	5	2.5	5	2.5
Burst diaphragm	3/8	0.5	1	0.5	1	0.5	1	0.5	1	0.5	1	0.5	1	0.5	2	1.0	1	0.5	1	0.5	1	0.5	1	0.5	1	0.5
Press filter	3/8	0.8	2	1.6	3	2.4	1	0.8	1	0.8	1	0.8	1	0.8	2	1.6	1	0.8	2	1.6	1	0.8	1	0.8	2	1.6
Orifice		0.5	1	0.5	2	1.0	2	1.0	1	0.5	2	1.0	2	1.0	2	1.0	3	1.5	2	1.0	2	1.0	2	1.0	2	1.0
Diffuser		1.0	2	2.0	2	2.0	2	2.0	2	2.0	2	2.0	2	2.0	2	2.0	2	2.0	3	3.0	3	3.0	4	4.0	4	4.0
Pressure and temperature switch		1.0	3	3.0	3	3.0	3	3.0	3	3.0	3	3.0	3	3.0	2	2.0	4	4.0	5	5.0	5	5.0	5	5.0	5	5.0
Lines (Aluminum)	3/8	0.03 $\frac{lb}{ft}$	45'	1.3	95'	2.8	50'	1.5	40'	1.2	45'	1.3	65'	2.0	50'	1.5	65'	2.0	65'	2.0	60'	1.8	80'	2.4	90'	2.7
Gas Generator (open air)	0.5 $\frac{lb}{sec}$						1	10.0	1	10.0	1	7.0	1	10.0			1	10.0			1	9.7				
Gas Generator (closed)	0.5 $\frac{lb}{sec}$						1	3.1							1	5.0							1	10.0	1	10.0
Heat Exchanger (gas generator)	1.0 $\frac{lb}{sec}$	9.2													1	4.0					2	12.0	1	9.2	1	2.0
Heat Exchanger (gas generator)	1.5 $\frac{lb}{sec}$	1.4																								
Heat Exchanger (Eng)	0.2 $\frac{lb}{sec}$	0.3	1	0.3	1	0.3	1	0.3	1	0.3	1	0.3	1	0.3	1	0.3	2	0.6	2	0.6						
Total				34.7		59.4		56.0		57.5		45.0		47.4		45.5		63.2		50.7		64.8		67.2		64.4

* Pump fed

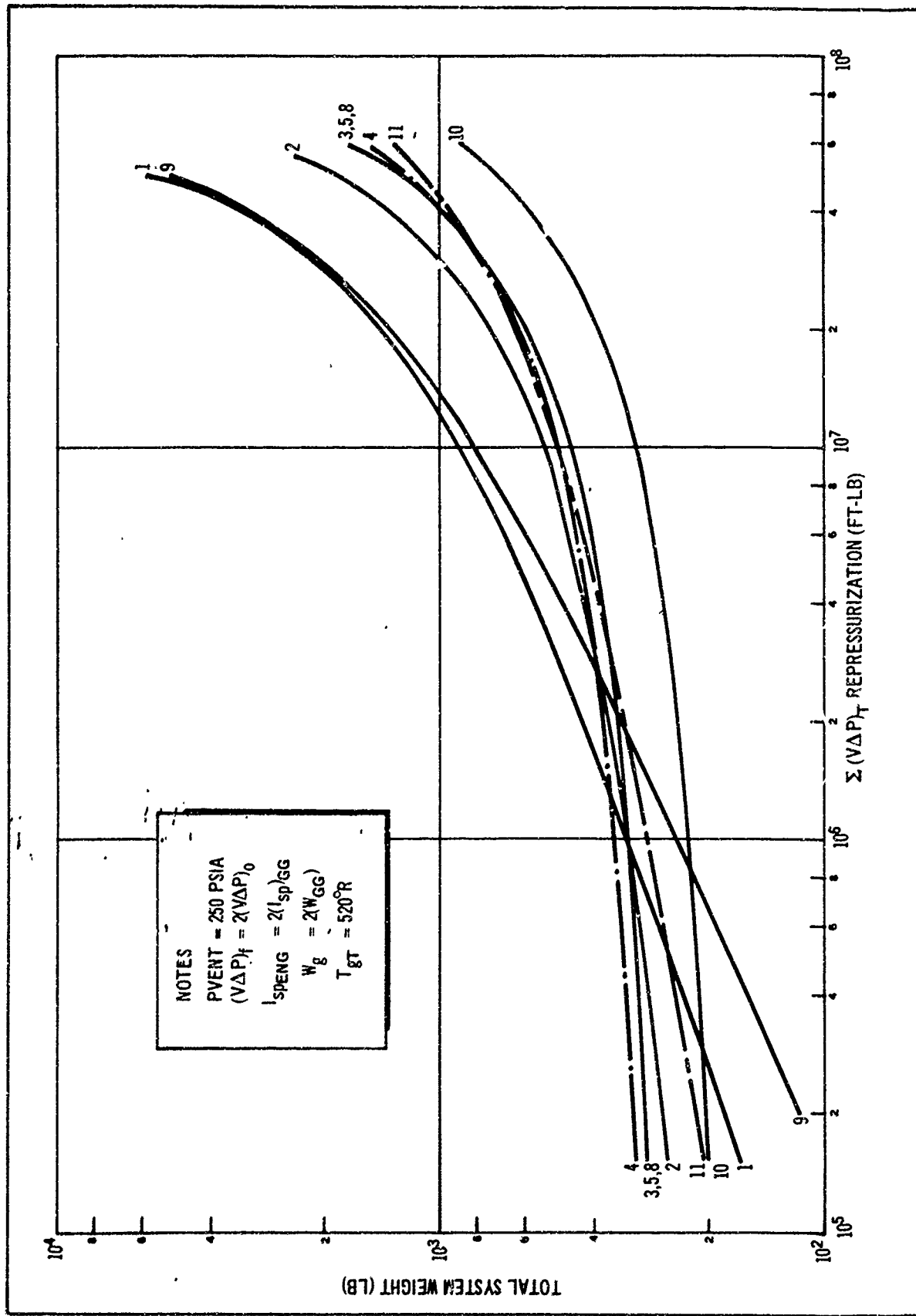


Figure 4-110. Pressurization System Weight as a Function of Summation of Repressurization $(V\Delta P)_T$ for Pressure-Fed Systems

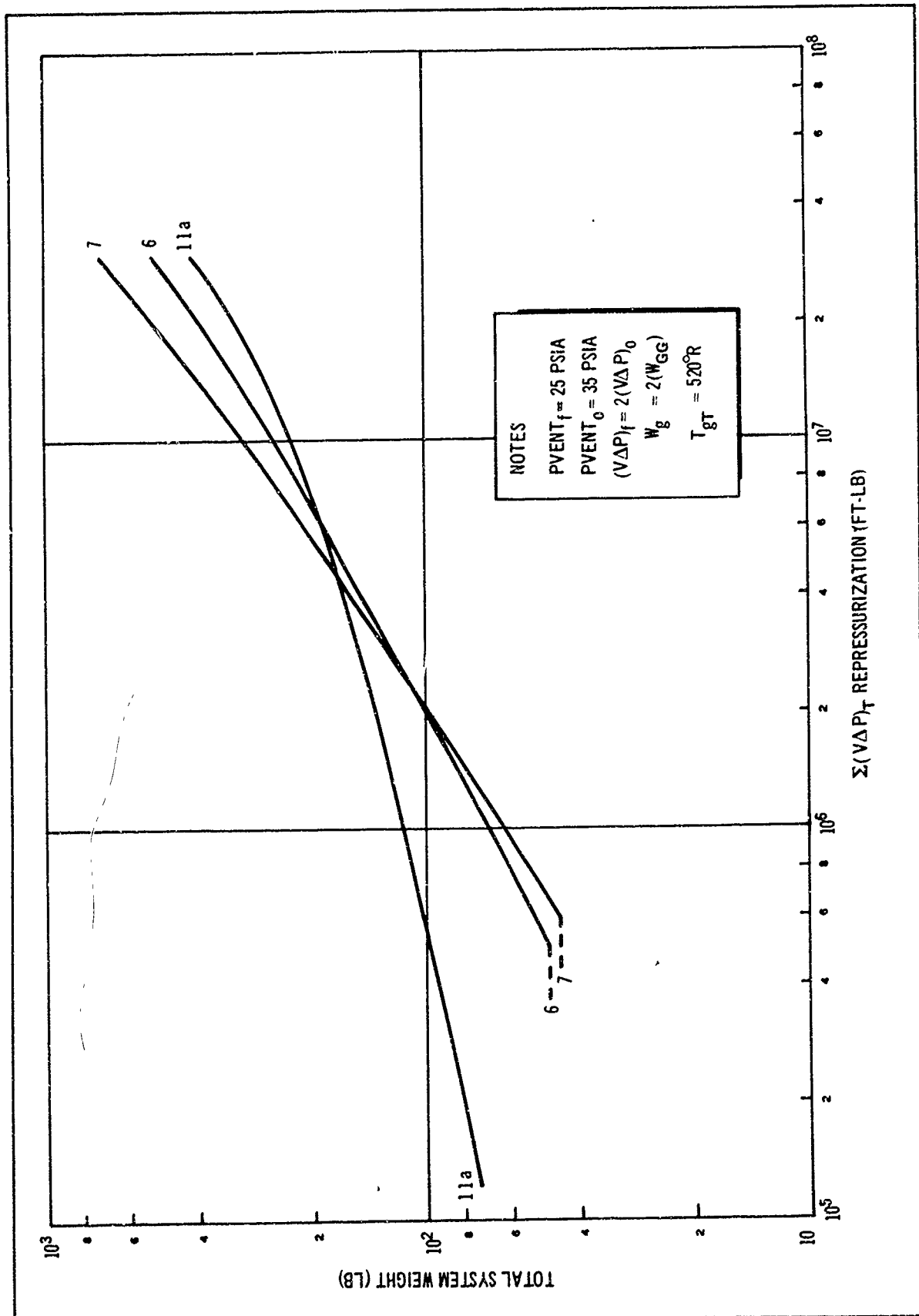


Figure 4-11.1. Pressurization System Weight as a Function of Summation of Repressurization $(V\Delta P)_T$ for Pump-Fed System

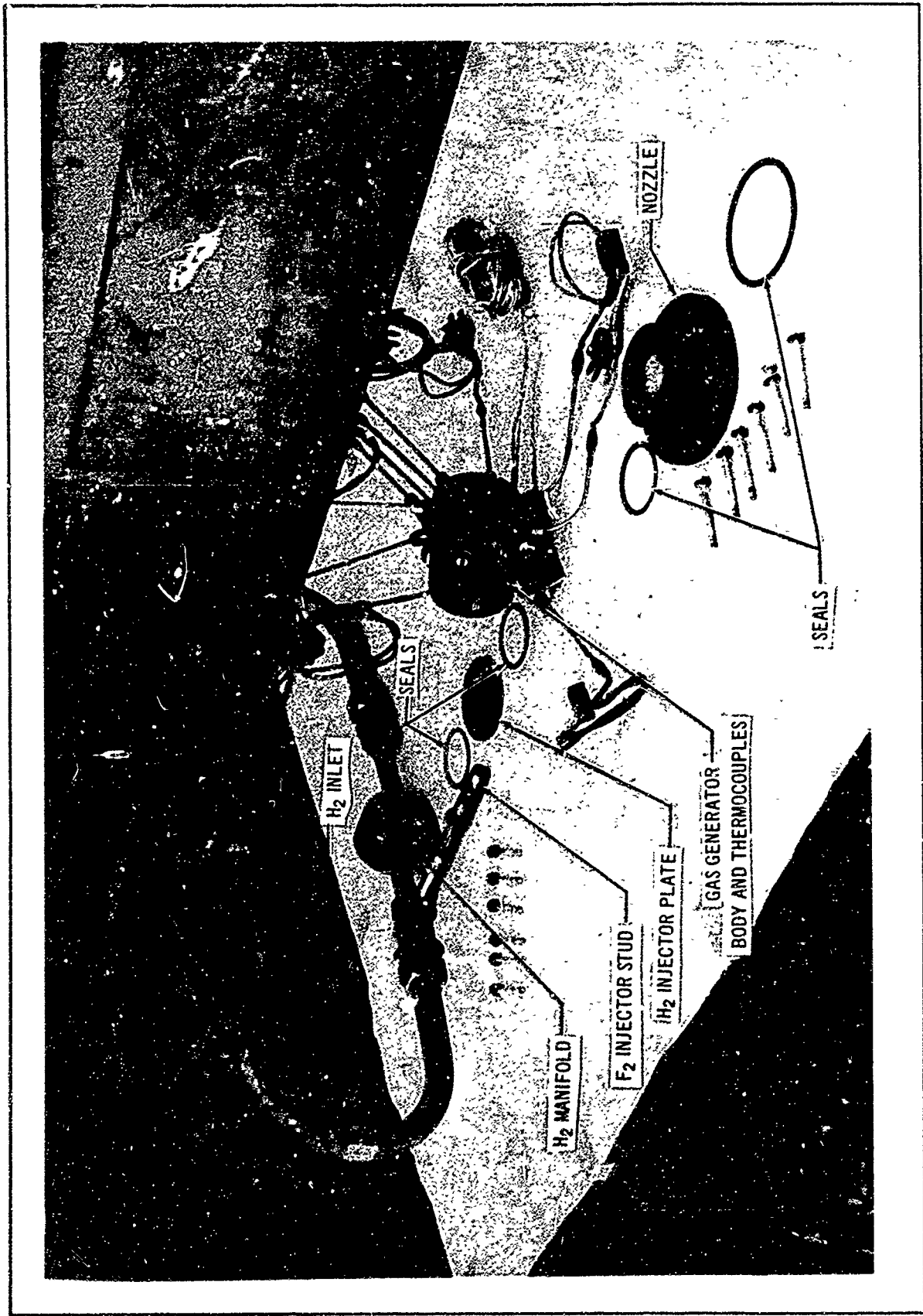


Figure 4-112. F₂/H₂ Gas Generator Hardware

b. Pressurant Requirement Analysis. As discussed previously, the total pressurant requirements for multiburn missions can be considerably higher than in the case of conventional single burn systems. Also the propellant heat input, contributed by the pressurant, can be significant relative to the total propellant heat input for highly insulated propellant tankage. Because of this importance, a careful, accurate pressurant gas analysis is mandatory. To accomplish this, a computerized pressurant gas analysis was developed as part of this program which would account for such factors as heat transfer to tank walls from the ullage gas, and heat and mass transfer across the liquid gas interface with independent variables such as inlet gas temperature, initial tank contents, expulsion rate and inlet gas composition.

Prior to describing the details of this analysis, it is appropriate to review the overall propellant tank fluid dynamic history for the missions of interest, because these define the initial conditions for pressurization.

(1) Propellant Thermodynamic History. Heat transfer to the stored liquid propellant, and the resulting temperature distributions and tank pressure variations, occur under many different operating modes. These would include the following:

- Ground-hold at 1-g. and a quiescent fluid state.
- Boost at g levels from 1 to 5 and some degree of fluid motion relative to the tank.
- Orbit at approximately 1×10^{-6} g.
- Powered operation at approximately 1-g. with some degree of fluid motion relative to the tank.

Modes 3 and 4 occur alternately with restarting of the stage. During the ground-hold period as well as boost, the propellant is held at the bottom of the tank and heat flow into the liquid is primarily controlled by free convection. The free convection results in propellant temperature stratification. That is, the heat is deposited at the top of the tank and a temperature gradient is established. Sloshing also will be present during boost. For example, in the Saturn S-IV, waves of 3 in. in height are experienced during boost (reference 6). As the stage goes into orbit and booster power is terminated, the transition from very high to very low-g. disperses liquid around the spherical tank wall. The factors responsible for this are (1) an order of magnitude increase in slosh wave height; (2) a structural spring back of the tank, and (3) the normal tendency of wetting fluids, such as LH₂ and LF₂, to climb container walls. These transient actions also mix the fluid, thereby destroying the temperature gradients established during high-g. flight. Tank pressure will also drop to some low equilibrium value. Once in 0-g., the propellants maintain the wall distributed minimum energy configuration, unless some type of settling device is employed.

At this point, the detailed understanding of the fluiddynamic and heat-transfer processes occurring in stored cryogenic fluids in a low-g. environment is not as fully developed as would be desired to accurately design

flight vehicle propellant storage and feed systems. Difficulties in simulating low-g. operation to facilitate appropriate research is primarily responsible for this technological deficiency. The most complete work carried out in this area has been by NASA-LeRC, involving suborbital experiments using a small (9 in.) radiant-heated sphere containing LH₂. Four flights have been run, which have been documented in references 31 through 36. The conclusion reached from these tests can be summarized as follows:

- LH₂ wets the spherical tank wall, when going into nearly zero-g.
- Nucleate boiling and localized wall drying occurs.
- Temperature stratification results.
- The tank pressure rise is slightly greater than that predicted by a homogeneous heating model, although it is below that corresponding to an all-vaporization or all-gas phase heating model, and always less than that corresponding to a 1-g. quiescent heating model.
- Temperature distributions are not easily destroyed by system oscillations.
- Vapor flashing and pressure increases occur when liquid is sloshed back over dry walls.

The lowest heat flux established in these low-g. tests was about 23 B. t. u. p. ft. ²-hr., which is nearly two orders of magnitude greater than that anticipated for a tank using a high-performance insulation system. The general consensus of Douglas engineers agree that for the low anticipated heat leak it would be appropriate to employ a homogeneous heating model to predict temperature and pressure rises during orbit. To bracket the problem, it would also be desirable to spot check results, using a 1-g. quiescent heating model for possible effects on the overall results. The homogeneous heating model is an integral part of the Douglas H109 propulsion system sizing computer program, which is the basic tool to be employed for the optimization stage of this study. A 1-g. quiescent model is being formulated under a Douglas IRAD program.

At, or just before engine startup, the propellants are settled. This causes limited mixing so that most of the temperature gradients are eliminated. Behavior during powered-stage operation is similar to that experienced during boost, and stratification will take place. However, outflow from the tank takes place. Computations have been run to assess the degree of stratification, assuming a single 200 sec. burn at 1-g. and 1 B. t. u. p. ft. ²-hr. heat input, that would empty the tank. These involved a boundary-layer analysis and indicated a LH₂ temperature rise at the surface of 0.2°R. just before propellant depletion. This should have a negligible effect on the overall system behavior. Therefore, on the basis of these calculations, radiant heating and stratification during tank outflow will be neglected in the study.

Following the first burn, propellant will once again be distributed around the tank wall. However, the tank wall will be heated during expulsion by the warm pressurizing gases and this stored heat must be absorbed by the propellant as it flows back over the walls. The quantity of heat stored in the wall is determined by the developed pressurant gas analysis program.

An unresolved point is how this heat is distributed in the propellant (direct vaporization, bulk heating or a combination). The most conservative approach would be to assume that all this heat went into flashing off propellant. After zero-g. stabilization, a new equilibrium is established and the process is repeated.

Equations in the Douglas program for propulsion system optimization predict pressure histories for multiburn duty cycles, including the tank pressure collapse after engine shutdown, as well as the pressure buildup during orbit coast (assuming the uniform mixed heating model). Program equations also predict pressurant requirements based on a simple model, assuming no heat transfer. An improved model for predicting the pressurant requirements to augment the H109 capabilities is required.

(2) Analytical Model Development. The required model and computational procedure must be general enough to handle the wide range of conditions to be encountered, and be rapid enough to permit many repetitive calculations to be performed in parametric surveys and system optimization.

While significant work has been done in this field, no existing analysis fully met the needs of this study. The most promising area for improvement is in the numerical solution of the system of equation. The computer program must provide an efficient balance between computational speed and accuracy. The nature of the study objectives permits some simplifications in the analysis, but the developed technique is still general.

To predict pressurant requirements for propellant tanks during pressurization and expulsion requires primarily an analysis of the heat and mass transfer processes occurring within the tank. These phenomena can be complex, and an exact mathematical description is extremely difficult to achieve. A simplified mathematical model must be used to ensure that the resulting equations can be solved practically. Attempts to obtain a closed-form solution require such highly simplified models that actual cases cannot be simulated accurately. More realistic models produce equations of such complexity that numerical solutions are required. Recent work has progressed to the point where non-viscous, one-dimensional models are being treated, which permit fluid properties and the initial and boundary conditions to be varied arbitrarily. The solution to the system of partial differential equations is approximated numerically by a digital computer program.

The current technology in ullage gas analysis is characterized by several basic assumptions. One such assumption is that all fluid flow is non-viscous, ignoring both kinetic energy and momentum, and the ullage pressure does not vary spatially. The most important simplification is the

elimination of radial and circumferential variation, making the system one-dimensional. The resulting partial differential equations are in two independent variables, time and axial distance. Heat transferred at the fluid boundaries is, therefore, distributed uniformly and instantaneously throughout the fluid volume at that axial location. An absence of significant radial temperature gradients has been observed experimentally, but the general validity of this assumption has not been fully established. The heat-transfer mechanism responsible for this behavior is not understood, but apparently the one-dimensional model is realistic in most cases. This is fortuitous, for a two or three-dimensional model would require a prohibitive amount of machine time for solution and would not be practical in the proposed program.

Two analyses of a non-viscous, one-dimensional, ullage gas model have appeared in the literature. The simpler, by Roudebush of NASA-LeRC (reference 37), includes heat transfer between a cylindrical tank wall and a one-component ullage, but ignores axial transfer processes. The finite-difference equations are in Eulerian form, using a fixed, evenly spaced net point system. The equations are obtained from an implicit type of derivation, but only single differences between two adjacent net points are involved. The resulting equations are explicit, giving the variable values at successive axial locations, starting from the current-time boundary conditions at the inlet plane. The computer program is straightforward and fast. Results have agreed with experiments despite the relative simplicity of the model. A more complete analysis has been developed by Epstein, Georgius, and Anderson of NAA (reference 38). The model includes an arbitrary tank geometry, two-component ullage, axial conduction and diffusion, and interface transfer. Because the ullage interacts with the propellant interface, the liquid temperature profile must also be calculated. In addition to the more complete ullage gas model, heat transfer through the wall and insulation is treated in detail and coupled equations for the pressurant supply system are included. The effects of mixing because of the nonuniform flow may be simulated by using effective transfer coefficients which are estimated from empirical data. The finite-difference equations are in explicit, Lagrangean form with the gas and liquid nodes changing volume and position relative to the tank. The computer program has been reported to be accurate, but it also requires more computation time, as would be expected with the more complicated equation system. By using empirical data, the program computations can be made to agree more closely with experimental results. It is difficult to determine these inputs, however, and often they are not available at all.

The model developed for the present analysis shares some features with that of both Roudebush and Epstein. It is as general as that of Epstein, but does not include the heat transfer through the tank insulation or the pressurant system characteristics. These factors would not be of immediate importance in this study.

The model has the following major features. An arbitrary tank geometry may be specified by giving the axial variation of the cross-sectional area of the ullage space and of the heat-transfer circumference for the tank wall and for the internal hardware. Heat transfer occurs between the ullage and both the tank wall and internal hardware. Axial conduction in the wall

and hardware is neglected. Axial conductions in the gas and heat and mass transfer at the interface is included. Anticipating relatively short outflow times and well insulated walls, the heat flow in the liquid is described by a simple conduction equation without wall heating. The ullage may be a binary mixture of condensable propellant vapor and non-condensable gas. The composition profile is governed by axial diffusion and evaporation/condensation at the interface. The ullage is an ideal mixture of real gases for which compressibility factors are functions of temperature and pressure. Specific heats are functions of temperature. Transport coefficients are assumed constant in deriving the equations but may be evaluated locally in their application.

For the problem solution, the gas composition and all temperature profiles must be given as initial conditions. The tank pressure, propellant outflow rate, and inlet gas temperature and composition may be varied arbitrarily with time. Heat addition externally to the wall and internally to the hardware is provided. At the interface, boundary conditions are the gas, wall and hardware temperatures, gas composition and velocity. The latter conditions are not set at problem initiation, but are determined throughout the solution from interaction of the gas and liquid at the interface.

c. The Temperature and Velocity Equations. It has been convenient to derive the equation system in the same general pattern as Roudebush. The present model is more extensive, but the development of some of the terms may be taken directly from reference 37.

The first law of thermodynamics for a fluid particle may be written as (reference 39 pg 189).

$$\frac{De}{Dt} + \frac{P}{J} \frac{D}{Dt} \left(\frac{1}{\rho} \right) = Q \quad (4-109)$$

where e is the energy and Q is the rate of heat addition to the fluid particle per unit mass. The concept refers to a one-dimensional coordinate system in which the Eulerian derivative is defined as

$$\frac{Df}{Dt} = \frac{df}{dt} + u \frac{df}{dx}$$

where $f(x, t)$ is a fluid property. The total heat addition to a fluid particle is made up of heat transfer from the tank wall and the internal hardware, and conduction from the adjacent fluid (reference 39 pg 337):

$$Q = Q_{\text{wall}} + Q_{\text{hardware}} + Q_{\text{conduction}} \quad (4-110)$$

$$Q_{\text{wall}} = \frac{C_W h_W}{A_p} (T_W - T) \quad (4-111)$$

$$Q_{\text{hardware}} = \frac{C_I h_I}{A_p} (T_I - T) \quad (4-112)$$

$$Q_{\text{conduction}} = \frac{k}{A_p} \frac{d}{dx} \left(A \frac{dT}{dx} \right) \quad (4-113)$$

Subscripts W and I denote wall and internal hardware properties, respectively. C is the heat-transfer circumference, A the ullage cross-section area, and h the heat-transfer coefficient. The conductivity k is assumed constant in the derivation.

The left-hand side of equation 4-109 is developed in the same manner as in reference 37 obtaining

$$C_p \frac{DT}{Dt} - \frac{T}{J} \left[\frac{d}{dT} \left(\frac{1}{\rho} \right) \right]_{p, \alpha} \frac{DP}{Dt} = Q \quad (4-114)$$

The equation of state for a real gas mixture is written as

$$MP = ZRT_p \quad (4-115)$$

in which the average molecular weight M and compressibility factor Z for the mixture are defined as

$$M = \alpha(M_V - M_{FG}) + M_{FG} \quad (4-116)$$

$$Z = \alpha(Z_V - Z_{FG}) + Z_{FG} \quad (4-117)$$

Properties of the vapor and the foreign gas species are indicated by the subscripts V and FG, respectively, and α is the mole fraction of propellant vapor.

From equation 4-115 is derived the term

$$\left[\frac{d}{dT} \left(\frac{1}{\rho} \right) \right]_{p, \alpha} = \frac{RZ_1}{MP} \quad (4-118)$$

in which

$$Z_1 = Z + T \frac{dZ}{dT} \quad (4-119)$$

Substituting equation 4-118 into equation 4-119 produces

$$C_p \frac{DT}{Dt} - \frac{RTZ_1}{JMP} \frac{DP}{Dt} = Q \quad (4-120)$$

which is expanded to give

$$C_p \left(\frac{dT}{dt} + u \frac{dT}{dx} \right) = \frac{ZRT}{MP} \left(\frac{C_W h_W}{A} (T_W - T) + \frac{C_I h_I}{A} (T_I - T) + \frac{Z_1}{JZ} \frac{dP}{dt} + \frac{k}{A} \frac{d}{dx} \left[A \frac{dT}{dx} \right] \right) \quad (4-121)$$

This is the energy equation from which the gas temperature is determined. It may also be obtained by simplifying the complete energy equation given in reference 40 pg 318.

The tank wall temperature is determined in the same manner as in reference

$$\frac{dT_W}{dt} = \frac{1}{l_W \rho_W C'_W} \left[h_W (T - T_W) + q_W \right] \quad (4-122)$$

where l_W is the wall thickness and C'_W the wall specific heat.

A similar equation is written for the internal hardware temperature as follows:

$$\frac{dT_I}{dt} = \frac{1}{l_I \rho_I C'_I} \left[h_I (T - T_I) + q_I \right] \quad (4-123)$$

The terms l_I in equation 4-123 and C_I from equation 4-112 are defined as the wall thickness and heat-transfer circumference for the internal hardware in the same general manner as for the external tank wall. If the hardware consists of pressure bottles, these terms are simple to use. If supports, baffles, and other hardware are to be included, a more careful definition of these parameters is necessary. All hardware across the width of the tank at each axial location is lumped together in the one-dimensional model. The proper effective values of L_I and C_I must be chosen to accurately represent their situation in the simple model. The values q_w and q_I are heat source terms for the wall and internal hardware. In reference x , q_w is determined by an analysis of heat conduction from the ambient through the tank insulation, and q_I is determined by the processes occurring within internally stored pressurant bottles. Here they are left as arbitrary boundary conditions.

The continuity equation for quasi-one-dimensional flow in a system of variable cross-section area is

$$A \frac{d\rho}{dt} + \frac{d}{dx} (\rho u A) = 0 \quad (4-124)$$

which yields

$$\frac{du}{dx} = \rho \frac{D}{Dt} \left(\frac{1}{\rho} \right) - \frac{u}{A} \frac{dA}{dx} \quad (4-125)$$

The second term can be written

$$\rho \frac{D}{Dt} \left(\frac{1}{\rho} \right) = \frac{\rho R}{MP^2} \left[-PZ_1 \frac{DT}{Dt} - TZ_2 \frac{DP}{Dt} + PZT \left(\frac{Z_3}{Z} - \frac{M_v - M_{FG}}{M} \right) \frac{D\alpha}{Dt} \right] \quad (4-126)$$

in which

$$Z_2 = Z - \rho \frac{dZ}{dP} \quad (4-127)$$

$$Z_3 = Z_v - Z_{FG} \quad (4-128)$$

Substituting equation 4-126 into equation 4-125 gives

$$\frac{du}{dx} = \frac{Z_1}{ZT} \left(\frac{dT}{dt} + u \frac{dT}{dx} \right) + \left(\frac{Z_3}{Z} - \frac{M_v - M_{FG}}{M} \right) \left(\frac{d\alpha}{dt} + u \frac{d\alpha}{dx} \right) - \frac{Z_2}{ZP} \frac{dP}{dt} - \frac{u}{A} \frac{dA}{dx} \quad (4-129)$$

for the gas velocity.

d. The Diffusion Equation. The Roudebush analysis does not include a two-component ullage and the diffusion equation given by Epstein is incorrect. Therefore, the derivation used in this analysis will be presented in detail. This development refers to basic equations in reference 40 pg 16.

The species continuity equation for the condensable vapor in quasi-one-dimensional form is

$$A \frac{d(c\alpha)}{dt} + \frac{d(N_v A)}{dx} = 0 \quad (4-130)$$

where the total molar concentration is given by $c = \rho/M$. The molar flux of condensable vapor N_v , relative to stationary coordinates, is given by

$$N_v = \alpha(N_v + N_{FG}) - c D^* \frac{d\alpha}{dx} \quad (4-131)$$

which is the sum of bulk flow and diffusion terms. The total molar flux is

$$N_v + N_{FG} = c u^* \quad (4-132)$$

Combining equations 4-130, 4-131, and 4-132 results in

$$A \frac{d(c\alpha)}{dt} + \frac{d}{dx} \left[cA \left(\alpha u^* - D^* \frac{d\alpha}{dx} \right) \right] = 0 \quad (4-133)$$

as the basic diffusion equation. It is noted that u^* is the molar average velocity and not the mass average velocity u which appears in the previous equations.

The molar average velocity is defined as

$$u^* = \alpha u_v + (1 - \alpha) u_{FG} \quad (4-134)$$

and the mass average velocity as

$$u = w u_v + (1 - w) u_{FG} \quad (4-135)$$

where u_v and u_{FG} are the velocities of the individual vapor and foreign gas species and w is the mass fraction of condensable vapor in the gas,

$$w = \frac{\alpha M_v}{\alpha M_v + (1 - \alpha) M_{FG}} = \frac{\alpha M_v}{M} \quad (4-136)$$

An expression relating u_v and u_{FG} is taken from reference 40 pg 502.

$$u_v - u_{FG} = - \frac{D^*}{\alpha(1 - \alpha)} \frac{d\alpha}{dx} \quad (4-137)$$

and substituted into equation 4-135 to give

$$u = u_v + \frac{(1 - w)}{\alpha(1 - \alpha)} D^* \frac{d\alpha}{dx} \quad (4-138)$$

Using equation 4-136 and solving for u_v gives

$$u_v = u - \frac{M_{FG}}{\alpha M} D^* \frac{d\alpha}{dx} \quad (4-139)$$

Equations 4-134, 4-137, and 4-139 combine and simplify to

$$u^* = u + \left(\frac{M_v - M_{FG}}{M} \right) D^* \frac{d\alpha}{dx} \quad (4-140)$$

which is the molar average velocity in terms of the mass average velocity, molecular weights and the mole fraction gradient. If the molecular weights are identical, or if there is no gradient, the two velocities are equal. If, for example, there is a negative gradient in the vapor mole fraction, then $u_v > u_{FG}$. Further, if the vapor molecular weight is greater than that of the foreign gas, then $u > u^*$, because u_v is weighted more heavily in u than in u^* . Equations 4-133 and 4-140 give

$$A \frac{d(c\alpha)}{dt} + \frac{d}{dx} \left\{ cA \left[\alpha u - \frac{M_{FG}}{M} D^* \frac{d\alpha}{dx} \right] \right\} = 0 \quad (4-141)$$

for the diffusion equation.

The basic diffusion equation will now be expanded into simple terms. Equation 4-141 is rewritten

$$A \frac{d}{dt} \left(\frac{\rho\alpha}{M} \right) + \frac{d}{dx} \left(\frac{\alpha\rho u A}{M} \right) - \frac{d}{dx} \left(cA \frac{M_{FG}}{M} D^* \frac{d\alpha}{dx} \right) = 0 \quad (4-142)$$

The left-hand terms become

$$\rho A \frac{d}{dt} \left(\frac{\alpha}{M} \right) + \frac{\alpha}{M} \left[A \frac{d\rho}{dt} + \frac{d}{dx} (\rho u A) \right] + \rho u A \frac{d}{dx} \left(\frac{\alpha}{M} \right)$$

in which the expression in square brackets is the continuity equation and equal to zero from equation 4-124. The remaining terms combine to give

$$cA \frac{M_{FG}}{M} \left(\frac{d\alpha}{dt} + u \frac{d\alpha}{dx} \right) - \frac{d}{dx} \left(cA \frac{M_{FG}}{M} D^* \frac{d\alpha}{dx} \right) = 0 \quad (4-143)$$

Expanding the right-hand term through the following steps

$$cA \frac{M_{FG}}{M} \left(\frac{d\alpha}{dt} + u \frac{d\alpha}{dx} \right) - c \frac{M_{FG}}{M} D^* \frac{d}{dx} \left(A \frac{d\alpha}{dx} \right) - AD^* \frac{d\alpha}{dx} \frac{d}{dx} \left(c \frac{M_{FG}}{M} \right) = 0$$

$$\frac{d\alpha}{dt} + u \frac{d\alpha}{dx} - \frac{D^*}{A} \frac{d}{dx} \left(A \frac{d\alpha}{dx} \right) - D^* \frac{d\alpha}{dx} \frac{d}{dx} \ln \left(\frac{c}{M} \right) = 0$$

we arrive at the final form of the diffusion equation

$$\frac{d\alpha}{dt} + u \frac{d\alpha}{dx} = \frac{D^*}{A} \frac{d\alpha}{dx} \left(A \frac{d\alpha}{dx} \right) - D^* \frac{d\alpha}{dx} \left[\frac{Z_1}{ZT} \frac{dT}{dx} + \left(\frac{Z_1}{Z} + \frac{M_v - M_{FG}}{M} \right) \frac{d\alpha}{dx} \right] \quad (4-144)$$

e. The Liquid Equations. To establish the interface conditions, it is necessary to calculate the heat flow into the propellant. Only axial conduction is considered in the energy equation. The equivalent of equation 4-121 for the liquid temperature equation, assuming constant density, is

$$\rho_L c_{PL} \left(\frac{dT_L}{dt} + u_L \frac{dT_L}{dx} \right) = \frac{k_L}{A} \frac{d}{dx} \left(A \frac{dT_L}{dx} \right) \quad (4-145)$$

The subscript L denotes liquid properties. The liquid velocity is

$$u_L = \frac{\dot{m}}{\rho_L A} \quad (4-146)$$

in which \dot{m} is the propellant mass outflow rate.

f. The Interface Equations. The gas-liquid interface provides a boundary value for both the liquid and gas temperature equations and for the gas composition and velocity equations. The evaporation rate is determined by the net heat supplied to the interface by conduction from the gas and into the liquid. When the ullage is composed of pure propellant vapor, the interface-temperature is the saturation temperature at tank pressure. With a two-component ullage, the heat and mass-transfer rates at the interface must be balanced to determine the interface conditions. The liquid and gas

temperatures are assumed equal at the interface and in equilibrium with the vapor partial pressure. The vapor pressure P_v is a temperature dependent property of the propellant, therefore

$$P_{v \text{ int}} = P_v (T_{\text{int}}) \quad (4-147)$$

where the subscript int denotes an interface condition. The interface vapor mole fraction is

$$\alpha_{\text{int}} = \frac{P_{v \text{ int}}}{P} \quad (4-148)$$

These equations relate T , T_L , and α at the interface in the expressions developed below.

Heat flux to the interface from the gas is

$$\dot{q}_{\text{in}} = -k \frac{dT}{dx} \quad (4-149)$$

and from the interface into the liquid is

$$\dot{q}_{\text{out}} = -k_L \frac{dT_L}{dx} \quad (4-150)$$

The net heat flux available for evaporation is

$$\dot{q}_{\text{net}} = \dot{q}_{\text{in}} - \dot{q}_{\text{out}} \quad (4-151)$$

resulting in a mass evaporation rate at the interface of

$$\dot{n} = -\rho_v u_{v \text{ rel}} A_{\text{int}} = \frac{\dot{q}_{\text{net}}}{l_v} A_{\text{int}} \quad (4-152)$$

where u_{vrel} is the vapor velocity (downward) relative to the interface, ρ_v is the vapor density, and l_v is the propellant heat of vaporization. In a pure vapor system, $u_{vrel} = u_{rel}$ and $\rho_v = \rho$, giving

$$u_{rel} = - \frac{\dot{q}_{net}}{\rho l_v} \quad (4-153)$$

The liquid interface velocity is

$$u_{L\ int} = \frac{\dot{m} + \dot{n}}{\rho_L A_{int}} \quad (4-154)$$

Therefore, the pure vapor interface gas velocity relative to the fixed coordinate system is

$$u_{int} = \frac{\dot{m} + \dot{n}}{\rho_L A_{int}} - \frac{\dot{q}_{net}}{\rho l_v} \quad (4-155)$$

This is the boundary value for the gas velocity equation.

With a two-component gas at the interface, the vapor velocity is determined by the diffusion rate

$$u_{v\ rel} = - \frac{D^*}{\alpha(1-\alpha)} \frac{d\alpha}{dx} \quad (4-156)$$

as obtained from equation 4-137 by setting $u_{FG\ rel} = 0$ at the interface.

The vapor density is

$$\rho_v = \alpha \rho \frac{M_v}{M} \quad (4-157)$$

For $u_{FG\ rel} = 0$, the relative gas velocity is

$$u_{rel} = \frac{\rho_v}{\rho} u_{v\ rel} \quad (4-158)$$

or, with equations 4-156 and 4-157

$$u_{rel} = -\frac{M_v}{M} \frac{D^*}{(1-\alpha)} \frac{d\alpha}{dx} \quad (4-159)$$

resulting in the two-component, interface, gas velocity

$$u_{int} = \frac{\dot{m} + \dot{n}}{\rho_L A_{int}} - \frac{M_v}{M} \frac{D^*}{(1-\alpha)} \frac{d\alpha}{dx} \quad (4-160)$$

This is used in place of equation 4-155 for two-component ullage problems.

To determine the interface temperature with a two-component ullage, equations (4-149) through (4-152) are combined with (4-156) and (4-157) to obtain

$$-\frac{M_v}{M} \frac{\rho_{lv}}{(1-\alpha)} D^* \frac{d\alpha}{dx} = k \frac{dT}{dx} - k_L \frac{dT_L}{dx} \quad (4-161)$$

which is the balance between the diffusion and evaporation rates. This equation, together with conditions given by equation 4-147 and 4-148, must be satisfied at the interface.

g. Program Solution. Equations 4-121, 4-122, 4-123, 4-129, 4-144, 4-145, and 4-146 are the final expressions for the gas temperature, tank wall temperature, hardware temperature, gas velocity, gas composition, liquid temperature, and liquid velocity. These Eulerian form equations were converted into difference equations suitable for programming. For example, the difference form of equation 4-122 for the wall temperature becomes

$$\frac{T_{w,i}^i - T_{w,i}}{\Delta t} = \left(\frac{1}{c_w \rho_w c_w^i} \right)_i \left[h_{w,i} (T_i^i - T_{w,i}^i) + q_{w,i} \right]$$

The solution of the equations must be performed in a specific sequence. The solution proceeds by determining the temperature and composition profiles and then the velocity profiles at each time step.

The equation system with boundary and input condition was programmed in Fortran IV language to yield Douglas computer code H225. Figure 4-113 summarizes the function and capabilities of the program. It analyzes the internal tank thermodynamics between points a and b in the pressure time history, which covers pre-pressurization/re-pressurization and pressurization during expulsion. Further details relative to the H225 program are contained in a special report as part of this contractual effort.

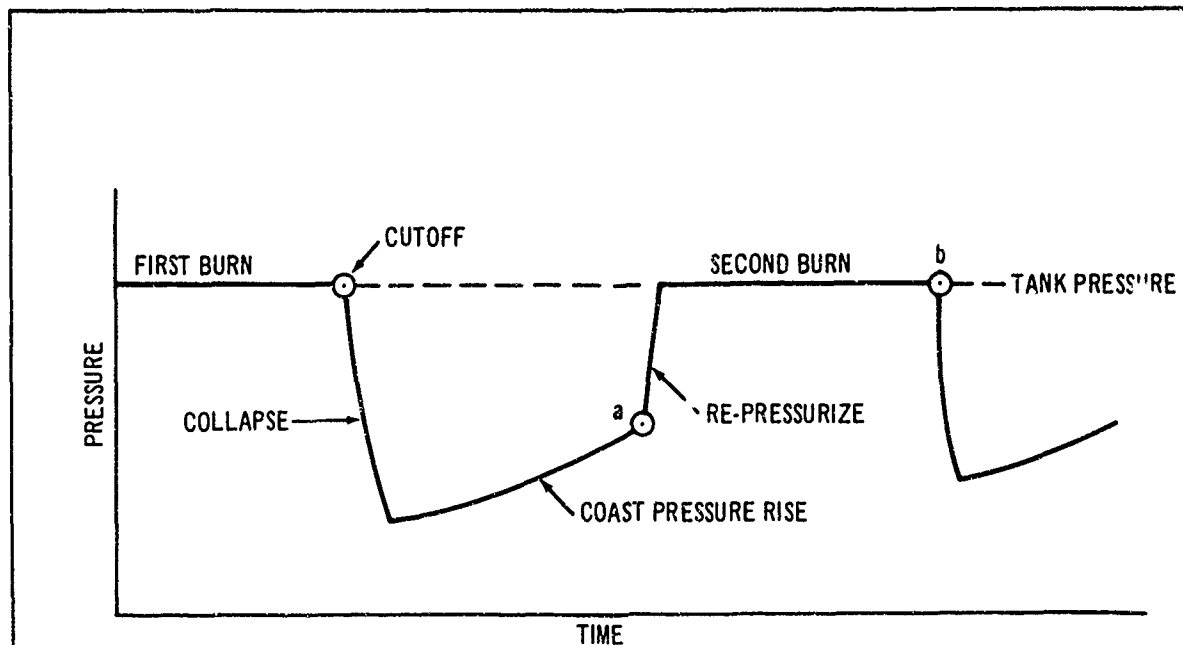
h. Typical Results. To illustrate the capabilities of the program and certain trends, a series of trial runs were made with the H225 program.

An example of the output generated by the tank pressurization program is illustrated in figures 4-114 and 4-115. The computations are based on the study vehicle configuration liquid hydrogen tank and includes the use of all tabular and calculated local properties and transfer coefficients provided by the program. Figure 4-114 shows the pressurant requirements during outflow at a constant pressure and flow rate for three inlet temperatures. Also shown are the ideal curves, representing the pressurant mass required if there were no cooling of the ullage gas. Figure 4-115 shows ullage gas temperature profiles at three times during the outflow at 500°R, inlet temperature. One wall temperature profile is included, which corresponds to the longest expulsion time. The irregular shape of the curves is caused by spherical pressure bottles mounted at the mid-section. The depression in the profiles near the center of the tank is caused by the additional cooling effect of these pressure bottles.

Figure 4-116 illustrates the general data trends. These computations were based on the study vehicle LH₂ tank with He pressurant. It was assumed that the tank initially contained half the maximum propellant volume and that propellant was expelled at a rate of 4.6 lb.p. sec. Uniform equilibrium initial conditions were assumed. The conditions were the tank pressure, temperature and ullage composition. Choosing any two determines the third value. In this example, the initial ullage composition was assumed to be pure propellant vapor. Choosing the initial pressure requires the initial temperature to be the corresponding saturation temperature.

To identify the degree of expulsion, the amount expelled is compared to the maximum total propellant volume, not the initial propellant volume. In this case, a 10 pct. expulsion indicates that one fifth of the initial propellant has been expelled, because the tank was initially half full. Fifty pct. expulsion means that the tank has been emptied. The initial conditions specify the propellant volume, but the outflow rate is specified in mass units. The density of LH₂ shows a pronounced decrease with increasing temperature resulting in higher volumetric outflow rates and lower expulsion times at the higher expulsion pressures.

Ideal curves, which assume there is no heat transfer from the gas, are shown for comparison. As the gas temperature is raised, the heat-transfer rates increase and the computer curves show a greater departure



INPUTS	OUTPUTS
<p>TIME VARIANTS: PROPELLANT OUTFLOW RATE TANK PRESSURE EXTERNAL WALL HEATING RATE INTERNAL HARDWARE HEATING RATE</p> <p>PROPERTY TABLES: WALL SPECIFIC HEAT INTERNAL HARDWARE SPECIFIC HEAT GAS SPECIFIC HEAT GAS COMPRESSIBILITY PROPELLANT VAPOR PRESSURE PROPELLANT HEAT OF VAPOR</p> <p>EFFECTIVE COEFFICIENTS: HEAT-TRANSFER COEFFICIENTS DIFFUSION COEFFICIENTS GAS CONDUCTIVITY LIQUID CONDUCTIVITY INTERFACE AREA</p> <p>BOUNDARY CONDITIONS: PROPELLANT TEMPERATURE AND COMPOSITION INTERFACE CALCULATIONS</p>	<p>TEMPERATURE PROFILES: GAS LIQUID TANK WALL INTERNAL HARDWARE</p> <p>COMPOSITION AND VELOCITY PROFILES FOR GAS</p> <p>TOTAL MASS OF ULLAGE GAS HEAT DISTRIBUTION: GAS LIQUID TANK WALL INTERNAL HARDWARE</p> <p>TOTAL EVAPORATION AND/OR CONDENSATION</p> <p>COLLAPSE FACTOR</p>

Figure 4-113. Program H225 Function.

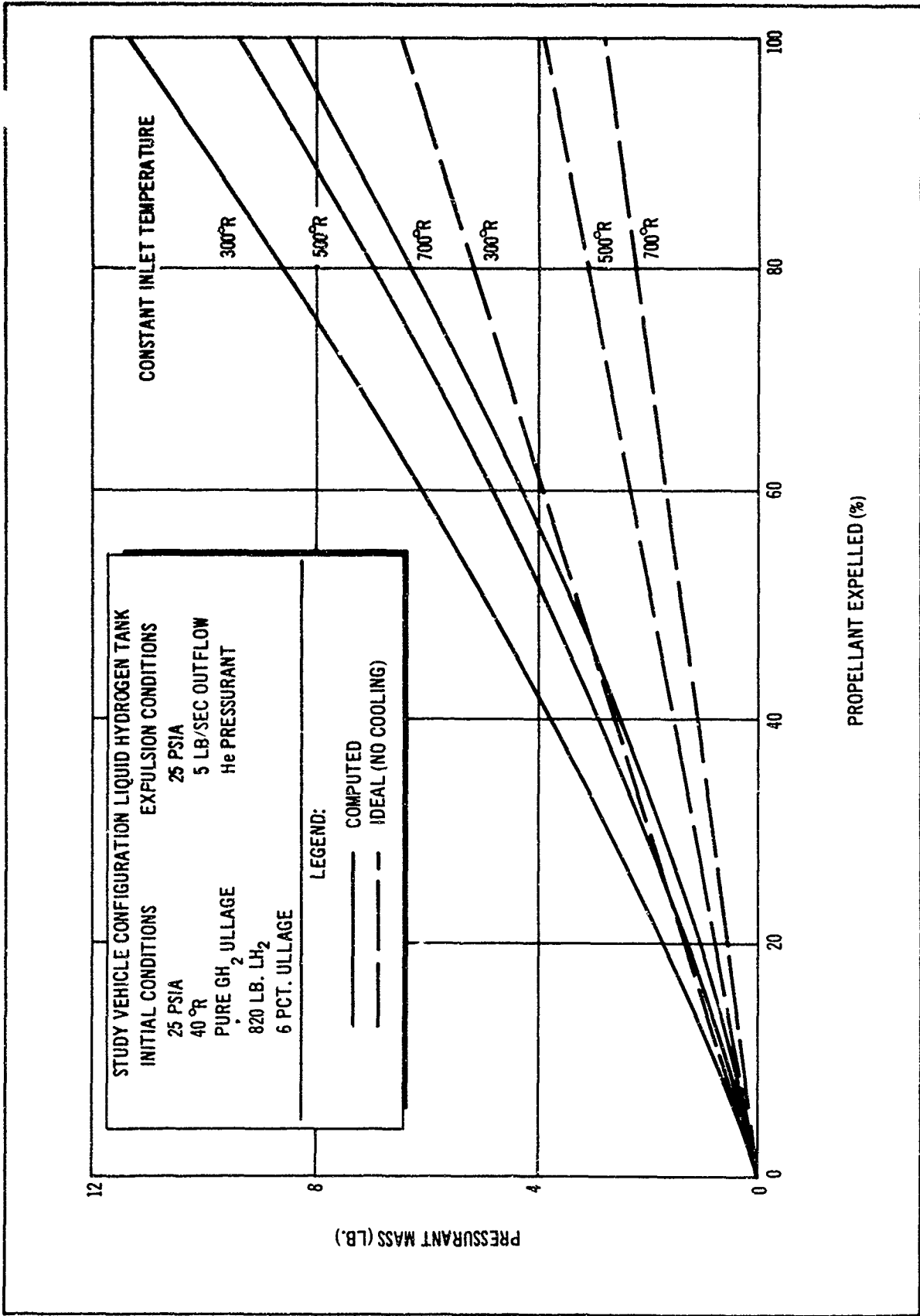


Figure 4-114. Pressurant Requirements During Outflow

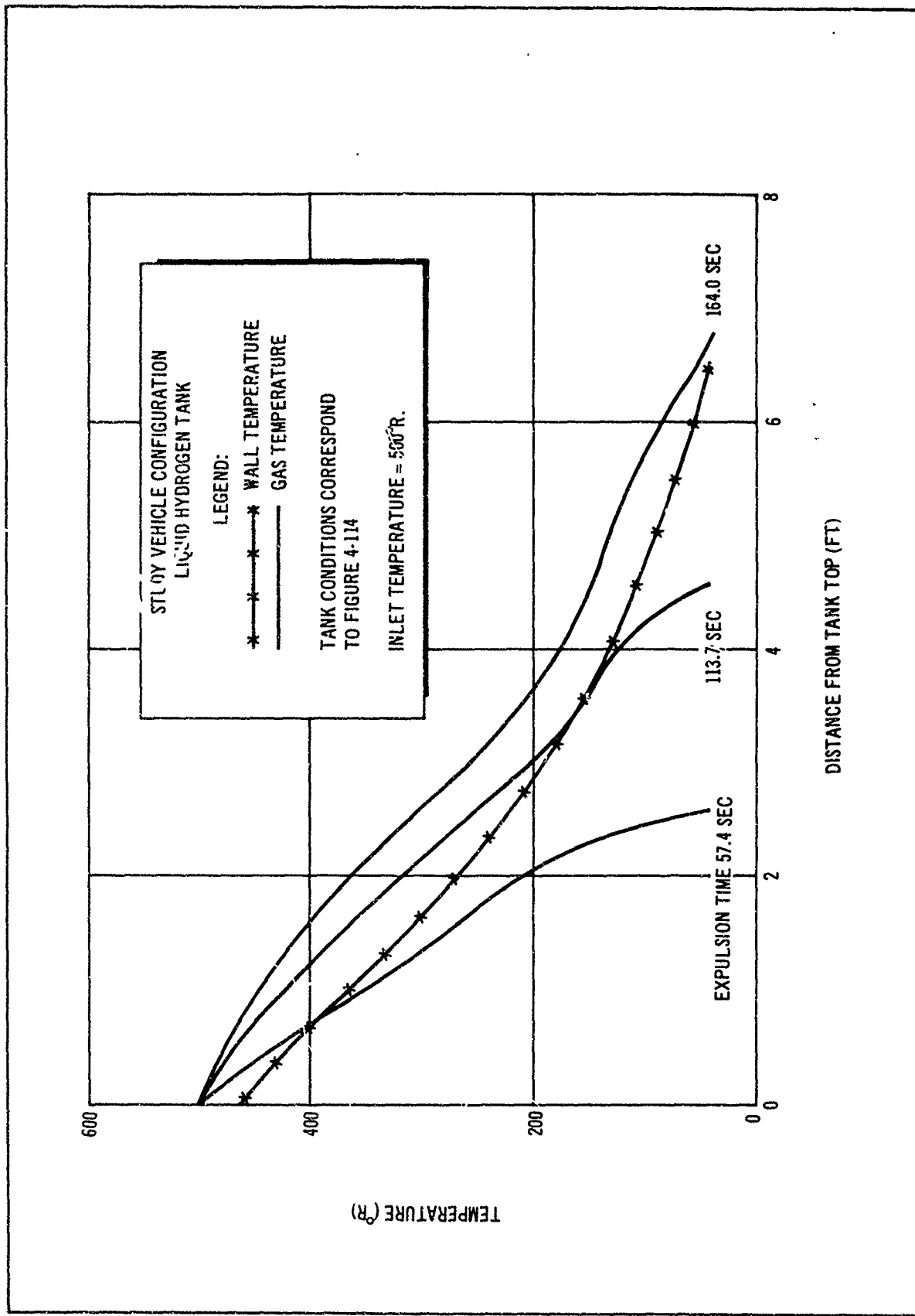


Figure 4-115. Ullage Temperature Profiles During Outflow

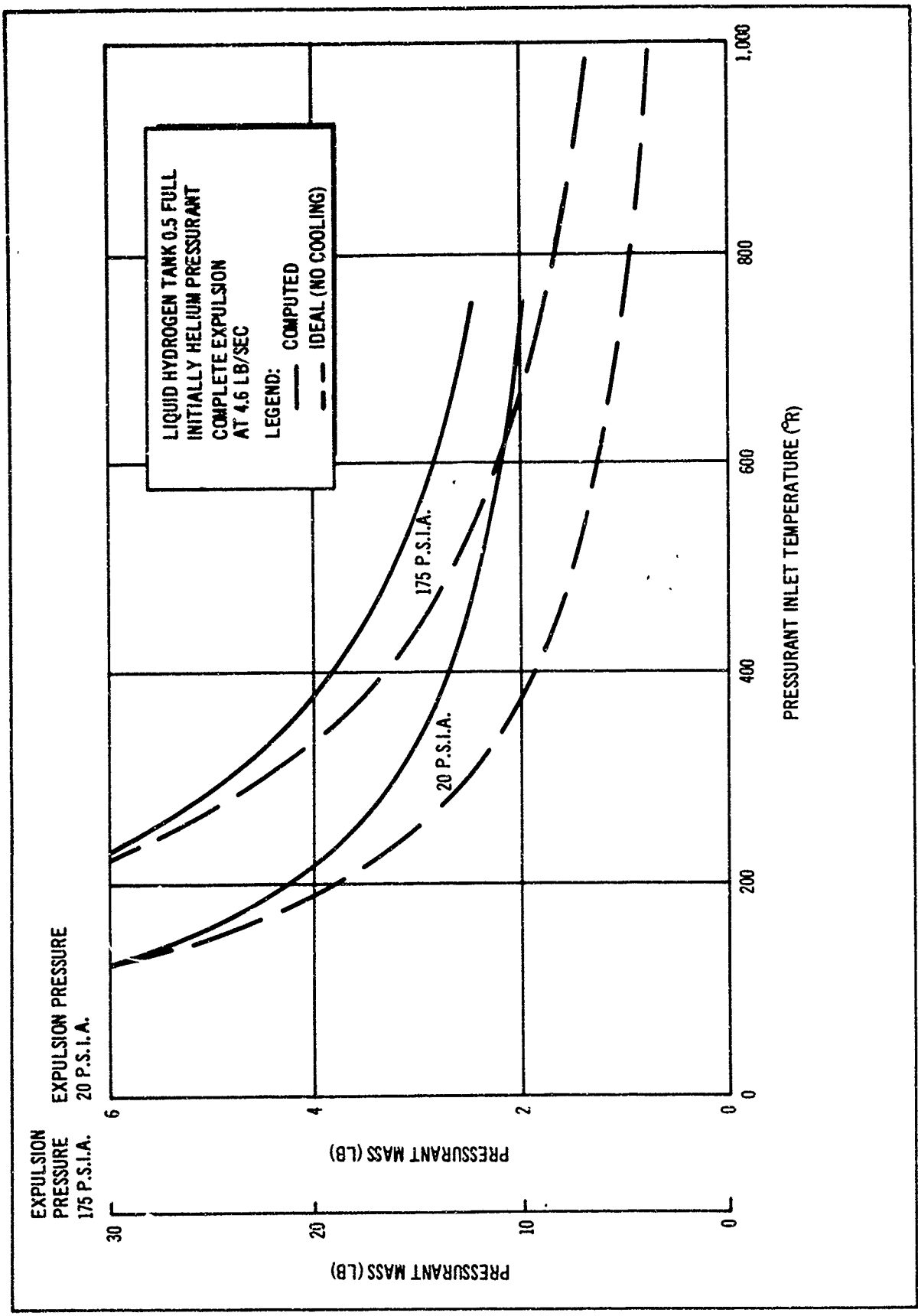


Figure 4-116. Pressurant Requirements During Expulsion

from the ideal. At a given inlet temperature, the relative departure from ideal decreases with increasing pressure because the heat required to raise the wall temperature becomes a smaller fraction of the total heat in the gas. In all cases, however, the curves are monotonically decreasing.

The influence of expulsion pressure is shown in figure 4-117 for an inlet temperature of 700°R. Pressurant requirement curves for expulsion preceded by pressurization have been added. The solid curves correspond to an initial pressure equal to the expulsion pressure without pressurization. Dashed curves extend from each which give the pressurant requirements when the expulsion process is preceded by a pressurization from initial pressures of 20, 40, and 90 p. s. i. a. The curves originating from the horizontal axis of the graph give the pressurant required for pressurization, alone, before expulsion begins.

i Determination of Pressurant Requirements. The evaluation of the pressurant requirements for the study ground-rule tank pressures and duty cycles required the generation of a large amount of parametric data. To accomplish this efficiently, a procedure combining the H225 and H109 program capabilities was used. The H109 program normally computes the pressurant requirements assuming no heat or mass transfer. However, provisions were incorporated into the program to permit inclusion of a correction factor to account for heat transfer. Therefore, the H225 program was used to generate required parametric correction factors. These factors were supplied to the H109 program, which generated the pressurant weights. At the same time, overall performance was computed for the pressurization system operating conditions optimization.

Figures 4-118 and 4-119 show typical examples of the parametric corrections factors generated by program H225.

Table 4-41 presents the overall computed pressurant requirements. Also shown are the usable propellant weights as computed by the H109 program.

j. Discussion of Results and Optimization. As shown in table 4-41, detailed computations were run for the two pressure extremes on the pressure-fed system and the pump-fed case (no booster pump) at three inlet gas temperatures, 300, 800, and 1,200°R. For the pump-fed system, only CH₂ pressurization of the LH₂ tank using pressurization system 6 (table 4-38) was considered. Both He and CH₂ pressurization of the LH₂ tank was considered for the pressure-fed systems using systems 4 and 10. This method was followed in comparing He versus CH₂ as a LH₂ tank pressurant. For some cases, using CH₂, particularly those at high-pressure and high-inlet gas temperature, it was impossible to obtain solutions because the LH₂ temperature would become critical at some point in the mission.

Because various levels of venting occur in certain cases, it is at times misleading to compare pressurant weight. However, some typical

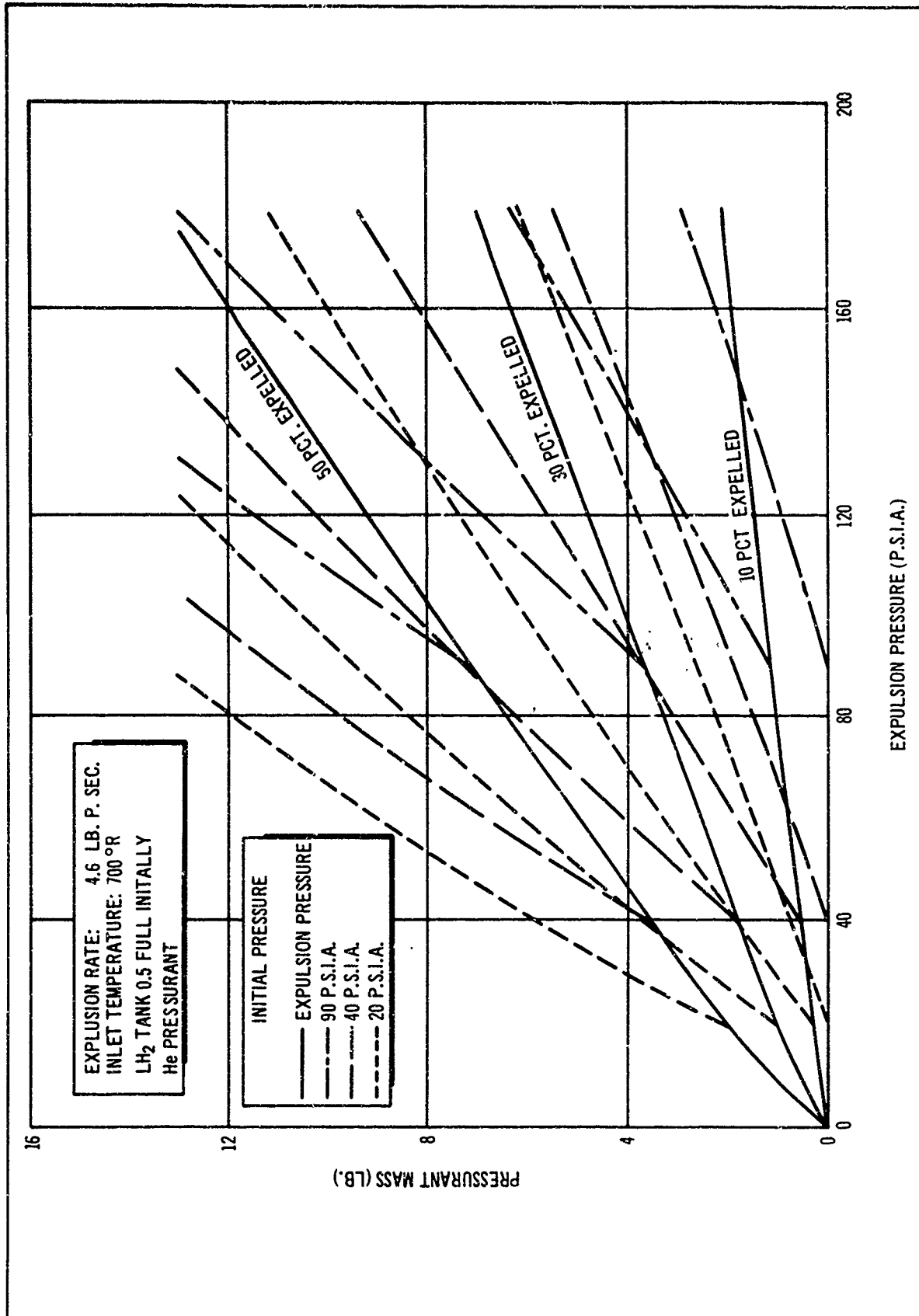


Figure 4-117. Pressurant Requirements for Pressurization and Expulsion

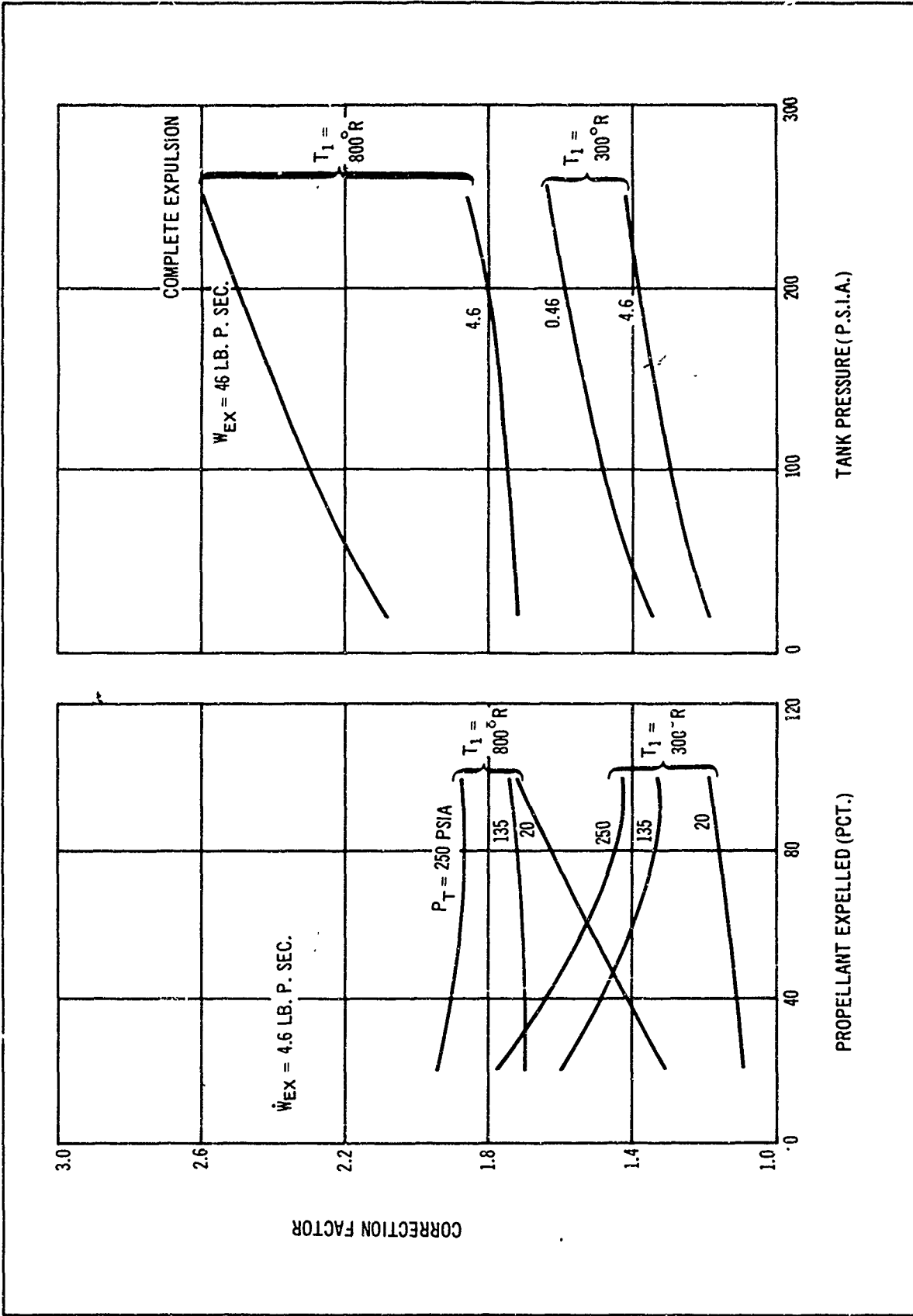


Figure 4-118 Pressurization Correction Factors for LH₂ Tank with Initial Ullage of 80 Pct.

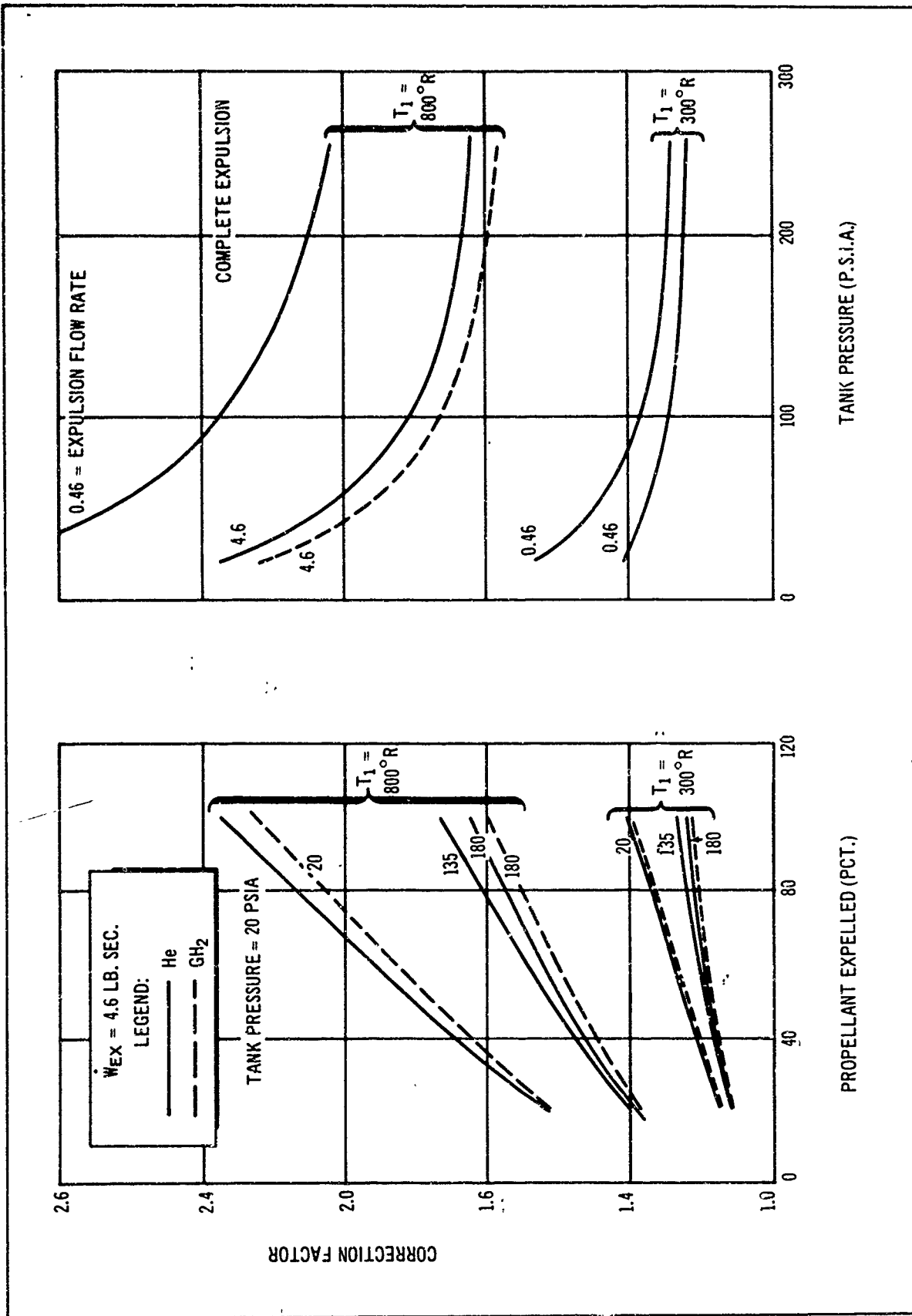


Figure 4-119. Pressurization Correction Factors for LH₂ Tank with Initial Ullage of 3 Pct.

Table 4-41 (page 1 of 10)
PF ESSURANT REQUIREMENTS

Duty Cycle	Tank Pressure p.s.i.a.	Inlet Gas Temperature °F.	Burn No.	LH ₂ Tank Gas Weight - (lb)				LF ₂ Tank Gas Weight				Total Gas Weights		Usable Propellant Weight - (lb)				
				Repressurization	He Expulsion	Total	Repressurization	GH ₂ Expulsion	Total	Repressurization	Expulsion	Total	All He	He/GH ₂	All He	He/GH ₂		
I	235	300	1	--	77.3	77.3	0	38.3	38.3	38.3	0	41.5	41.5	118.8	79.8	12,232	12,424	
				--	51.8	51.8	0	20.9	20.9	20.9	0	23.2	23.2	75.0	44.1	12,393	12,522	
	100	300	1	--	43.3	43.3	0	17.4	17.4	17.4	0	16.9	16.9	60.2	34.3	12,448	12,548	
				--	36.5	36.5	0	17.2	17.2	17.2	0	19.2	19.2	55.7	36.4	12,719	12,814	
	P	800	1	--	25.7	25.7	0	9.7	9.7	9.7	0	10.9	10.9	36.6	20.6	12,792	12,855	
				--	22.3	22.3	0	8.2	8.2	8.2	0	8.1	8.1	30.4	16.3	12,815	12,867	
	235	300	1	--	--	--	0	8.	8.6	8.6	0	13.0	13.0	--	21.6	--	12,986	--
				--	--	--	0	6.1	6.1	6.1	0	7.7	7.7	--	13.8	--	13,009	--
	100	800	1	--	--	--	0	5.	5.2	5.2	0	6.0	6.0	--	11.2	--	13,016	--
				0	37.4	37.4	0	19	19	19	0	24.8	24.8	--	--	--	--	--
100	300	2	12.4	41.0	90.8	4.9	22.1	46.8	3.6	23.1	51.7	3.6	23.1	142.5	98.5	12,145	12,352	
			0	21.9	--	0	1.6	--	--	0	14.1	--	0	14.1	--	--	--	--
100	800	2	4.5	25.0	51.4	1.3	3.6	26.5	3.1	14.1	31.3	3.1	14.1	82.7	57.6	12,315	12,425	
			0	16.6	--	0	8.8	--	--	0	10.9	--	0	10.9	--	--	--	--
100	300	2	3.7	18.3	38.6	1.6	9.6	20.0	1.3	10.1	22.3	1.3	10.1	60.9	47.3	12,679	12,776	
			0	10.6	--	0	5.6	--	--	0	6.2	--	0	6.2	--	--	--	--
100	800	2	1.2	11.6	23.4	0.3	6.0	11.9	0.3	6.2	13.6	0.3	6.2	37.0	25.5	12,763	12,812	
			0	9.4	--	0	4.9	--	--	0	5.1	--	0	5.1	--	--	--	--
100	300	2	0.6	10.2	20.2	0	5.6	10.5	0.95	5.3	11.4	0.95	5.3	31.6	21.9	12,781	12,806	
			--	--	--	0	3.8	--	--	0	6.9	--	0	6.9	--	--	--	--
100	800	2	--	--	--	0.8	4.0	8.6	0.5	6.4	13.8	0.5	6.4	--	22.4	--	12,949	
			--	--	--	0	2.3	--	--	0	3.9	--	0	3.9	--	--	--	--
100	300	2	--	--	--	0.3	2.4	5.0	0.7	3.9	8.5	0.7	3.9	--	13.5	--	12,968	
			--	--	--	0	1.9	--	--	0	3.2	--	0	3.2	--	--	--	--
100	800	2	--	--	--	0.2	2.1	4.2	0.5	3.3	7.0	0.5	3.3	--	11.2	--	12,945	
			--	--	--	0	28.9	--	--	0	32.8	--	0	32.8	--	--	--	--
100	300	2	13.8	19.2	90.5	4.2	11.3	44.4	7.9	10.9	51.6	7.9	10.9	142.1	96.0	12,043	12,248	
			0	37.5	--	--	--	--	--	0	20.0	--	0	20.0	--	--	--	--
100	800	2	0	15.6	53.1	--	--	--	4.	6.5	31.1	4.	6.5	84.2	--	12,122	--	
			0	37.5	--	--	--	--	--	0	18.4	--	0	18.4	--	--	--	--
100	300	2	0	14.6	52.1	--	--	--	3.	5.4	26.9	3.	5.4	79.0	--	12,044	--	
			0	14.6	52.1	--	--	--	--	3.	5.4	26.9	3.	5.4	79.0	--	12,044	--

Table 4-41 (page 2 of 10)

PRESSURANT REQUIREMENTS

Duty Cycle	Tank Pressure p.s.i.a.	Inlet Gas Temperature °F.	Burn No.	LH ₂ Tank Gas Weight - (lb)				LF ₂ Tank Gas Weight				Total Gas Weight		Usable Propellant Weight - (lb)				
				Repressurization	He Expulsion	Total	Repressurization	GH ₂ Expulsion	Total	Repressurization	Expulsion	Total	All He	He/GH ₂	All He	He/GH ₂		
K	100	300	1	0	26.6	--	0	13.3	--	0	14.8	--	--	--	--	--	--	
			2	1.7	8.1	36.4	0.6	4.4	18.3	2.5	4.5	21.8	58.2	40.1	12.629	12.713		
	800	1	0	17.9	--	--	0	8.6	--	0	9.6	--	--	--	--	--	--	
		2	0	4.4	22.3	0	2.4	11.0	1.7	2.6	13.9	36.2	24.9	12.667	12.684			
P	300	300	1	0	18.0	--	--	--	--	0	6.5	--	--	--	--	--	--	
			2	0	3.6	21.6	--	--	--	1.2	2.2	12.9	34.5	--	12.640	--		
	800	1	--	--	--	--	0	6.8	--	0	10.3	--	--	--	--	--	--	
		2	--	--	--	--	1.2	1.5	9.5	0.3	2.7	13.3	--	22.8	--	12.880		
C	235	300	1	--	--	--	0	4.8	--	0	7.0	--	--	--	--	--	--	
			2	--	--	--	0.5	0.8	6.1	0.7	1.5	9.2	--	15.3	--	12.862		
	800	1	--	--	--	0	4.1	--	--	0	5.6	--	--	--	--	--	--	
		2	--	--	--	0.3	0.6	5.0	0.6	1.3	7.5	--	12.5	--	12.855			
100	1,200	300	1	0	13.7	--	0	7.0	--	0	8.5	--	--	--	--	--	--	
			2	7.0	6.9	--	2.6	3.8	--	2.4	4.2	--	--	--	--	--	--	
			3	9.0	8.2	--	3.4	4.7	--	2.6	5.3	--	--	--	--	--	--	--
			4	10.0	14.4	--	4.0	8.0	--	2.1	9.2	--	--	--	--	--	--	--
			5	11.5	34.7	115.4	4.9	19.7	58.1	2.8	23.9	51.1	60.9	176.3	119.0	12.027	12.291	
100	1,200	300	1	0	7.9	--	0	3.9	--	0	5.1	--	--	--	--	--	--	
			2	2.7	3.3	--	0.8	1.8	--	1.4	2.1	--	--	--	--	--	--	
			3	3.7	4.3	--	1.0	2.4	--	1.9	3.2	--	--	--	--	--	--	--
			4	4.3	7.0	--	1.2	3.8	--	2.2	4.6	--	--	--	--	--	--	--
			5	5.1	21.6	59.9	1.3	12.0	28.2	3.2	13.9	37.6	97.5	65.8	12.265	12.389		
100	300	300	1	0	6.1	--	0	3.1	--	0	3.7	--	--	--	--	--	--	
			2	3.0	2.8	--	1.2	1.5	--	0.9	1.9	--	--	--	--	--	--	
			3	3.9	3.6	--	1.7	2.0	--	1.0	2.2	--	--	--	--	--	--	
			4	4.5	6.2	--	2.0	3.3	--	0.9	3.7	--	--	--	--	--	--	
			5	4.4	14.7	57.2	2.1	7.9	24.8	1.3	9.3	24.8	82.0	49.6	12.647	12.751		

Table 4-41 (page 3 of 10)

PRESSURANT REQUIREMENTS

Duty Cycle	Tank Pressure P.s.i.a.	Inlet Gas Temperature °F.	Burn No.	LH ₂ Tank Gas Weight - (lb)				LF ₂ Tank Gas Weight				Total Gas Weights		Usable Propellant Weight - (lb)					
				Repressurization	He Expulsion	Total	Repressurization	GH ₂ Expulsion	Total	Repressurization	Expulsion	Total	All He	He/GH ₂	All He	He/GH ₂			
C	100	600	1	0	3.7	--	0	1.8	--	0	2.2	--	--	--	--	--	--		
			2	1.2	1.5	--	0.3	0.8	--	0.6	0.9	--	--	--	--	--	--		
			3	1.6	2.0	--	0.5	1.1	--	0.8	1.2	--	--	--	--	--	--	--	
			4	1.9	3.0	--	0.6	1.6	--	1.0	1.9	--	--	--	--	--	--	--	
			5	2.0	8.1	25.0	0.6	4.2	11.5	4.2	5.4	15.4	40.4	26.9	12.755	12.791	--	--	
		1,200	1	0	3.1	--	0	1.5	--	0	2.0	--	--	--	--	--	--		
			2	0.8	1.2	--	0.2	0.6	--	0.4	0.7	--	--	--	--	--	--	--	
			3	1.1	1.8	--	0.3	1.0	--	0.6	1.1	--	--	--	--	--	--	--	
			4	1.3	2.4	--	0.3	1.3	--	0.7	1.4	--	--	--	--	--	--	--	--
			5	1.3	7.4	20.4	0.3	3.8	9.3	3.8	4.7	12.7	33.1	22.0	12.775	12.800	--	--	
P		300	1	--	--	--	0	1.3	--	0	2.4	--	--	--	--	--	--		
			2	--	--	--	1.1	0.6	--	0.5	1.1	--	--	--	--	--	--		
			3	--	--	--	1.4	0.8	--	0.6	1.3	--	--	--	--	--	--	--	
			4	--	--	--	1.6	1.4	--	0.6	2.4	--	--	--	--	--	--	--	
			5	--	--	--	0.6	3.1	11.9	3.1	5.4	14.8	26.7	--	--	12.940	--	--	
		600	1	--	--	--	0	0.7	--	0	1.4	--	--	--	--	--	--		
			2	--	--	--	0.4	0.3	--	0.4	0.6	--	--	--	--	--	--		
			3	--	--	--	0.5	0.4	--	0.5	0.8	--	--	--	--	--	--	--	
			4	--	--	--	0.6	0.6	--	0.6	1.1	--	--	--	--	--	--	--	
			5	--	--	--	0.2	1.7	5.4	1.7	3.1	9.3	14.7	--	--	12.970	--	--	
		1,200	1	--	--	--	0	0.6	--	0	1.3	--	--	--	--	--	--		
			2	--	--	--	0.3	0.2	--	0.2	0.4	--	--	--	--	--	--		
			3	--	--	--	0.3	0.3	--	0.3	0.6	--	--	--	--	--	--	--	
			4	--	--	--	0.4	0.5	--	0.4	0.9	--	--	--	--	--	--	--	
			5	--	--	--	0.2	1.3	7.1	1.3	2.7	7.5	11.6	--	--	12.974	--	--	
235		300	1	0	6.2	--	--	--	--	0	4.1	--	--	--	--	--	--		
			2	3.7	6.8	--	--	--	--	1.2	4.1	--	--	--	--	--	--	--	
			3	6.3	6.9	--	--	--	--	1.8	4.1	--	--	--	--	--	--	--	
			4	8.4	7.0	--	--	--	--	2.2	4.4	--	--	--	--	--	--	--	
			5	9.6	8.9	--	--	--	--	2.2	5.8	--	--	--	--	--	--	--	
			6	10.0	9.8	--	--	--	--	1.5	6.5	--	--	--	--	--	--	--	
			7	9.1	8.2	--	--	--	--	7.1	5.5	--	--	--	--	--	--	--	
			8	8.5	11.0	--	--	--	--	7.2	8.6	--	--	--	--	--	--	--	
			9	6.0	9.5	--	--	--	--	0	6.6	--	--	--	--	--	--	--	
			10	3.9	10.7	130.5	--	--	--	--	9.7	82.6	233.1	--	--	11.823	--	--	

Table 4-4: (page 4 of 10)
PRESSURANT REQUIREMENTS

Duty Cycle	Tank Pressure P.s.i.a.	Inlet Gas Temperature CR.	Burn No.	LF ₂ Tank Gas Weight - (lb)				LF ₂ Tank Gas Weight				Total Gas Weights		Usable Propellant Weight - (lb)						
				Repressurization	He Expulsion	Total	Repressurization	CH ₂ Expulsion	Total	Repressurization	Expulsion	Total	All He	He/CH ₂	All He	He/CH ₂				
		800	1	0	3.7	--	--	--	--	0	2.5	--	--	--	--	--	--			
			2	1.4	3.7	--	--	--	--	0.7	2.6	--	--	--	--	--	--	--		
			3	2.6	3.3	--	--	--	--	1.3	2.1	--	--	--	--	--	--	--	--	
			4	3.5	3.4	--	--	--	--	1.8	2.2	--	--	--	--	--	--	--	--	
			5	4.2	4.6	--	--	--	--	2.2	3.6	--	--	--	--	--	--	--	--	
			6	1	5.0	--	--	--	--	2.3	4.1	--	--	--	--	--	--	--	--	--
			7	4.4	4.0	--	--	--	--	2.3	3.1	--	--	--	--	--	--	--	--	--
			8	4.1	5.8	--	--	--	--	2.4	5.5	--	--	--	--	--	--	--	--	--
			9	2.3	4.9	--	--	--	--	1.8	3.9	--	--	--	--	--	--	--	--	--
			10	0.4	6.8	72.6	--	--	--	1.3	6.1	51.8	124.4	--	--	12.07	--	--	--	--
		1,200	1	0	3.2	--	--	--	--	0	2.3	--	--	--	--	--	--	--		
			2	0.9	3.5	--	--	--	--	0.5	2.3	--	--	--	--	--	--	--	--	
			3	1.6	2.7	--	--	--	--	0.9	1.6	--	--	--	--	--	--	--	--	--
			4	2.3	2.9	--	--	--	--	1.4	1.7	--	--	--	--	--	--	--	--	--
			5	2.8	4.2	--	--	--	--	1.7	2.7	--	--	--	--	--	--	--	--	--
			6	2.9	4.6	--	--	--	--	2.0	2.9	--	--	--	--	--	--	--	--	--
			7	2.7	3.3	--	--	--	--	2.1	2.1	--	--	--	--	--	--	--	--	--
			8	2.3	5.0	--	--	--	--	2.2	4.0	--	--	--	--	--	--	--	--	--
			9	0.3	4.3	--	--	--	--	2.0	2.9	--	--	--	--	--	--	--	--	--
			10	0	5.5	55.7	--	--	--	1.7	5.0	42.0	97.7	--	--	12.030	--	--	--	--
P	100	300	1	0	2.8	--	--	--	--	0	1.8	--	--	--	--	--	--	--	--	
			2	1.5	3.0	--	--	--	0.6	1.6	2.0	--	--	--	--	--	--	--	--	
			3	2.7	2.8	--	--	--	1.1	1.5	1.8	--	--	--	--	--	--	--	--	
			4	3.6	3.1	--	--	--	1.6	1.7	1.8	--	--	--	--	--	--	--	--	
			5	4.3	3.9	--	--	--	1.9	2.2	2.4	--	--	--	--	--	--	--	--	
			6	4.5	4.2	--	--	--	2.1	2.4	2.8	--	--	--	--	--	--	--	--	
			7	4.3	3.4	--	--	--	2.1	2.0	2.3	--	--	--	--	--	--	--	--	
			8	3.8	4.6	--	--	--	1.9	2.7	3.4	--	--	--	--	--	--	--	--	
			9	2.8	3.8	--	--	--	1.4	2.2	2.8	0	--	--	--	--	--	--	--	
			10	2.1	4.9	66.1	--	--	0.8	2.8	34.0	0	4.1	35.2	101.3	69.2	12.539	12.642	--	--
		800	1	0	1.7	--	--	--	--	0	1.2	--	--	--	--	--	--	--	--	
			2	0.6	1.8	--	--	--	0.2	0.9	1.2	--	--	--	--	--	--	--	--	
			3	1.1	1.5	--	--	--	0.3	0.8	0.9	--	--	--	--	--	--	--	--	
			4	1.5	1.5	--	--	--	0.5	0.8	0.9	--	--	--	--	--	--	--	--	
			5	1.9	2.0	--	--	--	0.6	1.1	1.3	--	--	--	--	--	--	--	--	

Table 4-41 (page 5 of 10)
PRESSURANT REQUIREMENTS

Duty Cycle	Tank Pressure p.s.i.a.	Inlet Gas Temperature °F.	Burst No.	LH ₂ Tank Gas Weight - (lb)						LF ₂ Tank Gas Weight				Total Gas Weight		Usable Propellant Weight - (lb)	
				Pressurization	He Expulsion	Total	Repressurization	GH ₂ Expulsion	Total	Repressurization	Expulsion	Total	All He	He/GH ₂	All He	He/GH ₂	
			6	2.0	2.1	--	0.6	1.2	--	1.0	1.4	--	--	--	--	--	--
			7	2.0	1.5	--	0.6	0.9	--	1.1	1.0	--	--	--	--	--	--
			8	1.9	2.2	--	0.5	1.3	--	1.2	1.7	--	--	--	--	--	--
			9	1.4	1.6	--	0.2	0.9	--	1.1	1.2	--	--	--	--	--	--
			10	1.1	2.1	31.5	0	1.2	13.5	1.0	2.9	20.6	52.1	34.1	12.654	12.678	
		1,200	1	0	1.3	--	0	0.8	--	0	1.1	--	--	--	--	--	--
			2	0.4	1.6	--	0.1	0.8	--	0.2	1.1	--	--	--	--	--	--
			3	0.7	1.2	--	0.2	0.6	--	0.4	0.7	--	--	--	--	--	--
			4	1.0	1.2	--	0.3	0.7	--	0.6	0.7	--	--	--	--	--	--
			5	1.2	1.8	--	0.3	1.0	--	0.7	1.1	--	--	--	--	--	--
			6	1.3	1.8	--	0.3	1.1	--	0.8	1.1	--	--	--	--	--	--
			7	1.4	1.2	--	0.3	0.7	--	0.9	0.8	--	--	--	--	--	--
			8	1.2	1.8	--	0.2	1.1	--	1.0	1.4	--	--	--	--	--	--
			9	0.8	1.3	--	0	0.8	--	1.0	1.0	--	--	--	--	--	--
			10	0.5	1.6	23.3	0	0.8	10.1	0.9	1.8	17.3	40.6	27.4	12.676	12.672	
P	P	300	1	--	--	--	0	0.6	--	0	1.3	--	--	--	--	--	--
			2	--	--	--	0.6	0.7	--	0.2	1.3	--	--	--	--	--	--
			3	--	--	--	1.0	0.6	--	0.3	1.1	--	--	--	--	--	--
			4	--	--	--	1.2	0.7	--	0.5	1.2	--	--	--	--	--	--
			5	--	--	--	1.5	0.8	--	0.5	1.4	--	--	--	--	--	--
			6	--	--	--	1.5	0.8	--	0.4	1.6	--	--	--	--	--	--
			7	--	--	--	1.4	0.7	--	0.2	1.4	--	--	--	--	--	--
			8	--	--	--	1.0	0.9	--	0.2	1.9	--	--	--	--	--	--
			9	--	--	--	0.5	0.8	--	0	1.6	--	--	--	--	--	--
			10	--	--	--	0.1	0.8	16.3	0	2.2	17.3	33.6	12.891			
		800	1	--	--	--	0	0.3	--	0	0.8	--	--	--	--	--	--
			2	--	--	--	0.2	0.3	--	0.2	0.8	--	--	--	--	--	--
			3	--	--	--	0.4	0.3	--	0.3	0.6	--	--	--	--	--	--
			4	--	--	--	0.5	0.3	--	0.4	0.6	--	--	--	--	--	--
			5	--	--	--	0.6	0.4	--	0.6	0.8	--	--	--	--	--	--
			6	--	--	--	0.6	0.4	--	0.6	0.8	--	--	--	--	--	--
			7	--	--	--	0.5	0.4	--	0.5	0.6	--	--	--	--	--	--
			8	--	--	--	0.4	0.5	--	0.7	1.0	--	--	--	--	--	--
			9	--	--	--	0.4	0.3	--	0.6	0.7	--	--	--	--	--	--
			10	--	--	--	0.5	0.4	7.7	0.6	1.0	12.3	20.0	12.915			

Table 4-41 (page 6 of 10)
PRESSURANT REQUIREMENTS

Duty Cycle	Tank Pressure P.s.i.a.	Inlet Gas Temperature °K.	Burn No.	LiH ₂ Tank Gas Weight - (lb)						LF ₂ Tank Gas Weight				Total Gas Weights		Usable Propellant Weight - (lb)	
				Repressurization	He Expulsion	Total	Repressurization	GH ₂ Expulsion	Total	Repressurization	Expulsion	Total	All He	He/GH ₂	All He	He/GH ₂	
																	Repressurization
		1,200	1	--	--	--	0	0.3	--	--	0	0.7	--	--	--	--	--
			2	--	--	--	0.2	0.3	--	--	0.1	0.7	--	--	--	--	--
			3	--	--	--	0.2	0.2	--	--	0.2	0.4	--	--	--	--	--
			4	--	--	--	0.3	0.3	--	--	0.3	0.4	--	--	--	--	--
			5	--	--	--	0.4	0.4	--	--	0.4	0.6	--	--	--	--	--
			6	--	--	--	0.4	0.4	--	--	0.5	0.6	--	--	--	--	--
			7	--	--	--	0.3	0.3	--	--	0.6	0.5	--	--	--	--	--
			8	--	--	--	0.2	0.4	--	--	0.6	0.8	--	--	--	--	--
			9	--	--	--	0.3	0.3	--	--	0.6	0.6	--	--	--	--	--
			10	--	--	--	0.3	0.3	--	--	0.6	1.0	--	--	10.2	16.0	12,917
	235	300	1	0	6.2	--	--	--	--	--	0	4.1	--	--	--	--	--
			2	3.7	1.4	--	--	--	--	--	1.2	0.8	--	--	--	--	--
			3	3.8	1.4	--	--	--	--	--	0.9	0.9	--	--	--	--	--
			4	3.8	1.5	--	--	--	--	--	0.7	0.9	--	--	--	--	--
			5	3.8	1.5	--	--	--	--	--	0.6	0.9	--	--	--	--	--
			6	3.8	1.5	--	--	--	--	--	0.5	0.9	--	--	--	--	--
			7	3.7	1.5	--	--	--	--	--	0.5	1.0	--	--	--	--	--
			8	3.6	1.5	--	--	--	--	--	0.4	1.0	--	--	--	--	--
			9	3.5	1.6	--	--	--	--	--	0.4	1.0	--	--	--	--	--
			10	3.4	1.7	--	--	--	--	--	0.4	1.0	--	--	--	--	--
			11	3.2	1.7	--	--	--	--	--	0.4	1.0	--	--	--	--	--
			12	2.1	23.4	--	--	--	--	--	0.2	13.4	--	--	--	--	--
			13	8.6	5.4	--	--	--	--	--	2.9	3.7	--	--	--	--	--
			14	6.9	5.9	--	--	--	--	--	1.4	4.1	--	--	--	--	--
			15	5.2	6.1	--	--	--	--	--	0.4	4.3	--	--	--	--	--
			16	3.6	6.2	--	--	--	--	--	0	4.9	--	--	--	--	--
			17	2.1	6.4	--	--	--	--	--	0	4.9	--	--	--	--	--
			18	0.8	6.6	--	--	--	--	--	0	4.7	--	--	--	--	--
			19	0	4.8	151.0	--	--	--	--	0	3.1	67.5	218.5	11,792	--	--
P	100	300	1	0	2.8	--	0	1.4	--	--	0	1.9	--	--	--	--	--
			2	1.6	0.6	--	0.6	0.3	--	--	0.5	0.4	--	--	--	--	--
			3	1.7	0.6	--	0.7	0.3	--	--	0.4	0.4	--	--	--	--	--
			4	1.7	0.6	--	0.8	0.3	--	--	0.3	0.4	--	--	--	--	--
			5	1.8	0.6	--	0.8	0.3	--	--	0.2	0.4	--	--	--	--	--
			6	1.8	0.7	--	0.9	0.4	--	--	0.2	0.4	--	--	--	--	--

Table 4-41 (page 7 of 10)
PRESSURANT REQUIREMENTS

Duty Cycle	Tank Pressure p.s.i.a.	Inlet Gas Temperature OR.	Burn No.	LH ₂ Tank Gas Weight - (lb)				LF ₂ Tank Gas Weight				Total Gas Weight		Usable Propellant Weight - (lb)		
				Repressur-isation	He Expulsion	Total	Repressur-isation	GH ₂ Expulsion	Total	Repressur-isation	Expulsion	Total	All He	He/GH ₂	All He	He/GH ₂
			7	1.8	0.7	--	1.0	0.4	--	0.2	0.4	--	--	--	--	--
			8	1.8	0.7	--	1.0	0.4	--	0.2	0.4	--	--	--	--	--
			9	1.7	0.7	--	1.1	0.4	--	0.2	0.4	--	--	--	--	--
			10	1.7	0.7	--	1.1	0.4	--	0.2	0.4	--	--	--	--	--
			11	1.7	0.7	--	1.1	0.4	--	0.15	0.4	--	--	--	--	--
			12	0.8	10.2	--	0.9	5.5	--	0.04	6.0	--	--	--	--	--
			13	3.1	2.3	--	1.6	1.4	--	1.1	1.5	--	--	--	--	--
			14	2.5	2.5	--	1.4	1.5	--	0.6	1.6	--	--	--	--	--
			15	1.8	2.5	--	1.1	1.5	--	0.2	1.8	--	--	--	--	--
			16	1.3	2.5	--	0.7	1.6	--	0	2.0	--	--	--	--	--
			17	0.7	2.6	--	0	2.2	--	0	2.0	--	--	--	--	--
			18	0.2	2.4	--	0	1.4	--	0	1.7	--	--	--	--	--
			19	0	1.9	64.0	0	1.1	36.0	0	1.2	28.2	92.2	64.2	12,532	12,622
		800	1	0	1.7	--	0	0.9	--	0	1.2	--	--	--	--	--
			2	0.6	0.4	--	0.2	0.2	--	0.3	0.2	--	--	--	--	--
			3	0.7	0.4	--	0.2	0.2	--	0.3	0.2	--	--	--	--	--
			4	0.7	0.4	--	0.2	0.2	--	0.3	0.2	--	--	--	--	--
			5	0.8	0.4	--	0.3	0.2	--	0.3	0.2	--	--	--	--	--
			6	0.8	0.4	--	0.3	0.2	--	0.3	0.2	--	--	--	--	--
			7	0.9	0.4	--	0.3	0.2	--	0.3	0.2	--	--	--	--	--
			8	0.9	0.4	--	0.3	0.2	--	0.3	0.3	--	--	--	--	--
			9	0.9	0.4	--	0.3	0.3	--	0.3	0.3	--	--	--	--	--
			10	0.9	0.4	--	0.3	0.2	--	0.3	0.2	--	--	--	--	--
			11	0.9	0.4	--	0.3	0.2	--	0.3	0.2	--	--	--	--	--
			12	0.7	6.0	--	0.3	3.2	--	0.3	3.5	--	--	--	--	--
			13	1.3	1.2	--	0.4	0.7	--	1.0	0.8	--	--	--	--	--
			14	1.1	1.2	--	0.3	0.8	--	1.0	0.9	--	--	--	--	--
			15	0.8	1.2	--	0.1	0.8	--	0.9	0.9	--	--	--	--	--
			16	0.6	1.2	--	0	0.8	--	0.7	1.0	--	--	--	--	--
			17	1.3	1.3	--	0	0.8	--	0.6	1.0	--	--	--	--	--
			18	1.4	1.4	--	0	0.8	--	0.5	1.0	--	--	--	--	--
			19	0	1.0	33.5	0	0.5	15.3	0.3	0.7	21.5	59.0	36.8	12,613	12,616

Table 4-41 (page 8 of 10)

PRESSURANT REQUIREMENTS

Duty Cycle	Tank Pressure p.s.i.a.	Inlet Gas Temperature °K.	Burn No.	LH ₂ Tank Gas Weight - (lb)				LF ₂ Tank Gas Weight				Total Gas Weight		Usable Propellant Weight - (lb)		
				Repressurization	He Expulsion	Total	Repressurization	GH ₂ Expulsion	Total	Repressurization	Expulsion	Total	All He	He/GH ₂	All He	He/GH ₂
		1,200	1	0	1.5	--	0	0.8	--	0	1.1	--	--	--	--	--
			2	0.4	0.3	--	0.1	0.2	--	0.2	0.2	--	--	--	--	--
			3	0.5	0.3	--	0.1	0.2	--	0.2	0.2	--	--	--	--	--
			4	0.5	0.3	--	0.1	0.2	--	0.2	0.2	--	--	--	--	--
			5	0.5	0.3	--	0.2	0.2	--	0.3	0.2	--	--	--	--	--
			6	0.6	0.3	--	0.2	0.2	--	0.5	0.2	--	--	--	--	--
			7	0.6	0.3	--	0.1	0.2	--	0.3	0.2	--	--	--	--	--
			8	0.6	0.4	--	0.2	0.2	--	0.3	0.2	--	--	--	--	--
			9	0.6	0.4	--	0.2	0.2	--	0.3	0.2	--	--	--	--	--
			10	0.6	0.4	--	0.2	0.2	--	0.3	0.2	--	--	--	--	--
			11	0.6	0.4	--	0.2	0.2	--	0.3	0.2	--	--	--	--	--
			12	0.5	5.5	--	0.2	2.8	--	0.3	3.2	--	--	--	--	--
			13	0.7	1.0	--	0.1	0.7	--	0.8	0.7	--	--	--	--	--
			14	0.5	1.3	--	0	0.7	--	0.8	0.7	--	--	--	--	--
			15	0.3	1.1	--	0	0.7	--	0.8	0.8	--	--	--	--	--
			16	0.1	1.1	--	0	0.7	--	0.7	0.9	--	--	--	--	--
			17	0	1.1	--	0	0.7	--	0.7	1.0	--	--	--	--	--
			18	0	1.2	--	0	0.7	--	0.5	0.8	--	--	--	--	--
			19	0	1.0	25.8	0	0.5	12.3	0.3	0.6	19.5	45.3	31.8	12,622	12,611
L	Pump	300	1	--	--	--	0	0.6	--	0	1.3	--	--	--	--	--
			2	--	--	--	0.6	0.13	--	0.22	0.25	--	--	--	--	--
			3	--	--	--	0.62	0.14	--	0.16	0.25	--	--	--	--	--
			4	--	--	--	0.65	0.14	--	0.13	0.25	--	--	--	--	--
			5	--	--	--	0.66	0.14	--	0.11	0.25	--	--	--	--	--
			6	--	--	--	0.67	0.14	--	0.10	0.25	--	--	--	--	--
			7	--	--	--	0.67	0.14	--	0.09	0.25	--	--	--	--	--
			8	--	--	--	0.67	0.15	--	0.09	0.25	--	--	--	--	--
			9	--	--	--	0.66	0.16	--	0.09	0.25	--	--	--	--	--
			10	--	--	--	0.64	0.16	--	0.87	0.25	--	--	--	--	--
			11	--	--	--	0.63	0.16	--	0.86	0.25	--	--	--	--	--
			12	--	--	--	0	2.24	--	0	3.92	--	--	--	--	--
			13	--	--	--	0.3	0.52	--	0.51	0.89	--	--	--	--	--
			14	--	--	--	0.03	0.52	--	0.25	0.95	--	--	--	--	--
			15	--	--	--	0	0.51	--	0.08	1.00	--	--	--	--	--
			16	--	--	--	0	0.51	--	0	1.00	--	--	--	--	--

Table 4-41 (page 9 of 10)

PRESSURANT REQUIREMENTS

Duty Cycle	Tank Pressure p.s.i.a.	Inlet Gas Temperature °f.	Burn No.	LH ₂ Tank Gas Weight - (lb)			LF ₂ Tank Gas Weight			Total Gas Weight		Usable Propellant Weight - (lb)	
				Repressurization	He Expulsion	Total	Repressurization	CH ₂ Expulsion	Total	All He	He/CH ₂	All He	He/CH ₂
			17	--	--	--	0	0.54	--	0	1.07	--	--
			18	--	--	--	1.39	0.48	--	0.33	1.01	--	--
			19	--	--	--	0.41	0.43	16.4	0.40	0.74	18.6	35.0
		800	1	--	--	--	0	0.30	--	0	0.81	--	--
			2	--	--	--	0.22	0.07	--	0.16	0.15	--	--
			3	--	--	--	0.24	0.07	--	0.17	0.15	--	--
			4	--	--	--	0.26	0.07	--	0.17	0.15	--	--
			5	--	--	--	0.28	0.07	--	0.17	0.15	--	--
			6	--	--	--	0.28	0.07	--	0.18	0.15	--	--
			7	--	--	--	0.31	0.07	--	0.18	0.15	--	--
			8	--	--	--	0.32	0.07	--	0.18	0.15	--	--
			9	--	--	--	0.33	0.08	--	0.18	0.15	--	--
			10	--	--	--	0.33	0.08	--	0.28	0.15	--	--
			11	--	--	--	0.33	0.08	--	0.18	0.15	--	--
			12	--	--	--	0.10	1.26	--	0.16	2.20	--	--
			13	--	--	--	0	0.27	--	0.6	0.46	--	--
			14	--	--	--	0.38	0.28	--	0.55	0.51	--	--
			15	--	--	--	0.19	0.28	--	0.50	0.52	--	--
			16	--	--	--	0.42	0.28	--	0.46	0.55	--	--
			17	--	--	--	0.50	0.28	--	0.37	0.57	--	--
			18	--	--	--	0.52	0.27	--	0.29	0.57	--	--
			19	--	--	--	0.56	0.20	9.70	0.16	0.44	12.85	22.55
		1,200	1	--	--	--	0	0.26	--	0	0.71	--	--
			2	--	--	--	0.14	0.06	--	0.12	0.14	--	--
			3	--	--	--	0.16	0.06	--	0.13	0.13	--	--
			4	--	--	--	0.17	0.06	--	0.14	0.13	--	--
			5	--	--	--	0.19	0.06	--	0.15	0.13	--	--
			6	--	--	--	0.19	0.06	--	0.15	0.13	--	--
			7	--	--	--	0.21	0.07	--	0.16	0.13	--	--
			8	--	--	--	0.21	0.07	--	0.17	0.13	--	--
			9	--	--	--	0.22	0.07	--	0.17	0.13	--	--
			10	--	--	--	0.22	0.07	--	0.18	0.13	--	--

Table 4-41 (page 10 of 10)

PRESSURANT REQUIREMENTS

Duty Cycle	Tank Pressure P.s.i.a.	Inlet Gas Temperature °K.	Burn No.	LH ₂ Tank Gas Weight - (lb)				LF ₂ Tank Gas Weight			Total Gas Weight		Usable Propellant Weight - (lb)			
				Repressurization	He Expulsion	Total	Repressurization	GH ₂ Expulsion	Total	Repressurization	Expulsion	Total	All He	He/GH ₂	All He	He/GH ₂
			11	--	--	--	0.22	0.07	--	0.18	0.13	--	--	--	--	--
			12	--	--	--	0.07	1.13	--	0.16	1.92	--	--	--	--	--
			13	--	--	--	0.23	0.23	--	0.48	0.39	--	--	--	--	--
			14	--	--	--	0.10	0.23	--	0.47	0.42	--	--	--	--	--
			15	--	--	--	0.25	0.23	--	0.45	0.45	--	--	--	--	--
			16	--	--	--	0.28	0.23	--	0.42	0.48	--	--	--	--	--
			17	--	--	--	0.34	0.23	--	0.38	0.51	--	--	--	--	--
			18	--	--	--	0.32	0.22	--	0.3	0.48	--	--	--	--	--
			19	--	--	--	0.38	0.17	7.5	0.20	0.36	11.4	--	18.9	--	12.840
F	Pump	800	1	--	--	--	0	4.80	--	0	7.00	--	--	--	--	--
			2	--	--	--	0.46	0.84	6.10	0.98	1.56	9.54	--	15.64	--	12.922
A			1	--	--	--	0	4.80	--	0	7.00	--	--	--	--	--
			2	--	--	--	0.45	0.84	6.09	1.10	1.56	9.66	--	15.75	--	12.947

values were extracted from table 4-41 and summarized in table 4-42. These apply to an inlet gas temperature of 300°R. It should be noted that duty cycles I, J, K, and L are 14-day missions. C is a 1-day and D is a 5-day mission. The gas requirements for expulsion are relatively constant, while the repressurization gas weight depends on the number of burns and the distribution of the expulsions. This is shown by comparing the two 2-burn cases, J and K. The repressurization gas weights for a 10- and 19-burn mission do not greatly differ, while the differences between a 2- and 5-burn and 5- and 10-burn are large. This is probably a result of the different venting for the various cases. Duty cycle L required significant venting. Examination of table 4-41 shows that GH₂ pressurization of the LH₂ tank nearly always results in lower total pressurant requirements as well as high usable propellant weight capabilities (figure 4-120). The effects of inlet gas temperature on required weight of pressurant are also evident. Higher temperatures result in lower gas weight, although the reduction in weight diminishes rapidly with increasing temperature. Of greater importance, however, is the effect on overall stage usable propellant. This is shown in figures 4-121 and 4-122 for pressure-fed and pump-fed systems. In most cases, there is relatively little performance gain in going to high inlet gas temperatures; in fact, there may be a performance loss.

For example, for an optimized pump-fed system designed for the most difficult duty cycle (cycle K, in this instance), the optimum inlet gas temperature would be approximately 300 to 400°R. Similarly, for a 100 p. s. i. a. pressure-fed system, the optimum inlet gas temperature would be approximately 600°R., while for 235 p. s. i. a. the optimum might be as high as 800°R.

The data presented in figures 4-121 and 4-122 do not include weight increases that would be needed in the tank structure. The tankage is normally designed to take advantage of the increased material strength at cryogenic temperatures. Therefore, the higher temperature environment would mean an increased tank wall thickness or the addition of internal tank wall insulation, with a structural weight increase.

Outputs from the H225 computer program indicate that the wall temperature increases significantly during expulsion, particularly in the vicinity of the upper tank dome. Time did not permit a detailed study of this problem; however, it appears that inlet gas temperatures in the area of 300°R. would, in general, be optimum for multiburn long-duration cryogenic stages.

Table 4-42
 COMPARISON OF PRESSURANT REQUIREMENTS
 LB. OF GAS

Duty Cycle	P _T = 235 PSIA			P _T = 100 PSIA			Pump		
	Repressurization	Expulsion	Total	Repressurization	Expulsion	Total	Repressurization	Expulsion	Total
I	0	79.8	79.8	0	36.4	36.4	0	21.6	21.6
J	8.6	89.9	98.5	2.9	39.4	42.3	1.3	21.1	22.4
K	12.1	83.9	96.0	3.1	37.0	40.1	1.5	21.3	22.8
C	24.8	94.2	119.0	11.0	38.6	49.6	6.9	19.8	26.7
D				23.5	45.7	69.2	11.2	22.4	33.6
L				19.3	44.9	64.2	12.9	22.1	35.0

CH₂ Pressurization of LH₂ Tank
 He Pressurization of LF₂ Tank
 Inlet Gas Temperature = 300°R.

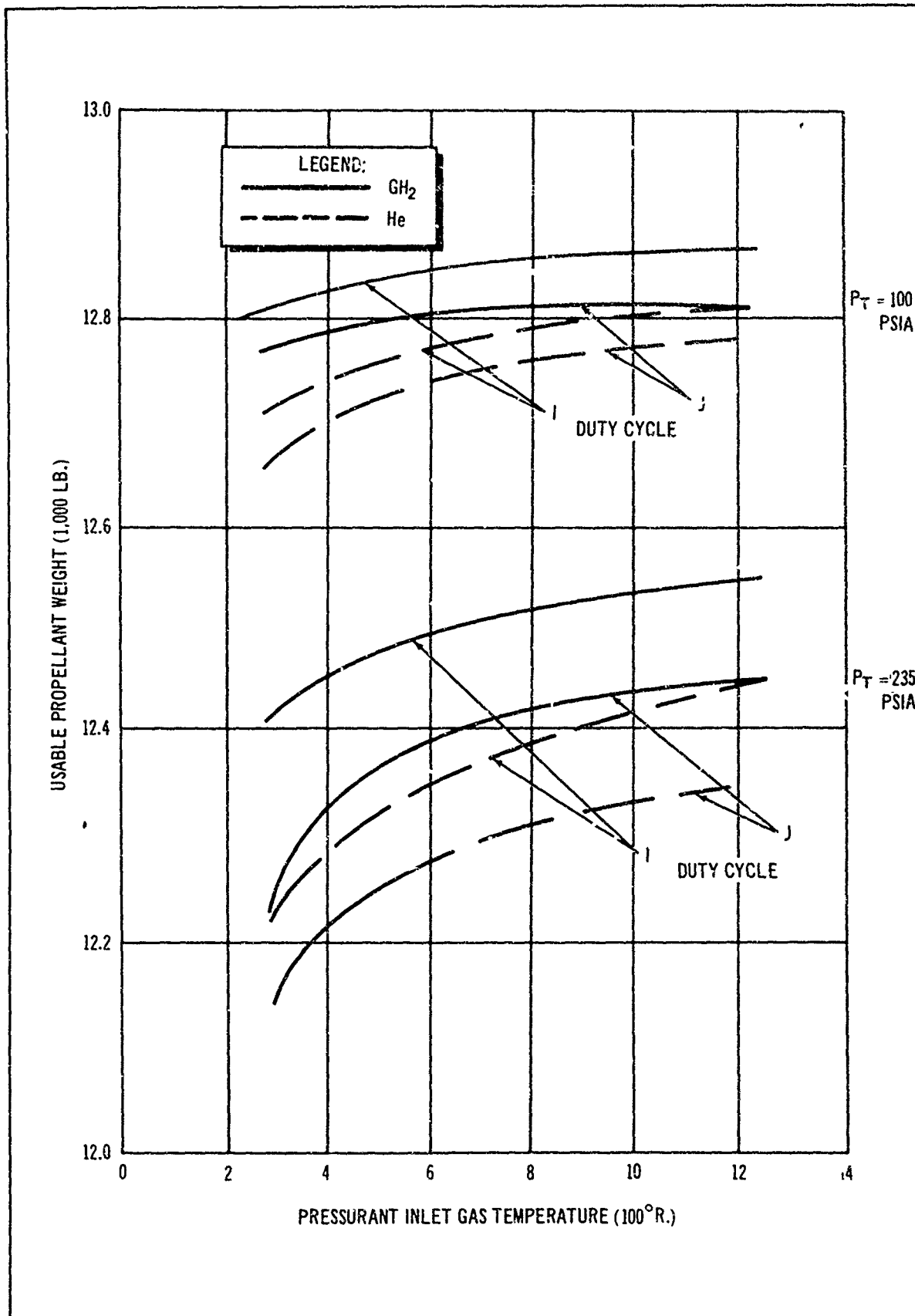


Figure 4-120. Effect of LH_2 Tank Pressurant on Stage Performance

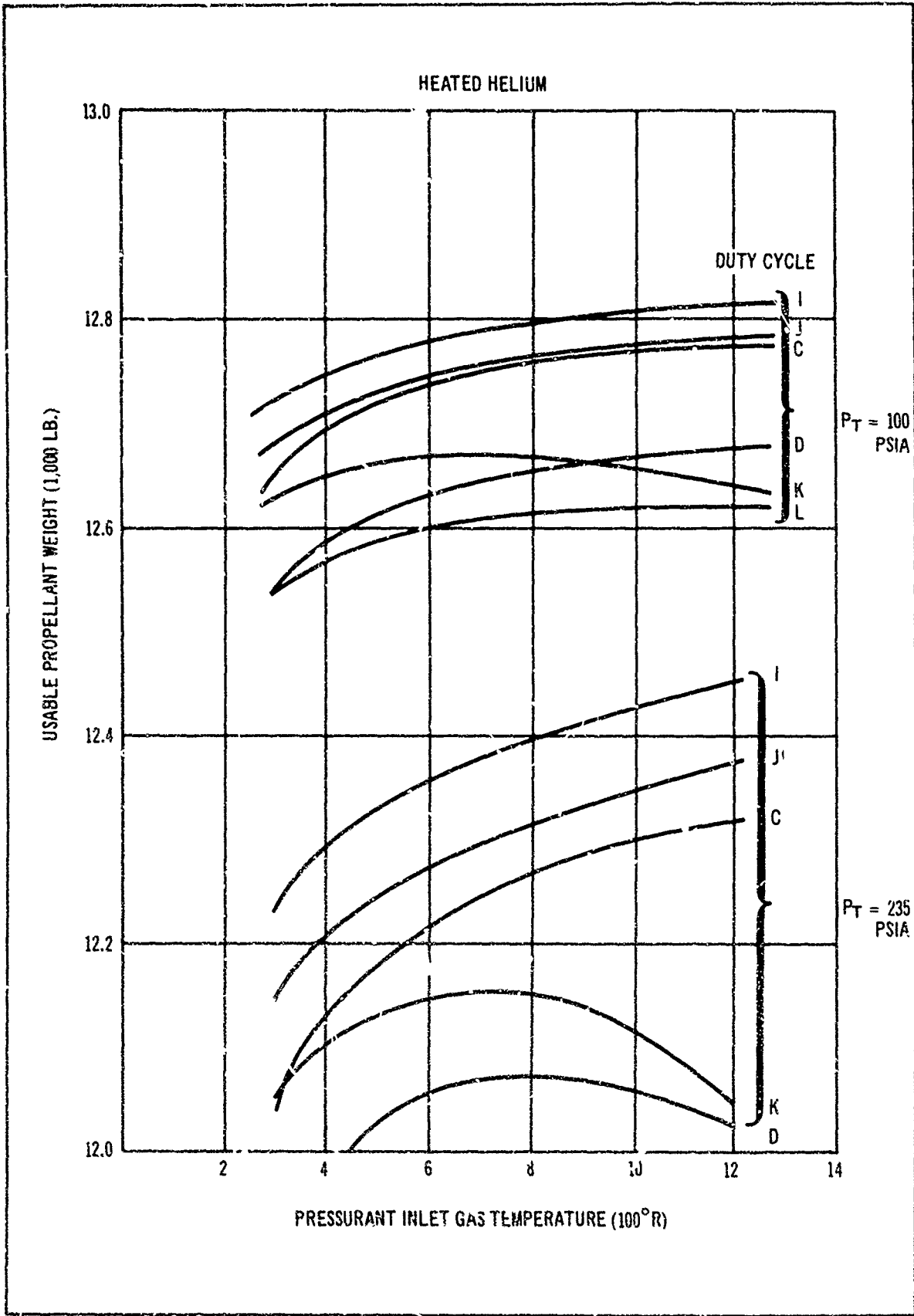


Figure 4-121. Effect of Pressurant Inlet Temperature on Performance of Pressure-Fed System

Heated GH_2 for Lita Tank
 " He. for LP Tank

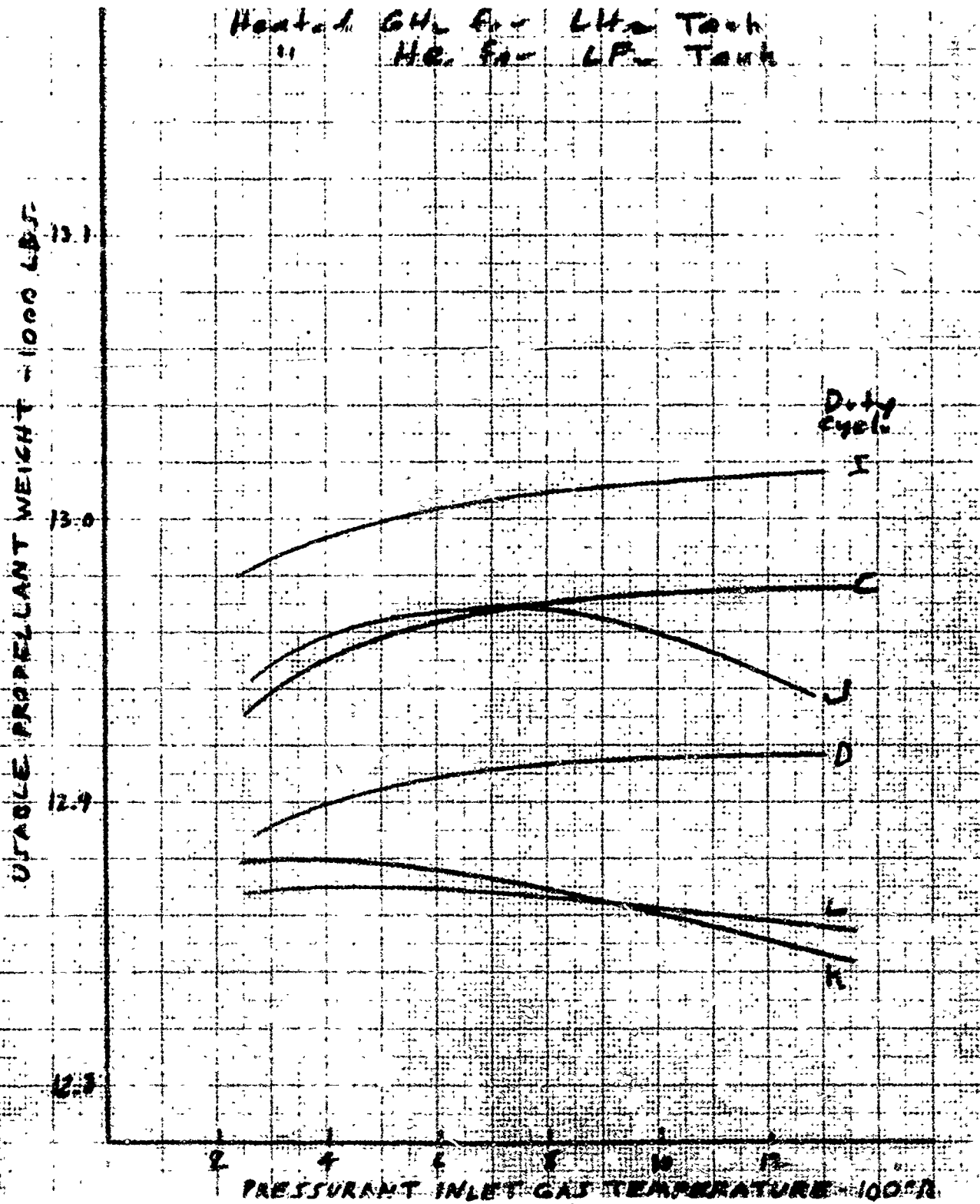


Figure 4-122. Effect of Pressurant Inlet Temperature on Performance of Pump-Fed System

8. Phase VIII--Test Apparatus Design and Fabrication. The previous seven study phases of this program defined many design features and parameters for a hypothetical LF_2/LH_2 space propulsion system. This was accomplished by performing analytical studies based on theoretical models and with limited small-scale experimental data from various unrelated programs. The validity of the conclusions reached are, therefore, strongly dependent upon the adequacy of the mathematical models and experimental data which were used.

A test apparatus was designed and fabricated for use at the EAFB space-simulation facility, which would provide data to correlate these analytical models, and to evaluate the concepts recommended to the extent possible in a structurally static one-g. space simulation facility. The problem areas which can be most readily evaluated by such testing include principally the steady state thermal performance of the propellant thermal protection concept and the thermodynamic performance of the tank pressurization system. Other problems such as liquid free zero-g. venting, tank pressure buildup during low gravity coast, and propellant tank pressure collapse following engine shutdown in zero-g. cannot be reasonably evaluated in a ground based test facility. The study of such problems must await a large-scale cryogenic space experiment. Therefore, the test apparatus was designed primarily to generate information on the steady-state heat transfer characteristics of the propellant storage system and of the parametric performance of the tank pressurization system.

To minimize scaling problems, it was decided at the beginning of the contract to design a full-scale, but nonflight weight, test article. This was to duplicate, as closely as possible, all the basic features of the flight type propellant storage and feed system including both propellant tanks, the structural shroud or shell, tank supporting structure, propellant feed and vent plumbing, pressurization system (using He and/or GH_2) and a high performance space insulation system. Further, the system was designed to permit variations in propellant flow rate, tank pressure, and pressurant inlet gas temperature, all with remote setting and control provisions. Of course, with a complex test article of this type it became necessary to make design compromises relative to simulating a flight system. These compromises arose from primarily four sources: (1) limitations imposed by safety requirements, (2) limitations imposed by cost restraints, (3) provisions for instrumentation, and (3) the necessity of ease of servicing. For example, facility limitations resulted in very heavy-walled tankage which was reflected throughout the entire system. Budgetary restraints were imposed primarily in componentry where development of new hardware items had to be held to a minimum. The general approach taken was to continually strive to duplicate a real system but to make those compromises that were essential, and to attempt to either minimize their influence on the system behavior or to provide instrumentation which would account for their influence as much as possible.

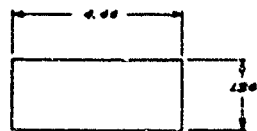
a. Sizing and Structural Design. Design of the test apparatus was started at the beginning of the contract with the first task the sizing of the pressurant storage bottles. Pressurant storage bottle volume had to be accounted for

in sizing the LH₂ tank so that a net LH₂ volume of 214.6 ft.³ would be maintained. Pressurant requirements were evaluated through approximate analysis techniques for a tank pressure of 250 p. s. i. a. and it was determined that 312 lb. of He were required for both LH₂ and LN₂ tank pressurization and that 33.5 lb. of LH₂ were needed to pressurize the LH₂ tank. A 3,000 p. s. i. a. pressure and a -420°F. temperature produces a helium volume of 26 ft.³ and a LH₂ volume of 7.5 ft.³. It was therefore decided to store the He in two 3,000 p. s. i. a. cylindrical bottles and the LH₂ in a single cylindrical bottle. Each of the three bottles is 23 in. in diameter. This size was selected to limit the manhole size in the tank, and because of the need for internal clearance. The two He bottles are 81 in. long and the auxiliary LH₂ tank is 51 in. long. Type 304 stainless steel was used as the material for the pressurant bottles because of good strength at cryogenic temperature, ease in forming and welding, and availability. A yield factor of safety of 1.5 and an ultimate factor of safety of 3 on the limit pressure of 3,000 p. s. i. required a sheet thickness of 1.5 in. The fabrication and proof testing of these tanks, per Douglas drawings, was subcontracted to FanSteel of Torrance, Calif.

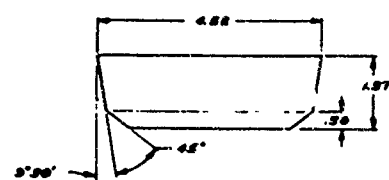
The He and auxiliary LH₂ bottles were positioned vertically inside the LH₂ tank. Fittings welded to the steel tanks rested on a beam structure across the bottom of the tank which had one end fixed and the other end floating to permit expansion/contraction. Steel straps with turnbuckles secured the bottles to the LH₂ tank wall.

At that point it was possible to size and design the propellant tankage. To reduce cost, it was decided to make the LN₂ and LH₂ tank bulkheads identical in both size and configuration. The bulkheads are nearly spherical. The LN₂ tank has a diameter of 74 in. and a length of 81 in. and the LH₂ tank has a diameter of 74 in. and a length of about 140 in. Type 6061-T6 aluminum alloy was chosen for the propellant tank material because of its good cryogenic strength, because it can be easily formed and welded, and because it is readily available. At 250 p. s. i. a. the required wall thickness is 1.0 in. It was originally planned to spin the tank domes in one piece, but it was found that the required circular blank would not be available in time. It was therefore necessary to go to a six gore dome design with the cylindrical sections formed from one piece with a single longitudinal weld. Manholes of 31 in. and 18 in. were provided in the LH₂ and LN₂ tank. These are sealed with a Creavey O-ring type of seal. After studying the fabrication problems, it was decided to subcontract fabrication and proof testing of the LN₂ and LH₂ tanks, per Douglas drawings, to FanSteel.

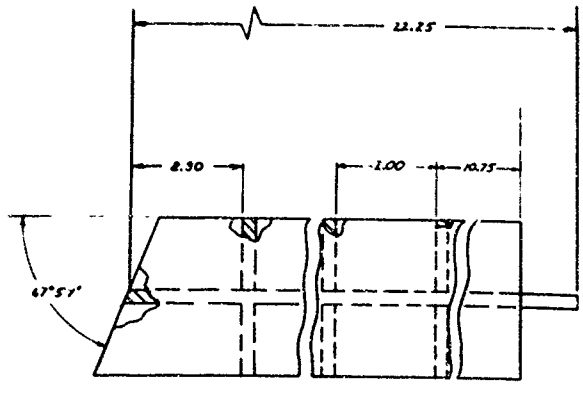
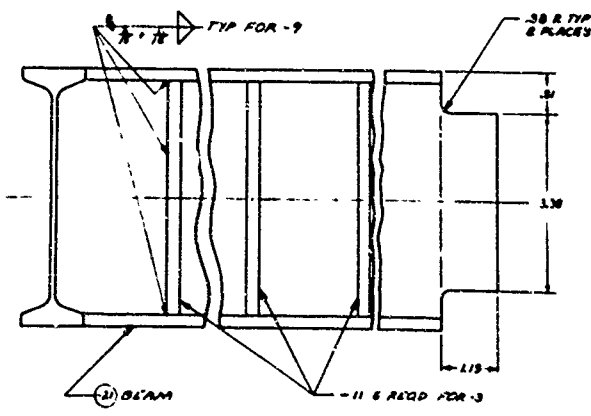
Douglas fabricated the tank penetration (including the top penetration cross which facilitates venting, pressurization and electrical feed-throughs, the outlet elbows) and the pressurization-line penetration section into the LH₂ tank. These were sent to FanSteel where they were installed and welded prior to proof-testing. Figure 4-123 shows the details of the LH₂ tank assembly. Figure 4-124 shows a photograph of the completed LN₂ tank with the mounted tank shutoff valve.



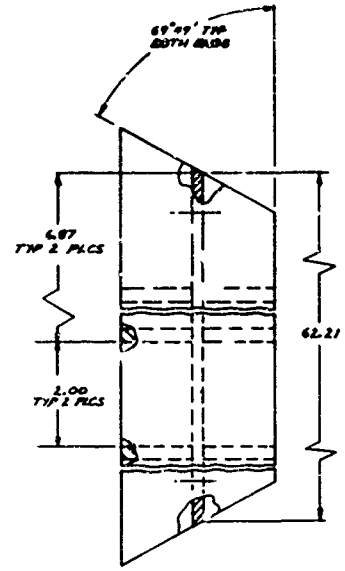
DETAIL -8
SCALE 1/1



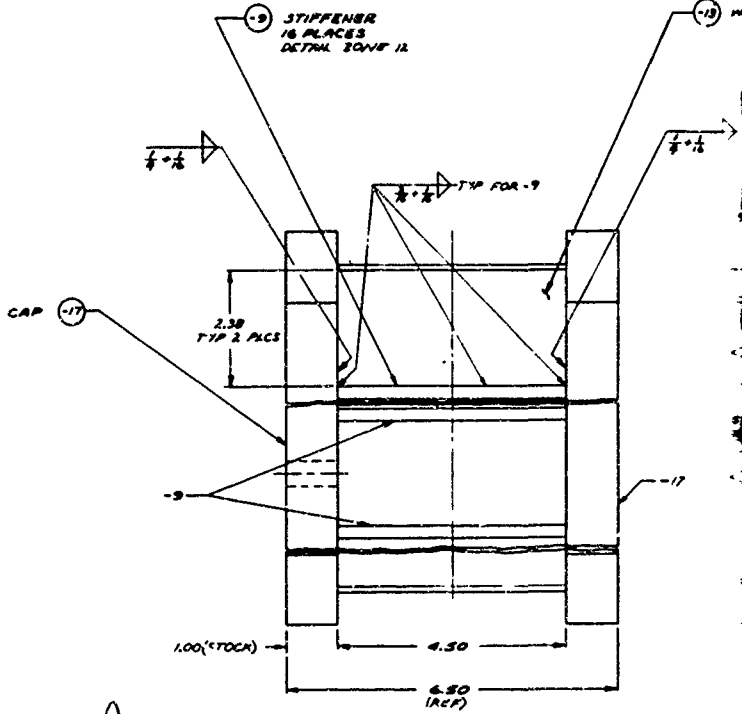
DETAIL -11
SCALE 1/1



-8 WELD ASSEMBLY
SCALE 1/1



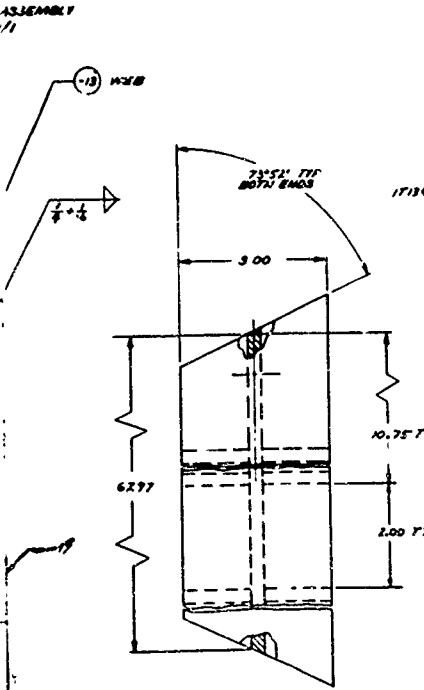
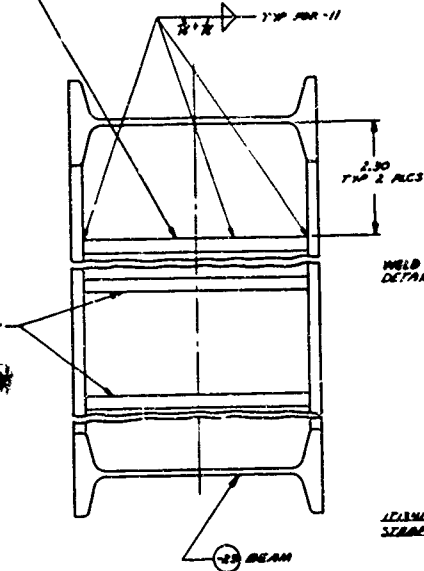
-7 WELD ASSEMBLY
SCALE 1/1



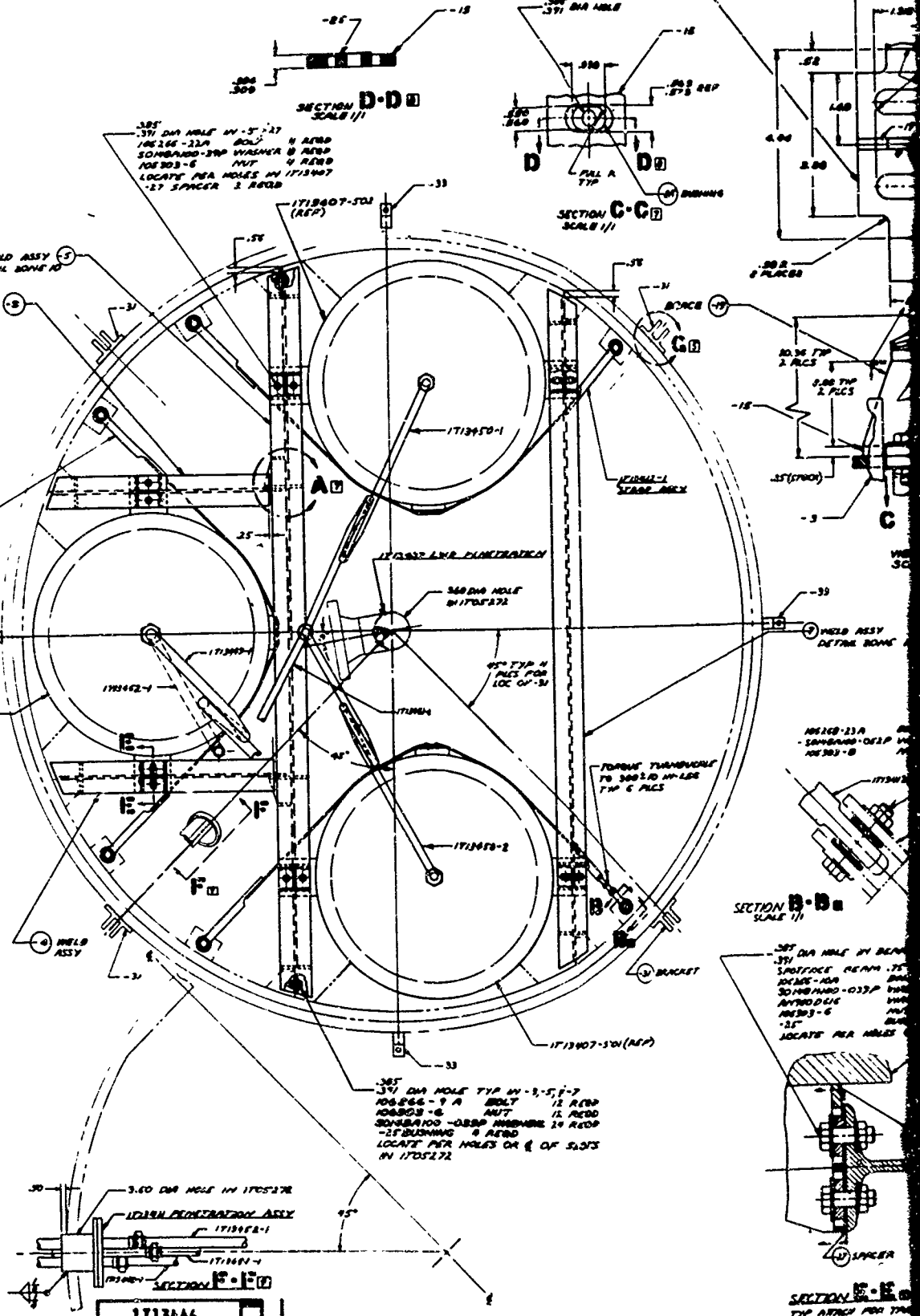
-5 WELD ASSEMBLY
SCALE 1/1

A

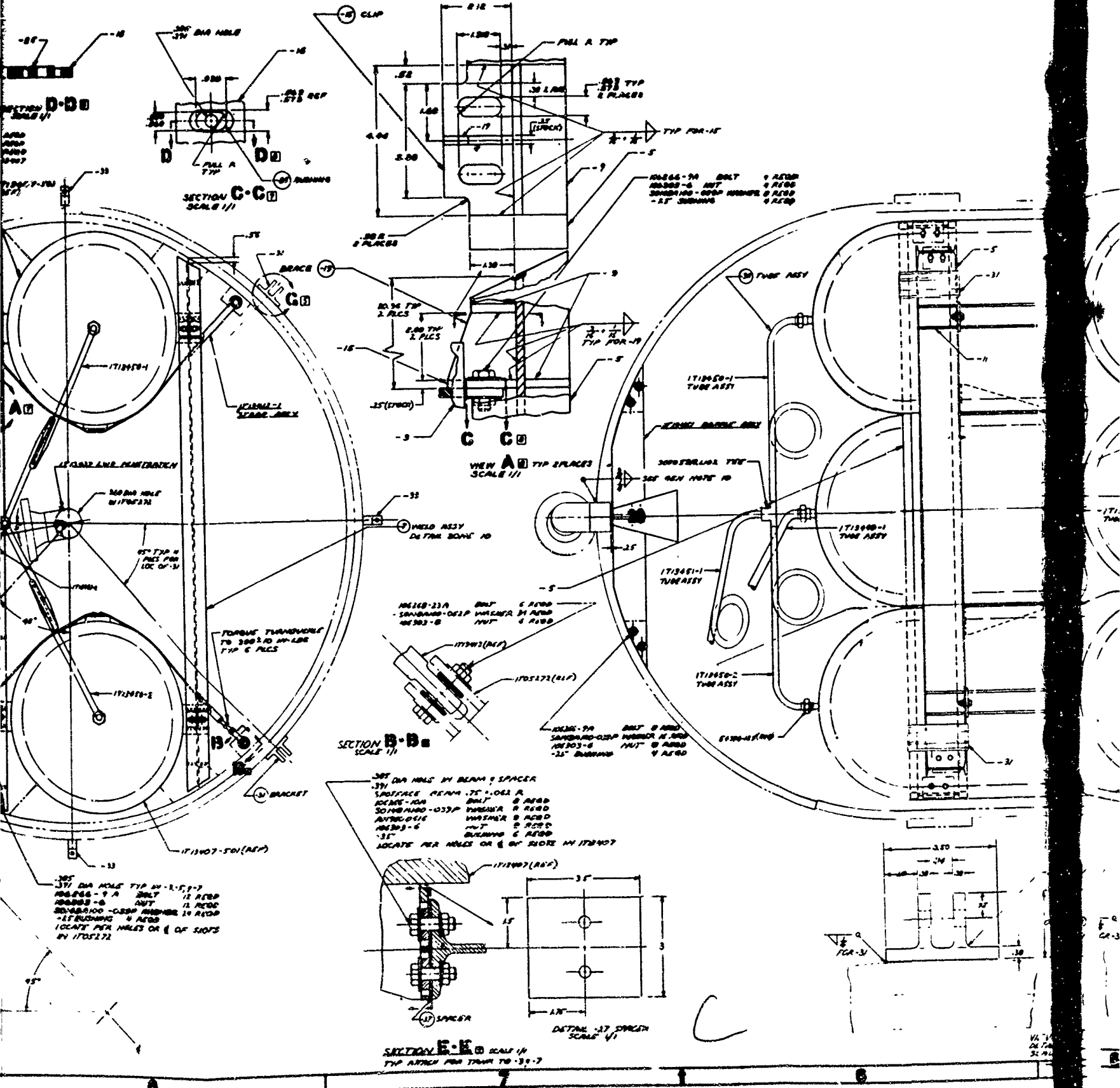
STIFFENER
12 ACOD PDA-7
DETAL SCOM 12



WELD ASSEMBLY
ALC 1/1



1713446



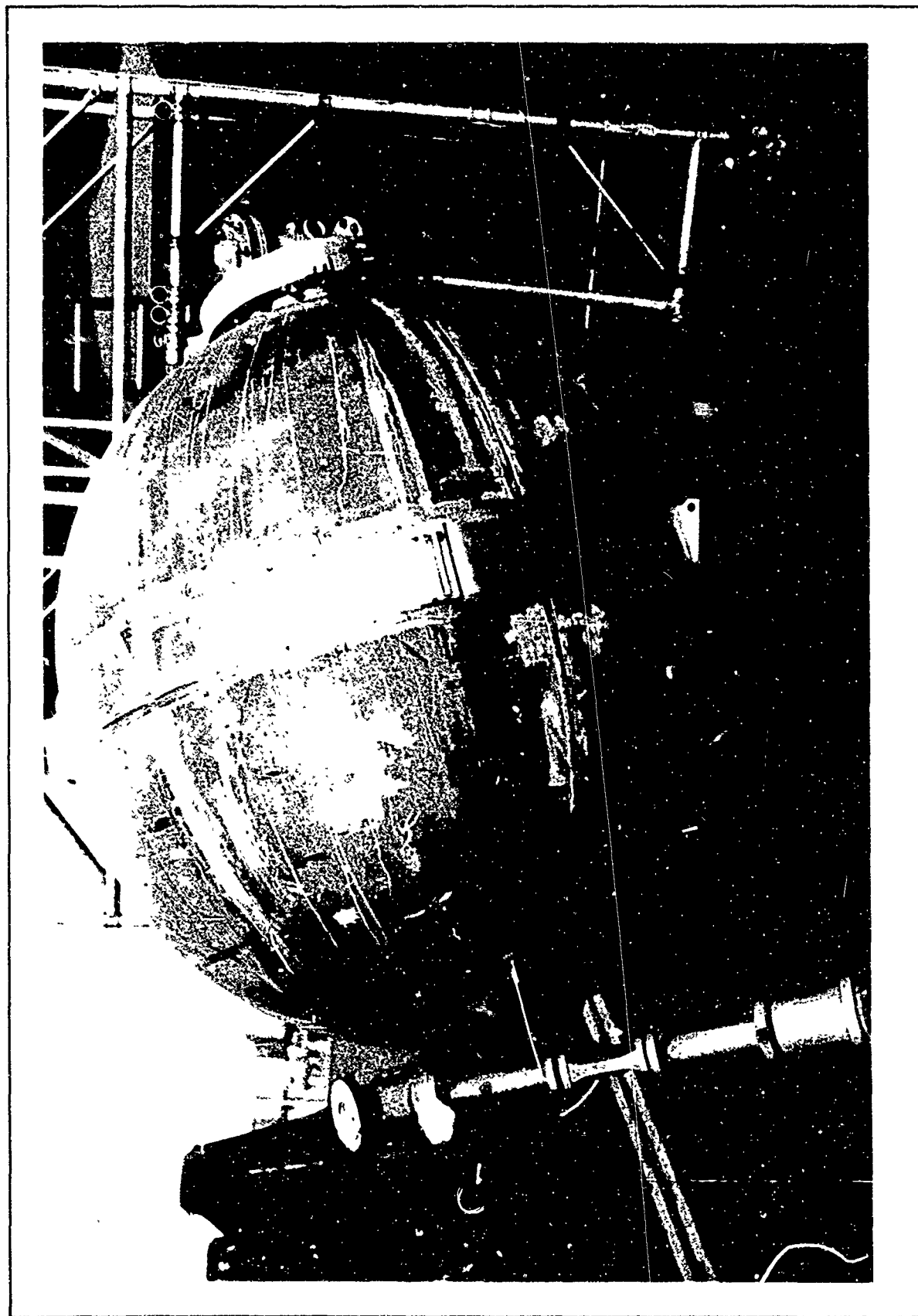


Figure 4-124. Completed LN₂ Tank Assembly

Prior to acceptance by Douglas, the tankage was tested at FanSteel. The tests included (1) radiographs of all welds according to MIL-STD-453 with inspection to Class III ABMA-PD-R-27, (2) hydrostatic tests to 375 p. s. i. a. on the aluminum tanks and 4,500 p. s. i. a. on the steel tanks, and (3) a gross leak-check with nitrogen at 100 p. s. i. a. for the aluminum and 1,500 for the steel tanks. All tests were passed.

After establishing the tankage configuration, design was begun on the simulated vehicle shell and tank support structure. To simplify fabrication, it was established that the shell have a constant diameter of 10 ft. and a length of 23 ft. Essentially it is a welded steel structure consisting of six circular 6 in. I-beams, 8 longerons made of 6 in. channels and 0.10 in. steel skin. The longerons are bolted to the ring frames at intersection points and the skin is welded to the beams and the longerons. Four all-welded support legs attach to the shell sides and mate to the vacuum chamber hard points on a 16 ft. diam. circle.

Two tank support systems are incorporated in the hardware: (1) a transport support system for the tanks which will take loadings during shipment, movement, and placement of the test article, and (2) a low-heat leak test support system which carries the static tank loads into the vacuum chamber after installation. The transport support system is essentially a truss work of pipes running between the tanks and the H-beam rings around the shell. After installation in the vacuum chamber, these supports are to be removed.

The results of the comparison of the flight vehicle tank support system, as discussed previously, indicated that the nine-rod glass fiber tension support system had maximum performance potential. Therefore, it was decided to apply this approach to the test apparatus. However, since the primary objective of this program is to evaluate thermal rather than structural/mechanical characteristics, only the thermal properties were simulated. Each tank was supported by four identical high-strength glass fiber support rods which were sized to yield a LH₂ tank support heat leak equivalent to that anticipated for the nine glass fiber rod system in the flight vehicle. Because of the compensating features of the high-boost-g. loading in the flight vehicle and the high tankage weight in this test apparatus, the total support rod cross-sectional areas for the two cases was very close. To reduce cost, identical glass fiber support rods were used for the LN₂ tank. The heat leak through the tank supports on the LN₂ tank is lower than would be anticipated for the flight vehicle, but this difference should be predictable.

Special tooling was set up to fabricate the support rods from one continuous length of glass fiber tape. The completed rods had a square cross-section with an area of 0.25 in.². These were cured at elevated temperatures to increase strength and to remove volatiles that might evaporate under the vacuum environment. The completed support rods were statically tested under tension to 5,800 lb. which was two times the maximum design load. One spare rod was tested to failure at 19,800 lb., nearly seven times the design load.

In the test apparatus, the tank positions were reversed relative to the flight vehicle to gain easier access to the interior of the LH₂ tank and its internal hardware. This was a fortuitous decision because it became necessary to gain access into the LH₂ tank during checkout testing.

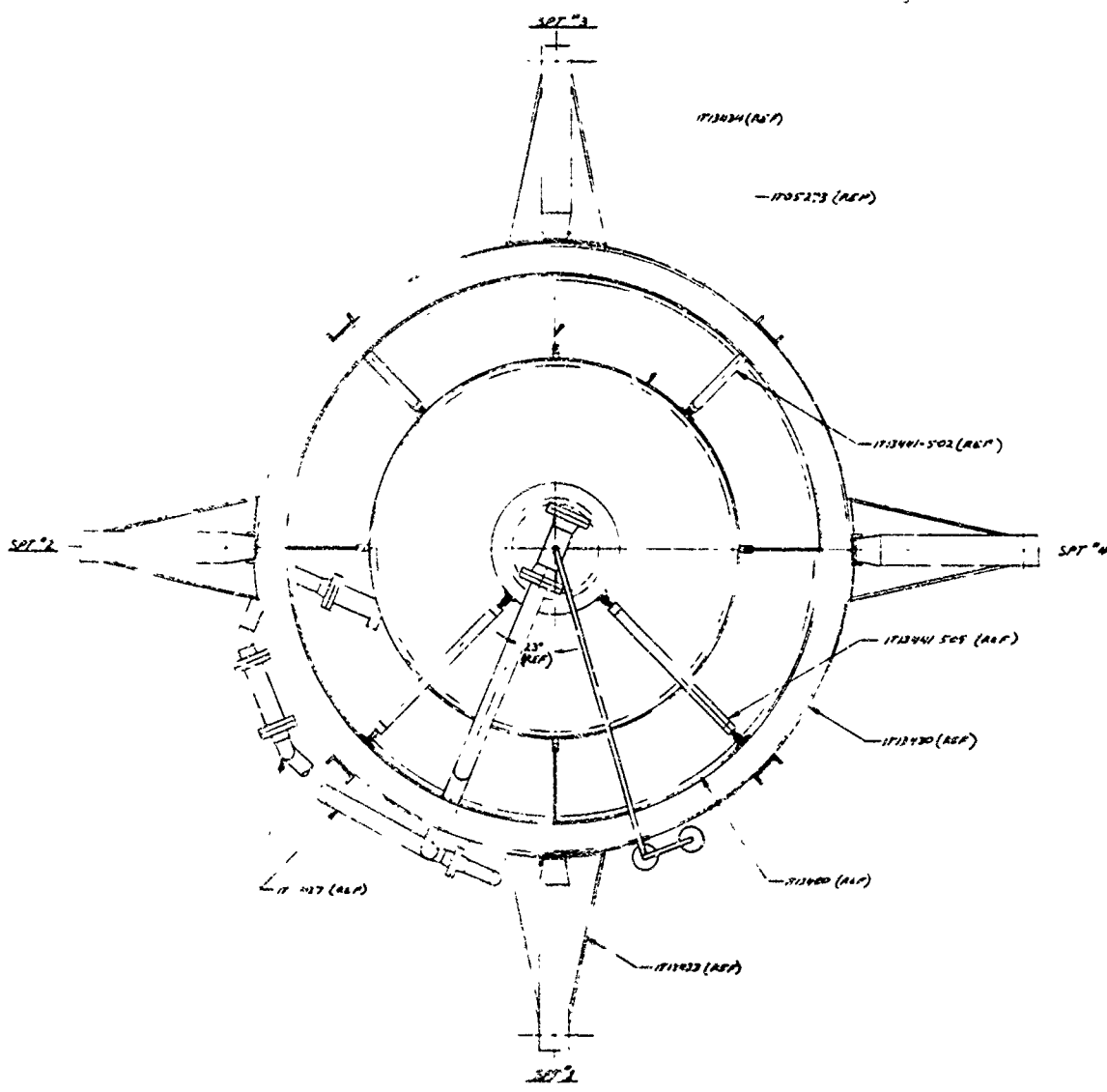
Removable aluminum skin and stringer type end closures are provided for both the top and bottom of the shell or shroud structures. These closures were designed to support a man at their centers. An access hatch about half way up the shell was also provided to gain access to the area between the two propellant tanks.

Figure 4-125 shows the overall test apparatus layout.

b. Insulation System. The results of the Phase VI insulation study indicated that there was little difference in overall insulation performance between aluminized Mylar, the NRC-2, or Dimplar type, and direct tank or shroud insulation mounting. Since shroud mounting had never been attempted on a large scale before, and since it has a number of interesting features, such as accessibility, it was mutually decided between Douglas and RPL to apply shroud-mounted Dimplar insulation to the test hardware. Further, to focus attention on the long duration pump fed engine case, 21 sheets of insulation were used per the results of optimization. Of the 21 sheets, 11 are flat 1/2 mil, while the other 10 are 1/2 mil, dimpled with a deep set. The greater thickness was used to facilitate rapid fabrication.

The insulation was applied to the shell sidewalls in eight 22-ft.-long blankets. Each blanket was 42 in. wide (standard material width), which resulted in eight longitudinal gaps, with an average gap width of about 1/2 in. Narrow strips of flat aluminized Mylar were interwoven and taped along the longitudinal gaps to form a continuous flat sheet around the shell. Figure 4-126 illustrates pertinent details of the insulation installation. Each blanket uses 20 Teflon studs to attach the insulation. It is recognized that probably a stud insulation attachment system would not be used for the flight vehicle. Some variation of a thread and button system would probably be used with a greater attachment density (points per square foot). Rough calculations showed that the heat leak with 20 studs per blanket is close to what would be expected for the flight type insulation attachment system. The insulation was placed on the inside faces of the H-beam rings and was held in place by 1/4 in. Teflon studs which passed through circular holes punched in the insulation blankets. The Teflon studs were screwed onto steel studs welded to the H-beam flange. A taped washer was screwed into the end of the Teflon stud to retain, but not compress the blanket. Slack was provided in the blanket between studs to permit contraction and expansion.

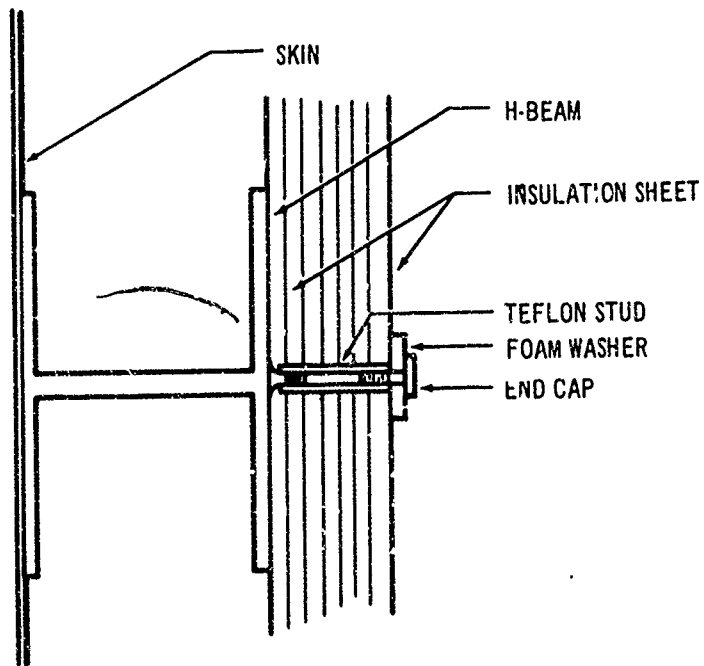
The junctures between the shell sidewall and the top and bottom covers posed a problem because it was desirable to have the end closure removable without having the insulation subject to damage. After considering various alternatives, molded glass fiber collar mating surfaces, were chosen which abut against the end of the insulation blankets at a 45° angle on both the shell sidewall and end closure (Figure 4-126). One collar were



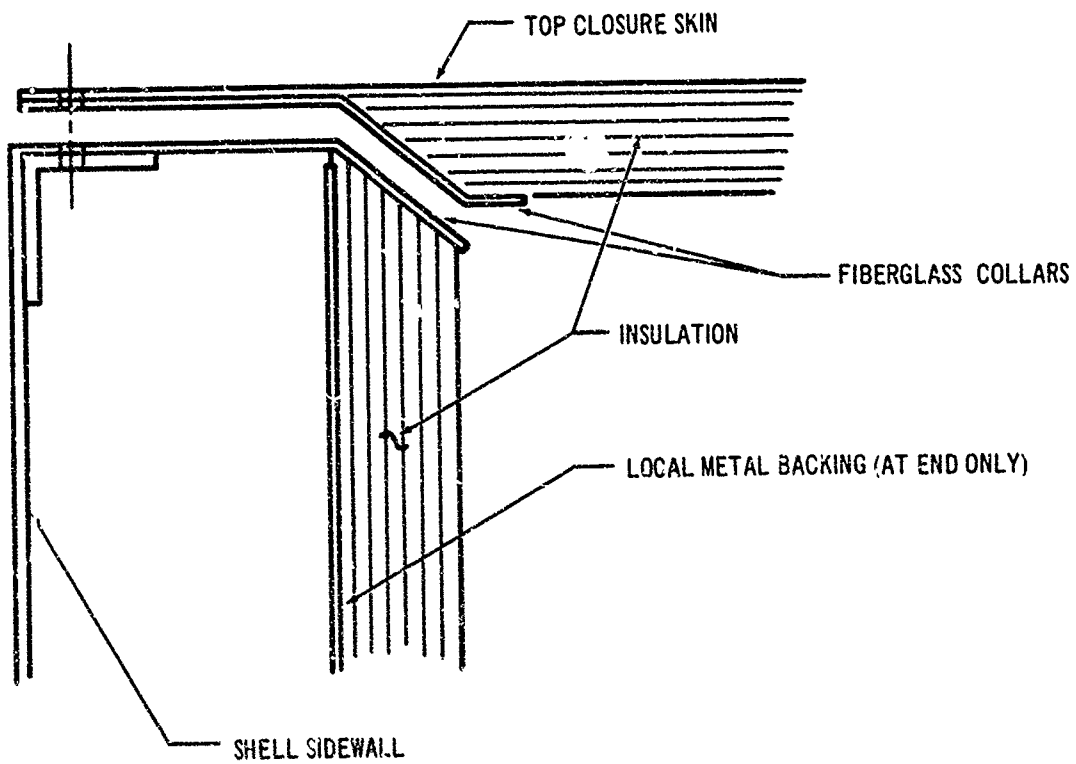
VIEW: LOOKING DOWN AT TOP OF LOG TANK.

1/5

A

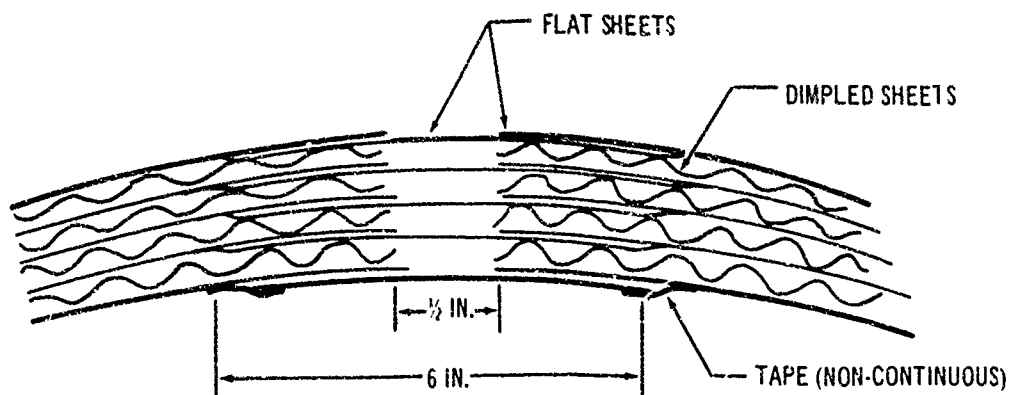


INSULATION ATTACHMENT

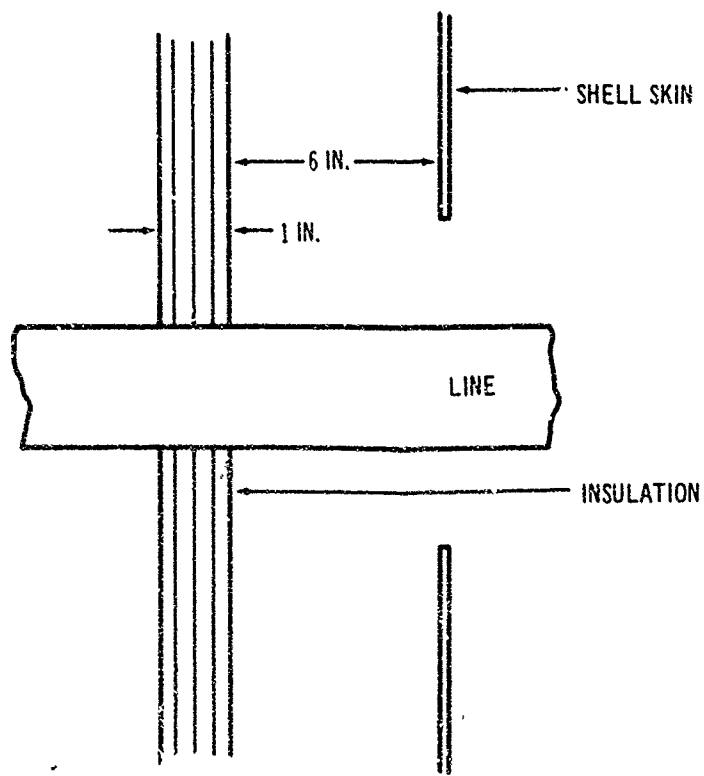


END JUNCTURE DESIGN

A



LONGITUDINAL INSULATION JOINT SPLICE



TYPICAL INSULATION PENETRATION

B

Figure 4-126. Insulation Installation Details

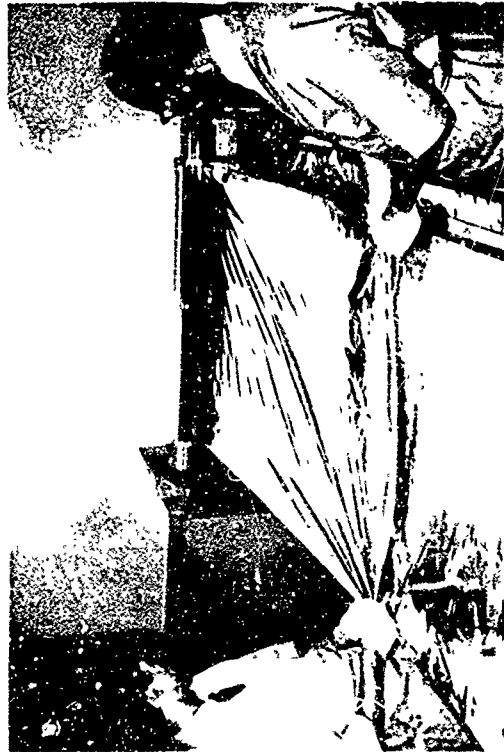
attached to the end closure and one to the edge of the shell cylinder. The collars were fabricated and installed so as to form a tight, close fit to minimize excessive heat leak through the joint. Glass fiber was used to minimize the blanket thermal degradation.

The 22-ft. -long insulation blankets were prefabricated in a controlled-atmosphere laboratory. Prefabrication included lay-up, thermocouple installation, cutting of the 45° mitred edge, and stitching where necessary. The blankets were then draped on the shroud sidewall with the test apparatus in its normal vertical position, and all internal hardware was installed, except for the LH₂ and LN₂ vent lines. Figure 4-127 illustrates the insulation fabrication and installation. Figure 4-128 shows the nearly completed insulation, as viewed from the top of the test apparatus, with the top closure removed. To preserve the insulation, the shell was kept closed as much as possible and desiccant containers were installed inside the shell.

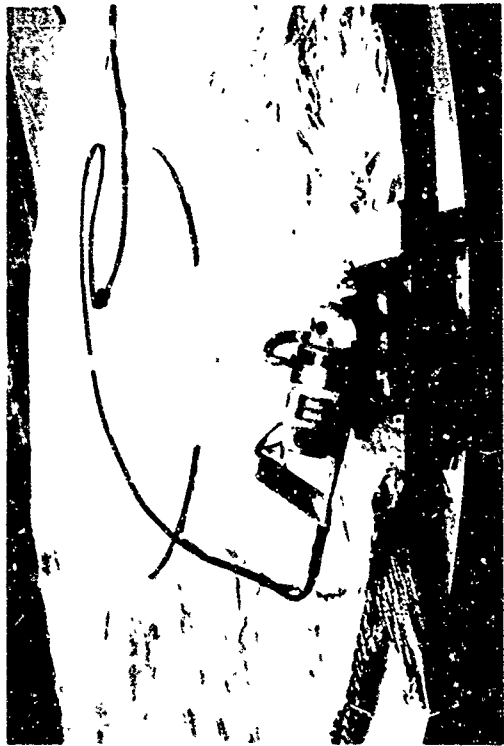
The study showed that the use of insulation on the lines with shroud-mounted insulation yielded only a small net performance gain. Theory also indicates that insulation shorting by penetrations with shroud mounting should be much less severe than is normally the case when insulation is placed directly on the cryogenic surface. Therefore, it was decided to test bare lines with simple butt joints where hardware penetrates the insulation blankets (Figure 4-126).

c. Propellant Feed and Pressurization System Design. Design of the feed, vent, and pressurization system involved solutions to extensive problems primarily because of the controlled variability required for the system. Figure 4-129 shows the finalized schematic of the propulsion system for the test apparatus. To conform with the phase II study findings, all lines were made of stainless steel, but to satisfy safety requirements, basic wall size had to be increased (for example, to 0.32 in. from 0.022 in. for the feed lines). Line diameters were also selected to represent flight vehicle conditions: 2.5 in. for feed lines, 3 in. for vent lines, and 3/4 or 1 in. for pressurization lines. It was possible to reasonably simulate line routing for the tank vent and the pressurization system, but feed line routing had to be compromised to facilitate flow meter instrumentation requirements and geometry limitations. Flex hose sections were welded into the lines to provide for contraction and expansion.

As indicated in the schematic, each feed line consists of a tank shut-off valve (per the conclusions reached in the phase II study), a flow meter, a controllable throttling valve, and a bypass section with a fill valve. The bypass was necessary to prevent reverse flow through the flow meter. The throttle valve represents the engine propellant flow control valve. Each propellant tank vent system consists of an on/off type vent valve which is triggered by a variable signal to permit venting at any desired pressure. A vent bypass with a safety burst disc is also included. There are two alternate pressurization systems: (1) both tanks are pressurized with heated He or (2) the LN₂ (simulated LF₂) tank is pressurized with heated He and the LH₂ tank is pressurized by GH₂. Both pressurants are stored in the



BLANKET LAY-UP



END CLOSURE INSULATION



BLANKET INSTALLATION



FITTING AROUND PENETRATION

Figure 4-127. Insulation Fabrication and Installation

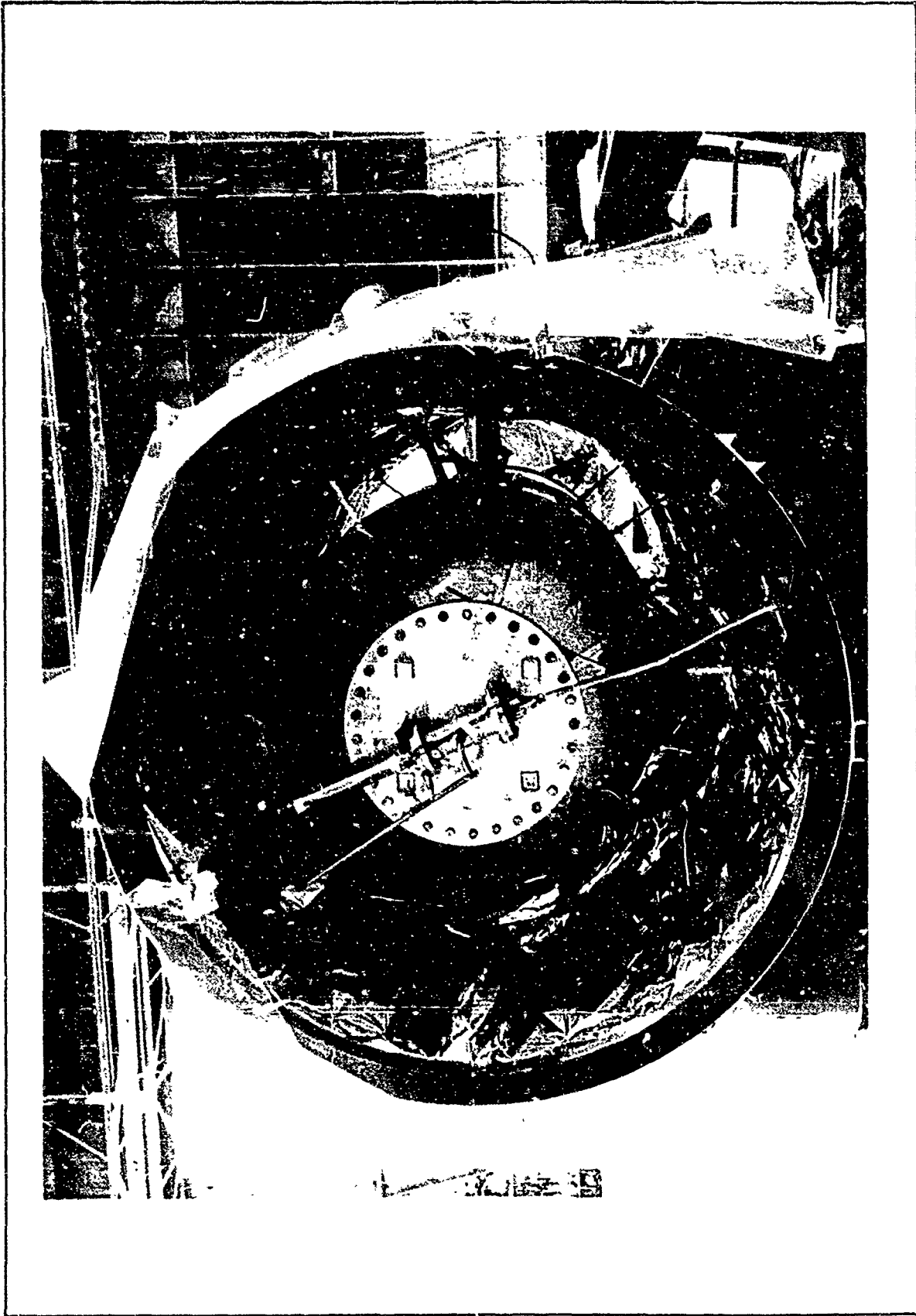
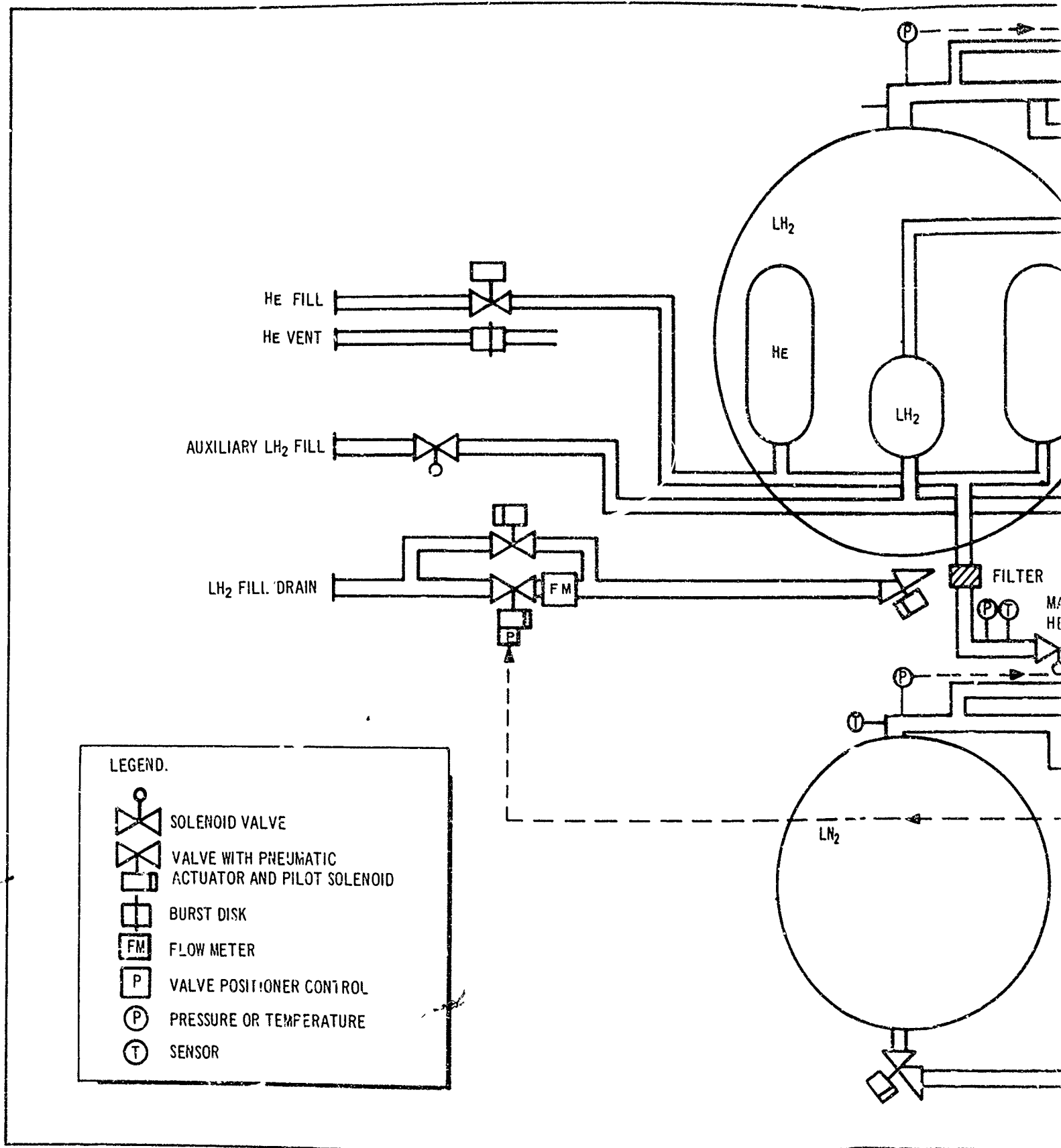


Figure 4-128. Nearly Completed Insulation



- LEGEND.**
-  SOLENOID VALVE
 -  VALVE WITH PNEUMATIC ACTUATOR AND PILOT SOLENOID
 -  BURST DISK
 -  **FM** FLOW METER
 -  **P** VALVE POSITIONER CONTROL
 -  **P** PRESSURE OR TEMPERATURE
 -  **T** SENSOR

7

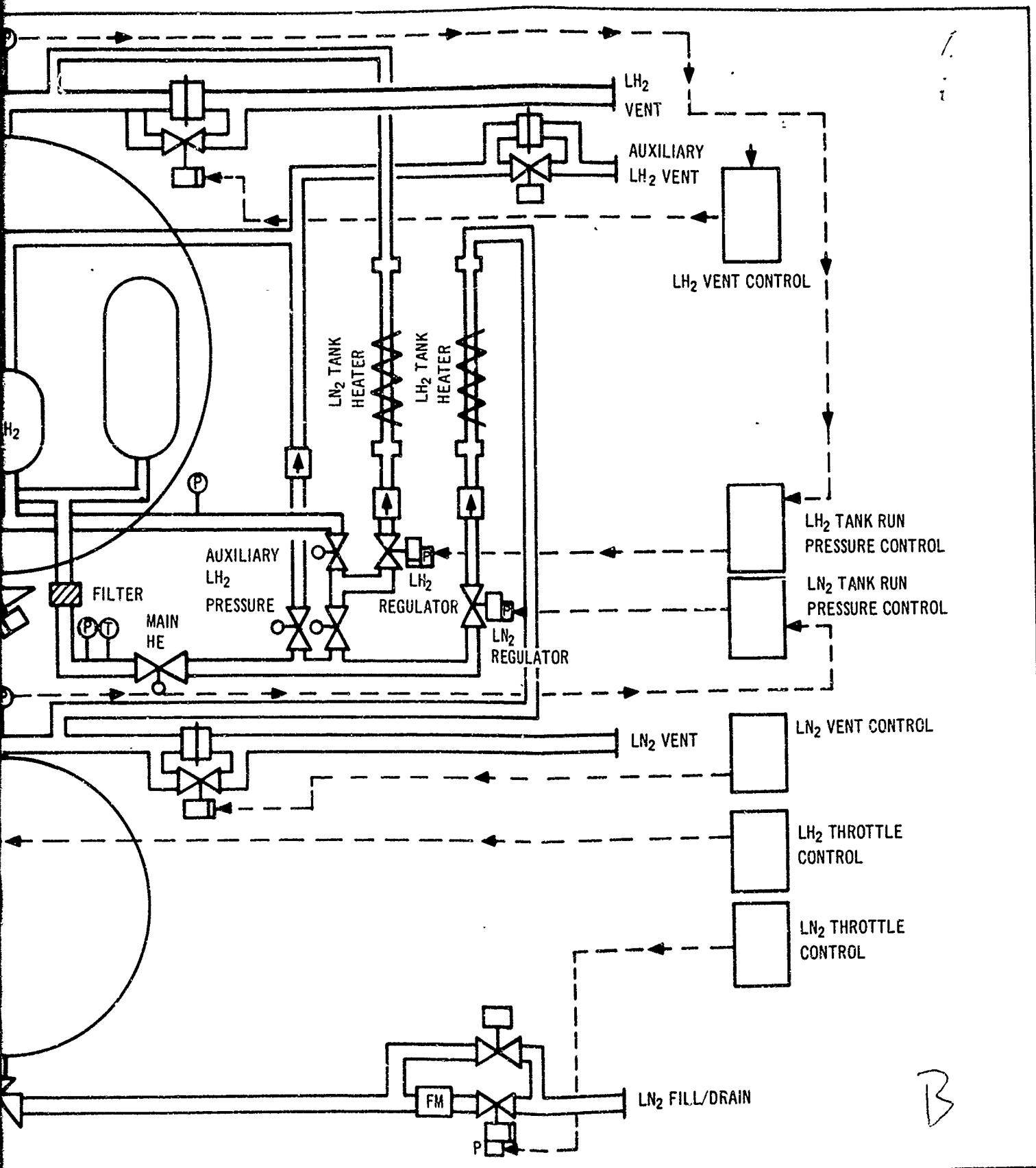


Figure 4-129. Test Apparatus Propulsion System

LH₂ tank at an initial 3,000 p. s. i. The desired pressurization system is selected by properly positioning the pressurant supply solenoids. Each propellant tank has an individual pressurant heater which uses externally-supplied d. c. electrical power as the heat source. Pressurant flow is controlled by variable throttling valves tied in with a closed-loop feedback control system. Pressurant inlet temperature is held constant at a desired level by a second feedback-type control which modulates the heater power input. Manual vent valves and safety burst discs are also used with each pressurant bottle.

The major problem area lay in component selection. The system components had to perform normal functions at cryogenic temperatures, produce negligible external leakage into the vacuum chamber, and be capable of functioning under variable conditions upon command from the control console 900 ft. from the vacuum chamber. These commands included 10:1 throttling, variabing tank pressures for 25 to 235 p. s. i. a. (venting and expulsion), and variabing inlet gas temperatures. Budgetary limitations restricted any extensive development efforts, and therefore, standard ground facilities componentry had to be used.

After considerable study and extensive discussions with component suppliers, the following general approach was adopted:

- Wherever possible, components were located on the outside of the shroud structure where the environmental temperature is higher and the mass and surface area of the components would not greatly interfere with the internal heat transfer to the tankage.
- Standard industrial components were used.
- Sealed-and-purged cans or modules were provided in which all components were placed which were limited with respect to low pressure, temperature, or leakage.

The most critical items were the cryogenic valve pneumatic actuators which are temperature sensitive and leak sensitive. The valves normally use long stem actuators which permit free convection to maintain the actuator above limiting temperature (which in a vacuum environment would not be present). Therefore, the conditioning module concept was applied by providing a purged cover for each large valve. The module consists of a flat machined plate, welded to the cryogenic valve stem about midway between the valve Y and the actuator, and an aluminum cylindrical cover, which is sealed and bolted to the plate. The plate contains fittings for actuation gas, purge gas, vent gas, and conduit for electrical wires which must serve the valve actuator. The plate and cover were designed and fabricated by Douglas, and the plate was adapted to the valve by the valve manufacturer, Calmec. Of the smaller 3/4 in. valves, two could be mounted into one module. Additional space remained in the modules for placement of other critical items such as pilot solenoids, pressure transmitters, positioners crossswitches, etc. The purge and vent lines from the eight modules were all routed to a

common manifold where they could be supplied with ambient or warm nitrogen from one inlet line into the vacuum chamber. Figure 4-130 shows the valve module arrangement schematically. Figure 4-131 is a photograph of the LN₂ valve complex with the cover removed. The throttle valve is on the left, the fill valve on the right, and the vent valve is above.

One component which could not be adopted in this manner was the tank shutoff valve which had to be inside the shroud and immediately below the propellant tank. In this case, a specially designed valve with dual metal bellows sealed with He actuation had to be used. This is shown installed on the LH₂ tank in figure 4-124.

The variable pressure, tank pressure regulation system had to be relatively complex. Attempts to locate an adjustable dome-loaded pressure regulator which could control He at -420°F. were unsuccessful. Although regulators have been designed for this type of service, they have been fixed-pressure regulators, custom-made for flight service for a particular application. The only dome-loaded regulator which came close to meeting the temperature requirements was limited to operation at -320°F. minimum. When tested with helium at lower temperatures, the regulator leaked. Although the low cost of the regulator made it attractive, there was no evidence that it could be made to work without further costly (in dollars and calendar time) development.

The elements of the selected regulator system are as follows:

- A pressure transducer to sense tank pressure and convert it to an electrical signal.
- A power supply to energize the pressure transducer.
- An automatic control station to accept the input signal from the pressure transducer, compare it with a preset pressure entered at the control station by the test operator, and transmit a correcting signal if the sensed pressure does not agree with the set pressure.
- An electro-pneumatic transducer to convert the electrical correcting signal from the automatic control station into a pneumatic signal.
- A throttling valve to control the flow of pressurizing gas from the high pressure supply tank to the propellant tanks.
- A valve positioner to position the valve as directed by the pneumatic signal.

In operation, the test operator sets the desired tank pressure with the dial on the automatic control station. The control station will then signal the throttle valve to open and permit enough gas to flow into the propellant tank to pressurize it to the required level. As the pressure sensor at the tank signals the rising pressure to the automatic controller, the controller in turn signals the valve to close and to hold the set pressure. As propellants

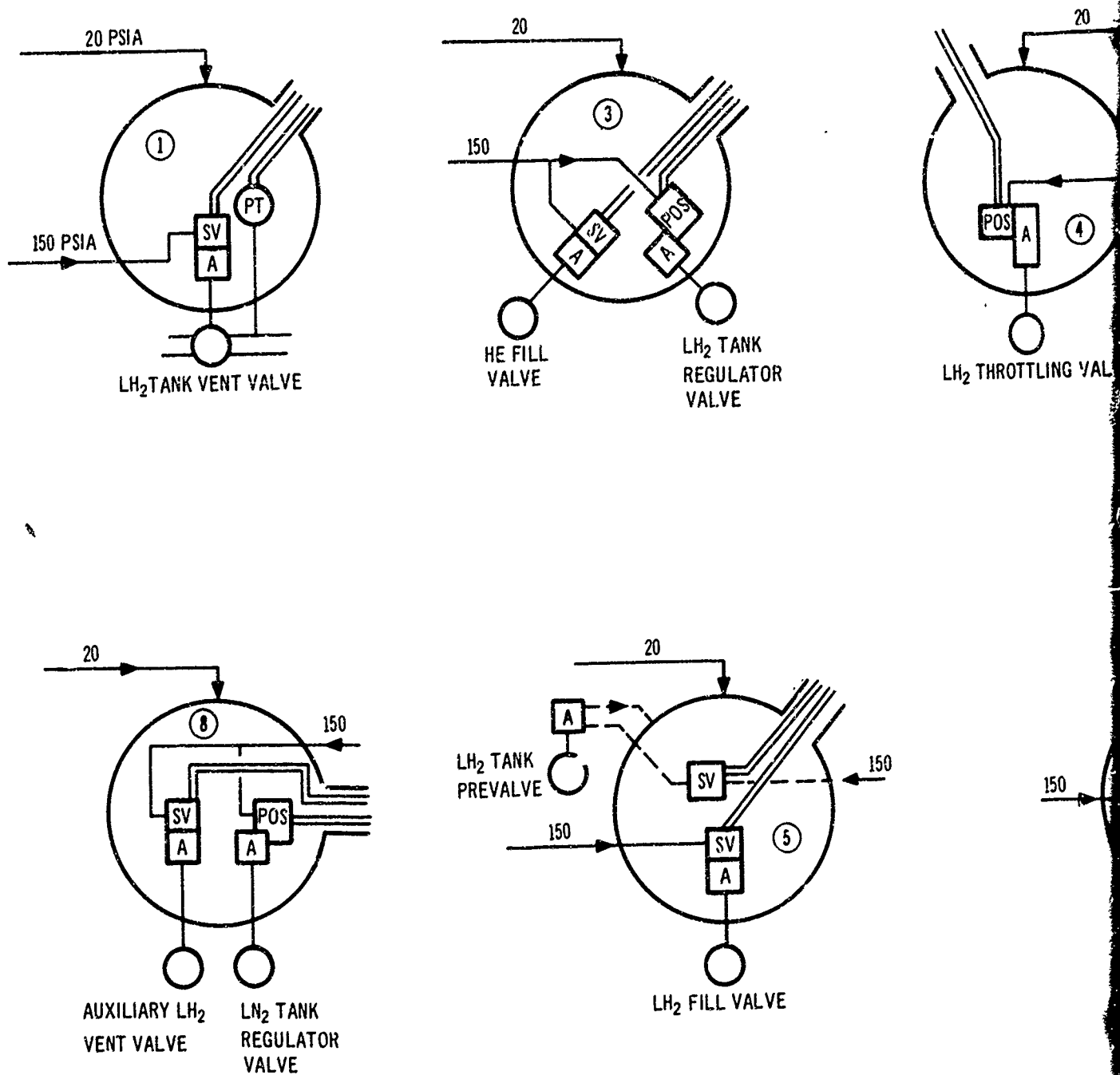
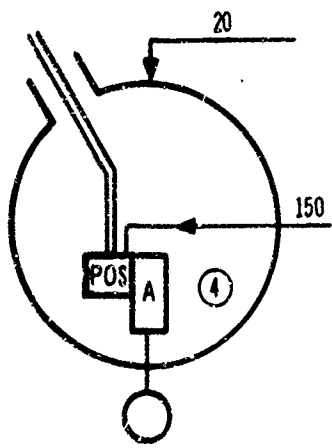
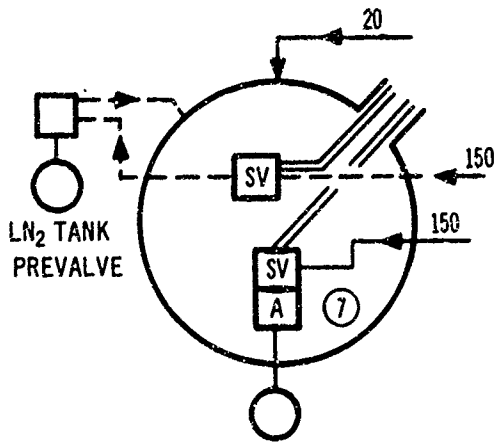


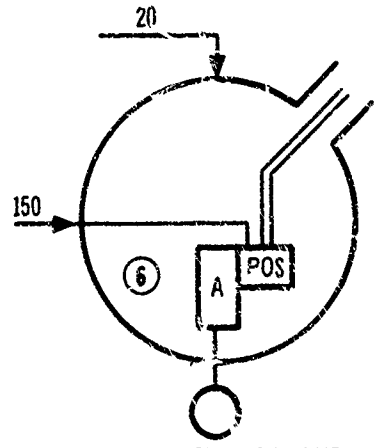
Figure 4-130. Valve Module



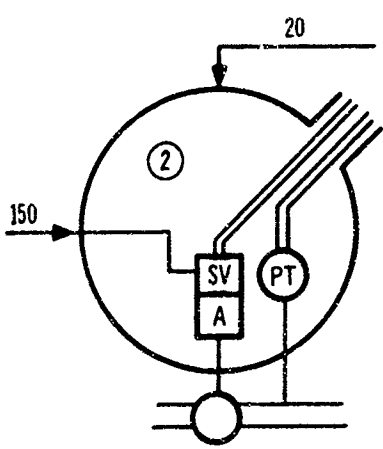
LH₂ THROTTLING VALVE



LN₂ FILL VALVE



LN₂ THROTTLING VALVE



LN₂ TANK VENT VALVE

LEGEND:

- GN₂
- - - - He
- ==== ELECTRICAL WIRER
- [A] PNEUMATIC ACTUATOR
- [SV] ELECTRICAL SOLENOID
- (PT) PRESSURE TRANSMITTER
- [POS] VALVE POSITIONER

B

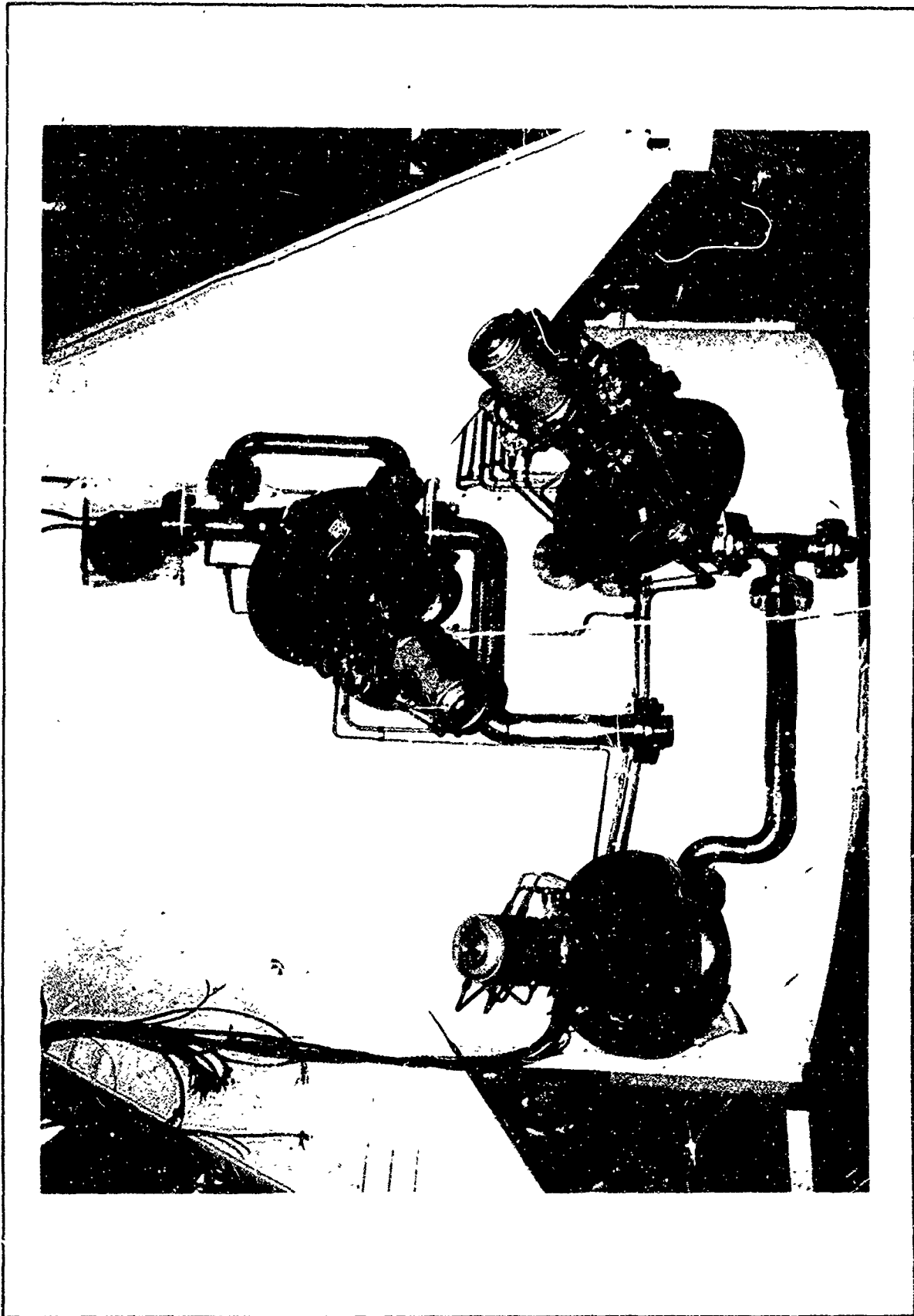


Figure 4-131. LN₂ Tank Valve Complex

flow from the tank, the automatic controller signals the pressurizing gas valve to open and close or hold in proper position to maintain constant tank pressure. This arrangement is shown schematically in figure 4-132. To shut down, the set point is reduced to zero. This closes the throttle valve and halts the flow of gas to the tank. The tank can now be vented.

The 1 to 5 ma. signal from the tank pressure transmitter is also used to control venting. The signal is sent to the vent valve pressure set control which is another bridge circuit with a relay. When the incoming signal matches that set into the control by the test operator, a relay will open terminating 28 v. d. c. power to the normally open vent valve, thus venting the tank to a lower pressure which will signal the vent valve to close. The pressure drop during venting can be controlled by adjusting the vent valve controller.

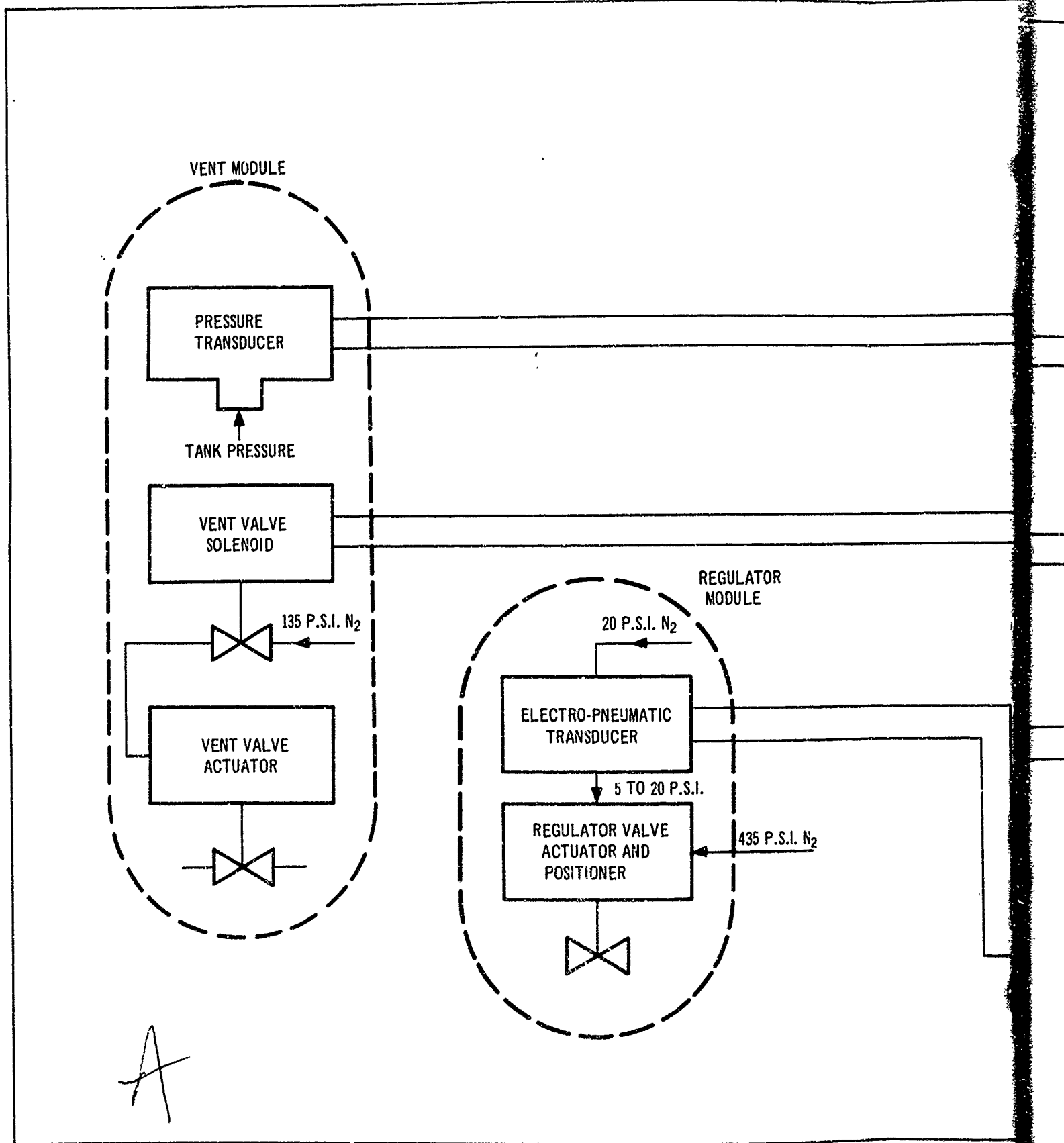
Throttling is achieved by using another electro-pneumatic transducer to position the valve. The signal to the transducer is supplied from a manually set control unit which puts out a 1 to 5 ma. signal.

The control units described above also have real-time readouts of tank pressure and valve positions as well as a set-point indications.

Other control features include resistance-type high and low liquid level sensors which provide light indications for full, and for near-empty tanks. The low level sensor may also be connected so that the tank shutoff valves are closed just before depletion, to prevent turbine flow meter overspin.

The simplest and most direct method of heating the pressurant is to use electrical resistance heating of the flow tubes prior to entry into the tank. Estimates showed that about 67 kw. of power would be needed for helium pressurization of the LN₂ tank, 97 kw. for helium pressurization of the LH₂ tank, and 193 kw. for GH₂ pressurization of the LH₂ tank. If it is assumed that the heaters are made of 5/8 in. 0.016 in. 310 stainless steel, and are powered with a maximum voltage of 80 v. d. c., heater lengths of about 8 ft. and 3 ft. for the LN₂ and LH₂ tanks, respectively, were estimated to be required. Figure 4-133 shows the estimated temperature capabilities for the heaters. Note that under certain operating conditions it is possible to get gas temperature above 800°R. which is about the limit that would be desired for these tests (as indicated by the phase VII study results). Table 4-43 lists the heater operating conditions.

Electrical power and control requirements for the heaters were quite severe. After reviewing the problems with various electrical equipment suppliers, it was recommended that a bank of standard arc welders be used for the primary power supply with a solid-state power manipulator to provide control with the use of platinum temperature elements in and on the heaters to provide signals for gas temperature control and over-temperature shutdown. This would permit the test operator to set a desired inlet gas temperature. Also a recommendation was made that control relays be used that would prevent the application of power to the heater unless gas were flowing through the system. Table 4-44 lists the feed and vent system components.



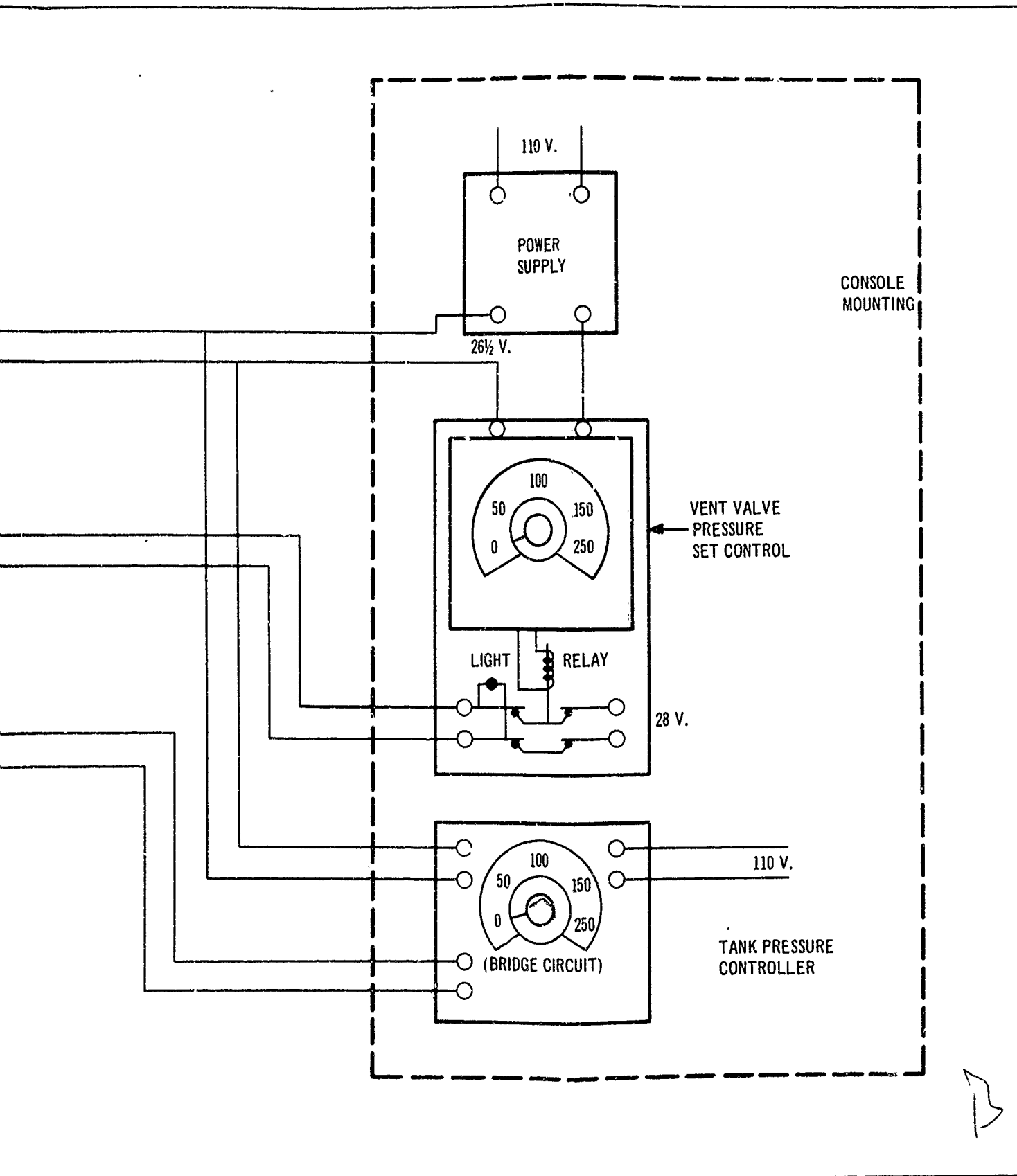


Figure 4-137. Tank Pressure Control System

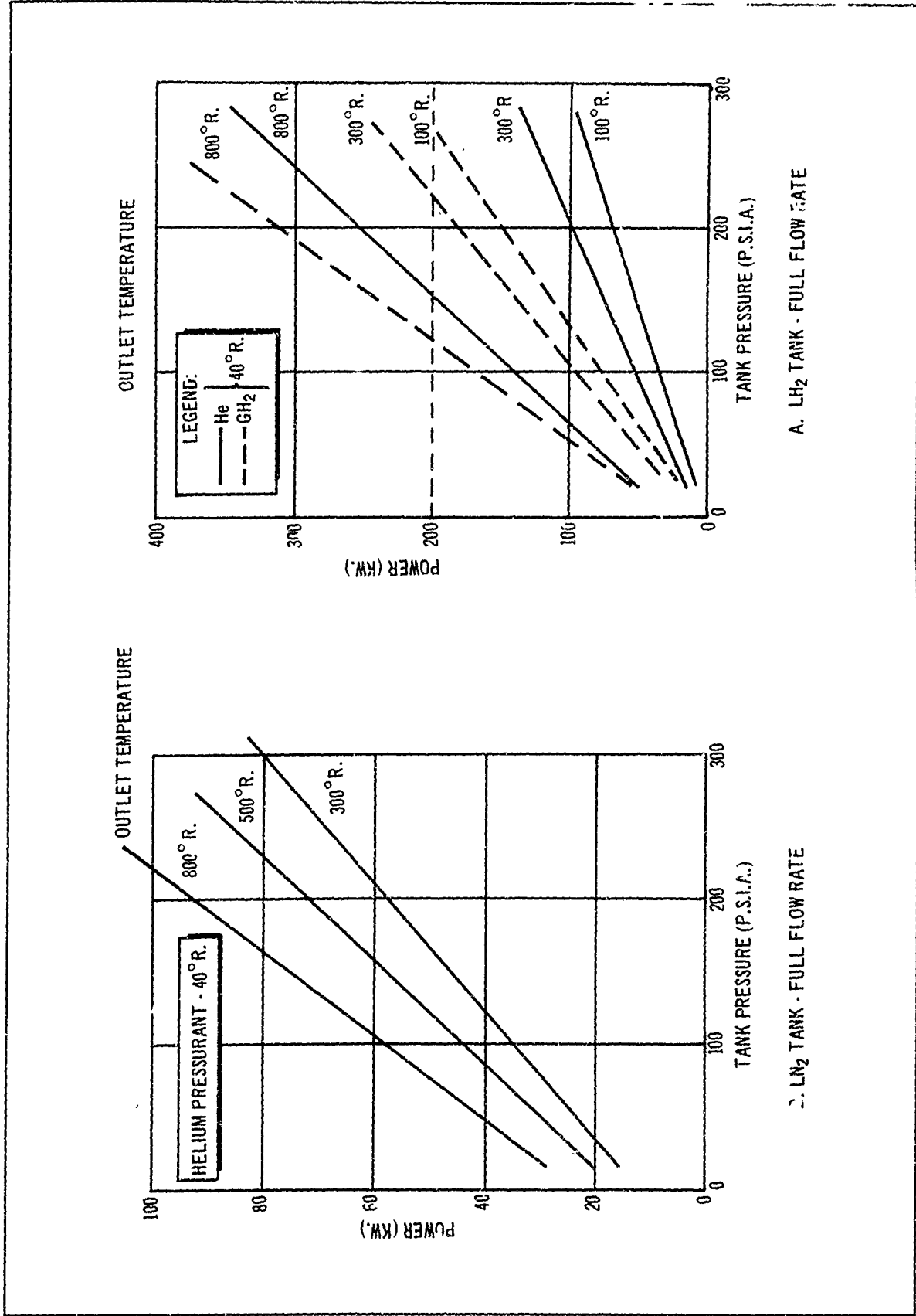


Figure 4-133. Estimated Pressurant Heater Capability

Table 4-43

PRESSURANT HEATER OPERATING CHARACTERISTICS

Characteristics	LN ₂ Tank Heater	LH ₂ Tank Heater
Tube length (in.)	64	33
Approximate resistance (ohms)	0.0935	0.0352
Nominal voltage (v.)	80	80
Nominal current (a.)	1,250	2,500
Nominal power (kw.)	100	200

d. Instrumentation System. The test apparatus instrumentation system must provide data to satisfy the following functions: (1) determine total heating rate into the LH₂ and LN₂, (2) determine the approximate distribution of the total heat load among the various heat leak paths, (3) evaluate the behavior and performance of the pressurization system, (4) monitor propellant expulsion behavior, (5) control normal operation of the test apparatus, and (6) provide safety override capabilities. Table 4-45 lists the various selected test data instrumentation items. These consist primarily of 170 Douglas-fabricated copper-constantin thermocouples (c-cT_C), 46 Thermal Systems, Inc., platinum resistance temperature sensors, 7 Hastings thermocouple vacuum gages, 6 Statham pressure transducers, and 2 Potter turbine flowmeters. The copper-constantin thermocouples were selected to survey temperature distributions (1) around the structural shell, (2) around the outside of the LH₂ and LN₂ tanks, (3) along all plumbing lines passing between the shell and the propellant tanks, (4) along the support legs and the tank support rods, (5) through the insulation blankets, (10 stations), and (6) in the pressurant gas stream.

The platinum elements were selected to sense liquid and gas temperature inside the cryogenic tanks. These were chosen over thermocouples to gain the greater accuracy inherent in platinum elements and to avoid the use of copper-constantine feed-throughs to accommodate passage of the internal tank instrumentation wires through the tank wall. All the internal instrumentation wires passed through plugs located in the tank upper-tee penetration. Platinum temperature sensors were also used on the pressurant gas heaters.

The strain gauge pressure transducers are used to record all tank and feed line pressures. The thermocouple vacuum gauges are used to measure the vacuum level within the insulation and the interstage.

Figure 4-134 shows the primary instrumentation locations for the system. There are four longitudinal planes (1P1 through 1P5) and seven horizontal planes (1PA through 1PE, 1PT and 1PL). The shell, insulation,

Table 4-44 (page 1 of 3)
FEED AND VENT SYSTEM COMPONENTS

Component	Supplier/ Part Number	Location	Actuation
<u>Feed Systems</u>			
LH ₂ tank outlet valve	Calmecc 279-A-E347	Bottom of LH ₂ tank	He gas (150 p.s.i.a.)
Solenoid pilot valve	Crescent, Model No. 11403-AH	Module 5	28 v.d.c.
LN ₂ tank outlet valve	Calmecc 279-A-E347	Bottom of LN ₂ tank	He gas (150 p.s.i.a.)
Solenoid pilot valve	Crescent, Model No. 11403-AH	Module 7	28 v.d.c.
LH ₂ fill & drain valve	Calmecc 279-A-E353	Module 5	N ₂ gas (150 p.s.i.a.)
Solenoid pilot valve	Crescent, Model No. 11403-AH	Module 5	28 v.d.c.
LN ₂ fill & drain valve	Calmecc 279-A-E353	Module 7	N ₂ gas (150 p.s.i.a.)
Solenoid pilot valve	Crescent, Model No. 11403-AH	Module 7	28 v.d.c.
LH ₂ throttling valve	Calmecc 279-A-E352	Module 4	N ₂ gas (150 p.s.i.a.)
Valve positioner	Fisher Type 3570	Module 4	N ₂ gas (150 p.s.i.a.)
Electro-pneumatic transducer	Fisher, Model No. 546	Module 4	
Manual loading	Robertshaw Model No. 541	Control console	110 v.a.c.
LN ₂ throttling valve	Calmecc 279-A-E352	Module 6	N ₂ gas (150 p.s.i.)
Valve positioner	Fisher Type 3570	Module 6	N ₂ gas (150 p.s.i.)
Electro-pneumatic transducer	Fisher, Model No. 546	Module 6	
Manual loading	Robertshaw Model No. 541	Control console	110 v.a.c.
Line check valve (2)	Lanagan	In feed line bleed	--
<u>Vent Systems</u>			
LH ₂ safety head	Black, Sivalls & Bryson 77-DOU-053	Parallel with Module 1	
LH ₂ vent valve	Calmecc 279-A-E353	Module 1	N ₂ gas (150 p.s.i.a.)
Solenoid pilot valve	Crescent, Model No. 11403-AH	Module 1	28 v.d.c.
Alarm relay	Robertshaw Model No. 552-A2	Control console	28 v.d.c.
LN ₂ safety head	Black, Sivalls & Bryson 77-DOU-053	Parallel with Module 2	
LN ₂ vent valve	Calmecc 279-A-E353	Module 2	N ₂ gas (150 p.s.i.a.)
Solenoid pilot valve	Crescent, Model No. 11403-AH	Module 2	28 v.d.c.
Alarm relay	Robertshaw Model No. 552-A2	Control console	28 v.d.c.

Table 4-44 (page 2 of 3)
FEED AND VENT SYSTEM COMPONENTS

Component	Supplier/ Part Number	Location	Actuation
<u>Pressurization System</u>			
LH ₂ tank regulator valve	Calmech 279-F-E358	Module 3	N ₂ gas (150 p.s.i.a.)
Valve positioner	Fisher Type 3570	Module 3	N ₂ gas (150 p.s.i.a.)
Electro-pneumatic transducer	Fisher, Model No. 546	Module 3	
Pressure transducer	Robertshaw No. 113-A3-R1-AL	Module 1	32 v.d.c.
Automatic indicating controller	Robertshaw Model No. 321-52	Control console	110 v.a.c./28 v.d.c.
Power supply	Robertshaw Model No. A312-1	Control console	110 v.a.c.
Voltage stabilizing transformer	Robertshaw	Control console	110 v.a.c.
LN ₂ tank regulator valve	Calmech 279-F-E358	Module 8	N ₂ gas (150 p.s.i.a.)
Valve positioner	Fisher Type 3570	Module 8	N ₂ gas (150 p.s.i.a.)
Electro-pneumatic transducer	Fisher, Model No. 546	Module 8	
Pressure transducer	Robertshaw No. 113-A3-R1-AL	Module 2	32 v.d.c.
Automatic indicating controller	Robertshaw Model A321-52	Control console	110 v.a.c./28 v.d.c.
Power supply	Robertshaw Model No. A312-1	Control console	110 v.a.c.
Hi-pressure LH ₂ tank safety head	Black, Sivalls & Bryson 77-DOU-055	Parallel with Module 8	
Hi-pressure LH ₂ tank vent valve	Calmech 279-F-E357	Module 8	N ₂ gas (150 p.s.i.a.)
Solenoid pilot valve	Crescent, Model No. 11403-AH	Module 8	28 v.d.c.
Helium tank fill & vent valve	Calmech 279-F-E357	Module 3	N ₂ gas (150 p.s.i.a.)
Solenoid pilot valve	Crescent, Model No. 11403-AH	Module 3	28 v.d.c.
Hi-pressure He tank safety head	Black, Sivalls & Bryson 77-DOU-055	Parallel with Module 3	
Hi-pressure He outlet valve	Fox Valve No. 610750	Outside shroud	28 v.d.c.
Hi-pressure H ₂ outlet valve	Fox Valve No. 610750	Outside shroud	28 v.d.c.
LH ₂ tank, He pressure regulator supply valve	Fox Valve No. 610750	Outside shroud	28 v.d.c.

Table 4-44 (page 3 of 3)
FEED AND VENT SYSTEM COMPONENTS

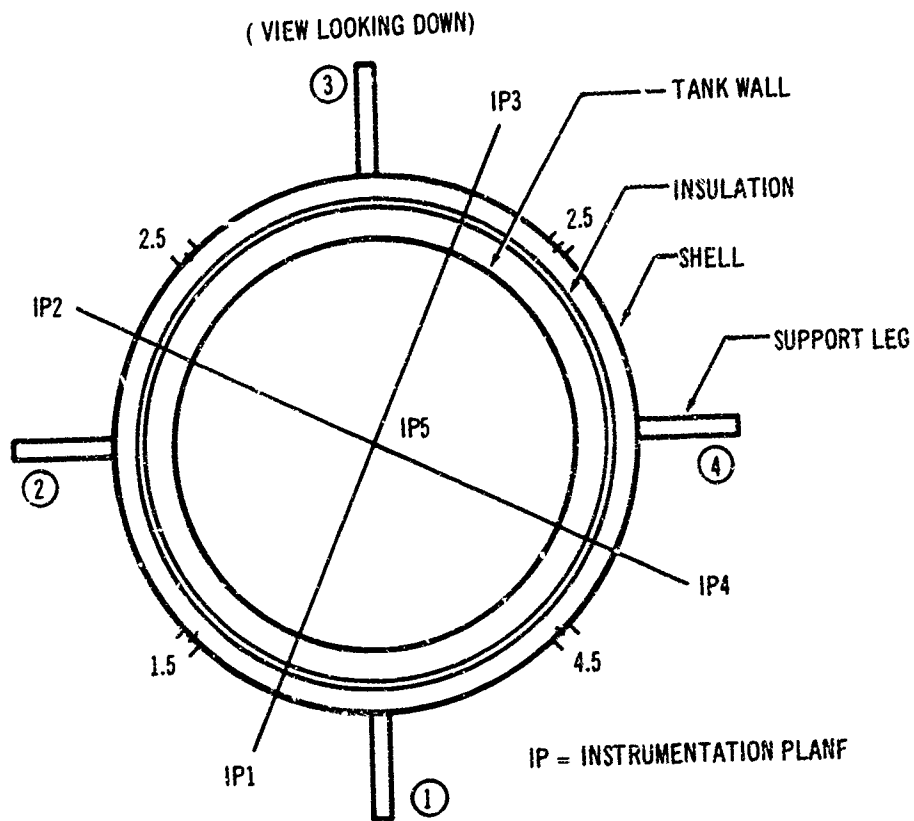
Component	Supplier/ Part Number	Location	Actuation
LN ₂ tank, He pressure regulator supply valve	Fox Valve No. 610750	Outside shroud	28 v.d.c.
Hi-pressure H ₂ tank fill & drain valve	Fox Valve No. 610750	Outside shroud	28 v.d.c.
LH ₂ tank check valve	Lanagan No. 90137	Outside shroud	
LN ₂ tank check valve	Lanagan No. 90137	Outside shroud	
Hi-pressure LH ₂ tank check valve	Lanagan No. 90137	Outside shroud	
Filter	Capital Westward No. 20606	Outside shroud	
<u>Control Instrumentatio.</u>			
Liquid level sensors (4)	United Control	On temp. rake	
Liquid level sensor power supplier (2)	United Control	In control console	
Heater temp. probes (2)	Thermal Systems	In heater tube	
Heater temp. sensors (4)	Thermal Systems	On heater tube	

Table 4-45 (page 1 of 2)
TEST DATA INSTRUMENTATION

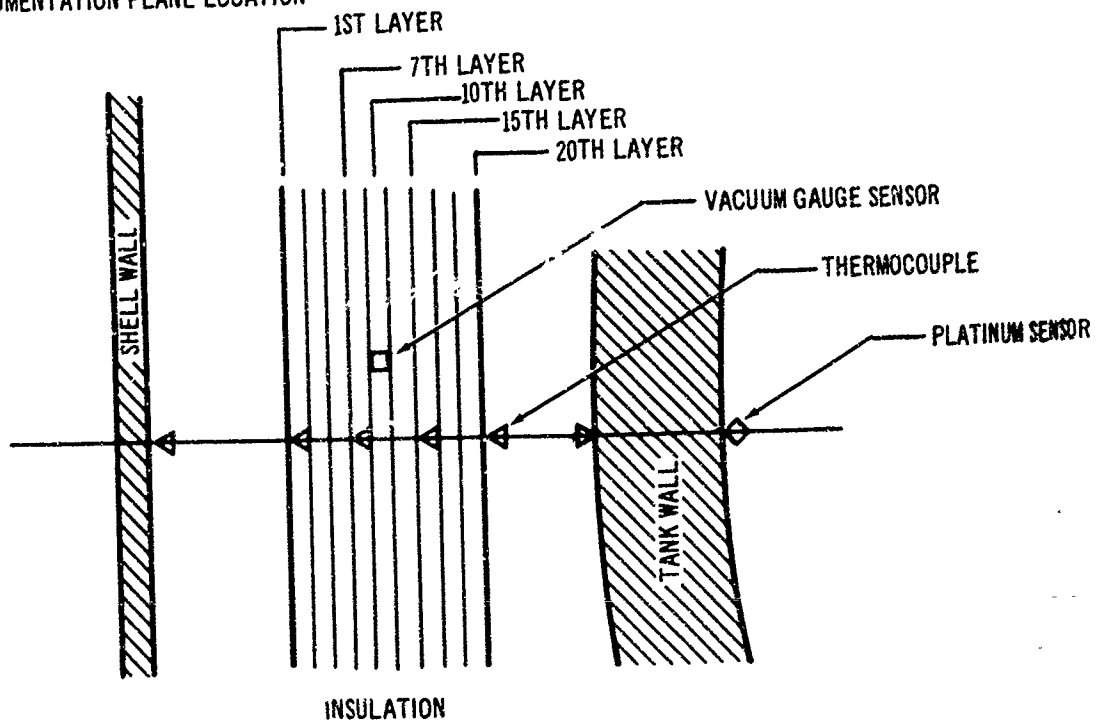
Component	Measurement	No.	Instrument	Environment	Output	Location
LH ₂ tank	Temperature -- internal tank wall	6	Platinum sensors (Thermal Systems Inc.) 1,380a	LH ₂ 37 - 200°R.		Inside tank wall
	Temperature -- external tank wall	15	c - c T _C (Douglas)	37 - 200°R.		Outside tank wall
	Tank pressure	1	Strain gage pres. transducer Statham PA750TC	25 to 260 p. s. i. a. 37 - 800°R.		Mounted off LH ₂ tank Manhole cover
LN ₂ tank	Temperature -- internal tank wall	4	Platinum sensors (Thermal Systems Inc.) 1,380a	LN ₂ 140 - 300°R.		Inside tank wall
	Temperature -- external tank wall	10	c - c T _C (Douglas)	140 - 300°R.		Outside tank wall
	Tank pressure	1	Strain gage pres. transducer Statham PA750TC	25 - 260 p. s. i. a. 140 to 800°R.		Mounted off LN ₂ tank Manhole cover
Primary insulation	Temperature -- insulation sheets	44	c - c T _C (Douglas)	37 to 500°R. v. a. c.		Within insulation
	Pressure within insulation	5	Thermocouple-type vacuum gages Hastings DV8	10 ⁻⁵ to 10 ⁻² torr.		Within insulation
LH ₂ tank pressure line	Temperature -- inlet gas	1	c - c T _C (Douglas)	100 to 800°R. 25 to 250 p. s. i. a.		Upstream of penetra- tion projecting into gas stream
	Temperature -- gas line	3	c - c T _C (Douglas)	100 to 800°R.		Along length of line
LN ₂ tank pressure line	Temperature -- inlet gas	1	c - c T _C (Douglas)	160 to 800°R. 25 to 250 p. s. i. a.		Upstream of penetra- tion projecting into gas stream
	Temperature -- gas line	3	c - c T _C (Douglas)	160 to 800°R.		Along length of line
LH ₂ tank vent line	Temperature -- vent line	3	c - c T _C (Douglas)	37 to 200°R.		Along length of line
LN ₂ tank vent line	Temperature -- vent line	3	c - c T _C (Douglas)	140 to 300°R.		Along length of line
He supply line	Temperature -- line segment	3	c - c T _C (Douglas)	37 to 500°R.		Along length of line
	Pressure helium tank	1	Strain gage pres. transducer Statham PA750TC	4,000 to 400 p. s. i. a. LH ₂ temperature		Immediately down- stream of penetration
	Temperature -- He gas flow	1	c - c T _C (Douglas)	37 to 70°R.		Immediately down- stream of penetration into gas stream

Table 4-45 (page 2 of 2)
TEST DATA INSTRUMENTATION

Component	Measurement	No.	Instrument	Environment	Output	Location
Auxiliary LH ₂ supply bottle system	Pressure -- auxiliary LH ₂ tank	1	Strain gage pres. transducer Statham PA740TC	4,000 to 400 p. s. i. a. LH ₂ temperature		Immediately downstream of penetration
LH ₂ tank rake	Temperature -- tank fluids	21	Platinum sensors (Thermal Systems, Inc.) 1,380a	37 to 600°R. 25 to 250 p. s. i. a.		On longitudinal rake 5 in. apart
LN ₂ tank rake	Temperature -- tank fluids	15	Platinum sensors (Thermal Systems, Inc.) 1,380a	140 to 700°R. 25 to 250 p. s. i. a.		On longitudinal rake 6 in. apart
Structure shell	Temperature -- shell skin	25	c - c T _c (Douglas)	300 to 600°R.		On skin
	Pressure -- interstage	2	Thermocouple-type vacuum gage - Hastings DV8	10 ⁻⁵ to 10 ⁻² torr.		With shell
	Temperature -- support point	4	c - c T _c (Douglas)	300 to 600°R.		On each support
LH ₂ feed line	Temperature -- line	8	c - c T _c (Douglas)	37 to 70°R.		Along length of line
	Pressure -- LH ₂ outlet	1	Pressure transducer Statham PA750TC	25 to 300 p. s. i. a.		Upstream of flow meter
	Flow -- LH ₂ rate	1	2-1/2 in. flow meter, 150 lb. flanges Potter 5000 series	LH ₂ 37 to 70°R. 25 to 300 p. s. i. a. 4.59 to 0.46 lb./sec.		Upstream of interface flange
LN ₂ feed line	Temperature -- line	4	c - c T _c (Douglas)	140 to 200°R.		Along length of line
	Pressure -- LN ₂ outlet	1	Pressure transducer Statham PA750TC	25 to 300 p. s. i. a.		Upstream of flow meter
	Flow -- LN ₂ rate	1	Flow meter, 150 lb. flanges Potter 5000 series	LN ₂ 140 to 200°R. 25 to 300 p. s. i. a. 33 to 3.3 lb./sec.		Upstream of interface flange
LH ₂ tank supports	Temperature	6	c - c T _c (Douglas)	37 to 500°R.		Along two support rods
LN ₂ tank supports	Temperature	6	c - c T _c (Douglas)	140 to 500°R.		Along two support rods



(a) INSTRUMENTATION PLANE LOCATION



(b) INSULATION THERMOCOUPLE ARRANGEMENT

A

NUM SENSOR

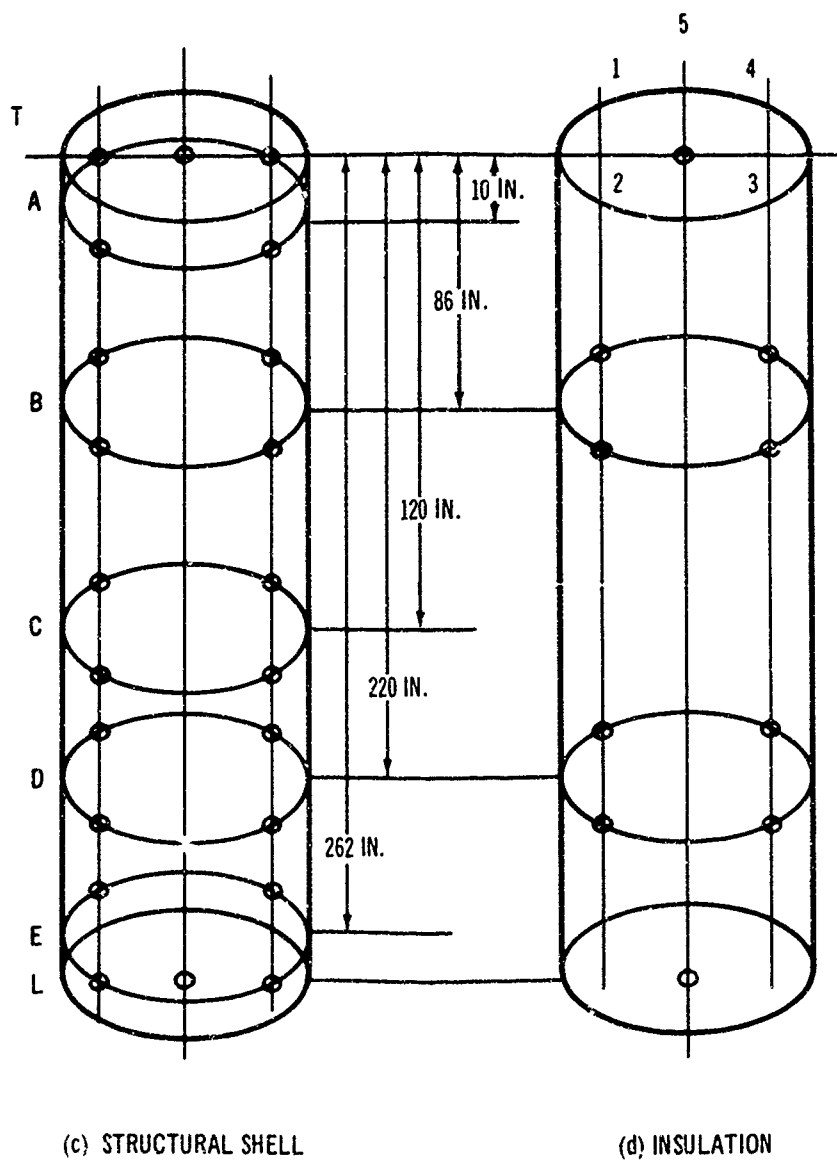
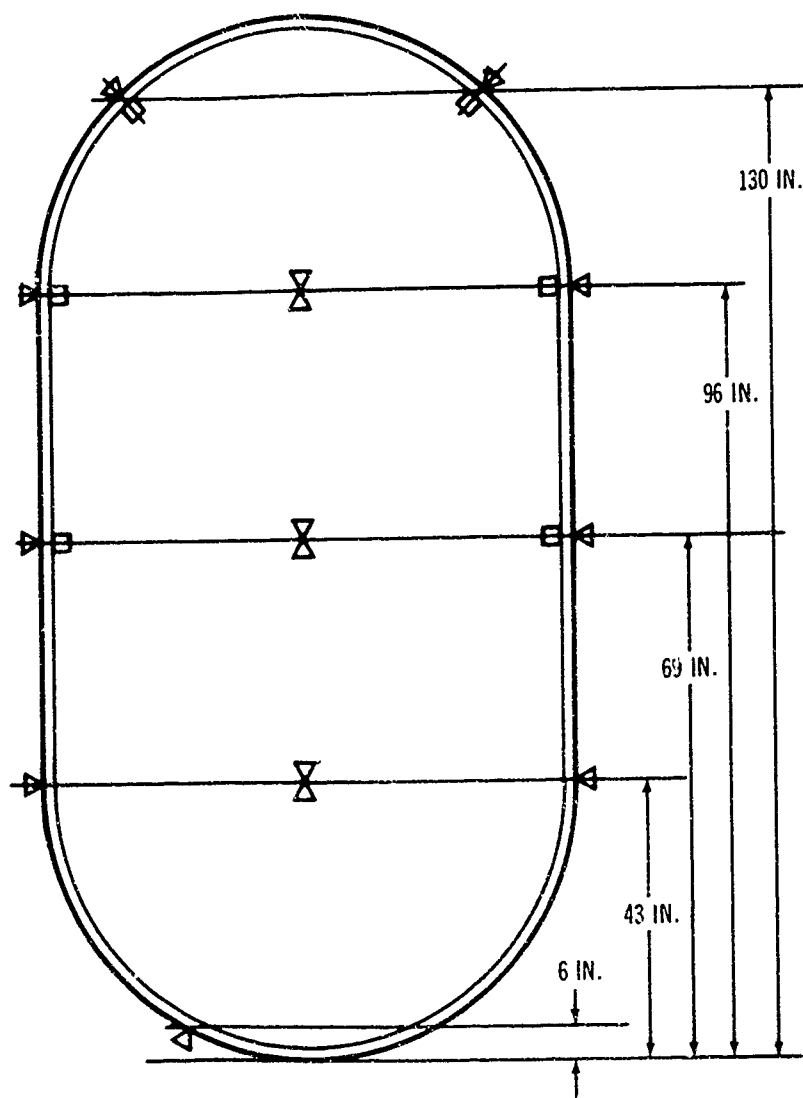


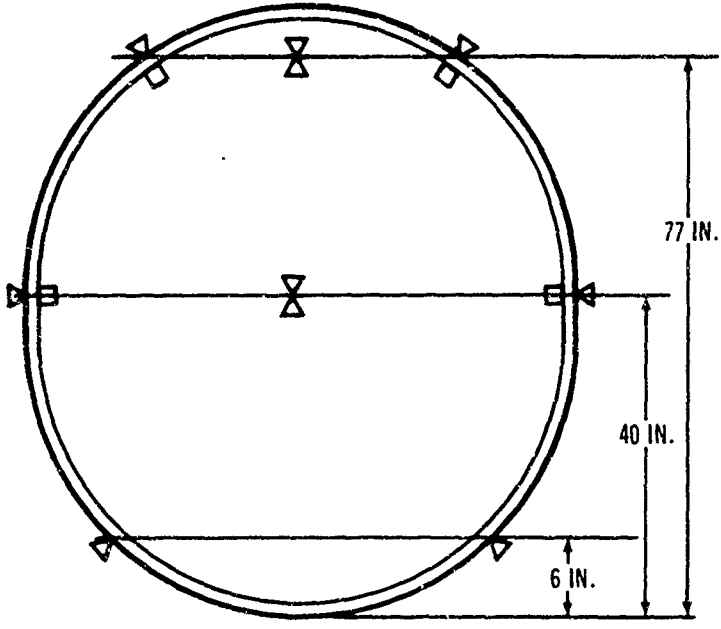
Figure 4-134. Basic Data Instrumentation Location



LH₂ TANK

A

- ▽ THERMOCOUPLES (OUTSIDE TANK)
- PLATINUM SENSORS (INSIDE TANK)



LN₂ TANK

3

Figure 4-134. Cont.

and tank instrumentation stations are aligned so that all stations fall in line with each other as indicated in figure 4-134. Figure 4-134 also indicates the location of the inside and outside tank wall temperature sensors. Figure 4-135 is a photograph of the LN₂ tank temperature probe as installed on the manhole cover. The level sensors can also be seen at the extreme ends of the phenolic probe.

In addition to the pressure transducers listed in table 4-45, there is an additional pressure transmitter connected to each propellant tank which is a part of the tank pressure control system and is therefore not an integral part of the test data instrumentation system.

Two vacuum-compatible Teflon terminal boards were provided on the exterior of the shroud to serve as electrical interfaces. In addition, there is a 37-pin electrical connector in valve module no. 2 to accommodate the valve wiring.

e. Assembly. The entire test apparatus was assembled in the Douglas Development Fabrication Laboratory at Santa Monica, California. Figures 4-136 and 4-137 show four views of the completed test apparatus.

f. Testing. To ensure adequacy of the test apparatus, an extensive series of tests was conducted which stressed leak checking and functional capability. As discussed in earlier sections of this document, the tankage was hydrotested by the manufacturer to 1.5 times its maximum operating pressure. This procedure was also used by Douglas on all fabricated items that were to be used under pressure. The glass fiber tank support rods were also load tested.

In addition to these normal structural tests, the following was performed:

- An ambient temperature He leak test at 2,250 p. s. i. a. was performed on the pressurant storage bottles as installed in the LH₂ tank.
- The LH₂ and LN₂ tank assemblies were leak checked with He as the pressurant. Tests were performed at ambient and near LH₂ temperatures at a pressure of 185 p. s. i. a. (this was the limit as permitted by Douglas safety requirements).
- An ambient and near-LN₂-temperature leak test was performed on the LH₂ and LN₂ feed line system as installed in the test apparatus at 185 p. s. i. a. A similar test was performed on the vent valve assemblies, and the vent line assemblies between the tank and the vent valve assembly. These items were not installed, however.
- Ambient temperature He leak tests were performed at 185 or 2,250 p. s. i. a. on all pressurization line assemblies.

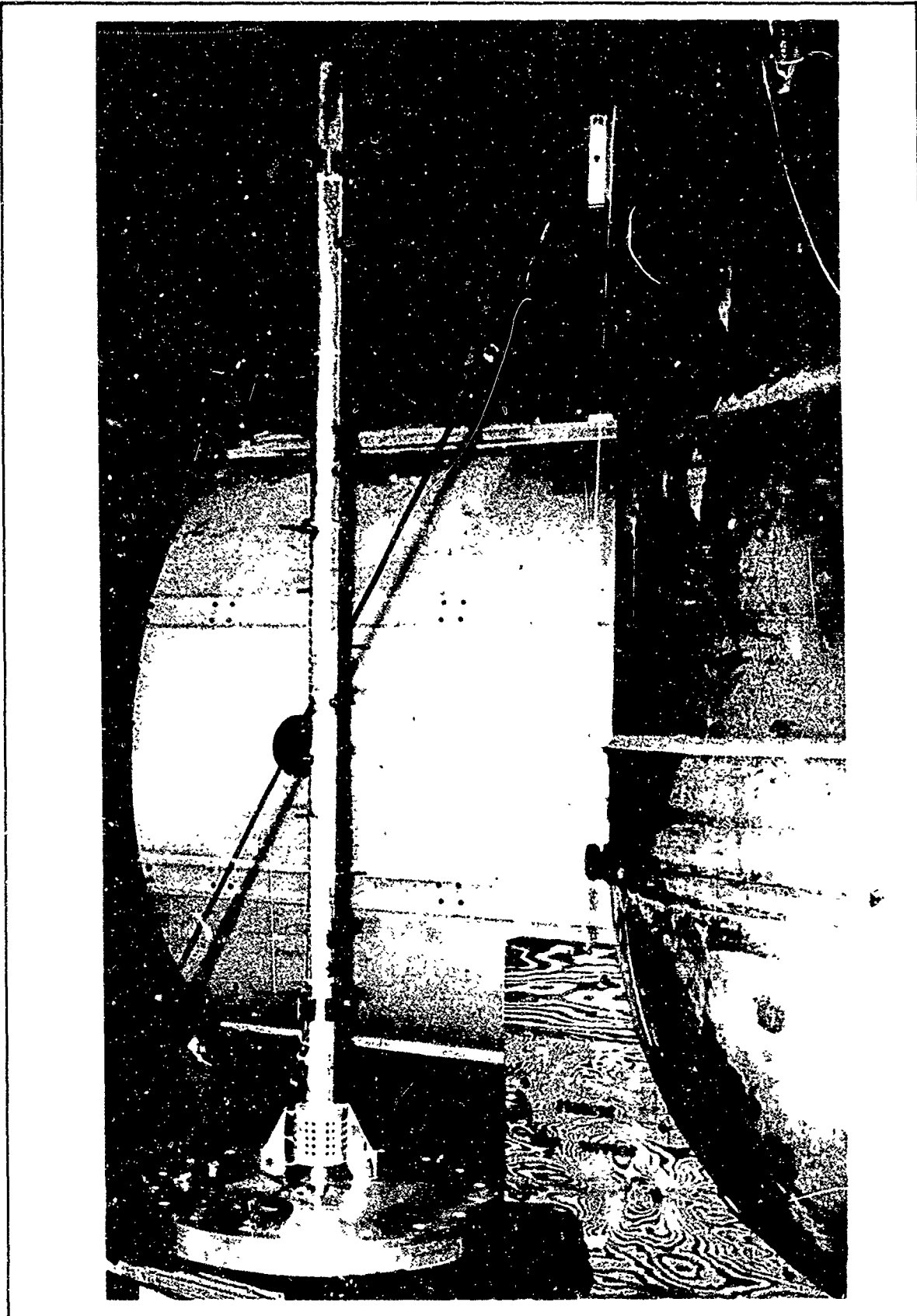


Figure 4-135. LN₂ Tank Temperature Rake

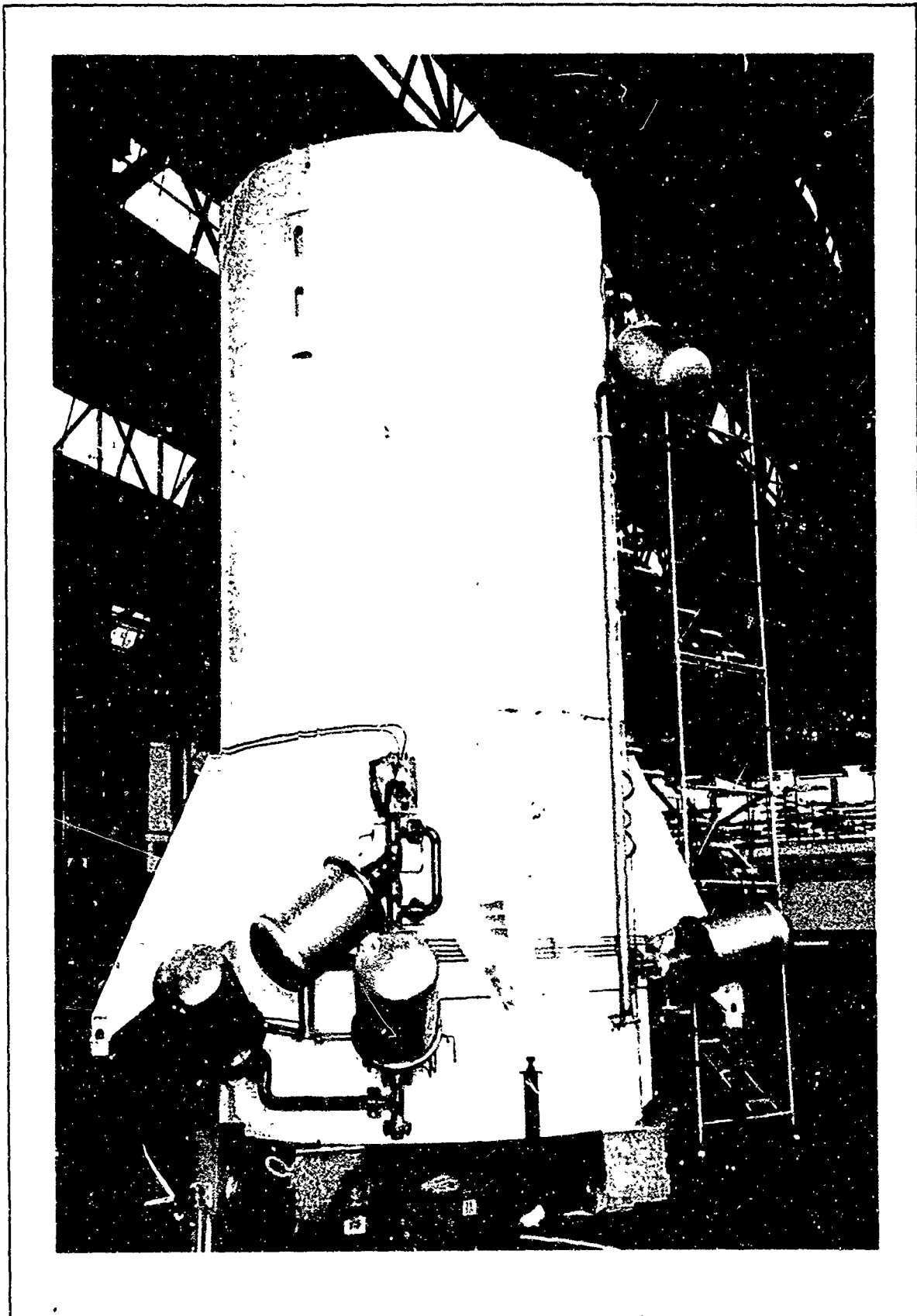


Figure 4-136. Completed Test Apparatus (Front View)

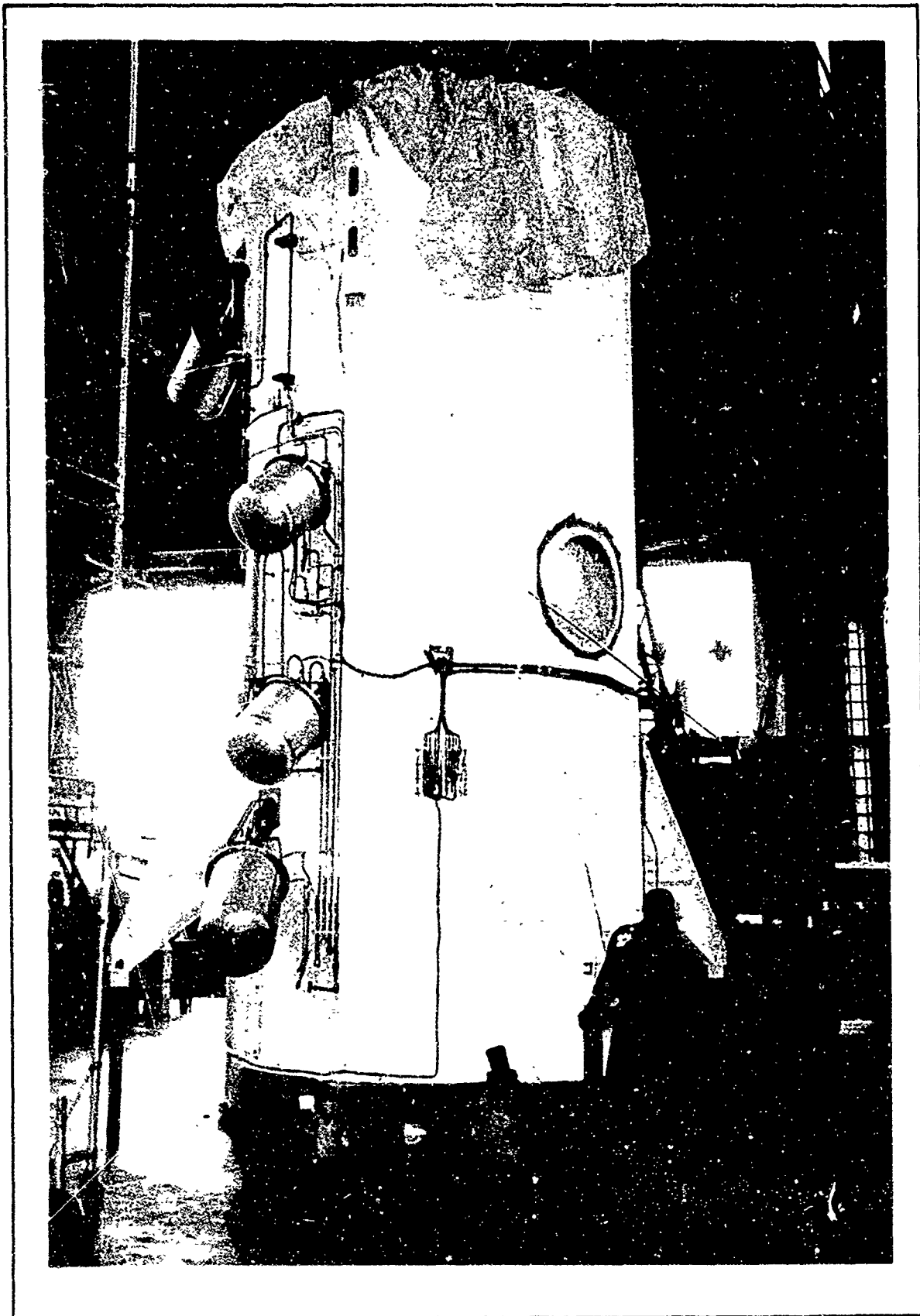


Figure 4-137. Completed Test Apparatus (Side View)

- After complete assembly of the test apparatus, an ambient He leak test was performed on the entire test apparatus at 185 p. s. i. a. downstream of the pressurant regulator valves and at 2,250 p. s. i. a. upstream of the regulator valve.
- The complete test apparatus was subjected to final a functional test including LN₂ and LH₂ loading, pressurization, venting and expulsion at 50 p. s. i. a. tank pressures. This was performed at atmospheric conditions in the Douglas LH₂ research laboratory at Santa Monica.

In all cases leakage was monitored with a mass spectrometer (the object was to get no significant readings on the instrument).

Difficulty was encountered in the pressurant bottle tests with Conoseal fitting leakage. It was found that this could be eliminated with the newer Teflon-coated seal rings.

In the tank assembly tests, a small amount of leakage was detected at the tank outlet flanges. This was corrected by increasing the number of bolt holes in the flange joint. The Creavey flange seals performed very well.

The most severe leakage was found in the burst disc assemblies. These were returned to the vendor for rework. Also the number of bolt holes in the mating flanges was increased, and a Teflon spray was used on the seal surfaces. These combinations eventually solved the problem.

The full-system leak checks went very smoothly. Leakage that did occur resulted from loose connections or improperly installed seals. In the process of running the total system leak tests, the test apparatus pressurization and vent system was operated. During operation, a structural failure, the result of vibration, occurred in the LH₂ tank pressurant heater turbulator. This damaged the heater and caused metal particles to be sent into the LH₂ tank. The turbulator was redesigned, tested and reinstalled after cleaning out the hydrogen system.

The test apparatus and its insulation system were primarily designed for vacuum chamber operation. However, since a loading and expulsion test had to be run prior to deliver, the system had to be capable of what was essentially a ground-hold operation. Since it was desirable at the same time to demonstrate the feasibility of a pure He purge for ground hold, no additional insulation (just for loading) was used. Prior to loading, the shell structure was sealed and was subjected to an ambient temperature He purge between the tankage and the insulation. LH₂ tank loading was attempted but had to be aborted when the purge failed to maintain positive pressure within the shell. Because of the purge failure, there was subsequent cryopumping into the insulation. Leakage in the LH₂ tank shutoff valve actuator also prevented proper valve operation. As a result of this failure, some moisture damage occurred to the insulation, although this was much less than would have been expected under the extensive cryopumping.

Prior to the second loading attempt, the following actions were taken:

- A new, larger capacity purge manifold was installed.
- Provisions for a cold He purge were made by plumbing into the facility LH₂-He heat exchanger.
- The shell was sealed more completely.
- A purge gas sampling system was installed.
- More instrumentation was connected.
- The LH₂ tank shutoff valve was repaired.

On 27 July, the filling and expulsion test was successfully completed. The shell structure was initially purged with ambient temperature He, and after about 1 hr. and 45 min., the proper He environment was established. 10,000 scf of He had been sent into the 3,300 ft.³ shell. A cold He purge was then initiated and shortly after the LN₂ tank was filled. This filling took about 10 min. The LN₂ tank was then pressurized and expelled, and system behaved satisfactorily.

The 1,500 gal. LH₂ tank was then filled. This took about 50 min. and required 5,000 gal of LH₂ which was less than expected, considering the mass of the LH₂ tank assembly. The LH₂ tank was then pressurized and the LH₂ was expelled. The only difficulty encountered was that no readout was received from the flow meters. This was later traced to an improper readout equipment connection.

This concluded the testing operations and the test apparatus was prepared for shipment to Edwards Air Force Base, 17 August 1966.

9. Phase IX--Space Simulation Testing. During the vacuum chamber space simulation testing, the following basic items are to be assessed for both LH₂ and LN₂ within the limits imposed by a 1-g. environment and structurally static test operations:

- 1) Space performance of the high-performance insulation system.
- 2) Structural heat leaks
 - a. Tank supports.
 - b. Feedlines.
 - c. Vent lines.
 - d. Pressurant supply lines.
 - e. Miscellaneous.
- 3) Pressurant gas requirements for initial LH₂ and LN₂ tank pressurization:
 - a. Influence of inlet gas temperature.
 - b. Influence of initial ullage volume.
 - c. Influence of initial propellant temperature.
 - d. Influence of pressurant type.
 - e. Influence of required pressure rise.
- 4) Pressurant gas requirements for expulsion of LH₂ and LN₂.
 - a. Influence of expulsion rate.
 - b. Influence of inlet gas temperature.
 - c. Influence of ullage volume.
 - d. Influence of propellant temperature.
 - e. Influence of pressurant type.
 - f. Influence of initial pressurization.
 - g. Influence of expulsion pressure.
- 5) Influence of blowdown on propellant state.

Items 1 and 2 are basically concerned with the system thermal protection while items 3, 4, and 5 are principally related to the pressurization system. They are all interrelated, however, when considering total propellant heat load. For example, the heat which is added to the pressurant during an expulsion eventually ends up in the propellant especially for a multiburn case. Thus, propellant heat load cannot be divorced from the pressurization system.

Items 1 and 2 are essentially independent of the duty cycle details. Conditions within the insulation should stabilize from 1/2 to 1 hr. after equilibrium chamber vacuum and shell temperatures are achieved. Total input to the propellant (B. t. u.) will vary with time, but once stabilization is achieved, the insulation heat flux (B. t. u. /ft.²-hr.) should not vary greatly with time. Second-order effects on heat flux will be introduced by variations

in propellant temperature and amount of propellant in the tanks, but data on these influences should automatically result by selecting the test runs to satisfy the pressurization test requirements which are more strongly influenced by duty cycle details.

To provide data to evaluate items 3, 4, and 5, tests must be run with the following varying conditions over the range indicated:

- Expulsion rates (100 to 10 pct. flow).
- Tank pressures (235 to 25 psia).
- Inlet gas temperatures (100 to 800°R.).
- Ullage volume (3 to 90 pct.).
- Propellant temperatures.

The test apparatus has the capabilities of directly controlling and varying the first four items above, and propellant temperature variations are obtained by altering the simulated coast duration (time between expulsions). The magnitude of the listed variables covers the range implied by the ground-rule duty cycles and tank pressures.

Since the objective of the test program is to generate data to permit necessary correlation and modification of the analytical techniques used in the study phases of the program, it is not essential that the individual duty cycles be run in detail. These objectives can be achieved as adequately, and with much less expense, by selecting a run sequence that will bracket the range of all critical variables. Costs can also be minimized by reducing the number of vacuum chamber pumpdowns. Barring component failures, the test apparatus is capable of running any sequence of tests within the range of specified operating conditions with a single chamber pumpdown. However, it is recommended that the testing be divided into at least two pumpdown sequences. The first would be relatively short and a preliminary data reduction would be made to ensure satisfactory operation. This is especially important since the testing must be conducted with a limited amount of real time readout.

a. Test Plan Development. A preliminary run sequence of 25 individual propellant tank loadings and expulsions was evolved. Specific conditions were established which would bracket the full range of operating conditions. Expulsion sequences were selected primarily to permit an evaluation of the pressurization systems and operating conditions. The thermal performance of the insulation and structure should naturally fall out from this testing.

The developed run sequence is shown in table 4-46. The first 24 runs had the same general propellant consumption schedule; that is, all runs were started with essentially a full tank and the propellant was expelled in five steps: step 1 expelling 20 pct. of the total initial load; step 2, 30 pct.; step 3, 10 pct.; step 4, 30 pct.; and step 5 expelling the remainder. The

Table 4-46

TESTING RUN SEQUENCE

Propellant Load Number	Time (hr.)	Tank Pressure	Ullage Volume (pct.)	Total Load Expelled (pct.)	Expulsion Rate (pct.)	Inlet Gas Temperature (°R.)	Pressurant Type	
1	t+1	100	Minimum	20	100	300	He	
	+2	100			30	100	300	He
	+3	100			50	100	300	He
	+4	100			60	100	300	He
	+5	100			90	100	300	He
2		100			50	300	He	
3		100			10	300	He	
4		25			100	300	He	
5		25			10	300	He	
6		235			100	300	He	
7		235			10	300	He	
8		100			100	800	He	
9		100			10	800	He	
10		25			100	800	He	
11		25			10	800	He	
12		100			100	150	He	

Table 4-46 (cont)

Propellant Load Number	Time (hr.)	Tank Pressure	Ullage Volume (pct.)	Total Load Expelled (pct.)	Expulsion Rate (pct.)	Inlet Gas Temperature (°R.)	Pressurant Type
13	t+1	100	Minimum	20	10	150	He
	+2						
	+3						
	+4						
	+5						
14	25	25	Minimum	20	100	150	He
15	235	235	50	10	10	150	He
16	100	100	90	30	100	300	GH ₂
17	100	100			10	300	GH ₂
18	25	25			100	300	GH ₂
19	235	235			100	300	GH ₂
20	100	100			100	800	GH ₂
21	25	25			100	800	GH ₂
22	100	100			100	150	GH ₂
23	25	25			100	150	GH ₂
24	235	235			10	150	GH ₂

Table 4-46 (cont)

Propellant Load Number	Time (hr.)	Tank Pressure	Ullage Volume (pct.)	Total Load Expelled (pct.)	Expulsion Rate (pct.)	Inlet Gas Temperature (°R.)	Pressurant Type
25	t+1	50	Minimum	10	50	350	GH ₂
	t+1+tb	50	10	40	50	350	GH ₂
	t+1+2tb	50	50	40	50	350	GH ₂
	t+1+3tb	50	90	10	50	350	GH ₂
26		50			50	350	GH ₂

system was allowed to come to equilibrium between each expulsion step. The equilibrium assumed that the tank pressure dropped to its minimum point and began to increase and that all temperatures were restabilized. It had been assumed that this would occur in about 1 hr.; however, this was difficult to estimate accurately. The conditions which varied between runs (or propellant loads) included tank pressure, expulsion rate, inlet gas temperature, and LH₂ tank pressurant. The general approach for selecting the values for these parameters was to test primarily at nominal conditions and check extremes. For example, most of the test runs (11) were made at a tank pressure of 100 p. s. i. a., which was representative of a pressure-fed case; nine test runs were made at 25 p. s. i. a. which was representative of a pump-fed case or a pressure-fed with booster pump case. The high pressure of 235 p. s. i. a. was checked at five points.

The 25 p. s. i. a. condition was considered to be the minimum possible tank pressure. It was found, however, that it may not be possible to achieve such low pressures because of the propellant storage facilities restrictions.

Run 25 was different from the preceding runs. The consumption schedule was slightly different and was in four separate expulsions rather than five. The time between expulsions, t_b , was such that venting and boil-off were assured, as well as stabilization. The low tank pressure level was selected to minimize the actual testing time. The test permits the most complete evaluation of the insulation performance and an evaluation of preconditioning prior to expulsion.

Measuring the boiloff during runs 25 and 26 was difficult because of varying tank pressure and temperature during the vent valve opening. GH₂ pressurization was used to minimize the problem. This eliminated the two-component gas problem. During run 26, tank blowdown and preconditioning to 5 p. s. i. NPSH was made for each expulsion cycle. These results will be compared with the results of run 25, which has no preconditioning. It is believed that this represents a minimum scope testing plan which should provide sufficient data to correlate the analytical models used throughout the study. It should be noted that, in all probability, the results obtained from these 26 runs will suggest additional tests.

Data sampling for the testing is an important consideration. It appears that, during expulsion and immediately following expulsion, data should be sampled every 1 to 2 sec. During simulated coasting periods, data should be sampled every 30 sec. The data testing times may be changed, after one or two tests, to permit a better indication of the system responses.

b. Operating Procedure.

(1) Initial loading and orbit simulation is accomplished as follows:

- Load facility with propellants and gases (F).^a
- Seal vacuum chamber and pump down to minimum possible pressure level (F).
- Apparatus control panel check (check list A).
- Set vent valve relief pressure.

Remove alarm relay cover.
Plug in milliampmeter.
Adjust potentiometer to desired meter reading
(1 to 5 ma. = 0-300 p. s. i. a.).
Unplug milliampmeter and replace alarm relay cover.

- Energize apparatus control panels.

Switch on 115 v. a. c. on rack A and B.
Switch on 28 v. d. c. on rack A and B.
- Set pressure and energize control gas supplies (F).

He control gas (150 p. s. i. a.)
N₂ control gas (150 p. s. i. a.)
- Purge propellant tanks with dry N₂ gas (F).
- Load propellants.

Place liquid level sensors in On position with selector switch in "HI" position.

Prepare liquid nitrogen tank.

- 1) Make sure than LN₂ vent valve light indicates valve "Open".
- 2) Set LN₂ throttle valve to "100 pct." closed.
- 3) Open apparatus fill and drain valve.
- 4) Open apparatus LN₂ prevalve.
- 5) Close supply tank vent valve (F).
- 6) Pressurize LN₂ supply tank to 15 p. s. i. a. (F).
- 7) Open LN₂ supply tank outlet valve (F).
- 8) Observe LN₂ tank "wet" light.
- 9) When "wet" light comes on, close LN₂ prevalve.

^a(F)Indicates USAF facility equipment.

Prepare LH₂.

- 1) Make sure that LH₂ vent valve light indicates valve "Open"
- 2) Set LH₂ throttle valve to "100 pct." closed.
- 3) Open apparatus LH₂ fill and drain valve.
- 4) Open apparatus LH₂ prevalve.
- 5) Close supply tank vent valve (F).
- 6) Pressurize LH₂ supply tank to 15 p. s. i. a. (F).
- 7) Open LH₂ supply tank outlet valve (F).
- 8) Observe LH₂ tank wet light.
- 9) When "wet" light comes on, close LN₂ prevalve.
- 10) Load pressurants.

Turn on instrumentation system to permit readout on pressurant bottle and line pressure levels.

Load GHe.

Close helium vent stack (F).
Open helium supply valve (F).
Open helium fill and vent valve.
Observe helium tank pressure level.
When 3,000 p. s. i. a. is indicated, close helium fill and vent valve.

Load LH₂ pressurant.

Open auxiliary LH₂ fill valve.
Flow for the required number of seconds to fill auxiliary LH₂ tank.
Close auxiliary LH₂ fill valve.

- Check top propellant tanks.

LN₂ tank

- 1) If LN₂ tank level sensor indicates "dry," open LN₂ tank pre-valve until "wet" light comes on, close prevalve. If "wet" light is still on, pass to step 2.
- 2) Close LN₂ fill and drain valve.
- 3) Close LN₂ supply tank valve (F).
- 4) Depressurize and vent LN₂ supply tank (F).

LH₂ tank

- 1) If LH₂ tank level sensor indicates "dry," open LH₂ tank pre-valve until "wet" light comes on and close prevalve. If "wet" light is still on, pass to step 2.

- 2) Close LN₂ fill and drain valve.
 - 3) Close LH₂ supply tank valve (F).
 - 4) Depressurize and vent LH₂ supply tank (F).
- Turn "Off" liquid level sensors.
 - Set LN₂ and LH₂ liquid level sensors to "Lo."
 - Turn on complete data system.
 - Initiate orbit heating.
 - Turn on heating lamps.
 - Observe skin temperature readouts.
 - Correct lamp energy to yield desired skin temperature.
 - Close tank vents.
 - Place manual LH₂ tank vent in closed position. Observe vent indicator light.
 - Place manual LN₂ tank vent in closed position. Observe vent indicator light.
 - (Automatic tank vent system is now operating.)
 - Close auxiliary LH₂ vent.
 - Apparatus control panel check. (checklist B)
- (2) General Expulsion Cycle (Non-Depletion).
- Set throttle valves to desired position.
 - LH₂ throttle valve.
 - LN₂ throttle valve.
 - Set temperature on LH₂ and LN₂ tank pressurant heater power controls (F).
 - Select LH₂ tank pressurant (He or GH₂).
 - Open main pressurant supply valves.
 - All He: open main He valve.
 - GH₂ LH₂-pressurant: open main He and main GH₂ valve simultaneously.
 - Set pressurant regulators to desired level.
 - Turn on pressurant heater power (F).

- Open tank prevalues.

LH₂ tank.
LN₂ tank.

- Check flow rate readings and readjust throttling valves, if necessary.
- Monitor inlet gas temperature and adjust power control, if necessary.
- Permit expulsion and specified number of seconds.
- After allotted expulsion time, shut down system.^a

Close LH₂ tank outlet valve and LN₂ tank outlet valve simultaneously.

Close main pressurant supply solenoids.

Close throttling valves.^a

Shut off pressurant heater power supply.

Vent all pressurant (LH₂ and He).^a

Set LH₂ and LN₂ tank regulators to zero.

Run apparatus control panel check (checklist C).

(3) General Expulsion Cycle (Depletion and Shutdown).

- Set throttle valves to desired position.

LH₂ throttle valve.
LN₂ throttle valve.

- Set temperature on LH₂ and LN₂ tank pressurant (F).
- Select LH₂ tank pressurant (He or GH₂).
- Open main pressurant supply valves.

He: open main He valve.

GH₂ LH₂-pressurant: open main He and main GH₂ valve simultaneously.

- Set pressurant regulators to desired level.
- Turn on pressurant heater power (F).
- Open tank prevalues.

LH₂ tank.
LN₂ tank.

^aFor long-term shutdown only.

- Check flow rate readings and re-adjust throttling valves, if necessary.
- Monitor inlet gas temperature and adjust power control, if necessary.
- Permit expulsion for specified number of sec.
- After allotted expulsion time, shutdown system.

Close LH₂ tank outlet valve.
Close LN₂ tank outlet valve.
Close main pressurant supply solenoids.
Open manual vent valves.
Open throttling valves.
Shut off pressurant heater power supply.
Vent all pressurant (LH₂ and He).
Set LH₂ and LN₂ tank regulators to zero.
Run apparatus control panel check (checklist A).

Checklist A

Rack A

115 v. a. c. power (off).
28 v. d. c. power (off).
LH₂ manual vent (open).
LN₂ manual vent (open).
Pressurant selector (null).
Main He valve (closed).
Main GH₂ valve (closed).
LH₂ tank regulator (off).
LN₂ tank regulator (off).

Rack B

115 v. a. c. power (off).
28 v. d. c. power (off).
Auxiliary LH₂ fill (closed).
Auxiliary LH₂ vent (open).^a
He fill (closed).^a
Level sensors (off).^a
Auto depletion switch (off).
Level sensor (high)
LH₂ fill (close).
LN₂ fill (close).
LH₂ pre valve (close).
LN₂ pre valve (close).
LH₂ throttle valve (close).
LN₂ throttle valve (close).

Checklist B

Rack A

115 v. a. c. power (on).
28 v. d. c. power (on).
LH₂ manual vent (closed).
LN₂ manual vent (closed).
Pressurant selector switch (null)
Main He valve (closed).
Main GH₂ valve (closed).
LH₂ tank regulator (zero).
LN₂ tank regulator (zero).

Rack B

115 v. a. c. power (on).
28 v. d. c. power (on).
Auxiliary LH₂ fill (closed).
Auxiliary LH₂ vent (closed).
Helium fill (closed).
Level sensors (off).
Automatic depletion switch (on).
Level sensor (low).
LH₂ fill (close).
LN₂ fill (close).
LH₂ pre valve (close).
LN₂ pre valve (close).
LH₂ throttle valve (close).
LN₂ throttle valve (close).

^aLong-term shutdown only.

Checklist C

Rack A

115 v. a. c. power (on).
28 v. d. c. power (on).
LH₂ manual vent (closed).
LN₂ manual vent (closed).
Pressurant selector (He).
Main He valve (closed).
Main GH₂ valve (closed).
Solenoid valve 3 (closed).
LH₂ tank regulator (zero).
LN₂ tank regulator (zero).

Rack B

115 v. a. c. power (on).
28 v. d. c. power (on).
Auxiliary LH₂ fill (closed).
Auxiliary LH₂ vent (open).^a
Helium fill (open).^a
Level sensors (off).^a
Auto depletion switch (on).
LH₂ level sensor (lo).
LH₂ fill (close).
LN₂ fill (close).
LH₂ pre valve (close).
LN₂ pre valve (close).
LH₂ throttle valve (close).
LN₂ throttle valve (close).

^aLong-term shutdown only.

Section V
NOMENCLATURE

A	Cross-sectional Area
B_o	Bond number
C	Heat-transfer circumference
C_p	Specific heat
D^*	Diffusion coefficient
D	Diameter
E	Electric field intensity
F	Force
F	Radiation configuration factor
G_r	Grashof number
H	Enthalpy
I_{sp}	Specific Impulse
J	Energy equivalent
K	Dielectric constant
L	Length
M	Average molecular weight
P_r	Prandtl number
Q	Heat transfer rate
R	Radius or universal gas constant
R_e	Reynolds number
S	Entropy

S_t	Stanton number
T	Temperature
U	Overall heat-transfer coefficient
V	Volume
W	Weight
W_e	Weber number
Z	Compressibility factor
a	Lineal dimension
b	Lineal dimension
c	Total molar concentration
d	Diameter
f	Friction factor
g	Gravitational constant
\underline{h}	Convective heat-transfer coefficient
h	Head
k	Thermal conductivity
\dot{m}	Propellant mass flow rate
n	Number of insulators
\dot{n}	Interface mass evaporation rate
p	Pressure
q	Heat flux per unit time
r	Radius
t	Time or thickness
v	Velocity
w	Vibration frequency
\dot{w}	Flow rate
x	Length dimension

ρ	Density
σ'	Surface tension
σ	Stefan Boltzman constant
λ	Vibration amplitude
μ	Viscosity
ϵ'	Capacitance
ϵ	Emissivity
β	Coefficient of expansion
γ	Specific heat ratio
ω	Rotational velocity

Section VI
REFERENCES

1. Liquid Hydrogen Boost Pump and Drive Analysis for Fluorine Maneuvering Stage Study, Final Report - Phase I Engineering Report No. 3513, Pesco Products, 8 September 1965.
2. A Compendium of the Properties of Materials at Low Temperature, Part I, WADD TR-60-56, July 1960.
3. A Compendium of the Properties of Materials at Low Temperature, Part II, WADD TR-60-56, July 1960.
4. Reynolds, W. C., Hydrodynamic Considerations for the Design of Systems for Very Low Gravity Environment, Stanford University, TR No. LG-1, September 1961.
5. Anliker, M. and Shih, P. Yen-Y, Effects of Geometry and Unidirectional Body Forces on the Stability of Liquid Layers, Stanford University Report SUDAER No. 150, March 1963.
6. Saturn V/S-S-IVB Stage Modifications for Propellant Control During Orbital Testing, Douglas Report SM-47177, April 1965.
7. Zero Gravity Vapor/Liquid Separator Design Review, Pesco Products Report.
8. Adelberg, M., "Cryogenic Problems in Space," Cryogenic Technology, Chapter 14, J. Wiley & Son (1963).
9. Kreith, F., "Principles of Heat Transfer," International Textbook Company (1958).
10. Blackmon, J. B., Collection of Liquid Propellants in Zero Gravity with Electric Fields. Journal of Spacecraft and Rockets, May 1965.
11. Blackmon, J. B., Propellant Orientation in Zero Gravity with Electric Fields. Douglas Paper No. 1468, January 1963.
12. Blackmon, J. B., Experimental Simulation of Propellant Orientation in Zero Gravity with Electrostatic Fields. Douglas Paper No. 1622, January 1963.
13. Development of Expulsion and Orientation Systems for Advanced Liquid Rocket Propulsion Systems SSD-TDR-62-172, December 1962.

14. Reynolds, J.M., H.T. Cho, R.L. Mela Design Study of a Liquid Oxygen Converter for use in Weightless Environment, Technical Document Report No. AMRL-TDR-63-42, June 1963.
15. Horwitz, M. and J.M. Reynolds, E.J. Fahimian, Zero Gravity Control of Hydrogen and Cesium by Electrical Phenomena, Technical Document Report No. APL-TDR-64-46, April 1964.
16. Carslaw, H.S., and Jaeger, J.C., "Conduction of Heat in Solids," Oxford Press (1947).
17. Neel, Carr B., Research on the Stability of Thermal-Control Coatings for Spacecraft, NASA TM-X-51, 196, October 1963.
18. Preliminary Results from the Ames Emmissivity Experiment on OSO II, Personal correspondence from B. D. Pearson.
19. Propellant Storability in Space, Contract AF04(611)-9078, General Electric TDR No. RPL-TDR-64-75.
20. Design Techniques for Structure-Cryogenic Insulation Integration, Martin Company Contract NAS 8-5268, Report No. CR-61038.
21. Development of Thermal Protection System for a Cryogenic Spacecraft Module, 1st Quarterly Report, Contract No. NAS 3-4199, Report No. LMSC-A703794.
22. Development of Thermal Protection System for a Cryogenic Spacecraft Module, 2nd Quarterly Report, Contract No. NAS 3-4199, Report No. LMSC-A729935.
23. Development of Thermal Protection System for a Cryogenic Spacecraft Module, 3rd Quarterly Report, Contract No. NAS 3-4199, Report No. LMSC-A744187.
24. Liquid Propellant Losses During Space Flight, Arthur D. Little Report No. 65008-00-04, October 1964.
25. Thomas, Jr., M., "The Practical Aspects of High Performance Insulation," Douglas Engineering Paper 3279, December 1964.
26. Basic Investigations of Multi-layer Insulation Systems, NASA CR-54191, October 1964.
27. Jones, P. and Terbo, W.H., (private communication), Quality Electric, Los Angeles, June 1965.
28. Guill, J.H., (private communication), LMSC, Sunnyvale, California, July 1965.
29. Jakob, M., "Heat Transfer," Wiley, New York, 1955, Vol. I, pp. 526-542.

30. Anderson and Merled, Thermal-Mechanical Environmental Experiments on Flight Type Insulation Systems for Space Cryogenic Storage Tanks, Preprint 224, 56 National Meeting, AIChE.
31. Knoll, R.H., Smolak, G.R., and Nananaker, R.R., Weightless Experiments with Liquid Hydrogen in Aerobee Sounding Rockets, Uniform Radiant Heat Addition, Flight No. 1, NASA Report No. TM X-484.
32. McArdle, J.G., R.C. Dillon, and D.A. Altmos, Weightless Experiments with Liquid Hydrogen in Aerobee Sounding Rockets, Uniform Radiant Heat Addition, Flight No. 2, NASA Report No. TM X-718, December 1962.
33. Nanaker, R.R., E.L. Coypas, and J. G. McArdle, Weightless Experiments with Liquid Hydrogen in Aerobee Sounding Rockets, Flight No. 3, NASA Report No. TM X-872.
34. Regetz, J.D., M.J. Conroy, and R.G. Jackson, Weightlessness Experiments with Liquid Hydrogen in Aerobee Sounding Rockets, Nonuniform Radiant Heat Addition, Flight No. 4, NASA Report TM X-873, February 1964.
35. Aydelott, J.C. E.L. Coupas, and R.P. Gruber, Comparison of Pressure Rise in a Hydrogen Dewar for Homogeneous, Normal g Quiescent and Zero g Conditions, NASA Report No. TM-1006.
36. A Study of Liquid Hydrogen in Zero Gravity, NASA Report No. TM X-0723, August 1963.
37. Roudebush, W.H., An Analysis of the Problem of Tank Pressurization During Outflow, NASA TND-2585, October 1964.
38. FORTRAN Program for the Analysis of a Single-Propellant Tank Pressurization System, Rocketdyne Report R-5727, 15 June 1964.
39. Liepman, H.W., and Roshko, A., Elements of Gasdynamics, John Wiley & Sons, Inc., 1957
40. Bird, R.B., Stewart, W.E., and Lightfoot, E.N., Transport Phenomena, John Wiley & Sons, Inc., 1960.

DISTRIBUTION LIST

	Copies
Central Intelligence Agency 2430 E. Street, N. W. Washington, D. C. 20505 Attn: OCD, Standard Dist.	1
Office of the Director of Defense Research and Engineering Washington, D. C. 20301 Attn: Dr. H. W. Schultz, Office of Assistant Director (Chemical Technology)	1
National Aeronautics and Space Administration Lewis Research Center 21000 Brookpark Road Cleveland, Ohio 44135 Attn: Library	1
National Aeronautics and Space Administration Manned Spacecraft Center P. O. Box 1537 Houston, Texas 77001 Attn: Library	1
National Aeronautics and Space Administration Langley Research Center Langley Air Force Base Virginia 23365 Attn: Library	1
Scientific and Technical Information Facility P. O. Box 5700 Bethesda, Maryland 20014 Attn: NASA Representative	1
National Aeronautics and Space Administration Lewis Research Center 21000 Brookpark Road Cleveland, Ohio 44135 Attn: Mr. D. Norred	1
National Aeronautics and Space Administration Goddard Space Flight Center Greenbelt, Maryland 20771 Attn: Library	1

National Aeronautics and Space Administration Marshall Space Flight Center Huntsville, Alabama 35800 Attn: Mr. C. Nevins	1
National Aeronautics and Space Administration Marshall Space Flight Center Huntsville, Alabama 35800 Attn: Mr. M. Nein	1
National Aeronautics and Space Administration Lewis Research Center 21000 Brookpark Road Cleveland, Ohio 44135 Attn: Mr. Dewitt	1
SSD (SSTA) Air Force Unit Post Office Los Angeles, California 90045	1
ASD (Library) Wright-Patterson Air Force Base, Ohio 45433	1
AFML (MAAE) Wright-Patterson Air Force Base, Ohio 45433	1
AFFDL (FDTS/Mr. L. Kelly) Wright-Patterson Air Force Base, Ohio 45443	1
Defense Documentation Center Cameron Station Alexandria, Virginia 22314	20
RTD (RTNP) Bolling Air Force Base Washington, D. C. 20332	1
AEDC (AEOIM) Air Force Systems Command Tullahoma, Tennessee 37389	1
AFSC (SCLT/Capt. S. W. Bowen) Andrews Air Force Base Washington, D. C. 20332	1
AFRPL (RPRPP/ Lt. Dahl) Edwards Air Force Base California 93523	20

AFFTC (FTBAT-2) Attn: Technical Library Edwards Air Force Base California 93523	1
Office of Research Analyses (OAR) Attn: RRRT Holloman Air Force Base, New Mexico 88330	1
Air Force Office of Scientific Research Washington, D. C. 20333 Attn: SREP, Dr. J. F. Masi	1
Linde Company Division of Union Carbide P. O. Box 44 Tonowando, New York 14152 Attn: Dr. L. C. Matsch	1
Lockheed California Company Missiles and Space Division Sunnyvale, California Attn: Mr. J. H. Guill	1
Marquardt Corporation 16555 Saticoy Street Box 2013, South Annex Van Nuys, California 91404	1
Martin-Marietta Corporation Martin Company Denver Division Denver, Colorado Attn: Kenneth P. Timmons	1
Minnesota Mining and Manufacturing Company 900 Bush Avenue St. Paul, Minnesota 55106 Attn: Code 0013 R&D Via: H. C. Zeman, Security Administrator	1
North American Aviation, Inc. Space and Information Systems Division 12214 Lakewood Blvd. Downey, California 90242 Attn: W. H. Morita	1
Quality Electric Super Temp Corporation Cryogenic Division 2411 S. Broadway Los Angeles, California 90007 Attn: Mr. W. Terbo	1

Rocketdyne 6633 Canoga Avenue Canoga Park, California 91304 Attn: Library, Dept. 576-306	1
Rocket Research Corporation 520 South Portland Street Seattle, Washington 98108	1
Republic Aviation Farmingdale, Long Island, New York Attn: Library	1
Stanford Research Institute Propulsion Science Division Menlo Park, California 94025	1
TRW Systems, Inc. Attn: Mr. Juan Elizalde One Space Park Redondo Beach, California 90200	1
Thiokol Chemical Corporation Reaction Motors Division Danville, New Jersey 07834 Attn: Librarian	1
United Aircraft Corporation Corporation Library 400 Main Street East Hartford, Connecticut 06118 Attn: Dr. David Rix	1
United Aircraft Corporation Pratt and Whitney Florida Research and Development Center Post Office Box 2691 West Palm Beach, Florida 33402 Attn: Library	1
Commanding Officer Picatinny Arsenal Liquid Rocket Propulsion Laboratory Dover, New Jersey 07801 Attn: Technical Library	1
Commander U. S. Naval Ordnance Test Station China Lake, California 93557 Attn: Code 45	1
Aerojet-General Corporation P. O. Box 296 Azusa, California 91703 Attn: Librarian	1

Aerojet-General Corporation Attn: Technical Library 2484-2015A P. O. Box 1947 Sacramento, California 95809	1
Aerojet-General Corporation Attn: Mr. G. K. Cornelius Von Karman Center Azusa, California	1
Aerospace Corporation P. O. Box 95085 Los Angeles, California 90045 Attn: Library-Documents	2
ARO, Inc. AEDC Arnold AFS, Tennessee 37389 Attn: Dr. B. H. Boethert, Chief Scientist	1
Arthur D. Little, Inc. Acorn Park Cambridge, Massachusetts Attn: Mr. F. E. Ruccia	1
Atlantic Research Corporation Shirley Highway and Edsall Alexandria, Virginia 22314 Attn: Security Office for Library	1
Bell Aerosystems Box 1 Buffalo, New York 14205 Attn: T. Reinhardt	1
Bell Aerosystems Box 1 Buffalo, New York 14205 Attn: Mr. J. Germano	1
The Boeing Company Aerospace Division P. O. Box 3707 Seattle, Washington 98124 Attn: R. R. Barber, Lib. Ut. Ch.	2
Chemical Propulsion Information Agency Applied Physics Laboratory 621 Georgia Avenue Silver Spring, Maryland 20910	3

Garrett Corporation
AiResearch Division
Phoenix, Arizona
Attn: Library 1

AiResearch Manufacturing Co.
Attn: Mr. John Kimball
9851 Sepulveda Blvd.
Los Angeles, California 1

General Dynamics/Convair
P. O. Box 1128
San Diego, California 92112
Attn: Mr. Mitchel 1

General Dynamics/Convair
P. O. Box 1128
San Diego, California 92112
Attn: Library and Information Services (128-00) 1

General Electric Company
Spacecraft Department
Valley Forge Space Technology Center
Philadelphia, Pennsylvania
Attn: Mr. A. Cohen 1

Grumman Corporation
Bethpage, Long Island, New York
Attn: Library 1

Jet Propulsion Laboratory
4800 Oak Grove Drive
Pasadena, California 91103 1

Appendix A

SPACE PROPULSION SYSTEM OPTIMIZATION PROGRAM

Douglas through its independent Research and Development program, initiated the development of a major computer program in 1964 to facilitate the efficient performance of tradeoff and optimization studies for advanced space propulsion systems. The program was primarily organized for studies of cryogenic stages requiring multiburn operation with extended times in orbit. The program became operational at the outset of this project and was employed extensively throughout the study.

This program essentially can take any given space propulsion system, as defined by the input condition, and quantitatively assess the influences on overall system performance of variation in any one selected design factor or parameter. A number of options are available for representing the overall stage performance. These include stage incremental velocity, maximum payload weight for a given propellant weight, maximum usable propellant weight for a fixed stage gross weight, and so forth. In addition to evaluating stage performance, the program also computes and prints out tank pressure history, venting requirements, and pressurant requirements for the overall mission as well as for each individual burn.

There are presently 1,500 input locations for the program. These include overall stage weights, engine geometry, engine mixture ratio, chamber pressure, tank pressures, initial propellant temperatures, propellant tankage stress and weight factors, stage geometry, tank insulation densities, sheet numbers and thermal performance factors, NPSH values, propellant and pressurant gas properties, correction factors for pressurant requirements, vehicle equilibrium temperatures, reaction control system weight and performance factors, refrigeration system weight and performance factors, pressurant inlet gas temperatures for repressurization and expulsion, thermal heat short factors, mission and duty cycle parameters, pressurization and feed system factors, and others.

Throughout this study, examples of the utilization and capabilities of the H109 program are in evidence. Without such a computer program, it would not have been possible to perform a study of this scope.

One area deserves special note. The propellant heating model for the H109 program is a separate subroutine which can be modified according to the physical heat transfer model which is desired.

The orbit heating equations incorporated into program H109 for this study assume a constant volume equilibrium process with uniform heating to a wall-oriented propellant. This results in the basic equation:

$$dQ = \Delta H - \frac{Vdp}{J} \quad (A-1)$$

or

$$\Delta Q = \Delta H - \frac{V\Delta P}{J} \quad (\text{for a small time increment})$$

For a tank volume containing liquid (subscript L), propellant vapor (subscript V), and noncondensable gas (subscript G) with propellant boiloff, W_{BO} , occurring during the time increment, the heat input to the propellant is given by:

$$\begin{aligned} \Delta Q &= \Delta H_L + \Delta H_V + \Delta H_G + \Delta H_{BO} - \frac{V\Delta P}{J} \\ &= (WC_p \Delta T)_L + (WC_p \Delta T)_V + (WC_p \Delta T)_G + (W_{BO} Q_V) - \frac{(V\Delta P)}{J} \quad (A-2) \end{aligned}$$

where

Q_V = propellant heat of vaporization

The boiloff weight can be found by equating the liquid and vapor volume changes from time points 1 to 2:

$$W_{BO} = \frac{W_{V_1} \frac{1}{\rho_{V_2}} - \frac{1}{\rho_{V_1}} - W_{L_1} \frac{1}{\rho_{L_1}} - \frac{1}{\rho_{L_2}}}{\frac{1}{\rho_{L_2}} - \frac{1}{\rho_{V_2}}} \quad (A-3)$$

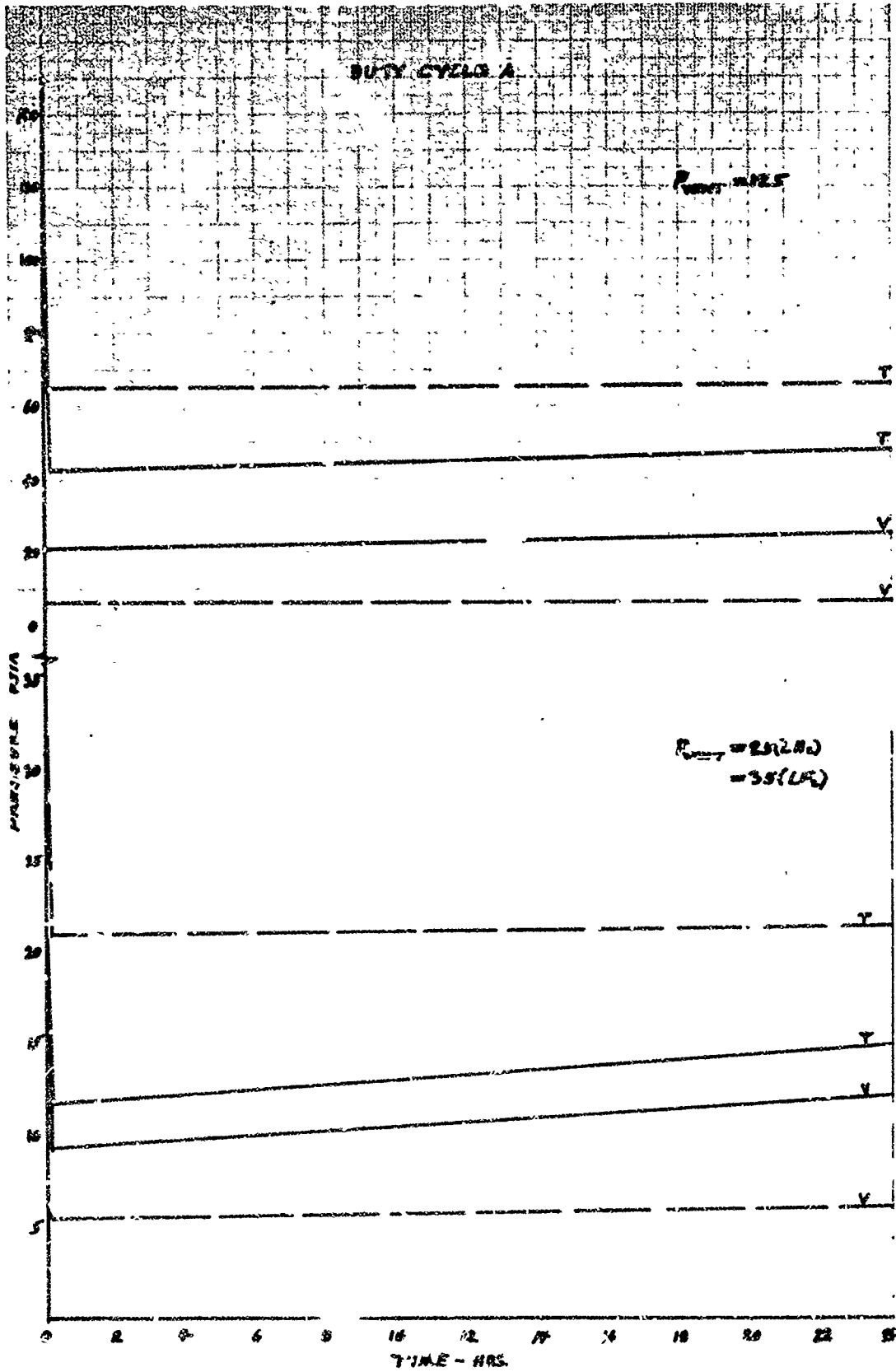
Also

$$\frac{V\Delta P}{J} = \frac{\rho_{V_2} (ZWRT)_{G_2}}{(W_{V_1} + W_{BO})} + P_{V_2} - (P_{V_1} + P_{G_1}) \frac{V_T}{J} \quad (A-4)$$

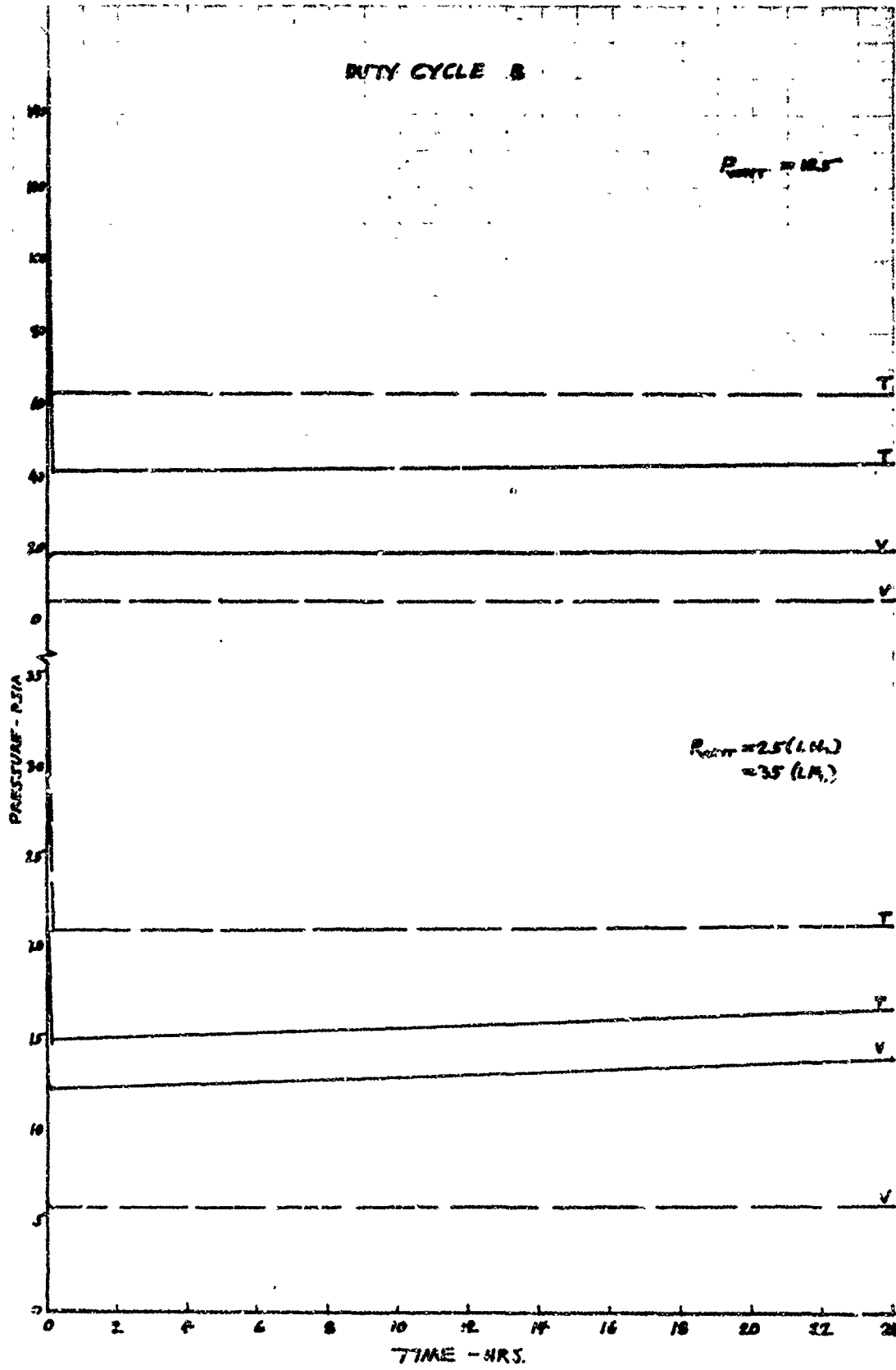
The heat transfer to the tank is programmed as the summation of a radiation and a conduction term with the radiation term accounting for the basic insulation behavior and the conduction term accounting for heat shorts and other sources of heat. These basic equations can be modified to consider the specific performance of various insulations and heat shorts. The analytical work of Phase VI was used to generate insulation performance equations which were then incorporated into the main H109 routine. The heat short predictions of Phase II and VI were used to appropriately modify the heat short conduction factors in the program.

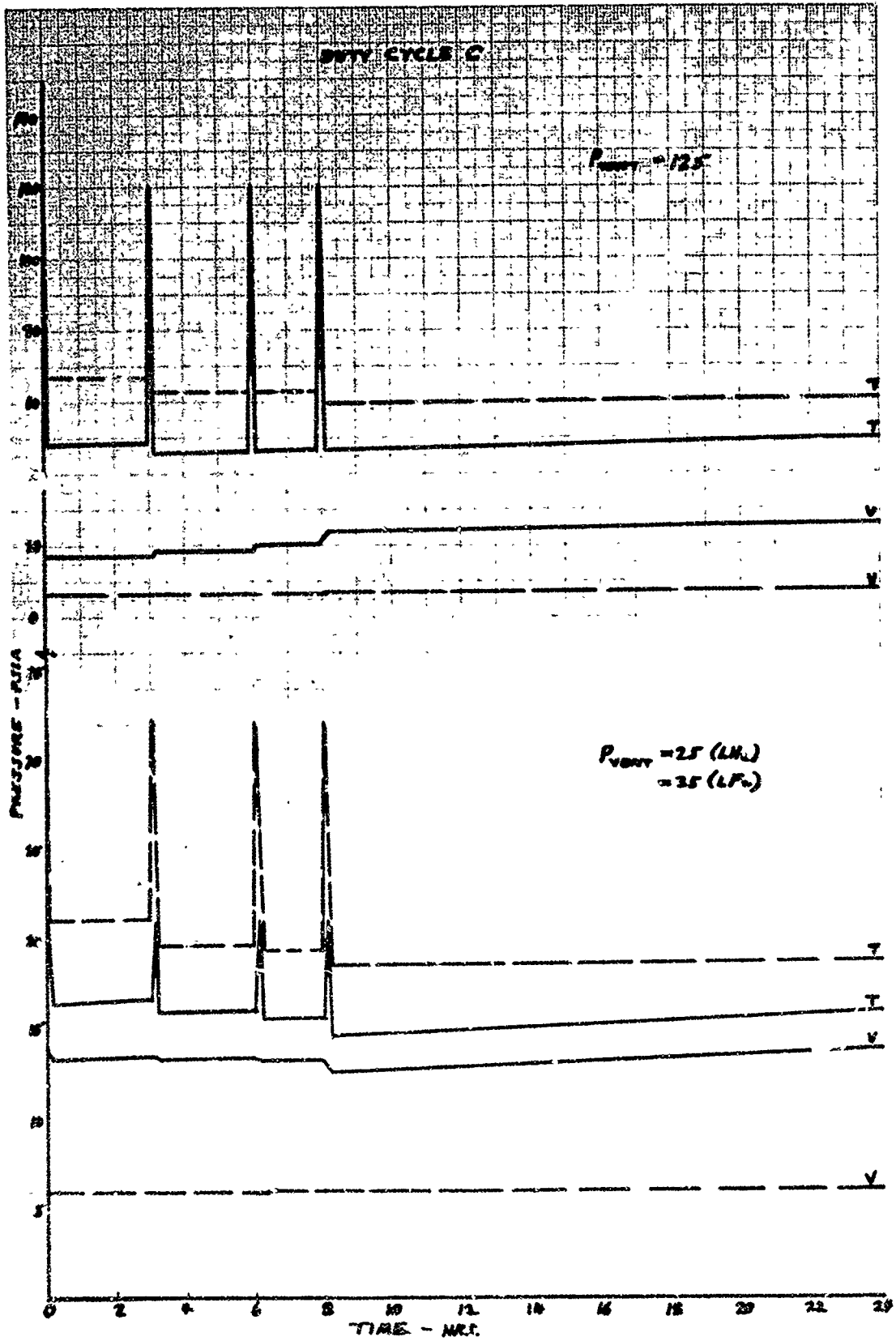
Appendix B
PRELIMINARY PRESSURE HISTORIES

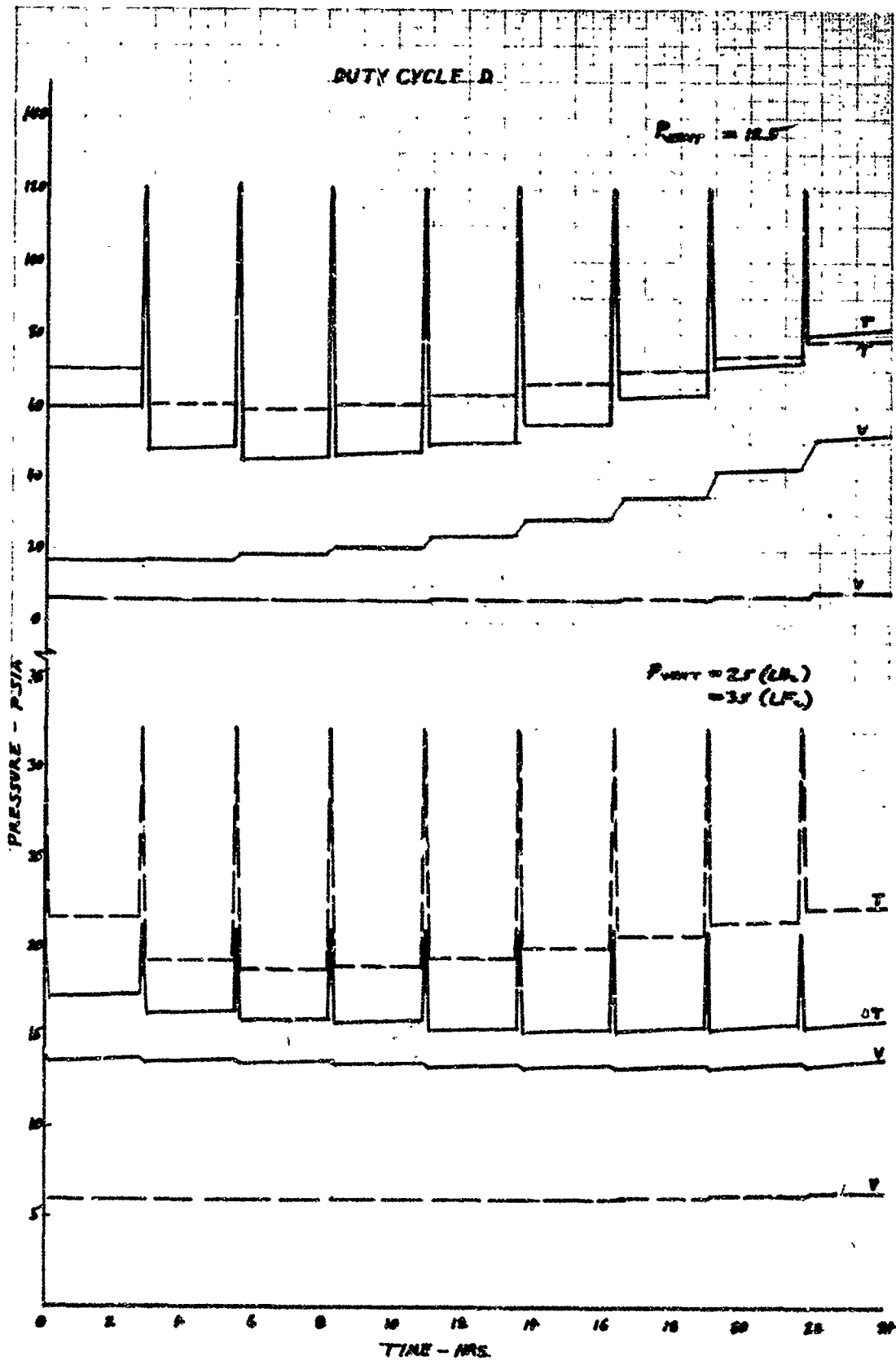
As discussed in Section 4, pressure histories were computed by the H109 computer program using first-order approximations for net propellant heat input values. The pressure histories, as computed, are presented in the following set of curves. In most cases, only the low pressure cases are shown since these show the significant trends. Both the LH_2 and LF_2 tank pressures are shown with the latter usually being designated by broken lines. In addition to the total pressure, the partial pressure of the propellant vapor is also shown. These are designated by T and V, respectively, in the graphs.

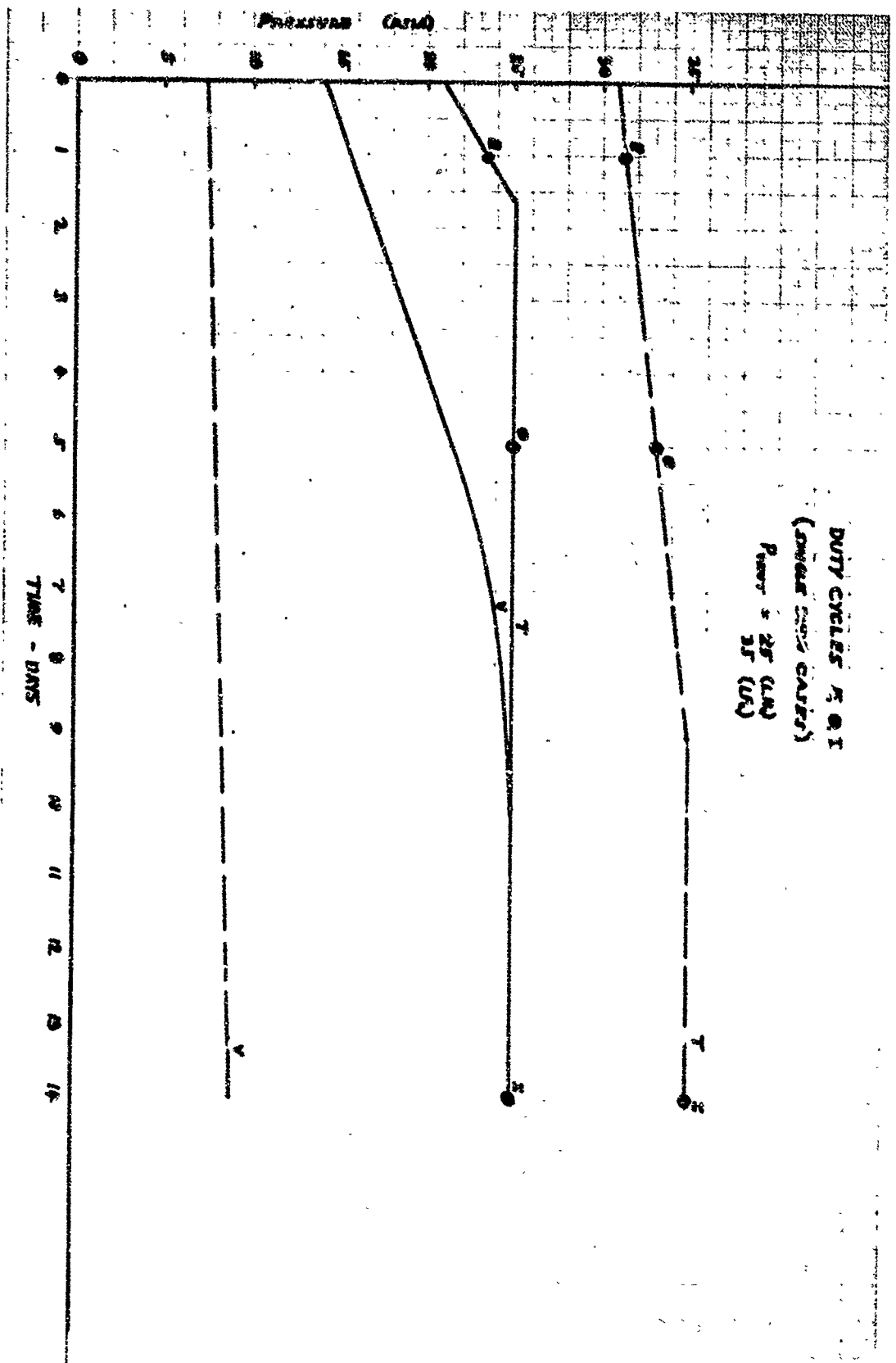


DUTY CYCLE B



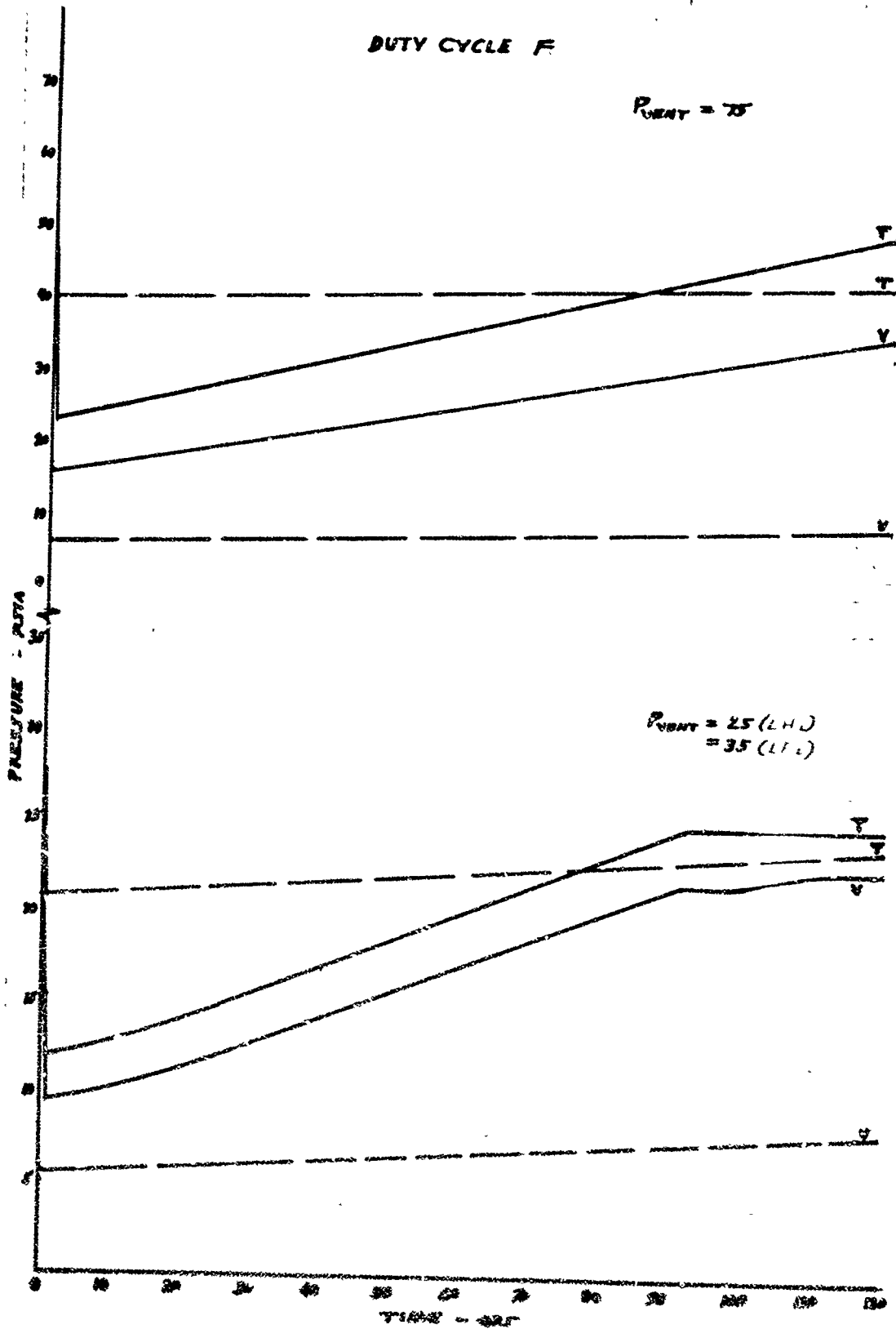




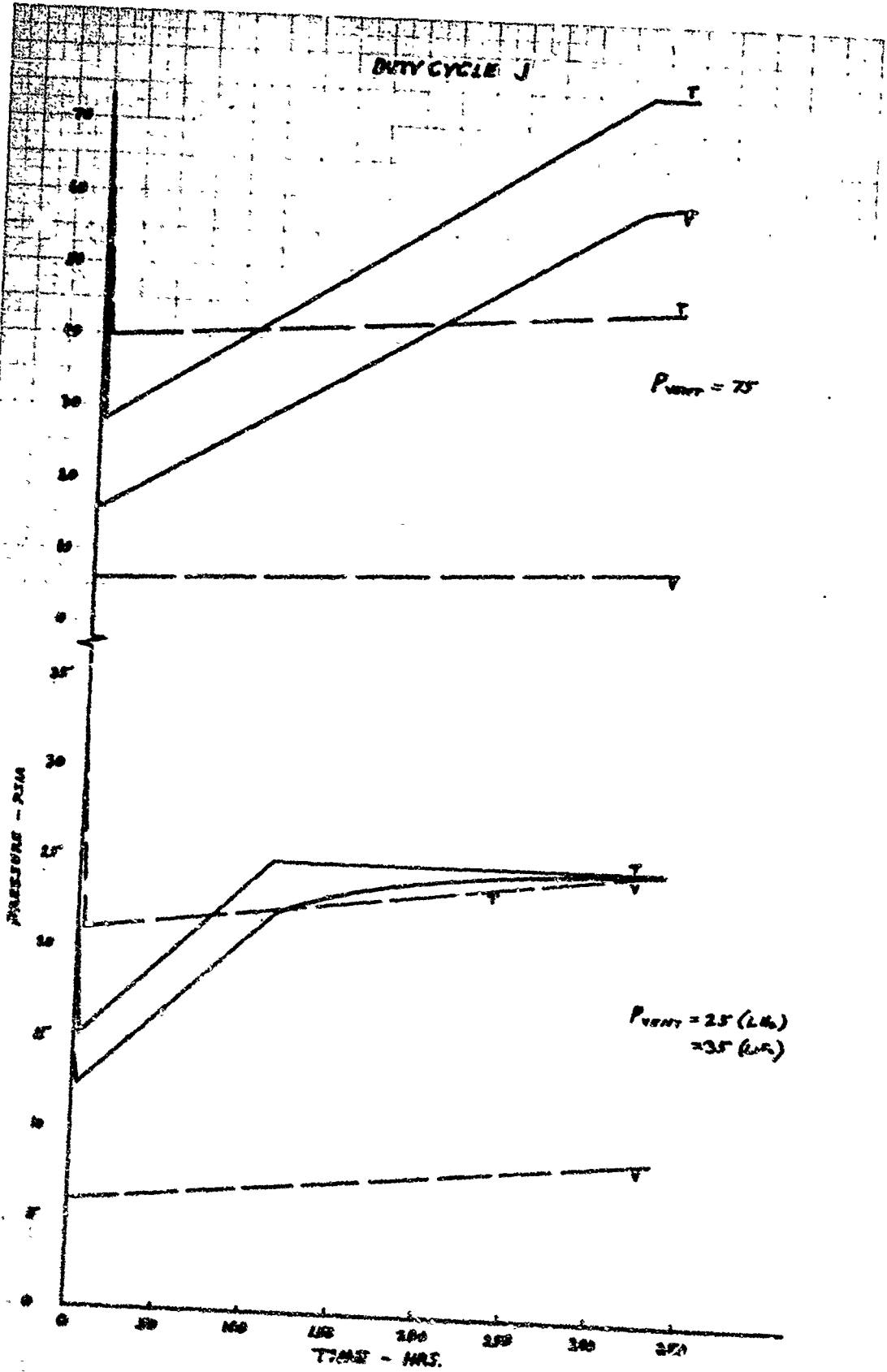


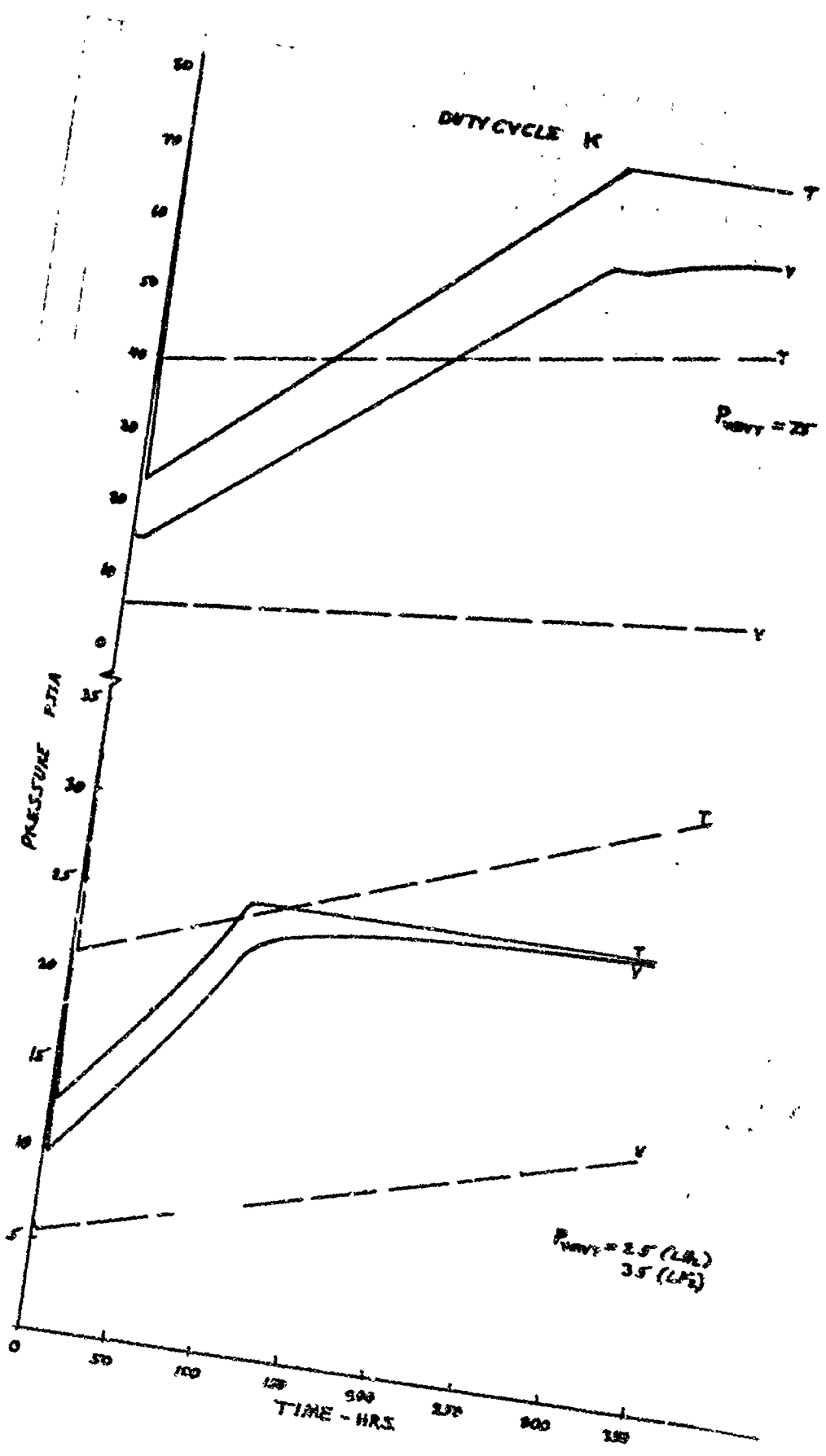
DUTY CYCLE F

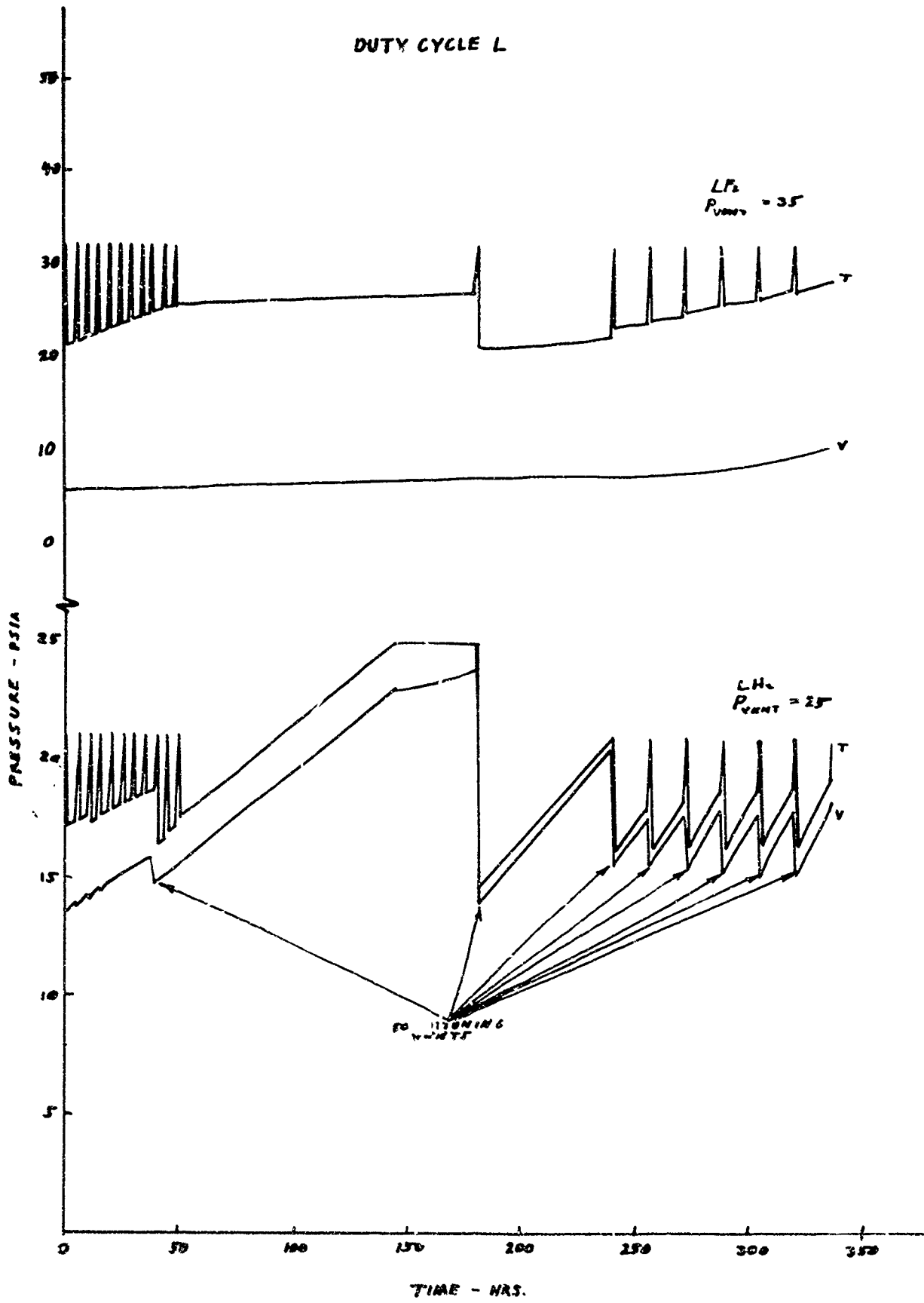
$P_{VENT} = 75$



$P_{VENT} = 25$ (L.H.)
 $= 35$ (R.H.)







Appendix C

OVERALL SYSTEM OPTIMIZATION APPROACH (LB)

The optimization study was performed by using the basic parametric data generated in the seven analytical phases of the program. The Douglas H109 space propulsion system optimization computer program was used.

1. Basic Information for Optimization. Table C-1 summarizes the system weight breakdown. Weights for the structural shell, thrust structure, secondary propulsion, thrust vectoring, trapped propellant, RCS propellant, and the pump-fed engine subsystem were taken directly from the work accomplished by Douglas under Contract AF04(611)-10745. Weights for the tankage and tankage supports were computed under the phase VI analysis. The optimum nine-rod glass fiber support system was assumed. Propellant feed and vent system, pressure-fed engine subsystem, and miscellaneous weights were estimated from component surveys. The P.U. system weight was supplied by RPL, and the zero-g. venting system weight was taken from the phase III results assuming a thermodynamic liquid/vapor separator. The insulation, pressurization, and booster pump systems are to be optimized using the basic data generated in phases VI, VII, and I, respectively. Table 4-28 summarizes the insulation weight and design factors for the three candidate insulation systems and the two possible locations. The insulation performance factors are as given in table 4-28 and are compatible with equations stored in program H109. Table C-2 lists the various heat leak values over and above the basic insulation for shroud-oriented and tank-mounted insulation. These values were evolved in phases II, III, or VI. These data along with surface temperatures evaluated in phase IV were provided (in the proper format) to the H109 optimization program.

2. Optimization Plan. The following general approach was taken in the optimization sequence:

- A system was selected with a nominal pressurization system weight and inlet gas temperature (400° R.), and using shroud-mounted Dimplar insulations. The number of insulation sheets was optimized for a 1-day and a 14-day mission for a selected duty cycle and for each ground-rule tank pressure with no booster pump in the system. The Douglas/Rocketdyne MANSAT study (AF04(611)-10745), showed that the 80/20 burn duty cycle represented one of the most severe cases in terms of propellant heating; therefore, this expulsion cycle for the 1-, and 14-day missions, A and K, respectively, were selected for detailed study.
- The booster pump optimization was performed with the optimum insulation for each tank pressure, and using each of the ground rule tank pressures as base points. Spot checks were made to assess the influence of mission duration and inlet gas temperatures.

Table C-1

WEIGHT BREAKDOWN
(LB)

Base Conditions: LH₂ Weight = 932.7
 LH₂ Tank Liquid Volume = 214.6 ft³.
 LH₂ Tank Diameter = 92 in.
 LF₂ Weight = 11,800 lb.
 LF₂ Tank Liquid Volume = 128.5
 LF₂ Tank Diameter = 75 in.

Tank Pressure (PSIA)	250	200	150	60	25
LH ₂ tank weight	422	338	255	139	139
LF ₂ tank weight	242	198	151	93	93
LH ₂ tank support	43	42	40	37	37
LF ₂ tank support	246	→ 246			
Structural shell	400	→ 400			
Thrust structure	100	→ 100			
Engine subsystem	455	461	560	482	482
Secondary propulsion	87	→ 87			
Thrust vectoring	70	→ 70			
Insulation system	← TBD →				
Propellant feed and vent	80	→ 80			
Pressurization system	← TBD →				
P. U. system	21	21	21	21	0
Miscellaneous	20	→ 20			
Zero-g. venting	9	→ 9			
Trapped propellants	10	→ 10			
P. U. residuals	56	56	56	98	114
Booster pump system	← TBD →				
R. C. S. propellant	278	→ 278			

Table C-2

HEAT LEAK ESTIMATES

Source	Design	B. t. u. /hr.
<u>Shroud-Mounted Insulation</u>		
<u>LH₂ Tank</u>		
Vent line	High-Performance Insulation (HPI) on steel line) (9-rod F-G, $\Sigma=0.1$) (bare steel)	0.56
Tank supports		0.31
Feed line		3.12
Radiation from LF ₂ line		0.08
Pressurization Line		0.40
Insulation attachments		<u>1.48</u>
		5.95
<u>LF₂ Tank</u>		
Vent line	(HPI on steel line) (9-rod F-G, $\Sigma=0.1$) (HPI on steel line)	0.93
Tank supports		1.44
Feed line		0.11
Pressurization line		0.20
Insulation attachment		<u>1.12</u>
<u>Tank-Mounted Insulation</u>		
<u>LH₂ Tank</u>		
Vent line	(HPI on steel line) (9-rod F-G, $\Sigma=0.1$) (Bare steel)	0.60
Tank supports		0.58
Feed line		3.30
Pressurization Line		0.50
Insulation attachments		<u>1.02</u>
<u>LF₂ Tank</u>		
Vent line	(HPI on steel line) (9-rod F-G, $\Sigma=0.1$) (HPI on steel line)	0.95
Tank supports		2.27
Feed line		0.20
Pressurization line		0.30
Insulation attachments		<u>0.68</u>

- The various insulation systems were then evaluated at each tank pressure. Each system and location was optimized and the data compared to select the best performing system. Influences of mission time and tank pressure were assessed.
- The pressurization systems variables for the best optimized insulation systems were optimized for a range of tank pressure. The influences of mission time and duty cycle were determined by spot checking.

The detailed optimization results are reported and discussed in the appropriate phase description.

Appendix D
HARDWARE TEST ITEMS

The basic test hardware items used in this program are shown in Table D-1.

Table D-1 (page 1 of 2)
 BASIC TEST HARDWARE ITEMIZATION

Item	Description	Material	Tests
Structural Shell	10 ft diam x 23 ft long: welded steel structure made up of six 6-in. H-beam rings, eight 2 - x 6-in. longerons, and 0.125 skins	Low-carbon steel	None
Shell and Closures	10 ft diam skin and stringer structure		None
Support Legs	Welded beam sections bolted to shell	Low-carbon steel	None
Tank Transport Support	3 ft diam rods with ball-and-socket and fixtures	Low-carbon steel	None
Static Tank Support	1/2 - x 1/2 - x 36-in. rods with steel insert	Fiberglas	Tensile load test at 5,800 lb (a) Load test to failure at 19,800 lb
LH ₂ Tank	6 ft diam x 12 ft long with six gore section spherical ends: 1-in. wall thickness with 1-1/2-in.-thick manhole	6061-T6 aluminum	Proof test to 375 psia (12/22/65) Ambient He leak test at 185 psia (3/31/65) and (6/22/66) LN ₂ temp. He leak test at 185 psia (4/7/66)
LN ₂ Tank	6 ft diam x 7 ft long with six gore section spherical ends: 1-in. wall thickness with 1-1/2-in.-thick manhole	6061-T6 aluminum	Proof test to 375 psia (12/10/65) Ambient He leak test at 185 psia (2/21/66) LN ₂ temp. He leak test at 185 psia (2/22/66)
He Bottles (2)	23-in. diam x 81-in. long: 1.5-in. wall thickness	304 stainless steel	Proof test to 4,500 psia (10/15/65) Ambient He leak test at 2,250 psia (3/22/66)

Table D-1 (page 2 of 2)

Item	Description	Material	Tests
Auxiliary LH ₂ Bottle	23-in. diam x 51-in. long; 1.5-in. wall thickness	304 stainless steel	Proof test to 4,500 psia (10/15/65) Ambient He leak test at 2,250 psia (3/22/66)
LH ₂ and LN ₂ Feedlines	2-1/2-in. diam flanged and welded tube and/or pipe sections	347 stainless steel	Proof tested to 375 psia (b) Ambient He leak test at 185 psia (4/27/66) LN ₂ temp. He leak test at 185 psia (4/27/66)
LH ₂ and LN ₂ Vent Lines	3-in. diam flanged and welded tube and/or pipe section	347 stainless steel	Proof tested to 375 psia (b) Ambient He leak test at 185 psia (5/18/66) (c) LN ₂ temp. He leak test at 185 psia (5/18/66) (c)
Pressurization Plumbing	3/4-in. or 1-in. diam tubing; 0.095- or 0.083-in. wall thickness	347 stainless steel	Proof tested to 1.5 times working pressure (b) Ambient He leak tested at 1.5 times working pressure (b)
Pressurant Heater for LN ₂ Tank	3/4-in. diam x 80-in. tube 0.016-in. wall	347 stainless steel	Proof tested to 375 psia Ambient He leak test at 185 psia (6/15/66)
Pressurant Heater for LH ₂ Tank	3-in. diam x 40-in. tube 0.016-in. wall	347 stainless steel	Proof tested to 375 psia Ambient He leak test at 185 psia (6/20/66)
LH ₂ and LN ₂ Vent Valve Assemblers	Valve with 2-in. burst disc and bypass	---	Ambient He leak test at 185 psia (5/20/66)

(a) 1 support only tested to failure

(b) Line sections and subassemblies tested as fabricated over a period of time

(c) The lines tested included those upstream of the vent valve

~~Unclassified~~
Security Classification

DOCUMENT CONTROL DATA - R&D

(Security classification of title, body of abstract and indexing annotation must be entered when the overall report is classified)

1. ORIGINATING ACTIVITY (Corporate author) Douglas Aircraft Company, Inc. Missile and Space Systems Division Santa Monica, California		2a. REPORT SECURITY CLASSIFICATION Unclassified	
		2b. GROUP Not Applicable	
3. REPORT TITLE System Effects on Propellant Storability and Vehicle Performance			
4. DESCRIPTIVE NOTES (Type of report and inclusive dates) Final Technical Report October 1966			
5. AUTHOR(S) (Last name, first name, initial)			
6. REPORT DATE October 3, 1966		7a. TOTAL NO. OF PAGES 350	7b. NO. OF REFS 40
8a. CONTRACT OR GRANT NO. AF04(611)-10750		9a. ORIGINATOR'S REPORT NUMBER(S) DAC-59314	
b. PROJECT NO. 6753			
c.		9b. OTHER REPORT NO(S) (Any other numbers that may be assigned this report)	
d.			
10. AVAILABILITY/LIMITATION NOTICES Qualified users may obtain copies of this report from the Defense Documentation Center. Defense Documentation Center release to the Office of Technical Services is not authorized.			
11. SUPPLEMENTARY NOTES		12. SPONSORING MILITARY ACTIVITY Air Force Rocket Propulsion Laboratory, Research and Technology Division, Air Force Systems Command, Edwards Air Force Base, California	
13. ABSTRACT The objective of this program was to investigate the tradeoff between propellant storability and vehicle performance for the propellant storage and feed subsystem of a hypothetical LF ₂ /LH ₂ space propulsion system. Detailed parametric analyses were conducted on such subsystem problem areas as booster-pump feed system utilization, feed line design, venting requirements and provisions, selection of thermal-control coatings, propellant utilization requirements, selection and design of insulation and tank supports, and pressurization system design. Each area was optimized for a spectrum of mission requirements and study ground rules including propellant tank pressures, mission duration, and propulsion system duty cycles. Design recommendations were derived on the basis of these results. A full-scale, non-flightweight test article was designed, fabricated, and tested to simulate the propellant storage and feed subsystem. This apparatus incorporated, wherever practical, the recommendations of the study effort. (The simulator, which uses LH ₂ and LN ₂ , will be tested in the Edwards Air Force Base Space Simulation Facility to obtain experimental data for correlating certain thermodynamic analytical models used in this study.)			

DD FORM 1473
1 JAN 64

Unclassified
Security Classification

Unclassified

Security Classification

14. KEY WORDS	LINK A		LINK B		LINK C	
	ROLE	WT	ROLE	WT	ROLE	WT
Propellant Storability Propellant Storage and Feed Subsystem LF ₂ /LH ₂ Space Propulsion System Booster-Pump Feed System Utilization Feed Line Design Venting Requirements Thermal-Control Coatings Propellant Utilization Pressurization System Design Insulation Design						

INSTRUCTIONS

1. **ORIGINATING ACTIVITY:** Enter the name and address of the contractor, subcontractor, grantee, Department of Defense activity or other organization (corporate author) issuing the report.

2a. **REPORT SECURITY CLASSIFICATION:** Enter the overall security classification of the report. Indicate whether "Restricted Data" is included. Marking is to be in accordance with appropriate security regulations.

2b. **GROUP:** Automatic downgrading is specified in DoD Directive 5200.10 and Armed Forces Industrial Manual. Enter the group number. Also, when applicable, show that optional markings have been used for Group 3 and Group 4 as authorized.

3. **REPORT TITLE:** Enter the complete report title in all capital letters. Titles in all cases should be unclassified. If a meaningful title cannot be selected without classification, show title classification in all capitals in parenthesis immediately following the title.

4. **DESCRIPTIVE NOTES:** If appropriate, enter the type of report, e.g., interim, progress, summary, annual, or final. Give the inclusive dates when a specific reporting period is covered.

5. **AUTHOR(S):** Enter the name(s) of author(s) as shown on or in the report. Enter last name, first name, middle initial. If military, show rank and branch of service. The name of the principal author is an absolute minimum requirement.

6. **REPORT DATE:** Enter the date of the report as day, month, year, or month, year. If more than one date appears on the report, use date of publication.

7a. **TOTAL NUMBER OF PAGES:** The total page count should follow normal pagination procedures, i.e., enter the number of pages containing information.

7b. **NUMBER OF REFERENCES:** Enter the total number of references cited in the report.

8a. **CONTRACT OR GRANT NUMBER:** If appropriate, enter the applicable number of the contract or grant under which the report was written.

8b, 8c, & 8d. **PROJECT NUMBER:** Enter the appropriate military department identification, such as project number, subproject number, system numbers, task number, etc.

9a. **ORIGINATOR'S REPORT NUMBER(S):** Enter the official report number by which the document will be identified and controlled by the originating activity. This number must be unique to this report.

9b. **OTHER REPORT NUMBER(S):** If the report has been assigned any other report numbers (either by the originator or by the sponsor), also enter this number(s).

10. **AVAILABILITY/LIMITATION NOTICES:** Enter any limitations on further dissemination of the report, other than those

imposed by security classification, using standard statements such as:

- (1) "Qualified requesters may obtain copies of this report from DDC."
- (2) "Foreign announcement and dissemination of this report by DDC is not authorized."
- (3) "U. S. Government agencies may obtain copies of this report directly from DDC. Other qualified DDC users shall request through _____."
- (4) "U. S. military agencies may obtain copies of this report directly from DDC. Other qualified users shall request through _____."
- (5) "All distribution of this report is controlled. Qualified DDC users shall request through _____."

If the report has been furnished to the Office of Technical Services, Department of Commerce, for sale to the public, indicate this fact and enter the price, if known.

11. **SUPPLEMENTARY NOTES:** Use for additional explanatory notes.

12. **SPONSORING MILITARY ACTIVITY:** Enter the name of the departmental project office or laboratory sponsoring (paying for) the research and development. Include address.

13. **ABSTRACT:** Enter an abstract giving a brief and factual summary of the document indicative of the report, even though it may also appear elsewhere in the body of the technical report. If additional space is required, a continuation sheet shall be attached.

It is highly desirable that the abstract of classified reports be unclassified. Each paragraph of the abstract shall end with an indication of the military security classification of the information in the paragraph, represented as (TS), (S), (C), or (U).

There is no limitation on the length of the abstract. However, the suggested length is from 150 to 225 words.

14. **KEY WORDS:** Key words are technically meaningful terms or short phrases that characterize a report and may be used as index entries for cataloging the report. Key words must be selected so that no security classification is required. Identifiers, such as equipment model designation, trade name, military project code name, geographic location, may be used as key words but will be followed by an indication of technical context. The assignment of links, rules, and weights is optional.

Unclassified

Security Classification